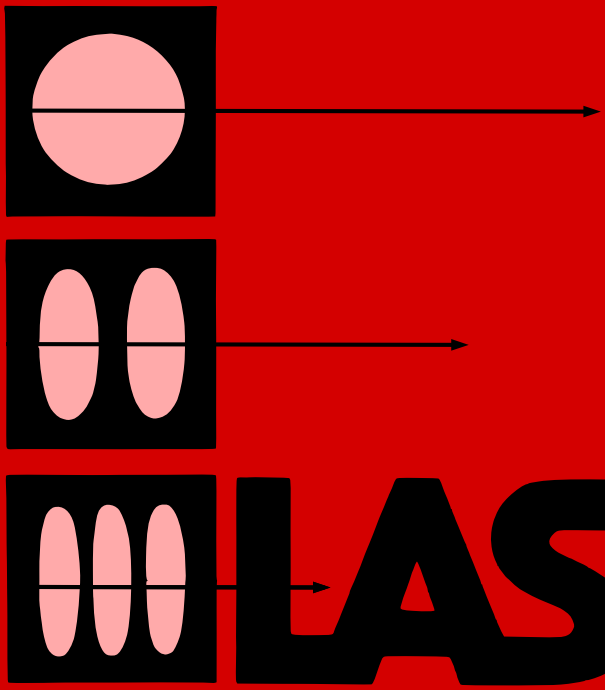
L.V. Tarasov



LASER PHYSICS

Mir
Publishers
Moscow

About the Book

The book aims at bringing the reader up-to-date with the latest achievements and trends in the physics of laser processes, as well as at providing sufficient information so that the reader can then independently make use of specialized literature in this field. It describes the present state of affairs in the development of laser technology from the point of view of research as well as applications in various branches of industry.


ИЗДАТЕЛЬСТВО
МИР

Л. В. Тарасов

ФИЗИКА ПРОЦЕССОВ В ГЕНЕРАТОРАХ КОГЕРЕНТНОГО ОПТИЧЕСКОГО ИЗЛУЧЕНИЯ

Издательство
«Радио и связь»
Москва

L.V. Tarasov

LASER PHYSICS

Translated from the Russian
by
Ram S. Wadhwa

MIR
Publishers
MOSCOW

First published 1983

Revised from the 1981 Russian edition



На английском языке

© Издательство «Радио и связь», 1981
© English translation, Mir Publishers, 1983

PREFACE

Lasers form the subject matter of a very wide range of scientific and industrial investigations. The number of scientists and engineers engaged in laser research and investigation of topics relating to laser technology is ever on the increase. Hence a need was felt to combine in a single book the physical concepts behind the laser processes with the present day state-of-the-art and the progress made in the field of laser engineering.

This book is intended to serve two purposes: to systematize and extend the reader's concepts on laser processes, and to provide information which could help the reader in further independent work involving specialized literature. The author has endeavoured to reflect the present day trends in laser engineering, and at the same time provide a systematic description of the methods employed in the theory of lasers and to discuss various approaches and approximations. As a result, the author feels that this book will be of interest not only to research workers and engineers, but will also provide a scientific and methodical background for specialized textbooks and lectures.

Three types of questions have been touched upon in this book: the methods of obtaining inverted active media, formation of the radiation field in a resonator, and the dynamics of laser processes.

The first chapter, dealing with the methods of creation of inversion in active media, describes the principles and peculiarities of different kinds of lasers: solid-state lasers, organic dye lasers, photodissociation lasers, gas-discharge lasers, ionization lasers, gasdynamic lasers, chemical lasers, and plasma lasers.

In the second chapter, the role of a resonator in the formation of a radiation field in a laser has been described, and the theory of open resonators has been discussed. The geometric optics approximation, the Fox-Li iteration method, the Gaussian beam model, and the $ABCD$ law have been employed. The effect of mirror apertures, the existence of a lens or a diaphragm inside a resonator, and the misalignment of elements in a resonator have been considered. Stable as well as unstable resonators of different geometries have been described. The thermal lens effect, the frequency pulling effect, and the hole-burning effect have been discussed for the case of active resonators. Special attention has been paid to the question of selection of longitudinal modes, as well as to the physics of waveguide resonators and thin-film lasers with a distributed feedback.

The third chapter begins with a review of various generation regimes in a laser, including the active and passive Q-switching in a resonator, the longitudinal and transverse mode locking, and the load modulation. The Statz-De Mars balance equations and their modifications have been introduced, analyzed, and applied to different cases. On the basis of these equations, different questions have been discussed concerning single mode lasers. These include transition processes leading to a damping of radiation power pulses, the emergence of undamped power pulses in the case of a weak modulation of losses, and the generation of giant pulses upon instantaneous switching. The electrooptical and the acoustooptic methods of active Q-switching have been compared. A detailed analysis has been carried out of the processes taking place in a bleachable filter laser. The longitudinal mode locking has been discussed by using the spectral as well as time-based approach. The question of self-mode locking in a bleachable filter laser has been discussed by using the time-based approach on the basis of fluctuation concepts. The time-based approach has also been used for the description of acoustooptic mode locking in a laser with a homogeneous broadening of the gain line. The methods of investigation of ultrashort light pulses have been discussed separately.

In the appendices, a systematic investigation has been carried out for the calculation of Hermite polynomials, Jones matrices, singular points in a plane dynamic system, etc.

The author expresses his deep sense of gratitude to V. G. Dmitriev, V. R. Kushnir, V. K. Novokreshchenov, E. A. Shalaev, V. N. Morozov, V. A. Dyakov, V. V. Nikitin, Yu. N. Pchelnikov, A. M. Amelyants, A. A. Solovyev, and V. F. Trukhin, who have read the manuscript and made valuable comments and suggestions. The author is also grateful to his wife A. N. Tarasova for the help rendered during the preparation of the manuscript for publication.

L. V. Tarasov

CONTENTS

Preface 5

Chapter 1. Population Inversion in Active Media 9

1.1 Some General Aspects 9
1.2 Optical Pumping. Solid-state Lasers 20
1.3. Organic Dye Lasers 30
1.4 Gas Lasers with a Wideband Optical Pumping 36
1.5 Pumping by Self-maintained Electric Discharge in Rarefied Gases 39
1.6 Electro-ionisation Lasers 50
1.7 Gasdynamic Lasers (Thermal Pumping) 54
1.8 Chemical Lasers 58
1.9 Plasma Lasers (Recombination Pumping) 64

Chapter 2. Formation of Radiation Field in a Laser Resonator . . . 73

2.1. Generation Condition 73
2.2 Optical Resonator and Laser Radiation (Preliminary Remarks) 78
2.3 General Remarks about Open Resonators 88
2.4 Lens Waveguides and Open Resonators (Geometrical Optics Approximation) 100
2.5 Detuning of an Open Resonator 112
2.6 Analysis of Open Resonators on the Basis of Fox-Li Iterative Method. Equivalent Resonators 116
2.7 Gaussian Beams 134
2.8 Transformation and Matching of Gaussian Beams 142
2.9 Gaussian Beams in Stable Resonators 151
2.10 Unstable Resonators 163
2.11 Frequency Selection 175
2.12 Hole burning Effect and Frequency Pulling Effect 183
2.13 Thermal Lens 190
2.14 Waveguide Resonators 195
2.15 Optical Radiation in a Thin-film Waveguide. Distributed Feedback 200

Chapter 3. Dynamics of Laser Processes 214

3.1 General Remarks about Laser Operating Conditions 215
3.2 Approximate Equations Describing the Dynamics of Laser Processes (Balance Equations) 229
3.3 Free Generation. Regular Damped Pulsations of Radiation Power 244
3.4 Unstable Resonator Laser. Undamped Pulsations of Radiation Power 256
3.5 Active Modulation of the Resonator Q-factor 262
3.6 Giant Pulse Generation in the Case of Active Modulation of the Resonator Q-factor 270
3.7 Bleachable Filter Lasers 283
3.8 Giant Pulse Generation for Passive Q-modulation of the Resonator 296

3.9 Longitudinal Mode Locking (Ultrashort Light Pulse Generation) 304
3.10 Measurement of Duration of Ultrashort Light Pulses 313
3.11 Analysis of Self-locking of Longitudinal Modes in a Bleachable Filter Laser Based on Fluctuation Concepts 319
3.12 Time-based Description of Active Longitudinal Mode Locking in a Laser with a Uniformly Broadened Gain Line 328

Appendices 336

References 345

Index 354

Chapter One

POPULATION INVERSION IN ACTIVE MEDIA

1.1. SOME GENERAL ASPECTS

Inversion of Active Medium as a Necessary Condition for Laser Generation. The generation of laser radiation is caused by transitions between certain energy levels of active centres. We shall call these levels the *laser levels*, and denote their population (per unit volume of the active medium) by n_1 (*lower* laser level) and n_2 (*upper* laser level) respectively. The difference

$$N = n_2 - (g_2/g_1)\, n_1 \tag{1.1.1}$$

is called the *inverse population density* of laser levels. Here, g_1 and g_2 represent the degeneracy of the corresponding levels. For the sake of simplicity, we assume that $g_1 = g_2$.

If the condition

$$N > 0 \tag{1.1.2}$$

is satisfied, an *inversion of the active medium* is said to take place. Since N is, in general, a function of time and space coordinates, the concept of inversion may be applied to definite time intervals and to specific regions of the active medium.

In a medium in thermodynamic *equilibrium*, N is a negative quantity, i.e. the lower level is more densely populated than the upper one. In order to create an inversion in the active medium, we must bring it to a *nonequilibrium* state.

Inversion of the active medium is a necessary condition for laser generation. It should be recalled that the *amplification factor* $\varkappa$ of a homogeneous medium is given by the expression[1]

$$\boxed{\varkappa = \sigma N} \tag{1.1.3}$$

where σ is the cross section of induced transitions between laser levels. It can be seen from Eq. (1.1.3) that the very fact of the amplification of radiation upon its passage through an active medium assumes that the condition (1.1.2) is satisfied, i.e. N is a *positive* quantity. The need for ensuring an inversion is physically apparent, since only for $N > 0$ (i.e. for $n_2 > n_1$) can the process of *induced emission* at the lasing transition dominate over the reverse process of *absorption* of radiation.

In order to create and sustain inversion, we have to excite (or pump) the active medium in some way. Several methods are avail-

[1] See, for example, Eqs. (5.6.9) and (5.6.10) in [1].

able for pumping and we shall be considering these in the following sections.

Quantum Yield and Efficiency of a Laser. The choice of the level diagram of an active centre and the method of pumping have a considerable effect on the efficiency of a laser.

Suppose that an active centre is represented by a four-level diagram (*four-level laser model*, Fig. 1.1), where *O* is the ground level, *1* and *2*—the lower and upper laser levels respectively, and *3*—the level populated as a result of pumping (excitation level). We assume that the entire pumping power is absorbed by the active

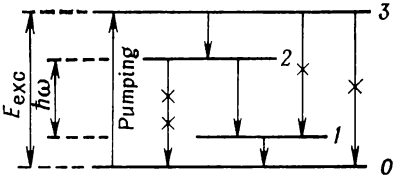


Fig. 1.1

centres and that the transitions which are crossed out in the figure do not take place. In this ideal case, the laser has maximum efficiency equal to the ratio of the energy $\hbar\omega$ of the emitted photon to the energy E_{exc} required to excite one active centre:

$$\eta' = \hbar\omega/E_{exc}. \qquad (1.1.4)$$

The quantity η' is called the *quantum yield* of the laser.

In actual practice, not all the pumping power is absorbed by the active centres. A part of the power is dissipated and another part is absorbed by inactive particles. Hence the expression for the efficiency of a laser must include a factor indicating the fraction of the pumping power actually absorbed by the active centres. We denote this fraction as γ. Besides, not all the excited active centres arrive at the upper laser level *2*, since a part of these directly goes from level *3* to level *1* or *0* (the transitions crossed out once in Fig. 1.1.) Consequently, the expression for the efficiency of a laser contains a factor indicating the fraction of the pumping power absorbed by the active centres, which is actually spent on "useful" excitation, i.e. on the excitation of such active centres which ultimately turn up at level *2*. This fraction is denoted by ν. Finally, not all the active centres at the level *2* undergo a laser transition, since a part of these directly comes to the ground level (the transition crossed twice in Fig. 1.1). This gives rise to yet another factor in the expression for the efficiency of a laser. This is the ratio f of the number of active centres undergoing a laser transition to the number of active centres excited to level *2*. The ultimate expression for laser

efficiency thus acquires the form

$$\eta = \gamma \nu f \hbar\omega / E_{\text{exc}}. \tag{1.1.5}$$

An increase in the fraction of pumping power absorbed by active centres leads to an increased value of the factor γ in Eq. (1.1.5). By employing active media in which "parasitic" transitions (which are crossed out in Fig. 1.1) are less probable, we can increase the factors ν and f. It should also be noted that the example of pumping considered in Fig. 1.1 is highly *selective*, since it causes a population of level *3* only. Pumping with a lower selectivity may lead, for example, to a population of level *1*. This results in a decreased value of ν.

Inversion Condition for the Four-level Model (Stationary Pumping). Figure 1.2 shows the four levels and such transitions among these

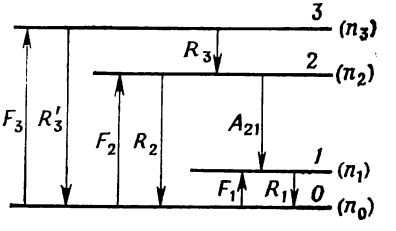


Fig. 1.2

which we shall be considering. Transition probabilities per unit time are indicated near the corresponding arrows in the figure. Since there is no generation, we shall be considering only spontaneous emission in the working channel *2-1* (A_{21} is Einstein's coefficient for spontaneous emission). The *balance equations* for stationary population density (stationary inversion) have the following form:

$$\text{For level } 3 \quad F_3 n_0 - (R_3 + R'_3)\, n_3 = 0; \tag{1.1.6a}$$

$$\text{For level } 2 \quad R_3 n_3 + F_2 n_0 - (R_2 + A_{21})\, n_2 = 0; \tag{1.1.6b}$$

$$\text{For level } 1 \quad F_1 n_0 + A_{21} n_2 - R_1 n_1 = 0. \tag{1.1.6c}$$

By way of an example, let us derive Eq. (1.1.6a). The rate of increase in population density of level *3* is equal to the number of transitions $0 \rightarrow 3$ per unit time per unit volume, i.e. equal to $F_3 n_0$. The rate of decrease in this population density is equal to the sum of transitions $3 \rightarrow 2$ and $3 \rightarrow 0$, i.e. equal to $(R_3 + R'_3)\, n_3$. For stationary pumping, the rate of increase and decrease in the population density of a level must be equal. This leads to Eq. (1.1.6a).

Introducing the notation $n_0/n_1 = x$, $n_2/n_1 = y$, and $n_3/n_1 = z$, we can rewrite the balance equations in the following form:

$$\left.\begin{aligned} &F_3 x = (R_3 + R'_3)\, z; \\ &F_2 x + R_3 z = (R_2 + A_{21}) y; \\ &F_1 x + A_{21} y = R_1. \end{aligned}\right\} \tag{1.1.7}$$

The inversion condition (1.1.2) in this case assumes the form

$$y > 1. \tag{1.1.8}$$

Substituting in Eq. (1.1.8) the expression for y obtained from Eq. (1.1.7), we get the following inequality:

$$R_1 > \left[A_{21} + F_1 \frac{A_{21} + R_2}{F_2 + F_3 R_3/(R_3 + R_3')} \right]. \tag{1.1.9}$$

The ratio $R_3/(R_3 + R_3')$ is the relative probability that an active centre goes from level *3* to level *2*. Consequently, $F_3 R_3/(R_3 + R_3')$ is the probability that level *2* is populated via level *3*. Since the transition $0 \to 2$ also leads to level *2*, the sum

$$F = F_2 + [F_3 R_3/(R_3 + R_3')] \tag{1.1.10}$$

is the total probability of populating the upper laser level. Further, we observe that the sum

$$R = A_{21} + R_2 \tag{1.1.11}$$

is apparently the total probability of depopulation (relaxation) of the upper level. Taking into account Eqs. (1.1.10) and (1.1.11) we can rewrite the *inversion condition* (1.1.9) in the form

$$\boxed{(R_1 - A_{21})/R > F_1/F}. \tag{1.1.12}$$

General Principles for Creating Inversion. In order to create inversion, the *selectivity* of population or depopulation of the corresponding levels of an active centre is of prime importance. In this connection, let us consider the condition (1.1.12), from which it can be seen that stationary inversion is attained under the assumption that the inequality

$$R_1 > A_{21} \tag{1.1.13}$$

is satisfied. In other words, the total probability of depopulation of the lower laser level must be higher than the probability of its population due to spontaneous transitions from the upper laser level.

It also follows from the inequality (1.1.12) that it is desirable to satisfy the following inequalities in order to create an inversion:

$$F \gg F_1, \tag{1.1.14}$$

$$R_1 \gg R. \tag{1.1.15}$$

These inequalities reflect the above-mentioned selectivity factor necessary for creating an inversion. The inequality (1.1.14) means that the total probability of populating the upper laser level must be considerably higher than the total probability of populating the lower laser level. The second inequality (1.1.15) means that the

total probability of relaxation of the lower laser level must be considerably higher than the total probability of relaxation of the upper laser level.

In actual practice, inversion can be created if at least one of these two inequalities is satisfied. In this connection, it should be remembered that inversion can be created not only through a preferential population of the upper laser level (in preference to the lower laser level), but also through a preferential depopulation of the lower laser level. Thus it is necessary to take into consideration the *relation* between the probabilities of population and depopulation mechanisms in laser levels while considering different methods for pumping.

Mechanisms for Population of Levels (Excitation Mechanisms). *Absorption of Light (Optical Pumping).* Pumping radiation with a specially selected spectrum can lead to a high selectivity of optical excitation on account of predominant population of the upper laser level: $F \gg F_1$.

Inelastic collisions with free electrons, where a part of kinetic energy of the electron is transferred to the active centre (electronic excitation). The exciting free electrons may be created by a self-sustained gas discharge, or by using ionising radiation in combination with an external electric field for accelerating electrons (non-self-sustained discharge). The latter case corresponds to *electro-ionisation pumping.* For the case of electronic excitation, the inequality $F < F_1$ is usually satisfied instead of the inequality (1.1.14)[2].

Inelastic collisions with auxiliary atoms and molecules with a resonant transfer of excitation energy from an atom (or molecule) to an active centre. The *resonance* mechanism of energy transfer assumes a high pumping selectivity due to predominant population of the upper laser level ($F \gg F_1$).

Chemical pumping corresponds to an excitation of levels through specially selected exothermic reactions. Chemical pumping is characterised by a highly pronounced selectivity ($F \gg F_1$).

Recombination pumping means an excitation of levels as a result of recombination of electrons and ions in a specially created plasma. The inequality (1.1.14) may not be satisfied when this method is applied for excitation.

Thermal pumping is the excitation of levels through heating of the active medium. In this case, $F < F_1$.

Mechanisms for Depopulation of Levels (Relaxation Mechanisms). *Radiative depopulation* by spontaneous emission. The selectivity of this mechanism is determined by the selection rules (a transition may be optically *allowed* or *forbidden*, depending on the properties of the levels under consideration) and the distance between the level

[2] The self-terminating transitions discussed later in this book are an exception to this.

being depopulated and the low-lying level at which the active centres arrive as a result of relaxation (in other words, on the energy $\hbar\omega$ of the spontaneously emitted photon). The higher the value of $\hbar\omega$, the higher the probability of radiative depopulation (subject, of course, to the condition that such a transition is optically allowed). It should be remembered that Einstein's coefficient A for spontaneous emission in the case of dipole (i.e. optically allowed) transitions is given by the expression[3]

$$A = \frac{4\omega^3}{3\hbar c^3} |(\mathbf{d})|^2, \tag{1.1.16}$$

where $(\mathbf{d})$ is the matrix element of the electric dipole moment of the radiating system, corresponding to a transition.

The mechanism of radiative depopulation may be characterised by a high selectivity. If the transition $2 \rightarrow 0$ is optically forbidden while the transition $1 \rightarrow 0$ is optically allowed[4] and has a fairly high frequency, then $R_1 \gg R$.

Inelastic collisions with free electrons, resulting in an increased kinetic energy of electrons (electronic de-excitation). This mechanism does not possess any special selectivity.

Inelastic collisions with auxiliary atoms and molecules, resulting in the energy transfer from an active centre to an atom (or a molecule). There are two mechanisms of energy transfer, namely, the *resonance* mechanism and the *gas-kinetic* mechanism. In the first case, specific atomic or molecular levels are excited. This mechanism has a fairly high selectivity ($R_1 \gg R$). In the second case, the kinetic energy of the atom (or molecule) increases. The gas-kinetic mechanism of energy transfer is considerably less selective and slower in comparison to the resonance mechanism.

As a special case, let us mention the de-excitation of active centres upon collisions with the walls of the reservoir containing an active medium (de-excitation at the walls).

De-excitation through adiabatic expansion of a gaseous active medium. The excitation energy of the active centres is converted into the kinetic energy of the particles of a rapidly expanding gas. This mechanism allows for a highly selective pumping due to predominant depopulation of the lower laser level ($R_1 \gg R$).

Chemical de-excitation through specially selected chemical reactions has a very high degree of selectivity ($R_1 \gg R$).

Transfer of excitation energy to the collective motions in a medium. In particular, this includes a transfer of energy to phonons (increase in the vibrational energy of atoms in a crystal lattice).

[3] See, for example, Eq. (2.5.34) in [1].

[4] The labelling of energy levels corresponds to the diagram shown in Fig. 1.1.

The above picture of physical mechanisms of excitation and relaxation of levels is not exhaustive and will be supplemented later It should be mentioned that most of the mechanisms described above are related to the *non-optical transitions* in matter[5].

The distinction between excitation and relaxation mechanisms is to a certain extent arbitrary. It should be remembered that the same mechanism, as a rule, leads to the population of certain levels and to the depopulation of certain other levels of an active centre.

Classification of Lasers on the Basis of Various Pumping Mechanisms. Traditionally, lasers are divided into four main categories, depending on the kind of active medium employed. These are: *gas* lasers, *liquid* lasers, *solid-state* lasers, and *semiconductor* lasers. A more precise classification should take into account not only the type of active medium, but also the pumping method. Such a classification is given in Fig. 1.3.[6] This diagram indicates various types of pumping: *optical pumping*, *pumping by self-sustained electric discharge*, *ionisation pumping*, *thermal pumping*, *chemical pumping*, and *recombination pumping*. These types have been mentioned above while describing different physical mechanisms of excitation. It should, however, be borne in mind that the problem of creating inversion should be considered by taking into account not only the excitation processes, but also the relaxation processes for energy levels.

In certain types of lasers, selective relaxation of laser levels plays an important role in creating inversion (in such lasers, $R_1 \gg R$). For example, in ion lasers, the comparatively fast radiative depopulation of lower laser levels plays an important role. In molecular and electro-ionisation lasers, the relaxation of lower laser levels by inelastic collisions is important. In gasdynamic lasers, it is the relaxation due to adiabatic processes that is of prime importance. The special role of relaxation processes in different types of lasers is shown in Fig. 1.3. The selective depopulation of laser levels, however, plays an important role in other types of lasers as well (for example, in plasma lasers and chemical lasers).

The *generation conditions* should also be taken into consideration. The question of depopulation of levels becomes specially important in the case of continuous-wave generation (stationary inversion) while in pulsed lasers one mainly considers the question of selective *population* of laser levels.

Some Problems Connected with Continuous-Wave Generation; Collision Lasers. We have mentioned above that one of the conditions for creating stationary inversion is expressed by the inequality

[5] Non-optical transitions and, in particular, inelastic collisions involving [electrons, atoms, and molecules have been discussed by Tarasov [1]. See also [2, 3].

[6] Semiconductor lasers have not been considered in this book.

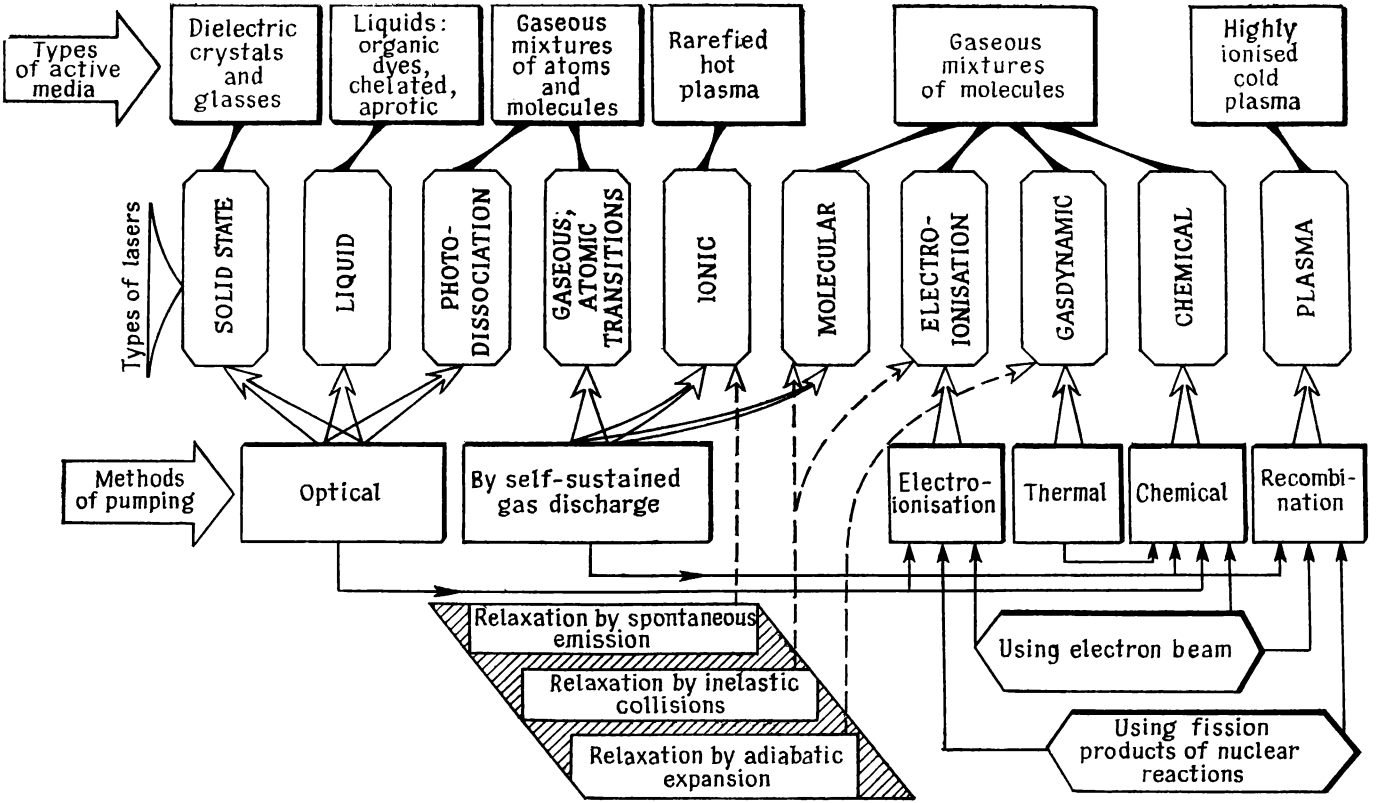

Types of active media
Dielectric crystals and glasses
Liquids: organic dyes, chelated, aprotic
Gaseous mixtures of atoms and molecules
Rarefied hot plasma
Gaseous mixtures of molecules
Highly ionised cold plasma
Types of lasers
SOLID STATE
LIQUID
PHOTO-DISSOCIATION
GASEOUS; ATOMIC TRANSITIONS
IONIC
MOLECULAR
ELECTRO-IONISATION
GASDYNAMIC
CHEMICAL
PLASMA
Methods of pumping
Optical
By self-sustained gas discharge
Electro-ionisation
Thermal
Chemical
Recombination
Relaxation by spontaneous emission
Relaxation by inelastic collisions
Relaxation by adiabatic expansion
Using electron beam
Using fission products of nuclear reactions

Fig. 1.3

(1.1.13). *A sufficiently fast relaxation of the lower laser level* is required in order to fulfil this condition. The inequality (1.1.13) considerably limits the choice of laser transitions which can create a stationary inversion, and hence a continuous-wave generation.

Suppose that relaxation of the lower laser level is caused by *spontaneous emission*. In this case, a high relaxation rate is ensured if the lower laser level is situated fairly high above the ground level, in accordance with (1.1.16). Consequently, a laser transition must take place between high levels, which means a fairly quantum yield $\eta' = \hbar\omega/E_{exc}$ of the laser. For a typical atomic gas laser operating in the CW mode, the energy $E_{exc} \approx 10\text{-}20$ eV, and, as a rule, η' does not exceed 0.1. Besides, the use of high levels means small values of the factors ν and f in the expression (1.1.5) for laser efficiency, since there is a probability of excitation of additional low-lying levels as well as a probability of relaxation of active centres to these levels. Hence it is not surprising that the efficiency of a CW atomic gas laser is just of the order of 10^{-3}.

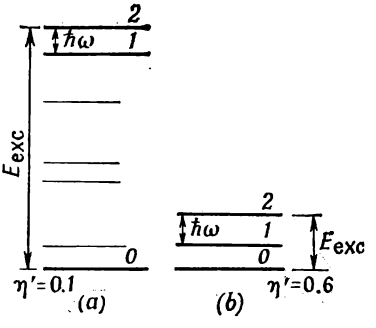


Fig. 1.4

Figure 1.4*a* shows a characteristic diagram of the laser levels under the condition that the lower level is depopulated by spontaneous emission. Here, *0* is the ground level, *1* and *2* are the laser levels. The other levels shown in the figure are parasitic levels in this case. For Fig. 1.4*a*, $\eta' = 0.1$. In order to improve the efficiency of the laser, we should go over from the diagram shown in Fig. 1.4*a* to the one in Fig. 1.4*b*, for which $\eta' = 0.6$. In other words, we should consider transitions between relatively low laser levels.

A decrease in the radiative depopulation of the lower laser level is unavoidable in this case, and hence supplementary mechanisms are necessary for relaxation of the lower level. One such supplementary mechanism may be the inelastic collisions of active centres with atoms and molecules specially introduced into the active gaseous medium. Such lasers are often called *collision lasers*.

Molecular and electro-ionisation lasers generating on vibrational transitions of a CO_2 molecule are examples of collision lasers. The cases shown in Fig. 1.3, where relaxation of the lower level by inelastic collisions plays an important role in creating inversion, also belong to this category of lasers.

Advantages of Pulsed Pumping; Generation on Self-terminating Transitions. For *pulsed* pumping, inversion is created just over certain time intervals and hence a fast depopulation of the lower

laser level is not significant. Suppose that when an excitation pulse is switched on, the upper laser level is populated at a faster rate than the lower laser level. In this case, the laser operates on account of inversion created at the *beginning of the excitation pulse*. Such a situation is illustrated in Fig. 1.5 where curves *1* and *2* describe the time variation of the population density of the lower and upper laser levels respectively, and curve *3* shows the excitation pulse. It can be seen from the figure that inversion is created at the beginning of the excitation pulse (in time t_1). Apparently, the rate of relaxation of the lower laser level in this case is not significant.

It follows from above that in the case of pulsed pumping, generation is possible in a *large number of media and for a larger number of transitions in any medium*, than for stationary pumping. In particular, generation is possible on the so-called *self-terminating* transitions.

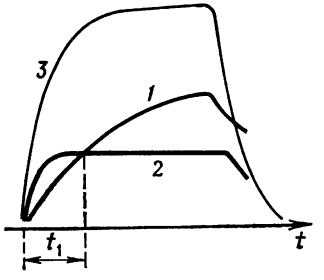


Fig. 1.5

Self-terminating transitions are ones for which the *first resonance* level of the active centre is the upper laser level, while the lower laser level is a *metastable* one. Metastability of the lower level forbids its depopulation by radiation and thus a stationary inversion is not possible for such transitions in spite of the fact that the first resonance level, as a rule, has the largest cross section of electronic excitation in a discharge. However, pulsed generation is possible for such transitions. This can happen at the beginning of the excitation pulse, when the rate of relaxation of the lower level is not significant, and the ratio of the population rates of laser levels is significant. Since the duration of generation is restricted in this case by the properties of the transition itself, such transitions are called self-terminating transitions.

The ratio of population rates of laser levels for self-terminating transitions is especially favourable on account of metastability of the lower laser level. As a matter of fact, the electron excitation cross sections for optically forbidden transitions are usually much lower than for the allowed ones [3]. Hence the probability of electronic excitation of the first resonance (upper laser) level is considerably higher than the probability of excitation of the metastable (lower laser) level. That is why the gain in lasers working on self-terminating transitions is very high[7].

[7] Owing to this circumstance, such lasers may operate in the superluminescence regime, i.e. without the resonator mirrors or with just one mirror (see Ch. 8 in [4]).

Another advantage of pulsed pumping is that from a technical point of view, it must be easier than continuous pumping. A continuous stable supply of energy to the active medium is, as a rule, more complicated than a pulsed supply. Besides, there is no need for a forced cooling of the heated active medium in the case of pulsed pumping.

Pulsed pumping leads to different *pulsed generation conditions*[8]. This helps in obtaining an exceptionally high concentration of the emitted optical energy in space and time. For example, operating conditions have been attained for generation of high-power ultrashort light pulses of duration 10^{-11}-10^{-12} sec and a peak power up to 10^{12} W.

In actual practice, pulse lasers are encountered much more frequently than CW-lasers. Solid-state and liquid lasers often operate in the pulsed regime by employing pulsed or continuous pumping. Gas lasers are characterised by a continuous operation, but even for such lasers, there is growing interest towards pulsed generation [5].

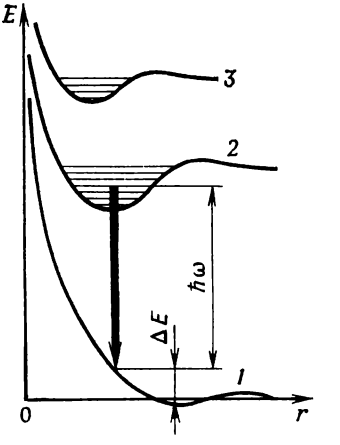


Fig. 1.6

Noble-gas Molecular Lasers. In conclusion of this section, we shall describe a fairly effective mechanism for depopulating the lower laser level. This mechanism is based on the use of the *noble-gas molecules* as active centres.

The ground state of a noble-gas molecule is unstable (repulsive). Such a molecule can exist only in electronically excited states. Upon a transition from an excited state into the ground state, it dissociates into atoms.

It is well known that the atoms of noble gases "do not like" to form molecules. In order to create the molecules Ar_2, Kr_2, or Xe_2, energy has to be expended. Such molecules exist only in the excited state and can be treated as disintegrating molecules.

Figure 1.6 shows the electron energy levels of a diatomic noble-gas molecule (as functions of the distance between the atomic centres). Here, level *1* corresponds to the ground state while *2* and *3* represent excited energy levels. In contrast to state *1*, states *2* and *3* are stable and the vibrational levels of molecules in these states are shown by horizontal lines. The vertical arrows indicate the transition $2 \rightarrow 1$; $\hbar\omega$ is the energy of a photon emitted during

[8] Pulsed generation conditions will be described in Ch. 3. It should be remembered that pulsed generation is possible even in the case of continuous pumping.

the transition and ΔE is the energy of the atoms into which the molecule disintegrates.

Suppose that noble-gas molecules are used as active centres in a laser, the energy levels *1* (ground state) and *2* (first electronic excited level) corresponding to the lower and upper laser levels respectively. Apparently, inversion on $2 \rightarrow 1$ transition will take place irrespective of the number of molecules excited to state *2*. As soon as a noble-gas molecule arrives at level *1*, it immediately leaves it on account of its dissociation into atoms. Thus an active medium consisting of noble-gas molecules is a medium in which the lower laser level is *continuously being emptied.*

Generation on transitions from a stable excited electronic state to the unstable ground state has been obtained in lasers based on molecules of noble gases and their halides (the so-called *excimer lasers*). Molecules of Ar_2, Kr_2, Xe_2, XeF, XeCl, KrF, ArF, etc. have been employed for this purpose. Such lasers are specially interesting because they also permit generation in the ultraviolet region of spectrum[9].

1.2. OPTICAL PUMPING. SOLID-STATE LASERS

Specific Properties of Optical Pumping. *Optical pumping* is based on excitation of active centres through absorption of the radiation from a certain special light source by the active medium. Optical pumping is widely used in different types of solid-state and liquid lasers as well as in gas lasers.

Optical pumping may be *coherent* or *incoherent*. For incoherent pumping, we use incoherent excitation radiation obtained from gas-discharge flash lamps, continuous glow lamps (incandescent or gas discharge lamps), spark gaps, flames, etc.[10]. For coherent pumping, an auxiliary laser is employed.

Optical pumping is characterised by the possibility of obtaining an exceptionally high selectivity of excitation. Pumping radiation with a specially selected spectrum helps in exciting a particular group of levels or even a *single* level. In coherent pumping, it is possible to "pump" energy to a particular line in the absorption spectrum of an active centre. To improve the selectivity of incoherent pumping excitation, it should be remembered that optical pumping is possible only for optically allowed transitions. Thus, for optical excitation, we get the most favourable conditions for satisfying the inequality (1.1.14). It can be assumed that $F_1 = 0$.

[9] For example, generation was observed at the wavelength 0.175 μm in an ArCl laser while for an Ar_2 laser, generation was observed at a wavelength 0.126 μm (see Ch. 9 in [4]).

[10] For pumping of lasers generating in the UV region, we can use the X-rays emitted by electrons in a synchrotron [6]. Such radiations are called synchrotron radiation or bremsstrahlung.

Optical pumping widens the scope of application of a laser. Thus, for coherent pumping, a laser may function as an amplifier of coherent radiation, or as an optical frequency converter.

Finally, a specific property of optical pumping is that it always initiates a *reverse* process in the excitation channel (in the transition between the ground level and the excited level), with nearly the same probability as the direct process involving absorption of radiation. The probability of absorption of pumping radiation per unit time is given by

$$w_p = B\rho_p, \qquad (1.2.1)$$

where ρ_p is the density of pumping radiation at the excitation frequency and B is Einstein's coefficient for absorption of radiation in the excitation channel. Besides absorption, the reverse process of induced emission also takes place and is initiated by the pumping radiation. The probability of this reverse process is

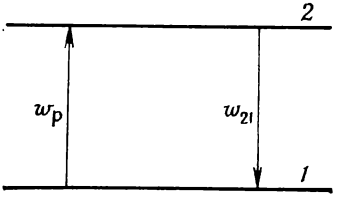


Fig. 1.7

$$w = B'\rho_p, \qquad (1.2.2)$$

where B' is Einstein's coefficient for this process. The coefficients B and B' are related through the well-known relation[11]

$$gB = g'B',$$

where g and g' represent the degeneracy of the ground level and the excited level respectively. This leads to the relation

$$w_p = (g'/g)\, w. \qquad (1.2.3)$$

The existence of two opposing processes whose probabilities are related through Eq. (1.2.3) means that the same channel cannot be used for excitation and generation in the case of optical pumping. Hence, in particular, the minimum number of levels necessary for an active centre under optical pumping is equal to three. We shall prove this below.

Conditions for Creating Stationary Inversion Under Optical Pumping. Let us start with a *two-level* case, depicted in Fig. 1.7. The probability w_{21} consists of two components, corresponding to the induced emission initiated by the pumping radiation and to the spontaneous emission:

$$w_{21} = w + A_{21} \qquad (1.2.4)$$

(we neglect the non-optical transition). We denote the stationary population density of levels *1* and *2* by n_{01} and n_{02} respectively (the subscript 0 means that the corresponding quantity is consider-

[11] See, for example, Eq. (2.1.6) in [1].

ed for the case when there is no generation), the total number of active centres per unit volume is denoted by n'.

The *balance equations* for the population densities of the levels have the form

$$n_{01}w_p - n_{02}w_{21} = 0; \quad n_{01} + n_{02} = n'.$$

Introducing the inverse population density $N_0 = n_{02} - (g_2/g_1)\, n_{01}$, we get

$$N_0 = n' \frac{w_p - (g_2/g_1)\, w_{21}}{w_p + w_{21}}. \tag{1.2.5}$$

Using Eqs. (1.2.4) and (1.2.3) (having replaced g by g_1 and g' by g_2, of course), we can rewrite (1.2.5) in the following form:

$$N_0 = -\frac{g_2}{g_1} n' \frac{A_{21}}{A_{21} + (1 + g_1/g_2)\, w_p}. \tag{1.2.6}$$

We introduce the term *pumping rate* Ω and define it as the probability that the active centres arrive at the upper laser level. In this

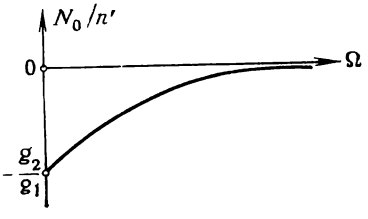


Fig. 1.8

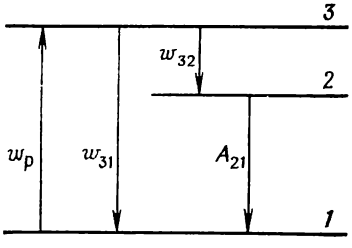


Fig. 1.9

case, $\Omega = w_p$. Using this term, Eq. (1.2.6) can be rewritten in the form

$$\frac{N_0}{n'} = -\frac{g_2}{g_1} \frac{A_{21}}{A_{21} + (1 + g_1/g_2)\, \Omega}. \tag{1.2.7}$$

Figure 1.8 shows the dependence of N_0/n' on Ω as defined by formula (1.2.7). It can be easily seen that irrespective of the pumping rate, the quantity N_0 remains negative, and so inversion is not created. This shows that a two-level diagram is not suitable for the case of optical pumping.

Let us now consider the *three-level* case shown in Fig. 1.9, where *1-3* is the excitation channel and *1-2* is the generation channel. The *balance equations* for the population densities of levels in this case have the form

$$\left.\begin{aligned} &-n_{02}A_{21} + n_{03}w_{32} = 0; \\ &n_{01}w_p - n_{03}(w_{31} + w_{32}) = 0; \\ &n_{01} + n_{02} + n_{03} = n'. \end{aligned}\right\} \tag{1.2.8}$$

Solving this system, we get

$$n_{01} = (n'/D)\, A_{21}\, (w_{31} + w_{32}); \quad n_{02} = (n'/D)\, w_p w_{32}, \tag{1.2.9}$$

where D is the determinant of the system of equations (1.2.8). From this, it follows that

$$\frac{N_0}{n'} = \frac{w_p w_{32} - (g_2/g_1)\, A_{21}\, (w_{31} + w_{32})}{A_{21}\, (w_p + w_{31} + w_{32}) + w_p w_{32}}. \tag{1.2.10}$$

The pumping rate Ω for this system of equations can be written in the form

$$\Omega = w_p w_{32}/(w_{31} + w_{32}). \tag{1.2.11}$$

Using (1.2.11), we can rewrite Eq. (1.2.10) in the following form:

$$\frac{N_0}{n'} = \frac{\Omega - (g_2/g_1)\, A_{21}}{A_{21} + \Omega\, (1 + A_{21}/w_{32})}. \tag{1.2.12}$$

Figure 1.10 shows the dependence of N_0/n' on Ω as given by formula (1.2.12). Of the two curves shown in this figure, the dashed one corresponds to the special case when $A_{21} \ll w_{32}$.

It can be easily seen that stationary inversion may be easily created in the case of a three-level diagram. For this, it is necessary that the condition

$$\Omega > (g_2/g_1)\, A_{21} \tag{1.2.13}$$

or,

$$w_p > (g_2/g_1)\, (w_{31} + w_{32})\, (A_{21}/w_{32}), \tag{1.2.14}$$

is satisfied. The quantity $\Omega_{inv} = (g_2/g_1)\, A_{21}$ is called the *inversion threshold* pumping rate. The smaller the value of A_{21}, the lower the inversion threshold.

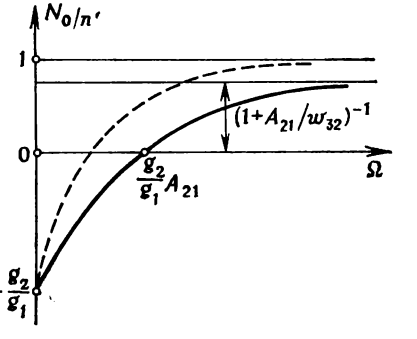


Fig. 1.10

For a three-level case, when the inequality

$$A_{21} \ll w_{32} \tag{1.2.15}$$

is satisfied, the magnitude of Ω_{inv} decreases and the limiting value of the ratio N_0/n' increases.

This leads to the conclusion that it is best to use such diagrams for which the value of A_{21} is the lowest. This conclusion, however, is not correct. It turns out that an extremely low value of A_{21} is not desirable. This question will be discussed in Sec. 2.1.

Solid-state Lasers. Practical Attainment of Optical Pumping, Operating Laser Diagrams[12]. Figure **1.11***a* shows a schematic for optical pumping in a solid-state laser. Here, *1* is the active element, *2*—the source of pumping radiation (for example, a gas discharge flash lamp); *3*—a reflector for focussing the pumping radiation on the active element; *4*—an optical resonator mirror, and *5*—the laser radiation. Figure 1.11*b* shows the laser cross section. The reflector surface in the cross section is represented by an ellipse at whose

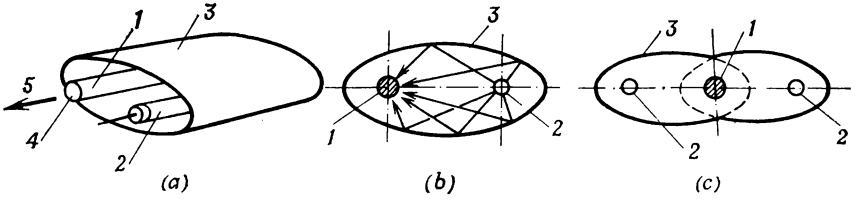


Fig. 1.11

foci lie the active element and the pumping source. In actual practice, reflectors of different forms and construction can be applied. Thus, a two-lamp reflector, whose cross section is shown in Fig. 1.11*c*, can be used. This type of construction increases the output power of radiation.

A solid-state active element consists of a *matrix* (*basis*) and an *activator* (active centre) introduced into the matrix in the form of impurity. The matrices employed may be crystalline or amorphous (glass-like).

The stimulated emission effect has so far been observed in more than 250 dielectric crystals activated by transition group ionic impurities. The most common among these are the oxide crystals having an ordered structure (for example, Al_2O_3 crystals with Cr^{3+} ion impurity, or $Y_3Al_5O_{12}$ and $YAlO_3$ crystals with Nd^{3+} ion impurity). We can also mention fluoride crystals having an ordered structure (for example, CaF_2 crystals with Dy^{2+} ion impurities).

The *efficiency* of optical pumping is determined by two main factors. Firstly, the pumping radiation must be absorbed effectively by the active centres and at the same time, it should not be absorbed by the matrix at all. Secondly, the *quantum efficiency* of pumping

[12] General problems concerning the working of solid-state lasers have been discussed in [7-9]. The basic theories of solid-state lasers have been described in [10-12]. Spectroscopic properties of activated laser crystals have been systematised by Herlich *et al.* [13] and Kaminskii [14]; see also [4]. Specific problems dealing with fabrication of lasers, and construction and properties of light sources have been described in [15]. The thermal conditions in solid-state lasers have been discussed in [16]. Finally, the preparation of solid-state active elements has been considered in [17].

must be high, and nearly all the active centres raised to the excitation level by pumping must come down to the upper laser level. Besides, it is desirable that the loss of energy at the secondary transitions should be minimum, for example, at the transition from the excitation level to the upper laser level.

In order to increase the efficiency of optical pumping, efforts are made to choose a *fairly wide* energy band or a group of levels as the excitation level, and thus ensure a *correspondence* between the transition frequency (frequencies) in the excitation channel and the maximum in the spectrum of pumping radiation. We can also use the

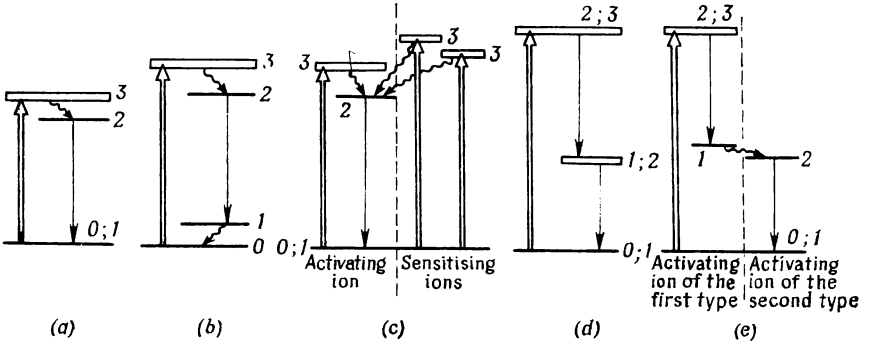


Fig. 1.12

sensitization method where, in addition to the basic (generating) ions, another type of ions (sensitizing ions) are introduced into the matrix. The sensitizing ions quite effectively absorb the pumping radiation and then transfer this absorbed energy to the activator ions[13]. Another method of increasing the efficiency of solid-state lasers envisages the use of mixed disordered systems (solid solutions) instead of simple compounds for the crystal matrix, which considerably broadens the absorption spectrum [20].

The energy level diagrams employed in solid-state lasers are quite diverse (see, for example, [14]). Some of these diagrams are shown in Fig. 1.12. The *ground* level, the *lower laser* level, the *upper laser* level, and the *excitation* level are denoted by *0*, *1*, *2*, and *3* respectively. A level designated by two digits performs two functions. For example, the level marked as *0* and *1* is simultaneously the ground level as well as the lower laser level. Transitions in the excitation channel have been shown by thick arrows, those in the generation channel by thin straight arrows, and the nonradiating transitions are indicated by undulating arrows. Figure 1.12*a* represents a normal three-level diagram, while a four-level diagram is shown

[13] The sensitization method has been presented in [18]. Possible mechanisms for the exchange of energy between ions in laser crystals are discussed in [19].

in Fig. 1.12*b*. A three-level diagram using sensitizing ions is indicated in Fig. 1.12*c*, and Figs. 1.12*d* and 1.12*e* show the *cascade* diagrams [21]. In this case, stimulated emission takes place simultaneously on several transitions (two transitions in this case). Cascade processes involve transitions between levels of the same activating ion (direct cascade diagram, Fig. 1.12*d*) or different types of activating ions (cascade diagram with an intermediate act of excitation

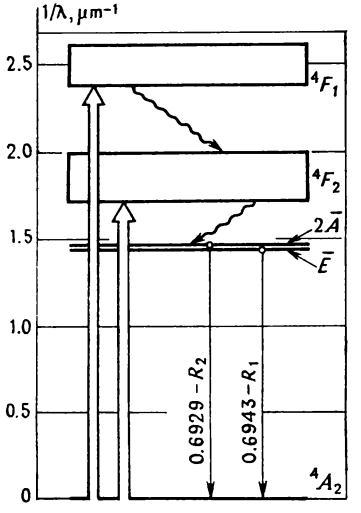


Fig. 1.13

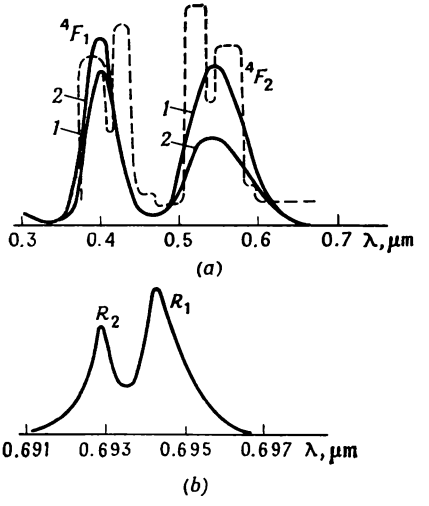


Fig. 1.14

energy transfer, shown in Fig. 1.12*e*). Cascade processes are particularly interesting, because they reduce the energy loss associated with secondary (nonradiating) transitions to a minimum.

Ruby Lasers. Laser generation was first observed in ruby [22]. Owing to the high mechanical strength and thermal conductivity of ruby crystals and the possibility of growing high quality optical samples, ruby lasers are widely employed even today.

Ruby is the aluminium oxide Al_2O_3 (matrix) doped with Cr^{3+} ion impurity (active centres). Pink ruby, containing 0.05% Cr (1.6×10^{19} ions cm^{-3} is normally used as laser material).

Figure 1.13 shows the *energy level diagram for a chromium ion in ruby*. The change from $1/\lambda$ to the energy E is accomplished through the formula $E = 2\pi\hbar c/\lambda$. The states $^4F_1$ and $^4F_2$ are excited as a result of pumping. Each of these states is shown in the form of an energy band in the figure. This is due to the broadening of the corresponding energy states (consequence of the small lifetime of active centres in these states). Active centres quickly pass on from the $^4F_1$ and $^4F_2$ states to two closely spaced metastable levels denoted by $2\bar{A}$ and $\bar{E}$

(the separation between these two levels is 0.003 μm^{-1}). These levels play the role of *upper* laser levels. Upon transition from the states $^4F_1$ and $^4F_2$ to the upper laser level, the chromium ions transfer a part of their energy to the crystal lattice (non-optical transitions are shown in the figure by undulating arrows). The *lower* laser level is denoted by $^4A_2$. This is also the *ground* state[14]. It is clear from the figure that ruby lasers may be represented by a *three-level* diagram.

Figure 1.14*a* shows the ruby *absorption spectrum* for the case when pumping radiation propagates parallel (curve *1*) and perpendicular (curve *2*) to the optical axis of the crystal[15]. In the absorption spectrum, two relatively broad lines with maxima at $\lambda = 0.41$ μm (blue absorption band) and $\lambda = 0.55$ μm (yellow-green absorption band) can be distinguished. These correspond to the excitation of states $^4F_1$ and $^4F_2$ respectively. The dashed curve shows the radiation spectrum of a mercury lamp which is the source of excitation. It can be easily seen that the spectrum of the mercury lamp coincides fairly well with the absorption bands of ruby, thus ensuring a high selectivity of excitation and increasing the fraction of gainfully consumed power of pumping radiation.

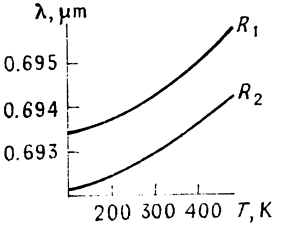


Fig. 1.15

Figure 1.14*b* shows the *luminescence spectrum* of chromium ions in ruby. Two lines can be observed in this spectrum: the R_1-line at 0.6943 μm corresponding to the transition $\bar{E} \rightarrow {}^4A_2$, and the R_2-line at 0.6929 μm corresponding to the transition $2\bar{A} \rightarrow {}^4A_2$. The curve shown in the figure has been obtained at a temperature of 300 K. On reducing the temperature, both lines shift towards the shorter wavelength region of the spectrum (Fig. 1.15).

Nd:YAG Laser. One of the most widely used solid-state lasers at present is that in which *Yttrium Aluminium Garnet* ($Y_3Al_5O_{12}$) serves as the matrix, while Nd^{3+} ions serve as the activator. This laser is known as Nd : YAG laser.

The Nd : YAG laser has a comparatively low excitation threshold and high thermal conductivity, which lead to generation at a high pulse frequency, as well as continuous operation. The efficiency of this laser is comparatively high (of the order of a few percent).

The main transitions of a neodymium ion in garnet are shown in Fig. 1.16. Transitions are accomplished between definite *atomic*

[14] The lower laser level consists of two sublevels separated by 4×10^{-5} μm^{-1}.

[15] Ruby crystal has a trigonal (rhombohedral) symmetry. Its optical axis has a three-fold symmetry.

energy levels[16] shown as energy bands in the figure. Each band (each energy level) has a corresponding group of closely spaced energy sublevels appearing as a result of a splitting of an energy level in the electric field of the crystal lattice of garnet (*Stark's splitting*).

As a result of pumping, the neodymium ions go over from the *ground* state corresponding to the energy level $^4I_{9/2}$ to three groups

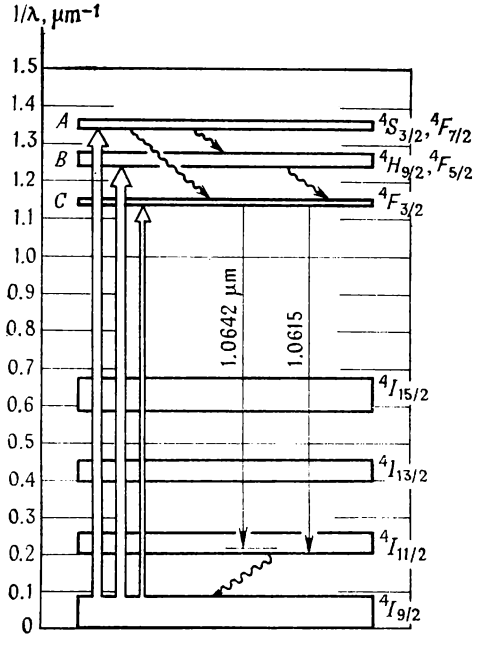


Fig. 1.16

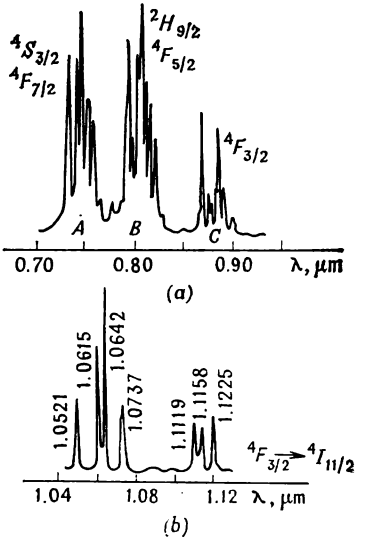


Fig. 1.17

of energy levels A, B, and C. Group A corresponds to the energy levels $^4F_{7/2}$ and $^4S_{3/2}$; group B to the levels $^4F_{5/2}$ and $^2H_{9/2}$; and group C to the level $^4F_{3/2}$. To these three groups of energy levels correspond three bands in the *absorption spectrum* of neodymium in garnet. These bands are represented in Fig. 1.17*a* as A. B, and C bands respectively. The fine structure of the absorption bands, which can be seen clearly in the figure, reflects Stark's splitting of energy levels.

The energy level $^4F_{3/2}$ is the *upper* laser "level". By omitting energy, the neodymium ions jump down from this level to the energy levels $^4I_{11/2}$, $^4I_{9/2}$, $^4I_{13/2}$, and $^4I_{15/2}$. The major part of this energy (60%) is omitted during the transition $^4F_{3/2} \rightarrow {}^4I_{11/2}$. Levels corresponding to the state $^4I_{11/2}$ are considered as *lower* laser levels.

[16] The notation used for designating atomic levels has been given in [7, 23]. See also Sec. 3.1 in [1].

Figure 1.17*b* shows the *luminescence spectrum* of Nd in garnet for the transition $^4F_{3/2} \rightarrow {}^4I_{11/2}$. This spectrum consists of 7 lines, the ones corresponding to 1.0615 μm and 1.0642 μm being the brightest of these. Wavelengths for 18 luminescence lines obtained by taking different transitions into consideration have been given in Table 1.1 [14]. The data given in this table have been obtained at a temperature of 300 K.

TABLE 1.1

Transitions	Luminescence line wavelength, μm	Relative intensity of transitions, %
$^4F_{3/2} \rightarrow {}^4I_{9/2}$	0.8910 0.8999 0.9385 0.9460	25
$^4F_{3/2} \rightarrow {}^4I_{11/2}$	1.0521 1.0615 1.0642 1.0737 1.1119 1.1158 1.1225	60
$^4F_{3/2} \rightarrow {}^4I_{13/2}$	1.3184 1.3331 1.3351 1.3381 1.3533 1.3572	14
$^4F_{3/2} \rightarrow {}^4I_{15/2}$	1.833	1

The Nd : YAG laser can be considered in a more simplified way by using the *four-level* diagram[17] consisting of the ground "level" $^4I_{9/2}$, the lower laser "level" $^4I_{11/2}$, the upper laser "level" $^4F_{3/2}$, and the excitation "levels" $^4F_{7/2}$ and $^4F_{5/2}$. It should be noted that the $F \rightarrow I$ transitions are forbidden in the dipole approximation (optically forbidden transitions), since the orbital quantum number for a neodymium ion changes by 3 in the case of such a transition. Thus, the states corresponding to F energy levels are metastable.

Krypton lamps are often employed for pumping Nd : YAG lasers. In some cases, chromium ions are introduced in the garnet lattice as sensitizers, and xenon lamps are used for pumping. Chromium has two broad absorption bands in garnet (corresponding to the wavelengths 0.43 μm and 0.59 μm). These coincide fairly well with the

[17] The four-level diagram is characteristic for solid-state lasers with Nd^{3+} ions as active centres.

emission spectrum from a xenon lamp. The excited chromium ions transfer their excitation energy to the active centres, i.e. to neodymium ions. The comparatively long time (about 6 msec) required for transferring the energy from chromium to neodymium restricts the application of this method of increasing pumping efficiency only to continuous laser emission.

Optical Pumping by a Semiconductor Laser or a Light-emitting Diode. At present, the *narrow-band* optical pumping method is used for an Nd : YAG laser. As pumping source, a GaAs injection laser or a $Ga_{1-x}Al_xAs$ light-emitting diode (LED) is used. In the former case, pumping is carried out at a wavelength of 0.88 μm

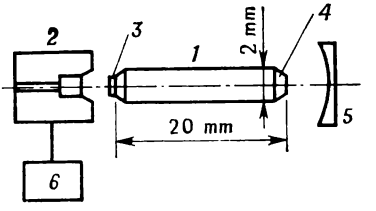


Fig. 1.18

(pumping to the *C*-group lines shown in Fig. 1.17*a*), while in the latter case, it takes place at a wavelength of 0.81 μm (pumping to the *B*-group lines in the same spectrum).

The pumping radiation is introduced at the end face of the active element. A laser using this kind of pumping is shown in Fig. 1.18 [24]. Here, *1* is the active element (garnet with neodymium), *2*—an injection laser, *3*—a dielectric mirror with reflection coefficient $R = 99.8\%$ for $\lambda = 1.06$ μm and $R \leqslant 5\%$ for $\lambda \approx 0.8$-0.9 μm, *4*—a dielectric antireflection coating with $R \leqslant 0.5\%$ for $\lambda = 1.06$ μm, *5*—an external spherical resonator mirror, and *6*—the power supply for the injection laser.

The method of narrow-band optical pumping at the end face of the active element lies behind the designing of miniature solid-state lasers with a relatively low generation threshold and a fairly high efficiency.

1.3. ORGANIC DYE LASERS

Optical pumping is also used for exciting *liquid lasers*. We shall now discuss lasers based on solutions of *organic dyes*[18].

[18] Besides solutions of organic dyes, liquids activated by ions of rare-earth elements (like Eu^{3+}, Nd^{3+}) are also used as active media. There are two types of such liquids: *organometallic* (chelated) and *inorganic* (aprotic); see, for example, Ch. 17 in [4].

Organic Dyes. *Dyes* are complex organic compounds with a branched system of conjugated bonds, and with strong absorption bands in the visible and near-ultraviolet regions of the spectrum[19]. Their chemical structure is characterised by a combination of benzene rings, pyridine rings, azine rings, pyrol rings, etc., located in the same plane. The most powerful luminescent dyes are divided into the following eight categories: *xanthenes*, *polymethines*, *oxazines*, *coumarins*, *anthracenes*, *acridines*, *azines*, and *phthalocyanines*.

As an example of practical importance, let us consider the dye *rhodamine 6G*, belonging to the class of xanthenes. Its structural

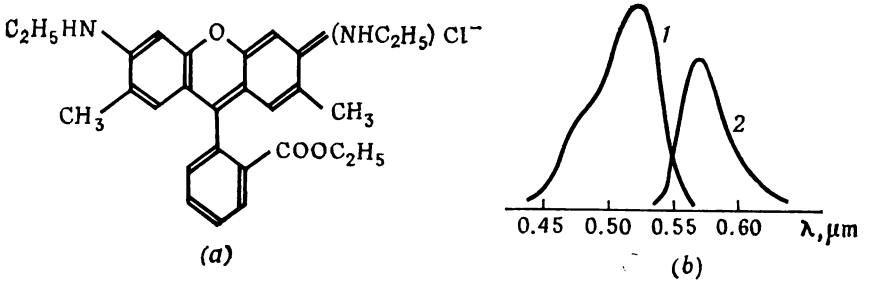


Fig. 1.19

formula, based on benzene rings, is shown in Fig. 1.19*a*. As a rule, xanthene dyes absorb and emit light in the visible spectral region. Figure 1.19*b* shows the *absorption* (curve *1*) and the luminescence (curve *2*) spectra of rhodamine 6*G*. This dye radiates in the band 0.55-0.6 μm. Uptill now, laser generation has been observed in more than 200 different dyes. The general wavelength band for these dyes is 0.3-1.3 μm. Laser radiation of almost any wavelength in this band can be obtained by a suitable choice of dyes.

The problems connected with the chemical and photochemical instability of dyes as well as the choice of suitable *solvents* have led to a search for new active media among dyes. Water, ethanol, methanol, cyclohexane, toluene, glycerine, benzene, acetone, etc. are the solvents commonly employed.

Significantly, the width of *luminescence lines* in the case of dye lasers is exceptionally large—of the order of 0.1 μm (see curve *2* in Fig. 1.19*b*), while the width of the *generated line* may be just of the order of 10^{-4} μm or even less. The wavelength generated by the laser may be changed continuously within the limits of the width of the luminescence line. In other words, a *continuous tuning* of the generation wavelength may be ensured over about 0.1 μm. Dye lasers

[19] The term "dye" does not necessarily mean a coloured material or one with colouring properties.

are an effective substitute for parametric light generators in the visible and near infrared regions of the spectrum.[20]

Optical Pumping of Dye Lasers. Most frequently, *coherent* pumping by radiation from solid-state *pulsed* lasers (Nd : YAG, Nd-glass, ruby, etc.) is used for excitation of dyes. Fundamental frequency as well as *harmonics* (for example, the second harmonic ($\lambda = 0.53$ μm) and the third harmonic ($\lambda = 0.35$ μm) of the Nd : YAG laser radiation) are used for pumping. The efficiency of dye lasers excited with the help of an auxiliary pulsed laser is of the order of tens percent. For a solution a rhodamine 6*G* in ethanol, an efficiency of 75% was achieved upon pumping by the second harmonic of a Nd-glass laser.

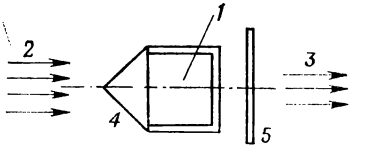


Fig. 1.20

Dye lasers employing coherent pumping may function as wide-band amplifiers in the optical region. They can also be used as relatively simple and efficient converters of optical frequencies.

Coherent pulsed pumping may be transverse or longitudinal. In the former case, the pumping radiation propagates perpendicular to the direction of dye oscillations, while in the latter case the two are parallel. As an example, one of the alternatives for longitudinal pumping is shown in Fig. 1.20. Here, *1* is the dye, *2*—the pumping radiation, *3*—the radiation generated by the dye; *4*—a totally reflecting prism, and *5*—the resonator mirror (opaque to the pumping radiation).

Besides pulsed pumping, *continuous* coherent pumping is also employed. For this purpose, an ionised argon laser is often used. In order to increase the generation threshold of the dye, the pumping radiation is focussed on the dye solution over a region of about 10 μm diameter. This is liable to produce thermooptical distortion in the active medium. In order to eliminate this risk, the dye solution is quickly circulated through the generation zone (a complete replacement of the solution in the generation zone is attained over a period of about 1 μsec). Circulation of the dye solution is important from other points of view too, for example, for removal of photodisintegration products from the generation zone.

[20] For a detailed description of organic dyes and lasers based on them, see [25-27], as well as Ch. 18 in [4].

Incoherent optical pumping is also applied to the dye lasers, by using, for example, flash tubes or coaxial flash lamps. Such lasers have an efficiency of about 1% and below.

Level Diagram and Basic Transitions. A dye molecule has a complex structure, is composed of a large number of atoms, and has a large number of states which are complicated mixtures of electronic, vibrational, and rotational states. Hence it is impossible to draw a sufficiently accurate energy level diagram. While considering the mechanism of creation of inversion in a dye laser an extremely simple, and to a certain extent, arbitrary level diagram is used, reflecting only some main aspects of quantum transitions in a dye molecule. This diagram is shown in Fig. 1.21.

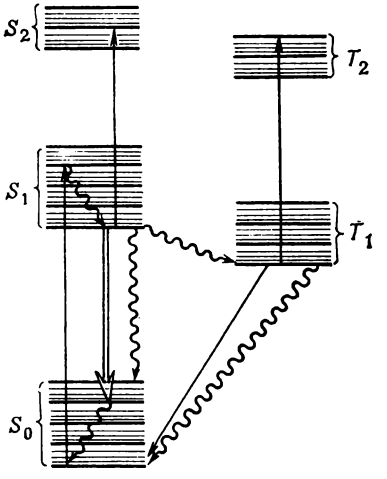


Fig. 1.21

The energy levels shown by thick and thin horizontal lines in Fig. 1.21 refer to *vibrational* and *rotational* states of the molecule respectively. The vibration-rotation states have been grouped together near the *electronic* states of the molecule, denoted in the figure as S_0, S_1, S_2, T_1, T_2, etc. The state corresponding to S_0 is the ground state.

An excitation leads to the transition of one of the electrons of the molecule to a more excited state. If the spin of this electron remains antiparallel to the spin of the rest of the molecule, the electronic state is called a *singlet* (states S_1, S_2, as well as the ground state S_0). If, however, excitation is accompanied by a spin flipping, rendering it parallel to that of the remaining molecule, the electronic states are called *triplets* (states T_1, T_2). The singlet-triplet transitions are associated with a flipping of the electron spin and are therefore less probable than the singlet-singlet or triplet-triplet transitions. Transitions are shown in Fig. 1.21 by arrows. The straight arrows indicate optical transitions (laser transition is indicated by a thick arrow), while the undulating arrows show nonoptical transitions.

Optical pumping excites a molecule from the electronic state S_0 to electronic state S_1. The excited molecule undergoes a nonradiative relaxation to the lower vibrational level of the state S_1 very quickly (over a period of about 10^{-11} sec), transferring its surplus energy to the solvent. This molecule may then undergo a radiative (laser) transition $S_1 \rightarrow S_0$, or one of the following three transitions competing with the laser transition: the transition $S_1 \rightarrow S_2$ associated with

an additional absorption of the pumping radiation; the nonradiative transition $S_1 \rightarrow S_0$ (*internal conversion*); or the nonradiative transition $S_1 \rightarrow T_1$ (*singlet-triplet conversion*). The singlet-triplet conversion may then be followed by additional absorption of pumping radiation for $T_1 \rightarrow T_2$ transition (*triplet-triplet absorption*). Besides this transition, the nonradiative and radiative $T_1 \rightarrow S_0$ transitions are also possible.

While considering the creation of inversion, all these transitions must be taken into account. The transitions $S_1 \rightarrow S_2$ and $T_1 \rightarrow T_2$ lead to additional expenditure of pumping energy. The nonradiative transition $S_1 \rightarrow S_0$ as well as the transitions $S_1 \rightarrow T_1 \rightarrow S_0$ decrease the number of molecules de-excited during the laser transition.

The unfavourable influence of the triplet-triplet absorption may be reduced if steps are taken to increase the probability of $T_1 \rightarrow S_0$ transitions. This probability (and hence the lifetime of the molecule in T_1 state, which is of the order of 1μsec) depends on the composition of the solvent. In order to increase this probability, certain special substances (the so-called extinguishers of the triplet state) are added to the dye solution. For example, addition of paramagnetic impurities (like oxygen) facilitates "mixing" of singlet and triplet states and consequently increases the rate of triplet-singlet transitions.

Tuning of Generation Wavelength; Selective Resonators. As has been mentioned above, tuning of generation wavelength is possible in dye lasers. For this we can use the dependence of the position of

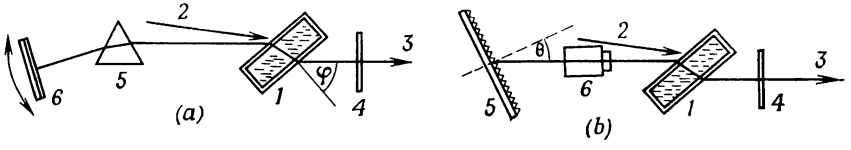


Fig. 1.22

dye generation line on the concentration of the dye molecules in the solution, temperature of the solution, and the reflection coefficients of the resonator mirrors. *Selective resonators* are often employed for tuning of the generation wavelength.

A selective resonator is one which contains a *spectral selective element* in addition to the active medium. Spectral optical filters, Fabry-Perot interferometers, dispersion prisms, or diffraction gratings can be employed as such elements.

Figure 1.22*a* shows a dye laser with a continuous tuning of the generation wavelength with the help of a *dispersion prism*. Here, *1* is the dye cuvette, *2*—the pumping radiation (from the auxiliary laser), *3*—the output radiation, *4*—the output resonator mirror, *5*—a prism, and *6*—a reflecting mirror rotating with respect to the prism. The cuvette is oriented in such a way that the perpendicular

to its wall forms Brewster's angle φ with the direction of the dye radiation. In this case, the generated radiation is linearly polarised (the vector **E** oscillates in the plane of the figure), and there are no losses due to reflections from the walls of the container. The prism plays the role of a selective element in this case. Depending on the orientation of the plane of mirror *6* with respect to the prism, a particular wavelength is generated. By rotating the plane of mirror *6*, the generation wavelength can be continuously varied (within the luminescence linewidth for the given dye).

Analogous effect can be obtained by using a *reflecting diffraction grating* instead of one of the resonator members. Figure 1.22*b* shows the schematic for such a laser. Here *1-4* are the same as in Fig. 1.22*a*, *5* is the reflecting diffraction grating, and *6* is a telescopic system for better separation of the narrow radiation beam. The diffraction angle θ is connected with the radiation wavelength λ through the well-known relation

$$2d \sin \theta = \lambda \qquad (1.3.1)$$

where d is the period of the grating. For a given value of the angle θ between the perpendicular to the grating and the resonator axis (for a given orientation of the grating in the resonator), radiation of wavelength λ will be generated in accordance with the formula 1.3.1[21]. Only for this wavelength, the radiation reflected by the grating will be propagated along the resonator axis. Rotation of the diffraction grating leads to a change in the angle θ and hence to a tuning of the generation wavelength.

The element which leads to a selection of the wavelength (prism, diffraction grating, etc.) performs two functions: it isolates the narrow generation line and also helps in changing the position of this line within the luminescence linewidth for the dye. Using one selective element, we can narrow the generation line to 10^{-3}-10^{-4} μm without significantly reducing the output power. Consequently, a very sharp and bright generation line is emitted instead of a broad and relatively low-intensity line. Figure 1.23 shows a qualitative comparison between these two lines (*1* is the luminescence line, and *2* is the generation line).

For a further narrowing of the generation line, combinations of several selective elements are used. This results in generation lines of width up to 10^{-6} μm if we take into account the considerable unavoidable losses of the output power.

Increasing the Tuning Range of the Generation Wavelength. In order to increase the tuning range of the generation wavelength for a given active dye solution, different methods may be employed. For example, we can use the change in the chemical structure of

[21] Of course, this wavelength must lie within the luminescence linewidth of the dye under consideration.

the dye as a result of chemical reactions occurring on addition of certain reagents to the active medium. Interaction of the dye molecules with the newly introduced reagents produces ionised forms of the dye with different spectral properties. Unfortunately, this method has very low tuning efficiency, and is also irreversible.

The method using *irreversible* variation of spectral properties of solutions of coumarine dyes by passing an electric current through them [28] is more interesting. It is observed that upon the passage of an electric current, the luminescence spectrum of the dye shifts by about 0.05 μm towards the long wavelength region, thus increasing (by 1.5-2 times) the tuning range of the generation wavelength for the given dye.

1.4. GAS LASERS WITH A WIDEBAND OPTICAL PUMPING

Optical Pumping of Gaseous Active Media. The efficiency of optical pumping in the case of solid-state and liquid lasers is mainly associated with the relatively large width of the absorption line for solid and liquid active media. In comparison to this width, which is of the order of 0.1 μm[22], the gaseous active media have *considerably narrower* absorption lines, which have a width of 10^{-6} μm or less. For optical excitation of a gas, it is necessary that the pumping radiation should have a line spectrum with sufficiently narrow lines and that the maximum of at least one bright spectral line of the pumping source should exactly coincide with the maximum of one of the absorption lines for an active centre.

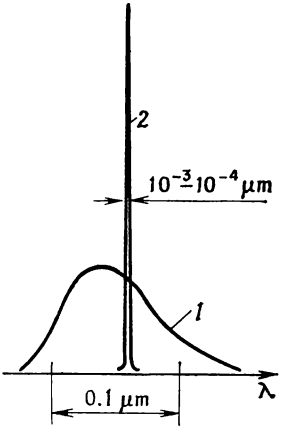


Fig. 1.23

An exactly similar situation exists for *Cs-laser* [29]. The Cs atoms are excited by radiation from a helium lamp whose spectrum contains a bright narrow line with $\lambda = 0.3888$ μm coinciding fairly accurately with the wavelength of one of the transitions in cesium.

In the case of gas lasers ordinary incoherent (wideband) optical pumping should apparently be extremely ineffective. On account of the fact that the absorption lines of gas particles are narrow, only an insignificant fraction of the optical power of the pumping source will be utilised in this case for the excitation of active centres. The main part of the optical radiation falling on the active medium will

[22] The absorption spectrum width for some specific media (solids and liquids) is shown in Figs. 1.14*a*, 1.17*a* and 1.19*b*.

be spent uselessly in heating the gas and surrounding objects. Hence wideband optical pumping is not employed for the case of gas lasers.

Possibility of Wideband Optical Pumping in Gases; Photodissociation Lasers. Exceptions to the rule are gaseous media containing molecules which dissociate under the influence of radiation. As a matter of fact, the absorption spectrum due to photodissociation of gaseous molecules is *continuous* and is comparable in width to the absorption spectra for solid and liquid active media. In this connection, we turn to Fig. 1.24.

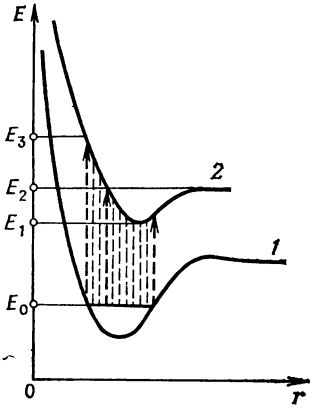


Fig. 1.24

The figure shows electronic energy levels of a diatomic molecule (curves *1* and *2*). Suppose that the molecule is in one of the vibrational states of level *1* (E_0 is the energy of the molecule). By absorbing the pumping radiation, the molecule may jump to the electronic energy level *2*. In accordance with the *Franck-Condon principle*[23], such transitions are shown in the figure by vertical arrows (dotted lines). It is evident from the figure that a transition $1 \rightarrow 2$ is possible upon absorption of photons whose energy is $\hbar\omega$ and satisfies the inequalities $(E_1 - E_0) < \hbar\omega < (E_3 - E_0)$. If $\hbar\omega < (E_2 - E_0)$, a transition takes place from the initial vibrational state of energy level *1* to one of the vibrational states of energy level *2*. The spectrum then consists of a number of narrow lines. If, however, $\hbar\omega > (E_2 - E_0)$, the transition $1 \rightarrow 2$ occurs, leading to the *dissociation* of the molecule. The absorption spectrum in this case will be *continuous* and its width will be equal to $E_3 - E_2$.

Owing to the continuous nature and comparatively large width of the absorption spectrum of photodissociating molecules, a wideband optical pumping can be employed for stimulating the photodissociation reaction:

$$AB + \hbar\omega \rightarrow A^* + B.$$

At least one of the products of molecular dissocisation is found to be in the excited state (A^*) and may be used for laser generation. Thus, wideband optical pumping in gas lasers is possible if molecular photodissociation is employed as the intermediate process[24]. Such gas lasers are called *photodissociation* lasers.

There are two types of photodissociation lasers. The first type employs one of the products of molecular dissociation as the excited

[23] See, for example, Sec. 3.7 in [1].

[24] The method of wideband optical pumping for laser generation in gases with dissociating molecules has been proposed in [30].

active centre (excitation in primary photoprocesses). In the second type, the excited active centres are formed as a result of chemical reactions involving the products of molecular dissociation (excitation in secondary chemical reactions). Such lasers are also called *photochemical lasers.*

At present, possibilities are being explored for creating gas lasers based on allowed electronic transitions of molecules with direct wideband optical pumping (without photodissociation of molecules). These possibilities are based on the relatively broad absorption spectra of a number of molecules (especially polyatomic) in the ultraviolet region of spectrum. The small magnitude of vibrational quanta may result in a nearly continuous absorption in this region[25].

Iodine Photodissociation Laser. As an example of a photodissociation laser, we consider the laser generating on transitions in *iodine atoms* [32]. Under the action of wideband optical pumping (with wavelength 0.27 μm), the CF_3I molecules dissociate: $CF_3I + \hbar\omega \rightarrow \rightarrow CF_3 + I^*$. The iodine atoms I* appear in the excited state $^2P_{1/2}$. On the transitions in these atoms to the state $^2P_{3/2}$, radiation with a wavelength 1.315 μm is emitted. In addition to CF_3I molecules, CH_3I molecules may also be used in this process.

The efficiency of photodissociation lasers is of the order of 0.5%. This efficiency may be increased in principle by broadening the absorption spectrum of dissociating molecules of a gaseous active medium as well as through chemical reactions corresponding to photodissociation. In this connection, we consider the problem of enlarging the class of active media applicable for use in photodissociation lasers [31].

Direct Conversion of Solar Energy into Laser Radiation. Holger et al. [33] have examined the possibility of creating a photodissociation laser excited by the solar radiation, and called the *sun-pumped laser.* The active medium of such a laser must satisfy a number of requirements: the absorption band must cover a considerable part of the solar spectrum, the quantum yield should be as high as possible, and the generation must take place for a relatively low-intensity continuous pumping.

A gaseous mixture containing cesium and xenon atoms has been proposed as active medium for a sun-pumped laser. The Cs_2 molecules are disintegrated into cesium atoms by absorbing solar radiation in the band 0.44 μm to 0.52 μm approximately. The products of dissociation contain excited cesium atoms in $7^2S_{1/2}$ state (denoted by Cs**). Laser oscillation may appear on transitions in these atoms into less excited states $6^2P_{3/2}$ and $6^2P_{1/2}$:

$$Cs^{**} \rightarrow Cs^* \begin{cases} 7^2S_{1/2} \rightarrow 6^2P_{3/2}, \\ 7^2S_{1/2} \rightarrow 6^2P_{1/2}. \end{cases}$$

[25] Wideband optical pumping in gas lasers with or without photodissociation of molecules has been described in [31].

These transitions correspond to the generation wavelengths 1.47 and 1.36 μm respectively.

The question of selective depopulation of the lower laser levels of cesium atoms (without deexciting the upper leser level) is of great importance in these lasers. A chemical depopulation mechanism has been proposed. It is based on active combination of Cs* atoms (and not Cs** atoms) with Xe atoms, leading to the creation of excited CsXe molecules. These molecules are dissociating molecules and their ground state is unstable. The molecules of CsXe, returning to the ground state, dissociate into unexcited Cs and Xe atoms.

1.5. PUMPING BY SELF-MAINTAINED ELECTRIC DISCHARGE IN RAREFIED GASES

Types of Gas Discharge Lasers. Pumping by *self-maintained* discharge in the active medium is often employed for excitation of gas lasers. Such lasers are called gas discharge lasers.[26] They operate in fairly rarefied gaseous media, the pressure being of the order of 1-10 mm Hg.

There are three types of gas discharge lasers: those operating on transitions between ionic levels (ion gas lasers or *ion lasers*); those operating on transitions between neutral atomic levels (neutral atom lasers, or *atomic lasers*); and those operating on transitions between molecular levels (*molecular lasers*). The active centres in these three types of lasers are free ions, free atoms, and free molecules respectively.

Ion lasers generate mainly in the visible as well as near ultraviolet region of the spectrum (from 0.3 to 1 μm approximately). *Atomic lasers* generate over a much wider range of wavelength—from 0.4 to 100 μm, the main laser transitions falling in the region 1-20 μm.

Molecular lasers have the widest range of generation wavelength. Lasers operating on transitions between rotational levels of the same electronic and vibrational state of a molecule (*purely rotational* transitions) generate in a wide infrared region from 10-20 μm up to several hundred micrometres. Molecular lasers operating on transitions between vibrational levels of the same electronic state of a molecule (*vibration-rotation* transitions) generate infrared radiation mainly in the range 5-50 μm. Molecular lasers may also generate on transitions between electronic states of a molecule. In this case, the generation wavelength is in the visible or ultraviolet region of the spectrum (nearly 0.2 to 1 μm)[27].

[26] Gas discharge lasers have been described in [34-36]. See also [4, 7, 8, 37, 38].

[27] As an example of this kind of lasers, we can mention the molecular lasers on transitions from a stable electron-excited state to the unstable ground state (excimer lasers).

The *vibration-rotation transitions* in molecular lasers obey the following selection rules:

$$\Delta v = \pm 1; \quad \Delta j = 0, \pm 1, \tag{1.5.1}$$

where v and j are the vibrational and rotational quantum numbers respectively, Δv and Δj represent the increments in these numbers upon transition. Transition corresponding to $\Delta j = 0$ is called a Q branch transition. Transitions from the rotational level $j - 1$ of the upper vibrational state to the level j of the lower vibrational state belong to the P branch. Transitions from the rotational level $j + 1$ of the upper vibrational state to the level j of the lower vibrational state belong to the R branch.

Electric Discharges Used in Gas-discharge Lasers. Gas-discharge plasma generated as a result of electric discharge serves as the active medium in a gas-discharge laser. If the pulse-rise time and the pulse-decay time of the current are less than the characteristic equilibrium time for the plasma, a *pulsed* electric discharge takes place. Besides pulsed discharge, *stationary* (quasi-stationary) electric discharges are also employed. Two types of stationary discharges are used in gas-discharge lasers: the *arc* discharge (in ion lasers) and the *glow* discharge (in molecular lasers and in atomic lasers).

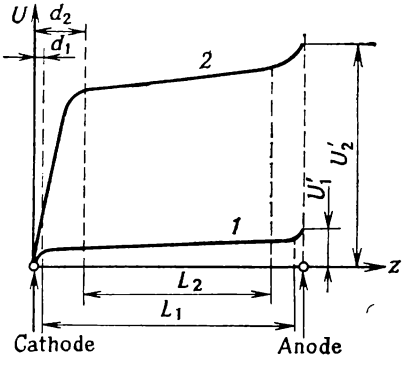


Fig. 1.25

The arc and glow discharges are compared in Fig. 1.25 which depicts the characteristic variation of potential over the length of the discharge gap for both types. The subscript (as well as the curve) *1* corresponds to the arc discharge, while the subscript (and the curve) *2* corresponds to the glow discharge, d is the length of the cathodic discharge region, L is the length of the discharge region, called the positive column in which the discharge characteristics are most stable and the field is uniform (this region is used as the working region for the active medium), U' is the operating voltage (potential difference between the anode and the cathode). It is clear from the figure that the following inequalities hold (for the same distance between the anode and cathode for both types of discharge):

$$d_1 \ll d_2, \quad U_1' \ll U_2', \quad L_1 > L_2. \tag{1.5.2}$$

Table 1.2 gives a comparison of characteristic parameters for the two types of discharge. Here, T_a is the temperature of the heavy plasmic component (discharge temperature), T_e is the temperature of the electron component (*electron temperature*), and n_e is the free electron concentration in the plasma. *Arc* discharge is a high-current high-temperature discharge with a relatively high plasma

TABLE 1.2

Discharge	Working voltage, V	Current density, A/cm^2	T_a, K	T_e, K	n_e, cm^{-3}	Relative ionisation, %
Arc	10-100	10^2-10^3	$\sim 10^3$	$\sim 10^4$	$\sim 10^{13}$	>1
Glow	$>10^3$	10^{-3}-0.1	$\sim 3\cdot10^2$	$>10^4$	10^9-11^{11}	10^{-4}-10^{-2}

ionisation ratio[28]. The *glow* discharge is a low-current, low-temperature discharge with a relatively low plasma ionisation ratio.

Stationary discharges are termed *a.c.* or *d.c.* excited discharges, depending on the method of their excitation. The former are excited by using an alternating current of 10-50 MHz frequency (in this case the electrodes are situated outside the discharge tube—Fig. 1.26*a*); the latter are excited by a direct current (the electrodes are located inside the tube—Fig. 1.26*b*). In these figures, *1* and *2* correspond to the discharge tube and the electrodes respectively.

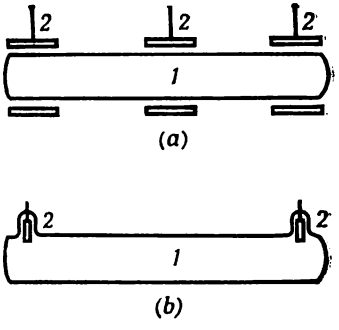


Fig. 1.26

Argon Laser [39]. As an example of *ion lasers*, we shall consider a laser operating on transitions in ArII (on transitions between levels of singly ionised Ar^+)[29]. This laser has been shown schematically in Fig. 1.27 where direct current excitation has been employed. Here, *1* is the anode, *2*—the cathode, *3*—the lasing volume of the tube, *4*—the water cooling system, *5*—the by-pass canal, *6*—the

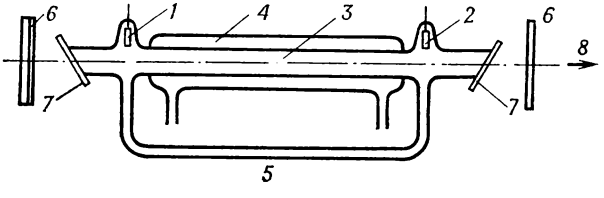


Fig. 1.27

resonator mirror (totally reflecting and transmitting), *7*—the output windows of the discharge tube, oriented at Brewster's angle with respect to the resonator axis, *8*—the output radiation. The by-pass

[28] The *degree of ionisation* of plasma is the ratio of the free-electron concentration in the plasma to the concentration of heavy particles.

[29] Roman numerals are used for spectroscopic notation of ionised gases. The numeral employed is higher than the degree of ionisation by one (e.g., ArII consists of Ar^+ ions, ArIII has Ar^{2+} ions, and so on).

canal is meant for maintaining a uniform pressure throughout the length of the discharge tube. In the absence of such a canal, there is a concentration of gas in the anodic part of the tube soon after the arc discharge is switched on.

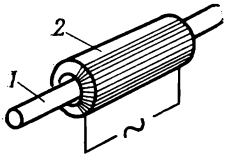


Fig. 1.28

For high-frequency excitation, the electrodes inside the tube are not used. The discharge may be excited with the help of a high-frequency choke mounted on the by-pass canal (Fig. 1.28). The by-pass canal and the choke are shown by *1* and *2* respectively.

The method of "squeezing" the discharge from the walls of a discharge tube with the help of a longitudinal magnetic field is fairly widely employed. As a result, the rate of relaxation of excited ionic states decreases on account of collisions with the walls of the tube. Consequently, the output power of the laser radiation increases.

Creation of Inversion in the Argon Laser. Figure 1.29 shows the most important transitions for an Ar^+ ion for creating inversion

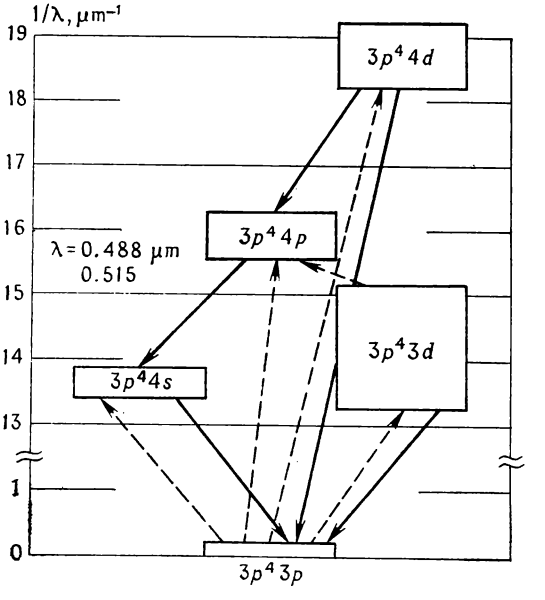


Fig. 1.29

in an argon laser. The dashed lines indicate transitions connected with electronic excitation, while the solid lines correspond to optical transitions. Five groups of levels are shown in the figure, and each one of these is characterised by a definite *electron configuration* (a

definite distribution of electrons in the ion over states with different principal and orbital quantum numbers, n and l respectively), namely $3p^44s$, $3p^44p$, $3p^43p$, $3p^43d$, and $3p^44d$. The group of levels with the electron configuration $3p^44s$ (four electrons in the state with $n = 3$, $l = 1$ and one electron in the state with $n = 4$, $l = 0$, i.e. four $3p$ electrons and one $4s$ electron) corresponds to the lower laser "level" which we shall designate as the "$4s$-level". The group of levels with the configuration $3p^44p$ corresponds to the upper laser "level" ("$4p$ level"). The group of levels with the configuration $3p^43p$ (i.e. with configuration $3p^5$) corresponds to the ground "level" ("$3p$-level"). The term "level" is used within inverted commas here since each electron configuration has several energy levels of the ion (several spectral terms)[30]. For example, the electron configuration $3p^44p$ has 15 terms, hence the "$4p$-level" actually consists of 15 energy levels. It is because of this that each electron configuration has a corresponding energy band of a definite width. Table 1.3 shows the

TABLE 1.3

Electron configuration	Spectral terms
$3p^43p$	$^2P_{1/2}{}^2P_{3/2}$
$3p^44s$	$^2P_{1/2}{}^2P_{3/2}{}^4P_{1/2}{}^4P_{3/2}{}^4P_{5/2}{}^2D_{3/2}{}^2D_{5/2}{}^2S_{1/2}$
$3p^44p$	$^2S_{1/2}{}^4S_{3/2}{}^2P_{1/2}{}^2P_{3/2}{}^4P_{1/2}{}^4P_{3/2}{}^4P_{5/2}$ $^2D_{3/2}{}^2D_{5/2}{}^4D_{1/2}{}^4D_{3/2}{}^4D_{5/2}{}^4D_{7/2}{}^2F_{5/2}{}^2F_{7/2}$

Lines in the argon luminescence spectrum ($4p \rightarrow 4s$ transition): 0.455 μm 0.466, 0.473, 0.477, 0.488, 0.497, 0.502, and 0.515 μm.

spectroscopic energy levels corresponding in this case to the ground, lower and upper laser "levels".

It should be noted that the energy bands in the level diagram shown in Fig. 1.16 (Nd: YAG laser) and Fig. 1 29 (argon laser) have different origins. Each band in Fig. 1.16 corresponds to one spectroscopic (atomic) energy level which is subjected to Stark's splitting into several sublevels under the action of the electric field of the crystal lattice. Each band in Fig. 1.29 corresponds to several unsplit spectroscopic energy levels.

Eight lines appear as a result of the $4p \rightarrow 4s$ transition. Their wavelengths are shown in Table 1.3. The blue line with wavelength 0.488 μm (relative intensity 45%) and the green line with wavelength 0.515 μm (relative intensity 35%) are the brightest ones. The upper laser "level" ("$4p$ level") is excited as a result of several processes:

[30] The connection between the electron configuration and the spectral terms corresponding to this configuration is explained, among others, by Landau and Lifshitz [40]. See Sec. 3.1 in [1].

(a) the transition $3p \rightarrow 4d \rightarrow 4p$, (b) the transition $3p \rightarrow 3d \rightarrow 4p$, and (c) the transition $3p \rightarrow 4p$ (the *cascade*, the *step-by-step*, and the *direct* electron excitation respectively).

It is interesting that the rate of electron excitation of the upper laser "level" (denoted by $F(4p)$) is less than the rate of electron excitation of the lower laser "level" ($F(4s)$). It turns out that $F(4s)/F(4p) \approx 2$. The inversion arises because the lower laser level states relax *considerably faster* than the upper ones:

$$R(4s)/R(4p) \approx 10.$$

The relaxation of the upper levels takes place mainly on account of spontaneous emission. Significantly, the transition $4p \rightarrow 3p$ is forbidden in the dipole approximation (optically forbidden transition), and the laser levels are situated fairly high in comparison with the ground state. Thus, inversion in the argon laser is created not due to the predominant population of the upper laser levels, but rather due to the predominant depopulation of the lower laser levels.

Helium-neon Laser; Creation of Inversion. *Helium-neon laser* is historically the first gas laser [41]. The generation takes place on transitions between levels of neutral *neon atoms*. Besides neon, the active gaseous medium contains *helium as the buffer gas*. The gaseous mixture has a pressure of about 1 mm Hg, the partial pressure of helium being about 5-10 times higher than the pressure of neon. The helium-neon laser employs a stationary glow discharge excited by a direct current.

Figure 1.30 shows the main transitions in the active medium of a helium-neon laser. The dashed lines show the transitions connected with electron excitation or deexcitation. The solid lines show the optical transitions, while the dotted line shows a transition connected with deexcitation at the walls. The curved arrows indicate the resonant transfer of excitation energy from helium atoms to neon atoms. As in the case of an argon laser, the energy bands shown in this figure for neon atoms correspond to specific electron configurations and are consequently composed of several levels (several spectral terms). Abbreviated notations of electron configurations (Paschen's notations) are used in the figure: 1*s*-band corresponds to the $2p^5 3s$ configuration, 2*s*-band to the $2p^5 4s$ configuration, 3*s*-band to the $2p^5 5s$ configuration, 2*p*-band to the $2p^5 3p$ configuration, and 3*p*-band to the $2p^5 4p$ configuration. Each *s*-band consists of four levels, while there are ten levels in each *p*-band.

The 3*s* and 2*s* bands play the role of upper laser levels, while 3*p* and 2*p* are the lower laser levels corresponding to these. The main laser transitions are $3s \rightarrow 3p$ (3.39 μm), $2s \rightarrow 2p$ (1.15 μm), and $3s \rightarrow 2p$ (0.6328 μm—red line).

Inversion in a helium-neon laser is due to the fact that the rate of population of the upper laser levels is considerably higher than

the rate of population of the lower laser levels. The decisive factor in this case is the *resonant* transfer of energy from helium to neon. Collision of a neon atom with a helium atom from the level 2^1S_0 may result in the excitation of one of the levels of the neon atom in the $3s$-band. Collision with a helium atom in the 2^3S_1 state may lead

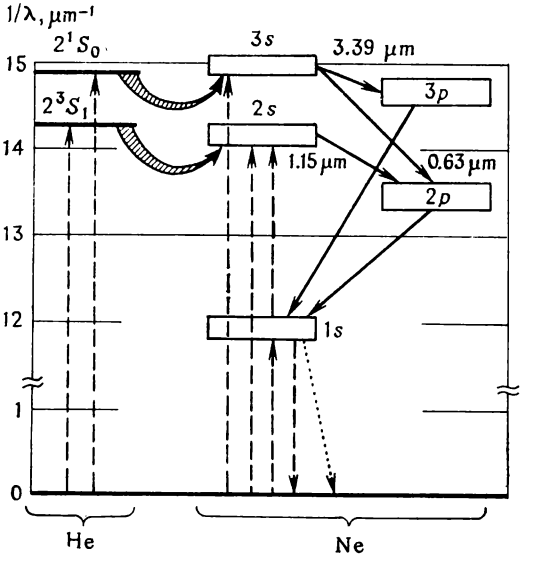


Fig. 1.30

to the excitation of the neon atom level in the $2s$-band. The process of resonant transfer of energy from helium to neon is facilitated by three factors: (i) closeness of the corresponding energy levels of helium and neon atoms, (ii) metastability of the 2^1S_0 and 2^3S_1 helium levels (thus making their relaxation by spontaneous emission impossible), and (iii) higher helium pressure in the gaseous mixture (thus reducing the possibility of a reverse transfer of energy from neon to helium).

The relaxation of lower laser levels ($3p$- and $2p$-bands) is caused by spontaneous emission, transferring neon atoms to the $1s$-band. Spontaneous transitions to the $1s$-band from higher laser levels ($3s$- and $2s$-bands) are forbidden in the dipole approximation. The relaxation of levels in the $1s$-band is the "bottleneck" of a helium-neon laser, and is caused by the deexcitation of electrons as well as the collisions of neon atoms with the walls of the tube. The latter are very significant, and that is why the generation power of helium-neon lasers is inversely proportional to the diameter of the discharge tube.

Copper-vapour Laser [5]. As another example of an atomic gas discharge laser, let us consider the *copper-vapour laser*. This laser is of special interest because it belongs to the type of lasers generating on *self-terminating* transitions. A pulse discharge is employed for evaporating copper and for creating inversion.

Figure 1.31 shows the energy-level diagram for a copper atom. The dashed lines indicate transitions connected with electron excitation, while the continuous lines correspond to the optical transitions for which laser generation is observed (0.51 μm and 0.58 μm). The

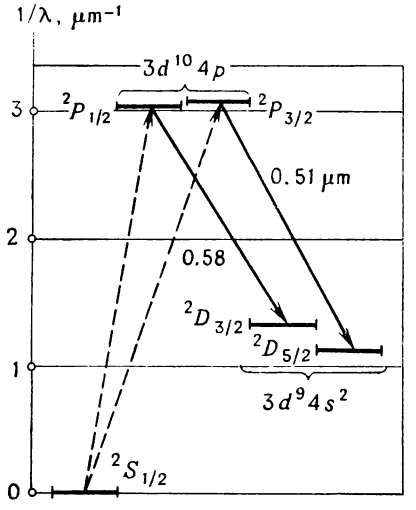


Fig. 1.31

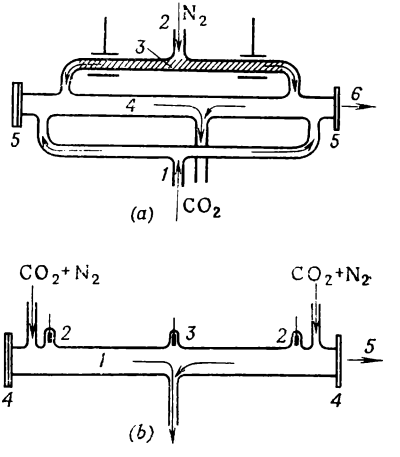


Fig. 1.32

upper laser level (atomic energy levels $^2P_{1/2}$ and $^2P_{3/2}$ corresponding to the electron configuration ($3d^{10}$) $4p$) is the first resonant energy level for a copper atom. The lower laser levels (the energy levels $^2D_{3/2}$ and $^2D_{5/2}$ corresponding to $3d^94s^2$ configuration) are metastable, and transitions between these levels and the ground level ($^2S_{1/2}$ level) are optically forbidden. It should be remembered that the probability of electron excitation for optically forbidden transitions is much lower than for the allowed ones. Hence the electrons from a gas-discharge plasma will quite effectively excite the upper laser levels of a copper atom leaving the lower laser states practically unexcited. Hence a strong inversion is observed at the laser transition right at the beginning of the excitation pulse.

CO_2 Laser. The *CO_2 laser*[31] gives a high power in CW generation (up to 10 kW and more) and have an exceptionally high efficiency (up to 40%). The active medium in a CO_2 laser is a mixture

[31] CO_2 laser was first created in 1964 [42]. Several reviews [43-46] deal with the CO_2 laser. See also [4, 8, 36].

of several components: carbon dioxide, nitrogen, and various additives like helium, water vapours, etc. The *active centres* are CO_2 molecules radiating on the transitions between vibrational levels of the electronic ground state. Nitrogen plays the role of a *buffer gas* and its molecules resonantly transfer the excitation energy to CO_2 molecules. A glow discharge is usually applied for exciting CO_2 lasers, although a pulse discharge can also be used.

Figure 1.32*a* shows the initial version of a CO_2 laser. Here, *1* indicates the system of CO_2 circulation, *2* is the nitrogen circulation system, *3* the region of high-frequency glow discharge, *4*—the lasing volume in which the excited nitrogen molecules are mixed with the unexcited CO_2 molecules, *5*—the resonator mirror, and *6*—the output radiation. In this version of the CO_2 laser, the discharge electrons excite only the nitrogen molecules, and the excited nitrogen molecules then transfer this energy to the active centres in another region.

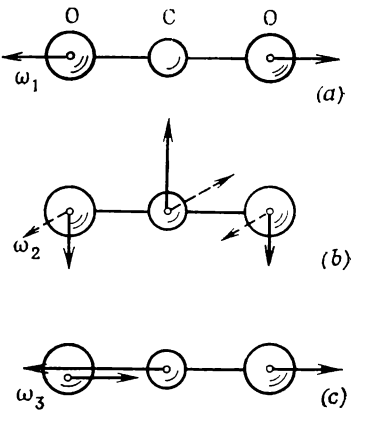


Fig. 1.33

Later versions of CO_2 laser employ a discharge in the $CO_2 + N_2$ mixture. For this, a d.c.-excited glow discharge is normally used. The schematic for such a CO_2 laser is shown in Fig. 1.32*b*, in which *1* is the lasing volume, *2* and *3* are the anode and cathode respectively, *4*—the resonator mirror, and *5*—the output radiation. Like the previous version, this system is also based on gas circulation, which helps in avoiding an undesirable change in the chemical composition of the active gaseous mixture, which takes place, in particular, as a result of the reaction $2CO_2 \rightarrow 2CO + O_2$.

At present, sealed CO_2 lasers are frequently employed (without any circulation of the gaseous mixture). The life of such tubes may be of the order of 1000 hours or more.

Creation of Inversion in a CO_2-Laser. The CO_2 molecule has four vibrational degrees of freedom, with three corresponding vibrational modes: the *symmetric* mode (Fig. 1.33*a*), the *deformation* mode (Fig. 1.33*b*), and the *asymmetric* mode (Fig. 1.33*c*)[32]. The vibrational frequencies corresponding to these are denoted by ω_1, ω_2, and ω_3 respectively, while $\hbar\omega_1 = 0.163$ eV, $\hbar\omega_2 = 0.078$ eV, $\hbar\omega_3 = 0.276$ eV, and $\omega_1 \approx 2\omega_2$.

[32] The energy of deformation mode is doubly-degenerate (a deformation mode has two vibrational degrees of freedom).

We shall represent the *vibrational states* of a CO_2 molecule through a set of three vibrational quantum numbers v_1, v_2, and v_3. These numbers are equal to the excitation factor of the symmetric, deformation, and asymmetric modes respectively of the CO_2 molecule. For example, the vibrational state (020) ($v_1 = 0$, $v_2 = 2$, $v_3 = 0$) is a state in which the deformation vibrations are doubly excited while the symmetric and asymmetric vibrations are not excited.

The mechanism of creation of inversion in the CO_2-laser is illustrated in Fig. 1.34 which shows the levels corresponding to the three different vibrational modes of a CO_2 molecule as well as the first

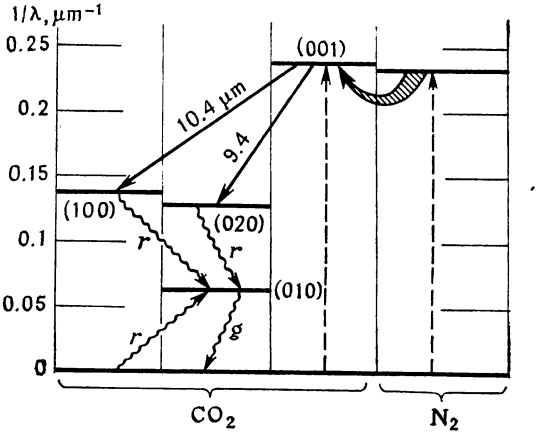


Fig. 1.34

excited vibrational level for an N_2 molecule. The *upper* laser level is (001), while the levels (020) and (100) form the *lower* laser level. Laser radiation of wavelength 10.4 μm is generated on the transition (001) → (100), while on the transition (001) → (020), radiation with wavelength 9.4 μm is generated. The excitation of the (001) level takes place as a result of inelastic collisions of CO_2 molecules with electrons (electronic excitation) and the excited N_2 molecules (resonant energy transfer) which are excited in collisions with electrons.

The relaxation of (020) and (100) levels mainly takes place as a result of *resonant* energy transfer to the unexcited CO_2 molecules, leading to the accumulation of CO_2 molecules in the (010) state (see the transition marked in Fig. 1.34 by the letter *r*):

$$CO_2(020) + CO_2(000) \rightarrow 2CO_2(010),$$
$$CO_2(100) + CO_2(000) \rightarrow 2CO_2(010).$$

The relaxation of the level (010) is the "bottleneck". The main relaxation mechanism for this level is the *gas kinetic* mechanism of

energy transfer to H_2O molecules or He atoms (see the transition indicated in Fig. 1.34 by the letter *g*). Thus, inelastic collisions of CO_2 molecules (010) with specially introduced additions to the gas mixtures play an important role in the creation of inversion. It should be recalled that CO_2 lasers belong to the class of *collision* lasers.

It should be observed that each vibrational level of a CO_2 molecule has a corresponding set of *rotational* sublevels. Hence the laser transitions (001) → → (100) and (001) → (020) must be treated as *vibration-rotation* transitions having the corresponding vibration-rotation bands in the laser generation spectrum.

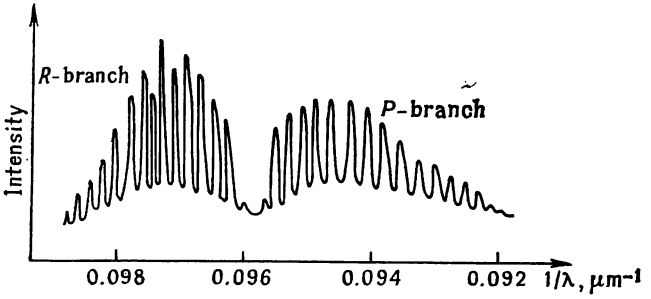


Fig. 1.35

These bands correspond to the *P* and *R* branches of transitions. These branches have been clearly indicated in Fig. 1.35 which shows the generation spectrum of a low-power CO_2 laser (for (001) → (100) transition). It should be noted that with increasing laser power, the number of lines generated simultaneously in *P* and *R* branches of transition decreases and may come down to just one or two lines (competition between transitions). In other words, the interaction (competition) between transitions may lead to generation mainly on one of the transitions in *P* and *R* branches only. Consequently, high-power CO_2 lasers have a highly coherent radiation.

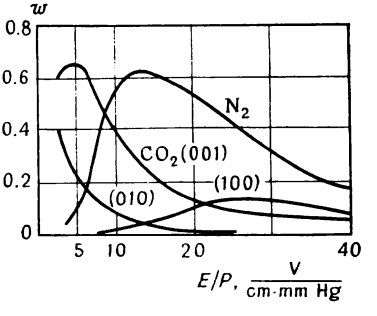


Fig. 1.36

Returning to the question of creation of inversion in a CO_2 laser, we mention the necessity for ensuring an *optimal* E/P ratio (E is the field intensity in the positive discharge column and P is the pressure of the gas mixture) for which the cross section of electron excitation of N_2 molecules and the (001) level of CO_2 molecules are sufficiently large and the cross sections of excitation of levels (100), (020), and (010) of CO_2 molecules are relatively small. As an example, Fig. 1.36 shows the dependence of the fraction w of energy,

transferred by the plasma electrons in different vibrational degrees of freedom, on the ratio E/P for the special case when the partial pressures of nitrogen and carbon dioxide are equal. The curves show that the optimal values of E/P lie in this case in the interval 5-10 $V \cdot cm^{-1}/mm$ Hg.

Thus, the selectivity of populating the upper laser level and depopulating the lower laser level necessary for creation of inversion in a CO_2 laser is ensured in practice by the introduction of nitrogen and special additives to the active medium (in a definite proportion), as well as by choosing an optimal value for E/P.

1.6. ELECTROIONISATION LASERS

Problem of Increased Pressure in a Gas Laser. As mentioned earlier, gas lasers, excited by *self-sustained* electric discharge (*gas-discharge* lasers) are characterised by a *low* pressure (of the order of 1-10 mm Hg) of the active gas mixture. This implies a relatively low concentration (10^{15}-10^{16} cm^{-3}) of the active centres, which is several orders lower than that in the solid-state or liquid lasers (10^{19}-10^{20} cm^{-3}). An increased concentration of active centres is highly desirable for increasing the radiation power emitted per unit volume of the active medium. Hence the endeavour to increase the pressure (and hence, the concentration of active centres) in the existing gas lasers is quite natural.

There are, however, two factors which hinder the pressure increase in gas-discharge lasers. Firstly, if the pressure is increased to the order of tens of mm Hg, the self-sustained discharge is practically ineffective for exciting any large volumes of the gas, since the discharge is *unstable*, and "twines" along the walls without affecting the inner part of the gas discharge tube. Secondly, the need for ensuring an *optimal* value for the ratio E/P from the point of view of excitation of the appropriate vibrational levels requires a corresponding increase in the field intensity E if we increase the pressure P. This, in turn, leads to an increase in the density of the electronic component of the discharge plasma. The surplus of electrons is a negative factor since this increases the probability of "extinguishing" collisions (in particular, collisions leading to a deexcitation of upper, and excitation of lower laser levels).

Electroionisation Method of Pumping High Pressure Gas Lasers. The *electroionisation pumping method* [47, 48] helped in solving the problem of increasing pressure in a gas laser. This method of pumping does not use the self-sustained discharge. In order to obtain fast electrons capable of effectively exciting the active centres, ionising radiation is used in conjunction with an external electric field. The ionising radiation generates free electrons in the active medium while the electric field accelerates them. Further on, the process follows the same course as in gas-discharge lasers: fast electrons excite

certain molecules (atoms), and this results in the creation of inversion under suitable conditions. Figure 1.37 illustrates the electroionisation pumping method. Here, *1* is the lasing volume (shaded in the figure), *2*—the resonator mirrors, *3*—the ionising radiation, *4*—the electrodes to which the electric voltage is applied, and 5—the output radiation.

The creation of one free electron requires energy of the order of several tens of electron volts. This energy is supplied by the ionising radiation. Each electron encounters up to 10^5 collisions with the

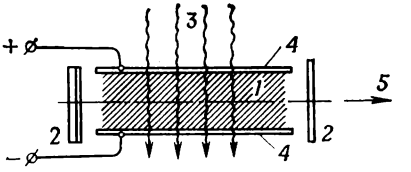


Fig. 1.37

particles of the active medium before recombining or leaving the lasing volume. In these collisions, the electron transfers energy of the order of 10^4 eV to the particles of the active medium. This is some three orders higher than the energy required for the creation of one free electron. Such a large amount of energy is taken from the external electric field. Thus, the electroionisation pumping method permits quite an effective (efficiency up to 30%) *direct* conversion of electric field energy into laser radiation.

While using this pumping method, it is not difficult to maintain the optimal value of the ratio E/P under increased pressure since the free electron concentration *does not depend* on the external field intensity E, but is rather determined by the intensity of the ionising radiation. This method permits an attainment of pressures up to tens of atmospheres (even up to 100 atmospheres). This led to the term "*compressed gas laser*".

In the electroionisation pumping process the passage of the electric current through the ionised gas is distinguished by a high stability irrespective of the pressure. A *non-self-sustained* discharge is created in the lasing volume, whose properties and structure remain constant under variations in the discharge volume over a wide range (volumes up to 100 litres were investigated).

Ionisation of the gas is necessary for maintaining the discharge, while the excitation of active centres is required for creating an inversion. Both these functions are accomplished simultaneously and by *the same* electrons in a gas-discharge laser. However, the energy distribution of electrons for the self-sustained discharge is not simultaneously optimal both for ionisation as well as excitation. In the electroionisation laser, these functions are *separately* fulfilled—

the ionisation of the gas is ensured by ionising radiation, while the electrons simply excite the active centres.

Electroionisation CO_2 Laser.[33] The electroionisation pumping method is applied in high pressure CO_2 lasers. The mechanism of creation of inversion for an electroionisation CO_2 laser is illustrated in Fig. 1.34 which also applies to a gas discharge CO_2 laser. The only difference is that the fast electrons exciting the vibrational degrees of freedom of N_2 and CO_2 molecules are generated not by the *self-sustained* discharge, but rather by the ionising radiation and the accelerating external electric field (*non-self-sustained* discharge). An

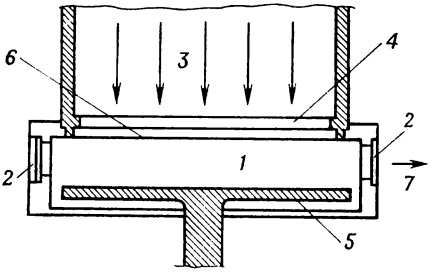


Fig. 1.38

electron beam from an accelerator (electron energy 100-500 KeV, current density of the beam $\sim 10^{-4}$ A/cm^2) is usually employed as ionising radiation.

Figure 1.38 shows the simplified version of an electroionisation CO_2 laser. Here, *1* is the lasing volume, *2*—the resonator mirrors, *3*—the electron beam (ionising radiation), *4* and *5*—the upper and lower electrons respectively, *6*—a metal foil which is transparent to fast electrons, and *7*—the laser radiation. It should be noted that the foil *6* is a fairly vulnerable place in an ionisation laser. It separates the evacuated accelerator space from the lasing volume which is under high pressure.

An increase in the pressure of the gas mixture leads to an increase in the power of laser radiation per unit volume of the active medium. Let us denote this power as W. Figure 1.39 shows the dependence of W on P. The experimental points A correspond to the gas-discharge CO_2 laser, while the points B correspond to the electroionisation CO_2 laser. This dependence is approximately quadratic: $W \propto \propto P^2$. In comparison with the gas discharge CO_2 laser, the power of laser radiation per unit volume of the active medium is 10^6 times more in an electroionisation laser.

[33] The first CO_2 lasers with non-self-sustained discharge operating at atmospheric pressure were created in 1971 [49, 50].

The Choice of an Active Medium. Besides the gas mixtures $CO_2 + N_2$ and $CO_2 + N_2 + He$, other active media can also be employed in electroionisation lasers [48]. For these, we consider the lasing transitions not only between vibrational states, but also between electronic states of molecules.

Electroionisation CO Laser. This laser operates on the transition between higher vibrational levels of a CO molecule ($v \approx 15$). The generated wavelength is equal to 5 μm. Usually, a mixture of gases $CO + N_2$ or $CO + N_2 + He$ is employed. This laser has an unusually high efficiency, up to 50%.

Electroionisation $Ar + N_2$ Laser. This laser operates on the transition between electronic states of an N_2 molecule. The generated wavelength is equal to 0.358 μm. Argon plays the role of a buffer gas, resonantly transferring energy to nitrogen.

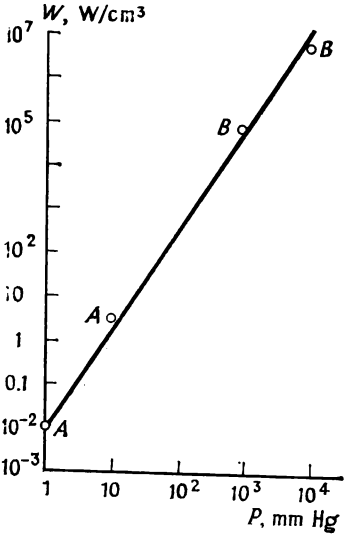


Fig. 1.39

Electroionisation Compressed Xenon Laser. This laser operates on a transition between the excited and ground electronic states of a disintegrating Xe_2 molecule. The generated wavelength is equal to 0.172 μm. Fast electrons excite the Xe atoms, which then form the excited Xe_2 molecules as a result of collision with unexcited atoms. Besides pure xenon, a mixture of Ar + Xe is also employed, argon playing the role of a buffer gas.

Methods of Ionisation. An *electron beam* is most frequently employed for ionisation. The method of ionisation through *ultraviolet radiation* (*photoionisation*), obtained, for example, through a spark discharge [51][34], is under intensive investigation. Also worth consideration is ionisation by the *heavy charged particles* created in nuclear reactions.

Laser generation has been obtained in an electroionisation CO_2 laser placed in the active zone of a stationary *nuclear reactor* [52]. An active gas mixture $CO_2 : N_2 : {}^3He$ of composition 1 : 4 : 5 was employed. The ionisation was caused by the products of the nuclear reaction

$$n + {}^3He \rightarrow p + T + 0.76 \text{ MeV}.$$

[34] Electroionisation lasers employing photoionisation are frequently called *photoionisation lasers.*

(where n is a neutron, p—a proton, and T—the tritium nucleus). The reaction was initiated by thermal neutrons created in the moderator of the reactor. The density of thermal neutrons was 10^{14} cm^{-2}sec^{-1}.

Possibilities are being considered for creating an electroionisation laser by using the energy generated by a nuclear reactor not only for ionisation, but also for accelerating free electrons appearing as a result of ionisation. Such a laser would directly transform nuclear energy into laser radiation.

1.7. GASDYNAMIC LASERS (THERMAL PUMPING)

Thermal Methods for Creating Inversion. *Thermal excitation* may be used as a fairly effective means of populating vibrational and rotational levels of a molecule. This involves heating the gas to temperatures around 1000-2000 K.

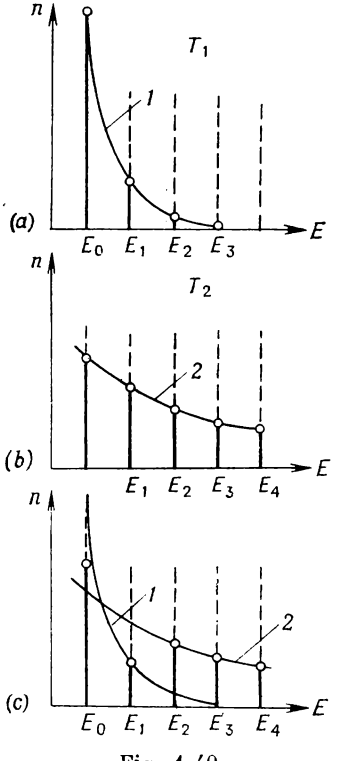


Fig. 1.40

Naturally, inversion cannot be created simply by heating a gas, which leads to a decrease in the population density of levels with increasing energy according to the Boltzmann law: $n \propto \exp(-E/kT)$. Figures 1.40*a* and *b* compare the population of vibrational levels at different temperatures (at temperatures T_1 and T_2, where $T_1 \ll T_2$). Curve *1* shows the dependence $n \propto \exp(-E/kT_1)$ while curve *2* shows the dependence $n \propto \exp(-E/kT_2)$. It can readily be seen that while an increase in temperature leads to a population of the higher levels, it *does not ensure a population inversion.*

Suppose that a gas heated to a temperature T_2 is *very rapidly cooled* to a temperature of T_1, τ being the time over which this temperature variation takes place. Further, we assume that the rate of relaxation of the first excited level (level E_1) is much higher than the relaxation rate of the levels E_2, E_3 More precisely, we assume that the relaxation time (τ_1) for the first level E_1 is much shorter than τ, while the relaxation time (τ_2) for the higher levels is, on the contrary, much longer than τ, i.e. $\tau_1 \ll \tau \ll \tau_2$. In this case, the population density of the E_1 level will follow the temperature variation upon cooling, while the population densities of other levels

remain *unchanged* upon a rapid cooling. This leads to a thermodynamic inequilibrium: the population density of the level E_1 will correspond to the *lower* temperature T_1 while the population density of the levels E_2, E_3, . . . will correspond to the *higher* temperature T_2 (see Fig. 1.40*c*). As can be readily seen from the figure, this situation results in inversion on transition between the first and second excited vibrational levels[35].

The process of *adiabatic expansion* of a gas upon its ejection from a narrow slit or a nozzle is the most convenient method for rapid cooling. This method of thermal pumping forms the basis of *gasdynamic lasers.*

It should be mentioned that inversion can also be created by *rapidly heating* a gas if the rate of thermal excitation of upper levels of a molecule is higher than for the lower levels. A fairly rapid heating may be obtained, for example, with the help of shock waves.

Gasdynamic CO_2 Laser[36]. The active medium for such a laser is a mixture of $CO_2 + N_2 + H_2O$, their characteristic proportions (by volume) being CO_2—8%, N_2—90%, and H_2O—2%. The molecules of CO_2 serve as the active centres.

A schematic version of a gasdynamic laser is shown in Fig. 1.41. Here, *1* is the combustion chamber, *2*—the nozzle array, *3*—the lasing volume (optical cavity volume), *4*—the diffuser, *5*—the resonator mirrors, and *6*—the laser beam. The active gas mixture in the initial state is prepared in the combustion chamber *1* (T_2 = = 1400-1600 K, P_2 = 20-30 atmospheres). The mixture passes through the nozzles *2* (the width of an individual slit at the exit is just 1 mm) and is expanded in the cavity volume *3* where the temperature and the pressure fall to the values T_1 = 250-300 K, P_1 = = 0.05-0.1 atmosphere. The speed of the gas coming out of the nozzles is 1200-1500 m/sec. The CO_2 molecules emit radiation in the cavity volume *3*. The purpose of the diffuser *4* is to decelerate the gas flow and to equalize its pressure with that of the surrounding atmosphere.

Existing gasdynamic CO_2 lasers give a record-high powered radiation up to 100 kW in CW operation. Unfortunately the efficiency of gasdynamic lasers is not high and does not exceed 1%.

Creation of Inversion in a Gasdynamic CO_2 Laser[37]. As in other types of CO_2 lasers, inversion in a gasdynamic CO_2 laser is created on the transitions (001) → (100) and (001) → (020) of a CO_2 mole-

[35] The possibility of creating inversion by rapid cooling in systems whose levels have different relaxation times has been considered by Basov *et al.* in [53-54].

[36] Gasdynamic lasers have been described in the monograph [55] by Losev. See also [56].

[37] The possibility of creating an inversion on vibrational levels of a CO_2 molecule upon a rapid expansion of the gas has been considered by Konyukhov *et al.* [57].

cule. The process of resonant transfer of excitation energy from a nitrogen molecule plays the main role in the population of the upper laser level (001). The introduction of additional components (like water vapours) in the mixture leads to a quicker relaxation (depopulation) of the (010) level.

Thermal pumping is characterised in this case by the population of vibrational levels of N_2 and CO_2 molecules as a result of *thermal*, and not *electronic*, excitation. As mentioned above, the *different* relaxation times for upper and lower levels play an important role in this case. Let us consider Fig. 1.42 which, in principle, is the same

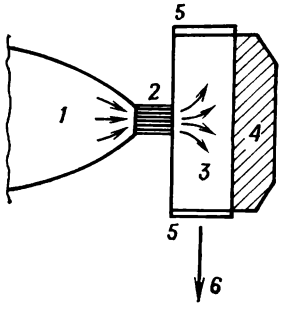


Fig. 1.41

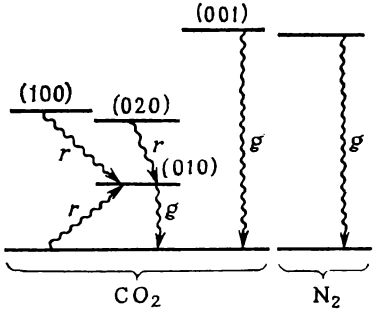


Fig. 1.42

as the level diagram shown in Fig. 1.34. Here, the resonant transitions are designated by r, while gas kinetic transitions are denoted by g. The relaxation of the excitation level of the N_2 molecule and the level (001) of the CO_2 molecule is achieved through *gas kinetic* mechanism of transferring energy (the resonant transfer of energy from nitrogen to carbon dioxide is not considered for the time being), while the relaxation of levels (100) and (020) of the CO_2 molecule takes place through *resonance* mechanism. Since the rate of resonant transfer of energy is considerably higher than for the gas kinetic case, it is apparent that the upper laser level of the CO_2 molecule must be depopulated more slowly than the lower laser levels[38]. The vibrational level of the N_2 molecule is depopulated even more slowly.

Let us assume that the $CO_2 + N_2$ mixture, heated to a temperature of about 1500 K, is rapidly expanded by passing it through a narrow nozzle (more precisely, through an array of nozzles). This leads to a sharp increase in the kinetic energy of the molecules (it should be recalled that the gas flow from the nozzle has a supersonic

[38] It should be recalled that in order to get rid of the "bottle neck" due to the relaxation of the (010) level, rapidly relaxing molecules (like H_2O molecules) are introduced in the gas mixture.

speed of about 1500 m/sec). The energy of *translational* motion of the molecules is supplied by the energy of *vibrational* motion. This means that the vibrational levels relax very rapidly at the exit from the nozzle. It is extremely significant that not all vibrational levels undergo a rapid relaxation, but only such levels for which the relaxation time is less, i.e. the lower laser levels (020) and (100) of the CO_2 molecule. As far as the (001) level of the CO_2 molecule and the vibrational level of the N_2 molecule are concerned, they *do not relax* to any considerable extent under a very rapid expansion of the gas. In the laser volume, i.e. under conditions of a sufficiently rarefied gas (the pressure does not exceed 0.1 atm) these levels practically do not relax at all, and "freezing" of higher vibrational degrees of freedom is observed.

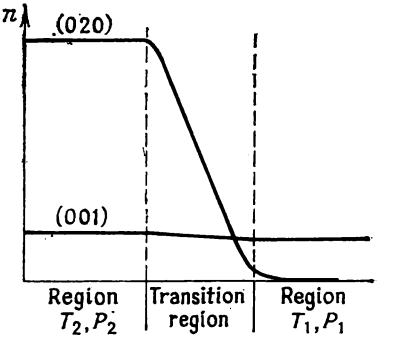


Fig. 1.43

Figure 1.43 shows the variation of the population densities of the levels (020) and (001) of a CO_2 molecule upon a passage of the gaseous mixture from the combustion chamber (the parameters of the mixture are T_2 and P_2) to the cavity (the mixture in the cavity has parameters T_1 and P_1). In the transition region (the nozzle), there is an almost complete depopulation of the (020) level and only a slight decrease in the population density of the (001) level. In the cavity, the population density of the (001) level practically freezes at values nearly corresponding to the initial temperature T_2. The population inversion of (001) and (020) levels is apparent.

Thus, the CO_2 molecules enter the cavity with nearly unpopulated lower laser levels (more precisely, the population density of these levels corresponds to the temperature T_1). As regards the upper laser level, it is populated as if the gas continued to be at a temperature T_2.

It is also important that the population density of the vibrational level of the N_2 molecules is "frozen". The excited N_2 molecules will resonantly give their excitation energy to CO_2 molecules and thus maintain the relatively high population density of the (001) level. It should be remembered that quantitatively, nitrogen constitutes the main component of the mixture—about 90% in a gasdynamic laser. Hence it may be considered that the laser energy is obtained mainly from the vibrational energy of nitrogen molecules.

Thus, the energy accumulated in the vibrational degrees of freedom of molecules in the combustion chamber is consumed during the passage of the gaseous mixture into the cavity through the nozzle according to the following procedure: part of energy accumulated

in *symmetric deformation* vibrations of CO_2 molecules is converted into the energy of *translational* motion of the flow through the nozzle. The energy accumulated in *asymmetric* vibrations of CO_2 molecules, and mainly in the *vibrations of* N_2 *molecules* is converted, excluding the losses in the cavity, into *laser radiation.*

Methods of Improving the Efficiency of Gasdynamic Lasers. The relatively low efficiency of gasdynamic lasers (not more than (1%) is due to a number of reasons. Firstly, the energy of the translational motion of the gas flowing from the nozzle is uselessly wasted (after deceleration and compression in the diffuser, the gas is found to be at high temperatures). Besides, a certain number of excited N_2 molecules are removed from the cavity by the gas flow before they have been able to convey their excitation energy to CO_2 molecules. Likewise, a certain number of excited CO_2 molecules are removed before they have been able to emit.[39]

In order to increase the efficiency of a gasdynamic laser, it is necessary to reduce the losses mentioned above. A reduction of losses caused by the removal of the excited molecules from the cavity is possible by optimising its parameters or by improving its construction. In order to avert the losses due to heating of the gas in the diffuser, some radical measures have to be taken. For example, it is possible to construct a gasdynamic laser with a *closed cycle* for the gas mixture. Such a laser must include two additional elements: a *compressor*, and a *heat-exchanger*. These are meant to impart the initial temperature and pressure to the gas mixture. Thus, the energy of the translational motion of gas flow may be used for bringing the gas into the initial state. In this case the gasdynamic laser is identical to a *heat engine* (whose working cycle is close to the Carnot cycle). Once such a laser starts generating, the subsequent supply of energy must simply compensate the losses due to the movement of the gas, losses in the resonator and the radiated light energy.

1.8. CHEMICAL LASERS

Chemical compounds are rich accumulators of energy. This energy may be partially liberated during a *rearrangement of chemical bonds* (in exoenergic chemical reactions). The idea of converting this energy into laser energy is quite tempting.

Chemical lasers are based on the realisation of this energy conversion.[40] The undiminishing interest to this type of lasers is due both to the practical importance of the problem of direct conversion of

[39] A premature removal of a certain number of excited nitrogen and carbon dioxide molecules from the cavity by the gas flow determines the type of losses in the resonator, which are typical of gasdynamic lasers.

[40] The possibility of creating a chemical laser was considered by Oraevskii [59] and Tal'roze [60]. Reviews by Tijoev *et al.* [61] and Basov *et al.* [62] have been devoted to chemical lasers. See also [8] and Ch. 7 in [4].

chemical energy into light, as well as to the possibility of using lasers for investigating chemical processes, the cross sections of reactions, and their kinetics.

The existing chemical lasers generate on *vibrational* (more precisely, *vibration-rotation*) transitions in molecules. The lower limit of the generation wavelength range in these lasers is about 2.5 μm. Investigations are being carried out to explore the possibilities of creating chemical lasers in the visible spectral region (i.e. lasers generating on transitions between *electronic* states of molecules).

Chemical Reactions. Initiation and Acceleration of Reactions. Most frequently, chemical lasers employ *substitution* reactions leading to formation of diatomic molecules in excited vibrational states. We shall call these molecules as *lasing active centres*. They either themselves emit, or cause emission in other molecules to which they transfer their excitation energy.[41] The following are the examples of substitution reactions used in lasers (the sign * indicates an excited molecule): $F + H_2 \rightarrow HF^* + H$; $F + D_2 \rightarrow DF^* + D$; $H + Cl_2 \rightarrow HCl^* + Cl$; $Cl + HI \rightarrow HCl^* + I$.

In order to initiate these reactions, a certain amount of energy has to be spent on obtaining *chemically active reagents* (F, H, Cl). Besides, it is essential to accelerate a chemical process since a chemical laser operates only on *fast reactions* which ensure a fairly rapid population of the upper laser level of the emitting molecules. The rate of a chemical reaction is proportional to the concentrations of the reagents taking part in it. Hence a sufficiently large amount of chemically active reagents is required in order to accelerate a reaction.

Various methods are employed for initiating and accelerating chemical reactions (in other wodrs, there are several different means of obtaining chemically active reagents). In particular, chemically active reagents are reagents in atomic state, obtained as a result of *dissociation* of molecules. The most widely used methods are *photodissociation*, *dissociation by electron impingement*, and *thermal dissociation* of molecules. In this context, the following methods for initiation (accelerating) of chemical reactions are employed: *photoinitiation*, *initiation by an electron beam* or *by an electric discharge pulse*, and *thermal initiation*.

Quartz flash lamps are often used as sources of radiation for *photoinitiation* of chemical reactions. For pumping at a shorter wavelength ($\lambda \leqslant 0.2$ μm), different types of open discharge (for example, spark discharge) are applied. One of the simplest means of initiating chemical reactions is the *self-sustained discharge* in a gas. However, this method is applicable only for relatively low pressures and small lasing volumes. Hence the method of initiation based on the application of an *electron beam* is more interesting. An electron beam

[41] In this context, we often speak of *direct* or *indirect* creation of inversion in chemical lasers (see later).

starts a reaction in a record short time of the order of 10^{-8}-10^{-7} sec (for self-sustained discharge, the duration of triggering pulse is not less than 10^{-6} sec). *Thermal* initiation of reactions is connected with thermal dissociation of molecules. This method can be conveniently employed for gasdynamic lasers which have an intensely heated gas (in order to obtain a high flow rate of the gas).

Chemically active reagents may also be produced as a result of specific *chemical reactions*. As an example, let us consider the reaction $NO + F_2 \rightarrow NOF + F$. The nitric oxide, which exists as a stable radical NO at normal temperatures, reacts with molecular fluorine, thus leading to the formation of chemically active atomic fluorine.

Chemical Chain Reactions. Chemical and Laser Length of a Chain. Chemical lasers work on *chain reactions* in which a chemically active centre (atom or radical) is *reproduced* during the course of the reaction. Suppose that chemically active centres, say F atoms, have been inoduced in a mixture of H_2 and F_2 molecules. The following chain reaction may be assumed to be taking place in this mixture:

$$F + H_2 \rightarrow HF^* + H \ (+30 \text{ kcal/mole});$$

$$H + F_2 \rightarrow HF^* + F \ (+100 \text{ kcal/mole});$$

$$F + H_2 \rightarrow HF^* + H \ (+30 \text{ kcal/mole}).$$

If a certain definite number of chemically active centres are created, this chain process may become sufficiently fast so that the condition for generation on transitions in HF* molecules is satisfied. Since this definite number of chemically active centres is conserved (reproduced) in the chain process, a possibility of involving an extremely large number of H_2 and F_2 molecules arises on account of *multiple* use of a certain number of *reproducible* chemically active centres, thus leading to the creation of many active laser centres. HF*. In this case, such a large amount of chemical energy contained in the $F_2 + H_2$ mixture may be converted into laser energy that it *compensates* the loss of energy in creating the chemically active centres.

In practice, however, it must be taken into account that the actual chain process is *not infinite*. Firstly, there is a loss of chemically active centres ($H + H \rightarrow H_2$, $F + F \rightarrow F_2$), hence the initial creation of N_0 such centres ensures the emergence of a limited number N_1 of active laser centres. The ratio $\nu_{chem} = N_1/N_0$ is called the *chemical length of the chain*. The existence of a *finite* chemical length of the chain means that not only a chemical reaction has to be initiated but it also has to be *maintained*, by creating new chemically active centres in exchange for those which have been excluded from the process.

Secondly, there is a loss of active laser centres on account of relaxation processes. In this context, we introduce the concept of *laser length* ν_{las} *of the chain* defined as the ratio of the rate of creation of

excited active laser centres to the rate of relaxation of these centres.[42] As a rule, the latter is higher than the rate of decrease of chemically active centres, so that $\nu_{las} < \nu_{chem}$. Hence the laser length of the chain normally defines the efficiency of a chemical laser.

A rapid decrease in the number of chemically active centres, and the relaxation processes may result in the chain process *not being realised at all.* For example, the process in the $Cl + H_2$ mixture is characterised by such a small laser chain length that it should be

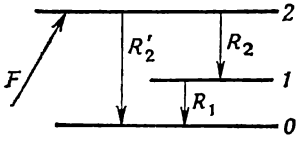


Fig. 1.44

considered essentially as a non-chain process. However, replacement of chlorine by the more active reagent fluorine in this mixture results in a chain process.

In order to extend the laser and chemical chains, it is expedient to use not simple but *branched* chain reactions in chemical lasers, i.e. such reactions which involve not a simple, but an *extensive* reproduction (multiplication) of chemically active centres. It is well known that at a particular pressure and temperature of the gaseous mixture $F_2 + H_2$, chemical reactions of the type $F_2 + HF \rightarrow HF + F + F$ might appear, thus ensuring *branching of the chains.* It may be assumed that such reactions may be used for creating a chemical laser in which the ratio of laser radiation energy to the energy spent in initiating and maintaining a chemical reaction is considerably higher than unity.

Lasers with Direct and Indirect Creation of Inversion. If the emitting molecules are a direct result of a chemical reaction, the inversion in the chemical laser is called *direct.* For creation of direct inversion, it is essential that these molecules appear in a particular excited state corresponding to the upper laser level.

Figure 1.44 shows a simplified level diagram for a molecule which is an active centre (the vibrational levels are considered). Here *1* and *2* are the lower and the upper level respectively, F denotes the rate of population of level *2* (rate of chemical reaction) while R_1, R_2, and R_2' are the relaxation rates for the corresponding levels. The specific nature of chemical pumping is manifested in the possibility of a high excitation selectivity. Unlike optical pumping, the excitation of level *2* is not accompanied by induced deexcitation, hence even *two-level* laser diagrams are possible in the case of chemical

[42] The concept of laser chain length has been introduced by Oraevskii [62].

pumping. The decisive factor in the creation of inversion is obviously the relationship between the rate of a chemical reaction and the relaxation rates for the levels. In particular, it is important that the inequality $R_1 > R_2$ be satisfied. In diatomic molecules this inequality is hard to satisfy on account of the fact that there is no process which would lead to a selective depopulation of the lower vibrational levels. On the contrary, the transitions $(v + 1) \rightarrow v$ take place, as a rule, at a faster rate than the transitions $v \rightarrow (v - 1)$. In this connection it is expedient to use an indirect inversion.

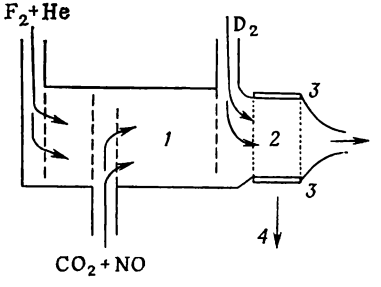


Fig. 1.45

In the *indirect* creation of inversion, the excited diatomic molecules appearing as a result of the chemical reaction resonantly transfer their excitation energy to the unexcited polyatomic (usually triatomic) molecules which then radiate in the resonator. In other words, inversion is created on the vibrational transitions of "cold" molecules forming the laser medium, as a result of resonant transfer of energy from the "hot" molecules produced in the chemical reaction. As a rule, CO_2 molecules are employed as "cold" molecules while the molecules of DF, HF, HCl, etc. serve as "hot" molecules. When energy is transferred to CO_2 molecules, the asymmetric vibrations of these molecules ((00n) levels) are most effectively excited.

DF-CO_2 Chemical Lasers with Indirect Creation of Inversion [63]. A high output power and a relatively long laser chain have made the $D_2 + F_2 + CO_2$ laser (deuterium, fluorine, and carbon dioxide mixture) as one of the most important chemical lasers. Chemical reactions are initiated in this laser by photolysis, electron beam, or with the help of the reaction $NO + F_2 \rightarrow NOF + F$. In the latter case, the laser is called a *purely chemical* DF—CO_2 laser.

A simplified version of such a laser is shown in Fig. 1.45. Here, *1* is the chamber in which the chemical reactions take place, *2* is an optical resonator, *3*—the resonator mirrors, and *4*—laser beam. A mixture of fluorine and helium[43] is first introduced into the chamber *1*. Carbon dioxide and nitric oxide are then injected into the flow through a number of holes. Atomic fluorine is created as the chemically active reagent as a result of the chemical reaction $NO + F_2 \rightarrow \rightarrow NOF + F$. When the concentration of atomic fluorine is sufficiently high, the following chain process takes place as deuterium

[43] Helium is introduced in order to prevent the overheating and spontaneous ignition of the fluorine-hydrogen mixture. Besides, helium facilitates the depopulation of the lower laser level in CO_2 molecules.

is injected into the mixture:

$$F + D_2 \rightarrow DF^* + D,\ D + F_2 \rightarrow DF^* + F;\ F + D_2 \rightarrow DF^* + D;\ldots$$

The excited DF* molecules transfer the excitation energy to CO_2 molecules which are then carried by the flow into the resonator where they radiate.

Carbon Disulphide Chemical Lasers (CO Chemical Lasers). The corrosive and highly toxic nature is the main drawback of the fluorine-hydrogen mixture. Hence other mixtures which are free from this drawback have been tried. Foremost among these are mixtures *based on carbon disulphide* (CS_2).

Let us first consider the mixture $CS_2 + O_2$ [64]. Upon irradiating this mixture with light of wavelength 0.18-0.22 μm, the following reactions take place in it[44]

$$CS_2 + \hbar\omega \rightarrow CS + S \text{ (photoinitiation)};$$

$$S + O_2 \rightarrow SO + O;$$

$$CS + O \rightarrow CO^* + S;\ CS_2 + O \rightarrow SO + CS.$$

Chemically active reagents CS, S, and O are formed in these reactions. Sulphur monoxide (SO) molecules and excited carbon monoxide (CO*) molecules are the end products of these reactions. The latter are used as active centres in the laser medium (direct creation of inversion). The observed emission spectrum is characterised by a wavelength range from 4.9 to 5.8 μm. The laser radiation is generated on vibrational transitions of CO molecules ($v \rightarrow v - 1$) where $v = 1, 2, \ldots, 16$.

More efficient chemical lasers involving lower losses in photoinitiated reactions are $CS_2 + SO_3$ lasers or $CS_2 + O_3$ lasers [65, 66]. In the $CS_2 + SO_3$ (carbon disulphide and sulphur trioxide) laser, the second of the above-mentioned reactions is replaced by the reaction $SO_3 + \hbar\omega \rightarrow SO_2 + O$ (the radiation wavelength must be less than 0.26 μm), while in the $CS_2 + O_3$ (carbon disulphide and ozone) laser, it is replaced by the reaction $O_3 + \hbar\omega \rightarrow O_2 + O$ ($\lambda_p \approx$ $\approx$ 0.22-0.28 μm).

In all chemical lasers based on carbon disulphide, CO molecules are the active centres of the laser medium. These lasers are often called CO *chemical lasers*. The main reaction $CS + O \rightarrow CO^* + S$ is a distinctly exoenergic reaction; energy of about 80 kcal/mole is liberated in this reaction, and 80% of this energy is used for exciting the vibrations of CO molecules. In order to increase the relaxation rate of lower vibrational levels of a CO molecule, we introduce agents (like nitrous oxide N_2O), to the gaseous mixtures of CO chemical lasers. Besides, thermal diluents like sulphur hexafluoride SF_6 are also introduced.

[44] The small length of the laser and chemical chain predetermines that the processes in this laser are not chain processes.

Chemical Lasers on Electronic Transitions of Molecules. As mentioned earlier, investigations are being carried out to create chemical lasers on *electronic* transitions of molecules (*chemical visible lasers*). One of the possibilities of creating such lasers is related to the excitation of electronic states of a molecule as a result of a *combination reaction* between an atom and a molecule. In particular, we can use the *oxidation reaction* [67] $Ge + N_2O \rightarrow N_2 + GeO$ (+130 kcal/mole), or $Sn + N_2O \rightarrow N_2 + SnO$ (+90 kcal/mole) leading to the creation of inversion on electronic transitions of GeO and SnO molecules. For initiating these reactions, we may use the thermal method, employing temperatures around 1000-1500 K. Another method of initiating envisages optical excitation by CO_2-laser radiation. This method gives rise to the possibility of an effective conversion of infrared radiation into visible radiation.

1.9. PLASMA LASERS (RECOMBINATION PUMPING)

Recombination Plasma as an Active Laser Medium. The recombination processes during collisions of free electrons with the positively charged ions in a plasma may lead to a sufficiently effective accumulation of atoms (ions) in excited states. In other words, it can be used, in principle, for pumping laser levels.

Let T_e denote the temperature of the electronic component of the plasma (electronic temperature), and T denote the equilibrium temperature at which the degree of ionisation coincides with the given value. Suppose that n_e and n_+ are the concentrations of electrons and ions respectively. The rate of decrease of n_+ on account of recombination electron-ion collisions is given by the equation

$$-dn_+/dt = \beta n_+ n_e^2 \tag{1.9.1}$$

where β is the coefficient of electron-ion recombination.[45] It increases with the decrease in electronic temperature T_e according to the relation

$$\beta = DT_e^{-9/2} \tag{1.9.2}$$

(D is a certain constant). It follows from Eq. (1.9.1) that

$$n_+(t) = n_+(0) \exp(-t/\tau_+), \tag{1.9.3}$$

where τ is obtained by taking into consideration Eq. (1.9.2),

$$\tau_+ = T_e^{9/2}/Dn_e^2. \tag{1.9.4}$$

The smaller the value of τ_e, the higher the rate of recombination, and hence the more effective the pumping. It can be easily seen that the recombination plasma must have a sufficiently high electron

[45] Here, we consider the recombination by triple collisions, since in a dense plasma the radiative recombination may be neglected [68].

concentration n_e and at the same time a sufficiently low electronic temperature T_e. Recombination plasma regime is a *dense, highly ionised* plasma whose electrons are "*supercooled*" so that the following inequality is satisfied

$$T_e < T. \tag{1.9.5}$$

Recombinating plasma is very attractive as an active laser medium. Unlike other active media, it does not change its aggregate state even upon the introduction of energy with the highest density. This opens the possibility for creating exceptionally powerful lasers. Besides, in the recombination plasma, we can use in principle laser transitions falling in the ultraviolet region, and even in the X-ray region.

The properties of *recombination plasma* are radically different from those of plasma used in gas-discharge lasers (this kind of plasma is called *ionised plasma*). A comparison of these properties is given in Table 1.4 where characteristic numerical values for plasmic parameters are given.

TABLE 1.4

Parameter	Plasma Regime		
	Ionisation		Recombination
	Glow discharge	Arc discharge	
n_e, cm^{-3}	10^9-11^{11}	$\sim 10^{13}$	10^{14}-10^{16}
T_e, K	$>10^4$	$\sim 10^4$	$\sim 10^2$
T_e/T	>100	10	0.1-1

Ionised plasma is characterised by a lower concentration of free electrons than in the recombination plasma, and a reverse relation between T_e and T as compared to (1.9.5). In the recombination plasma, electrons are "supercooled" while in the ionised plasma, they are "superheated". Deviations from thermodynamic equilibrium in *opposite* direction are apparent here.

It should be observed that a recombination plasma is characterised by a *downward* displacement of excited atoms (ions) on the energy scale. This facilitates a predominated excitation of upper levels. For the ionisation plasma laser, the population of levels takes place in the reverse (*upward*) direction, thus increasing the probability of parasitic excitation of lower levels.

Basic Problems of Creating Recombination Plasma Laser. Theoretical and experimental aspects of the creation of recombination plasma lasers are subjects of active investigation at the present time. These lasers are called *plasma lasers* or *recombination lasers.*[46]

[46] Plasma lasers have been reviewed by Gudzenko *et al.* [69]. See also [70, 71].

Let us emphasize the main difference between the plasma laser and the gas-discharge laser. During its operation, the degree of ionisation of plasma *increases* in a gas-discharge laser, while in the case of a plasma laser, the degree of ionisation *falls*. In this sense, the gas-discharge laser works on conversion of the medium *from gas to plasma*,[47] while the plasma laser works on conversion *from plasma to gas*.

Continuing the comparison between the plasma laser and the gas-discharge laser, let us consider the pulse pumping. Pulse gas-discharge lasers start emitting when a sufficiently high pulsed current intensity is reached in the discharge at the pulse front. The pulsed plasma laser starts emitting after the passage of the pulse current, i.e. only after a sufficiently high degree of plasma ionisation is attained, and a "cooling" of free electrons has taken place. In other words, the plasma laser generates in the *afterglow of the discharge*.

Two problems have to be solved in order to create a plasma laser. The *first* one is connected with the generation of a dense, highly ionised plasma with "supercooled" electrons, while the *second* one deals with the depopulation of the lower laser level.

The first problem is especially complicated and various methods have been investigated for solving it. These differ from one another in the method of introduction of excitation energy to the active medium and in the methods of cooling the electrons. If the plasma is stationary as a whole, there are two effective methods of cooling free electrons: cooling at the walls (in tubes of relatively small diameters), and cooling on account of elastic collisions with the atoms of the buffer gas, for example, helium or hydrogen. In a plasma which moves as a whole, the gasdynamic mechanism of cooling by adiabatic expansion of the gas mixture is also possible.

Depending on the methods of ionisation of the medium, cooling of electrons, and the depopulation of lower levels, plasma lasers are divided into different types: *pulsed* lasers, *electron beam* lasers, *nuclear pumping* lasers, *plasmadynamic* lasers, and *plasmachemical* lasers.

"Open" Two-level Model of a Plasma Laser. The two-level laser diagram corresponding to this simplest model is shown in Fig. 1.46. Here, *1* and *2* are the lower and upper laser levels respectively, F is the probability of population of the upper level, while R_1 and R_2 are the probabilities of depopulation of levels *1* and *2* respectively. Denoting the population densities of the laser levels by *1* and *2* respectively, and the ionic concentration by n_+, the balance equation for the stationary case may be written as

$$\left.\begin{aligned} dn_2/dt &= n_+/\tau_+ - n_2R_2 = 0; \\ dn_1/dt &= n_2R_2 - n_1R_1 = 0. \end{aligned}\right\} \qquad (1.9.6)$$

[47] An inordinate increase in the degrees of ionisation of the plasma in a gas-discharge laser may lead to a breakdown in generation.

The rate of population of level *2* is the rate of recombination of ions. It should be recalled that $\tau_+ = T_e^{9/2}/Dn_e^2$.

Using Eqs. (1.9.6), we get the following expressions for the inverse population density of laser levels:

$$n_2 - n_1 = n_2 (1 - n_1/n_2) = (n_+/R_2\tau_+) (1 - R_2/R_1). \quad (1.9.7)$$

In this case, formula (1.1.3) for the amplification factor assumes the form

$$\varkappa = \sigma (n_2 - n_1) = (\sigma n_+/R_2\tau_+) (1 - R_2/R_1), \quad (1.9.8)$$

or

$$\varkappa = \frac{\sigma D}{R_2} \frac{n_+ n_e^2}{T_e^{9/2}} \left(1 - \frac{R_2}{R_1}\right). \quad (1.9.9)$$

As can be seen from Eq. (1.9.9), this simplified model of a plasma laser reflects its main features: the necessity to create high concentrations n_e and n_+ in the plasma, "cooling" of electrons, and ensuring a rapid depopulation of the lower level (in order that the inequality $R_2 < R_1$ is satisfied).

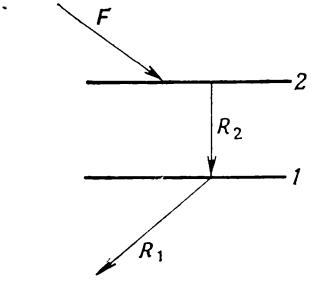


Fig. 1.46

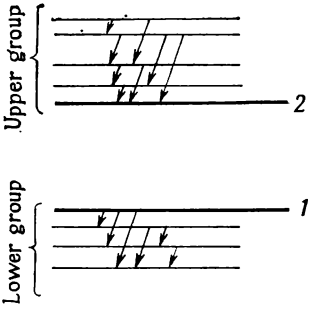


Fig. 1.47

Depopulation of the Lower Laser Level. The main mechanisms of depopulation of the lower laser level in plasma lasers are: radiation, deexcitation by cold free electrons, inelastic collisions with atoms of special additives, and chemical depopulation.

Radiative depopulation (depopulation by *spontaneous emission*) is effective when the lower laser level is quite high, the plasma is not too dense, and the lasing volume is not very large. In the contrary situation, the depopulation on account of *collisions* of active centres with the cooled free electrons is more important. The effectivity of this mechanism depends on the electron concentration and the degree of their cooling. It should be observed that the cooling of electrons is necessary to ensure recombination (and hence the population of the upper laser level) and for accelerating the process of depopulation of the lower laser level.

Inversion of electronic deexcitation takes place, in particular, when the levels of the active centre are divided into two groups of closely-spaced levels, the lowest level in the upper group is the upper laser level while the uppermost level in the lower group is the lower laser level (see Fig. 1.47; *1* and *2* are the laser levels). As a matter of fact, the probability of electronic deexcitation between levels of different groups is considerably smaller than between the closely-spaced levels of the same group. Hence collisions with electrons lead, within the limits of each group of levels, to a predominant population of the lower, and depopulation of the upper levels (as indicated by arrows in the figure). Thus, conditions are ensured

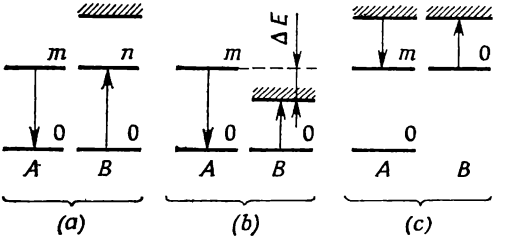


Fig. 1.48

for creating inversion between the lower level of the upper group and the upper level of the lower group even when the total population density of the lower group exceeds the population density of the upper group.

Inelastic collisions of active centres (let us denote these centres as A) with the atoms of special additives (denoted as B) may also be used for depopulation of lower levels. Figure 1.48 shows the transitions corresponding to different collision processes (the ionisation level of the atom is shaded), Fig. 1.48*a* showing the *resonant transfer of excitation*

$$A\ (m) + B\ (0) \rightarrow A\ (0) + B\ (n).$$

Figure 1.48*b* shows the *ionisation of an impurity atom upon transfer of excitation* (Penning effect)

$$A\ (m) + B\ (0) \rightarrow A\ (0) + B^+ + e;$$

(where e is an electron whose energy is indicated by ΔE in the figure). Figure 1.48*c* shows the *resonant charge transfer*[48]

$$A^+ + B\ (0) \rightarrow A\ (m) + B^+.$$

By a special choice of the additive (impurity), a predominant depopulation of the lower levels can be ensured. This is illustrated

[48] It can be easily seen that this process leads not to depopulation, but rather to population of the m-th level of the atom A.

in Fig. 1.49 where the population densities of laser levels n_1 and n_2 are plotted against the impurity concentration (n_{imp}). It can be seen that when the impurity concentration exceeds a certain value (the value $\bar{n}$ in the figure), a population inversion in laser levels takes place.

Effective depopulation of lower levels in plasma lasers is also possible through special chemical reactions. *Chemical depopulation* can lead to inversion even on transitions to the ground state.[49]

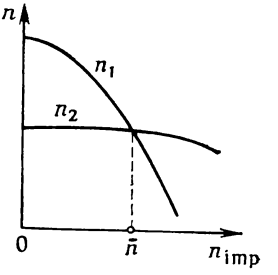


Fig. 1.49

Pulsed Plasma Lasers. For ionisation of the active medium in these lasers, rapidly decaying pulses of electric discharge with the following characteristic parameters are used: voltage up to 20 kV, current up to 300 A, and pulse duration of about 0.1-1 μsec. Pulse generation takes place in an *afterglow discharge.*

A mixture of an active laser component ionised and an auxiliary (buffer) component which cannot be easily ionised is used as active medium. The latter component is required mainly to ensure a sufficiently rapid cooling of free electrons in plasma.

Under the action of a powerful excitation pulse, plasma is generated with a high concentration of free electrons and ions of various multiplicities. On termination of the excitation pulse, a rapid cooling of free electrons takes place on account of collisions with atoms of the buffer gas. This is followed by an intensive *recombination of ions and electrons* which effects a pumping of laser levels in active centres consisting of atoms or ions (normally singly charged) of easily ionisable component of the mixture. The electronic deexcitation of lower laser levels plays an important role in the creation of inversion.

Pulsed plasma lasers have been created, in particular, *with ionised vapours of alkaline-earth metals* Mg, Ca, Sr, and Ba. As an example, let us consider the *Sr-He plasma laser* generating on transitions in SrII, i.e. on transitions between the levels of singly charged Sr^+ ions. Helium plays the role of buffer gas. The excitation pulse generates a plasma with a high concentration of doubly charged strontium ions (Sr^{2+}). The recombination processes lead to the formation of excited singly charged Sr^+ ions which play the role of active centres. Generation is attained on a number of transitions of Sr^+ ions. The principal lines are at 0.416 μm ($6^2S_{1/2} \rightarrow 5^2P_{1/2}$ transition) and at 0.431 μm ($6^2S_{1/2} \rightarrow 5^2P_{3/2}$ transition) [71].

Plasma Lasers Using Hard Ionising Agents. Reactor Laser. Some of the most promising methods of creating recombination plasma

[49] Chemical depopulation will be described in detail later in this book.

are based on the use of hard ionising agents like a *fast electron beam* introduced from outside into the cold dense gas, or *fission fragments of atomic nuclei*, formed in a nuclear reactor [69]. In the first case, we get an *electron-beam plasma laser*, while in the second case we get a *plasma laser with nuclear pumping* or, in other words, a *reactor laser*. Pulsed plasma lasers work on freely recombining plasma created after the termination of the ionising pulse discharge and the ensuing of rapid cooling of plasma electrons. Plasma lasers using hard ionised agents may operate on stationary supercooled plasma in which inversion may be persistently maintained. Let us discuss the principle behind a reactor laser.

It is well known that the energy released inside a nuclear reactor as a result of fission of uranium and plutonium nuclei is mainly the kinetic energy of "nuclear fragments". These fragments are *multiply charged ions*[50]. The ionic fragments fly apart with very high velocities in a comparatively cold medium[51] and may be used for creating an intense recombination plasma. Thus it is possible to obtain a direct transformation of nuclear energy into energy of laser radiation (along the "chain": kinetic energy of fission fragments, energy of highly ionised dense plasma, energy of laser radiation).

The schematic of a reactor laser is fairly simple. It is a set of parallel tubes called the *energy-liberating elements* (ELE) around which the coolant flows. Each ELE is filled with a mixture of a gaseous component of uranium (for example, uranium hexafluoride UF_6) and the active laser component (for example, helium). The tube has mirrors at its end faces. For UF_6 concentrations of around 10^{19} cm^{-3}, the mass of the nuclear fuel may become critical, and conditions for the fission chain reaction for uranium nucleus may be fulfilled. The concentration of helium should be about 10^{21} cm^{-3}. For such a density of the gas, the ionic fragments will effectively ionise helium in tubes having a radius not less than 1 cm. The plasma is cooled by the coolant flowing around the ELE tube[52]. Thus, in each ELE tube an intensely recombining plasma may be created for pumping laser levels in helium. As a result, these tubes are converted into *radiating active laser elements.*

Plasmadynamic Lasers. In this type of plasma lasers, the plasma moves as a whole. In the course of its motion, a transition in the recombination mode is attained. Various types of macroscopic motions of the plasma are being studied. These include *expansion*, *compression*, and a *uniform jet flow* [70].

[50] For example, the fission fragments of U^{235} most frequently include Sr^{20+} ions and Xe^{22+} ions.

[51] The velocity of the fragments is of the order of 10^7 m/sec and their energy is around 100 MeV.

[52] The heated coolant may be used in the steam generator of the atomic power plant.

A *rapid (adiabatic) expansion* of a dense plasma, heated beforehand by electric discharge, results in a cooling of the medium, thus ensuring favourable conditions for recombination. From a steady plasma jet through a narrow slit or a nozzle, a continuous laser generation may be obtained under certain specific conditions.

A *rapid constriction* of plasma can introduce into it energy of high density. This method of introducing energy into plasma may be practically accomplished in devices based on *pinch effect*[53]. Pinching of plasma column by an external longitudinal magnetic field ensures a record-high concentration of free electrons (more than 10^{17} cm^{-3}). Such a pinching of plasma leads, in principle, to recombination, since significant losses of energy in bremsstrahlung (this process is effective in a plasma containing multiply charged ions) may considerably hinder the rise in electron temperature, while the concentration of electrons will increase during pinching. Thus, in a rapidly constricted plasma, an effective recombinative population of upper laser levels may take place while the lower levels will be depopulated through an efficient collision mechanism under such conditions.

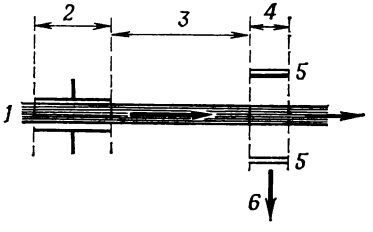


Fig. 1.50

The interesting possibility of obtaining a *CW-mode* in the afterglow discharge arises if we use a plasma mixture in the form of a *uniform jet-flow*. It should be recalled that three consecutive processes take place in a pulsed plasma laser. The first of these is the production of a highly ionised plasma. This is followed by the cooling of free electrons in the plasma, and finally by the recombination of the plasma (pumping of laser transitions). If the plasma is macroscopically stationary, these processes are accomplished at the same region of space and hence they must take place one after the other, thus leading to an unavoidable *pulsed* operation of the laser. If the plasma flows as a jet, all the above mentioned processes may be realised *simultaneously but in different regions of space* (different parts of the jet). Figure 1.50 illustrates this. Here, *1* is the gas jet, *2*—the region in which transverse discharge is accomplished, and a highly ionised plasma is produced, *3*—the region in which cooling of free electrons takes place, *4*—the recombination region, *5*—the optical resonator mirrors, and *6*—the laser beam. Such an unfolding of consecutive processes in space (along the jet flow) may lead, in principle, to a simultaneous realisation of these processes.

[53] Pinch effect is the compression of a discharge under the action of a current flowing through it. For details, see [72].

Plasmachemical Lasers. Unlike chemical lasers where chemical energy is used for exciting upper laser levels, the main function of chemical reactions in plasma lasers is to *depopulate the lower laser levels.* Investigations of plasmachemical lasers have two basic aspects: a study of chemical reactions which remove atoms (ions) from certain states, and an investigation of media based on dissociating molecules [69].

The first aspect envisages the investigation of kinetics of population and depopulation of energy levels in the course of some chemical reactions taking place in plasma mixtures. As an example, let us consider the chemical reactions which ensure a rapid removal of hydrogen atoms from the ground state [73]:

$$H + F + HF \rightarrow 2HF; \quad H + Cl + HCl \rightarrow 2HCl;$$

$$H + F + F_2 \rightarrow HF + F_2; \quad H + Cl + Cl_2 \rightarrow HCl + Cl_2.$$

By making use of these reactions, generation may be achieved on transitions corresponding to the Lyman series lines in the hydrogen spectrum.

In a plasma laser based on *noble-gas molecules*, the processes taking place in the recombinating plasma lead to the formation of electronically excited dissociating molecules. These molecules may be formed, for example, as a result of recombination of atoms in the ground state [denoted as A (0)] with the atoms in the excited state [denoted as A (1)]: $2A\ (0) + A\ (1) \rightarrow A_2\ (1) + A\ (0)$. Here A_2 (1) is the dissociating molecule in the electronically excited state.

Plasma lasers based on electronic transitions of noble-gas molecules apparently belong to the most promissing type of plasma lasers already in operation, since the problem of depopulation of the lower laser level can be easily solved for them, and also the choice of emitting molecules is varied. In particular, the compounds based on heavy inert gases (Ar, Kr, Xe) and the elements having a high affinity for electrons (halogens, oxygen) offer bright perspectives.

Chapter Two

FORMATION OF RADIATION FIELD IN A LASER RESONATOR

Besides the active medium and excitation (pumping) system, the *optical cavity* (*resonator*) is one of the main elements of a laser. To create laser oscillations, the inversion of the active medium should ensure a *gain* which is higher than the total loss in the resonator. By changing the level and nature of losses in a resonator, one can exercise *control* over laser processes. Depending on the specific nature of the resonator used in a laser, radiation is generated with definite spectrum and a definite structure in space and time. The main function of the optical resonator in a laser is *to create the radiation field with a definite structure.*

2.1. GENERATION CONDITION

Relation Between Initial Gain and Loss Coefficients. It is well known that as light propagates in the inverted active medium an increase in the optical flux density is accompanied by the equalization of population densities of laser levels. This leads to the effect called *gain saturation.* The gain $\varkappa(z)$ at the point z (the flux propagates along z-axis) is expressed in terms of the optical flux density $S(z)$ in the following form

$$\varkappa(z) = \frac{\varkappa_0}{1+(\alpha/v)\,S(z)}, \qquad (2.1.1)$$

where v is the velocity of light in the active medium; α is the parameter of nonlinearity of the laser transition; and $\varkappa_0$ is the initial gain[1]. The nonlinearity parameter characterises the rate of equalization of the population densities of laser levels upon increasing the optical flux density. The initial gain is defined by the inverse population density N_0 of the laser levels in the absence of generation, i.e. for $S = 0$:

$$\varkappa_0 = (B_{21}\hbar\omega/v)\,[n_{02} - (g_2/g_1)\,n_{01}] = \sigma N_0. \qquad (2.1.2)$$

Here, ω is the frequency of the generated radiation; B_{21} is the Einstein's coefficient; $\sigma = B_{21}\hbar\omega/v$ is the cross section of induced emission in the laser transition; and $N_0 = n_{02} - (g_2/g_1)\,n_{01}$ (we have already encountered this quantity in Sec. 1.2). It should be observed that a substitution of (2.1.2) in (2.1.1) leads to the result (1.1.3):

$$\varkappa(z) = \sigma\frac{N_0}{1+(\alpha/v)\,S(z)} = \sigma N(z).$$

[1] Sec. 5.6 in [1].

The optical power generated by the active centres in a unit volume is given by the expression[2]

$$W(z) = \varkappa(z)\, S(z). \tag{2.1.3}$$

Eliminating $S(z)$ from Eqs. (2.1.1) and (2.1.3), we get

$$W(z) = (v/\alpha)\,[\varkappa_0 - \varkappa(z)]. \tag{2.1.4}$$

We denote by W_{gen} the optical power generated in the total volume of the active medium of the laser:

$$W_{\text{gen}} = s \int_0^L W(z)\, dz \tag{2.1.5}$$

where s is the area of cross section of the active medium and L is the length of the resonator (for the sake of simplicity, we assume that the active medium completely fills the resonator and that physical quantities do not depend on transverse coordinates). Substituting Eq. (2.1.4) in Eq. (2.1.5), we get

$$W_{\text{gen}} = (vLs/\alpha)\,[\varkappa_0 - \langle\varkappa\rangle], \tag{2.1.6}$$

where $\langle\varkappa\rangle = \frac{1}{L}\int_0^L \varkappa(z)\, dz$ is the gain averaged over the length of the resonator.

For the case of stationary generation, the following relation is valid[3]:

$$\langle\varkappa\rangle = \eta_1 + \eta_2, \tag{2.1.7}$$

where η_1 and η_2 are linear coefficients of attenuation of optical flux corresponding to the unfavourable and favourable losses respectively[4]. *The favourable losses* are due to removal of a part of energy from the active medium in the form of laser radiation. The coefficient of favourable losses η_2 is given by the expression

$$\eta_2 = (1/L) \ln \sqrt{1/R_1 R_2}, \tag{2.1.8}$$

where R_1 and R_2 are the reflection coefficients of the resonator mirrors of the laser. The *unfavourable losses* may be caused by absorption of radiation by atoms (molecules) which are not active centres, by scattering of radiation through the lateral face of the active medium, by diffraction effects, or due to other reasons.

By using Eq. (2.1.7), we can rewrite (2.1.6) in the following form

$$W_{\text{gen}} = (vLs/\alpha)\,[\varkappa_0 - (\eta_1 + \eta_2)]. \tag{2.1.9}$$

[2] See, for example, Eq. (4.1.17) in [1].
[3] See, for example, Eq. (5.6.23) in [1].
[4] In order to explain the physical sense of these coefficients, one has to consider Bouguer's differential law: $dS = -(\eta_1 + \eta_2)\, S(z)\, dz$.

This result leads to a very important conclusion (which is valid not only for stationary generation, but for the general case as well): the following inequality must be satisfied in order to ensure generation:

$$\boxed{\varkappa_0 > (\eta_1 + \eta_2)}. \qquad (2.1.10)$$

In other words, the *initial gain must be higher than the loss level in the resonator*, which is defined as the sum of the coefficients of unfavourable and favourable losses. The larger the difference $[\varkappa_0 - (\eta_1 + \eta_2)]$, the higher the optical power generated. The *generation threshold* is defined by the equality

$$\varkappa_0 = \eta_1 + \eta_2. \qquad (2.1.11)$$

Initial Gain for Optically Allowed and Forbidden Transitions. It should be recalled that dipole transitions (transitions that are allowed in the dipole approximation) are called *optically allowed* transitions. The matrix element of the electric dipole moment of the system is nonzero for these transitions. If the matrix element is equal to zero, the corresponding transition is *optically forbidden.* Such a transition may be allowed in higher approximations like the magnetic dipole approximation, the quadrupole approximation, etc.

By considering the interaction of optical radiation with an electron of the atom, we can obtain expressions for Einstein's coefficient B_{21}, appearing in Eq. (2.1.2), for different types of transitions[5]. These expressions are given in Table 2.1. They lead to the following

TABLE 2.1

Dipole transition	$B_{D21} = \frac{4\pi^2}{3\hbar^2} \left\| (\mathbf{d})_{21} \right\|^2$	$\mathbf{d} = -e\mathbf{r}$
Magneto-dipole transition	$B_{M21} = \frac{4\pi^2}{3\hbar^2} \left\| (\mathbf{n}\times\boldsymbol{\mu})_{21} \right\|^2$	$\boldsymbol{\mu} = -\frac{e}{2mc}(\mathbf{r}\times\mathbf{p})$
Quadrupole transition	$B_{Q21} = \frac{4\pi^2}{3\hbar^2} \left\| (\mathbf{k}Q)_{21} \right\|^2$	$Q = -\frac{e}{2}\begin{pmatrix} x^2 & xy & xz \\ yx & y^2 & yz \\ zx & zy & z^2 \end{pmatrix}$

$\mathbf{d}$ — electric dipole moment of the electron;
$\boldsymbol{\mu}$ — magnetic dipole moment of the electron;
Q — electric quadrupole moment of the electron;
$\mathbf{k}$ — wave vector of the radiation, $\mathbf{n} = -\mathbf{k}/k$;
$(\ldots)_{21}$ — matrix element for the $2 \to 1$ transition.

estimates (for radiation wavelength of the order of 1 μm):

$$B_{Q21}/B_{D21} \approx 10^{-6}; \quad B_{M21}/B_{D21} \approx 10^{-4}.$$

[5] The expressions for Einstein's coefficient A_{21} describing spontaneous emission have been derived by Tarasov (Sec. 2.5 in [1]). Using the well known relation $B_{21} = A_{21}\pi^2c^3/\hbar\omega^3$, we can get the corresponding values of B_{21} from A_{21}.

Thus the factor B_{21} appearing in the initial gain is smaller (by a factor of 10^4-10^6) for optically forbidden transitions than for optically allowed transitions. It follows from this that the metastability of the upper laser level associated with the creation of inversion has its disadvantages.

However, while estimating the value of the initial gain, one has to consider not only the factor B_{21}, but also the product $B_{21}N_0$. The factors appearing in this product have opposite tendencies: an increase in the lifetime of the upper laser level leads to an increase in N_0, but to a decrease in B_{21}. On the other hand, a decrease in lifetime results in a higher value for B_{21}, but reduces N_0. Decrease in N_0 in the latter case is due to the fact that an increase in B_{21} also results in an increase in Einstein's coefficient A_{21}. In other words, spontaneous transitions become more frequent in the generation channel.

One may ask the question: which working transitions should one use, the ones that are optically allowed, or the ones that are forbidden? In other words, what is more important—an increase in N_0 (for optically forbidden transitions), or an increase in B_{21} (for optically allowed transitions)?

It turns out that it is advisable to use optically *forbidden* transitions. The decrease in the coefficient B_{21} due to the metastability of the upper level is often effectively compensated by an increase in the inverse population density N_0 of the levels. Significantly, however, the lifetime of the upper laser level should not be too large. An excessive decrease in the value of B_{21} may render the above mentioned compensation impossible.

Dependence of the Initial Gain on Pumping Rate. A three-level diagram identical to the one shown in Fig. 1.9 is depicted in Fig. 2.1. Unlike Fig. 1.9, additional transitions are stimulated by the laser radiation on the channel *2-1*. The probabilities of these transitions are given by $w_{21} = A_{21} + B_{21}\rho_{gen}$ and $w_{12} = B_{12}\rho_{gen}$ (where ρ_{gen} is the laser radiation density).

Substituting (1.2.12) in (2.1.2) (we assume for the sake of simplicity that $g_1 = g_2$), and using the inequality (1.2.15), we get the following expression for the initial gain:

$$\varkappa_0 = (B_{21}/v)\hbar\omega n' (\Omega - A_{21})/(\Omega + A_{21}). \qquad (2.1.12)$$

It should be recalled that here n' is the total number of active centres per unit volume and $\Omega = w_p w_{32}$: $(w_{31} + w_{32})$ is the *pumping rate* for this case. Using the relations between B_{21} and A_{21}, we can rewrite Eq. (2.1.12) in the following form:

$$\varkappa_0 = bA_{21} (\Omega - A_{21})/(\Omega + A_{21}), \qquad (2.1.13)$$

where b represents the factor $\pi^2 c^3 n'/v\omega^2$. Figure 2.2 shows the dependence $\varkappa_0$ vs. Ω as described by Eq. (2.1.13). The straight line AA corresponds to the loss level. Intersection of the curve $\varkappa_0$ (Ω) with

the x-axis determines the *inversion threshold* Ω_{inv}, while the intersection with the straight line AA determines the *generation threshold* Ω_{gen}. It can be easily seen that

$$\Omega_{inv} = A_{21}; \quad \Omega_{gen} = A_{21}\frac{bA_{21}+(\eta_1+\eta_2)}{bA_{21}-(\eta_1+\eta_2)}; \quad \Omega_{gen} > \Omega_{inv}.$$

If $\Omega \gg A_{21}$, the magnitude of the initial gain approaches its *limiting* value

$$\varkappa_{0\,lim} = bA_{21}. \tag{2.1.14}$$

Let us compare a few curves $\varkappa_0$ vs. Ω for different values of A_{21} (considering that the inequality (1.2.15), which assumes the metastability of level 2, is satisfied). Figure 2.3 shows four curves, numbereed in order of decreasing value of A_{21}. It can be seen from this figure that the lower the value of A_{21} (the higher the lifetime of level 2), the easier the creation of inversion. However, this results in a decrease in the limiting value of the initial gain. This reflects the negative aspect of the metastability of the upper laser level as mentioned above.

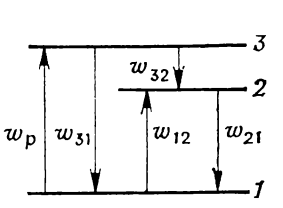


Fig. 2.1

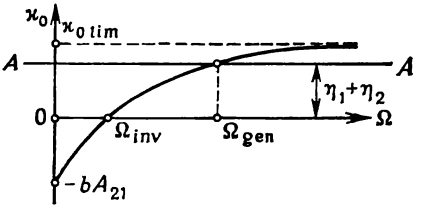


Fig. 2.2

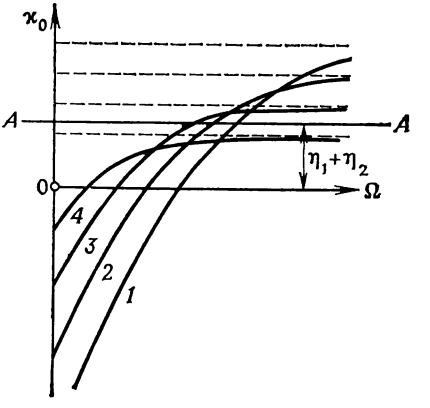


Fig. 2.3

The straight line AA in Fig. 2.3 defines the loss level. It can be seen that for a value of A_{21} corresponding to the curve 4, generation is not possible at all (an excessive decrease in the value of A_{21} has brought the limiting value of gain below the loss level). Thus, the lower limit of values of A_{21} is determined by the amount of loss. In accordance with (2.1.14) and (2.1.10), the following condition must be satisfied:

$$A_{21} > (\eta_1 + \eta_2)/b. \tag{2.1.15}$$

Frequency Dependence of the Initial Gain. In order to consider the frequency dependence of the initial gain, we start with Eq. (2.1.2), replacing B_{21} by Einstein's spectral coefficient $B_{21}(\omega)$. It should be recalled that $B_{21}(\omega) = B_{21}F(\omega)$ where $F(\omega)$ is a function defining the *shape of emission spectrum line.*[6] Thus,

$$\varkappa_0(\omega) = B_{21}F(\omega)\hbar\omega N_0/v. \qquad (2.1.16)$$

The factor B_{21} appearing in (2.1.16) is independent of frequency for dipole and magnetic dipole transitions, while $B_{21} \propto \omega^2$ for quadrupole transitions (see Table 2.1). Consequently, $\varkappa_0(\omega) \propto \propto \omega F(\omega)$ for dipole and magnetic dipole transitions, while $\varkappa_0(\omega) \propto \propto \omega^3 F(\omega)$ for quadrupole transitions. The qualitative form of the dependence $\varkappa_0(\omega)$ is determined by the function $F(\omega)$, i.e. by the shape of the emission spectrum line for the active centre. If, for example, the spectral line is *Lorentzian* in shape (*uniformly* broadened line) and if the dipole transitions are considered, we get

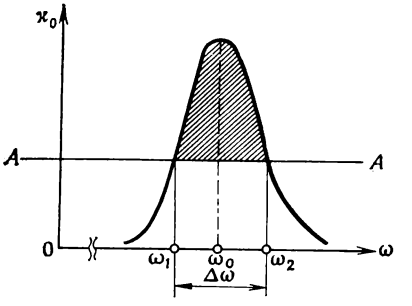


Fig. 2.4

$$\varkappa_0(\omega) \sim [\omega\Delta/[(\omega-\omega_0)^2+\Delta^2], \qquad (2.1.17)$$

where ω_0 is the frequency corresponding to the peak, and Δ is the halfwidth of the line at the middle of its maximum height. Figure 2.4 shows the dependence $\varkappa_0(\omega)$ as described by formula (2.1.17). The straight line AA corresponds to the loss level. Only the shaded part of the function $\varkappa_0(\omega)$, called the *gain line*, is operative during generation. The frequency of radiation generated on a given transition lies within the limits of the gain line width: $\omega_1 < \omega < \omega_2$. We have mentioned in the preceding chapter the selective resonators with a redistribution of the radiation frequency within the limits of the luminescence line width. As a modification, it may be observed that the range of redistribution is determined not by the luminescence line width, but by the gain line width (the width of the luminescence line at the loss level).

2.2. OPTICAL RESONATOR AND LASER RADIATION (PRELIMINARY REMARKS)

Optimisation of Favourable Losses. It follows from (2.1.9) that in order to increase W_{gen}, it is sufficient to *reduce the losses* in a resonator (reduce the sum $\eta_1 + \eta_2$). In particular, the favourable

[6] Einstein's spectral coefficients and the shape of a spectral line have been described by Tarasov (Sec. 4.7 in [1]).

loss level can be decreased. For this purpose, it is necessary to increase R_1R_2 in accordance with (2.1.8). However, an excessive increase in the reflection coefficient of resonator mirrors is not desirable, since a reduced η_2 means a decrease in the fraction of generated radiation converted into laser radiation. This fraction is defined as the ratio $\eta_2/(\eta_1 + \eta_2)$. Taking Eq. (2.1.9) into account, the *laser radiation power* is given by the expression

$$W = \frac{\eta_2}{\eta_1+\eta_2} W_{gen} = \frac{vLs}{\alpha} [\varkappa_0 - (\eta_1 + \eta_2)] \frac{\eta_2}{\eta_1+\eta_2}. \qquad (2.2.1)$$

A decrease in η_2 means a decrease in $\eta_2/(\eta_1 + \eta_2)$ but an increase in the factor $[\varkappa_0 - (\eta_1 + \eta_2)]$. Consequently, there should be an *optimal* value η_{2opt} for the coefficient of favourable losses, which gives the *maximum* output power.

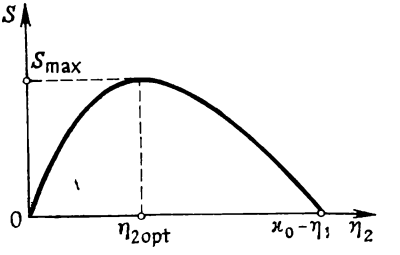


Fig. 2.5

Usually, one considers not the output power W, but rather the density S of the light flux emerging from the resonator. The quantities W and S are connected by the relation

$$S = W/s \qquad (2.2.2)$$

where s is the area of cross-section of the light beam (for the sake of simplicity, we assume it to be equal to the area of cross section of the active medium).

In view of the above, we can rewrite Eq. (2.2.1) in the form

$$S = (vL/\alpha) [\varkappa_0 - (\eta_1 + \eta_2)] \eta_2/(\eta_1 + \eta_2). \qquad (2.2.3)$$

Figure 2.5 shows the S vs. η_2 dependence defined by the expression (2.2.3). The threshold value of the coefficient of favourable losses is equal to $\varkappa_0 - \eta_1$. In order to find the value of η_{2opt}, let us differentiate the function S (η_2) and equate the derivative to zero. This gives

$$\boxed{\eta_{2opt} = \sqrt{\varkappa_0\eta_1} - \eta_1}. \qquad (2.2.4)$$

Hence

$$S_{max} = \frac{v}{\alpha} (\sqrt{\varkappa_0 L} - \sqrt{\eta_1 L})^2. \qquad (2.2.5)$$

Thus, for given values of $\varkappa_0$ and η_1, there is an optimal value for the coefficient of favourable losses, which is given by the relation (2.2.4). The maximum density of the emerging optical flux corresponding to it is given by the formula (2.2.5). A further increase in S_{max} requires an increase in $\varkappa_0$ and a decrease in η_1.

Suppose that the laser radiation emerges from one of the resonator mirrors, while the other mirror is totally reflecting. From

Eqs. (2.2.4) and (2.1.8), we get the *optimal reflection coefficient* for the output resonator mirror

$$R_{\text{opt}} = \exp\left[-2L\left(\sqrt{\varkappa_0\eta_1} - \eta_1\right)\right]. \tag{2.2.6}$$

For a sufficiently high gain, as is characteristic, for example, for neodymium lasers with pulsed pumping, the value of R_{opt} may be relatively low (10-20%). In the case of helium-neon lasers, where the gain is small, R_{opt} attains a value of 99%. Such a high reflectivity is obtained by using multilayer dielectric mirrors, which are obtained by applying (by spray coating) several thin dielectric layers on the substrate, each layer having an optical thickness equal to one fourth of the radiation wavelength, but differing in refractive index from the others.[7]

If both the resonator mirrors are output mirrors, the following relation holds instead of (2.2.6)

$$(R_1R_2)_{\text{opt}} = \exp\left[-2L\left(\sqrt{\varkappa_0\eta_1} - \eta_1\right)\right]. \tag{2.2.7}$$

Suppose that S_1 is the density of flux leaving the mirror with reflection coefficient R_1, and S_2 is the corresponding value for the mirror with reflection coefficient R_2; $S_1 + S_2 = S$. It can be shown[8] that

$$\frac{S_2}{S_1} = \frac{1-R_2}{1-R_1}\sqrt{\frac{R_1}{R_2}}. \tag{2.2.8}$$

Resonance Frequencies. Within the width of the gain line, the optical resonator isolates a set of *resonance* wavelength λ_q (or resonance frequencies ω_q). Assuming that the field inside a resonator is described approximately by a set of plasma waves propagating along the resonator axis, the resonance condition can be written in the form

$$L = q\lambda_q/2. \tag{2.2.9}$$

Here, q are positive numbers ($q \gg 1$) and L is the length of the resonator. The condition (2.2.9) means that an integral number of half-waves should cover the length of the resonator. This condition also means that the *phase shift* (or, in other words, the *phase advance*) of a wave accomplishing a round trip through the resonator (or, from one mirror to the other and back) is a multiple of 2π. As a matter of fact the phase advance for a plane wave which has traversed a distance z, is equal to $2\pi z/\lambda$. For a distance $2L$, this advance is $4\pi L/\lambda$. Assuming that this phase advance is a multiple of 2π, i.e. $4\pi L/\lambda = 2\pi q$, we arrive at the condition (2.2.9).

Considering that the radiation wavelength and frequency are connected through the relation

$$\lambda = 2\pi v/\omega = 2\pi c/n\omega, \tag{2.2.10}$$

[7] Multilayer dielectric coatings are described in Ch. 24, Vol. II of [2].
[8] See, for example, [3].

where n is the refractive index of the medium occupying the resonator, Eq. (2.2.9) can be rewritten in the form

$$L = q\pi c/n\omega_q. \tag{2.2.9a}$$

Thus the resonance frequencies of an optical resonator are given by the expression

$$\boxed{\omega_q = q\pi c/Ln}. \tag{2.2.11}$$

It should be observed that the expression (2.2.11) is *approximate*. It assumes that firstly, the field in a resonator is described by plane waves and secondly, the dispersion of the refractive index is insignificant. Both these simplifications will be withdrawn in the following.

According to Eq. (2.2.11), the resonance frequency spectrum is *equidistant*, i.e. the difference between adjacent frequencies is constant and is equal to

$$\Delta\omega' = \pi c/Ln. \tag{2.2.12}$$

Dividing the gain line width $\Delta\omega$ by $\Delta\omega'$, we find the total number of resonance frequencies in the spectrum of a laser

$$M = \Delta\omega/\Delta\omega' = \Delta\omega Ln/\pi c. \tag{2.2.13}$$

The number M increases with increasing optical length Ln of the resonator and with increasing gain line width $\Delta\omega$. The latter is greater, the wider the luminescence line of the active centres and the lower the loss level in the resonator.

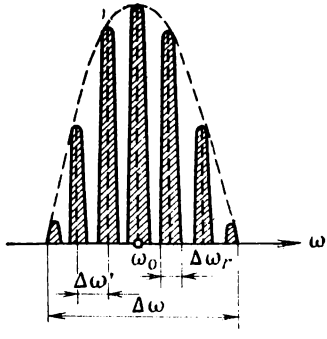


Fig. 2.6

Isolating the set of resonance frequencies, the resonator transforms the gain line shown in Fig. 2.4 into a set of narrow lines called the *spectral lines of the resonator* (Fig. 2.6). The maxima of these lines correspond to resonance frequencies while the width of a line depends on the losses in the resonator. Denoting the width of a spectral line of the resonator as $\Delta\omega_r$, we define the ratio

$$Q = \omega_0/\Delta\omega_r \tag{2.2.14}$$

as the *Q-factor of the resonator*[9]. The smaller the losses in a resonator, the higher its Q (the lower the value of $\Delta\omega_r$).

For resolution of narrow lines in the generation spectrum, it is essential that the condition $\Delta\omega_r < \Delta\omega'$ should be satisfied. With the help of relations (2.2.12) and (2.2.14), this condition may be transformed into the inequality

$$Q > \omega_0 Ln/\pi c. \tag{2.2.15}$$

[9] The Q-factor of an optical resonator will be discussed in detail in Sec. 2.3.

Putting $\omega_0/\pi \approx 10^{15}$ sec^{-1}, $Ln \approx 10$ cm, we get $Q > 10^6$ from (2.2.15). The values obtained in practice for the Q-factor of laser resonators usually satisfy the condition (2.2.15).

Under actual conditions, additional factors crop up, influencing the resolution of narrow spectral lines. One of such factors is the non-uniformity of the refractive index of solid-state active media. By using (2.2.11), it can be easily shown that the fluctuation δn in the refractive index causes a fluctuation $\delta\omega \approx \omega\delta n/n$ in the resonance frequency. For resolution of narrow lines in the frequency spectrum, it is necessary that $\delta\omega < \delta\omega'$. Consequently, besides condition (2.2.15), the condition $\delta n/n < \pi c/\omega Ln$ must be satisfied. It follows from this that $\delta n/n < 10^{-6}$. This inequality is not always satisfied in solid-state lasers.

Vibrational Modes of an Optical Resonator. As has been shown above, the resonator of a laser has a considerable influence on the power of laser radiation as well as on its spectral properties. In actual practice, the influence of the resonator on the properties of laser radiation is even more significant and fundamental. As a matter of fact, the resonator forms definite states in the radiation field. These are called *vibrational modes* of the resonator.

An individual mode is designated as TEM_{mnq}. TEM stands for transverse electromagnetic modes (the electrogmagnetic vibrations in an optical resonator may be considered as transverse). m and n are the *transverse* indices of the mode and q is the *longitudinal* one. Each mode is characterised by a definite *spatial* field configuration (a definite amplitude and phase distribution) in a direction perpendicular to the resonator axis, in particular at the mirror surfaces of the resonator. The specific nature of this configuration is determined by the transverse mode indices m and n. Besides, each mode is characterised by a definite phase shift at the resonator axis upon a round-trip in the resonator. This phase shift is equal to $2\pi q$, where q is the longitudinal mode index.

It should be observed that the phase shift is considered *at the resonator axis* due to the fact that, strictly speaking, a mode is not a plane wave. Clearly, such a restraint would be unnecessary for a plane wave since the distance from the resonator axis of any point in a plane wave front is the same. For each definite combination of indices m and n reflecting a definite transverse field configuration in a resonator, there is a number of corresponding modes with different values of q. These are called *longitudinal* modes (also called *axial* modes). For each one of them, there is a corresponding narrow line in the generation spectrum. The set of longitudinal modes with a given combination of indices m and n is termed a *transverse* mode. Obviously, the transverse mode is characterised by only transverse indices (and is denoted by TEM_{mn}).

Each type of transverse mode has a definite structure of the luminous spot on the resonator mirror. Figure 2.7*a* shows the structure of intensity pattern obtained in a circular mirror for the simplest

(lowest) transverse modes. The corresponding nature of change in the sign of amplitude of the field on the mirror surface is shown in Fig. 2.7*b*. It is evident from the figure that the index m indicates the number of times the field amplitude changes sign in the radial direction, while n indicates the number of times it changes sign upon a rotation by 180° around the centre of the mirror.

The transverse mode TEM_{00} is called the *lowest-order* mode. It is characterised by the simplest structure of the spot. It is apparent from Fig. 2.7*a* that the smaller the value of transverse indices, the more concentrated is the mode field near the centre of the mirror.

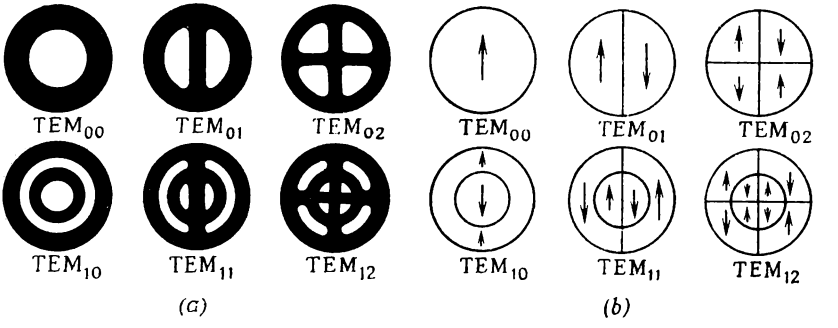


Fig. 2.7

An intensity pattern, as observed under actual conditions, is often a superposition of several transverse modes (*multimode* generation). The spectrum of the generated radiation usually contains several narrow lines (*multifrequency* generation)[10].

The Role of an Optical Resonator in a Laser. According to Gerrard *et al.* [4], the main function of an optical resonator is to impart a definite shape and definite mode structure to optical waves radiated by a laser. The mode pattern of a laser radiation field is formed in the resonator during the process of successive reflections of the radiation at the resonator mirrors. In some resonators the field configuration is formed after a *large* number of passages from one mirror to the other (*multipass* resonators), while in some other resonators this process takes place after just *a few* passes.[11]

In order to understand the role of a resonator in a laser, it is convenient to use the *quantum* concept, since it takes into account the nature of the laser generation process in the optical spectral region in the best possible way. In particular, the fact that optical radiation

[10] The mode patterns for solid-state lasers may be distorted on account of nonuniformity of the refractive index of the solid active medium.

[11] For a sufficiently large gain, the inversion of the active medium can be removed in a single pass. Such lasers may work without mirrors in the *superluminescence* regime.

is generated as a result of a large number of acts of emission by atoms or molecules performing quantum transitions from one state into another is very well reflected by using the quantum concept. In a certain sense, an individual emitting atom (molecule) may be compared with a certain "resonator", or a certain oscillatory system. In the words of Academician L. I. Mandelshtam [5], "We imagine that there is an optical resonator of a certain frequency in each gas molecule. The luminescence of the gas is due to the fact that the resonators oscillate at the same frequency and the gas emits light of this frequency".

Obviously, in order to get coherent beams of light, it is essential that the acts of emission by a large number of resonators are mutually correlated, not only in the radiation frequency, but also in the direction of its propagation and in polarisation. In other words, it is essential that the principle of self-regulation or, in the language of electronics, the principle of *positive feedback* be followed. The possibility of such a correlation (the possibility of attaining a positive feedback) is inherent in the *very nature* of induced emission: the secondary photon is *in the same state* as the primary photon which induces the creation of the secondary photon. In order to realise this in actual practice, a *selective* population of photon states[12] must be ensured in the course of induced transitions. In other words, certain states must be *isolated* in actual practice. In these states, photons are accumulated while in all the remaining states spontaneously created photons must be eliminated as quickly as possible.

The selectivity of population of photon states is also ensured by the optical resonator in a laser. "The possibility of a positive feedback, inherent in the induced emission process, is realised in a laser with the help of an optical resonator" [6]. Primarily, a resonator isolates a certain direction in space in which generation predominantly takes place. Besides, the resonator also performs a frequency and polarisation selection of the radiation. The parallel plates used frequently in resonators are oriented to the resonator axis at Brewster's angle, and thus ensure the selectivity of the generated photons, according to their polarisation. It may be said that the main function of an optical resonator is to isolate certain photon states in which predominant laser generation takes place. The coherence properties of laser radiation (directionality, monochromatism, degree of polarisation) depend on how well the resonator ensures the selectivity of population of photon states.

Considering the question as to how a resonator ensures selectivity of the population of photon states, it should be emphasized that this is attained on account of *selective losses* for different states. These losses should be small for some states while for the other states these

[12] Photon states are characterised by a definite energy, momentum, and polarisation of the photon.

must be large, on the contrary. In accordance with the condition (2.1.10), generation is possible only in such states for which losses are comparatively low.

Inspite of a certain degree of sketchiness, the quantum concept gives a proper representation, from a *physical* point of view, of the main function of an optical resonator. It may be stated that by ensuring the selectivity of population of photon states, a resonator forms in the long run the monochromatic optical beam. This determines the energy, spectral, spatial, and other properties of radiation generated by the laser.

Before concluding this description of an optical resonator, let us consider a rather delicate question. The most "prominent" function of a resonator is *to return* a part of the radiation of the active medium with the help of mirrors. Naturally, this means a more effective removal of inversion. But how important is this? Can a resonator ensure the selective population of photon states, and thus eventually form the radiation field, without returning a part of radiation to the active medium?

A straightforward answer to this question is apparently difficult to give. Of course, there do exist lasers without mirrors. The selectivity of the photon momentum according to directions is attained in such lasers through a special configuration of the active element. It is also well known that there is a practically complete analogy between the structure of transverse modes of a resonator with mirrors (where the radiation is returned) and a lens waveguide (where the radiation propagates in one direction) [7]. At the same time, it is well known that the degree of selectivity of population of photon states (and hence the coherence of the radiation) realised in a mirrorless laser is, as a rule, considerably lower than for lasers employing mirrors. As regards the analogy between a resonator with mirrors and a lens waveguide, it exists only for the spatial properties, and not for spectral properties of radiation, since a lens waveguide does not have resonant frequencies.

It should be emphasized that the *amplification* of the active medium must be taken into account while considering the question raised above. It should be recalled that the optimal value of the reflection coefficient for an output resonator mirror depends on the initial value of the gain. The higher the value of $\varkappa_0$, the lower the R_{opt} and hence the less significant the reflecting properties of the mirror. On the other hand, for small values of $\varkappa_0$, when R_{opt} is close to 100%, the role of the mirror becomes significant.

It may be stated that the presence of reflecting mirrors is not necessary for *sufficiently high* values of gain for the active medium. That is why lasers working on self-terminating transitions, in particular, the copper vapour laser (see Ch. VIII in [8]), as well as hydrogen and nitrogen lasers generating in the ultraviolet spectral region (see Ch. IX in [8]) can work in the superluminescence regime (without

mirrors). These lasers are characterised by fairly high values of gain.

This circumstance plays a significant role in solving the problem of creating lasers in the X-ray and γ-ray regions where the reflecting mirrors are simply not available. In this connection, Dr. Yu. A. Ilyinskii says, "In earlier works on gamma-ray lasers, considerable attention was paid to the cavity which amplifies the intensity of laser radiation as a result of multiple passes through the active medium upon reflection at the mirror. Creation of mirrors for hard γ-rays is an independent problem which has not been solved as yet. It became clear in the seventies that this is not the main problem, because by that time ultraviolet lasers had been created without any mirrors. Such lasers give a directional and monochromatic radiation under the condition that the gain in the active medium is sufficiently high. In this case, the active body of the laser is chosen in the form of a rod whose length ensures the required amplification of radiation during its single passage in the laser "(from the article "Problems of Gamma-ray Laser", published in *Priroda* in 1978).

As regards lasers with a relatively *low* gain, their field structure is formed by the noise from a *large number* of passes of radiation through the cavity. In this case, the reflecting mirrors are apparently of great importance.

Passive and Active Resonators. If there is no amplifying active medium inside a cavity, it is called a *passive* resonator. In the case of an amplification, the cavity is called an *active* resonator.

A laser cavity is an active resonator. However, in order to study the process of radiation field formation in laser cavities passive resonators are considered to begin with. Most of theoretical investigations deal only with passive resonators. This is due not only to the fact that an investigation of active resonators involves serious amplifications. As a matter of fact, a passive resonator provides a fully realistic picture, *to first approximation*, of the process of the optical field formation in a laser cavity.

On the basis of studies carried out for passive resonators, it is possible to investigate the damping of different modes, identify the slowly damping modes characterised by the lowest losses (high Q modes), determine the field configuration for these modes, as well as estimate the influence of aperture effects and lens systems. In the presence of an amplifying active medium, it is the high Q modes that are amplified primarily, since the results obtained for passive resonators are applicable for lasers *in the vicinity of the generation threshold*. For low gain values, an active resonator is characterised by practically the same amplitude and phase distributions of the field at the mirror surfaces, as well as the losses due to diffraction effects, as in a passive resonator.

It should be observed that highly effective *computational methods* have been worked out for passive resonators. These methods may

also be used for solving a large number of problems concerning active resonators.

At the same time, it should be remembered that an amplifying active medium imparts certain properties to the process of field formation in a resonator (see, for example, [9]). To begin with, we can mention the *mode competition*, leading to a reallocation of the generated power from some modes to others. This reallocation may take place on the frequency scale (between longitudinal modes) as well as in space (between transverse modes). The active medium causes mode competition on account of the nonlinear optical effect of *gain saturation*. Gain saturation for certain frequencies may lead to the appearance of "holes" in the profile of gain curve (*hole burning effect*). Another consequence of gain saturation is that higher transverse modes (modes with comparatively large values of transverse indices) rather than lower ones may have a higher Q. Let us consider this in greater detail.

In a passive resonator, it is the lower transverse modes, and above all the lowest-order mode TEM_{00}, which have the lowest loss characteristics as a rule. These modes are the ones to be excited in the first place in the case of an amplification. The field intensity in these modes will rise and may attain saturation. This means that the gain will be minimum in the part of the active medium that is effectively covered by lower modes (i.e. in the vicinity of the resonator axis[13]). Consequently, the inverse density near the resonator axis may turn out to be lower than in the periphery. In this case the higher order transverse modes which occupy large volumes in the active medium (covering, among others, the peripheral region as well) get excited first. A reallocation of power from the lower modes to the higher ones may lead to a significant change in the field configuration in a resonator.

Besides the gain saturation effect, there are other factors which influence the formation of radiation field in an active resonator. For example, a dispersion of the refractive index of the active medium may lead to the so-called effect of *frequency pulling* [10], because of which the resonance frequency spectrum is no longer equidistant: resonance frequencies are more closely spaced near the centre of the amplification line. Heating of the active medium through absorption of the pumping radiation leads to a change in its refractive index. As a result the so-called *thermal lens* effect takes place: the active element works as a converging or a diverging lens for the radiation inside a resonator (see, for example, [11]).

In a resonator filled with solid (crystal, glass) active medium, *supplementary* modes may be excited. Their emergence is due to the effect of total internal reflection at the lateral face of the active

[13] In accordance with Eq. (2.1.1), we get $\varkappa_{min} = \varkappa_0/[1 + (\alpha/v)\, S_{sat}]$, where S_{sat} is the saturation flux density.

element. Denoting by θ the angle between the direction of propagation of a mode and the optical axis of a resonator, we can bifurcate these modes into two groups. The modes with $\theta = \pi/2$ circulate in the cross section of the active element (*circular* modes), see Fig. 2.8*a*. Modes with $\theta \neq \pi/2$ shift in the direction of optical axis as shown in Fig. 2.8*b*. The modes of the first group are parasitic modes. Modes of the second group may be used for creating *waveguide* resonators [12]. Supplementary modes in the filled resonators have been considered by Stepanov *et al.* [3] and Mikaelyan *et al.* [13].

In actual practice, an active resonator usually contains a certain set of elements (including the active element) which are separated from one another. Consequently, while considering such a resonator one has to take into account a whole set of reflecting surfaces which

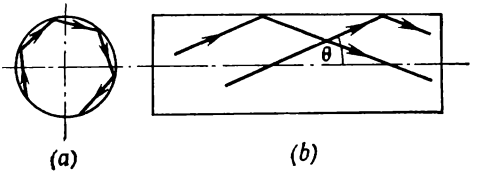


Fig. 2.8

include, besides the resonator mirrors, the end faces of the elements in the resonator (including the end faces of the active element). In this case, the resonator is equivalent to several *coupled* resonators. The interference effects arising in a system of coupled resonators may significantly influence the resonance frequency spectrum.

In this chapter, main attention will be devoted to *passive* resonators. The questions dealing with the effects of the *active medium* on the generation spectrum (hole burning effect and frequency pulling effect) and on the configuration of radiation field (thermal lens effect) will be considered separately. Waveguide resonators and thin-film lasers will also be described later. It should be emphasized that field formation in active resonators is closely related to the *dynamics of the processes* in generating lasers. This is an important and fundamental problem, and the third chapter of this book will be devoted to its analysis.

2.3. GENERAL REMARKS ABOUT OPEN RESONATORS

Resonators used in lasers belong to the class of open resonators[14]. They are considerably different from the cavity resonators used in the SHF band.

[14] The waveguide resonators and thin-film lasers with a distributed feedback are important examples of this class of resonators (see Secs. 2.14 and 2.15).

The theory of open resonators has been described by a number of authors [4, 9, 13-15]. See also [3, 7, 16, 17] and Chs. 22 and 23 in [2].

Impossibility of Using Cavity Resonators in Optical Band. Let us consider a rectangular cavity resonator with conducting walls, shown schematically in Fig. 2.9*a*. Here L and D are linear dimensions of the resonator. We shall represent the resonator modes simply in the form of plane waves satisfying certain boundary conditions

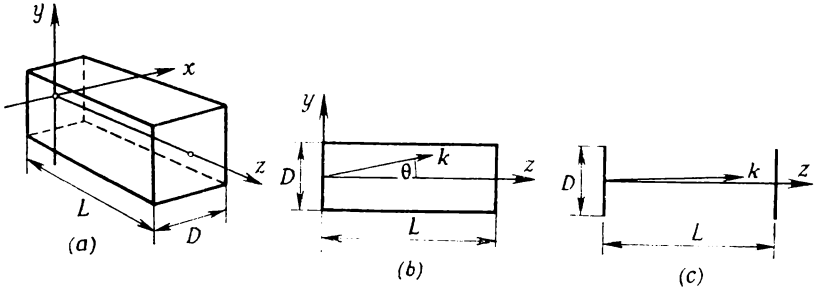


Fig. 2.9

at the cavity walls. Using the boundary conditions for a standing wave, we find that the component modes of the wavevector are of the form

$$k_x = \pi m/D; \quad k_y = \pi n/D; \quad k_z = \pi q/L, \tag{2.3.1}$$

where m, n, and q are integers (mode indices). The relations (2.3.1) lead to the following expression for the resonance wavelength λ_{mnq}:

$$\frac{1}{\lambda_{mnq}} = \sqrt{\left(\frac{m}{2D}\right)^2 + \left(\frac{n}{2D}\right)^2 + \left(\frac{q}{2L}\right)^2}. \tag{2.3.2}$$

The mode with indices 0, n, q propagates in the yz-plane (for this mode, $k_x = 0$) as an angle θ to the resonator axis, which is determined by the numbers n and q (Fig. 2.9*b*). According to (2.3.1), $k \sin\theta = \pi n/D$ and $k \cos\theta = \pi q/L$. Consequently,

$$\sin\theta = n\lambda/2D; \quad \cos\theta = q\lambda/2L. \tag{2.3.3}$$

Further, it should be recalled that for the volume V of the resonator, the number of plane waves, taken over the frequency interval between ω and $\omega + \Delta\omega$, is proportional to ω^2:

$$M \propto V\omega^2\Delta\omega. \tag{2.3.4}$$

It should also be recalled that the Q-factor of a resonator, determined by the Joule losses in the conducting walls, is proportional to $\sqrt{\omega}$:

$$Q \propto \sqrt{\omega}. \tag{2.3.5}$$

The above information is quite sufficient to show that it is practically impossible to use cavity resonators for high frequency radiation. An increase in frequency causes a condensation of the resonance frequency spectrum: the separation between the centres of spectral lines of a resonator, i.e. the ratio $\Delta\omega/M$, decreases with frequency (in accordance with (2.3.4) $\Delta\omega/M \propto 1/\omega^2$). At the same time, an increase in frequency leads to a broadening of the spectral line: the ratio ω/Q, defining the width of a spectral line, increases with frequency (in accordance with (2.3.5), $\omega/Q \propto \sqrt{\omega}$). Obviously, for sufficiently *high* frequencies, the spectral lines of a cavity resonator will completely *overlap* and thus the resonator will lose its resonance properties.

In order to ensure the excitation of a relatively small number of laser modes, one should use cavity resonators whose dimensions, in accordance with (2.3.2), are of the order of radiation wavelength. It should be observed that if the volume of a resonator is given by $V \approx \lambda^3 \approx 1/\omega^3$, the number of plane waves excited in it will decrease, and not increase, with increasing frequency: $M \propto V\omega^2\,\Delta\omega \propto \Delta\omega/\omega$. However, in this case we shall have to use cavity resonators having a volume of the order of 1 μm^3 only if we go over to the optical region. Leaving the technical problems associated with the construction of a resonator of such dimensions aside, it may be remarked that such a reduction in the volume of the resonator, and consequently in the volume of the active medium, is not permissible from the point of view of the magnitude of output radiation power. A solution to this problem was found in 1958 when the idea of using *open* resonators instead of cavity resonators in the optical region was put forward[15].

Open Resonator. Constructionally, an open resonator differs from a cavity resonator in two main aspects. Firstly, the conducting side-walls are removed while the end-face reflectors, which fix the resonator axis in space, are retained. Secondly, the dimensions of the resonator are larger than the radiation wavelength.

Since the side walls have been removed, the only modes that can be excited in the resonator either propagate along the resonator axis, or deviate very slightly from it (Fig. 2.9*c*). In other words, $\sin\theta \ll 1$ for open resonator modes. Taking into consideration (2.3.3), it can be concluded that

$$n\lambda/D \ll 1; \quad q\lambda/L \approx 1. \tag{2.3.6}$$

Since $\lambda \ll D$ and $\lambda \ll L$, only such modes will be excited in an open resonator for which

$$m,\ n \gtrsim 1; \quad q \gg 1, \tag{2.3.7}$$

[15] This fruitful idea was first suggested by A. M. Prokhorov [18] and, independently, by R. Dicke [19], and A. Shawlow and Ch. Townes [20].

in accordance with (2.3.6). This result means that upon a changeover from a cavity resonator to an open resonator, a *decrease* of the number of excited modes is observed: only the modes with m, $n \geqslant 1$ and $q \gg 1$, propagating along the resonator axis, are left. The three-dimensional picture is now practically replaced by *one-dimensional*. In this connection, it is worthwhile to recall that while $M \propto \omega^2 \Delta\omega$ in the three-dimensional case, $M \propto \omega \Delta\omega$ in the two-dimensional case and $M \propto \Delta\omega$ in the one-dimensional case. Thus in an open resonator, which in essence corresponds to the one-dimensional case, the number of resonance frequencies is *independent* of frequency. In this connection, it should be recalled that in accordance with (2.2.13), $M = \Delta\omega L n/\pi c$.

Thus, unlike a cavity resonator, the resonance frequency spectrum in an open resonator does not undergo a condensation with increasing frequency, but is considerably *rarefied* instead, on account of the fact that a relatively small number of modes is retained.

One more difference between an open resonator and a cavity resonator is worth mentioning. As a matter of fact, retention of only the reflecting end faces and the smallness of the wavelength (which causes a decrease in the diffraction effects) together lead to a considerable *distinction* in losses for different modes. This circumstance permits, on the one hand, a *further* reduction (selection) of modes right down to a single-mode, and on the other, ensures a fairly high Q-factor for certain modes, or even for a single mode.

Q-factor of a Resonator. Let U (0) denote the energy of radiation field in a passive resonator at the moment $t = 0$. Since the resonator is a passive one, this energy will decrease (attenuate) with time on account of different types of losses. We shall assume that the process of attenuation of energy is continuous and a reduction $-dU$ in the energy in the time interval between t and $t + dt$ is proportional to the energy U (t) and the duration dt of this interval. Thus

$$-dU = (1/\tau)\, U\, dt. \tag{2.3.8}$$

It follows from this that the field energy in a passive resonator must attenuate exponentially with time:

$$U\ (t) = U\ (0) \exp\ (-t/\tau). \tag{2.3.9}$$

The parameter $1/\tau$ characterises the rate of attenuation of field energy in a resonator. It may be treated as the width $\Delta\omega_r$ of the spectral line of the resonator ($1/\tau = \Delta\omega_r$).

The Q-factor of a resonator is inversely proportional to the rate of decrease of field energy in the resonator:

$$Q = \omega\tau = \omega/\Delta\omega_r \tag{2.3.10}$$

(cf. (2.2.14)). Using (2.3.10), we can rewrite (2.3.8) in the form

$$-dU/dt = U\omega/Q \tag{2.3.11}$$

or

$$Q = \omega U \Big/ \left(-\frac{dU}{dt}\right). \tag{2.3.12}$$

Thus, the Q-factor of a passive resonator may be defined as the product of the radiation frequency and the ratio of energy stored in the resonator to the energy lost by the resonator per unit time. The ratio (2.3.12) reflects quite well the relation between the Q-factor of a resonator and the losses inherent in it.

Losses characteristic for an open resonator can be divided into three groups: (i) losses due to transmission through the output mirror of the resonator, (ii) diffractional losses due to finite apertures of the mirrors and all elements inside the resonator, and (iii) losses due to partial absorption of radiation inside the resonator by its mirrors, as well as due to scattering of radiation through the lateral surface of the active element. In Secs. 2.1 and 2.2, losses were divided into two categories, the favourable and the unfavourable ones. Apparently, the losses pertaining to the *first* of the above-mentioned three groups belong to the favourable losses (relation (2.1.8) for the coefficient of favourable losses describes losses connected with the transmission through resonator mirrors). Losses corresponding to the *third* group are apparently unfavourable. As regards the *diffractional losses*, they may be favourable in some cases, and unfavourable in some others.

We observe that in the so-called unstable resonators (which will be considered later), the diffractional losses cause an extraction of laser radiation from the resonator and hence must be treated as favourable losses. In the case of stable resonators, the diffractional losses are, as a rule, unfavourable. However, even in this case, there may be situations when diffractional losses may be considered, at least partially, as favourable losses (for example, in resonators where a reflecting mirror with a hole in the centre is used as the output mirror).

Let us denote the linear coefficient of losses as η without specifying the nature of these losses. We shall find a relation between the loss coefficient η and the Q-factor of a resonator. For this purpose, let us consider the dependence of the field energy U on the longitudinal coordinate z instead of time (this is identical to the process of attenuation of light flux propagating in the absorbing medium):

$$U(z) = U(0) \exp(-\eta z). \tag{2.3.13}$$

Here, $1/\eta$ is the length over which the quantity U decreases to $1/e$ of its value. The attenuation time corresponding to this is given by

$$\tau = 1/\eta v = n/\eta c, \tag{2.3.14}$$

where n is the refractive index of the medium filling the resonator. Substituting (2.3.14) in (2.3.10), we get

$$Q = \omega n/\eta c = 2\pi/\eta\lambda. \tag{2.3.15}$$

Let Q_i denote the Q-factor of a resonator, connected with the i-th type of losses, and let Q denote the total Q-factor. If different types of losses can be considered independently of one another, we get

$$-dU/dt = \sum_i (-dU/dt)_i.$$

Taking (2.3.11) into account, this gives

$$1/Q = \sum_i 1/Q_i. \tag{2.3.16}$$

The result (2.3.15) is in accordance with (2.3.16):

$$\frac{1}{Q} = \frac{\lambda}{2\pi}\eta = \frac{\lambda}{2\pi}\sum_i \eta_i = \sum_i \frac{\lambda\eta_i}{2\pi} = \sum_i \frac{1}{Q_i}.$$

Q-factor of a Resonator due to Transmission Through the Output Mirror. The process of attenuation of field energy in a resonator on account of transmission through the output mirror may be conveniently considered by observing the propagation of radiation

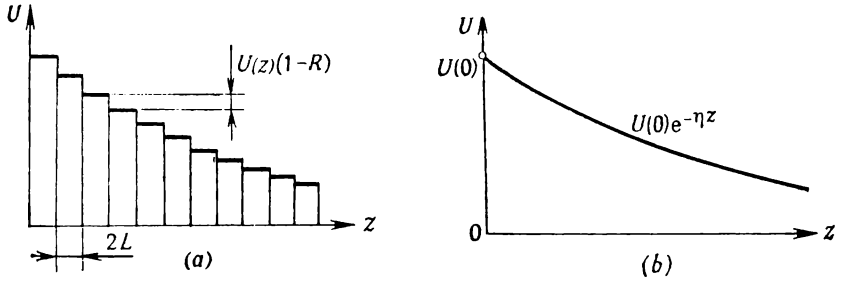


Fig. 2.10

inside the resonator from one mirror to another. We shall assume that only one resonator mirror is the output mirror (with reflection coefficient R), and the other totally reflects the radiation. If the radiation traverses a path of length Δz inside a resonator of length L, it means that it is reflected $\Delta z/2L$ times at the output mirror. On each such reflection, the resonator loses a part of the energy, equal to $1 - R$. Consequently, in traversing the path Δz, the loss of energy by the radiation is given by

$$-\Delta U = (U\Delta z/2L)(1 - R). \tag{2.3.17}$$

The dependence of U on z is shown in Fig. 2.10*a*. This dependence is step-shaped, the height of a single step being equal to $U(z)(1 - R)$. For the sake of comparison, the continuous U vs z curve corresponding to the relation (2.3.13) is shown in Fig. 2.10*b*. In order that the relation (2.3.13) describes approximately the case shown in

Fig. 2.10*a*, it is necessary to assume that the difference $1 - R$ defining the height of a "step" is small. This means that the output mirror must have a reflection coefficient fairly close to unity. We can write

$$R = 1 - \xi, \quad \text{where} \quad \xi \ll 1. \tag{2.3.18}$$

In this case, we can revert from (2.3.17) to a relation of the type (2.3.13), which will have the form

$$U(z) = U(0) \exp[-(1 - R)\, z/2L]. \tag{2.3.19}$$

It follows from this that the coefficient of favourable losses due to transmission through the output mirror of the resonator may be expressed as

$$\eta = (1 - R)/2L. \tag{2.3.20}$$

Substituting (2.3.20) in (2.3.15), we get

$$Q = 2\omega Ln/c\,(1 - R) = 4\pi L/\lambda\,(1 - R). \tag{2.3.21}$$

We have given earlier the expression (2.1.8) for the coefficient of favourable losses. Considering that the resonator has only one output mirror, this expression may be rewritten in the form

$$\eta = (1/2L) \ln (1/R). \tag{2.3.22}$$

Using (2.3.18), we can write

$$\ln (1/R) = \ln [1/(1 - \xi)] \approx \ln (1 + \xi) \approx \xi = 1 - R.$$

Consequently, the expression (2.3.22) turns into the expression (2.3.20) obtained above.

Q-factor and Modes of an Open Resonator. So far, we have been considering the Q-factor of a resonator without taking into account the mode structure of radiation. However, as mentioned earlier, the losses in an open resonator may strongly vary from one mode to another. Hence, strictly speaking, one should consider the Q-factor not of an entire resonator, but of a *given mode in a given resonator.* It should be emphasized that it is the difference in losses for different modes that leads to the formation of laser radiation field. This point has been mentioned in Sec. 2.2 while discussing the role of a resonator in a laser.

Let us somehow excite different modes in a passive resonator and observe the process of their gradual attenuation with time. Different losses for different modes lead to different damping rates for them, and so the *mode structure* of a field changes with time. The most dominating modes in this structure are characterised by the lowest losses. Thus, a resonator is similar to some sort of a "filter", isolating from any radiation field such components that correspond to modes with the lowest losses. In the case of an amplifying active medium, high-Q modes of a passive resonator will be characterised apparently by the largest difference $(\varkappa_0 - \eta)$. These modes will be the first to be amplified.

Diffractional Losses. Fresnel Number. Diffractional losses are due to a *finite aperture* of the resonator mirrors. They have a considerable dependence on the aperture, form and the alignment of mirrors, the geometry of the resonator defined, in particular, by its length and the radii of curvature of the mirrors employed. The diffractional losses are quite sensitive to the transverse structure of the radiation field. These losses increase rapidly with increasing

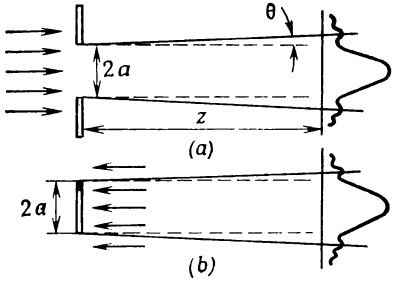


Fig. 2.11

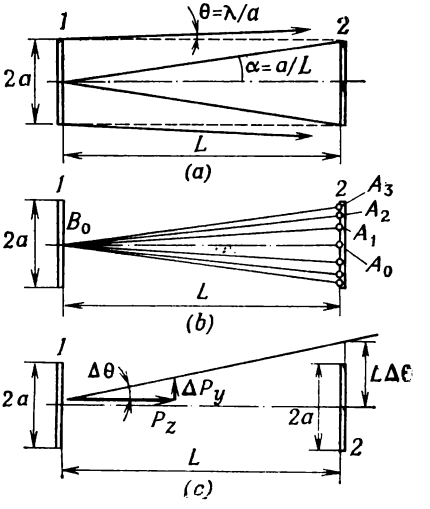


Fig. 2.12

transverse mode indices m and n. Apparently, a consideration of diffractional losses is a fundamentally important and at the same time a very complicated problem.

Let us start with the simplest approach to this problem. First we consider the familiar problem of Fraunhofer diffraction at a circular aperture (see, for example, [21]). A plane light wave is normally incident on a circular aperture of radius a (Fig. 2.11a). The diffraction pattern in a far zone (for $z \gg a$) will be characterised by a number of diffraction rings, the angular radius of the first diffraction ring is given by the diffraction angle $\theta \approx \lambda/a$. An analogous diffraction pattern emerges if a plane reflecting a mirror of radius a is used in place of the aperture with radius a, and if the diffraction is considered not in the transmitted, but in reflected light (Fig. 2.11b).

Let us consider a resonator of length L, formed by two ideally aligned plane reflecting circular mirrors with radius of aperture a (Fig. 2.12a). A light wave reflected from mirror *1* is diffracted at an angle $\theta \approx \lambda/a$. The lower this angle in comparison to the angle $\alpha = a/L$ at which mirror *2* can be seen from the centre of mirror *1*, the more effective the mirror *2* in "capturing" the radiation propagat-

ing from mirror *1*, and hence, the smaller the radiation losses on account of diffraction. Thus, in order to reduce the diffractional losses, the following condition must be satisfied:

$$\lambda/a \ll a/L.$$

This condition can be rewritten in the form

$$\boxed{a^2/L\lambda \gg 1}. \tag{2.3.23}$$

The quantity

$$N = a^2/L\lambda \tag{2.3.24}$$

is called the *Fresnel number*. In order to explain the physical meaning of this important parameter of the resonator, we divide the surface of mirror *2* into Fresnel zones as seen from the centre of mirror *1*. This division is shown in Fig. 2.12*b* by points A_1, A_2, A_3, ... ($A_1A_0 = \rho_1$ is the radius of the first zone, $A_2A_0 = \rho_2$ is the external radius of the second zone, and so on). Fresnel zones are defined by the relations

$$A_1B_0 - A_0B_0 = \lambda/2; \quad A_2B_0 - A_1B_0 = \lambda/2;$$
$$A_3B_0 - A_2B_0 = \lambda/2; \ \ldots$$

It can be easily seen that

$$L^2 + \rho_1^2 = (A_1B_0)^2 = \left(A_0B_0 + \frac{\lambda}{2}\right)^2 = \left(L + \frac{\lambda}{2}\right)^2$$
$$= L^2 + L\lambda + \frac{\lambda^2}{4} \approx L^2 + L\lambda.$$

Thus, the area of the first Fresnel zone seen from the centre of mirror *1* on the surface of mirror *2* is equal to $\pi\rho_1^2 = \pi L\lambda$. It can be seen that the second, third, and other Fresnel zones will have the same area. Consequently, the total number of Fresnel zones contained on the surface of mirror *2* is given by the ratio $\pi a^2/\pi L\lambda$, i.e. the Fresnel number. Thus, the *Fresnel number* is the number of Fresnel zones seen on the surface of one mirror of a finite aperture from the centre of the other. The larger the number of Fresnel zones covering the resonator mirror, the smaller the diffraction losses.

The *quantum representation* gives a fairly good visual explanation for the condition (2.3.23) that the diffractional losses be small [9]. Let us suppose that a photon is reflected at mirror *1* in the resonator. The photon coordinate transverse to the resonator axis (y-coordinate) has an uncertainty of the order of the aperture of the mirror ($\Delta y \approx a$), and in accordance with the uncertainty relation, the y-component of the photon momentum must have an uncertainty $\Delta P_y \approx \hbar/\Delta y \approx \hbar/a$. This means that the direction of motion of the photon is characterised by the uncertainty $\Delta\theta \approx \Delta P_y/P_z$ (Fig. 2.12*c*). Since $P_z = \hbar\omega/c = 2\pi\hbar/\lambda$, we get $\Delta\theta \approx \lambda/a$. On reaching mirror *2*, the trans-

verse photon coordinate will have an uncertainty of the order of $l\Delta\theta \approx L\lambda/a$. Mirror *2* must effectively capture the photons reflected at mirror *1*. For this purpose, it is necessary that the aperture of the mirror be considerably larger than the uncertainty, i.e. $a \gg L\lambda/a$. This is the condition (2.3.23).

As mentioned above, the question of diffractional losses is quite complicated. Naturally, it does not end with the condition (2.3.23) or the Fresnel number. Two resonators with the Fresnel numbers may have, for the same transverse mode, quite different values of diffraction losses depending on the geometry of the resonator taking into account the radii of curvature of the mirrors. For example, while in a plane-parallel resonator with $N \approx 1$ the power losses due to diffraction may be around 10-20% for a single pass, the power losses due to diffraction in a confocal resonator (resonator with spherical concave mirrors with radii of curvature equal to the length of the resonator) are an order of magnitude smaller (they do not exceed 1%) for the same values of the Fresnel number [22]. It follows, in particular, from this that while taking into account the diffractional losses, one should consider other resonator parameters as well besides the Fresnel number.

Main Parameters of a Passive Resonator Consisting of Two Mirrors (Spherical or Plane). We shall use the notation: L—the length of the resonator along its optical axis, r_1 and r_2—the radii of curvature of the mirrors. For a concave mirror $r > 0$, while for a convex mirror $r < 0$. Considering the aperture of the mirrors, we can isolate three quantitatively different cases:

1. The apertures of the mirrors are *infinitely large* (in effect, this means that the radius of the luminous spot on the mirror is much smaller than the aperture of the mirror). In this case, the Fresnel number has an infinitely large value. Diffractional losses are assumed to be completely absent. The main parameters of the resonator are[16]

$$\boxed{g_1 = 1 - L/r_1; \quad g_2 = 1 - L/r_2}. \tag{2.3.25}$$

2. The apertures of the mirrors are *finite and equal* (a is the radius of aperture of the mirror). The main parameters of the resonator in this case are

$$\boxed{N = a^2/L\lambda; \; g_1 = 1 - L/r_1; \; g_2 = 1 - L/r_2}. \tag{2.3.26}$$

3. The apertures of the mirrors are *finite and unequal.* Let a_1 and a_2 denote the radii of aperture of mirrors with the radii of curvature r_1 and r_2 respectively. The main parameters of the resonator

[16] The role of the parameters g_1 and g_2 will be explained later.

in this case are (see [15, 23])

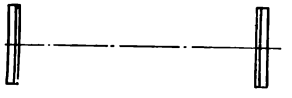
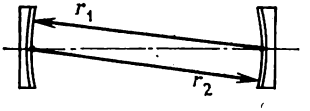
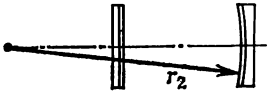
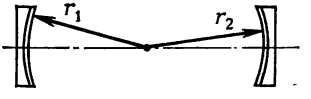
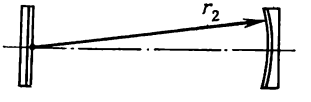
$$\boxed{N=\frac{a_1a_2}{L\lambda};\ G_1=\frac{a_1}{a_2}\ g_1=\frac{a_1}{a_2}\left(1-\frac{L}{r_1}\right);\quad G_2=\frac{a_2}{a_1}\ g_2=\frac{a_2}{a_1}\left(1-\frac{L}{r_2}\right)}. \tag{2.3.27}$$

It should be observed that

$$G_1G_2 = g_1g_2. \tag{2.3.28}$$

In the general case, it is necessary to take into account the *product* and *ratio* of the apertures of the resonator mirrors besides the geometry of the resonator. Parameters for some specific resonators are given in Table 2.2.

TABLE 2.2

	Plane-parallel resonator $r_1=r_2=\infty$ $\boxed{g_1=1,\ g_2=1}$
	Confocal resonator $r_1=r_2=L$ $\boxed{g_1=0,\ g_2=0}$
	Semiconfocal resonator $r_1=\infty,\ r_2=2L$ $\boxed{g_1=1,\ g_2=1/2}$
	Concentric resonator $r_1=r_2=L/2$ $\boxed{g_1=1,\ g_2=-1}$
	Semiconcentric resonator $r_1=\infty,\ r_2=L$ $\boxed{g_1=1,\ g_2=0}$

In addition to the two-mirror resonators, *ring resonators* are also used. The light beam in such resonators circulates along a closed circuit formed by three or more mirrors. Ring resonators and optical quantum gyroscopes based on them have been discussed in [24-26], see also Ch. 23 in [2].

Geometrical Approximation[17]. Strictly speaking, geometrical optics is a limiting case of wave optics, for $\lambda \to 0$. Since the diffraction effects are in principle not possible for $\lambda = 0$, geometrical-optics approximation is sometimes said to be valid only when diffraction can be neglected. However, such a condition on the applicability of geometrical optics is too stringent. *Geometrical* representation by no means excludes *diffractional phenomena.* In the modern theory of diffraction it is shown that "a violation of the laws of geometrical optics takes place only in the narrow transition bands where diffractional fields not envisaged by these laws are formed. Further propagation of these fields, away from the place of their excitation, is again described by the laws of geometrical optics" (Borovikov *et al.* [27]). This led, among other things, to a special term—*geometrical theory of diffraction.*

We shall be using the following rule for the applicability of geometrical optics approach. Firstly, it is necessary that the wavefront of the radiation field should be sufficiently smooth, i.e. the constant-phase surfaces should be sufficiently smooth. This is necessary so that we can speak of the existence of *light rays* or lines which are perpendicular to the constant-phase surface at every point. Secondly, it is necessary that these rays should be *straight lines* in an optically homogeneous medium.

From this, it follows that the geometrical optics deals not only with *plane* waves (constant-phase surfaces are planes), but also with *spherical* waves, i.e. waves with spherical constant-phase surfaces which have a common centre.

It is sometimes said that relatively small diffractional losses form the criterion for the applicability of geometrical approach for open resonators. Generally speaking, such a view is not correct. For example, unstable resonators are characterised by large diffractional losses. Yet most of the results for these generators have been obtained in the geometrical approximation. While considering the question of applicability of geometrical optics, one should take into account not the smallness of diffractional losses, but the rules formulated above.

A rigorous consideration of the process of radiation field formation in a resonator obviously requires the application of *wave theory.* However, a large number of questions on the theory of open resonators may be successfully investigated in the geometrical approximation. In particular, these include the derivation of stability conditions for resonators, estimation of various losses, selection of transverse modes, consideration of misalignment of resonator elements, etc. Geometrical approximation is a good approach for describing unstable resonators. In the case of stable resonators, we may use the connection that apparently exists between geometrical optics and the Gaussian optics, which is frequently employed for describing such resonators. According to Gerrard and Berch [4], one of the most

[17] The term *geometrical optics approximation* is also used sometimes.

widely accepted surprises of modern optics is the ease with which the methods of geometrical transformation of rays may be applied for a description of generation and propagation of laser radiation.

2.4. LENS WAVEGUIDES AND OPEN RESONATORS (GEOMETRICAL OPTICS APPROXIMATION)

While considering the passage of light in a lens waveguide or in an open resonator, we shall be using the *paraxial approximation*, i.e. we shall assume that the angle α, which a light ray forms with the optical axis of the waveguide (resonator), is so small that the relation $\tan\alpha \approx \sin\alpha \approx \alpha$ is always satisfied.

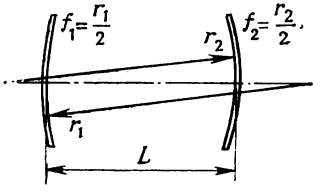


Fig. 2.13

Lens Waveguide and Open Resonator. There is a close resemblance between a *lens waveguide* and an *open resonator* [7, 15].

Consider a resonator of length L, formed by two concave spherical mirrors with radii of curvature r_1 and r_2 (Fig. 2.13). The focal lengths of these mirrors are equal to $f_1 = r_1/2$ and $f_2 = r_2/2$ respectively. A concave mirror with focal length f_i is optically equivalent to a combination of a plane mirror and a plane-convex lens with focal length $2f_i$. Thus the resonator shown in Fig. 2.13 may be replaced by the resonator shown in Fig. 2.14, which uses combinations of a plane mirror and a plane-convex lens instead of concave mirrors.

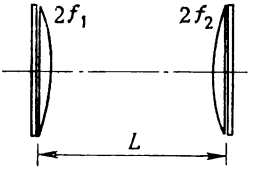


Fig. 2.14

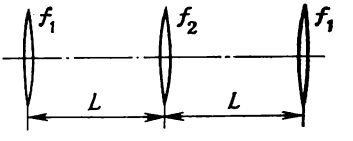


Fig. 2.15

Next, we go over from the resonator shown in Fig. 2.14 to the lens waveguide consisting of double convex lenses with focal lengths f_1 and f_2 alternatingly. The distance between adjacent lenses is equal to L (Fig. 2.15). The system shown in Fig. 2.15 is optically equivalent to the system shown in Fig. 2.14 and hence, to the one shown in Fig. 2.13. Of course, the light wave *changes* the direction of its propagation in systems shown in Figs. 2.13 and 2.14 each time it reaches the mirror, while in the system shown in Fig. 2.15, the light wave always propagates in the *same* direction.

Thus, an open resonator consisting of spherical mirrors with radii of curvature r_1 and r_2 is *optically equivalent* to a lens waveguide consisting of lenses with alternating focal lengths $f_1 = r_1/2$ and $f_2 = r_2/2$. The waveguide has a step (distance between adjacent lenses) equal to the length of the resonator. The concave mirror in a resonator is equivalent to the converging lenses in a waveguide, while the convex mirror is equivalent to the diverging lenses.

The difference between a lens waveguide and a resonator is that while the resonator isolates *certain discrete* frequencies, the waveguide has a *continuous frequency spectrum*. In all other respects, a resonator and a waveguide are alike. Certain transverse modes are excited and maintained in a waveguide just as in the case of a resonator.

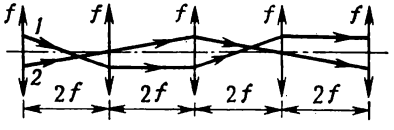


Fig. 2.16

The lens waveguide shown in Fig. 2.16 is analogous to a confocal resonator. This waveguide is called a *confocal lens waveguide*. All the lenses of such a waveguide have the same focal length f, and the step of the waveguide is equal to twice the focal length ($L = 2f$). As an example, two light rays (*1* and *2*) propagating in a confocal waveguide are shown in the figure. It can be seen by following the course of these rays that a confocal waveguide is capable of conducting light since it contains light rays which do not leave the waveguide (through the lateral face).

A lens waveguide which can contain the radiation in the vicinity of the optical axis is called a *stable waveguide*. It corresponds to a *stable open resonator*. Besides stable waveguides, there are such waveguides in which the light rays deviate to any extent from the axis as they propagate. As a result, they leave the waveguide. Such waveguides are called *unstable* and correspond to the *unstable open resonators*. An apparent example of an unstable waveguide is the one consisting of divergent lenses. The resonator corresponding to this waveguide is made up of convex mirrors.

Stability Condition for a Lens Waveguide with Alternating Lenses.[18] We shall derive a condition for the parameters of a lens waveguide (parameters L, f_1, f_2) under which the waveguide is stable. First of all, let us recall the equation for a thin lens. For this purpose, we

[18] We shall henceforth confine the discussion to light rays which are in planes passing through the optical axis of the waveguide or the resonator (sagittal rays are not considered). Besides, we assume that a waveguide has cylindrical symmetry. In this case, it is possible to consider a two-dimensional (plane) problem.

consider Fig. 2.17 where two parallel light rays forming an angle α with the optical axis OO pass through the lens and are focussed at the point A in the focal plane. We assume that the angles α and α' are sufficiently small so that $\tan\alpha \approx \alpha$ and $\tan\alpha' \approx \alpha'$ (paraxial approximation). In this case, $f\alpha = f\alpha' + y$ (see figure). Thus

$$\alpha' - \alpha = -y/f. \tag{2.4.1}$$

This is the *equation for a thin lens.* It expresses the difference between the angles a ray forms with the axis after and before passing

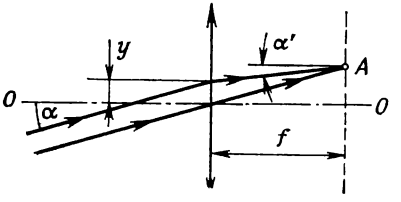


Fig. 2.17

through a lens, in terms of the focal length f and the distance y between the optical axis and the point where the ray comes in contact with the lens.

Let us now consider a lens waveguide with alternating focal lengths f_1, f_2, f_1, f_2, . . . of the lenses. The passage of a light ray

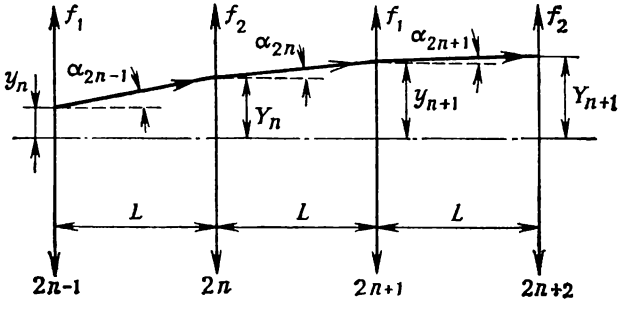


Fig. 2.18

through such a waveguide is shown in Fig. 2.18. Using Eq. (2.4.1), we write

$$\alpha_{2n} - \alpha_{2n-1} = -Y_n/f_2; \tag{2.4.2}$$

$$\alpha_{2n+1} - \alpha_{2n} = -y_{n+1}/f_1. \tag{2.4.3}$$

It follows from purely geometrical considerations (see Fig. 2.18) that

$$Y_n = y_n + L\alpha_{2n-1}; \tag{2.4.4}$$

$$y_{n+1} = Y_n + L\alpha_{2n}; \tag{2.4.5}$$

$$Y_{n+1} = y_{n+1} + L\alpha_{2n+1}. \tag{2.4.6}$$

Subtracting (2.4.4) from (2.4.5) and taking (2.4.2) into account, we get

$$y_{n+1} + y_n = Y_n (2 - L/f_2). \tag{2.4.7}$$

Subtracting (2.4.5) from (2.4.6) and taking (2.4.3) into account, we get

$$Y_{n+1} + Y_n = y_{n+1} (2 - L/f_1). \tag{2.4.8}$$

Replacing n by $n - 1$ in (2.4.8) and adding the resulting equation to (2.4.8), we get

$$Y_{n+1} + 2Y_n + Y_{n-1} = (y_{n+1} + y_n) (2 - L/f_1).$$

Substituting the result (2.4.7) into this expression, we get an equation connecting the positions of the ray only at even lenses (lenses with focal length f_2):

$$Y_{n+1} - 2 [2 (1 - L/2f_1) (1 - L/2f_2) - 1] Y_n + Y_{n-1} = 0. \tag{2.4.9}$$

It can be easily seen that the equation connecting the positions of the ray at odd lenses will be similar in form.

The solution of Eq. (2.4.9) may be expressed in the form

$$Y_n = A \exp (in\varphi) + B \exp (-in\varphi). \tag{2.4.10}$$

In order to determine the parameter φ, we substitute the first term from the right-hand side of Eq. (2.4.10) into Eq. (2.4.9). This gives

$$[\exp (i\varphi) + \exp (-i\varphi)]/2 = 2 (1 - L/2f_1) (1 - L/2f_2) - 1. \tag{2.4.11}$$

Stability of a waveguide means that for any n, the values of Y_n (as well as y_n) must remain within the limits of the bounded region near zero. Consequently, the parameter φ must be *real* (otherwise (2.4.10) will contain a term which increases indefinitely with increasing n). For real values of parameter φ, $[\exp (i\varphi) + \exp (-i\varphi)]/2 = \cos \varphi$. Thus for a *stable waveguide*, Eq. (2.4.11) assumes the form

$$\cos \varphi = 2 (1 - L/2f_1) (1 - L/2f_2) - 1. \tag{2.4.12}$$

This leads to the *condition for the stability of a waveguide*: $-1 \leqslant \cos \varphi \leqslant 1$. This can be written in the form

$$\boxed{0 \leqslant (1 - L/2f_1) (1 - L/2f_2) \leqslant 1}. \tag{2.4.13}$$

Stable and Unstable Open Resonators. Stability Diagram. We shall make use of the analogy between a lens waveguide with parameters L_1, f_1, and f_2, and an open resonator with the parameters L, $r_1 = 2f_1$, and $r_2 = 2f_2$. We introduce the parameters g_1 and g_2 (see (2.3.25)). This analogy turns the condition (2.4.13) for the stability of a waveguide into the *condition for the stability of a resonator*:

$$\boxed{0 \leqslant g_1 g_2 \leqslant 1}. \tag{2.4.14}$$

If the parameters g_1 and g_2 of an open resonator satisfy the condition (2.4.14), such a resonator is capable of containing the radiation within itself. If this condition is not satisfied, the resonator does not contain the radiation (even if both the mirrors are totally reflecting).

The stability condition (2.4.14) is often represented graphically on a coordinate plane on whose axes the values of g_1 and g_2 are plotted (see Fig. 2.19). If a resonator is represented by a corresponding point

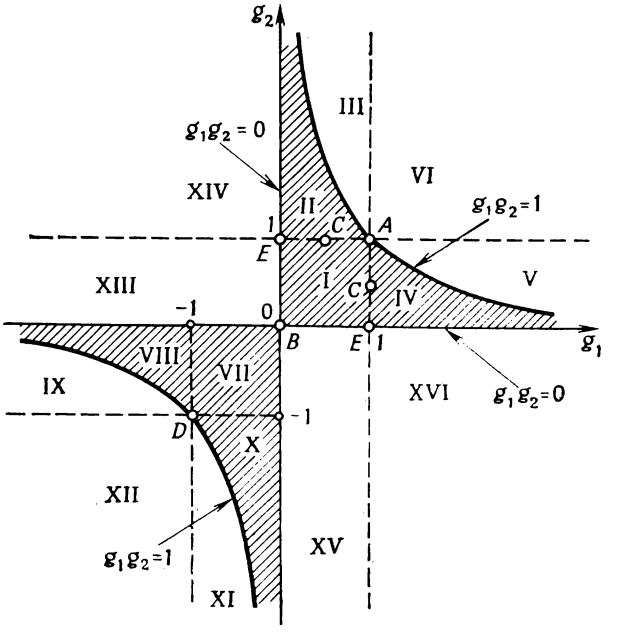
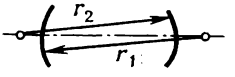
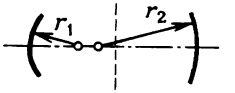
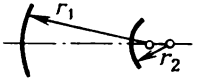
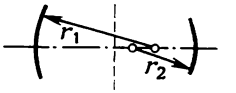
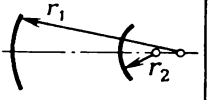
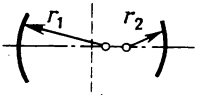
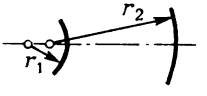
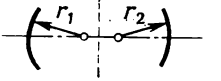
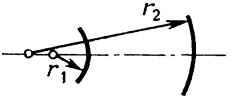
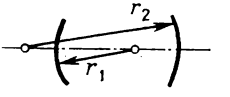
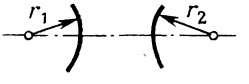
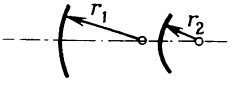
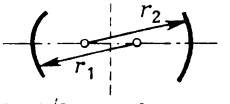
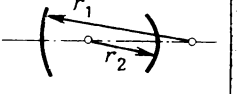
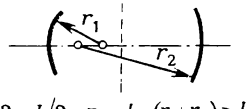
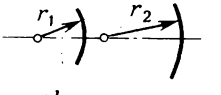


Fig. 2.19

(g_1, g_2) in this plane, then, in accordance with (2.4.14), the stable resonators fall within the shaded area, including its boundaries described by the curves $g_1g_2 = 1$ and $g_1g_2 = 0$. Figure 2.19 is called the *stability diagram* of resonators. The plane g_1g_2 in Fig. 2.19 is divided into 16 regions denoted by Roman numerals from I to XVI. To each region there corresponds a definite type of configuration of the resonator. Table 2.3 shows the different configurations of resonators.

It should be observed that from a physical point of view, stability of a lens waveguide or an open resonator is connected with the relative *smallness* of diffractional losses. Thus, a considerable increase in diffractional losses means leaving the shaded area in Fig. 2.19. The curves $g_1g_2 = 1$ and $g_1g_2 = 0$ separate the regions of low and high

TABLE 2.3

I  $r_1 > L$, $r_2 > L$	IX  $0 < r_1 < L/2$, $L/2 < r_2 < L$, $(r_1+r_2) < L$
II  $r_1 > L$, $r_2 < 0$, $(r_1-L) < \lvert r_2 \rvert$	X  $L/2 < r_1 < L$, $0 < r_2 < L/2$, $(r_1+r_2) > L$
III  $r_1 > L$, $r_2 < 0$, $(r_1-L) > \lvert r_2 \rvert$	XI  $L/2 < r_1 < L$, $0 < r_2 < L/2$, $(r_1+r_2) < L$
IV  $r_1 < 0$, $r_2 > L$, $(r_2-L) < \lvert r_1 \rvert$	XII  $0 < r_1 < L/2$, $0 < r_2 < L/2$
V  $r_1 < 0$, $r_2 > L$, $(r_2-L) > \lvert r_1 \rvert$	XIII  $0 < r_1 < L$, $r_2 > L$
VI  $r_1 < 0$, $r_2 < 0$	XIV  $0 < r_1 < L$, $r_2 < 0$
VII  $L/2 < r_1 < L$, $L/2 < r_2 < L$	XV  $r_1 > L$, $0 < r_2 < L$
VIII  $0 < r_1 < L/2$, $L/2 < r_2 < L$, $(r_1+r_2) > L$	XVI  $r_1 < 0$, $0 < r_2 < L$

diffractional losses. It should be noted that a very sharp transition between these regions takes place for large values of the Fresnel number (see [28]).

Point A in Fig. 2.19 corresponds to a plane-parallel resonator; point B corresponds to a confocal resonator while C, D, and E represent a semiconfocal, concentric, and semiconcentric resonators respectively. The plane-parallel, confocal, concentric, and semiconcentric resonators fall on the boundary of stability region. This means that the diffractional losses in these resonators are sensitive (especially for large numbers) to the deviations of parameters from theoretically ideal values. Hence in actual practice, it is preferable to deliberately deviate a bit towards the stability region by slightly changing the length of the resonator. Obviously, this is not possible in the case of a plane-parallel resonator.

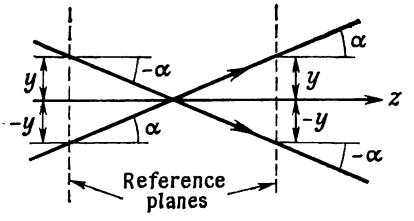


Fig. 2.20

Transfer Matrix for a Light Ray. As *reference plane*, we choose the plane $z = z_1$ perpendicular to the optical axis (z-axis) and at a certain distance z_1 from the origin. A light ray passing through the reference plane $z = z_1$ is characterised by two parameters: the distance y (z_1) from the optical axis and the tangent of the angle of inclination α (z_1) to the axis. In the paraxial approximation the parameter α (z) may be simply considered as the angle between the ray and the axis. In order to describe the transformation of the ray upon its propagation from the reference plane $z = z_1$ up to the reference plane $z = z_2$, we must indicate the law of transition from parameters y (z_1), α (z_1) to the parameters y (z_2), α (z_2).

Figure 2.20 shows two rays and two reference planes. This figure clearly shows the situations when one parameter of the ray is positive or negative.

While considering the transformation of a ray during its propagation from one reference plane to the other, we shall denote the initial reference plane by P_1 (y_1 and α_1 are the parameters of the ray) and the final, by P_2 (the parameters of the ray being y_2 and α_2). The transformation of the ray as it propagates from P_1 to P_2 is described by the relations

$$y_2 = Ay_1 + B\alpha_1; \quad \alpha_2 = Cy_1 + D\alpha_1. \tag{2.4.15}$$

In the matrix form, these relations can be represented as

$$\begin{pmatrix} y_2 \\ \alpha_2 \end{pmatrix} = \begin{pmatrix} A & B \\ C & D \end{pmatrix} \begin{pmatrix} y_1 \\ \alpha_1 \end{pmatrix}. \tag{2.4.16}$$

The matrix $\begin{pmatrix} A & B \\ C & D \end{pmatrix}$ is called the *transfer matrix* (transformation matrix) for the ray.

Suppose that a light ray passes through free space extending over a length d (Fig. 2.21*a*). In this case

$$y_2 = y_1 + \alpha_1 d; \quad \alpha_2 = \alpha_1. \tag{2.4.17}$$

Comparing (2.4.17) and (2.4.15), we find that $A = 1$, $B = d$, $C = 0$ and $D = 1$. Thus

$$M(d) = \begin{pmatrix} A & B \\ C & D \end{pmatrix} = \begin{pmatrix} 1 & d \\ 0 & 1 \end{pmatrix}, \tag{2.4.18}$$

where $M(d)$ denotes the transfer matrix of the ray for a free space of length d.

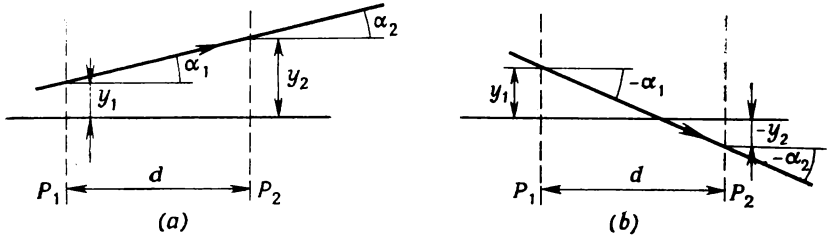


Fig. 2.21

The form of the matrix $M(d)$ is independent of the choice of light ray. For example, let us consider the ray shown in Fig. 2.21*b*. In this case,

$$y_1 + (-y_2) = (-\alpha_1)\, d; \quad -\alpha_2 = -\alpha_1.$$

It can be easily seen that this system of equations is equivalent to the system (2.4.17).

Figure 2.22*a* illustrates the transformation of a light ray in a thin convergent lens. Taking into account the equation (2.4.1) for a thin lens, we can write

$$y_2 = y_1; \quad \alpha_2 = (-1/f)\, y_1 + \alpha_1. \tag{2.4.19}$$

Thus, the transfer matrix $M(f)$ for a ray in the case of a thin lens with focal length f is of the form

$$M(f) = \begin{pmatrix} 1 & 0 \\ -1/f & 1 \end{pmatrix}. \tag{2.4.20}$$

If the lens is convergent, $f > 0$. For a divergent lens, $f < 0$.

Figure 2.22*b* shows the transformation of a ray upon successive passage through free space stretching over d and then through a thin

lens with a focal length f. It can be easily seen that

$$y_2 = y_1 + \alpha_1 d; \quad \alpha_2 = (-1/f)\, y_2 + \alpha_1 = (-1/f)\,(y_1 + \alpha_1 d) + \alpha_1$$

or

$$y_2 = y_1 + \alpha_1 d; \quad \alpha_2 = (-1/f)\, y_1 + (1 - d/f)\, \alpha_1. \qquad (2.4.21)$$

Thus, the transfer matrix of a ray in this case (we denote it as $M\ (d \to f)$) has the form

$$M\,(d \to f) = \begin{pmatrix} 1 & d \\ -1/f & 1 - d/f \end{pmatrix}. \qquad (2.4.22)$$

The same result is obtained if we multiply the matrix $M\ (f)$ by the matrix $M\ (d)$:

$$\begin{pmatrix} 1 & 0 \\ -1/f & 1 \end{pmatrix}\begin{pmatrix} 1 & d \\ 0 & 1 \end{pmatrix} = \begin{pmatrix} 1 & d \\ -1/f & 1 - d/f \end{pmatrix}.$$

Consequently,

$$M\ (d \to f) = M\ (f)\ M\ (d). \qquad (2.4.23)$$

Thus, the matrix corresponding to two successively accomplished transformations is equal to the *product* of the matrices of the corresponding transformations. The law of multiplication of transfer matrices for a ray is applicable to more complex systems as well.

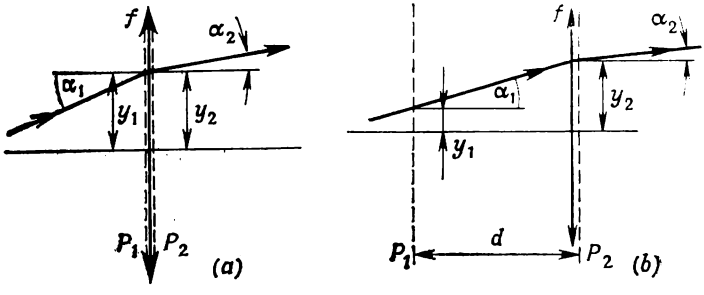


Fig. 2.22

Let us suppose, for example, that a light ray passes through a system of thin lenses shown in Fig. 2.23. The ray proceeds from left to right, i.e. from the reference plane P_1 to the reference plane P_2. The transformation matrix of light ray from P_1 to P_2 is defined as the product of elementary transfer matrices of the type $M\ (d)$ and $M\ (f)$:

$$M\ (d_1 \to f_1 \to d_2 \to f_2 \to d_3) = M\ (d_3)\ M\ (f_2)\ M\ (d_2)\ M\ (f_1)\ M\ (d_1). \qquad (2.4.24)$$

It should be emphasized that the order of the factors in the right-hand side of the relation (2.4.24) is *opposite* to the order in which the transformations are performed on the light ray (as if the right-hand side of the relation (2.4.24) were read not from left to right but, on the contrary, from right to left). This situation has already been indicated in the relation (2.4.23).

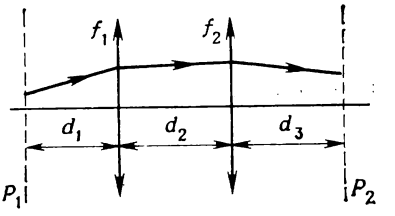


Fig. 2.23

The above remark is quite significant, since the product of matrices is *not commutative*. The *associative* law is valid for the product of matrices. Hence multiplication of matrices in pairs may be carried out in different ways. For example, the matrices in (2.4.24) may be multiplied in the following way:

$$M(d_3)\{M(f_2)[M(d_2)(M(f_1)M(d_1))]\},$$

we can choose the following pattern:

$$[M(d_3)(M(f_2)M(d_2))][M(f_1)M(d_1)]$$

or, alternatively,

$$[M(d_3)M(f_2)][(M(d_2)M(f_1))M(d_1)]$$

or some other pattern. The only important thing is that the sequence of matrices in the product should remain the same, for example, as in the relation (2.4.24).

Table 2.4 shows six transformation matrices for a ray. The first three have been considered above. The last three (describing the refraction of a ray at the boundary of two media) may be dealt with by the reader independently. It can be mentioned in conclusion of this discussion that for all transformation matrices of a ray, the following relation is satisfied:

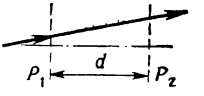
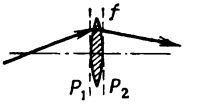
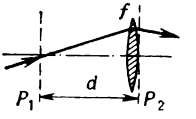
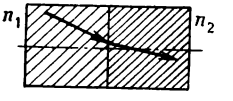
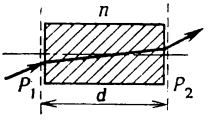
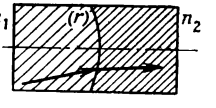
$$AD - BC = n_1/n_2, \qquad (2.4.25)$$

where n_1 is the refractive index of the medium in which the initial reference plane is situated, while n_2 is the corresponding value for the final reference plane. Equation (2.4.25) reflects the property of *reversibility* of light rays.

Transfer Matrix for a Ray in the Case of a Round-trip through the Resonator. First of all, let us find the transformation matrix for a ray upon reflection from a mirror with radius of curvature r. It can be seen from Fig. 2.24 that

$$-\alpha_2 = \alpha_1 + 2\beta; \quad (\alpha_1 + \beta)\, r = y_1.$$

TABLE 2.4

Nature of transformation	Diagram of transformation	Transformation matrix
Free space of length d		$\begin{pmatrix} 1 & d \\ 0 & 1 \end{pmatrix}$
Thin lens of focal length f		$\begin{pmatrix} 1 & 0 \\ -\frac{1}{f} & 1 \end{pmatrix}$
Combination of free space and a thin lens		$\begin{pmatrix} 1 & d \\ -\frac{1}{f} & 1-\frac{d}{f} \end{pmatrix}$
Refraction at the plane interface between two media (n_1, n_2)		$\begin{pmatrix} 1 & 0 \\ 0 & \frac{n_1}{n_2} \end{pmatrix}$
Medium of length d with refractive index n (plane end faces)		$\begin{pmatrix} 1 & \frac{d}{n} \\ 0 & 1 \end{pmatrix}$
Refraction at the spherical interface between two media (n_1, n_2)		$\begin{pmatrix} 1 & 0 \\ \frac{n_2-n_1}{n_2} & \frac{1}{r}\ \frac{n_1}{n_2} \end{pmatrix}$

Eliminating β, we get $\alpha_2 = -(2y_1/r) + \alpha_1$. Considering that $y_1 = y_2$, we get the following expression for the required matrix:

$$M(r) = \begin{pmatrix} 1 & 0 \\ -2/r & 1 \end{pmatrix}. \qquad (2.4.26)$$

For a concave mirror $r > 0$, while for a convex mirror $r < 0$. Matrix (2.4.26) may be represented in the form (2.4.20) so that the mirror

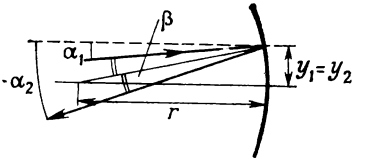


Fig. 2.24

with radius of curvature r has a focal length $f = r/2$. This leads to the analogy between a lens waveguide and resonator formed by spherical mirrors.

Let us consider a resonator of length L with mirrors having radii of curvature r_1 (left mirror) and r_2 (right mirror). We choose the

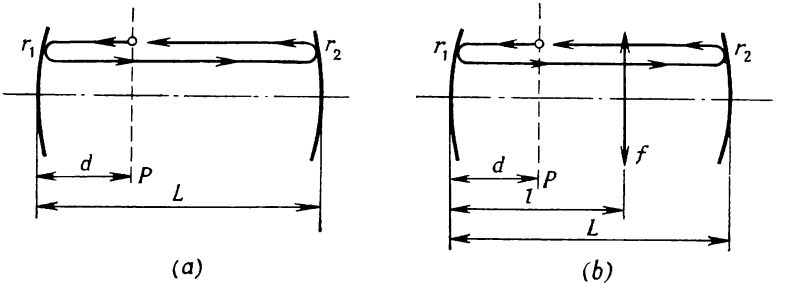


Fig. 2.25

reference plane P at a distance d from the left mirror. The transfer matrix of the ray for a round-trip through the resonator from the plane P (as shown by arrows in Fig. 2.25a) may be expressed in the form of the product

$$M(d \to r_1 \to L \to r_2 \to (L-d)) = M(L-d)\, M(r_2) \times \times M(L)\, M(r_1)\, M(d). \qquad (2.4.27)$$

Using (2.4.18) and (2.4.26), we carry out the multiplication of matrices:

$$\begin{pmatrix}1 & L-d\\ 0 & 1\end{pmatrix}\left[\begin{pmatrix}1 & 0\\ -2/r_2 & 1\end{pmatrix}\begin{pmatrix}1 & L\\ 0 & 1\end{pmatrix}\right]\left[\begin{pmatrix}1 & 0\\ -2/r_1 & 1\end{pmatrix}\begin{pmatrix}1 & d\\ 0 & 1\end{pmatrix}\right]$$
$$=\begin{pmatrix}1 & L-d\\ 0 & 1\end{pmatrix}\left[\begin{pmatrix}1 & L\\ -2/r_2 & 1-2L/r_2\end{pmatrix}\begin{pmatrix}1 & d\\ -2/r_1 & 1-2d/r_1\end{pmatrix}\right]$$
$$=\begin{pmatrix}1 & L-d\\ 0 & 1\end{pmatrix}\times\begin{pmatrix}1-\frac{2L}{r_1} & L+d-\frac{2dL}{r_1}\\ \frac{4L}{r_1r_2}-\frac{2}{r_1}-\frac{2}{r_2} & 1+\frac{4Ld}{r_1r_2}-\frac{2d}{r_1}-\frac{2}{r_2}(L+d)\end{pmatrix}.$$

As a result, we get the following transfer matrix of a ray for a round-trip shown in Fig. 2.25*a*[19].

$$\begin{Bmatrix} 1+\frac{4L}{r_1r_2}(L-d)-\frac{2}{r_1}(2L-d)-\frac{2}{r_2}(L-d) \\ 2L+\frac{4Ld}{r_1r_2}(L-d)-\frac{2d}{r_1}(2L-d)-\frac{2}{r_2}(L^2-d^2) \\ \frac{4L}{r_1r_2}-\frac{2}{r_1}-\frac{2}{r_2} \quad 1+\frac{4Ld}{r_1r_2}-\frac{2d}{r_1}-\frac{2}{r_2}(L+d) \end{Bmatrix}. \quad (2.4.28)$$

Suppose that a lens of focal length f is introduced in the resonator. This lens is located on the right side of the plane P at a distance l from the left mirror (Fig. 2.25*b*). In this case the following relation should be used instead of (2.4.27) for calculating the matrix for a round-trip through the resonator from the plane P:

$$M\,(d\to r_1\to l\to f\to (L-l)\to r_2\to (L-l)\to f \to (l-d)) = M\,(l-d)\,M\,(f)\,M\,(L-l)\,M\,(r_2)\,M\,(L-l) \times M\,(f)\,M\,(l)\,M\,(r_1)\,M\,(d). \quad (2.4.29)$$

The geometrical optics approximation is not applicable for considering the field in a resonator even for large apertures of the mirrors. Nevertheless, the transfer matrices obtained in the framework of geometrical optics are found to be quite useful. It will be shown in Sec. 2.8 that *similar matrices describe the transformation of Gaussian beams*[20].

2.5. DETUNING OF AN OPEN RESONATOR[21]

The geometrical optics approximation is useful for considering the detuning effects in an open resonator, caused by the fact that

[19] It can be easily seen that the determinants of all the transfer matrices of rays considered here are equal to unity ($AD - BC = 1$).

[20] For example, the matrix (2.4.28) will be used in Sec. 2.9 to consider the field in a resonator forming a Gaussian beam.

[21] This section has been written in collaboration with V. R. Kushnir.

individual optical elements (lenses, mirrors, etc.) in a resonator turn out to be *misaligned* to a certain extent.[22]

Misalignment of an Optical Element. The misalignment of an element may be caused by a slight *displacement* with respect to the optical axis of the resonator, or by a slight *rotation* with respect to the resonator axis. For an ideally aligned element, its optical axis *coincides* with the optical axis of the resonator. Such a coincidence no longer exists when the optical element is misaligned. We denote by y_1, α_1 and y_2, α_2 the parameters of a light ray at the entrance and exit of the element relative to its optical axis. The corresponding parameters for the same element relative to the optical axis of the resonator are expressed through y_1', α_1' and y_2', α_2'. The transformation from y_1, α_1, to y_2, α_2 is accomplished with the help of the transfer matrix of a ray for the element under consideration:

$$\begin{pmatrix} y_2 \\ \alpha_2 \end{pmatrix} = \begin{pmatrix} A_e & B_e \\ B_e & D_e \end{pmatrix} \begin{pmatrix} y_1 \\ \alpha_1 \end{pmatrix} \tag{2.5.1}$$

Our task is to find the method of transformation from y_1', α_1' to y_2', α_2' in the case of misalignment of an element.

Displacement of an Optical Element. Suppose that the optical axis O_1O_1 of an element is displaced by a very small distance Δy from the optical axis OO of a resonator (Fig. 2.26*a*). In this case

$$y_1 = y_1' - \Delta y; \quad \alpha_1 = \alpha_1'; \quad y_2 = y_2' - \Delta y; \quad \alpha_2 = \alpha_2'. \tag{2.5.2}$$

Substituting (2.5.2) into (2.5.1), we get

$$\begin{pmatrix} y_2' - \Delta y \\ \alpha_2' \end{pmatrix} = \begin{pmatrix} A_e & B_e \\ C_e & D_e \end{pmatrix} \begin{pmatrix} y_1' - \Delta y \\ \alpha_1' \end{pmatrix}$$

or

$$y_2' = A_e y_1' + B_e \alpha_1' + (1 - A_e)\,\Delta y; \quad \alpha_2' = C_e y_1' + D_e \alpha_1' - C_e \Delta y$$

or

$$\begin{pmatrix} y_2' \\ \alpha_2' \end{pmatrix} = \begin{pmatrix} A_e & B_e \\ C_e & D_e \end{pmatrix} \begin{pmatrix} y_1' \\ \alpha_1' \end{pmatrix} + \begin{pmatrix} (1 - A_e)\,\Delta y \\ -C_e \Delta y \end{pmatrix}. \tag{2.5.3}$$

Inclination of an Optical Element. Suppose that the optical axis O_1O_1 of an element is turned through a very small angle $\Delta\alpha$ with respect to the optical axis OO of a resonator (Fig. 2.26*b*). In this case

$$\begin{aligned} y_1 &\approx y_1' + l\,\Delta\alpha/2; \quad \alpha_1 = \alpha_1' - \Delta\alpha; \\ y_2 &\approx y_2' - l\,\Delta\alpha/2; \quad \alpha_2 = \alpha_2' - \Delta\alpha. \end{aligned} \tag{2.5.4}$$

[22] The effects caused by the non-ideal alignment of a resonator have been discussed, for example, by Gerrard *et al.* [4]. Marconze [7] has described lens waveguides with a random displacement of lenses.

Substituting (2.5.4) in (2.5.1), we get

$$\begin{pmatrix} y_2' - \frac{l}{2}\Delta\alpha \\ \alpha_2' - \Delta\alpha \end{pmatrix} = \begin{pmatrix} A_e & B_e \\ C_e & D_e \end{pmatrix} \begin{pmatrix} y_1' + \frac{l}{2}\Delta\alpha \\ \alpha_1' - \Delta\alpha \end{pmatrix}$$

or

$$\begin{pmatrix} y_2' \\ \alpha_2' \end{pmatrix} = \begin{pmatrix} A_e & B_e \\ C_e & D_e \end{pmatrix} \begin{pmatrix} y_1' \\ \alpha_1' \end{pmatrix} + \begin{pmatrix} \left[(1+A_e)\frac{l}{2} - B_e\right]\Delta\alpha \\ \left[1 + C_e\frac{l}{2} - D_e\right]\Delta\alpha \end{pmatrix}. \quad (2.5.5)$$

The inclination shown in Fig. 2.26*b* is in the anticlockwise direction. For an inclination in the clockwise direction, $\Delta\alpha$ in (2.5.5) should be replaced by $-\Delta\alpha$.

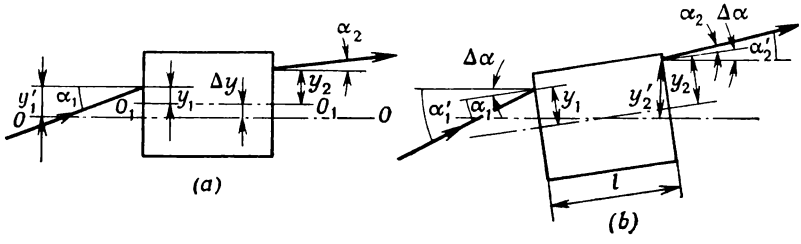


Fig. 2.26

General Case. Comparing the results (2.5.3) and (2.5.5), we conclude that a transformation of the ray from parameters y_1', α_1' to parameters y_2', α_2' may be represented by the expression

$$\begin{pmatrix} y_2' \\ \alpha_2' \end{pmatrix} = \begin{pmatrix} A_e & B_e \\ C_e & D_e \end{pmatrix} \begin{pmatrix} y_1' \\ \alpha_1' \end{pmatrix} + \Delta\varepsilon \begin{pmatrix} \Lambda_1 \\ \Lambda_2 \end{pmatrix}. \quad (2.5.6)$$

Here, $\Delta\varepsilon$ is Δy or $\Delta\alpha$, while Λ_1 and Λ_2 are expressed through the elements of the transfer matrix of the ray for the optical element under consideration in accordance with (2.5.3) or (2.5.5). For a simultaneous displacement and rotation of the optical element, Eq. I2.5.6) assumes the form

$$\begin{pmatrix} y_2' \\ \alpha_2' \end{pmatrix} = \begin{pmatrix} A_e & B_e \\ C_e & D_e \end{pmatrix} \begin{pmatrix} y_1' \\ \alpha_1' \end{pmatrix} + \Delta y \begin{pmatrix} \Lambda_1 \\ \Lambda_2 \end{pmatrix} + \Delta\alpha \begin{pmatrix} \Lambda_1' \\ \Lambda_2' \end{pmatrix}. \quad (2.5.7)$$

it should be emphasized that both Δy and $\Delta\alpha$ are assumed to be fairly small.

Resonator with a Misalignment Optical Element. Let us consider a resonator formed by two spherical mirrors with radii of curvature r_1 (left mirror) and r_2 (right mirror). An optical element with transformation matrix M_e of the ray is placed inside the resonator.

In an ideally aligned resonator, the axis of the light beam is a *straight line* with parameters 0, 0. This straight line coincides with the optical axis of the resonator (see Fig. 2.27*a*). If the optical element in the resonator is somehow misaligned, the axis of the beams will be a *bent line* in this case. The initial and final transverse coordinates of the beam axis will not be equal to zero: $y_1 \neq 0$, $y_2 \neq 0$ (Fig. 2.27*b*). It may be said that a resonator with a misaligned element (elements) is characterised by a bent optical axis with coordinates y_1 and y_2 at the left and the right mirror respectively.

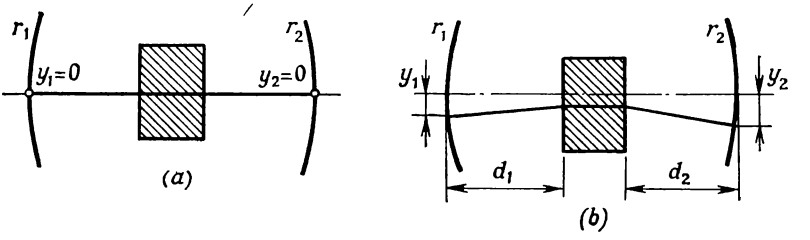


Fig. 2.27

Significantly, the axis of the light beam must form a *right angle* with the left as well as the right resonator mirror irrespective of the alignment or misalignment of the element. This means that the parameters of the beam axis on the mirrors will have the following form in a general case.

$$y_1,\ -y_1/r_1 \text{ (left mirror)}; \quad y_2,\ y_2/r_2 \text{ (right mirror)}.$$

Let us express y_1 and y_2 through the transfer matrix M_e of the ray characterising the optical element placed in the resonator, as well as through the parameters describing the misalignment of the element. For the sake of simplicity, we assume that the element is only displaced and not inclined. Besides the transfer matrix M_e we shall also use the matrices $M(d_1)$ and $M(d_2)$ describing the transformation of a light ray upon its propagation from the left resonator mirror to the optical element and from the optical element to the right mirror respectively (these matrices are described by relations of the type (2.4.18)).

The parameters of the axis of the light beam on the left mirror (parameters y_1, $-y_1/r_1$) are transformed as a result of its passage through resonator in the following way (if we take into account Eq. (2.5.6)):

$$M(d_2)\left[M_e M(d_1)\begin{pmatrix} y_1 \\ -y_1/r_1 \end{pmatrix} + \Delta y \begin{pmatrix} \Lambda_1 \\ \Lambda_2 \end{pmatrix}\right].$$

Equating the parameters obtained from this with the parameters of the axis of the beam on the right mirror (parameters y_2, y_2/r_2),

we get

$$\begin{pmatrix} y_2 \\ y_2/r_2 \end{pmatrix} = M(d_2)\left[M_e M(d_1)\begin{pmatrix} y_1 \\ -y_1/r_1 \end{pmatrix} + \Delta y \begin{pmatrix} \Lambda_1 \\ \Lambda_2 \end{pmatrix}\right].$$

This equation can be rewritten in the following form:

$$\begin{pmatrix} y_2 \\ y_2/r_2 \end{pmatrix} = M\begin{pmatrix} y_1 \\ -y_1/r_1 \end{pmatrix} + \Delta y M(d_2)\begin{pmatrix} \Lambda_1 \\ \Lambda_2 \end{pmatrix}. \qquad (2.5.8)$$

Here $M = M(d_2)\, M_e M(d_1)$ is the transfer matrix of the ray through the aligned system (from the left mirror to the right mirror).

Relation (2.5.8) is a system of two linear equations in y_1 and y_2

$$\left.\begin{aligned} y_2 &= Ay_1 - (By_1/r_1) + \Delta y\,(A_2\Lambda_1 + B_2\Lambda_2); \\ y_2/r_2 &= Cy_1 - (Dy_1/r_1) + \Delta y\,(C_2\Lambda_1 + D_2\Lambda_2), \end{aligned}\right\} \qquad (2.5.9)$$

where A, B, C and D are elements of the matrix M; A_2, B_2, C_2, and D_2 are elements of the matrix $M(d_2)$. Considering that in accordance with (2.4.18) $A_2 = 1, B_2 = d_2$, $C_2 = 0$, and $D_2 = 1$, we can rewrite (2.5.9) in the form

$$\left.\begin{aligned} y_2 &= Ay_1 - (By_1/r_1) + \Delta y\,(\Lambda_1 + d_2\Lambda_2); \\ y_2/r_2 &= Cy_1 - (Dy_1/r_1) + \Delta y\Lambda_2. \end{aligned}\right\} \qquad (2.5.9a)$$

By solving the system of equations (2.5.9a) we can easily find y_1 as well as y_2. The expression for y_1 is of the form

$$y_1 = \Delta y \frac{(-1/r_2)\,\Lambda_1 + (1 - d_2/r_2)\,\Lambda_2}{(1/r_2)\,(A - B/r_1) - (C - D/r_1)}. \qquad (2.5.10)$$

Knowing the value of y_1, we can find the displacement of the bent axis of the misaligned resonator with respect to the optical axis of an ideally aligned resonator for any reference plane. For this purpose, we have to operate on the column of initial parameters $\begin{pmatrix} y_1 \\ -y_1/r_1 \end{pmatrix}$ by the transfer matrix of a ray describing the transfer of the ray from the left mirror to the reference plane under consideration.

2.6. ANALYSIS OF OPEN RESONATORS ON THE BASIS OF FOX-LI ITERATIVE METHOD. EQUIVALENT RESONATORS

The main properties of open passive resonators are determined by diffraction parameters. While considering these phenomena we shall use the *scalar theory of diffraction*, i.e. we shall describe the field by a scalar function of spatial coordinates for which purpose one of the components of the electrical intensity vector[23] may be

[23] The fundamentals of scalar theory of diffraction have been described, for example, in [7, 29].

used. Besides, we shall assume diffraction angles to be very small (paraxial approximation).

Kirchhoff-Huygens Diffraction Integral. Let us consider an optical system of two parallel planes, separated by a distance L (plane-parallel resonator of length L); see Fig. 2.28. Suppose that the light field on the left plane (plane P_1) is described in the scalar form by a certain function $u(\mathbf{R}_1)$. Propagating from left to right, the field reaches the right plane (plane P_2) where it will be described by some other function $v(\mathbf{R}_2)$. The diffraction theory provides a representation of the function v in terms of u. For this purpose, we can use the following integral, which is a modification of *Kirchhoff-Huygens diffraction integral* (see [7]):

$$v(\mathbf{R}_2) = \frac{-i}{2\lambda} \int_{P_1} u(\mathbf{R}_1) \frac{\exp(ikl)}{l} (1 + \cos\theta)\, ds_1. \qquad (2.6.1)$$

Here l is the distance between a certain point $\mathbf{R}_1(x_1, y_1)$ on the P_1 plane to a point $\mathbf{R}_2(x_2, y_2)$ on the P_2 plane, and θ is the angle between the optical axis and the straight line joining these points.

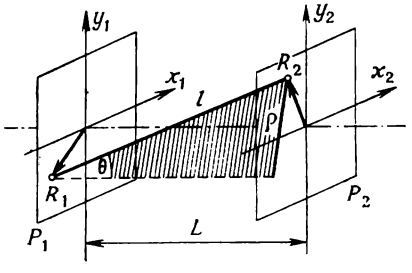


Fig. 2.28

For sufficiently small values of θ, the integral (2.6.1) assumes a form actually predicted by Huygens in the end of the 17th century. According to Huygens, the expression $u \exp(ikl)/l$ must appear under the integral sign. In this case $v(\mathbf{R}_2)$ is the result of summation of spherical waves $\exp(ikl)/l$, propagating from each element in the P_1 plane, at the point $\mathbf{R}_2$. In other words, the plane P_1 is identical to a set of elementary sources of spherical waves. The intensity of these sources is "regulated" by the given field $u(\mathbf{R}_1)$ on the P_1 plane. Subsequent development of the diffraction theory introduced some corrections to Huygens' formula, but the basic diffraction integral defined by the Huygens-Fresnel wave theory did not undergo any significant change.

We put

$$l = (L^2 + \rho^2)^{1/2}. \qquad (2.6.2)$$

The significance of parameter ρ is clear from Fig. 2.28:

$$\rho^2 = (\mathbf{R}_2 - \mathbf{R}_1)^2 = (x_2 - x_1)^2 + (y_2 - y_1)^2. \qquad (2.6.3)$$

Taking (2.6.2) into account, we can rewrite (2.6.1) in the form

$$v(\mathbf{R}_2) = \frac{-i}{2\lambda} \int_{P_1} u(\mathbf{R}_1) \exp\left[ikL\sqrt{1 + (\rho/L)^2}\right] \times \frac{1 + \cos\theta}{l}\, ds_1. \qquad (2.6.4)$$

Applying the diffraction integral to open resonators, it may be assumed that l may be larger than the transverse dimensions of the field. Consequently, the expression (2.6.4) can be considerably sim-

plified, since we can put

$$\cos\theta \approx 1; \quad 1/l \approx 1/L, \tag{2.6.5a}$$

while the phase multiplier can be written in the form

$$\exp\left[ikL\sqrt{1+(\rho/L)^2}\right] \approx \exp\left[ikL\left(1+\frac{\rho^2}{2L^2}\right)\right]$$
$$= \exp(ikL)\exp\left(ik\frac{\rho^2}{2L}\right). \tag{2.6.5b}$$

(It is assumed that $\rho \ll L$.) In this case the diffraction integral assumes the form (*Fresnel diffraction*)

$$v(\mathbf{R}_2) = \frac{-i}{\lambda L}\exp(ikL)\int\limits_{P_1} u(\mathbf{R}_1)\exp\left(i\frac{\pi}{\lambda L}\rho^2\right)ds_1. \tag{2.6.6}$$

Fox-Li Integral Equation. Fox and Li have proposed an iterative method for finding the transverse modes in an open resonator [30]. Suppose an arbitrary field $u(\mathbf{R}_1)$ is given at the left resonator mirror. Substituting this field in (2.6.6), we can calculate the field $v(\mathbf{R}_2)$ at the right mirror. Using the relation (2.6.6) again, we substitute the computed value of the field v in the integral. This gives a value u_1 of the field at the left mirror caused by the field v at the right mirror. We use the relation (2.6.6) again and return to the right mirror and find the value of the field v_1 for it, caused by the field u_1 on the left mirror, and so on. Fox and Li showed that after a large number of passages in the resonator from one mirror to another, the structure of the field or its dependence on the transverse coordinates starts getting *reproduced*, repeating itself after every passage of radiation through the resonator. This means that after a large number of transitions the field on the surface of the mirror is described by the function u which is a solution of the *Fox-Li integral equation*:

$$\boxed{\frac{i}{\lambda L}\int\limits_{P_1} u(\mathbf{R}_1)\exp\left(i\frac{\pi}{\lambda L}\rho^2\right)ds_1 = \gamma u(\mathbf{R}_2).} \tag{2.6.7}$$

Irrespective of the transverse coordinates the complex factor γ takes into account the *phase shift* in the field for a passage (including the purely geometrical phase incursion over a distance L, given by the factor $\exp(-ikL)$ in γ) as well as the *decrease in the amplitude* u of the field as a result of losses in the resonator. We assume that light power reflected by the left mirror in the direction of the right mirror is given by

$$\int\limits_{P_1} |u(\mathbf{R}_1)|^2 ds_1 = W.$$

On account of the losses in the resonator, the right mirror will reflect less light power back to the left mirror:

$$\int_{P_2} |\gamma u(\mathbf{R}_2)|^2 ds_2 = |\gamma|^2 W.$$

For every passage through the resonator, the power reflected by the mirror will decrease (its magnitude will be multiplied every time by $|\gamma|^2$) (see Fig. 2.29). The fraction of the light power lost during a single passage is given by

$$\Delta W/W = (W - |\gamma|^2 W)/W = 1 - |\gamma|^2. \quad (2.6.8)$$

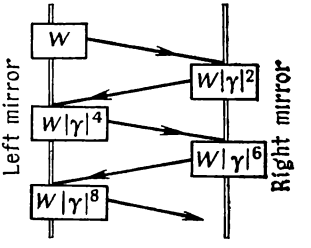


Fig. 2.29

We denote

$$|\gamma| = \exp(-\beta). \quad (2.6.9)$$

Assuming that the losses associated with the passage are small, we write $\Delta W/W = 1 - |\gamma|^2 \approx 1 - (1 - 2\beta) = 2\beta$. In this case, the linear loss coefficient is given by

$$\eta = 2\beta/L. \quad (2.6.10)$$

Transverse Modes in an Open Resonator. Let us write the integral equation (2.6.7) in the form

$$\boxed{\hat{L}u(\mathbf{R}_1) = \gamma u(\mathbf{R}_2)}. \quad (2.6.11)$$

Here $\hat{L}$ is an integral operator describing the transformation of the field in the resonator for one pass; γ are the *eigenvalues* of the operator $\hat{L}$, and u are its *eigenfunctions.*

The spectrum of eigenvalues of the operator $\hat{L}$ is *discrete.* In order to fix various eigenvalues, we make use of a couple of integral indices m and n ($m, n = 0, 1, 2, \ldots$). The eigenfunction of the operator $\hat{L}$, corresponding to the eigenvalue γ_{mn} is denoted by u_{mn}. This is the mn-th *transverse mode* for a given resonator.

Thus, following Fox and Li, if we assume that after passing through the resonator (from mirror to mirror), the field can *reproduce* its structure, we arrive at the concept of transverse modes in a resonator in the most natural way: *transverse modes* represent a field which reproduces its structure after passage through the resonator. Mathematically, the transverse modes are eigenfunctions of the operator $\hat{L}$ defined by the integral equation (2.6.7).

Taking into consideration the above remarks, we can rewrite (2.6.9) and (2.6.10) in the form

$$|\gamma_{mn}| = \exp(-\beta_{mn}), \qquad (2.6.9a)$$

$$\eta_{mn} = 2\beta_{mn}/L. \qquad (2.6.10a)$$

Substituting (2.6.10*a*) into (2.3.15), we get an expression for the Q-factor of the mn-th mode:

$$Q_{mn} = \pi L/\lambda\beta_{mn}. \qquad (2.6.12)$$

If we know the eigenvalues γ_{mn} of the operator $\hat{L}$ describing a given resonator, we can find the losses for mn-th mode, which are equal to $1 - |\gamma_{mn}|^2$ in accordance with (2.6.8). Besides, we can also find the phase shift of mn-th mode defined by $\arg \gamma_{mn}$. Equating the phase-shift for a pass through the resonator to the product of π and an integer q, we can determine the spectrum of resonance frequencies for the transverse mode under consideration.

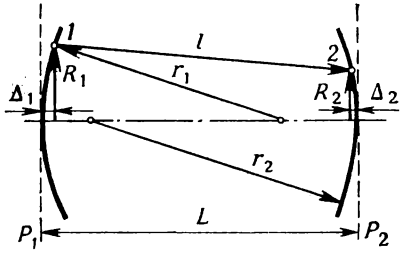


Fig. 2.30

Resonator Consisting of Two Spherical Mirrors. Figure 2.30 shows a cross section along the optical axis of a resonator of length L, formed by spherical mirrors with radii of curvature r_1 (left mirror) and r_2 (right mirror). Any point on the left mirror is given by the vector $\mathbf{R}_1$ lying in the plane passing through the given point and perpendicular to the optical axis. Similarly, vector $\mathbf{R}_2$ represents a point on the right mirror[24]. Points *1* and *2* in Fig. 2.30 are chosen so that the vectors $\mathbf{R}_1$ and $\mathbf{R}_2$ lie in the same plane (of the figure). In actual practice, however, these vectors do not necessarily lie in the same plane.

From Fig. 2.30, it can be seen that the length l of the straight line joining the points corresponding to vectors $\mathbf{R}_1$ and $\mathbf{R}_2$ is given by the expression

$$l = [(L - \Delta_1 - \Delta_2)^2 + (\mathbf{R}_2 - \mathbf{R}_1)^2]^{1/2}. \qquad (2.6.13)$$

(In particular, if vectors $\mathbf{R}_1$ and $\mathbf{R}_2$ lie in the same plane as shown in the figure, we should replace $(\mathbf{R}_2 - \mathbf{R}_1)^2$ in (2.6.13) by $(R_2 - R_1)^2$). Since $(\Delta_1 + \Delta_2) \ll L$, we get

$$(L - \Delta_1 - \Delta_2)^2 = L^2\left(1 - \frac{\Delta_1 + \Delta_2}{L}\right)^2 \approx L^2 - 2L(\Delta_1 + \Delta_2).$$

[24] Strictly speaking, the vectors $\mathbf{R}_1$ and $\mathbf{R}_2$ define the *transverse* coordinates of the corresponding points (coordinates of the projections of the points on the planes P_1 and P_2; see Fig. 2.30).

Consequently,

$$l = (L^2 + [(\mathbf{R}_2 - \mathbf{R}_1)^2 - 2L(\Delta_1 + \Delta_2)])^{1/2}. \quad (2.6.14)$$

Comparing (2.6.14) and (2.6.2), we conclude that we should use the expression $(\mathbf{R}_2 - \mathbf{R}_1)^2 - 2L(\Delta_1 + \Delta_2)$ instead of ρ^2 in the integral equation (2.6.7). Besides, the difference in the radii of curvature of the mirrors violates the symmetry of the resonator. In such a resonator the field structure is reproduced not after *one*, but after *two* passes through the resonator. Consequently, we should now consider the following *system* of two integral equations instead of the integral equation (2.6.7):

$$\frac{i}{\lambda L}\int_{P_1} u(\mathbf{R}_1) K(\mathbf{R}_1; \mathbf{R}_2)\, ds_1 = \gamma' v(\mathbf{R}_2); \quad (2.6.15a)$$

$$\frac{i}{\lambda L}\int_{P_2} v(\mathbf{R}_2) K(\mathbf{R}_1; \mathbf{R}_2)\, ds_2 = \gamma'' u(\mathbf{R}_1), \quad (2.6.15b)$$

where

$$K(\mathbf{R}_1; \mathbf{R}_2) = \exp\left(i\frac{\pi}{\lambda L}[(\mathbf{R}_2 - \mathbf{R}_1)^2 - 2L(\Delta_1 + \Delta_2)]\right]. \quad (2.6.16)$$

Since vectors $\mathbf{R}_1$ and $\mathbf{R}_2$ give only the *transverse coordinates* of points on the mirror surface, it may be considered that integration in (2.6.15) is carried out over the planes P_1 and P_2 shown in Fig. 2.30. The curvature of the mirror surface is taken into account in the expression (2.6.16) for the kernel of the integral equation.

It should be observed that the functions $u(\mathbf{R}_1)$ and $v(\mathbf{R}_2)$ must satisfy the condition

$$\int_{P_1} |u(\mathbf{R}_1)|^2 ds_1 = \int_{P_1} |v(\mathbf{R}_2)|^2 ds_2. \quad (2.6.17)$$

This condition has been introduced in order that the eigenvalues γ' and γ'' should have a similar meaning as the eigenvalue γ in (2.6.7). Denoting $\int_{P_1} |u(\mathbf{R}_1)|^2 ds_1$ by W and taking (2.6.17) into account, we find that the fraction of the light power lost in a single pass through the resonator *from the left mirror to the right one* is equal to

$$(W - |\gamma'|^2 W)/W = 1 - |\gamma'|^2.$$

The fraction of power lost in a single pass *from the right mirror to the left one* is equal to $1 - |\gamma''|^2$. The fraction of power lost as a result of a round-trip through the resonator is equal to $1 - |\gamma'\gamma''|^2$. In this case, Fig. 2.31 is analogous to Fig. 2.29, applied to a symmetrical resonator.

From Fig. 2.30 it is apparent that $R_1^2 = r_1^2 - (r_1 - \Delta_1)^2 \approx r_1^2 - r_1^2(1 - 2\Delta_1/r_1) = 2\Delta_1 r_1$, and similarly $R_2^2 = r_2^2 - (r_2 - \Delta_2)^2 \approx 2\Delta_2 r_2$. Thus $2(\Delta_1 + \Delta_2) = (R_1^2/r_1) + (R_2^2/r_2)$. From this it follows

that

$$(\mathbf{R}_2-\mathbf{R}_1)^2-2L(\Delta_1+\Delta_2)=\left(1-\frac{L}{r_1}\right)R_1^2$$
$$+\left(1-\frac{L}{r_2}\right)R_2^2-2\mathbf{R}_1\mathbf{R}_2=g_1R_1^2+g_2R_2^2-2\mathbf{R}_1\mathbf{R}_2. \quad (2.6.18)$$

Thus the kernel of the integral equations (2.6.15) may be represented in the form

$$K(\mathbf{R}_1;\ \mathbf{R}_2)=\exp\left[i\frac{\pi}{\lambda L}(g_1R_1^2+g_2R_2^2-2\mathbf{R}_1\mathbf{R}_2)\right]. \quad (2.6.19)$$

Using *Cartesian coordinates* ($\mathbf{R}_1(x_1, y_1)$; $\mathbf{R}_2(x_2, y_2)$), we can rewrite Eqs. (2.6.15) and (2.6.19) in the following form:

$$\frac{i}{\lambda L}\int\limits_{P_1}\int u(x_1, y_1)K(x_1y_1;\ x_2y_2)\,dx_1\,dy_1=\gamma' v(x_2, y_2); \quad (2.6.20a)$$

$$\frac{i}{\lambda L}\int\limits_{P_2}\int v(x_2, y_2)K(x_1, y_1;\ x_2, y_2)\,dx_2\,dy_2=\gamma'' u(x_1, y_1); \quad (2.6.20b)$$

$$K(x_1, y_1;\ x_2, y_2)=\exp\left(i\frac{\pi}{\lambda L}[g_1(x_1^2+y_1^2)\right.$$
$$\left.+g_2(x_2^2+y_2^2)-2(x_1x_2+y_1y_2)]\right). \quad (2.6.21)$$

We assume that the aperture of mirrors is *much larger* than the size of the luminous spot. Then, irrespective of the actual form of

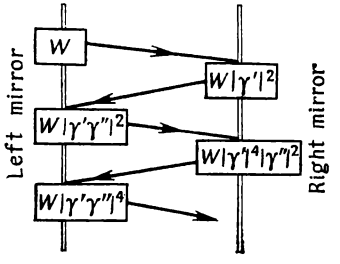


Fig. 2.31

mirrors, we can separate the variables in (2.6.20) and carry out integration between symmetrical infinite limits. Introducing the indices m, n of a mode, we can write

$$\left.\begin{aligned} u_{mn}(x_1, y_1)&=u_m(x_1)\,u_n(y_1); \quad \gamma'_{mn}=\gamma'_m\gamma'_n;\\ v_{mn}(x_2, y_2)&=v_m(x_2)\,v_n(y_2); \quad \gamma''_{mn}=\gamma''_m\gamma''_n. \end{aligned}\right\} \quad (2.6.22)$$

It can be easily seen that the system of equations (2.6.20) breaks up into two identical systems of equations—a system of equations for the functions u_m and v_m, and another system of equations for

the functions u_n and v_n. We shall consider only the first of these systems of equations:

$$\frac{\sqrt{i}}{\sqrt{\lambda L}} \int_{-\infty}^{\infty} u_m(x_1)\, K(x_1;\, x_2)\, dx_1 = \gamma'_m v_m(x_2); \qquad (2.6.23a)$$

$$\frac{\sqrt{i}}{\sqrt{\lambda L}} \int_{-\infty}^{\infty} v_m(x_2)\, K(x_1;\, x_2)\, dx_2 = \gamma''_m u_m(x_1), \qquad (2.6.23b)$$

where

$$K(x_1;\, x_2) = \exp\left[i \frac{\pi}{\lambda L} (g_1 x_1^2 + g_2 x_2^2 - 2x_1 x_2) \right]. \qquad (2.6.24)$$

The condition (2.6.17) then assumes the form

$$\int_{-\infty}^{\infty} |\, u_m(x_1)\,|^2\, dx_1 = \int_{-\infty}^{\infty} |\, v_m(x_2)\,|^2\, dx_2. \qquad (2.6.25)$$

Confocal Resonator ($g_1 = g_2 = 0$, $r_1 = r_2 = L$). Since this resonator is symmetrical, it is sufficient to have just one integral equation. It has the form

$$\frac{\sqrt{i}}{\sqrt{\lambda L}} \int_{-\infty}^{\infty} u_m(x_1) \exp\left(-i \frac{2\pi}{\lambda L} x_1 x_2 \right) dx_1 = \gamma_m u_m(x_2). \qquad (2.6.26)$$

The left-hand side of Eq. (2.6.26) describes the Fourier transform of the function u_m. The solutions of such an equation are functions having the following property: Fourier transformation leaves these functions *unchanged* (with an accuracy up to a constant multiplier). *Hermite-Gauss polynomials*[25] are familiar functions of this kind.

A Hermite-Gauss polynomial of the m-th order may be represented in the form

$$\psi_m(t) = (2^m m!\, \sqrt{\pi})^{-1/2}\, H_m(t) \exp(-t^2/2), \qquad (2.6.27)$$

where $H_m(t) = \exp(t^2)\, (-1)^m \frac{d^m}{dt^m} \exp(-t^2)$ is a Hermite polynomial of the m-th order. The polynomials $\psi_m(t)$ satisfy the orthonormalisation condition

$$\int_{-\infty}^{\infty} \psi_m(t)\, \psi_n(t)\, dt = \delta_{mn}. \qquad (2.6.28)$$

[25] Hermite polynomials and Hermite-Gauss polynomials are described in Appendix 1.

The first few Hermite-Gauss polynomials are given by

$$\psi_0(t) = (\sqrt{\pi})^{-1/2} \exp(-t^2/2);$$
$$\psi_1(t) = (2\sqrt{\pi})^{-1/2} 2t \exp(-t^2/2);$$
$$\psi_2(t) = (2\sqrt{\pi})^{-1/2} (2t^2 - 1) \exp(-t^2/2).$$

Curves corresponding to these polynomials are shown in Fig. 2.32.

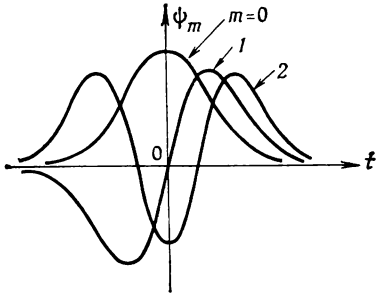


Fig. 2.32

Hermite-Gauss polynomials satisfy the following integral equation [31]:

$$\frac{1}{\sqrt{2\pi}} \int_{-\infty}^{\infty} \psi_m(t) \exp(-it\tau)\, dt = i^m \psi_m(\tau). \qquad (2.6.29)$$

We introduce the notation

$$x_1 = t\sqrt{\lambda L/2\pi}; \qquad x_2 = \tau\sqrt{\lambda L/2\pi}.$$

Equation (2.6.29) assumes a form coinciding with Eq. (2.6.26):

$$\frac{1}{\sqrt{\lambda L}} \int_{-\infty}^{\infty} \psi_m\left(x_1\sqrt{\frac{2\pi}{\lambda L}}\right) \exp\left(-i\,\frac{2\pi}{\lambda L}\, x_1 x_2\right) dx_1 = i^m \psi_m\left(x_2\sqrt{\frac{2\pi}{\lambda L}}\right).$$

It follows from this that

$$u_m(x_1) = \text{const}\, \psi_m\left(x_1\sqrt{\frac{2\pi}{\lambda L}}\right)$$
$$= \text{const}\, H_m\left(x_1\sqrt{\frac{2\pi}{\lambda L}}\right) \exp\left(-\frac{\pi}{\lambda L}\, x_1^2\right). \qquad (2.6.30)$$

Figure 2.33*a* shows the curves for the functions $u_m(x_1)$ for $m = 0, 1, 2$ obtained for values of $2\pi a^2/\lambda L$ equal to 25 (curves *1*) and 200 (curves *2*) [22]. These curves correspond to the curves of Hermite-Gauss polynomials shown in Fig. 2.32. Figure 2.33*b* shows the forms of luminous spots for modes TEM_{00}, TEM_{10} and TEM_{20}. The intensity of the light field of the mode TEM_{m0} vanishes along

the x_1-axis at points where the amplitude of $u_m(x_1)$ changes sign. The number of such points is equal to m.

Aperture of Resonator Mirrors. Let us assume that the mirrors have quadratic apertures, and denote the apertures of the left and

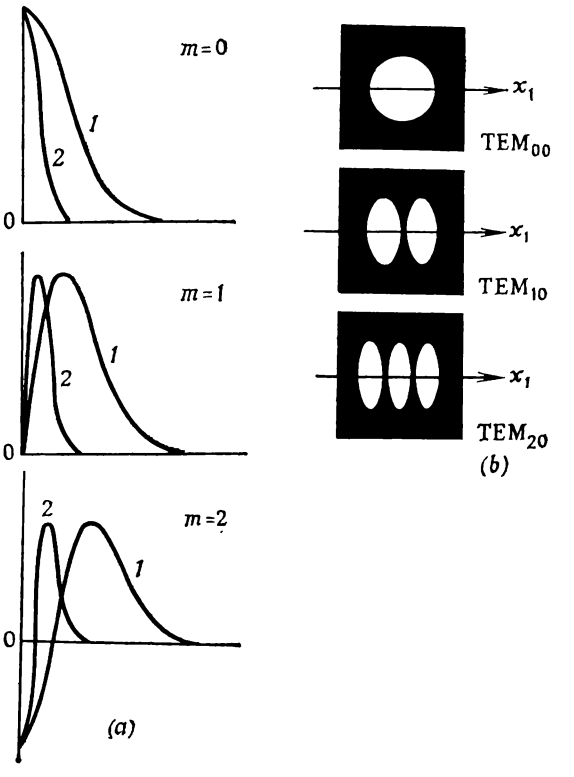


Fig. 2.33

the right mirror by $2a_1$ and $2a_2$ respectively (Fig. 2.34). Since the aperture of the mirror is quadratic, *Cartesian coordinates* can be used as before for separation of variables in integral equations. However, unlike large apertures, the limits of integration in the corresponding integrals are not infinite. Instead of (2.6.23), we now have

$$\frac{\sqrt{i}}{\sqrt{\lambda L}} \int_{-a_1}^{a_1} u_m(x_1)\, K(x_1; x_2)\, dx_1 = \gamma'_m v_m(x_2); \qquad (2.6.31a)$$

$$\frac{\sqrt{i}}{\sqrt{\lambda L}} \int_{-a_2}^{a_2} v_m(x_2)\, K(x_1; x_2)\, dx_2 = \gamma''_m u_m(x_1), \qquad (2.6.31b)$$

where $K(x_1, x_2)$ is defined by the expression (2.6.24). In this case, the condition (2.6.25) assumes the form

$$\int_{-a_1}^{a_1} |u_m(x_1)|^2 dx_1 = \int_{-a_2}^{a_2} |v_m(x_2)|^2 dx_2. \quad (2.6.32)$$

Following Gordon and Kogelnik [23], we obtain the dimensionless variables

$$\xi_1 = x_1/a_1; \quad \xi_2 = x_2/a_2. \quad (2.6.33)$$

In accordance with (2.6.32), we introduce the functions

$$U_m(\xi_1) = u_m(\xi_1 a_1)\sqrt{a_1}; \quad V_m(\xi_2) = v_m(\xi_2 a_2)\sqrt{a_2}. \quad (2.6.34)$$

Consequently, the system of equations (2.6.31) is transformed into

$$\sqrt{iN}\int_{-1}^{1} U_m(\xi_1) K(\xi_1; \xi_2) d\xi_1 = \gamma'_m V_m(\xi_2); \quad (2.6.35a)$$

$$\sqrt{iN}\int_{-1}^{1} V_m(\xi_2) K(\xi_1; \xi_2) d\xi_2 = \gamma''_m U_m(\xi_1), \quad (2.6.35b)$$

where

$$K(\xi_1; \xi_2) = \exp[i\pi N(G_1\xi_1^2 + G_2\xi_2^2 - 2\xi_1\xi_2)]. \quad (2.6.36)$$

It should be recalled (see (2.3.27)) that

$$N = a_1 a_2/\lambda L; \quad G_1 = (a_1/a_2)(1 - L/r_1);$$
$$G_2 = (a_2/a_1)(1 - L/r_2).$$

It can be seen from (2.6.35)-(2.6.36) that a passive resonator consisting of two spherical mirrors may be completely described *with the help of only three parameters* N, G_1, and G_2.

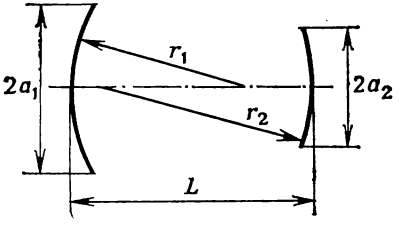


Fig. 2.34

Although these results have been obtained for quadratic apertures which allow a separation of variables in Cartesian coordinates, the conclusion about the existence of only three parameters N, G_1 and G_2 of a resonator is valid even for other forms of apertures, including circular ones.

For *circular* apertures (of radii a_1 and a_2), we make use of *polar coordinates* $\mathbf{R}_1\,(R_1,\,\Phi_1)$, $\mathbf{R}_2\,(R_2,\,\Phi_2)$. The system of integral equations (2.6.15) then assumes the form

$$\frac{i}{\lambda L}\int_0^{2\pi}\int_0^{a_1} u_{mn}(R_1,\Phi_1)\,K(R_1,\Phi_1;\,R_2,\Phi_2)\,R_1\,dR_1\,d\Phi_1 = \gamma'_{nm}v_{mn}(R_2,\Phi_2); \tag{2.6.37a}$$

$$\frac{i}{\lambda L}\int_0^{2\pi}\int_0^{a_2} v_{mn}(R_2,\Phi_2)\,K(R_1,\Phi_1;\,R_2,\Phi_2)\,R_2\,dR_2\,d\Phi_2 = \gamma''_{mn}u_{mn}(R_1,\Phi_1), \tag{2.6.37b}$$

where

$$K(R_1,\Phi_1;\,R_2,\Phi_2) = \exp\left(i\frac{\pi}{\lambda L}\left[g_1R_1^2+g_2R_2^2-2R_1R_2\cos(\Phi_1-\Phi_2)\right]\right). \tag{2.6.38}$$

Here,

$$\int_0^{2\pi}\int_0^{a_1} |\,u_{mn}(R_1,\Phi_1)\,|^2\,R_1\,dR_1\,d\Phi_1 = \int_0^{2\pi}\int_0^{a_2} |\,v_{mn}(R_2,\Phi_2)\,|^2\,R_2\,dR_2\,d\Phi_2. \tag{2.6.39}$$

Introducing new variables and amplitudes:

$$\zeta_1 = R_1/a_1; \quad \zeta_2 = R_2/a_2;$$
$$U_{mn}(\zeta_1,\,\Phi_1) = u_{mn}(\zeta_1 a_1,\,\Phi_1)\,a_1;$$
$$V_{mn}(\zeta_2,\,\Phi_2) = v_{mn}(\zeta_2 a_2,\,\Phi_2)\,a_2;$$

the system of equations (2.6.37)-(2.6.38) can be transformed as follows:

$$iN\int_0^{2\pi}\int_0^{1} U_{mn}(\zeta_1,\Phi_1)\,K(\zeta_1,\Phi_1;\,\zeta_2,\Phi_2)\,\zeta_1\,d\zeta_1\,d\Phi_1 = \gamma'_{mn}V_{mn}(\zeta_2,\Phi_2); \tag{2.6.40a}$$

$$iN\int_0^{2\pi}\int_0^{1} V_{mn}(\zeta_2,\Phi_2)\,K(\zeta_1,\Phi_1;\,\zeta_2,\Phi_2)\,\zeta_2\,d\zeta_2\,d\Phi_2 = \gamma''_{mn}U_{mn}(\zeta_1,\Phi_1), \tag{2.6.40b}$$

where

$$K(\zeta_1,\Phi_1;\,\zeta_2,\Phi_2) = \exp\left(i\pi N\left[G_1\zeta_1^2+G_2\zeta_2^2 - 2\zeta_1\zeta_2\cos(\Phi_2-\Phi_1)\right]\right). \tag{2.6.41}$$

It is apparent from (2.6.40)-(2.6.41) that for circular apertures also, the resonator is described by three parameters N, G_1 and G_2.

Equivalent Resonators[26]. Thus, the nature of the operator $\hat{L}$ and hence its eigenvalues γ and eigenfunctions u are defined in integral equation (2.6.11) through three parameters N, G_1 and G_2. This means that the *field distribution* at the mirrors (described by the

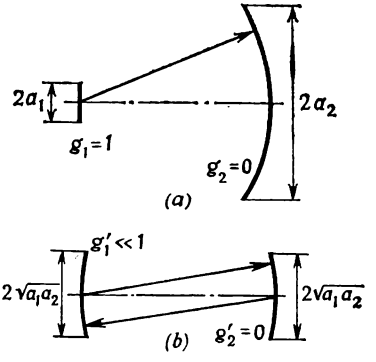


Fig. 2.35

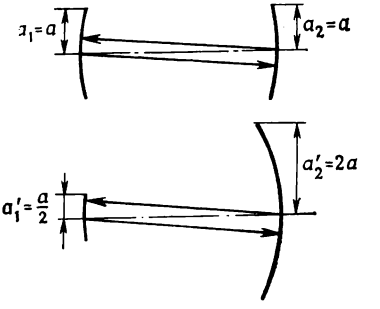


Fig. 2.36

functions u) as well as *diffraction losses* and *resonance frequencies* (expressed in terms of eigenvalues γ) are fully defined by the parameters N, G_1 and G_2.

Resonators with identical diffraction losses, resonance frequencies and field distribution at mirrors are called *equivalent* (*identical*) resonators. From the above discussion it follows that equivalent resonators must have identical Fresnel numbers N, identical values of G_1 and of G_2. Suppose that one of the resonators is described by the parameters

$$N=\frac{a_1a_2}{\lambda L};\quad G_1=\frac{a_1}{a_2}\left(1-\frac{L}{r_1}\right);\quad G_2=\frac{a_2}{a_1}\left(1-\frac{L}{r_2}\right),$$

while another resonator is described by the parameters

$$N'=\frac{a_1'a_2'}{\lambda L'};\quad G_1'=\frac{a_1'}{a_2'}\left(1-\frac{L'}{r_1'}\right);\quad G_2'=\frac{a_2'}{a_1'}\left(1-\frac{L'}{r_2'}\right).$$

The *equivalence condition* for these resonators is given by

$$\boxed{N=N';\quad G_1=G_1';\quad G_2=G_2'}. \tag{2.6.42}$$

It follows from (2.6.42) that if the transverse dimensions of a resonator (parameters a_1 and a_2) are increased ε-fold, and at the same time the longitudinal dimensions (parameters L, r_1, and r_2) are increased ε^2-fold, the resonator thus obtained will be equivalent

[26] Equivalence of resonators has been discussed in [23, 15].

to the initial one. It should be noted that in these resonators, not only parameters G, but also parameters g are identical.

An identity of parameters g is, of course, not a must for equivalence of resonators. For example, let us consider a semiconcentric resonator ($g_1 = 1$, $g_2 = 0$), in which $a_1 \ll a_2$ (Fig. 2.35*a*). In accordance with (2.6.42), its equivalent resonator has the same length and $a_1' = a_2' = \sqrt{a_1 a_2}$, $g_1' = a_1/a_2$ and $g_2' = 0$ (Fig. 2.35*b*). Since $a_1 \ll a_2$, we have $g_1' \ll 1$. Hence the resonator in Fig. 2.35*b* is nearly confocal. Thus a semiconcentric resonator in which the aperture of the plane mirror is much smaller than that of the spherical mirror ($a_1 \ll a_2$), is in fact equivalent to a confocal resonator of the same length, in which the apertures a_1' and a_2' of mirrors are identical, and $a_1' = a_2' = \sqrt{a_1 a_2}$.

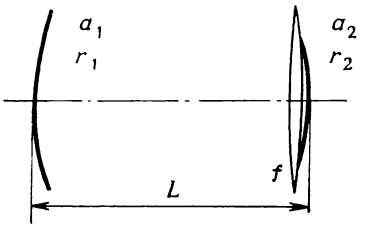


Fig. 2.37

Strictly speaking, a *confocal resonator* may be equivalent only to a confocal resonator. This is so because if $g_1 = g_2 = 0$, the equivalence conditions can be satisfied only for $g_1' = g_2' = 0$. It should be noted that two confocal resonators may be equivalent *irrespective* of the ratio of mirror apertures as long as they have the same Fresnel number. In other words, the condition of equivalence of two confocal resonators has the form

$$\boxed{a_1 a_2 / L = a_1' a_2' / L'} . \qquad (2.6.43)$$

By way of example, two equivalent confocal resonators of the same length ($a_1 a_2 = a_1' a_2'$) are shown in Fig. 2.36.

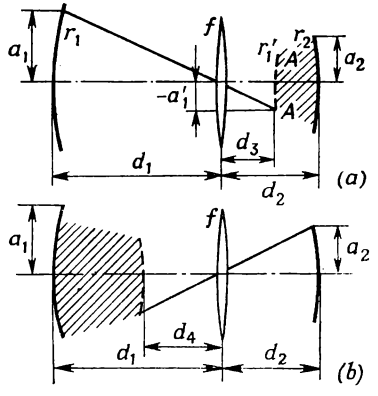


Fig. 2.38

Resonator Equivalent to a Resonator with an Integral Lens. Let us first consider a resonator in which a thin lens with focal length f and an indefinitely large aperture is placed directly in front of one of the mirrors, say the right one (Fig. 2.37). A combination of a mirror of radius r_2 and a lens of focal length f is optically equivalent to a mirror of radius $r_2 f/(r_2 + f)$. Consequently, the resonator with a lens shown in Fig. 2.37 is equivalent to a resonator without a lens, whose right mirror has a radius of curvature $r_2 f/(r_2 + f)$. The param-

eters of this resonator are given by

$$N=\frac{a_1a_2}{\lambda L};\quad G_1=\frac{a_1}{a_2}\left(1-\frac{L}{r_1}\right);\quad G_2=\frac{a_2}{a_1}\left(1-L\frac{r_2+f}{r_2f}\right). \tag{2.6.44}$$

A more interesting situation arises when the lens is situated at some distance from the mirrors [32]. Such a resonator is shown in Fig. 2.38*a*. Here d_1 and d_2 represent the distance of the lens from the left and right mirror respectively. The image of the left mirror produced by the lens (together with the field distribution on it) is shown in the figure by the dashed curve AA, situated at a distance d_3 from the lens. Let us denote the radius of curvature of the curve AA by r_1'. Then a_1 is transformed into a_1' by the lens (see figure). The shaded resonator of length $d_2 - d_3$ in the figure is a resonator without a lens equivalent to the initial resonator with a lens. Taking into consideration the relations

$$d_3 = d_1f/(d_1 - f);\quad a_1/a_1' = -d_1/d_3 = 1 - d_1/f,$$

we obtain the following parameters for the equivalent resonator without a lens

$$N=\frac{a_1'a_2}{\lambda(d_2-d_3)}=\frac{a_1a_2}{\lambda(d_1+d_2-d_1d_2/f)}; \tag{2.6.45}$$

$$G_2=\frac{a_2}{a_1'}\left(1-\frac{d_2-d_3}{r_2}\right)=\frac{a_2}{a_1}\left[1-\frac{d_1}{f}-\frac{1}{r_2}\left(d_1+d_2-\frac{d_1d_2}{f}\right)\right]. \tag{2.6.46}$$

In order to determine the parameter G_1, one should first find r_1'. However, we shall not do this, but rather consider another equivalent resonator without a lens. This resonator is shown in Fig. 2.38*b* (shaded region). We shall use the analogy with the case considered earlier. Since

$$d_4 = d_2f/(d_2 - f);\quad a_2/a_2' = -d_2/d_4 = 1 - d_2/f,$$

we get

$$N=\frac{a_1a_2'}{\lambda(d_1-d_4)}=\frac{a_1a_2}{\lambda(d_1+d_2-d_1d_2/f)}; \tag{2.6.47}$$

$$G_1=\frac{a_1}{a_2'}\left(1-\frac{d_1-d_4}{r_1}\right)=\frac{a_1}{a_2}\left[1-\frac{d_2}{f}-\frac{1}{r_1}\left(d_1+d_2-\frac{d_1d_2}{f}\right)\right]. \tag{2.6.48}$$

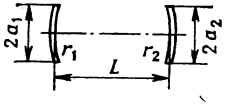
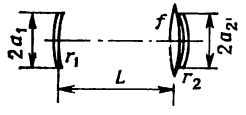
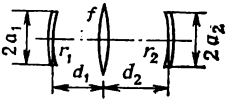
As expected, the results (2.6.47) and (2.6.45) are identical. Since each lensless resonator shaded in Fig. 2.38 is equivalent to the initial resonator with a lens, these two lensless resonators are equivalent to each other. Using (2.6.45), (2.6.46), and (2.6.48), we can write down the parameters for the equivalent resonator without

a lens:

$$\left.\begin{aligned} N &= \frac{a_1 a_2}{\lambda (d_1 + d_2 - d_1 d_2 / f)}; \\ G_1 &= \frac{a_1}{a_2}\left[1 - \frac{d_2}{f} - \frac{1}{r_1}\left(d_1 + d_2 - \frac{d_1 d_2}{f}\right)\right]; \\ G_2 &= \frac{a_2}{a_1}\left[1 - \frac{d_1}{f} - \frac{1}{r_2}\left(d_1 + d_2 - \frac{d_1 d_2}{f}\right)\right]. \end{aligned}\right\} \qquad (2.6.49)$$

Table 2.5 gives a comparison of three resonators: one without a lens, another with a lens placed directly in front of a mirror, and

TABLE 2.5

	$\begin{pmatrix} 1 & L \\ 0 & 1 \end{pmatrix}$	$N = \frac{a_1 a_2}{\lambda}\,\frac{1}{L}$ $G = \frac{a}{a_2}\left(1 - \frac{1}{r_1} L\right)$ $G_2 = \frac{a_2}{a_1}\left(1 - \frac{1}{r^2} L\right)$
	$\begin{pmatrix} 1 & L \\ -\frac{1}{f} & 1 - \frac{L}{f} \end{pmatrix}$	$N = \frac{a_1 a_2}{\lambda}\,\frac{1}{L}$ $G_1 = \frac{a_1}{a_2}\left(1 - \frac{1}{r_1} L\right)$ $G^2 = \frac{a_2}{a_1} \times$ $\times \left[\left(1 - \frac{L}{f}\right) - \frac{1}{r_2} L\right]$
	$\begin{pmatrix} 1 - \frac{d_2}{f} & d_1 + d_2 - \frac{d_1 d_2}{f} \\ -\frac{1}{f} & 1 - \frac{d_1}{f} \end{pmatrix}$	$N = \frac{a_1 a_2}{\lambda}\,\frac{1}{d_1 + d_2 - d_1 d_2 / f}$ $G_1 = \frac{a_1}{a_2}\left[\left(1 - \frac{d_2}{f}\right) - \right.$ $\left. - \frac{1}{r_1}\left(d_1 + d_2 - \frac{d_1 d_2}{f}\right)\right]$ $G_2 = \frac{a_2}{a_1}\left[\left(1 - \frac{1}{f}\right) -\right.$ $\left. - \frac{1}{r_2}\left(d_1 + d_2 - \frac{d_1 d_2}{f}\right)\right]$

the third one with a lens placed at a certain distance from the mirrors. The transfer matrices for a ray passing from the left mirror to the right one are given for these resonators. The first two matrices were considered in Sec. 2.4 (see (2.4.18) and (2.4.22)), while the third is the matrix $M(d_1 \to f \to d_2) = M(d_2)\, M(f)\, M(d_1)$. The

table also gives the parameters N, G_1 and G_2 for equivalent lensless resonators. These values have been obtained by using (2.6.44) and (2.6.49).

Looking at the table, we can easily perceive a certain *general rule*. Suppose that a ray passing from the left mirror (with radius of curvature r_1) to the right mirror (with radius of curvature r_2) is transformed in accordance with a certain matrix $\begin{pmatrix} A & B \\ C & D \end{pmatrix}$. This matrix takes into account both the free space inside the resonator, as well as the possible optical elements in the resonator, deployed in a certain manner along its optical axis. The general rule states that this resonator is equivalent to an "empty" resonator with the following parameters [32]:

$$N=\frac{a_1a_2}{\lambda B};\quad G_1=\frac{a_1}{a_2}\left(A-\frac{B}{r_1}\right);\quad G_2=\frac{a_2}{a_1}\left(D-\frac{B}{r_2}\right). \qquad (2.6.50)$$

Diaphragm Resonator. Let us suppose that inside a resonator of length L there is a *diaphragm* or an absorbing surface with a hole of diameter $2a$. We assume the apertures of the mirrors to be *indefinitely large*. The distance of the left mirror (radius of curvature r_1) and the right mirror (radius of curvature r_2) from the diaphragm is denoted by d_1 and d_2 respectively, $d_1 + d_2 = L$.

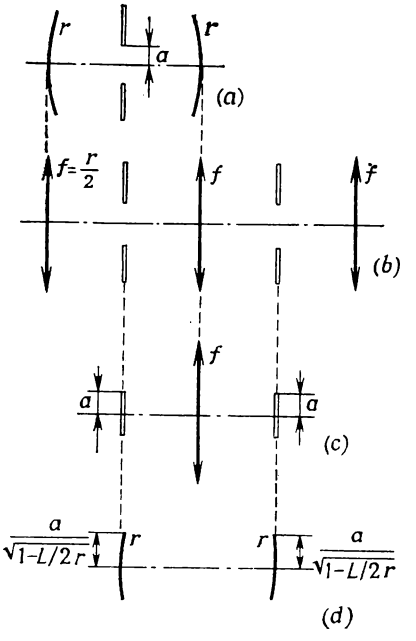


Fig. 2.39

In the special case of a *symmetric resonator* (when $d_1 = d_2 = L/2$ and $r_1 = r_2 = r$), it is convenient to use the analogy between an open resonator and a lens waveguide. The diaphragm resonator shown in Fig. 2.39*a* is optically equivalent to the lens waveguide shown in Fig. 2.39*b*. This waveguide, in turn, is equivalent to the plane-parallel resonator with a lens in the middle, as shown in Fig. 2.39*c*. The apertures of the mirrors of this resonator are equal to the aperture of the diaphragm of the initial resonator, and the focal length of the lens is $f = r/2$. Using (2.6.49), we obtain the parameters of the lensless resonator, equivalent to the resonator shown in Fig. 2.39*c*, and hence to

the resonator shown in Fig. 2.39*a*:

$$N=\frac{a^2}{\lambda L\,(1-L/2r)}\,;\quad G_1=G_2=1-\frac{L}{r}\,. \tag{2.6.51}$$

This lensless resonator is shown in Fig. 2.39*d*. Unlike the initial diaphragm resonator, it has mirrors with a *finite aperture* whose radius is equal to $a\sqrt{1-L/2r}$, where a is the radius of the aperture of the diaphragm of the initial resonator.

It should be noted that the result (2.6.51) may be obtained from (2.6.50), if we consider that the matrix $\begin{pmatrix} A & B \\ C & D \end{pmatrix}$ for the resonator in Fig. 2.39*c* has the form

$$M\left(\frac{L}{2}\right)M(f)\,M\left(\frac{L}{2}\right)=\begin{pmatrix} 1-\frac{L}{2f} & L-\frac{L^2}{4f} \\ -\frac{1}{f} & 1-\frac{L}{2f} \end{pmatrix}$$

$$=\begin{pmatrix} 1-\frac{L}{r} & L-\frac{L^2}{2r} \\ -\frac{2}{r} & 1-\frac{L}{r} \end{pmatrix}.$$

We should then put $a_1=a_2=a$, and $1/r_1=1/r_2=0$ in (2.6.50).

An *asymmetric diaphragm resonator does not have*, generally speaking, an equivalent "empty" resonator. However, it can be shown [33] that in the general case of an asymmetric diaphragm resonator (with indefinitely large mirror apertures), the *diffraction losses* as well as *field amplitude distribution* at the mirrors are determined by *three parameters*. The following combinations of a, d_1, d_2, r_1 and r_2 serve as these three parameters:

$$\gamma=\frac{a^2}{4\lambda}\left[\frac{r_1}{d_1\,(r_1-d_1)}+\frac{r_2}{d_2\,(r_2-d_2)}\right]; \tag{2.6.52a}$$

$$\bar{g}=\frac{(r_1-2d_1)\,d_2\,(r_2-d_2)+(r_2-2d_2)\,d_1\,(r_1-d_1)}{r_1d_2\,(r_2-d_2)+r_2d_1\,(r_1-d_1)}\,; \tag{2.6.52b}$$

$$\beta=\frac{r_1d_2\,(r_2-d_2)-r_2d_1\,(r_1-d_1)}{r_1d_2\,(r_2-d_2)+r_2d_1\,(r_1-d_1)}\,. \tag{2.6.52c}$$

The result (2.6.52) follows from the corresponding integral equations describing the propagation of radiation in a diaphragm resonator.

For $r_1=r_2=r$ and $d_1=d_2=L/2$, (2.6.52) leads to

$$\gamma=\frac{a^2}{\lambda L\,(1-L/2r)}\,;\quad \bar{g}=1-\frac{L}{r}\,;\quad \beta=0. \tag{2.6.53}$$

Comparing (2.6.53) and (2.6.51), we conclude that for a symmetric diaphragm resonator, the parameter γ is identical to the Fresnel number N, while the parameter $\bar{g}$ coincides with the parameters G_1 and G_2 for an equivalent lensless resonator.

Let us consider a confocal resonator ($r_1 = r_2 = L$) with a diaphragm placed arbitrarily along its axis. In this case, the relation (2.6.52) is considerably simplified:

$$\gamma = a^2 L/[2\lambda d_1 (L - d_1)]; \quad \bar{g} = 0; \quad \beta = 0. \qquad (2.6.54)$$

It can be seen from this that two confocal diaphragm resonators have identical diffraction losses and identical field amplitude distributions at the mirrors, if the following condition is satisfied:

$$a^2 L/[d_1 (L - d_1)] = (a')^2 L'/[d_1' (L' - d_1')] \qquad (2.6.55)$$

(where a, L, and d_1 are the parameters of one resonator, while a', L', and d_1' are the parameters of the other resonator).

It should be recalled that a confocal resonator without a diaphragm, consisting of mirrors with finite (and unequal) apertures, is characterised by the parameters $N = a_1 a_2/\lambda L$, $G_1 = 0$, $G_2 = 0$. The parameter $\gamma = a^2 L/2\lambda d_1 (L - d_1)$ in a confocal diaphragm resonator with mirrors of infinitely large apertures plays the same role as the Fresnel number $N = a_1 a_2/\lambda L$ in a confocal resonator without a diaphragm and with finite apertures of the mirrors. Both γ and N define the diffraction losses in the respective confocal resonators. A large value of these parameters ($N \gg 1$, $\gamma \gg 1$) means small diffraction losses.

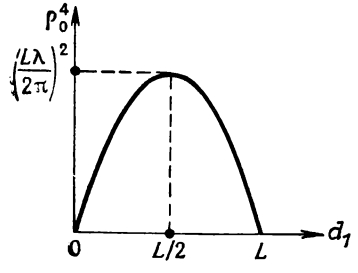


Fig. 2.40

Using the relation (2.6.54), let us consider the dependence of $1/\gamma$ on d_1 for given values of L and a (Fig. 2.40). It can be easily seen that the biggest diffraction losses in a confocal resonator take place when the diaphragm is placed in the middle of the resonator ($d_1 = L/2$). If we bring the diaphragm closer to the mirror, the diffraction losses start decreasing rapidly (in spite of the fact that the aperture of the diaphragm remains unchanged). By placing the diaphragm indefinitely close to the mirror, we can make the parameter γ indefinitely large. This fact has an interesting physical explanation (see Sec. 2.9).

2.7. GAUSSIAN BEAMS

General Remarks. Gaussian Beam Shape. In order to describe the field structure of a light beam originating in a stable resonator, the *Gaussian beam* model is frequently employed. Such beams are characterised by a rapid decrease in the amplitude of field as we move away from the beam axis. The amplitude decreases in accordance with the *Gaussian function* $A \exp(-x^2/\rho^2)$ (Fig. 2.41). The parameter ρ plays the role of the effective radius of the beam.

The simplest type of Gaussian beam corresponds to the fundamental transverse mode. The dependence of the modulus of the field amplitude of the fundamental mode on the transverse coordinate is completely described by the Gaussian function

$$|u(x, y)| \propto \exp\left(-\frac{x^2+y^2}{\rho^2}\right). \tag{2.7.1}$$

For higher-order modes, the field amplitude of a Gaussian beam is usually expressed through the product of the Gaussian function and Hermitian polynomials (i.e. through *Hermite-Gauss polynomials*):

$$|u_{mn}(x, y)| \propto H_m\left(\sqrt{2}\,\frac{x}{\rho}\right) H_m\left(\sqrt{2}\,\frac{y}{\rho}\right) \exp\left(-\frac{x^2+y^2}{\rho^2}\right). \tag{2.7.2}$$

Figure 2.42 shows schematically, for a certain resonator, the shape of a Gaussian beam, as determined by the parameter ρ. The radius ρ

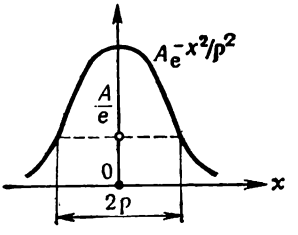


Fig. 2.41

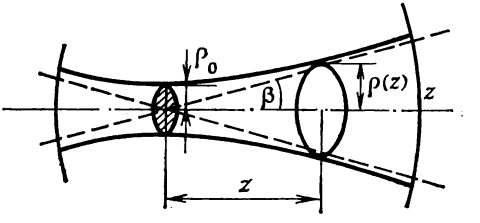


Fig. 2.42

of the beam changes along the length of the resonator (along the beam axis). At a certain point on the axis, the beam radius assumes its minimum value which we shall denote as ρ_0. The reference plane passing through the point is called the *construction plane of the beam* (or the "neck" of the beam) (see the shaded cross section in Fig. 2.42). We shall consider the beam radius as a function of distance z measured from the constriction. It will be shown later that

$$\rho^2 = \rho_0^2 + (\lambda/\pi)^2 (z^2/\rho_0^2). \tag{2.7.3}$$

Relation (2.7.3) is the equation of a surface bounding the Gaussian beam field in space. This surface is called the *caustic surface* or, simply the *caustic*. It is a hyperboloid of revolution and its cross section by the plane passing through the beam axis is a hyperbola (see the solid lines in Fig. 2.42).

The asymptotes of this hyperbola are shown by dashed lines. Let β be the angle between an asymptote and the beam axis. In order to find this angle, we should first transform Eq. (2.7.3) to a canonical form

$$(\rho^2/a^2) - (z^2/b^2) = 1. \tag{2.7.4}$$

Comparing Eqs. (2.7.4) and (2.7.3), we conclude that $a = \rho_0$ and $b = \pi\rho_0^2/\lambda$. The ratio a/b is the tangent of the angle β. Thus

$$\tan \beta = \lambda/\pi\rho_0. \tag{2.7.5}$$

It is assumed that the Gaussian beams considered here have a rotational symmetry around the beam axis (*circular Gaussian beams*). Such beams are found in resonators consisting of ideally spherical mirrors under the condition that there are no elements inside the resonator to violate the rotational symmetry around the optical axis. In practice, however, the sphericity of resonator mirrors may be violated or even deliberately distorted (*astigmatic resonators*). Besides, the rotational symmetry of the resonator may be violated by elements inside it, for example, inclined plane-parallel plates (in particular, Brewster windows in a gas-discharge tube). In such cases, the cross section of the light beam is not circular but elliptical. Such beams are called *elliptical*. Figure 2.43 shows an elliptical Gaussian beam in an astigmatic resonator.

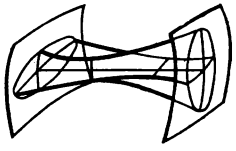


Fig. 2.43

The theory of Gaussian beams has been described in [22, 32, 34, 35, 17]; see also [4, 7, 15]. Goncharenko [17] has discussed both circular as well as elliptical Gaussian beams.

Propagation of a Gaussian Beam in Free Space. We make use of the fact that the constriction plane of a Gaussian beam is a constant-phase plane. In other words, the Gaussian beam has a *plane wavefront* at the point on the axis corresponding to the constriction. This is in accordance with the symmetrical form of the Gaussian beam with respect to the constriction plane.

Let us consider only the *fundamental mode* for the present. The Gaussian beam field in the constriction plane P_0 is written in the form

$$u(\xi, \eta) = A \exp[-(\xi^2 + \eta^2)/\rho_0^2]. \tag{2.7.6}$$

Here ξ and η are the Cartesian coordinates in the P_0 plane. Since the wavefront is plane, there is no phase factor of the type $\exp[i\Phi(\xi, \eta)]$ in the expression for $u(\xi, \eta)$.

If the Gaussian beam field is specified in a certain plane (for example, in the constriction plane), the field for this beam may be determined at any other reference plane by considering, in accordance with the diffraction theory, the propagation of radiation from the initial plane to the reference plane chosen by us. Let us choose the reference plane P_z at a distance z from the constriction plane P_0. The field $u(x, y, z)$ of the Gaussian beam in the P_z plane is given by the diffraction integral (2.6.6) into which the value of the field (2.7.6) is substituted, and L is replaced by z. Thus,

$$u(x, y, z) = -\frac{i}{\lambda z} A \exp\left(i \frac{2\pi}{\lambda} z\right)$$

$$\times \iint_{P_0} \exp\left(-\frac{\xi^2+\eta^2}{\rho_0^2}\right) \exp\left(\frac{i\pi}{\lambda z}[(x-\xi)^2+(y-\eta)^2]\right) d\xi\, d\eta. \tag{2.7.7}$$

Using (2.7.7), we get an expression for the *complex amplitude* of the fundamental mode field of the Gaussian beam at a distance z from the constriction plane of the beam[27]:

$$u(x, y, z) = A \frac{(i\pi\rho_0^2/\lambda z)}{(i\pi\rho_0^2/\lambda z) - 1} \exp\left(i \frac{2\pi}{\lambda} z\right)$$
$$\times \exp\left[i \frac{(x^2+y^2)\,\pi/\lambda z}{1+(\pi\rho_0^2/\lambda z)^2}\right] \exp\left[-\frac{(x^2+y^2)\,(\pi\rho_0/\lambda z)^2}{1+(\pi\rho_0^2/\lambda z)^2}\right]. \quad (2.7.8)$$

The transverse dimensions of the beam are determined by the factor

$$\exp\left[-\frac{(x^2+y^2)\,(\pi\rho_0/\lambda z)^2}{1+(\pi\rho_0^2/\lambda z)^2}\right]$$

in (2.7.8), which decreases rapidly with increasing distance from the beam axis. From the form of this factor, it follows that the radius ρ of the Gaussian beam at a distance z from the constriction is given by the expression (2.7.3):

$$\rho^2(z) = \frac{1+(\pi\rho_0^2/\lambda z)^2}{(\pi\rho_0/\lambda z)^2} = \rho_0^2 + \left(\frac{\lambda}{\pi}\right)^2 \frac{z^2}{\rho_0^2}.$$

It should be noted that

$$\exp(i \arctan \alpha) = \cos(\arctan \alpha) + i \sin(\arctan \alpha) = \frac{1+i\alpha}{\sqrt{1+\alpha^2}}. \quad (2.7.9)$$

Taking (2.7.9) into account, we get

$$\frac{(i\pi\rho_0^2/\lambda z)}{(i\pi\rho_0^2/\lambda z)-1} = \frac{1}{1+i\,(\lambda z/\pi\rho_0^2)} = \frac{\exp\left[-i \arctan\,(\lambda z/\pi\rho_0^2\right.}{\sqrt{1+(\lambda z/\pi\rho_0^2)}}.$$

In accordance with (2.7.3),

$$[1 + (\lambda z/\pi\rho_0^2)]^{-1/2} = \rho_0/\rho\,(z).$$

Consequently, the expression (2.7.8) may be rewritten in the form

$$u(x, y, z) = A \frac{\rho_0}{\rho\,(z)} \exp\left[-(x^2+y^2)/\rho^2(z)\right]$$
$$\times \exp\left\{i\left[\frac{2\pi}{\lambda} z - \arctan\left(\frac{\lambda z}{\pi\rho_0^2}\right) + \frac{(x^2+y^2)\,\pi/\lambda z}{1+(\pi\rho_0^2/\lambda z)^2}\right]\right\}. \quad (2.7.10)$$

Radius of Curvature of the Constant-phase Surface. It follows from (2.7.10) that the propagation of a Gaussian beam from P_0 plane to P_z plane is accompanied by a *phase shift* given by

$$\Phi = \frac{2\pi}{\lambda} z - \arctan\left(\frac{\lambda z}{\pi\rho_0^2}\right) + \frac{(x^2+y^2)\,\pi/\lambda z}{1+(\pi\rho_0^2/\lambda z)^2}. \quad (2.7.11)$$

Upon propagation from P_0 to P_z, the initially *plane* wavefront of the beam becomes *spherical*. Hence the expression describing the

[27] For detailed calculation, see Appendix 2.

phase shift acquires a term depending on transverse coordinates

$$\varphi(x, y, z) = \frac{(x^2+y^2)\,\pi/\lambda z}{1+(\pi\rho_0^2/\lambda z)^2}. \qquad (2.7.12)$$

Let us denote by $R(z)$ the radius of curvature of the constant-phase surface, intersecting the beam axis at the point z (at a distance z from the constriction), see Fig. 2.44. It can be seen from the figure that the phase shift at the point x, y of the P_z plane, compared to the point 0,0 in the same plane, is $(2\pi/\lambda)\,d(x, y)$. Since this phase shift is defined by the expression (2.7.12), we get

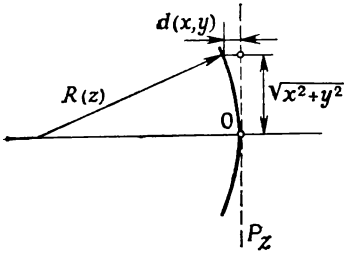


Fig. 2.44

$$d(x, y) = \frac{(x^2+y^2)/2z}{1+(\pi\rho_0^2/\lambda z)^2}. \qquad (2.7.13)$$

Further, we take into account that $R^2 - (x^2 + y^2) = [R - d(x, y)]^2$ (see figure). Since $d \ll R$, it follows that $(R - d)^2 \approx R^2(1 - 2d/R) = R^2 - 2Rd$ and hence $2Rd \approx x^2 + y^2$. Substituting this result into (2.7.13), we get the following expression for the radius of curvature $R(z)$ of the constant-phase surface:

$$\boxed{R(z) = z\,[1+(\pi\rho_0^2/\lambda z)^2]}. \qquad (2.7.14)$$

Taking (2.7.14) into consideration, we can rewrite (2.7.10) in the form

$$\boxed{u(x, y, z) = A\frac{\rho_0}{\rho(z)}\exp\left[-\frac{x^2+y^2}{\rho^2(z)}\right] \times \exp\left\{i\left[\frac{2\pi}{\lambda}z - \arctan\left(\frac{\lambda z}{\pi\rho_0^2}\right) + \frac{(x^2+y^2)\,\pi}{\lambda R(z)}\right]\right\}}. \qquad (2.7.15)$$

It follows from (2.7.14) that at large distances from the beam constriction, for which the inequality

$$z \gg \pi\rho_0^2/\lambda \qquad (2.7.16)$$

is satisfied, the radius of curvature of the constant-phase surface may be given by the expression $R(z) \approx z$ (here, we speak of a "far region"). Thus in a *far region*, the Gaussian beam is converted into a spherical wave and may be considered in the geometrical approximation. This approximation is not valid for the *near region* ($z \leqslant \pi\rho_0^2/\lambda$); *the light rays in this region are not straight lines* (see Fig. 2.45*a*. Here the light rays are shown by solid lines while the cross sections of the constant-phase surfaces are shown by dashed

lines). The dependence R vs. z, obtained from the relation (2.7.14), is shown in Fig. 2.45*b*.

Basic Relations Between Parameters of a Gaussian Beam. The parameters of a Gaussian beam are the radius ρ of the beam and the radius of curvature R of the constant-phase surface, at a distance z

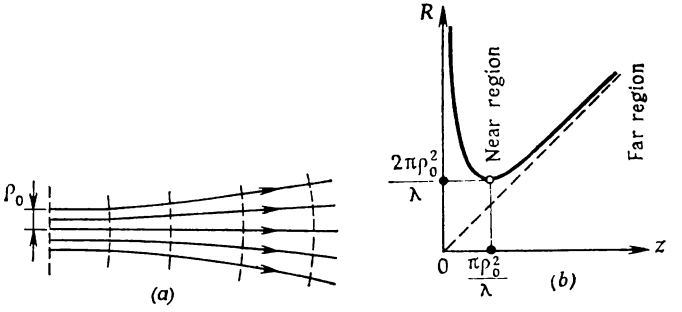


Fig. 2.45

from the beam constriction of radius ρ_0 (see Fig. 2.46). The results obtained above lead to a number of relations connecting ρ, R, z, and ρ_0. These relations can be written as

$$\boxed{\rho^2 = \rho_0^2 + (\lambda/\pi)^2 (z^2/\rho_0^2)}\ ; \tag{2.7.3}$$

$$\boxed{\rho_0^4 = (\lambda/\pi)^2 z (R - z)}\ ; \tag{2.7.17}$$

$$\boxed{\rho^2\rho_0^2 = (\lambda/\pi)^2 Rz}\ . \tag{2.7.18}$$

The relation (2.7.17) follows directly from (2.7.14), while (2.7.18) follows from (2.7.3) by substituting into it the value of z^2 obtained from (2.7.17).

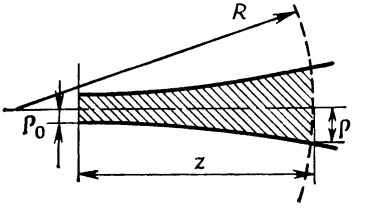


Fig. 2.46

Complex Parameters of a Gaussian Beam. The expression (2.7.15) for the field amplitude u (x, y, z) may be expressed in a more com-

pact form if we introduce the *complex parameters* $q(z)$ and $R(z)$ of the beam, as proposed by Kogelnik [32]. These parameters are defined as follows:

$$\boxed{1/q = 1/R + i\lambda/\pi\rho^2}\ ; \tag{2.7.19}$$

$$\boxed{P = -\arctan(z\lambda/\pi\rho_0^2) - i\ln(\rho_0/\rho)}\ . \tag{2.7.20}$$

Using these parameters, we can rewrite (2.7.15) in the form

$$\boxed{u(x, y, z) = A\exp\left\{i\left[P(z) + (x^2+y^2)\frac{\pi}{\lambda q(z)}\right]\right\} \times \exp\left(i\frac{2\pi}{\lambda}z\right)}\ . \tag{2.7.21}$$

Gaussian Beam as a Solution of a Parabolic Equation. The expression (2.7.21) describes the fundamental mode field. Keeping in view the subsequent generalisation of results for higher-order modes, we shall prove on the example of the fundamental mode that the Gaussian beam is a solution of a *parabolic* equation.

Let us first write the familiar wave equation for a monochromatic electromagnetic wave propagating in a charge free space:

$$\nabla^2 u(x, y, z) + (4\pi^2/\lambda^2)\, u(x, y, z) = 0. \tag{2.7.22}$$

The wave amplitude $u(x, y, z)$ is written in the form

$$u(x, y, z) = U(x, y, z)\exp(i\,2\pi z/\lambda). \tag{2.7.23}$$

Substituting (2.7.23) into (2.7.22), we get the equation

$$\frac{\partial^2 U}{\partial x^2} + \frac{\partial^2 U}{\partial y^2} + \frac{\partial^2 U}{\partial z^2} + i\frac{4\pi}{\lambda}\frac{\partial U}{\partial z} = 0. \tag{2.7.24}$$

We assume that the function $U(x, y, z)$ depends relatively weakly on the coordinate z, so that the following inequality is valid:

$$\left|\frac{\partial^2 U}{\partial z^2}\right| \ll \frac{4\pi}{\lambda}\left|\frac{\partial U}{\partial z}\right|. \tag{2.7.25}$$

Equation (2.7.24) can then be transformed into

$$\frac{\partial^2 U}{\partial x^2} + \frac{\partial^2 U}{\partial y^2} + i\frac{4\pi}{\lambda}\frac{\partial U}{\partial z} = 0. \tag{2.7.26}$$

This equation is called a *parabolic equation.*

We shall now show that the function $U(x, y, z)$ having the form (see (2.7.21))

$$U(x, y, z) = A\exp\{i[P(z) + (x^2 + y^2)\,\pi/\lambda q(z)]\}, \tag{2.7.27}$$

is a solution of the parabolic equation (2.7.26). Substituting (2.7.27) into (2.7.26), we get

$$\frac{4\pi}{\lambda}\left[\frac{dP}{dz}-\frac{i}{q(z)}\right]+\frac{4\pi^2(x^2+y^2)}{\lambda^2 q^2(z)}\left(1-\frac{dq}{dz}\right)=0.$$

This equation must be satisfied for all values of x and y. Consequently, the following equations must be valid:

$$dP/dz - i/q(z) = 0; \quad 1 - dq/dz = 0. \tag{2.7.28}$$

It can be easily shown by using Eqs. (2.7.19) and (2.7.20) that Eqs. (2.7.28) are actually satisfied.

Generalisation to Higher-order Modes. Using (2.7.21) and (2.7.2), we can write the field amplitude for the mn-th mode of a Gaussian beam in the following form:

$$u_{mn}(x, y, z) = AH_m\left(\sqrt{2}\,\frac{x}{\rho(z)}\right)H_n\left(\sqrt{2}\,\frac{y}{\rho(z)}\right)$$
$$\times \exp\left\{i\left[P(z)+(x^2+y^2)\frac{\pi}{\lambda q(z)}+\Phi_{mn}(z)\right]\right\}\exp\left(i\frac{2\pi}{\lambda}z\right), \tag{2.7.29}$$

where Φ_{mn} is yet to be determined.

Assuming that, like the fundamental mode, the mn-th mode is a solution of the parabolic equation, we substitute (2.7.29) (without the factor $\exp(i2\pi z/\lambda)$) into (2.7.26). This substitution transforms Eq. (2.7.26) into

$$\frac{1}{H_m}\left(\frac{d^2H_m}{dX^2}-2X\frac{dH_m}{dX}\right)+\frac{1}{H_n}\left(\frac{d^2H_n}{dY^2}-2Y\frac{dH_n}{dY}\right)$$
$$-\frac{2\pi}{\lambda}\rho^2\frac{d\Phi_{mn}}{dz}=0, \tag{2.7.30}$$

where

$$X=\sqrt{2}\,x/\rho; \quad Y=\sqrt{2}\,y/\rho.$$

Further, we consider that the Hermite polynomial $H_m(X)$ of the m-th order satisfies the differential equation[28]

$$\frac{d^2H_m}{dX^2}-2X\frac{dH_m}{dX}+2mH_m=0. \tag{2.7.31}$$

Comparing (2.7.30) and (2.7.31), we conclude that the phase shift Φ_{mn} must satisfy the equation

$$\frac{\pi}{\lambda}\rho^2(z)\frac{d\Phi_{mn}}{dz}=-(m+n). \tag{2.7.32}$$

Taking (2.7.3) into account, we get

$$\int_0^z d\Phi_{mn}=-\frac{m+n}{\pi\rho_0^2/\lambda}\int_0^z\frac{dz}{1+(\lambda z/\pi\rho_0^2)^2}=-(m+n)\arctan\left(\frac{\lambda z}{\pi\rho_0^2}\right).$$

[28] See Appendix 1.

Since $\Phi_{mn}(0) = 0$, it follows that

$$\Phi_{mn}(z) = -(m + n) \arctan(\lambda z/\pi\rho_0^2). \qquad (2.7.33)$$

Using this result in (2.7.29) and changing over from parameters q and P to parameters ρ and R, we get the following expression for the field amplitude of the mn-th mode:

$$u_{mn}(x, y, z) = A\frac{\rho_0}{\rho(z)} H_m\left(\sqrt{2}\,\frac{x}{\rho(z)}\right) H_n\left(\sqrt{2}\,\frac{y}{\rho(z)}\right) \times \exp\left[-\frac{x^2+y^2}{\rho^2(z)}\right] \exp\left\{i\left[\frac{2\pi}{\lambda} z - (m+n+1) \times \arctan\left(\frac{z\lambda}{\pi\rho_0^2}\right) + \frac{(x^2+y^2)\pi}{\lambda R(z)}\right]\right\}. \qquad (2.7.34)$$

It should be noted that the radius ρ of the beam and the radius of curvature R of the constant-phase surface (and hence the parameter q) are *independent* of mode indices m and n. This means that while using these parameters of a Gaussian beam, it is sufficient to consider just the fundamental mode.

2.8. TRANSFORMATION AND MATCHING OF GAUSSIAN BEAMS

In order to describe the transformation of a Gaussian beam upon its propagation from the reference plane $z = z_1$ to the reference plane $z = z_2$, we must indicate the rule for change-over from parameters $\rho(z_1)$, $R(z_1)$ to parameters $\rho(z_2)$, $R(z_2)$, or, in other words, the rule for change-over from $q(z_1)$ to $q(z_2)$.

Transformation of a Gaussian Beam in Free Space. Let us first prove that

$$q = z - i\pi\rho_0^2/\lambda. \qquad (2.8.1)$$

As a matter of fact, we get from (2.7.19)

$$q = R\frac{1 - i(\lambda R/\pi\rho^2)}{1 + (\lambda R/\pi\rho^2)^2}.$$

It follows from (2.7.18) that $\lambda R/\pi\rho^2 = \pi\rho_0^2/\lambda z$. Hence

$$q = R\frac{1 - i(\pi\rho_0^2/\lambda z)}{1 + (\pi\rho_0^2/\lambda z)^2}.$$

This leads to the result (2.8.1) if we take into account the relation (2.7.14).

The rule for transformation of a Gaussian beam in free space follows from (2.8.1). If the beam propagates from $z = z_1$ to $z = z_2$,

we get

$$\boxed{q_2 = q_1 + d}, \tag{2.8.2}$$

where $q_1 = q(z_1)$, $q_2 = q(z_2)$, and $d = z_2 - z_1$.

Lens as a Phase Corrector. By changing the phase of an optical wave, a lens can serve as a *phase corrector*. Let us consider a double convex lens characterised by the radius of curvature r of its surface and the radius a of its aperture (Fig. 2.47). Let d_0 be the maximum thickness of the lens, $d(x, y)$ — its thickness at the point xy in the aperture plane, n— its refractive index, and f— its focal length. Suppose that $u_1(x, y)$ is the field in the initial reference plane P_1 and $u_2(x, y)$ is the field corresponding to the final reference plane P_2. Assuming that the modulus of the field amplitude does not change upon passing through the lens, we put

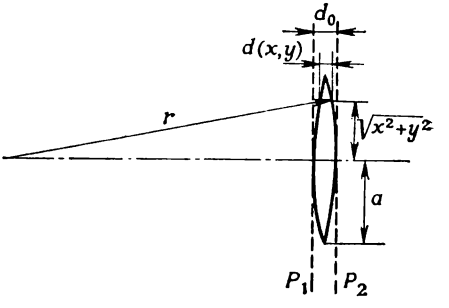


Fig. 2.47

$$u_2(x, y) = u_1(x, y) \exp \times$$
$$\times [i(2\pi d_0/\lambda) + i\varphi(x, y)] \tag{2.8.3}$$

where $(2\pi/\lambda)\, d_0$ is the phase advance at a distance d_0 between P_1 and P_2 planes, and $\varphi(x, y)$ is the additional phase shift due to the lens. Obviously, the total phase shift is equal to the sum of phase shifts inside and outside the lens:

$$\frac{2\pi}{\lambda} d_0 + \varphi(x, y) = \frac{2\pi}{\lambda} nd(x, y) + \frac{2\pi}{\lambda} [d_0 - d(x, y)].$$

Thus

$$\varphi(x, y) = (2\pi/\lambda)(n - 1)\, d(x, y). \tag{2.8.4}$$

Taking into consideration the relation $1/f = (n - 1)\, 2/r$, we can transform (2.8.4) into

$$\varphi(x, y) = (\pi r/\lambda f)\, d(x, y). \tag{2.8.5}$$

It follows from geometrical considerations (see Fig. 2.47) that

$$d(x, y) = 2\left[\frac{d_0}{2} - \left(r - \sqrt{r^2 - (x^2 + y^2)}\right)\right]$$
$$\approx d_0 - 2r\left[1 - \left(1 - \frac{x^2 + y^2}{2r^2}\right)\right] = d_0 - \frac{x^2 + y^2}{r}.$$

Since the function $d(x, y)$ vanishes for $x^2 + y^2 = a^2$, we get $d_0 = a^2/r$. Finally, we get

$$\varphi(x, y) = (\pi/\lambda f)\,[a^2 - (x^2 + y^2)]. \qquad (2.8.6)$$

It can be seen that a lens serves as a *quadratic phase corrector*.

Transformation of a Gaussian Beam in a Lens. Let us denote the parameters of a Gaussian beam by ρ_1, R_1 and q_1 just in front of the lens and by ρ_2, R_2, q_2 just behind the lens. Let f be the focal length of the lens. Being a phase corrector, the lens changes the *curvature* of the wave front ($R_2 \neq R_1$). The radius of the beam remains unchanged ($\rho_2 = \rho_1$).

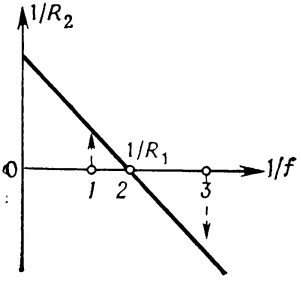


Fig. 2.48

The curvature of the wavefront in (2.7.15) is connected with the term $\pi(x^2 + y^2)/\lambda R$ in the exponent of the phase factor, which depends on transverse coordinates x and y. Considering the passage of a Gaussian beam through a lens, we should supplement this term with $-\pi(x^2 + y^2)/\lambda f$ in accordance with (2.8.6). Thus,

$$\pi(x^2 + y^2)/\lambda R_2 = [\pi(x^2 + y^2)/\lambda R_1] - [\pi(x^2 + y^2)/\lambda f]$$

or

$$\boxed{1/R_2 = (1/R_1) - (1/f)}. \qquad (2.8.7)$$

Figure 2.48 shows the dependence of $1/R_2$ on $1/f$, as defined by the formula (2.8.7). Three cases have been indicated in the figure: (a) $1/f < 1/R_1$ (point *1*); in this case $R_2 > R_1 > 0$; (b) $1/f = 1/R_1$, (point *2*); in this case $R_2 = \infty$; (c) $1/f > 1/R_1$ (point *3*); in this case $R_2 < 0$.

These situations have been illustrated in Fig. 2.49. Here, *1* and *2* are the constant-phase surfaces (wavefronts) in front of the lens and behind it respectively. The point $z = 0$ fixes the position of the plane wavefront (constriction) for the beam as it enters the lens, while point A corresponds to the wavefront as the beam leaves the lens. It can be seen from Fig. 2.49*a* that the lens somewhat decreases the divergence of the beam. In Fig. 2.49*b* the lens gives rise to a plane wavefront at the position where it is placed. In Fig. 2.49*c*, the lens reverses the wavefront.

Since $\rho_2 = \rho_1$ the rule (2.8.7) can be apparently generalised for the parameter q:

$$\boxed{1/q_2 = (1/q_1) - (1/f)}. \qquad (2.8.8)$$

Transformation of a Gaussian Beam in a Lens System. In Fig. 2.50, a Gaussian beam propagates from plane P_1 to plane P_2, passing

through a lens with focal length f; d_1 is the distance from P_1 to the lens, while d_2 is the distance from the lens to P_2. The beam is first

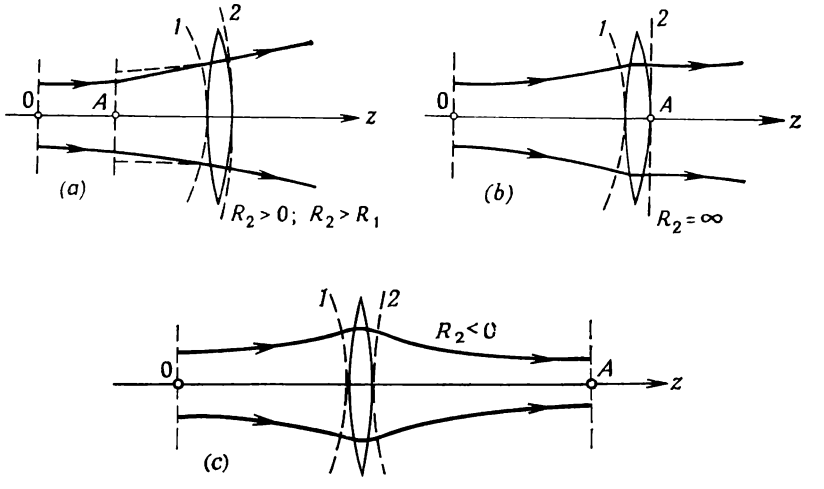


Fig. 2.49

transformed in the free space between P_1 and the lens. In accordance with (2.8.7), we have

$$q_2 = q_1 + d_1. \tag{2.8.9}$$

The beam is then transformed in the lens. In accordance with (2.8.8), we have

$$1/q_3 = (1/q_2) - (1/f)$$

or

$$q_3 = \frac{q_2}{-q_2/f + 1}. \tag{2.8.10}$$

Finally, the beam is transformed in the free space between the lens

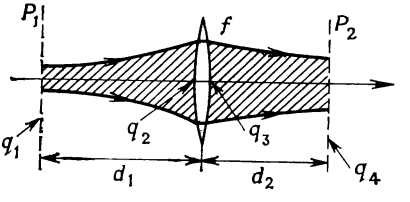


Fig. 2.50

and P_2. In accordance with (2.8.7), we have

$$q_4 = q_3 + d_2. \tag{2.8.11}$$

Combining (2.8.9)-(2.8.11), we get the following rule for transformation of a beam as it propagates from plane P_1 (beam parameter q_1) to plane P_2 (beam parameter q_4):

$$q_4 = \frac{q_1 + d_1}{(-1/f)(q_1 + d_1) + 1} + d_2 = \frac{(1 - d_2/f) q_1 + (d_1 + d_2 - d_1 d_2/f)}{(-1/f) q_1 + (1 - d_1/f)}. \quad (2.8.12)$$

***ABCD* Law—the Law of Transformation of Gaussian Beams in Lens Systems.** Any transformation of a Gaussian beam in a lens system may be expressed in the form

$$\boxed{q_2 = (Aq_1 + B)/(Cq_1 + D)}, \quad (2.8.13)$$

where q_1 and q_2 are the initial and final parameters of the beam respectively. The matrix $\begin{pmatrix} A & B \\ C & D \end{pmatrix}$ describes a system ensuring this transformation of the beam.

For example, the following matrix accounts for the transformation of a beam in free space extending over a length d (cf. 2.8.7) and (2.8.13)):

$$M(d) = \begin{pmatrix} 1 & d \\ 0 & 1 \end{pmatrix}. \quad (2.8.14)$$

The transformation of the beam in a lens with focal length f is given by the matrix (cf. (2.8.10) and (2.8.13))

$$M(f) = \begin{pmatrix} 1 & 0 \\ -1/f & 1 \end{pmatrix}. \quad (2.8.15)$$

The transformation of a beam in the lens system shown in Fig. 2.50 is given by the matrix (cf. (2.8.12) and (2.8.13))

$$M(d_1 \to f \to d_2) = \begin{pmatrix} 1 - \frac{d_2}{f} & d_1 + d_2 - \frac{d_1 d_2}{f} \\ -\frac{1}{f} & 1 - \frac{d_1}{f} \end{pmatrix}. \quad (2.8.16)$$

If the transformation of a Gaussian beam is a *chain* of several transformations, its matrix is a product of matrices of the component transformations written in an order *opposite* to the one in which these transformations are accomplished. It can be easily verified, for example, that

$$M(d_1 \to f \to d_2) = \begin{pmatrix} 1 & d_2 \\ 0 & 1 \end{pmatrix} \begin{pmatrix} 1 & 0 \\ -1/f & 1 \end{pmatrix} \begin{pmatrix} 1 & d_1 \\ 0 & 1 \end{pmatrix} = M(d_2) M(f) M(d_1). \quad (2.8.17)$$

The *ABCD law* expressed by the relation (2.8.13) can be used to determine the transformation law for a Gaussian beam in any lens system. The *ABCD* matrix of the corresponding transformation is

defined as the product of matrices of the type (2.8.14) and (2.8.15) written in a definite order. Keeping in mind the analogy between a lens waveguide and an open resonator, the *ABCD* law can be extended to a resonator, if the light beams in these resonators are Gaussian. The matrix describing the transformation of a Gaussian beam upon its reflection at a spherical mirror with radius of curvature r is of the form

$$M(r)=\begin{pmatrix} 1 & 0 \\ -2/r & 1 \end{pmatrix},$$

which follows from (2.8.15), if $f = r/2$.

Comparing the results obtained in this section with the results obtained in Sec. 2.4 while considering the transformation of a light

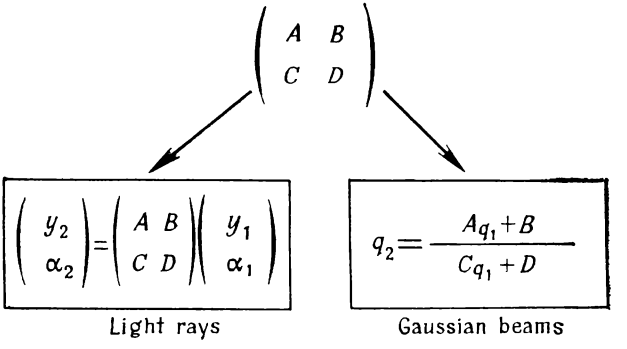


Fig. 2.51

ray, an interesting *analogy* is obtained between the Gaussian beam optics and geometrical optics. As a matter of fact, the *ABCD*-matrix, employed in the *ABCD* law for Gaussian beams and describing a certain optical system, *is identical* to the transfer matrix for the light rays, describing the same system. This matrix is expressed as a product of "elementary" matrices (for free space, lens, and spherical mirror), written in a certain order and having the same form in geometrical optics as well as Gaussian optics[29]. We can obtain the *ABCD*-matrix by considering the behaviour of *light rays* in an optical system, and then apply this matrix to *Gaussian beams*. The transfer matrices for a ray given in Table 2.4 are applicable for Gaussian beams.

The analogy between geometrical optics and Gaussian optics, however, should not be exaggerated. The analogy exists only as long as we speak about the *form* of the *ABCD*-matrix for the optical system under consideration. The *nature* of the transformation accomplished by an *ABCD*-matrix for a ray and a Gaussian beam is different. The transformation of a ray is described by the relation

[29] Compare (2.8.14) and (2.4.18), (2.8.15) and (2.4.20), (2.8.18) and (2.4.26).

(2.4.16) while a Gaussian beam is transformed in accordance with the *ABCD* law expressed through the relation (2.8.13); see Fig. 2.51.

In conclusion of this discussion, it should be noted that the *ABCD* law is also applicable when a Gaussian beam propagates in a medium whose refractive index changes in a direction perpendicular to the optical axis according to the quadratic law:

$$n(x, y) = n_0 - n_2 (x^2 + y^2)/2. \qquad (2.8.19)$$

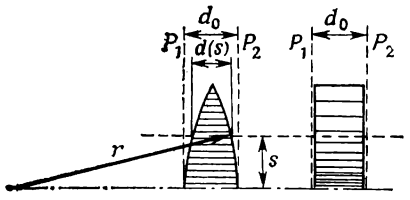


Fig. 2.52

For media with an arbitrary (nonquadratic) law of variation of refractive index, the *ABCD* law is not applicable. It is also not applicable in cases when lens aberrations have to be taken into account. In all these cases, the light beam after transformation is no longer Gaussian [7].

Transformation of a Gaussian Beam in a Quadratic Medium. A quadratic medium is one whose refractive index varies in accordance with the law (2.8.19)[30]. The applicability of the *ABCD* law to quadratic media is explained by the fact that such media may be considered as a set of a large number of lenses stacked together[31]. Let us compare a lens and a plane-parallel thin layer of a quadratic medium (Fig. 2.52). The thickness d_0 of the layer is chosen equal to the maximum thickness of the lens. The refractive index of the lens is equal to n_0, while the refractive index of the layer is given by the relation (2.8.19):

$$n(s) = n_0 - n_2 s^2/2,$$

where $s^2 = x^2 + y^2$. Let us compare the phase shifts as a result of the propagation of light from the plane P_1 to the plane P_2 at a distance s from the optical axis for the case of a lens and a layer of quadratic medium (Fig. 2.52). The required shift for the layer is given by

$$\varphi_{\text{layer}}(s) = \frac{2\pi}{\lambda} n(s) d_0 = \frac{2\pi}{\lambda} n_0 d_0 - \frac{\pi}{\lambda} n_2 s^2 d_0, \qquad (2.8.20)$$

and for a lens, we have

$$\varphi_{\text{lens}}(s) = \frac{2\pi}{\lambda} n_0 d(s) + \frac{2\pi}{\lambda} [d_0 - d(s)]. \qquad (2.8.21)$$

[30] An example of such a medium is an optical fibre with a radial gradient of refractive index. A quadratic medium may also be created by a radial temperature gradient in the active element upon absorption of pumping radiation (*thermal lens effect*).

[31] The propagation of light in a quadratic medium is quite identical to the propagation in a lens waveguide [36, 7].

Since $d_0 - d(s) = 2(r - \sqrt{r^2 - s^2}) \approx s^2/r$ (where r is the radius of curvature of the lens, $s \ll r$), the result (2.8.21) may be rewritten in the form

$$\varphi_{\text{lens}}(s) = \frac{2\pi}{\lambda} n_0 d_0 - \frac{2\pi}{\lambda}(n_0 - 1)\frac{s^2}{r}$$

or, if we take into account the fact that $1/f = (n_0 - 1)\,2/r$ (f is the focal length of the lens), we get

$$\varphi_{\text{lens}}(s) = \frac{2\pi}{\lambda} n_0 d_0 - \frac{\pi s^2}{\lambda f}. \tag{2.8.22}$$

Comparing (2.8.22) and (2.8.20), we conclude that the phase shift for a light beam as it passes through a thin layer of a quadratic medium of thickness d_0 is *exactly the same* as for a thin lens with focal length

$$f = 1/n_2 d_0. \tag{2.8.23}$$

The $ABCD$-matrix transforming the beam upon its passage through a quadratic medium of thickness d is of the form [15]

$$\begin{pmatrix} \cos\left(\sqrt{\frac{n_2}{n_0}}\,d\right) & \frac{1}{\sqrt{n_2 n_0}}\sin\left(\sqrt{\frac{n_2}{n_0}}\,d\right) \\ -\sqrt{n_2 n_0}\sin\left(\sqrt{\frac{n_2}{n_0}}\,d\right) & \cos\left(\sqrt{\frac{n_2}{n_0}}\,d\right) \end{pmatrix} \tag{2.8.24}$$

It can be easily seen that as $n_2 \to 0$, the matrix (2.8.24) turns into matrix $\begin{pmatrix} 1 & d/n_0 \\ 0 & 1 \end{pmatrix}$ given in Table 2.4. If d tends to zero in (2.8.24), and if we consider that the C-element of the matrix tends to $-1/f$ in accordance with (2.8.23) (for sufficiently small values of d, we have $-\sqrt{n_2 n_0}\sin\left(\sqrt{\frac{n_2}{n_0}}\,d\right) \approx -n_2 d$), we arrive at the matrix (2.8.15) describing the transformation of the beam in a thin lens.

Matching of Gaussian Beams. The problem of matching of Gaussian beam may have various practical applications. For example, suppose that it is required to introduce a Gaussian beam emerging from a laser into a lens waveguide, another laser (for pumping the latter), to a parametric light generator cavity, etc. In all these cases, it is required to introduce a Gaussian beam emerging from *one* resonator into *another*. It is important that for this purpose, the initial beam should be properly transformed, or *matched*, with the receiving resonator. For this purpose, a lens is placed at a definite point between the first and the second resonator (matching lens).

Figure 2.53 shows a typical matching diagram. Here, *1* is the first resonator, *2*—the second resonator, *3*—the matching lens (focal length f). A and B are points in primary and secondary Gaussian beams at which the beams have a plane wavefront (the constriction points of the beams). The radii of the beams at the points A

and B are denoted by ρ_{10} and ρ_{20} respectively, d_1 and d_2 are the distances between the matching lens and points A and B respectively. The problem of matching of beams may be presented in the following way: given ρ_{10}, ρ_{20}, and f; it is required to find d_1 and d_2. By solving this problem, we can find out the distance by which the centres of matched resonators should be separated, and the position where the matching lens should be placed[32].

Let us consider the reference planes P_1 (beam parameter q_1) and P_2 (beam parameter q_2), see Fig. 2.53. These planes coincide with the

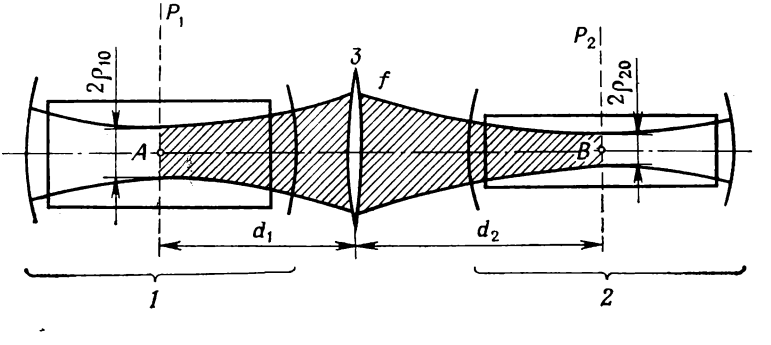


Fig. 2.53

constriction planes of the beams. Consequently, the parameters q_1 and q_2 should be purely imaginary (as soon as $1/R_1 = 0$ and $1/R_2 = 0$). In accordance with (2.8.1), we put

$$q_1 = -i\pi\rho_{10}^2/\lambda \equiv -iQ_1;$$
$$q_2 = -i\pi\rho_{20}^2/\lambda \equiv -iQ_2. \qquad (2.8.25)$$

Using the $ABCD$ law, we write: $q_2 = (Aq_1 + B)/(Cq_1 + D)$ or, otherwise, $Aq_1 + B = Cq_1q_2 + Dq_2$. Substituting (2.8.25) in it, we get $-iAQ_1 + B = -CQ_1Q_2 - iDQ_2$, or

$$\left.\begin{aligned} CQ_1Q_2 + B &= 0; \\ AQ_1 - DQ_2 &= 0. \end{aligned}\right\} \qquad (2.8.26)$$

Further, we use the specific form of the $ABCD$-matrix for transforming a beam from P_1 to P_2. This is the matrix (2.8.16), using which we can rewrite the system of equations (2.8.26) in the form

$$\left.\begin{aligned} (-Q_1Q_2/f) + (d_1 + d_2 - d_1d_2/f) &= 0; \\ (1 - d_2/f)\,Q_1 - (1 - d_1/f)\,Q_2 &= 0. \end{aligned}\right\} \qquad (2.8.27)$$

[32] It is also necessary to know the distances from resonator mirrors at which the constriction points of beams are situated. This question will be discussed in Sec. 2.9.

This system of equations (considered for the unknowns d_1 and d_2) has two solutions. The first solution is given by

$$d_1 = f + \sqrt{\frac{Q_1}{Q_2}}\sqrt{f^2 - f_0^2}; \quad d_2 = f + \sqrt{\frac{Q_2}{Q_1}}\sqrt{f^2 - f_0^2}. \quad (2.8.28a)$$

The second solution is

$$d_1 = f - \sqrt{\frac{Q_1}{Q_2}}\sqrt{f^2 - f_0^2}; \quad d_2 = f - \sqrt{\frac{Q_2}{Q_1}}\sqrt{f^2 - f_0^2}. \quad (2.8.28b)$$

Here $f_0 = (\pi/\lambda)\,\rho_{10}\rho_{20}$ is the so-called *characteristic length*. For matching, it is necessary that the following inequality be satisfied

$$f > f_0. \quad (2.8.29)$$

This inequality imposes certain conditions on the choice of a matching lens.

Taking into account Eqs. (2.8.25), we can rewrite Eqs. (2.8.28) in the following form

$$d_1 = f + \frac{\rho_{10}}{\rho_{20}}\sqrt{f^2 - f_0^2}; \quad d_2 = f + \frac{\rho_{20}}{\rho_{10}}\sqrt{f^2 - f_0^2}; \quad (2.8.30a)$$

$$d_1 = f - \frac{\rho_{10}}{\rho_{20}}\sqrt{f^2 - f_0^2}; \quad d_2 = f - \frac{\rho_{20}}{\rho_{10}}\sqrt{f^2 - f_0^2}. \quad (2.8.30b)$$

2.9. GAUSSIAN BEAMS IN STABLE RESONATORS

Self-reproduction of a Gaussian Beam Upon Reflection from a Spherical Mirror. Figure 2.54*a* shows a Gaussian beam propagating from the constriction plane P_0 in the positive direction of z-axis. Here, the solid lines with arrows show the light rays while the dashed lines indicate the cross sections of constant phase surfaces (it should be recalled that a light ray is perpendicular to the constant phase surface at every point). The radius (ρ_0) of the beam at the constriction plane is assumed to be given.

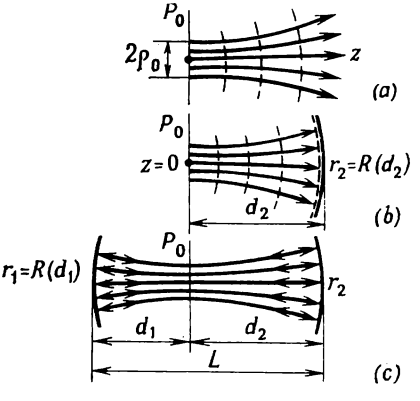


Fig. 2.54

Using a concave spherical mirror of a sufficiently large aperture, the light beam may be reflected in such a way that it *reproduces itself* (is reflected back along the same path). For this purpose, it is necessary that each light ray in the beam should strike the reflecting surface of the mirror at right angles. In other words, it is necessary that the surface of the mirror should *coincide* with one of the constant phase surfaces of the beam (Fig. 2.54*b*).

Assuming that the mirror is placed at a distance d_2 from the constriction plane P_0, the radius of curvature of the constant phase surface for $z = d_2$ will be given, in accordance with (2.7.14), by

$$R(d_2) = d_2 [1 + (\pi\rho_0^2/\lambda d_2)^2].$$

In order that the light beam reproduces itself upon reflection, the radius of curvature r_2 of the mirror should be equal to this quantity. Thus

$$r_2 = d_2 [1 + (\pi\rho_0^2/\lambda d_2)^2]. \qquad (2.9.1)$$

The relation (2.9.1) can be rewritten in the following form:

$$\rho_0^4 = (\lambda/\pi)^2 d_2 (r_2 - d_2). \qquad (2.9.2)$$

(This is the same as relation (2.7.17) for $z = d_2$ and $R = r_2$.)

Considering the propagation of a Gaussian beam from the constriction plane P_0 not only in positive direction, but also in the negative direction of the z-axis, we place another concave mirror across the beam axis at a distance d_1 to the left of the P_0-plane. In order that the beam reproduces itself upon reflection at this mirror, we require that the following relation, analogous to (2.9.2), be satisfied

$$\rho_0^4 = (\lambda/\pi)^2 d_1 (r_1 - d_1), \qquad (2.9.3)$$

where r_1 is the radius of curvature of the mirror. The light beam is now "blocked" from *both* sides in such a way that upon each reflection (from left to right, or from right to left), it reproduces itself (Fig. 2.54*c*). This means that the Gaussian beam is a *mode of a resonator* consisting of mirrors whose radii of curvature have been chosen in accordance with the relations (2.9.2) and (2.9.3).

Gaussian Beam in a Resonator (Large Mirror Apertures). The above discussion concerns a certain Gaussian beam with a given value of ρ_0, and mirrors are chosen for this beam (for two points on its axis) in such a way that they reflect the beam back into itself. In actual practice, however, it is not the beam which is the main factor of such a resonator but rather the mirrors, since it is the mirrors which form the Gaussian beam, reproducing itself upon reflections.

Let us consider a resonator of length L, formed by two mirrors with radii of curvature r_1 (left mirror) and r_2 (right mirror) and with quite large apertures. Let d_1 and d_2 denote the respective distances from the left and right mirrors of the constriction plane of the Gaussian beam formed in the resonator (see Fig. 2.54*c*). Taking into account Eqs. (2.9.2) and (2.9.3), we can write the following system of equations for determining d_1 and d_2:

$$d_1 (r_1 - d_1) = d_2 (r_2 - d_2); \quad d_1 + d_2 = L. \qquad (2.9.4)$$

Eliminating d_2, for example, we get

$$d_1 (r_1 + r_2 - 2L) = L (r_2 - L). \qquad (2.9.5)$$

Assuming[33] that

$$r_1 + r_2 - 2L \neq 0, \tag{2.9.6}$$

we get from (2.9.5)

$$\boxed{d_1 = L(r_2 - L)/(r_1 + r_2 - 2L)}. \tag{2.9.7a}$$

Similarly, we can find that

$$\boxed{d_2 = L(r_1 - L)/(r_1 + r_2 - 2L)}. \tag{2.9.7b}$$

Substituting (2.9.7a) in (2.9.3), we get an expression for the beam radius in the constriction plane:

$$\rho_0^4 = \left(\frac{\lambda}{\pi}\right)^2 \frac{L(r_1 - L)(r_2 - L)(r_1 + r_2 - L)}{(r_1 + r_2 - 2L)^2}. \tag{2.9.8}$$

In order to determine the beam radius at the resonator mirrors (ρ_1 and ρ_2 for left and right mirrors, respectively), we make use of the relation (2.7.18), which in this case assumes the form

$$\rho_i^2 \rho_0^2 = (\lambda/\pi)^2 r_i d_i \quad \text{for} \quad i = 1, 2. \tag{2.9.9}$$

Using (2.9.8), we can find

$$\rho_1^2 = \frac{\lambda r_1}{\pi} \sqrt{\frac{L(r_2 - L)}{(r_1 - L)(r_1 + r_2 - L)}};$$
$$\rho_2^2 = \frac{\lambda r_2}{\pi} \sqrt{\frac{L(r_1 - L)}{(r_2 - L)(r_1 + r_2 - L)}}. \tag{2.9.10}$$

For a *symmetric* resonator ($r_1 = r_2 = r$), we get

$$d_1 = d_2 = \frac{L}{2}; \quad \rho_0^4 = \left(\frac{\lambda}{2\pi}\right)^2 L(2r - L); \quad \rho_1^2 = \rho_2^2$$
$$= \frac{\lambda r}{\pi} \sqrt{\frac{L}{2r - L}}. \tag{2.9.11}$$

Using the parameter g ($g = 1 - L/r$), we can rewrite the result for ρ_0^4. Thus, in a symmetric resonator

$$\rho_0^4 = (\lambda L/2\pi)^2 (1 + g)/(1 - g). \tag{2.9.12}$$

It follows from (2.9.12) that the parameter g must satisfy the condition $-1 < g < 1$, since it is only for these values that ρ_0^4 is positive (Fig. 2.55). It can be easily seen that ρ_0 increases (for a given length of the resonator) with increasing value of the parameter g, i.e. with increasing radius of curvature of the mirrors.

We have thus arrived at the question as to which resonators may give rise to a Gaussian beam. From the example of symmetric resonators it is apparent that *unstable* resonators (for which $g > 1$ or

[33] The case when $r_1 + r_2 - 2L = 0$ will be considered separately.

$g < -1$) do not form Gaussian beams. Strictly speaking, Gaussian beams are also not formed in resonators that are at the boundaries of the stability region, i.e. in plane-parallel resonators ($g = 1$) and in concentric resonators ($g = -1$). The impossibility of reproducing a Gaussian beam in these resonators is evident[34].

Returning to the general case of *asymmetric* resonators, let us consider the basic relations (2.9.2) and (2.9.3). In order that a self-reproducing Gaussian beam be formed in a resonator, it is necessary that the right-hand sides of these relations be positive, i.e. it is necessary that the following inequalities be satisfied:

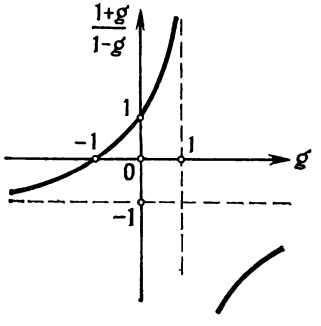


Fig. 2.55

$$d_1 (r_1 - d_1) > 0,$$
$$(L - d_1)(r_2 - L + d_1) > 0. \quad (2.9.13)$$

Substituting (2.9.7a) in either of these inequalities, we get

$$L \frac{(r_1 - L)(r_2 - L)(r_1 + r_2 - L)}{(r_1 + r_2 - 2L)^2} > 0.$$

Thus, it is necessary that the following inequality be satisfied:

$$(r_1 - L)(r_2 - L)(r_1 + r_2 - L) > 0. \quad (2.9.14)$$

In terms of parameters g_1 and g_2, this inequality can be rewritten in the following form:

$$g_1 g_2 (1 - g_1 g_2) > 0$$

Hence,

$$\boxed{0 < g_1 g_2 < 1}. \quad (2.9.15)$$

This inequality may be considered as the necessary condition for the existence of a self-reproducing Gaussian beam in a resonator.

Comparing the relation (2.9.15) with the stability condition (2.4.14) for resonators, we conclude that Gaussian beams cannot be formed in *unstable* resonators. Besides, they are also not formed in resonators which are at the boundary of the stability region (i.e. for which $g_1 g_2 = 1$ or $g_1 g_2 = 0$). An important exception is the confocal resonator (with $g_1 = 0$, $g_2 = 0$).[35]

The Effect of Mirror Aperture. It has been assumed above that the apertures of resonator mirrors are *quite large*:

$$(N = a_1 a_2 / \lambda L) \gg 1.$$

[34] We are speaking of "empty" resonators. It is possible to get a Gaussian beam in a plane-parallel resonator with an internal lens.

[35] The confocal resonator requires to be considered separately, since it belongs to the case when the condition (2.9.6) is not satisfied.

In this case, there is a physically well defined boundary between the stability and instability regions of resonators: upon a transition from unstable to stable resonators, there is a *sharp decrease* in diffraction losses. In such a case, this boundary provides a *clear* distinction between resonators with Gaussian and non-Gaussian beams.

A decrease in the aperture of mirrors means a decrease in the Fresnel number. This leads to a gradual *smoothing* of the difference between diffraction losses in stable and unstable resonators located near the boundary of the stability region. Simultaneously, the boundary between resonators with Gaussian and non-Gaussian beams will be smeared. This means that with decreasing Fresnel number, the "non-Gaussian resonator" region will become wider than the region corresponding to unstable resonators. The description of the field in stable resonators will become to a considerable extent approximate or even incorrect.

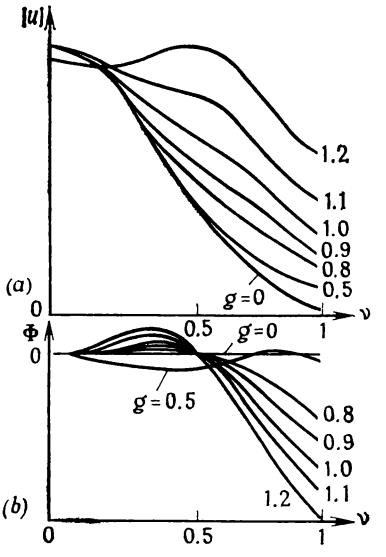


Fig. 2.56

Under these conditions, the field structure in a resonator may be revealed as a result of numerical solution of corresponding integral equations on the basis of the Fox-Li iterative method (see Sec. 2.6). The Fox-Li method permits a calculation of field in a resonator for any values of the parameters N, G_1, G_2. Figure 2.56 shows the field distribution on the surface of a mirror with a circular aperture, obtained by the numerical iterative method for symmetric resonators ($r_1 = r_2$, $a_1 = a_2$) for different values of the parameter $g = 1 - L/r$ [15]. The field distributions have been calculated for the fundamental mode for relatively small mirror apertures, i.e. for $N = 1$. The curves depicted here have been obtained for the modulus of the field amplitude $|u|$ (Fig. 2.56*a*) and for the phase Φ of the field (Fig. 2.56*b*) for different values of the parameter g. These field characteristics have been plotted as functions of the ratio of the distance of the mirror from the centre to the radius of its aperture (this ratio is denoted by ν). The parameter g was varied from 0 (confocal resonator) to unity (plane-parallel resonator) and a little higher, going into the region of unstable resonators with convex mirrors ($0 \leqslant g \leqslant 1.2$).

The dependences shown in the figure demonstrate the absence of a sharp change in the field amplitude distribution for $N = 1$ upon

transition from stable to unstable resonators. Consequently, there is no sharp change in the magnitude of diffraction losses. For a *confocal* resonator ($g = 0$), the distribution $|u(\nu)|$ is quite aptly described by the *Gaussian function*, while the phase of the field remains practically *unchanged* over the surface of the mirror. This means that even for $N = 1$, a confocal resonator forms a *Gaussian beam*. With an increase in the value of g, the distribution $|u(\nu)|$ gradually loses its similarity to a Gaussian function, while the phase of the field changes more and more strongly over the mirror surface. Even in the stability region, the Gaussian beam model is no longer applicable.

It should also be noted that the curves in Fig. 2.56*a* illustrate the remark made earlier, that diffraction losses are determined not only by the Fresnel number, but also by other parameters of the resonator. For the same value of the Fresnel number ($N = 1$), diffraction losses considerably increase with an increasing value of the parameter g. The confocal resonator is characterised by *minimum* diffraction losses.[36]

We find that the condition (2.9.15) is in general *necessary* but not *sufficient* for forming a Gaussian beam in the resonator. In order to form a Gaussian beam, it is necessary that *diffraction losses be small*. Consequently the region of "Gaussian resonators" will practically coincide with the stability region of resonators only for sufficiently large Fresnel numbers (for large apertures of mirrors). In this connection, the condition (2.9.15) should be modified:

$$\boxed{0 < g_1 g_2 < 1;\ N \gg 1}. \qquad (2.9.15a)$$

If the inequality $N \gg 1$ is not satisfied, the region of "Gaussian resonators" will be smaller than the region defined by the inequalities $0 < g_1 g_2 < 1$. There are no sharp criteria in this case. It can simply be stated that with decreasing Fresnel number (with decreasing aperture of the mirrors) the region of "Gaussian resonators" will rapidly shrink to the point $g_1 = 0$, $g_2 = 0$ corresponding to a confocal resonator. For sufficiently small values of Fresnel number, Gaussian beams are not formed even in a confocal resonator.

Phase Shift for a Gaussian Beam and Resonance Frequency Spectrum. It has been mentioned in Sec. 2.2 that in order to find the *frequency spectrum* of a resonator, we must make use of the fact that the phase shift in the radiation for one pass through the resonator is an integral multiple of π, the phase shift being considered at the optical axis of the resonator. If the light beam formed in the resonator is Gaussian, the resonance frequency spectrum can be determined with the help of relation (2.7.34). According to (2.7.34), the phase shift for the *mn*-th mode of a Gaussian beam as it propagates from

[36] Upon a change in the sign of the parameter g, the dependences $|u(\nu)|$ will be similar to the curves shown in Fig. 2.56*a* if these are considered for $|g|$.

the constriction plane ($z = 0$) to a certain reference plane $z = z_1$ is equal (for $x = y = 0$) to

$$\varphi_{mn}(z_1) = (2\pi/\lambda)\, z_1 - (m + n + 1) \arctan (z_1\lambda/\pi\rho_0^2). \qquad (2.9.16)$$

The phase shift of the mn-th mode for one pass of radiation through the resonator, shown for example in Fig. 2.54*c* from the left mirror to the right mirror, is $\varphi_{mn}(d_2) - \varphi_{mn}(-d_1)$. This phase shift is a multiple of π:

$$\varphi_{mn}(d_2) - \varphi_{mn}(-d_1) = \pi q. \qquad (2.9.17)^{37}$$

Using (2.9.16), we can rewrite (2.9.17) in the form

$$\frac{2\pi}{\lambda}(d_1 + d_2) - (m + n + 1)\left[\arctan\left(\frac{\lambda d_2}{\pi\rho_0^2}\right) + \arctan\left(\frac{\lambda d_1}{\pi\rho_0^2}\right)\right] = \pi q. \qquad (2.9.18)$$

With the help of (2.9.9), we can write

$$\lambda d_i/\pi\rho_0^2 = \pi\rho_i^2/\lambda r_i \quad \text{for} \quad i = 1, 2.$$

Substituting the result (2.9.10) in this, we get

$$\frac{\lambda d_1}{\pi\rho_0^2} = \sqrt{\frac{L(r_2 - L)}{(r_1 - L)(r_1 + r_2 - L)}};$$
$$\frac{\lambda d_2}{\pi\rho_0^2} = \sqrt{\frac{L(r_1 - L)}{(r_2 - L)(r_1 + r_2 - L)}} \qquad (2.9.19)$$

We then transform the sum of arc tangents in the relation (2.9.18) as per formula

$$\arctan\alpha + \arctan\beta = \arccos\left(\frac{(1 - \alpha\beta)^2}{1 + \alpha^2 + \beta^2 + \alpha^2\beta^2}\right)^{1/2}.$$

Using this formula and taking into account (2.9.19), we transform the relation (2.9.18) into the following form:

$$\frac{2\pi}{\lambda} L - (m + n + 1) \arccos \sqrt{\left(1 - \frac{L}{r_1}\right)\left(1 - \frac{L}{r_2}\right)} = \pi q.$$

Thus

$$\frac{2\pi}{\lambda} L - (m + n + 1) \arccos \sqrt{g_1 g_2} = \pi q. \qquad (2.9.20)$$

Using (2.2.10), we get the following expression for resonance frequencies of the mn-th mode of a Gaussian beam:

$$\boxed{\omega_{mnq} = \frac{\pi c}{L}\left[q + (m + n + 1)\frac{1}{\pi} \arccos \sqrt{g_1 g_2}\right]}. \qquad (2.9.21)$$

[37] Here, q is a positive integer (longitudinal mode index). This mode index should not be confused with the complex parameter of a Gaussian beam.

Application of the *ABCD*-law for Considering the Resonator Field. Let us denote as q the parameter of a Gaussian beam on a certain reference plane P chosen inside a resonator. We suppose that the transformation of the beam upon its propagation from the left resonator mirror (with radius of curvature r_1) to the plane P is given by an $A_1B_1C_1D_1$-matrix, while the transformation upon propagation of the beam from plane P to the right mirror (with radius of curvature r_2) is given by an $A_2B_2C_2D_2$-matrix (see Fig. 2.57). We mentally conceive a round-trip through the resonator—from P to the left mirror, and further as shown by arrows in the figure. The *ABCD*-matrix for such a pass may be represented by the product

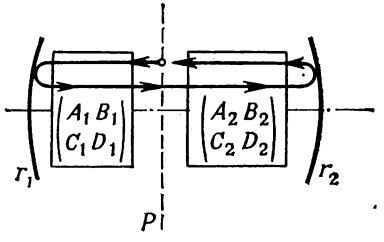


Fig. 2.57

$$\begin{pmatrix} A & B \\ C & D \end{pmatrix} = \begin{pmatrix} A_2 & B_2 \\ C_2 & D_2 \end{pmatrix} \begin{pmatrix} 1 & 0 \\ -\frac{2}{r_2} & 1 \end{pmatrix} \times \begin{pmatrix} A_2 & B_2 \\ C_2 & D_2 \end{pmatrix} \begin{pmatrix} A_1 & B_1 \\ C_1 & D_1 \end{pmatrix} \begin{pmatrix} 1 & 0 \\ -\frac{2}{r_1} & 1 \end{pmatrix} \begin{pmatrix} A_1 & B_1 \\ C_1 & D_1 \end{pmatrix}. \quad (2.9.22)$$

Using the *ABCD*-law for Gaussian beams (2.8.13), we find the parameter q' of the beam, obtained as a result of a round-trip through the resonator:

$$q' = (Aq + B)/(Cq + D). \quad (2.9.23)$$

Since the beam structure must be *reproduced* as a result of a round-trip through the resonator, we get

$$q' = q. \quad (2.9.24)$$

Substituting (2.9.24) in (2.9.23) we get an equation for the parameter q of the beam in the reference plane P chosen by us

$$\boxed{q = (Aq + B)/(Cq + D)}. \quad (2.9.25)$$

The parameter q is *complex-valued*, hence Eq. (2.9.25) is equivalent to a system of two equations which can be used for finding the radius of the light beam and the radius of curvature of its wavefront in the transverse cross section chosen by us for the resonator. We represent

$$1/q = g + ih, \quad (2.9.26)$$

where, in accordance with (2.7.19),

$$g = 1/R; \quad h = \lambda/\pi\rho^2. \quad (2.9.27)$$

Substituting (2.9.26) into (2.9.25) we get

$$(g^2 - h^2)\,B - g\,(D - A) - C + ih\,[2gB - (D - A)] = 0.$$

Thus

$$\left.\begin{aligned}&(g^2 - h^2)\,B - g\,(D - A) - C = 0;\\ &2gB - (D - A) = 0.\end{aligned}\right\} \qquad (2.9.28)$$

Taking into consideration the relation $AD - BC = 1$, we can write the solution of the system of equations (2.9.28) in the form

$$g = \frac{D-A}{2B}; \quad h = \frac{1}{B}\sqrt{1 - \left(\frac{D+A}{2}\right)^2}.$$

Taking (2.9.27) into account, we finally get

$$\boxed{R = \frac{2B}{D-A}; \quad \rho^2 = \frac{\lambda}{\pi} B \left[1 - \left(\frac{D+A}{2}\right)^2\right]^{-1/2}}. \qquad (2.9.29)$$

In Sec. 2.4, we obtained the $ABCD$-matrix (2.4.28) for a round-trip through an "empty" resonator from any arbitrarily chosen reference plane. Using this matrix, we can easily obtain the relation (2.9.7) determining the position of the constriction plane in a resonator.

Let us choose the *constriction plane* of the beam as reference plane, from which we start a round of the resonator. Since $1/R = 0$ in this plane, the matrix of a round-trip must have, in accordance with (2.9.29), the following property:

$$A = D. \qquad (2.9.30)$$

Using the result (2.4.28), we can rewrite (2.9.30) in the following form (after replacing d by d_1):

$$1 + \frac{4L}{r_1 r_2}(L - d_1) - \frac{2}{r_1}(2L - d_1) - \frac{2}{r_2}(L - d_1)$$
$$= 1 + \frac{4Ld_1}{r_1 r_2} - \frac{2d_1}{r_1} - \frac{2}{r_2}(L + d_1).$$

It can be easily verified that this equation is equivalent to the relation (2.9.5).

Indefiniteness of the Caustic of a Confocal Resonator with Infinite Mirror Apertures. In accordance with (2.9.5), the position of the constriction plane of a Gaussian beam formed in a certain resonator *is fixed* by the "longitudinal configuration" of the resonator (i.e. by parameters r_1, r_2, L). The position of the constriction plane for a symmetric resonator ($r_1 = r_2$) is fixed at the middle of the resonator ($d_1 = L/2$). A symmetric resonator has a symmetric caustic corresponding to it.

This statement is valid for all resonators forming Gaussian beams except the *confocal* resonator ($r_1 = r_2 = L$). One of the most interesting properties of this resonator is that the position of the constric-

tion plane of the beam and hence the form of the caustic in the resonator *are not fixed* by the "longitudinal configuration" of the resonator (see, for example, [37]).

As a matter of fact, for $r_1 = r_2 = L$ the relation (2.9.5) assumes the form $d_1 \cdot 0 = L \cdot 0$. Hence d_1 may assume any value from the interval $0 < d_1 < L$. This interval is determined by the relation (2.9.3) which has the following form for a confocal resonator of length L:

$$\rho_0^4 = (\lambda/\pi)^2 d_1 (L - d_1). \tag{2.9.31}$$

If the apertures of the confocal resonator mirrors are infinitely large, there are no factors that could fix the caustic. The caustic in such a resonator is *indefinite*. It may be symmetric or asymmetric, to a certain degree, with respect to the mirrors.

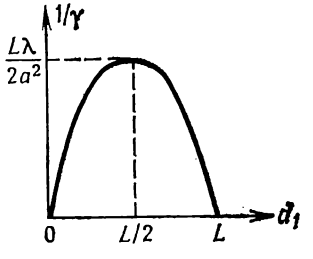


Fig. 2.58

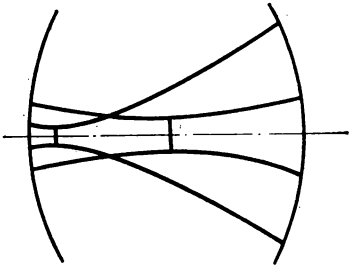


Fig. 2.59

A change in the form of the caustic is accompanied by a change in the radius of the beam on the constriction plane (radius ρ_0). It can be seen from (2.9.31) that ρ_0 assumes a maximum value for the case of a symmetric caustic (for $d_1 = L/2$):

$$\rho_{0\,\max} = \sqrt{\lambda L/2\pi}, \tag{2.9.32}$$

If d_1 tends to zero or to L, the radius ρ_0 will decrease and tend to zero (Fig. 2.58).

Irrespective of the form of the caustic, the product of the beam radii at the mirrors remains constant. This can be easily verified by using the relation (2.7.18). We denote the radii on the left and right mirror by ρ_1 and ρ_2, respectively. In accordance with (2.7.18), we have

$$\rho_1^2 = (1/\rho_0^2)(\lambda/\pi)^2 L d_1; \quad \rho_2^2 = (1/\rho_0^2)(\lambda/\pi)^2 L (L - d_1). \tag{2.9.33}$$

Taking (2.9.31) into account, we get

$$\rho_1 \rho_2 = \lambda L/\pi. \tag{2.9.34}$$

Figure 2.59 shows, by way of an example, two caustics of a confocal resonator with infinite mirror apertures. One of these caustics is symmetric, while the other is asymmetric.

Confocal Resonator with Finite Mirror Apertures. Let us go over from a purely speculative confocal resonator with infinite apertures to a real confocal resonator whose mirrors have apertures a_1 (for the left mirror) and a_2 (for the right mirror). The independence of the form of the caustic of a confocal resonator from its "longitudinal configuration" makes the caustic of such a resonator capable of *adjustment* according to its "transverse configuration" determined by the ratio of its mirror apertures. Unlike other resonators the form of the caustic in a confocal resonator is fixed by the mirror apertures, which also determine the position of the constriction plane of the beam.

Suppose that a resonator has mirrors with identical apertures (radius of aperture is a). A symmetric caustic is fixed in this case, since only such a caustic will correspond to the *lowest* diffraction losses. The caustic of a symmetric confocal resonator is characterised by the following parameters:

$$d_1 = L/2; \quad \rho_0 = \sqrt{\lambda L/2\pi}; \quad \rho = \sqrt{\lambda L/\pi}. \tag{2.9.35}$$

where ρ is the beam radius at the mirrors.

Let us now consider another confocal resonator of the same length but with $a_1 = a/2$, $a_2 = 2a$. Both the resonators considered here have the same product of mirror apertures: $a_1 a_2 = a^2$. Hence they are *equivalent* resonators characterised, in particular, by identical diffraction losses. This result follows from the equivalence condition (2.6.43) of confocal resonators.

It is well known that the ratio of the radius of light beam on a mirror to the radius of the mirror aperture serves as a measure of diffraction losses. The fact that diffraction losses of a confocal resonator do not change upon halving the aperture of one mirror and simultaneously doubling the aperture of the other means a corresponding change in the radii of the beam at the mirrors:

$$\rho_1 = \rho/2; \quad \rho_2 = 2\rho. \tag{2.9.36}$$

(It should be noted that $\rho_1 \rho_2 = \rho^2$ in accordance with (2.9.34).) Taking into account the relation (2.9.35), we can rewrite (2.9.36) in the following form:

$$\rho_1 = \sqrt{\lambda L/\pi}/2; \quad \rho_2 = 2\sqrt{\lambda L/\pi}. \tag{2.9.37}$$

Thus, the fact that diffraction losses in a confocal resonator remain constant in spite of a change in the ratio of mirror apertures (for the same value of the product $a_1 a_2$) is explained by a corresponding change in the caustic shape and its *readjustment according to new apertures.*

Using (2.9.37) we can find the distance d_1' between the left mirror and the constriction plane. We substitute (2.9.37) in (2.9.33) and take into account (2.9.31). Consequently, the first of the relations (2.9.33) assumes the form $\lambda L/4\pi = \lambda L d_1'/\pi \sqrt{d_1'(L - d_1')}$. Hence $d_1' = L/17$.

Both confocal resonators considered here are shown in Fig. 2.60, which also shows their caustics.

As mentioned earlier, the caustic shape in a *non-confocal* resonator is fixed by the "longitudinal configuration" of the resonator. The existence of a Gaussian beam in stable resonators whose parameters are not close to the point $g_1 = g_2 = 0$ is possible only for large apertures of the mirrors. A decrease in the aperture cannot change a *fixed* caustic in these resonators. It can only lead to higher diffraction losses so that the beam is finally no longer Gaussian. The caustic of a *confocal* resonator, on the other hand, is capable of *readjustment* according to mirror apertures. Besides, a confocal resonator is characterised by the *lowest* value of $\rho_1\rho_2$ (for a given L)[38]. These two circumstances mean that the diffraction losses in a confocal resonator are the *lowest* in comparison to other types of resonators (for the same value of Fresnel number). For this reason, a confocal resonator is capable of forming a Gaussian beam even for *relatively small* values of Fresnel numbers.

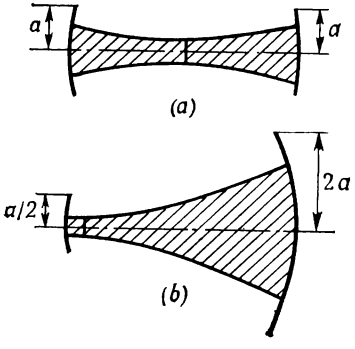


Fig. 2.60

Confocal Diaphragm Resonator. If the mirror apertures are sufficiently large, the decisive factor in the caustic shape of a confocal resonator may turn out to be the *diaphragm* introduced into the resonator. For large mirror apertures, the beam constriction is fixed at the same point where the diaphragm is deployed.

It was mentioned in Sec. 2.6 that the highest diffraction losses in a confocal diaphragm resonator[39] take place when the diaphragm is located in the middle of the resonator. If the diaphragm is displaced towards one of the mirrors, the diffraction losses will decrease. This is explained by a *readjustment* of the caustic as a result of this displacement. Consequently the beam constriction *follows the diaphragm*. In accordance with (2.9.31), the maximum radius ρ_0 of constriction is attained for $d_1 = L/2$. If d_1 tends to zero or L, the radius ρ_0 of constriction decreases (Fig. 2.58). Thus, as the

[38] In accordance with (2.9.11) we get the relation $\rho^2 = \lambda L/\pi \sqrt{1 - g^2}$ for symmetric nonconfocal resonators. The corresponding relation for a confocal resonator is given by $\rho^2 = \lambda L/\pi$.

[39] We are speaking of diffraction at the edge of the diaphragm hole.

diaphragm approaches a mirror, the ratio ρ_0/a (a is the radius of the diaphragm hole) will *decrease*, thus causing a decrease in the diffraction losses. Figure 2.61 illustrates this situation.

If the caustic were fixed and incapable of readjustment according to the diaphragm, a displacement of the diaphragm would lead not to a decrease, but rather to an *increase* in the ratio ρ_0/a. Consequently, there would be a rise in diffraction losses and probably a conversion of the Gaussian beam into non-Gaussian.

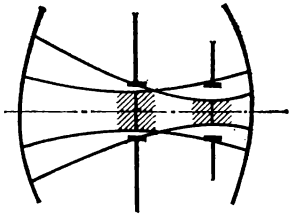


Fig. 2.61

2.10. UNSTABLE RESONATORS

In 1962, Boyd and Kogelnik showed that resonators whose parameters satisfy the condition (2.4.14) are characterised by small diffraction losses for large values of Fresnel number, and that a violation of this condition leads to a sharp *increase* in losses [28]. Resonators for which the condition (2.4.14) is not satisfied were termed *unstable*[40] resonators. At that time, laser generation was considered impossible for large diffraction losses, hence not much attention was paid by specialists to the unstable resonators for some time. Interest to these resonators was revived in late sixties after Siegman [38, 39] and a number of other authors [40-42] considered these resonators for laser applications.

These investigations demonstrated the viability of lasers with unstable resonators. It was shown that it is expedient to use such resonators for sufficiently large values of gain of the active medium—not less than 10-20% for a pass [43]. It turned out that unstable resonators have a number of advantages over stable ones (see [44], as well as Ch. 23 in [2]).

Homocentricity of a Beam Extracted from an Unstable Resonator. It was mentioned, in Sec. 2.3, that most of the results for unstable resonators can be obtained in the geometrical approximation. The idea of *geometrical* calculations for unstable resonators was put forward by Siegman [38]. According to him, the field inside a resonator is treated as a superposition of two *spherical* waves (or a spherical and a plane wave in certain resonators) which are propagating in opposite directions and are transformed *into each other* upon reflection at the mirrors.

Consider an unstable resonator of length L, formed by convex mirrors with radii of curvature r_1 and r_2 and apertures a_1 and a_2 (Fig. 2.62*a*). The dashed lines in the figure show cross sections of constant phase surfaces of two divergent spherical waves. We shall

[40] Different types of unstable resonators have been compiled in Table 2.3 (positions III, V, VI, IX, XI-XVI). See Sec. 2.4.

designate the wave propagating *from left to right* as wave *1* and the one propagating *from right to left* as wave *2*. Point A_1 is the common centre of constant phase surfaces for wave *1* while point A_2 is the corresponding point for wave *2*. While propagating from the left mirror to the right one, wave *1* partially leaves the resonator in the form of a *homocentric* light beam with centre at A_1, is partially reflected at the right mirror and is thus transformed into wave *2*. Wave *2*, propagating from the right mirror to the left one, partially leaves the resonator in the form of a homocentric light beam with centre at A_2, is partially reflected at the left mirror and is thus transformed into wave .

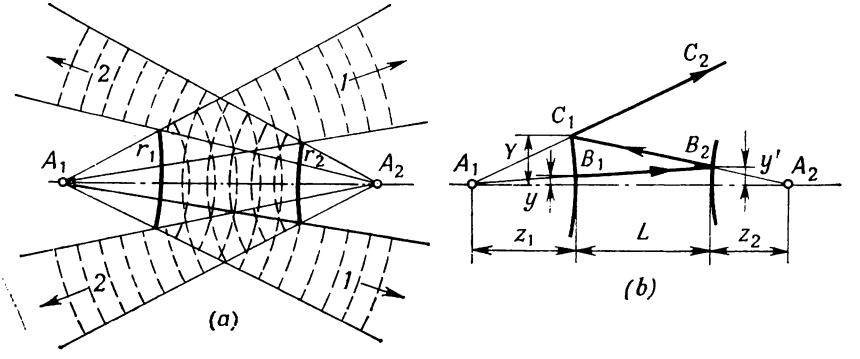


Fig. 2.62

In order that wave *1* be transformed into wave *2* and wave *2* into wave *1* upon reflection at the mirrors, it is necessary that point A_2 should be the image of point A_1 in the right mirror, and point A_1 should be the image of point A_2 in the left mirror. This can be clearly seen if we consider two successive reflections of any light ray corresponding to wave *1* or *2*. Figure 2.62*b* shows the ray B_1B_2 propagating from the left mirror to the right one. Since the ray corresponds to wave *1*, its continuation beyond the left mirror must intersect the optical axis at the point A_1. This ray is reflected at the right mirror and is converted into the ray B_2C_1. Continuation of this ray beyond the right mirror defines the image of point A_1, i.e. point A_2, in this mirror. Since the ray B_2C_1 must correspond to wave *2*, point A_2 must be the centre of wave *2*. Upon reflection at the left mirror, the ray B_2C_1 is converted into ray C_1C_2. Since the ray C_1C_2 corresponds to wave *1*, its continuation must pass through the point A_1. Consequently, the point A_1 must be the image of point A_2 in the left mirror.

We denote the distance between the point A_1 and the left mirror by z_1, and between the point A_2 and the right mirror by z_2. In order to find these distances we use the formula for constructing an image

in a convex mirror:

$$(1/d') - (1/d) = 2/|\, r \,|, \tag{2.10.1}$$

where d is the distance of the object from the mirror, d' is the distance of the image from the mirror, and r is the radius of curvature of the mirror. Considering the point A_2 as the image of the point A_1 in the right mirror, let us write down the relation (2.10.1) for this mirror (Fig. 2.62*b*):

$$(1/z_2) - [1/(z_1 + L)] = 2/|\, r_2 \,|. \tag{2.10.2a}$$

Considering the point A_1 as the image of the point A_2 in the left mirror, we can write down, for this mirror,

$$(1/z_1) - [1/(z_2 + L)] = 2/|\, r_1 \,|. \tag{2.10.2b}$$

Considering that $|\, r_1 \,| = -r_1$, $|\, r_2 \,| = -r_2$ and using the familiar relations $L/r_1 = 1 - g_1$, $L/r_2 = 1 - g_2$, we arrive at the system of equations

$$\left.\begin{aligned} (1/z_1) - [1/(z_2 + L)] &= -2\,(1 - g_1)/L; \\ (1/z_2) - [1/(z_1 + L)] &= -2\,(1 - g_2)/L. \end{aligned}\right\} \tag{2.10.3}$$

Solving this system, we get

$$\begin{aligned} z_1 &= L\,\frac{\sqrt{g_1 g_2\,(g_1 g_2 - 1)} - g_1 g_2 + g_2}{2 g_1 g_2 - g_1 - g_2}\,; \\ z_2 &= L\,\frac{\sqrt{g_1 g_2\,(g_1 g_2 - 1)} - g_1 g_2 + g_1}{2 g_1 g_2 - g_1 - g_2}\,. \end{aligned} \tag{2.10.4}$$

For a symmetric resonator ($g_1 = g_2 = g$), this result assumes the form

$$z_1 = z_2 = \frac{L}{2}\left(\sqrt{\frac{g+1}{g-1}} - 1\right). \tag{2.10.5}$$

Geometrical Optics Losses in an Unstable Resonator. Losses in stable resonators due to finite aperture of mirrors are, as a rule, unfavourable and undesirable. In unstable resonators, however, these losses are *favourable*, since they are responsible for the extraction of the light beam from the resonator[41]. The homocentricity of the beam suggests that these losses may be described within the framework of geometrical optics. A special term *geometrical optics losses* is sometimes used to describe these losses.

Let y be the transverse coordinate on the left mirror for one of the rays in an unstable resonator (Fig. 2.62*b*). In passing from the left mirror to the right one, the ray deviates from the axis. Let us denote its coordinate on the right mirror by y'. Upon returning to

[41] The radiation is extracted from the resonator because of the fact that the diameter of the light beam turns out to be more than the aperture of the mirror (Fig. 2.62). Such a method of extracting radiation from the resonator is called *circular*, and is characteristic of unstable resonators.

the left mirror (after reflection at the right mirror), the ray will have coordinate Y. The ratio

$$M = Y/y \tag{2.10.6}$$

showing the number of times the distance between the light ray and axis has increased for a round-trip through the resonator is called the *coefficient of transverse broadening* of the beam. From Fig. 2.62*b*, it can be seen that

$$y'/y = (z_1 + L)/z_1; \quad Y/y' = (z_2 + L)/z_2. \tag{2.10.7}$$

This gives

$$M = \frac{z_1 + L}{z_1} \frac{z_2 + L}{z_2}. \tag{2.10.8}$$

The factor $(z_1 + L)/z_1$ in (2.10.8) defines the increase in the transverse dimensions of the beam upon its passage *from the left mirror to the right mirror*, while the factor $(z_2 + L)\, z_2$ defines the same quantity as the beam passes *from the right mirror to the left mirror*.

Substituting (2.10.4) in (2.10.8), we get

$$M = \frac{g_1 g_2 + \sqrt{g_1 g_2 (g_1 g_2 - 1)}}{g_1 g_2 - \sqrt{g_1 g_2 (g_1 g_2 - 1)}}. \tag{2.10.9}$$

For a symmetric resonator ($g_1 = g_2 = g$), the relation (2.10.9) assumes the form

$$M = (g + \sqrt{g^2 - 1})^2. \tag{2.10.10}$$

In this case we usually consider the coefficient of expansion for a *single* pass through the resonator instead of a round-trip:

$$M_s = \sqrt{M} = g + \sqrt{g^2 - 1}. \tag{2.10.11}$$

The radius of the light beam reflected at the left mirror is equal to the radius of aperture a_1 of this mirror. After passing through the resonator (from left mirror to right mirror), the radius of the beam increases $(z_1 + L)/z_1$ times and becomes equal to $a_1 (z_1 + L)/z_1$. If the radius of aperture a_2 of the right mirror is less than $a_1 (z_1 + L)/z_1$, only a *part* of the light flux reflected by the left mirror will be reflected by the right mirror. The ratio of the light flux reflected by the right mirror to that reflected by the left mirror is equal to [42]

$$\gamma_{2/1} = a_2^2/[a_1 (z_1 + L)/z_1]^2. \tag{2.10.12a}$$

Thus, the fraction of light flux lost during a passage from the left mirror to the right one is equal to

$$\Gamma_{1\to 2} = 1 - \gamma_{2/1} = 1 - (a_2/a_1)^2 [z_1/(z_1 + L)]^2. \tag{2.10.13a}$$

The ratio of light flux reflected by the left mirror to that reflected by the right mirror is defined in a similar manner:

$$\gamma_{1/2} = a_1^2/[a_2 (z_2 + L)/z_2]^2. \tag{2.10.12b}$$

[42] It is assumed that the field intensity in the beam cross section is practically constant.

The fraction of light flux lost during a passage from the right mirror to the left one is given by

$$\Gamma_{2\to 1} = 1 - \gamma_{1/2} = 1 - (a_1/a_2)^2\,[z_2/(z_2 + L)]^2. \qquad (2.10.13b)$$

With the help of (2.10.12a) and (2.10.12b), we can find the fraction of light flux lost during a round-trip through the resonator. This fraction is equal to

$$\Gamma = 1 - \gamma_{2/1}\gamma_{1/2} = 1 - \left[\frac{z_1 z_2}{(z_1+L)(z_2+L)}\right]^2. \qquad (2.10.14)$$

Using (2.10.8), we can rewrite (2.10.14) in the following form:

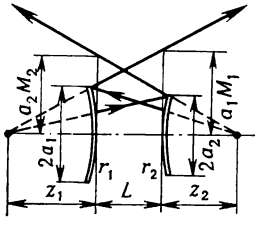
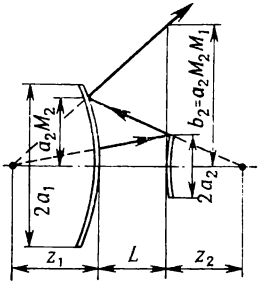
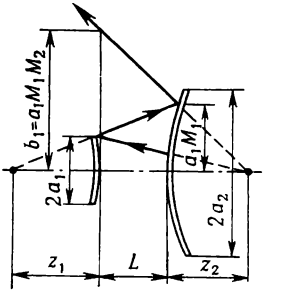
$$\boxed{\Gamma = 1 - (1/M^2)}. \qquad (2.10.15)$$

In a symmetric resonator, we can consider the fraction of the light flux lost during a single pass through the resonator:

$$\Gamma_s = 1 - (1/M_s^2). \qquad (2.10.16)$$

It should be emphasized that the geometrical optics losses in an unstable resonator do not depend on the aperture of the mirrors. The ratio of the mirror apertures may affect only the *nature of extraction* of radiation from the resonator: through both mirrors, through the left mirror, or through the right mirror. These three cases are illustrated in Table 2.6.

TABLE 2.6

Radiation emerging from both mirrors	Radiation emerging from the right mirror	Radiation emerging from the left mirror
		
$\gamma_{2/1} = \dfrac{a_2^2}{(a_1 M_1)^2}$	$\gamma_{1/2} = 1$	$\gamma_{2/1} = 1$
$\gamma_{1/2} = \dfrac{a_1^2}{(a_2 M_2)^2}$	$\gamma_{2/1} = \dfrac{a_2^2}{b_2^2} = \dfrac{a_2^2}{(a_2 M_2 M_1)^2}$	$\gamma_{1/2} = \dfrac{a_1^2}{b_1^2} = \dfrac{a_1^2}{(a_1 M_1 M_2)^2}$
$\gamma_{2/1}\gamma_{1/2} = \dfrac{1}{M_1^2 M_2^2} = \dfrac{1}{M^2}$	$\gamma_{2/1}\gamma_{1/2} = \dfrac{1}{(M_2 M_1)^2} = \dfrac{1}{M_2}$	$\gamma_{2/1}\gamma_{1/2} = \dfrac{1}{(M_1 M_2)^2} = \dfrac{1}{M^2}$

Application of *ABCD* Law to Unstable Resonators. A more general and elegant geometrical optics treatment of unstable resonators is based on the application of the *ABCD law.*

It can be easily seen that the *ABCD* law is applicable to *spherical* waves. The radius of curvature of the wavefront of a homocentric beam is transformed upon propagation in free space over a length d according to the obvious relation (Fig. 2.63)

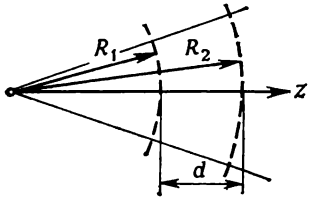


Fig. 2.63

$$R_2 = R_1 + d. \qquad (2.10.17)$$

A thin lens of focal length f changes the radius of curvature of the spherical front according to the relation (2.8.7):

$$1/R_2 = (1/R_1) - (1/f). \qquad (2.10.18)$$

Comparing (2.10.17) with (2.8.2) and (2.10.18) with (2.8.8), we find that in ideal lens systems (including systems with spherical mirrors) the parameter R of a *homocentric* beam is transformed *exactly in the same way* as the parameter q of a *Gaussian* beam. In other words, the *ABCD* law described for Gaussian beams by relation (2.8.13) may be applied to the radius of curvature R of the wavefront of a homocentric beam:

$$\boxed{R_2 = (AR_1 + B)/(CR_1 + D)} \quad . \qquad (2.10.19)$$

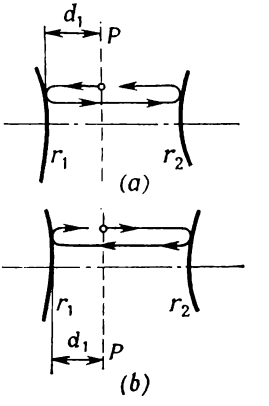


Fig. 2.64

Let us isolate a reference plane P in an unstable resonator at a distance d_1 from the left mirror. For this plane, let us denote by $R\,(d_1)$ the radius of curvature of the spherical wavefront propagating from the right mirror to the left one. The radius of curvature of the wavefront propagating in the reverse direction is denoted by $R'(d_1)$. These radii $R\,(d_1)$ and $R'\,(d_1)$ may be found from the condition of reproducibility of the field for a round-trip through the resonator:

$$R\,(d_1) = [AR\,(d_1) + B]/[CR\,(d_1) + D]; \qquad (2.10.20a)$$

$$R'\,(d_1) = [A'R'\,(d_1) + B']/[C'R'\,(d_1) + D']. \qquad (2.10.20b)$$

Here, $\begin{pmatrix} A & B \\ C & D \end{pmatrix}$ is the matrix corresponding to a round-trip through the resonator, starting from the plane P to the left mirror (Fig. 2.64*a*), while $\begin{pmatrix} A' & B' \\ C' & D' \end{pmatrix}$ is the matrix corresponding to a round-trip through

the resonator starting from the plane P to the right mirror (Fig. 2.64*b*)

$$\begin{pmatrix} A & B \\ C & D \end{pmatrix} = \begin{pmatrix} 1 & L-d_1 \\ 0 & 1 \end{pmatrix} \begin{pmatrix} 1 & 0 \\ -\frac{2}{r_2} & 1 \end{pmatrix} \times \begin{pmatrix} 1 & L \\ 0 & 1 \end{pmatrix} \begin{pmatrix} 1 & 0 \\ -\frac{2}{r_1} & 1 \end{pmatrix} \begin{pmatrix} 1 & d_1 \\ 0 & 1 \end{pmatrix}; \quad (2.10.21a)$$

$$\begin{pmatrix} A' & B' \\ C' & D' \end{pmatrix} = \begin{pmatrix} 1 & d_1 \\ 0 & 1 \end{pmatrix} \begin{pmatrix} 1 & 0 \\ -\frac{2}{r_1} & 1 \end{pmatrix} \times \begin{pmatrix} 1 & L \\ 0 & 1 \end{pmatrix} \begin{pmatrix} 1 & 0 \\ -\frac{2}{r_2} & 1 \end{pmatrix} \begin{pmatrix} 1 & L-d_1 \\ 0 & 1 \end{pmatrix}. \quad (2.10.21b)$$

Confining ourselves to the case when the round through the resonator is along the path indicated in Fig. 2.64*a* (in other words, confining ourselves to Eq. 2.10.20a), we get the following two solutions of Eq. (2.10.20a):

$$R = (1/2C)\,[A - D + \sqrt{(A+D)^2 - 4}]; \quad (2.10.22a)$$

$$\overline{R} = (1/2C)\,[A - D - \sqrt{(A+D)^2 - 4}]. \quad (2.10.22b)$$

It can be shown that one of the solutions is *stable* (the small perturbation in the radius R of the front will be attenuated as the wave propagates through the resonator), while the other is *unstable*[43]. The stable solution describes a *divergent* spherical wave while the unstable one describes a *convergent* wave. If $(A + D) > 2$ the stable (divergent) wave is given by (2.10.22a), if $(A + D) < -2$, this wave is described by (2.10.22b).

The $ABCD$-matrix of a round-trip through the resonator shown in Fig. 2.64*a* is already familiar to us—it is described by the relation (2.4.28). Suppose that $d_1 = L$ (the reference plane touches the right mirror). In this case, the matrix (2.4.28) assumes the form

$$\begin{pmatrix} A & B \\ C & D \end{pmatrix} = \begin{pmatrix} 1 - \frac{2L}{r_1} & 2L - \frac{2L^2}{r_1} \\ \frac{4L}{r_1 r_2} - \frac{2}{r_1} - \frac{2}{r_2} & 1 + \frac{4L^2}{r_1 r_2} - \frac{2L}{r_1} - \frac{4L}{r_2} \end{pmatrix}. \quad (2.10.23)$$

The matrix (2.10.23) is used for determining the radius of curvature of the light front immediately after reflection at the right mirror. In other words, it is used for finding the distance z_2 between the right mirror and the centre of the spherical wave propagating through a resonator from the right mirror to the left one. In the present case

$$A + D = 2\,(2g_1 g_2 - 1). \quad (2.10.24)$$

[43] See Appendix 3.

We assume that we are considering unstable resonators for which $g_1g_2 > 1$ and hence $(A + D) > 2$. The stable (divergent) wave in such resonators is described by the relation (2.10.22a). Using (2.10.23), we get the following relation from (2.10.22a):

$$R(d_1 = L) = z_2 = L\frac{\sqrt{g_1g_2(g_1g_2-1)} - g_1g_2 + g_1}{2g_1g_2 - g_1 - g_2}.$$

This is a familiar result (see (2.10.4)).

Laser with an Unstable Telescopic Resonator. This resonator is shown in Fig. 2.65. Here, *1* is the active medium, *2*—a concave mirror with radius of curvature r_1, *3*—a convex mirror with radius of curvature r_2, and *4*—the output radiation. The concave and the convex mirror have a common focus; $r_1 = 3L$, $r_2 = -L$. For this resonator,

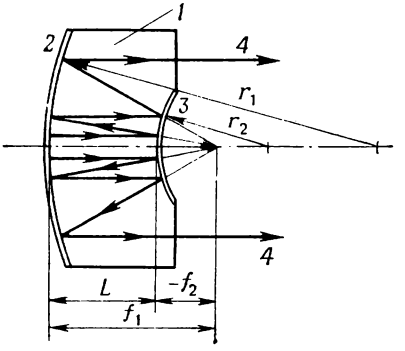


Fig. 2.65

$$g_1 = 2/3; \quad g_2 = 2. \quad (2.10.25)$$

The field inside a telescopic resonator is described as a superposition of *plane* and *spherical* waves. A divergent spherical wave propagates in the resonator from the convex mirror to the concave one, while a plane wave propagates from the concave mirror to the convex one. The light rays corresponding to these waves are shown in Fig. 2.65. It can be easily seen that in this case

$$z_1 = \infty; \quad z_2 = L/2; \quad M = 3. \quad (2.10.26)$$

The laser considered here is analogous to the cascade laser shown in Fig. 2.66*a*, which is a highly efficient *selective* system. The notation used in Fig. 2.66*a* is as follows: *1*—the driving generator, *2*—the matching telescopic system, and *3*—the active medium. For driving generator, we use a low-power laser for which a selection of the fundamental transverse mode can be easily made. This mode is then amplified at every cascade.

The system shown in Fig. 2.66*a* is highly efficient but, unfortunately, quite complicated from a technical point of view. It is better to use a laser with an unstable telescopic resonator which is *identical* to the system under consideration. The analogy between the two can be easily seen if we slightly modify the system shown in Fig. 2.66*a* and consider the lens waveguide shown in Fig. 2.66*b*. The waveguide consists of alternate *converging* (focal length f_1) and *diverging* (focal length f_2) lenses, for which $f_1 = 3\,|f_2|$. Lenses are separated by a gap $2\,|f_2|$ which is filled with the active medium. There is

no driving generator in this case, and the region near the axis of the active elements performs the function of the driving generator. It can be easily seen that this lens waveguide is optically equivalent to a telescopic resonator. It should be noted that the shaded area in Fig. 2.66*b* shows a light beam corresponding to an unstable (convergent) wave.

It can be easily seen from Fig. 2.66*b* that generation in a telescopic resonator (as in any other unstable resonator) starts in the *axial*

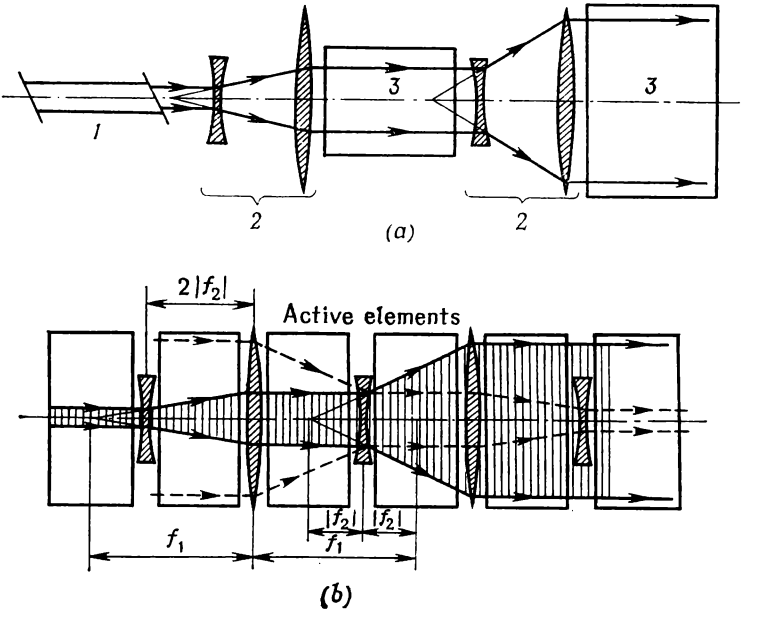


Fig. 2.66

region of the active element. For each round-trip of the radiation through the resonator, the transverse dimension of the optical beam increases M times. The higher the coefficient M of expansion of the beam, the faster the formation of radiation field in the resonator. This may be accomplished in just a few passes through the resonator.

Mirror-Edge Diffraction. Equivalent Fresnel Number. A rigorous treatment of losses in unstable resonators is based on the use of integral equations of the type (2.6.20) (see, for example, [39, 41, 42]). Such a treatment shows that the result (2.10.15) obtained within the framework of geometrical optics is approximate. In actual practice, losses depend on the product of the apertures of the mirrors. With variation in a_1a_2, the magnitude of losses oscillates around the geometrical optics value.

Figure 2.67 shows results of loss calculations based on the iterative method [45]. Calculations were carried out for symmetric resonators ($a_1 = a_2 = a$, $g_1 = g_2 = g$). The apertures of mirrors were chosen in the form of infinite bands of width $2a$. The curves in the figure show the dependence of losses Γ on Fresnel number $N = a^2/\lambda L$ for different values of the parameter g ($g = 0.8$-1.2). For the sake of comparison, the dashed lines show the results obtained on the basis of geometrical considerations [38].

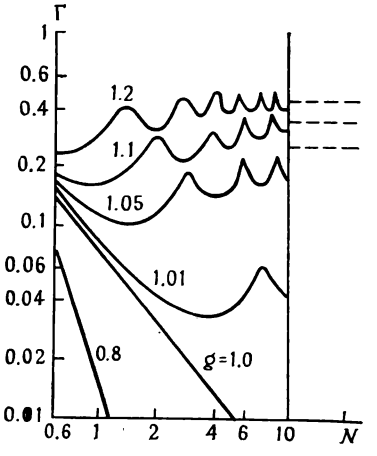


Fig. 2.67

Periodic variation of losses with variations in the value of a^2, shown in Fig. 2.67 is due to the *edge effect*, or the mirror-edge diffraction of radiation ([40, 42]; see also [44]).

In this connection, let us consider Fig. 2.68, where the edge-ray BB_1 is transformed upon reflection into the ray B_1C. The mirror-edge diffraction results in the emergence of an *auxiliary* diffraction wave, shown by the ray B_1D in the figure, in addition to the reflected wave. The periodic variation of losses upon variation of a^2 may be explained if we consider the interference of a divergent wave falling on the

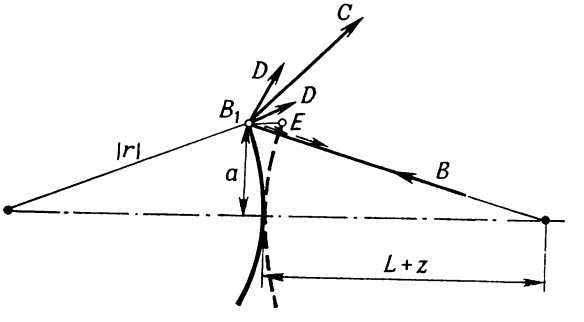


Fig. 2.68

edge of the mirror, and the diffracted wave propagating in a direction *opposite* to the divergent wave. For a mutual amplification of these waves, it is necessary that the path $2d$ (a) from a point F of the wave front to the edge B_1 of the mirror and back (see figure) should be a multiple of the wavelength λ: $2d$ (a) $= \lambda p$ where p is an integer. In this case, the phase shift of the diffracted wave relative to the

phase of the wave incident on the mirror edge will be a multiple of 2π.

The distance $d(a)$ (between F and B_1) may be represented in the form

$$d(a) = (|r| - \sqrt{r^2 - a^2}) + (L + z - \sqrt{(L+z)^2 - a^2}).$$

Since $a \ll |r|$, and $a \ll (L + z)$, we have

$$\sqrt{r^2 - a^2} \approx |r|(1 - a^2/2r^2), \quad \sqrt{(L+z)^2 - a^2} \approx (L+z)\left[1 - \frac{a^2}{2(L+z)^2}\right],$$

Thus,

$$d(a) = \frac{a^2}{2L}\left[\frac{L}{|r|} + \frac{1}{(z/L)+1}\right].$$

Using (2.10.5) and considering that $L/|r| = -L/r = g - 1$, we get

$$d(a) = \frac{a^2}{2L}\left(g - 1 + \frac{2}{\sqrt{(g+1)/(g-1)}+1}\right) = \frac{a^2}{2L}\sqrt{g^2 - 1}.$$

The condition $2d(a) = \lambda p$ now assumes the form

$$(a^2/\lambda L)\sqrt{g^2 - 1} = p. \tag{2.10.27}$$

It follows from (2.10.27) that a change in the properties of an unstable resonator with a change in the Fresnel number $a^2/\lambda L$ must be characterised by the *period* $1/\sqrt{g^2 - 1}$. Curves in Fig. 2.67 confirm this result (see curves for $g = 1.05$, 1.1, 1.2).

The quantity

$$\boxed{N_{eq} = (a^2/\lambda L)\sqrt{g^2 - 1}} \tag{2.10.28}$$

is called the *equivalent Fresnel number*. According to (2.10.27), losses in an unstable resonator must have the same value for equivalent Fresnel numbers differing by any *integer*. It can be easily seen (see (2.10.11)) that

$$N_{eq} = (a^2/2\lambda L)(M_s - 1/M_s). \tag{2.10.29}$$

In order to counter the edge effect in unstable resonators, steps are taken to reduce the intensity of the diffracted wave. For this purpose, we use *smooth-edge mirrors*, i.e. mirrors whose reflection coefficient falls not abruptly at the edge of the mirror, but gradually over a band of width not less than a/N_{eq} [46]. Smooth-edge mirrors weaken the dependence of losses on the mirror aperture, and then the geometrical optics treatment of losses in an unstable resonator is more correct.

Advantages of Unstable Resonators. "Unstable resonators are used most frequently to select the transverse oscillatory modes and to reduce the angular divergence of radiation. This method of selec-

tion is most promising for large volumes of active media, since it neither complicates the laser system nor reduces the efficiency of the laser to any appreciable extent" [44].

The example of a telescopic resonator clearly demonstrates the enhanced *selective* properties of unstable resonators forming light beams with a high degree of spatial coherence. Obviously, from the point of view of angular selection, it is better to choose conditions in which diffraction losses are relatively *large* since diffraction ensures a breakdown of oscillations primarily in higher order modes. Since diffraction (geometrical) losses are always high for an unstable resonator, we do not have to take any steps for auxiliary selection of transverse modes if we use an unstable resonator. A laser with an unstable resonator usually generates only the *fundamental* transverse mode (TEM_{00} mode), and the diffractional divergence limit is frequently attained. It should be observed that from the point of view of directionality of radiation, it is preferable to have higher values for the coefficient of expansion M (higher values of N_{eq}).

By way of an example, it should be noted that by using an unstable resonator in an Nd-glass laser an angular divergence of 2×10^{-5} rad was observed for the radiation whose beam width was 15 cm [47]. The unstable resonator had parameters $M = 2$, $N \approx 56\,000$, $N_{eq} = 7000$.

An important advantage of lasers with unstable resonators is an effective filling of the active medium by the radiation field. Even for relatively small resonator lengths, the volume occupied by the field of fundamental mode is quite large. Unlike stable resonators, the light beam in an unstable resonator has no constriction, hence there is no risk that the optical energy density of the beam may increase at certain points in the active medium to values corresponding to the disintegration threshold of the medium.

Unstable resonators are quite promising for creating lasers which have *stringently prescribed* spectral and time characteristics. As mentioned above, generation in a laser with an unstable resonator starts in the axial region of the active medium and then spreads to the entire volume. If inside the resonator of the laser we introduce, directly along its optical axis, radiation from an auxiliary generator with definite spectral and time properties at low power, we can effectively *control* the formation of radiation and thus obtain the desired output parameters for the optical beam [48].

It should be observed that the role of the axial region of the active element in the generation process has its disadvantages as well: lasers with unstable resonators are sensitive to different types of irregularities and defects in the active medium or in reflective coatings in the region immediately near the optical axis of the resonator.

A rapid development of the generator process in the direction from the axis to the periphery means, in particular, that the spatial growth (in the direction perpendicular to the axis) of a *giant pulse*

in the Q-spoiled mode takes place much more rapidly in lasers with unstable resonators than in lasers with stable resonators. Consequently, the duration of the light pulse generated by the laser is considerably *reduced.* It should be emphasised that the application of an unstable resonator may have a considerable effect on the dynamics of a laser process [49].

2.11. FREQUENCY SELECTION

Angular and *frequency* mode selections are also called transverse and longitudinal mode selections, respectively[44]. In order to separate any mode it is necessary that the losses for this mode be lower than for other modes. Transverse mode selection is based on the difference in the transverse field structure of different order modes, while the longitudinal mode selection is based on the difference in frequencies.

A difference in the field structure for transverse modes leads to a difference in diffraction losses. In unstable resonators, diffraction losses are so high that only the fundamental transverse mode oscillations are usually realised. In stable resonators, diffraction losses are relatively small, and hence special measures have to be taken in order to obtain a preferential increase in losses for higher order modes. For this purpose, either a diaphragm is introduced into the resonator[45] or the resonator configuration (parameters G_1 and G_2) is chosen in such a way that the Fresnel number decreases, and hence the difference between losses for the fundamental (primary) mode and other modes increases. We shall now discuss the frequency selection principles in detail.

Various Types of Frequency Selection. Let us suppose that two laser transitions between two pairs of energy levels take place in an active medium. Frequencies ω_1 and ω_2 at which these transitions take place correspond to the *maxima* in the luminescence curves for these transitions. In order to describe the spectral lines, we shall be using the frequency dependence of the initial gain (i.e. the $\varkappa_0$ vs. ω dependence).

Figure 2.69*a* shows the luminescence curve for two laser transitions. Here $\Delta\omega_l$ is the effective luminescence line-width (width at half the maximum height of the luminescence curve), $\Delta\omega$ is the separation between the maxima of lines ($\Delta\omega = \omega_2 - \omega_1$). The quantity $\Delta\omega$ assumes values in the interval 10^{12}-10^{16} $\sec^{-1}$ approximately, while $\Delta\omega_l$ lies between 10^{10} $\sec^{-1}$ (for gaseous media) and 10^{14} $\sec^{-1}$ (for organic dyes). For the case of a resonator, each luminescence line has (in the laser generator spectrum) a set of *spectral lines of the*

[44] Mode selection methods have been described in [50]. See also [9, 13, 51] and Ch. 23 in [2].

[45] A comparison of selective properties in various diaphragm resonators has been carried out in [33]. It is shown that the confocal resonator is the most selective one.

resonator, corresponding to resonance frequencies (Fig. 2.69*b*). In accordance with (2.2.12), the separation between the maxima of neighbouring lines for a resonator[46] is given by $\Delta\omega' = \pi v/L$, where l is the length of the resonator and v is the velocity of light in the medium filling the resonator. The width of an individual resonator line $\Delta\omega_r$ is of the order of 10^7-10^9 $\sec^{-1}$.

With the help of Fig. 2.69, we can separate three types of frequency selection in a laser. The first type is the selection over a relatively

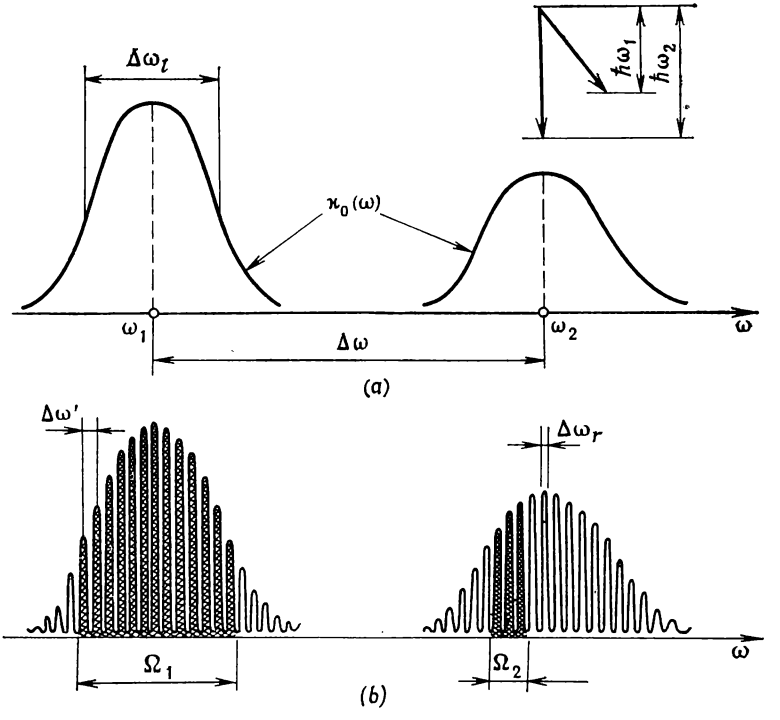


Fig. 2.69

wide frequency band where the undesirable transitions are suppressed and generation is ensured only on a single transition. Oscillations in this case are generated over a frequency band of width Ω_1 (see Fig. 2.69*b*). Selection of the *second* type ensures a generation over a narrower frequency band, for example, the frequency band Ω_2 (Fig. 2.69*b*). By varying the position of this frequency interval within the luminescence line width, a continuous frequency tuning of the laser radiation[47] may be attained. The *third* type of selection

[46] The frequency pulling effect will be considered in Sec. 2.12.

[47] Such a frequency tuning is made, for example, in organic dye lasers (See [52], as well as Sec. 1.3).

is the selection of longitudinal modes. This ensures generation of an individual spectral line (usually, the central line). In this case, the selection is carried out over a fairly narrow frequency interval—of the order of 10^9 sec^{-1} or less.

Application of Wide-band Absorption Filters and Dispersive Elements. For carrying out a frequency selection of the first type,

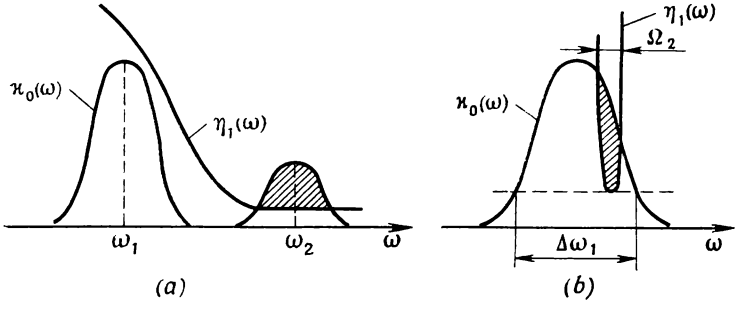


Fig. 2.70

we can use relatively wide-band *absorption filters* inside the resonator. For example, the output windows of the discharge tube of a helium-neon laser are made of a special type of glass which absorbs infrared radiation. Thus transitions with $\lambda = 3.39$ μm and 1.15 μm are suppressed and the laser generates only on a transition with $\lambda = 0.63$ μm. Such a selection is illustrated in Fig. 2.70*a*. It is based on a suitable choice of frequency dependence of the unfavourable loss coefficient ($\eta_1(\omega)$). Generation takes place on the transition corresponding to frequency ω_2 although this transition is characterised by a lower gain factor in comparison to the transition at frequency ω_1.

For a narrower frequency selection, either *dispersive elements* (for example, a prism) are introduced into a resonator, or the resonator mirror is replaced by a reflection grating. Examples of such a selection were given in Sec. 1.3 while describing *selective resonators*. The frequency dependence curve for the loss coefficient ($\eta_1(\omega)$ curve) of a selective resonator has a sharp and narrow dip of width $\Omega_2 \approx$ $\approx 10^{12}$-10^{13} sec^{-1} (Fig. 2.70*b*). By tilting the prism or the reflection grating, we can control the position of this dip on the frequency scale and thus tune the oscillation frequency over the luminescence line width at a constant loss level (within the limits of the line width $\Delta\omega_1$; see the figure).

For an even narrower band selection, a *Fabry-Perot interferometer* is used as the dispersive element. This interferometer is a system of closely spaced plane parallel mirrors, and helps in isolating an individual longitudinal mode.

General Remarks about Selection of Longitudinal Modes. For selection of longitudinal modes, a fairly *narrow-band* filter, capable of isolating an interval less than 10^9 sec^{-1}, is required. In order to consider the general principles of selection of longitudinal modes, let us turn to Fig. 2.71 (dashed lines indicate the contour of the luminescence curve). This figure illustrates the possible methods of carrying out such selection.

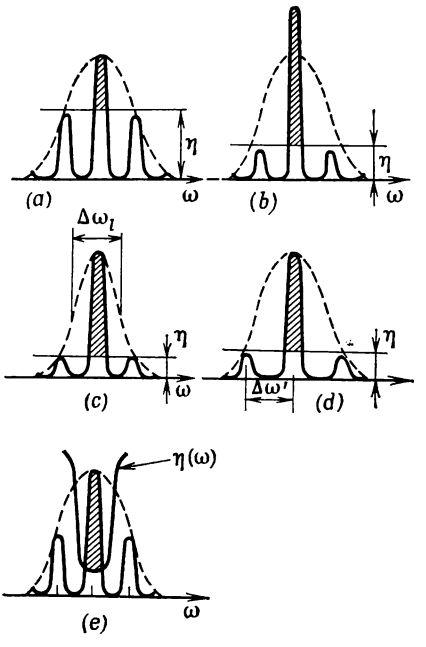


Fig. 2.71

In the first place, we can simply *raise the loss level* so that the difference $\varkappa_0 - \eta$ (η is the total loss coefficient) is positive only for the central longitudinal mode (Fig. 2.71*a*). Of course, the laser power is considerably reduced in this case. It is better to *change* the relation between the maximum values of the initial gain factor of the central mode and the other longitudinal modes (in favour of the central mode) (Fig. 2.71*b*). A similar result may be attained *by changing the contour of the luminescence curve*, i.e. to decrease the width $\Delta\omega_l$ (Fig. 2.71*c*)[48]. We can also increase the frequency interval between the maxima of longitudinal modes *by decreasing the length of the resonator* (Fig. 2.71*d*). Naturally, decreasing the length of the resonator has its own disadvantages like less gain per pass, lower output power, and increased divergence of radiation[49]. Finally, we can try to get a fairly narrow-band selectivity of the loss coefficient (Fig. 2.71*e*).

All these methods of mode selection are used in actual practice. The simplest methods of selection are based on decreasing the length of the resonator. The selection methods using *interference*, *polarisation*, and *nonlinear optical* effects are more interesting. We shall now describe these methods in detail.

Interference Methods of Longitudinal Mode Selection. These methods are based on the use of resonators with *auxiliary* (additional) mirrors (*coupled* resonators), see, for example, [54-56].

[48] A significant narrowing of the luminescence curve should take place in atomic beam lasers [53].

[49] These negative factors may be eliminated by using unstable resonators.

Let us consider the laser shown in Fig. 2.72 [54]. Here, *1* is the discharge tube with windows inclined at Brewster's angle (active element), *2*—a double-refraction crystal, splitting a light ray into extraordinary (linearly polarised in the plane of the figure) and

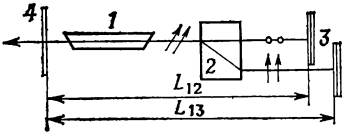


Fig. 2.72

ordinary (linearly polarised perpendicular to the plane of the figure) parts, *3*—totally reflecting mirrors, and *4*—the output mirror. In

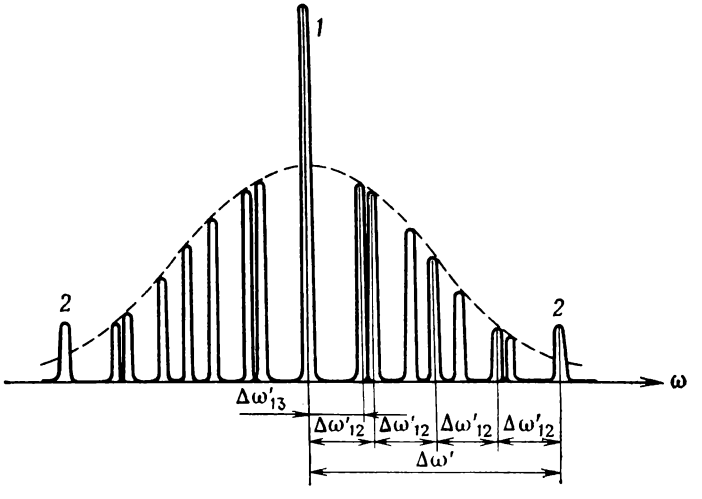


Fig. 2.73

fact we have two resonators in this case with different lengths L_{12} and L_{13}. The intermode separations for these resonators are respectively equal to

$$\Delta\omega'_{12} = \pi c/L_{12} \quad \text{and} \quad \Delta\omega'_{13} = \pi c/L_{13}. \tag{2.11.1}$$

If we assume that the inequality

$$\Delta\omega_r < (\Delta\omega'_{12} - \Delta\omega'_{13}) \tag{2.11.2}$$

is satisfied, the spectral lines of the resonator will have the form shown in Fig. 2.73. The lines marked as *1* and *2* are found to be

amplified much more than the neighbouring lines, since they correspond to frequencies for which the resonance condition is simultaneously satisfied in resonators of length L_{12} and L_{13}. Appearance of such lines is apparently due to interference effects. The separation between them is given by

$$\Delta\omega' = \pi c/(L_{13} - L_{12}). \quad (2.11.3)$$

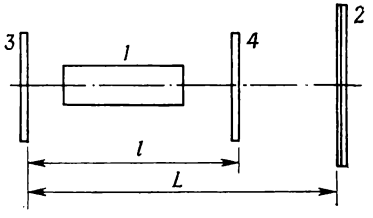


Fig. 2.74

For a sufficiently small difference $(L_{13} - L_{12})$, the magnitude of $\Delta\omega'$ may be increased ($\Delta\omega'$ may exceed the luminescence line width).

Another alternative interference mode selection is connected with the use of a three-mirror linear resonator (Fig. 2.74). Here, *1* is the active element, *2* — a totally reflecting mirror, *3* — the output mirror, and *4*—an auxiliary mirror. The interference of light waves formed in resonators of length l and L leads, as in the previous case, to a change in the correlation between the mode intensities. Calculations have been carried out by Mikaelyan *et al.* [13] for $l/L = 3/4$ and $R' = 0.65$ (R' is the reflection coefficient of the auxiliary mirror). Figure 2.75 illustrates the results of calculations. Three modes are shown in the figure. For the sake of comparison, dashed lines show the corresponding modes in the absence of an auxiliary mirror. It can be seen that interference effects lead to a preferential population of the central mode and to an increase in the mode separation.

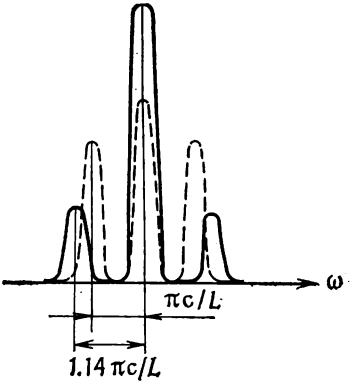


Fig. 2.75

Various methods are used in actual practice for interference selection of longitudinal modes, e.g., different types of four-mirror coupled resonators, where the mirror axes are at right angle to each other, are used (see Ch. 23 in [2]). One such resonator is shown in Fig. 2.76.

Resonators with Anisotropic Elements. For selection of longitudinal modes, the *polarisation* properties of a resonator with *anisotropic* elements may be used. The resonator shown in Fig. 2.77 is an example of this kind of a resonator. Here, *1* is a linear polariser, *2*—a double-refraction slab which ensures a phase difference $\Delta\varphi$ between ordinary and extraordinary rays, and *3*—the resonator mirrors. The optical axis of slab *2* is perpendicular to the optical axis of the resonator and is inclined at an angle α to the direction of polarisation determined by the polariser *1*.

Suppose that the polarisation of a light ray in the reference plane P (Fig. 2.77) is described by the *Jones vector*[50] $\begin{pmatrix} E_x \\ E_y \end{pmatrix}$. The x-axis is so chosen that it coincides with the direction of polarisation fixed by the polariser. The *Jones matrix* for a round-trip through the resonator from the reference plane P has the following form:

$$M = M_1 M(-\alpha)\, M(\varphi)\, M(\varphi)\, M(\alpha)\, M_1. \qquad (2.11.4)$$

The matrices appearing in (2.11.4) have the following sense (see Appendix 4):

$$M_1 = \begin{pmatrix} 1 & 0 \\ 0 & 0 \end{pmatrix} \qquad (2.11.5)$$

is the Jones matrix for a *linear polariser* which fixes the direction of

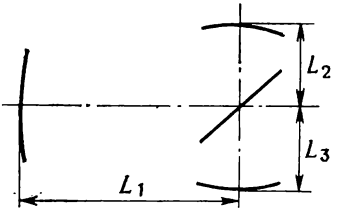


Fig. 2.76

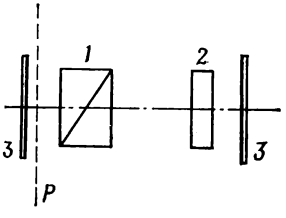


Fig. 2.77

polarisation along the coordinate axis corresponding to the first component of the Jones vector (along x-axis);

$$M(\alpha) = \begin{pmatrix} \cos\alpha & \sin\alpha \\ -\sin\alpha & \cos\alpha \end{pmatrix} \qquad (2.11.6)$$

is the matrix for transforming the Jones vector to new axes (*inclined* at an angle α to the initial coordinate axes); and

$$M(\varphi) = \begin{pmatrix} e^{i\varphi_1} & 0 \\ 0 & e^{i\varphi_2} \end{pmatrix} \qquad (2.11.7)$$

is the Jones matrix for a *double-refraction slab*, ensuring a phase advancement φ_1 for the x-component of the Jones vector and a phase advancement φ_2 for the y-component. Suppose that the extraordinary ray is polarised along the x-axis while the ordinary ray is polarised along the y-axis. If $\Delta\varphi = \varphi_1 - \varphi_2$ is the phase difference between the extraordinary and ordinary rays after passing through the double-refraction slab, we can rewrite (2.11.7) in the form

$$M(\varphi) = e^{i\varphi_2} \begin{pmatrix} e^{i\Delta\varphi} & 0 \\ 0 & 1 \end{pmatrix}. \qquad (2.11.8)$$

[50] Application of the Jones vector and matrix for *polarised* light rays is described in [4,57]. See also [58].

It should be observed that

$$\Delta\varphi = \omega\,(n_e - n_o)\,d/c, \tag{2.11.9}$$

where n_e and n_o are refractive indices for extraordinary and ordinary rays respectively, and d is the thickness of the slab.

Substituting (2.11.5), (2.11.6), and (2.11.8) in (2.11.4), we get the following expression for the Jones matrix for a round-trip through the resonator from P plane (see Fig. 2.77):

$$\begin{aligned} M &= \begin{pmatrix} 1 & 0 \\ 0 & 0 \end{pmatrix} \begin{pmatrix} \cos\alpha & -\sin\alpha \\ \sin\alpha & \cos\alpha \end{pmatrix} \begin{pmatrix} e^{2i\Delta\varphi} & 0 \\ 0 & 1 \end{pmatrix} \\ &\times \begin{pmatrix} \cos\alpha & \sin\alpha \\ -\sin\alpha & \cos\alpha \end{pmatrix} \begin{pmatrix} 1 & 0 \\ 0 & 0 \end{pmatrix} e^{i2\varphi_2} \\ &= \begin{pmatrix} \cos^2\alpha e^{i2\Delta\varphi} + \sin^2\alpha & 0 \\ 0 & 0 \end{pmatrix} e^{i2\varphi_2}. \end{aligned} \tag{2.11.10}$$

Denoting by $\begin{pmatrix} E'_x \\ E'_y \end{pmatrix}$ the Jones vector for a light wave after a round-trip through the resonator, we write

$$\begin{pmatrix} E'_x \\ E'_y \end{pmatrix} = e^{i2\varphi_2} \begin{pmatrix} \cos^2\alpha e^{i2\Delta\varphi} + \sin^2\alpha & 0 \\ 0 & 0 \end{pmatrix} \begin{pmatrix} E_x \\ E_y \end{pmatrix}. \tag{2.11.11}$$

Due to the existence of a linear polariser, only the x-component of the Jones vector passes through the resonator. In accordance with (2.11.11), the relative losses for a round-trip can be expressed by

$$\begin{aligned} \Gamma &= 1 - |E'_x|^2/|E_x|^2 \\ &= 1 - |\cos^2\alpha e^{i2\Delta\varphi} + \sin^2\alpha|^2. \end{aligned} \tag{2.11.12}$$

Thus

$$\Gamma = \sin^2 2\alpha \sin^2\Delta\varphi. \tag{2.11.13}$$

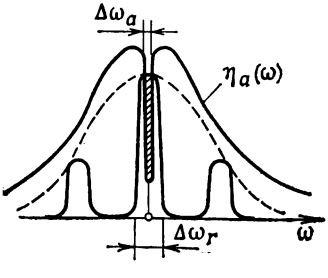


Fig. 2.78

In accordance with (2.11.9), the quantity $\Delta\varphi$ depends on the radiation frequency. Consequently, the losses expressed by (2.11.12) must *vary periodically* with frequency. This variation of losses with frequency may be used for selection of longitudinal modes in the resonator under consideration.

Nonlinear Optics Method for Frequency Selection. Suppose that an *absorbing* element with the following properties is placed in a resonator: it absorbs on the laser transition frequency for a given active medium; in the case of a sufficiently high intensity radiation, a *saturation* of absorption takes place at the laser transition frequency near the centre of the absorption line (in other words, the nonlinear

optical effect of *bleaching* of medium takes place). As a result of this nonlinear effect, the shape of the absorption line (dependence of the absorption coefficient η_α on frequency ω) changes: a dip, which may have a quite *narrow band*, appears. The width $\Delta\omega_a$ of the dip may be less than the width $\Delta\omega_r$ of the spectral line of the resonator. In this case we cannot only separate one longitudinal mode, but also further narrow down the width of the generated line (Fig. 2.78).

A cell filled with a gas at low pressure can be used as the absorbing nonlinear element. For pressures around 10^{-2} mm Hg, we get $\Delta\omega_a = 10^5$-10^6 sec^{-1}, which is about two orders less than the width $\Delta\omega_r$ of the mode [59].

Assuming $\Delta\omega_a \ll \Delta\omega_r$ and considering that the position of the dip in the absorption spectrum of the gas cell is *fixed* on the frequency scale, it may be concluded that this method is not only the method of frequency selection but also the method of *stabilisation* of laser radiation frequency (the stability of the centre of the absorption line may be around 10^{-11}).

2.12. HOLE-BURNING EFFECT AND FREQUENCY PULLING EFFECT

It was remarked earlier (see Sec. 2.2) that the presence of an active (amplifying) medium influences the process of radiation field formation in a resonator. In particular, the energetic and spectral properties of the radiation are changed. In this connection, let us consider the hole-burning effect and the frequency pulling effect. A rigorous treatment of these effects is given in [60]; see also [9, 10].

Homogeneous and Inhomogeneous Broadening of Spectral Lines. The luminescence line for a laser transition in the active medium is formed by adding the contributions from different active centref undergoing this transition. We assume that the contribution os each active centre corresponds to the *entire frequency band* characterising the luminescence line of the medium. In this case, the broadening of the luminescence line is called *homogeneous*. Amplification of *different* frequencies of homogeneously broadened line is brought about by *the same* active centres.

If different active centres (or groups of active centres) contribute in *different* frequency regions of the luminescence line, the line broadening is called *inhomogeneous*. Amplification at *different* frequencies of an inhomogeneously broadened line is brought about by *different* groups of active centres.

Homogeneous broadening is connected with relaxation of levels due to spontaneous emission and different types of collisions, since the probability of these processes is the same for all active centres. It is well known that these processes are responsible for the *Lorentzian* form of the luminescence line[51]. A Lorentzian line profile is given by

[51] See, for example, Sec. 4.7 in [1].

the formula

$$F_1(\omega) = \frac{\Delta}{\pi} \frac{1}{(\omega-\omega_0)^2+\Delta^2}. \qquad (2.12.1)$$

Here, ω_0 is the fundamental frequency corresponding to the maximum in the line, Δ is the line half-width, $\Delta = \Delta_\gamma + \Delta_{col.}$, where Δ_γ is the natural half-width (due to spontaneous emission) and $\Delta_{col.}$ is the collision half-width. It should be noted that the function $F_1(\omega)$ is normalised to unity, i.e. $\int_0^\infty F_1(\omega)\, d\omega = 1$.

The equal probability of relaxation processes for all active centres means that the shape of the luminescence line *coincides* with the shape of the line for an individual active centre. In other words, the function (2.12.1) describing the shape of the line for an individual active centre also describes the shape of a homogeneously broadened line for the medium.

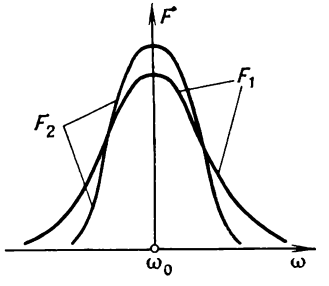


Fig. 2.79

In a general case, such a coincidence does not exist. The actual luminescence lines for the medium are more or less inhomogeneously broadened. The *inhomogeneous* broadening may be caused by various factors: Doppler effect, spatial inhomogeneity of the medium, overlapping of Lorentzian lines and various fundamental frequencies (for example, in Stark splitting of laser levels) etc. *Doppler effect* is the main cause of inhomogeneous broadening of lines in gaseous media. Apparently, the active centres having different velocities will contribute in different frequency intervals of the luminescence line of the medium. In this case, the line has a *Gaussian* shape

$$F_2(\omega) = \frac{\sqrt{\ln 2}}{\Delta_D \sqrt{\pi}} \exp\left[-\frac{(\omega-\omega_0)^2 \ln 2}{\Delta_D^2}\right], \qquad (2.12.2)$$

where ω_0 is the fundamental frequency, Δ_D is the line half-width; the function F_2 is normalised to unity just like the function F_1.

The functions $F_1(\omega)$ and $F_2(\omega)$ have been shown in Fig. 2.79. For the sake of convenience of comparison, they have been reduced to the same half-width. It can be seen from the figure, in particular, that a Gaussian line is characterised by a more rapid fall with increasing $|\omega - \omega_0|$.

Gain Saturation for Homogeneous and Inhomogeneous Line Broadening. Hole-burning Effect. It has been mentioned earlier[52] that

[52] See Sec. 2.1 as well as Sec. 5.6 in [1].

with increasing density of light flux propagating in an inverted active medium, the gain $\varkappa$ decreases gradually from its initial value $\varkappa_0$ up to the value

$$\varkappa_{sat} = \eta, \tag{2.12.3}$$

where η is the linear coefficient of total losses. This results in a stationary process characterised by a saturated gain $\varkappa_{sat}$ and a saturated light flux density S_{sat}, determined from (2.1.1) with the help of (2.12.3).

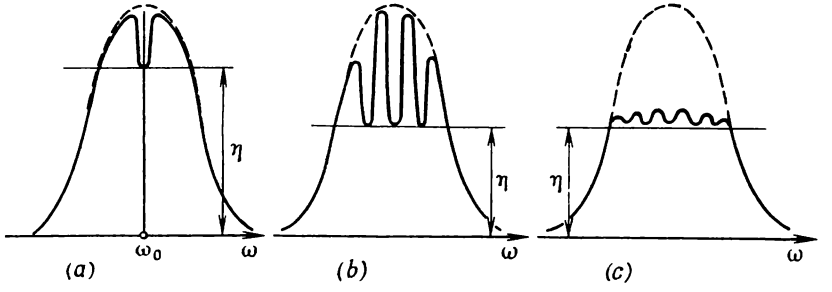


Fig. 2.80

Taking into consideration the frequency dependence of gain let us consider the cases when $\varkappa_0(\omega)$ corresponds to *homogeneous* and *inhomogeneous* broadening respectively. We assume the loss level to be so high that a selection of the central longitudinal mode takes place.

For *inhomogeneous* broadening of the line $\varkappa_0(\omega)$, only those active centres will take part in laser transitions which contribute in the frequency interval near ω_0 corresponding to the central longitudinal mode. Consequently, a *selective* removal of conversion of active medium will take place within this frequency interval. In this case, a *dip* ("hole burning") will be observed on the profile of the curve showing the frequency dependence of the gain. Figure 2.80*a* illustrates this situation. Here, the dashed line shows the inhomogeneous broadening of the $\varkappa_0(\omega)$ curve, while the continuous line shows the $\varkappa_{sat}(\omega)$ curve. In accordance with (2.12.3),

$$\varkappa_{sat}(\omega_0) = \eta, \tag{2.12.4}$$

which defines the *depth* of the burnt hole. The hole *width* corresponds to the line width of an individual active centre, i.e. the Lorentzian width 2Δ which in this case is considerably less than the width $2\Delta_D$ of the $\varkappa_0(\omega)$ curve.

If the hole width is smaller than the intermode frequency separation, i.e. if

$$2\Delta < \pi c/Ln, \tag{2.12.5}$$

a lowering of the loss level will lead to a burning of additional holes corresponding to various longitudinal modes (Fig. 2.80*b*). It should be emphasised that in this case, generation of *different* longitudinal modes is accomplished on account of emission by *different* groups of active centres. This means that a laser may generate on several modes *simultaneously* and *independently*.

If the condition (2.12.5) is not satisfied, a mutual *overlapping* of burnt holes takes place. In this case practically the entire profile of the gain curve may burn out (Fig. 2.80*c*).

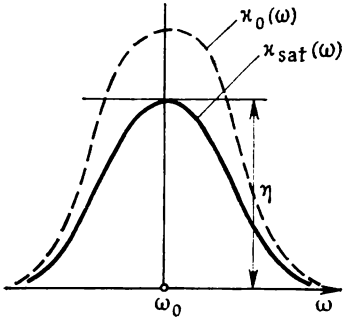


Fig. 2.81

For a *homogeneous* broadening of $\varkappa_0(\omega)$ curve, the hole-burning effect is not observed. We assume that for sufficiently high losses, a laser generates only the central longitudinal mode. Since the contribution to the radiation of this mode is made by *all* the active centres, an *all-round* change in the profile of the $\varkappa(\omega)$ curve takes place (Fig. 2.81). Thus, the excitation of one (central) mode leads to an all-round depletion of inversion of the active medium, which in turn hinders the excitation of other modes. Figures 2.80 and 2.81 very well illustrate the qualitative difference between homogeneous and inhomogeneous broadening. In the case of an inhomogeneous broadening when a single mode is generated, only a *part* of the energy stored in the inverted active medium is utilised. Hence the intensity of the generated mode for an inhomogeneously broadened transition line is *considerably lower* than for homogeneous broadening. Besides, it should be remembered that for a homogeneous broadening the gain saturation effect prevents an excitation of additional longitudinal modes.

Gain Saturation for the Inhomogeneous Broadening of a Transition Line. The gain for an active centre contributing in the vicinity of the frequency ω' may be expressed, in accordance with (2.1.1), in the form

$$\varkappa(\omega';\ \omega) = \frac{\varkappa_0(\omega';\ \omega)}{1+(1/\nu)\,\alpha(\omega';\ \omega)\,S}, \qquad (2.12.6)$$

where

$$\varkappa_0(\omega';\ \omega) = \varkappa_0 F_1(\omega';\ \omega);$$

$$\alpha(\omega';\ \omega) = \alpha F_1(\omega';\ \omega);$$

$$F_1(\omega';\ \omega) = \frac{\Delta}{\pi}\,\frac{1}{(\omega-\omega')^2+\Delta^2}.$$

The gain factor of the active medium for an inhomogeneous line broadening due to Doppler effect is expressed through the following

integral which takes into account the contribution from different active centres:

$$\varkappa(\omega) = \int_0^\infty \varkappa(\omega';\ \omega)\, F_2(\omega')\, d\omega', \tag{2.12.7}$$

where

$$F_2(\omega') = \frac{\sqrt{\ln 2}}{\Delta_D \sqrt{\pi}} \exp\left[-\frac{(\omega' - \omega_0)^2 \ln 2}{\Delta_D^2} \right].$$

Substituting (2.12.6) in (2.12.7) we get

$$\varkappa(\omega) = \sqrt{\frac{\ln 2}{\pi^3}} \frac{\varkappa_0}{\Delta_D \Delta} \int_0^\infty \frac{\exp\left[-(\omega' - \omega_0)^2 \ln 2/\Delta_D^2\right]}{1 + \left(\frac{\omega - \omega'}{\Delta}\right)^2 + \frac{\alpha}{v\pi\Delta} S}\, d\omega'. \tag{2.12.8}$$

Equating $\varkappa(\omega)$ to the linear coefficient of total losses, we get an equation for determining the saturation value for the light flux density S.

Frequency Pulling Effect. The resonance frequency spectrum of a *passive* resonator has the following form in accordance with (2.9.21) (for the fundamental mode of the Gaussian beam):

$$\omega_q = \frac{\pi c}{Ln}\left[q + \frac{1}{\pi} \arccos \sqrt{g_1 g_2} \right], \tag{2.12.9}$$

where n is the refractive index of the medium filling the resonator. The frequency spectrum is *equidistant*, and the separation between adjacent frequencies is given by $\Delta\omega' = \pi c/Ln$.

For an *active* (*amplifying*) medium, the frequency spectrum in a resonator changes. It loses its property of equidistantness on account of the frequency dependence of the refractive index of the amplifying medium. The nature of this dependence near the natural frequency of the laser transition ω_0 is shown in Fig. 2.82. It is evident from the figure that if $\omega < \omega_0$, then $n(\omega) < n(\omega_0)$. In accordance with (2.12.9), we conclude that the frequencies ω_q lying to the left of ω_0 are shifted to the right. If, however, $\omega > \omega_0$, then $n(\omega) > n(\omega_0)$ and hence the frequencies ω_q lying to the right of ω_0 are shifted to the left. Consequently, the entire set of resonance frequencies corresponding to the profile of the gain curve is *shifted* towards the natural transition frequency. The frequencies are sort of "pulled" towards the centre of the gain curve.

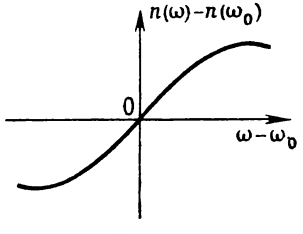


Fig. 2.82

Frequency Pulling for Homogeneous and Inhomogeneous Broadening. It is well known (see, for example, [9]) that an absorbing medium

may be described by the complex refractive index

$$n_{\text{compl.}} = n + in_1.$$

The imaginary component n_1 is expressed in terms of the linear absorption coefficient η_a

$$n_1 = \eta_a c/2\omega. \tag{2.12.10}$$

The dependences n vs. ω and n_1 vs. ω, corresponding to a *uniform* (Lorentzian) broadening of the luminescence line, may be found within the framework of the classical *dispersion theory of dielectric susceptibility* by considering the model of a harmonic oscillator with a natural frequency ω_0 and damping factor γ. For a gaseous medium, these dependences can be written in the form[53]

$$n - 1 = D\frac{\omega_0^2 - \omega^2}{(\omega_0^2 - \omega^2)^2 + \gamma^2\omega^2}; \tag{2.12.11a}$$

$$n_1 = D\frac{\gamma\omega}{(\omega_0^2 - \omega^2)^2 + \gamma^2\omega^2}, \tag{2.12.11b}$$

where D is a constant factor whose form is not important in this case. Assuming that the frequency ω is fairly close to ω_0, such that

$$\omega_0^2 - \omega^2 \approx 2\omega(\omega_0 - \omega), \tag{2.12.12}$$

we can rewrite (2.12.11) in the form

$$n - 1 = D\frac{(\omega_0 - \omega)/2\omega}{(\omega_0 - \omega)^2 + \gamma^2/4}; \tag{2.12.13a}$$

$$n_1 = D\frac{\gamma/4\omega}{(\omega_0 - \omega)^2 + \gamma^2/4}. \tag{2.12.13b}$$

Taking into account (2.12.10), we get the following frequency dependence of the absorption coefficient from (2.12.13b):

$$\eta_a(\omega) = D\frac{\gamma/2c}{(\omega_0 - \omega)^2 + \gamma^2/4}. \tag{2.12.14}$$

It can be easily seen that the absorption line η_a vs. ω is *Lorentzian* in shape.

Dividing (2.12.13a) by (2.12.14), we get

$$n(\omega) = 1 + \eta_a(\omega)(\omega_0 - \omega)\, c/\gamma\omega. \tag{2.12.15}$$

In order to use (2.12.15) to explain the frequency pulling effect, it should be remembered that the natural frequency ω_0 of the oscillator corresponds (upon quantum mechanical generalisation of relations (2.12.13)) to the natural transition frequency while the damping factor γ may be considered to be the Lorentzian width 2Δ. Besides, in order to consider the gain, we must replace the absorption coefficient $\eta_a(\omega)$ in (2.12.15) by the gain $\varkappa(\omega)$ but with *opposite*

[53] See, for example, Sec. 4.5 in [1].

sign (*gain* is considered as *negative absorption*). Thus

$$n(\omega) = 1 - \varkappa(\omega)(\omega_0 - \omega)\, c/2\omega\Delta. \qquad (2.12.16)$$

In the case of a stationary generator, the gain factor is equal to the loss factor: $\varkappa = \eta$. Taking into account (2.3.10) and (2.3.15), we find that

$$\varkappa = \Delta\omega_r/c, \qquad (2.12.17)$$

where $\Delta\omega_r$ is the width of the resonator spectral line. Substituting (2.12.17) in (2.12.16), we find that

$$n(\omega) = 1 - \frac{\omega^2 - \omega_0^2}{2\omega}\frac{\Delta\omega_r}{\Delta}. \qquad (2.12.18)$$

It can be easily seen that the frequency dependence of the refractive index, described by the relation (2.12.18), corresponds to the dependence given by Fig. 2.82 for values of ω close to ω_0.

Let ω_q be a resonance frequency of a *passive* resonator (for $n = 1$) and ω_q' be the corresponding resonance frequency of an *active* resonator. It follows from (2.12.9) that

$$\omega_q/\omega_q' = n(\omega_q'). \qquad (2.12.19)$$

Substituting (2.12.18) in (2.12.19), we get

$$\frac{\omega_q}{\omega_q'} = 1 - \frac{\omega_0 - \omega_q'}{\omega_q'}\frac{\Delta\omega_r}{2\Delta}.$$

Finally, we get the relation

$$(\omega_q' - \omega_q)/(\omega_0 - \omega_q') = \Delta\omega_r/2\Delta. \qquad (2.12.20)$$

It is evident from this that if the frequency is taken from the left of the centre of the gain curve ($\omega_0 - \omega_q' > 0$), then $\omega_q' > \omega_q$ and hence the frequency shift in an active resonator takes place to the right. If the frequency is taken from the right of the centre of the gain curve ($\omega_0 - \omega_q' < 0$), then $\omega_q' < \omega_q$ and the frequency shifts to the left.

For the case of an *inhomogeneously broadened transition line*, only such active centres are operative, whose frequencies differ from ω_0 by not more than Δ (not more than half-width of a homogeneously broadened line). The fraction of such active centres is approximately Δ/Δ_D where Δ_D is the half-width of the inhomogeneously broadened line. Consequently, the gain on an inhomogeneously broadened transition must be Δ_D/Δ times *smaller* than for a homogeneous broadening. This means that the following relation should be used instead of (2.12.17):

$$\varkappa = (\Delta\omega_r/c)(\Delta/\Delta_D).$$

Consequently, we get, instead of (2.12.20),

$$(\omega_q' - \omega_q)/(\omega_0 - \omega_q') = \Delta\omega_r/2\Delta_D. \qquad (2.12.21)$$

For a more rigorous approach, the right-hand side of the relation (2.12.21) acquires an additional term giving a nonlinear contribution to the frequency pulling effect [9].

2.13. THERMAL LENS

Thermal Lens Effect. By absorbing pumping radiation, an active medium gets heated. Consequently, its refractive index changes. Let $n(0)$ be the refractive index of the medium at a certain point in the absence of pumping radiation. If the temperature of the medium increases by ΔT at this point due to the presence of radiation, the refractive index becomes equal to

$$n(\Delta T) = n(0) + (dn/dT)\,\Delta T, \tag{2.13.1}$$

where dn/dT is a physical property of the medium, called *thermal coefficient* of its refractive index.

Upon extraction of heat through the lateral face of an active sample, a preferential cooling of its peripheral region is observed. Hence the temperature of the sample rises to its maximum value near its axial region and gradually falls in the direction from the axis to the periphery. It follows from this that if the inequality

$$dn/dT > 0 \tag{2.13.2}$$

as satisfied, the region near the axis of the active sample is optically *denser* than the peripheral region, in accordance with (2.13.1). If, on the contrary, the inequality

$$dn/dT < 0 \tag{2.13.3}$$

is satisfied, the region near the axis of the active sample is optically *rarer*.

In optically inhomogeneous media, light rays are deflected into the region with a *higher* refractive index; hence for $dn/dT > 0$, the laser radiation propagating along the active sample will be *focussed*, while for $dn/dT < 0$ it will be *defocussed*. In the former case the active sample is identical to a *convergent* lens, while in the latter case it is identical to a *divergent* lens. This is the *thermal lens effect*.

Ruby and YAG crystals have *positive* thermal coefficients of the refractive index. Hence a thermal lens formed in these crystals is convergent. For ruby $dn/dT = 1.4 \times 10^{-5}\ K^{-1}$, for garnet $dn/dT = 7.3 \times 10^{-6}\ K^{-1}$ [61]. The divergent thermal lens effect is observed in some types of glasses.

While considering the thermal lens effect in the active sample of a solid-state laser, the absorption of *laser radiation* in it may be neglected in the first approximation, since the power of this radiation is about two orders of magnitude lower than the *pumping radiation* power. In this case, a situation arises where a thermal lens

created by the absorption of *one* radiation (pumping radiation) influences the formation of the field of *another* radiation (radiation generated in the active laser medium). The role of laser radiation in a thermal lens becomes significant when the radiation is the only factor responsible for heating of the medium. A nonlinear crystal for parametric frequency transformation using laser radiation for pumping may be mentioned as an example.

In such cases, a thermal lens formed due to the absorption of a certain radiation (laser beam) in the medium influences *the same* radiation. The thermal lens effect serves as a *nonlinear* effect here; it is called the *thermal nonlinearity* effect or just *thermal self-focussing*[54]. If, for example, a laser beam forms a convergent thermal lens in any element, the density of the beam will increase as a result of thermal focussing in the axial region of the element, and hence the absorption of radiation in this region will also increase. Thus the focussing properties of such a thermal lens will be enhanced.

Thermoelastic Stress. Thermal Distortion of a Resonator. The relation (2.13.1) may be rewritten in the form

$$n(\Delta T) - n(0) = \Delta n_T + \Delta n_\sigma = (\partial n/\partial T)_\sigma \Delta T + \Delta n_\sigma. \quad (2.13.4)$$

This notation shows that the total change in the refractive index at a certain point in the medium consists of purely thermal variation $\Delta n_T = (\partial n/\partial T)_\sigma \Delta T$, and the variation Δn_σ caused by *thermoelastic* stresses in the non-uniformly heated medium. To be more precise, the variation Δn_σ in the refractive index is caused by the *photoelastic* effect (also called the *piezooptic* effect) resulting from thermoelastic stresses in the medium. The coefficient $(\partial n/\partial T)_\sigma$ is the thermal coefficient of the refractive index, measured under conditions of uniform heating of a solid without any stress (it can be easily seen that for $\Delta n_\sigma = 0$, we get $dn/dT = (\partial n/\partial T)_\sigma$[55]).

The quantity Δn_σ is expressed in terms of elastooptic constants of the medium and elastic deformations caused by nonuniform heating. Both Δn_T and Δn_σ have the same order of magnitude. Thus, for example, for the lithium niobate ($LiNbO_3$) crystal placed in the path of a laser beam, the following values have been obtained [63]: $\Delta n_T = 1.4 \times 10^{-5} \times \Delta T$; $\Delta n_\sigma = 0.66 \times 10^{-5} \times \Delta T$. If, in particular, $\Delta n_T < 0$, and $\Delta n_\sigma > 0$, both $(\Delta n_T + \Delta n_\sigma) < 0$ as well as $(\Delta n_T + \Delta n_\sigma) > 0$ are possible.

Significantly, thermoelastic stresses do not simply lead to an additional contribution to the change in the refractive index. These stresses influence the *optical indicatrix* of the sample through the photoelastic effect[56]. If in the initial state, a sample is optically isotropic (liquid, glass or crystal with a cubic symmetry), it acquires, under the action of thermoelastic stresses, properties

[54] The theory of thermal self-focussing effect is described, for example, in [62].

[55] The term $(\partial n/\partial T)_\sigma$ is often encountered in literature.

[56] See, for example, Sec. 4.3 in [1] for a description of optical indicatrix. Photoelasticity is discussed in Sec. 4.4, *ibid.*

of a uniaxial double-refraction crystal, and its optical indicatrix assumes the form of an ellipsoid of revolution instead of a sphere. YAG crystal has a cubic symmetry. As a result of absorption of pumping radiation, thermally induced double-refraction takes place in this crystal leading, in particular, to a depolarisation of laser radiation in YAG. If the sample in its initial state is a uniaxial or biaxial crystal, the changes in the optical indicatrix may be quite complicated: the principal axes of the optical indicatrix are rotated, the values of principal refractive indices are changed, and a uniaxial crystal assumes the properties of a biaxial crystal.

Photoelastic effect is not the only effect connected with thermoelastic stresses. Another effect is the thermal expansion of the sample and the subsequent warping of its lateral faces, which naturally affects the divergence of generated radiation. Effects caused by thermoelastic stresses, along with a purely thermal variation of the refractive index, together describe the thermal distortion of a resonator.

Thermal distortions in a resonator have been described in [11, 64, 65]. While considering the effect of thermal distortion on laser radiation, it is necessary in general to simultaneously take into account a number of effects, for example, scattering by the inhomogeneities in the refractive index. The combined effect of scattering and the thermal lens on the divergence of a light beam is discussed in [66].

Focal Length and Principal Planes of a Thermal Lens. Investigations show that the dependence of the refractive index on transverse coordinates x and y, connected with the thermal lens formation, is *quadratic* to a fairly high degree of precision [11]:

$$n(x, y) = n_0 \pm n_2 (x^2 + y^2)/2. \qquad (2.13.5)$$

Here, n_0 is the refractive index on the sample axis ($x = y = 0$): the plus sign refers to a *divergent* and the minus sign to a *convergent* thermal lens. Thus, a sample with a thermal lens may be treated as a *quadratic medium.*

In order to find the focal length of a thermal lens, we assume that the refractive index of the medium is described by the formula

$$n(s) = n_0 - n_2 s^2/2, \qquad (2.13.6)$$

where $s^2 = x^2 + y^2$. Suppose that a light ray parallel to the OO axis and at a distance s_1 from it is directed towards the end face of a heated sample of length d (Fig. 2.83*a*). The transformation of this ray as a result of its passage through the sample may be described by a relation of type (2.4.16)

$$\begin{pmatrix} s_2 \\ \alpha_2 \end{pmatrix} = \begin{pmatrix} A & B \\ C & D \end{pmatrix} \begin{pmatrix} s_1 \\ 0 \end{pmatrix}, \qquad (2.13.7)$$

where the result (2.8.24) is used for the $ABCD$-matrix. Taking into account this result, we get the following parameters for the

ray as it leaves the sample

$$s_2 = As_1 = s_1 \cos\left(\sqrt{\frac{n_2}{n_0}}\, d\right),$$
$$\alpha_2 = Cs_1 = -s_1 \sqrt{n_2 n_0} \sin\left(\sqrt{\frac{n_2}{n_0}}\, d\right). \qquad (2.13.8)$$

Figure 2.83*a* shows f as the distance along OO axis between the intersection of the emergent ray with the axis and the reference plane H passing through the point of cross section of extensions of incident and emergent rays (the extensions of rays have been shown by dashed lines in the figure). It can be easily seen that

$$f = -s_1/\alpha_2. \qquad (2.13.9)$$

Substituting (2.13.8) in (2.13.9), we find that

$$\boxed{\frac{1}{f} = -C = \sqrt{n_2 n_0} \sin\left(\sqrt{\frac{n_2}{n_0}}\, d\right)}. \qquad (2.13.10)$$

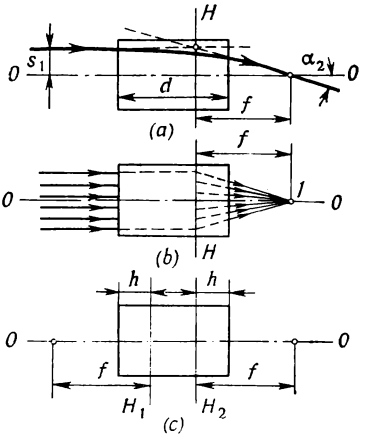


Fig. 2.83

The quantity f does not depend on s_1. This means that any ray propagating parallel to the OO axis intersects this axis at the same point after passing the sample, i.e. the point *1* in Fig. 2.83*b*. In other words, a thermal lens may be considered as an ideal lens system. The plane H is apparently one of the *principal planes* of this system and f is the *focal length*.

Figure 2.83*c* shows both the principal planes of a thermal lens—planes H_1 and H_2. The distance h between a principal plane and the corresponding end face of the sample is apparently defined by the relation

$$h = f - s_2/(-\alpha_2).$$

Using (2.13.8), we find that

$$h = \frac{1-A}{-C} = \frac{1}{\sqrt{n_0 n_2}} \operatorname{tg}\left(\frac{d}{2}\sqrt{\frac{n_2}{n_0}}\right). \qquad (2.13.11)$$

In solid-state lasers, the inequality

$$d\sqrt{n_2} \ll 1 \qquad (2.13.12)$$

is usually satisfied. Using this inequality, the relations (2.13.10) and (2.13.11) can be written in the form

$$1/f = n_2 d; \quad h = d/2n_0. \qquad (2.13.13)$$

Thermal Lens and Laser Systems. Suppose that a thermal lens with known parameters f and h is created in an active element. In order to take into account this thermal lens, the active element must be replaced by an ideal lens system consisting of a thin lens of focal length f and two segments of length h each in the free space. Figure 2.84*a* shows the initial resonator consisting of mirrors with radii of curvature r_1 and r_2. An active element of length d is placed incide the resonator, the distance of the left and right faces of the element from the nearest mirrors being given by l_1 and l_2 respectively. The dashed lines show the principal planes of the thermal lens in the active element. Figure 2.84*b* shows an equivalent resonator with a thin lens. It has similar mirrors as the initial resonator, but has a different length. The length of the initial resonator $L = l_1 + d + l_2$, while the length of the equivalent resonator with a thin lens is given by $L' = l_1 + 2h + l_2$.

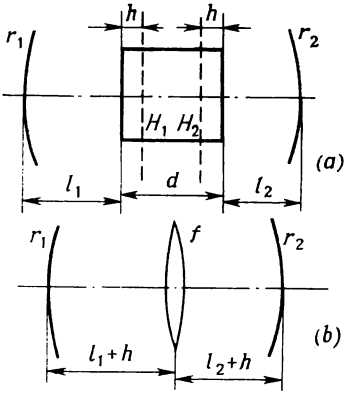


Fig. 2.84

The conversion of a resonator with an internal thermal lens into a resonator with an ordinary (thin) lens permits a consideration of an equivalent lensless resonator (see Sec. 2.6).

The thermal lens effect usually plays an important role in the formation of radiation field in a solid-state laser[57]. This may lead to a considerable decrease in the effective extraction of energy per unit volume of the active medium and even a breakdown of radiation. One of the methods of overcoming the thermal lens effect is to compensate this effect by introducing additional elements in the resonator to correct the wavefront of the generated radiation (for example, an additional lens may be introduced). Other methods are connected with a weakening of thermal distortion in a resonator by taking specific constructional and technical steps for a specific laser.

If the parameters f and h of a thermal lens are known for a given active sample and given pumping conditions, the thermal lens effect may be taken into account and used, by an appropriate choice of the type of resonator and its geometric parameters including the distance of the end faces of the sample from the mirrors. By *matching* the thermal lens with the resonator mirrors, we can ensure in prin-

[57] A thermal lens may also play a significant role in high-power gas lasers (for example, in molecular CO_2-lasers).

ciple the maximum occupation of the active element by generated radiation and thus increase the output laser power.

The radius of the light beam on the left face of the active sample in the resonator shown in Fig. 2.84*a* may be expressed in accordance with (2.9.29) through the elements of the matrix $M = \begin{pmatrix} A & B \\ C & D \end{pmatrix}$ for a round-trip through the resonator (in Fig. 2.84*b*) from the reference plane situated at a distance of l_1 from the left mirror of the resonator. This matrix is defined as

$$M = M(h)\, M(f)\, M(h + l_2)\, M(r_2)\, M(h + l_2)\, M(f)\, M \times \times (h + l_1)\, M(r_1)\, M(l_1). \quad (2.13.14)$$

Consequently, the required radius of the light beam is described in terms of the geometric parameters l_1, l_2, r_1, r_2 of the resonator and in terms of the parameters f and h of the thermal lens. By a proper choice of geometric parameters, the maximum beam radius may be obtained.

The problem of matching the thermal lens of an active sample with the resonator mirrors has been discussed, for example, in [67, 68]. Kushnir *et al.* [68] have investigated, on the example of a resonator with two active samples, the dependence of the output laser power on the mutual position of active samples and resonator mirrors by taking into account the thermal lens effect.

In actual practice the focal length f of a thermal lens created in a solid-state active element is found to depend not only on the power and spatial distribution of pumping, but also on the generated radiation power. The parameter h practically remains unchanged for different values of the pumping power. Hence the resonator of an actual solid-state laser may be considered as a resonator with an internal lens whose position is fixed but whose *optical strength* changes over a certain interval of values. In this connection, the search for such generators acquires a great practical value, whose configuration would ensure the least sensitivity of the field caustic to variation in the optical strength of the internal lens. This question has been analysed in [69] where plano-spherical resonators have been described. The analysis carried out in [69] leads to computations for resonators in solid-state lasers, which are insensitive to the optical strength of a thermal lens created in an active element.

2.14. WAVEGUIDE RESONATORS

There is a very effective method for countering the distortion in the wavefront of the generated radiation, caused by the thermal lens effect and by warping of the active element as a result of its thermal expansion. This method is based on the application of so-called *waveguide* resonators in which such modes can be realised

that retain the wavefront form in spite of thermal distortions in the resonator[58].

Waveguide Resonator; Waveguide Modes. A waveguide resonator is shown in Fig. 2.85, which shows the longitudinal cross section of the active element in the form of a rectangular parallelepiped. Here, *1* are the polished upper and lower lateral faces of the element, *2*—the medium around the lateral face of the element (for example, a coolant), *3*—the resonator mirrors inclined at an angle α to the end faces of the active element; L—the length of the active element, d—its transverse dimension in the plane of the figure. The figure also

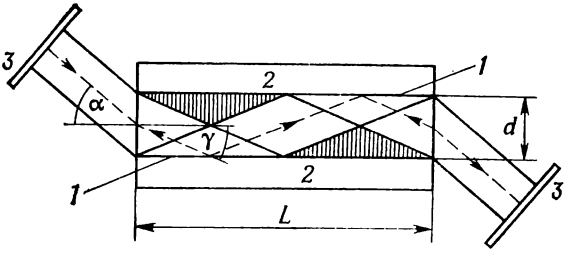


Fig. 2.85

shows a light beam which is subjected twice to total internal reflection from the face *1* of the active element (in place of a light beam, we can consider a ray of light, as indicated by the dashed lines). The shaded portions in the figure correspond to the volume of the active element not taking part in the generation. This volume amounts to 1/4 of the total volume of the element. Angles α and γ are the angles of incidence and refraction respectively for the end face. They are connected by the familiar relation

$$\sin \alpha / \sin \gamma = n, \tag{2.14.1}$$

where n is the refractive index of the active element.

It is important to note that the angle α (and hence angle γ), which determines the orientation of the resonator mirror with respect to the end face of the active element, cannot be chosen arbitrarily. It is necessary that the product $L \tan \gamma$ should be a multiple of d:

$$L \tan \gamma_m = md. \tag{2.14.2}$$

In this case, a light ray passing through an active element undergoes m total internal reflections at the lateral faces and leaves the element at the same angle α_m at which it entered it. Figure 2.86 illustrates this situation.

[58] Waveguide resonator lasers were first suggested in 1972 [70]. For a description of such lasers, see [12].

If the resonator mirrors are oriented with respect to the end face of the active element at an angle $\alpha = \alpha_m$ defined by the relations (2.14.1) and (2.14.2), the waveguide mode of the m-th type is excited in the waveguide resonator. In the case shown in Fig. 2.85, a waveguide mode of type *2* is excited, while Fig. 2.86 indicates the excitation of the waveguide mode of type *5*[59].

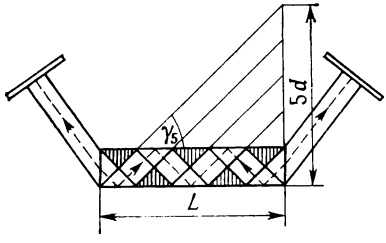


Fig. 2.86

Number of Waveguide Modes in a Resonator. The number of possible waveguide modes is restricted by the condition of total internal reflection at the lateral faces of the active element

$$\cos\gamma \geqslant n_1/n, \quad (2.14.3)$$

where n_1 is the refractive index of the medium covering the lateral faces of the element ($n_1 < n$). If $\cos\gamma < n_1/n$, the radiation emerges from the active element through the end faces.

The inequality (2.14.3) can be rewritten in the form

$$1/(1 + \tan^2\gamma) \geqslant (n_1/n)^2.$$

Substituting (2.14.2) in it, we get the condition limiting the possible values of m for waveguide modes excited in the resonator under consideration:

$$m \leqslant \frac{L}{d}\sqrt{\left(\frac{n}{n_1}\right)^2 - 1}. \quad (2.14.4)$$

The modes defined by the condition (2.14.4) may contain modes which undergo a total internal reflection not only at the lateral faces of the active element, but at the end faces as well. Such modes circulate within the element and hence are *parasitic modes*. These modes satisfy the condition $\sin\gamma_m \geqslant 1/n$ or $\tan^2\gamma_m/(1 + \tan^2\gamma_m) \geqslant 1/n^2$. Substituting (2.14.2) in it, we get

$$m \geqslant \frac{L}{d}\frac{1}{\sqrt{n^2-1}}. \quad (2.14.5)$$

If

$$\frac{1}{\sqrt{n^2-1}} > \sqrt{\left(\frac{n}{n_1}\right)^2 - 1}, \quad (2.14.6)$$

the parasitic modes do not appear and the number of waveguide modes that may be used as laser modes is determined by the condi-

[59] Figures 2.85 and 2.86 correspond to a *plane* waveguide resonator, since we consider a reflection not at all the four lateral faces of the active element, but just at two opposite faces (upper one and lower one). In a more general case, we must take into consideration reflection at the other pair of lateral faces as well (waveguide *cavity* resonator). Each waveguide mode will then be characterised by *two* indices instead of one.

tion (2.14.4). Otherwise, the number of laser waveguide modes is determined by the inequality

$$m < \frac{L}{d} \frac{1}{\sqrt{n^2-1}}. \qquad (2.14.7)$$

While speaking of the number of waveguide modes, it should be remembered that the angle α may be positive or negative. Hence the number of modes defined by the condition (2.14.4) (or by the condition (2.14.7)) must be multiplied by 2. In this connection,

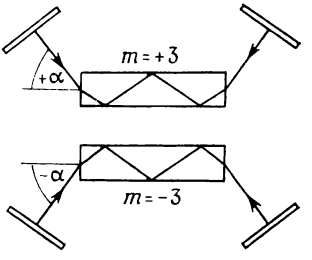


Fig. 2.87

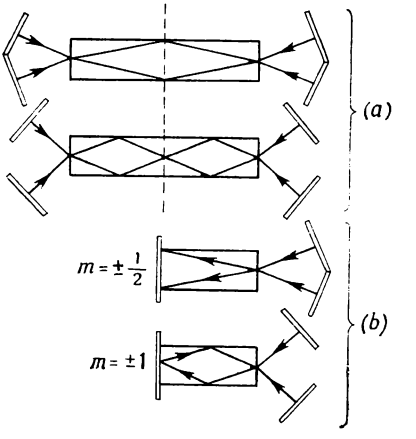


Fig. 2.88

we distinguish between $+m$ type modes and $-m$ type modes, depending on the sign of the angle α. Figure 2.87 shows modes of $+3$ type and -3 type by way of an example.

Half Waveguide Resonator. By using a *four-mirror* system, we can simultaneously excite two waveguide modes in a resonator, having the same magnitude of the index m but different signs. Figure 2.88*a* shows two such cases: for $|m| = 1$ and for $|m| = 2$. It can be easily seen that the volume of the active elements is completely utilised.

The dashed line in Fig. 2.88*a* indicates the cross section of the symmetry plane: the right half of the figure is the mirror image of the left half. It follows from this that the passage of light rays in the right half remains unchanged if we remove the left half and replace the symmetry plane by a totally reflecting mirror (Fig. 2.88*b*). Resonators shown in Fig. 2.88*b* are called *half waveguide* resonators. In the first case, modes with a *fractional* index ($m = +1/2$ and $m = -1/2$) are excited. While in the second case, *integral* index modes ($m = +1$ and $m -1$) are excited.

It should be noted that for excitation of modes with a fractional index in a half waveguide resonator, it is enough to have just *one* mirror inclined at an angle of α (Fig. 2.89*a*). For excitation of modes with an integral index, *both* inclined mirrors are necessary (Fig. 2.89*b*). This means that the integral modes $+m$ and $-m$ (including the modes $+1$ and -1) in a half waveguide resonator are mutually coupled.

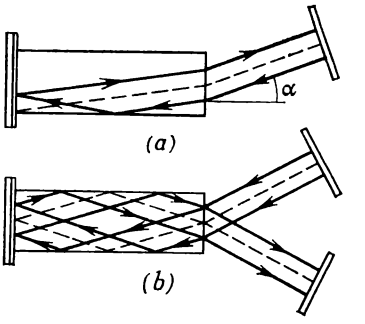


Fig. 2.89

Advantages of a Waveguide Resonator. By using a waveguide resonator, we can avoid distortions in the shape of radiation wavefront due to the thermal lens effect in the active element. This possibility is clearly illustrated in Fig. 2.90 showing a half waveguide resonator with mode $m = \pm 1$. The thermal lens assumes the dependence of the refractive index on the transverse coordinate y: $n = n(y)$. Let us consider a thin layer of the active medium, confined by the planes y and $y + \Delta y$ (see the figure). It can be easily seen that any light ray in the mode $m = \pm 1$ crosses this layer twice, following *the same path* with optical length $n(y)\,\Delta y/\sin\gamma$ (three light rays, indicated as *1*, *2*, and *3*, are shown in the figure).

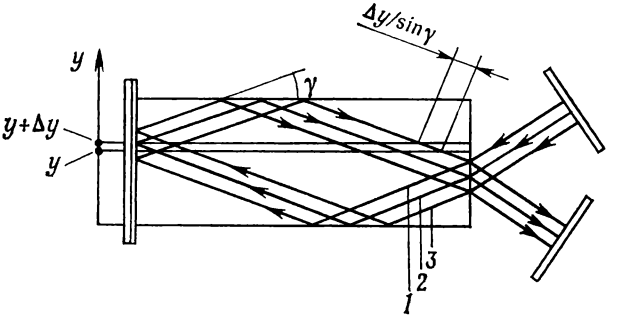


Fig. 2.90

The position of the layer along y-axis is arbitrarily chosen. Hence if the entire active element is divided into parallel thin layers, the remarks made above about the equality of optical paths for *all* light rays in a mode will be valid for *each* layer, and hence for the entire active element. In other words, for the case indicated in Fig. 2.90, each light ray in the waveguide mode traverses an optical path of *the same* length in the active element. It follows from this

that the thermal lens of an active element cannot distort the wavefront of the optical beam in this case.

It should be observed that we can choose such combinations of waveguide modes in waveguide resonators, which are insensitive not only to the thermal lens, but also to other thermal distortions of the active element (for example, to the bending of the active element due to thermal expansion). In any case, a *mutual compensation* can be attained for the changes in the wavefront of the light beam arising during its passage through the deformed active element.

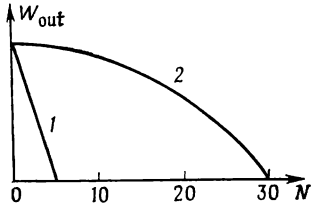


Fig. 2.91

The advantage of a waveguide resonator over an ordinary plane-parallel resonator is shown in Fig. 2.91 [12], which gives two experimental curves describing the dependence of the laser output power W_{out} on the number of flashes N of the excitation lamp. Curve *1* corresponds to an ordinary resonator, while curve *2* corresponds to a waveguide resonator (in both these cases the active element was not cooled, which led to a rapid heating). It can be seen from the figure that while thermal distortions lead to a comparatively rapid breakdown of generation in an ordinary resonator, the curve corresponding to a waveguide resonator has a rather slow fall (it should be noted that this fall is by no means due to thermal distortions of the element, but rather due to a deterioration in its generation properties with increasing temperature).

Investigations of lasers with waveguide resonators revealed highly *selective* properties of these resonators both with respect to a selection of *transverse* modes as well as with respect to the *frequency* selection. Practically all types of waveguide resonators are characterised by a single frequency generation (the central longitudinal mode is selected). Investigations in a Nd:YAG waveguide laser have shown [71] that a single frequency generation may be realised right up to the pumping power which ruptures the crystal. In the same laser, generation of one transverse mode was observed. The value of the Fresnel number in this case was higher than 10^4.

2.15. OPTICAL RADIATION IN A THIN-FILM WAVEGUIDE. DISTRIBUTED FEEDBACK

A thin-film optical waveguide is a dielectric film, whose thickness d is of the order of radiation wavelength ($d \approx 1\mu m$), deposited on a substrate (Fig. 2.92). We shall consider the two-dimensional case, assuming that the light rays do not leave the yz plane (y-axis is perpendicular to the interface between the substrate and the thin film, while z-axis corresponds to the direction along which radiation

propagates in the thin-film waveguide). As in an ordinary dielectric waveguide, propagation of light in the film is based on total internal reflection for which it is essential that the inequalities

$$n > n_1 \text{ and } n > n_2 \qquad (2.15.1)$$

are satisfied, n, n_1, and n_2 having the refractive indices of the film, substrate, and the medium over the film respectively. Since the film is usually in the air, we shall assume that $n_2 < n_1$.

Figure 2.92 shows a light ray inside the film undergoing total internal reflection at its boundaries. Let θ be the angle of incidence of the ray on the film boundary. The ray traverses a zigzag path inside the film. In this connection, the term zigzag rays (zigzag light waves) is often employed. A consideration of such rays (waves) provides an answer to a number of fundamental questions connected with the propagation of light in thin-film waveguides.

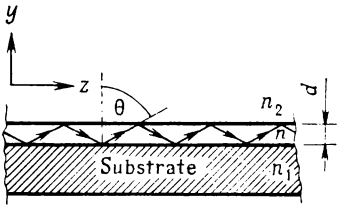


Fig. 2.92

A rigorous treatment of optics of dielectric films based on Maxwell's equations is given, for example, in [72]. Optical effects in thin-film waveguides have been thoroughly analysed in [73-77]. See also Ch. 28 in [2].

Dielectric thin films are used not only as *passive* elements intended for optical signal communication, but also as *active* elements (*thin-film lasers*). Besides, they are used for non-linear interactions of light waves, i.e. for generation of optical harmonics, parametric generation of light, induced Raman scattering of light. It has been remarked in [73], in particular, that "the use of thin-film dielectric waveguides opens the way for creation of miniature laser equipment, optical modulators, filters, parametric generators, and other elements for communication systems having large information capacity, high-speed computers, and for optical processing of information... . Such a perspective laid the foundation for a new branch of investigation at the confluence of microwave engineering and optics, called *integrated optics*."

In this section, we shall consider only a few problems of propagation of light in a thin-film waveguide, introduction of radiation in a film, as well as thin-film lasers with distributed feedback.

Waveguide Modes in a Thin Film. In accordance with two possible polarisations of light, there are two types of modes, TM and TE, propagating in a thin-film waveguide. These modes are illustrated in Fig. 2.93. In Fig. 2.93*a*, the following components of field vectors are non-zero: E_y, E_z, and H_x (the last component is oriented perpendicular to the plane of vectors **E** and **k**). This is the *transverse magnetic* mode, or the TM mode. The vector **H** in this mode is perpendic-

ular to the direction of propagation of radiation in the waveguide. In Fig. 2.93*b* the non-zero components are H_y, H_z, and E_x. This is the *transverse electrical* mode, or the TE mode. The vector **E** is perpendicular to the direction of propagation of radiation. Since the boundary conditions at the interface between two media are independent of each other for the field components perpendicular and parallel to the boundary, the modes TM and TE may be considered as independent. This means, in particular, that they are not transformed into each other as a result of reflection at the film boundary.

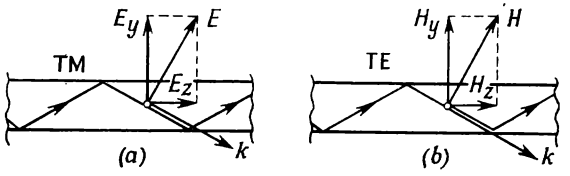


Fig. 2.93

Let us take the TE mode, for example, and consider the time and space coordinates dependence of the scalar function describing one component of the mode field, say E_x. Let us denote this function by $u\ (y,\ z,\ t)$. It should be noted that we could choose the component H_y or H_z (or for that matter, the components of the TM mode).

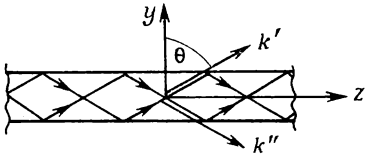


Fig. 2.94

The radiation field in a waveguide may be represented in the form of superposition of two plane monochromatic waves, whose wave vectors ($\mathbf{k}'$ and $\mathbf{k}''$) are shown in Fig. 2.94 ($|\,\mathbf{k}'\,| = |\,\mathbf{k}''\,| = kn$; $k = \omega/c$):

$$u\ (y,\ z,\ t) = U\ [\exp\ (i\mathbf{k}'\mathbf{r}) + \exp\ (i\mathbf{k}''\mathbf{r})]\ \exp\ (-i\omega t). \qquad (2.15.2)$$

Considering (see Fig. 2.94) that

$$\mathbf{k}'\mathbf{r} = k'_y y + k'_z z = kn\ (y \cos\theta + z \sin\theta);$$
$$\mathbf{k}''\mathbf{r} = k''_y y + k''_z z = kn\ (-y \cos\theta + z \sin\theta),$$

we can rewrite (2.15.2) in the form

$$u(y, z, t) = U[\exp(ikny\cos\theta) + \exp(-ikny\cos\theta)] \times \\ \times \exp(iknz\sin\theta)\exp(-i\omega t). \quad (2.15.3)$$

Introducing the notation

$$\beta = kn\sin\theta; \quad b = kn\cos\theta, \quad (2.15.4)$$

the expression (2.15.3) may be written in the form

$$u(y, z, t) = U[\exp(iby) + \exp(-iby)]\exp(i\beta z - i\omega t). \quad (2.15.5)$$

It should be noted that if the result (2.15.5) is applied, for example, to the component H_z of the TE mode instead of the component E_x, the amplitude U must be replaced by the amplitude $Un\sin\theta$ (this follows from the relation between the vectors **E** and **H** in a plane wave). Thus, there is simply a change in the amplitude of the component of the field, which depends neither on the space coordinates nor on time.

It can be seen from (2.15.5) that radiation propagates along the film in the direction of the z-axis with a velocity

$$v = \omega/\beta = ck/\beta = c/n\sin\theta, \quad (2.15.6)$$

while a standing wave

$$w(y) = U[\exp(iby) + \exp(-iby)] = 2U\cos(by) \quad (2.15.7)$$

is created in the direction of the y-axis. This means that the *resonance* condition must be satisfied in the direction of the y-axis (by

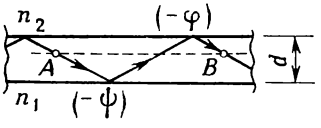


Fig. 2.95

analogy with the standing wave in an ordinary resonator). This condition indicates the allowed values of the parameter b, and hence of angle θ, for waveguide modes which may propagate in a given film.

In order to find the resonance condition, we must consider the propagation of a zigzag wave, say, from point A to point B (Fig. 2.95), traversing twice the thickness d of the film. Here, in addition to the geometrical plane advance along the y-axis, which is obviously given by $2bd$, we must also take into consideration the change in the phase of the wave upon a total internal reflection at the upper and lower boundaries of the film. Denoting these changes by $-\psi$ and $-\varphi$ respectively, we can show (see, for example, [72]),

that

$$\psi = 2 \arctan \frac{\sqrt{\beta^2 - (kn_1)^2}}{b}; \qquad (2.15.8a)$$

$$\varphi = 2 \arctan \frac{\sqrt{\beta^2 - (kn_2)^2}}{b}. \qquad (2.15.8b)$$

The total change in the phase of the wave (in the direction of the y-axis) upon traversing the film thickness must be a multiple of 2π:

$$2bd - \psi - \varphi = 2\pi m; \quad m = 0, 1, 2, \ldots \qquad (2.15.9)$$

The relation (2.15.9) expresses the required resonance condition.

Each integer m has a definite angle of incidence of the light ray at the film boundary (angle θ_m) corresponding to it, and hence definite values of the parameters β_m, b_m, ψ_m, and φ_m (since all these parameters are functions of θ in accordance with (2.15.4) and (2.15.8)). Hence the relation (2.15.9), strictly speaking, should be written in the form

$$\boxed{2b_m d - \psi_m - \varphi_m = 2\pi m}. \qquad (2.15.10)$$

The index m determines the *order* of the waveguide mode. Waveguide modes of different orders have different values of angle θ, which can assume only discrete values θ_m[60] in accordance with the resonance condition described above. In order to find θ_m, we must solve the transcendental equation (2.15.10).

With increasing m, the angle θ_m decreases. From this it follows that the value of the parameter b_m increases while, on the contrary, the parameter β_m decreases; see (2.15.4). The latter circumstance means that with increasing m, the velocity of propagation (2.15.6) of radiation in the film along the z-axis increases. It can be seen from (2.15.8) that with increasing m, the parameters ψ_m and φ_m decrease. Thus,

$$\theta_0 > \theta_1 > \theta_2 > \ldots; \quad \beta_0 > \beta_1 > \beta_2 > \ldots; \quad b_0 < b_1 < b_2 < \ldots;$$
$$\psi_0 > \psi_1 > \psi_2 > \ldots; \quad \varphi_0 > \varphi_1 > \varphi_2 > \ldots. \qquad (2.15.11)$$

Number of Waveguide Modes in a Film. The decrease in the value of the angle θ_m with increasing m (as well as the change in other parameters) cannot be indefinite. Apparently, the angle θ_m cannot become smaller than the *limiting* angle θ_{lim} for the total internal reflection at the interface between the film and the substrate, given by the familiar relation

$$\sin \theta_{lim} = n_1/n. \qquad (2.15.12)$$

The difference $\beta^2 - (kn_1)^2$ for $\theta = \theta_{lim}$ is equal to

$$\beta^2 (\theta_{lim}) - (kn_1)^2 = (kn)^2 \sin^2 \theta_{lim} - (kn_1)^2 = 0.$$

[60] It will be shown later that modes of different orders also differ in the distribution of field along the y-axis.

Thus, if the angle θ decreases and becomes equal to θ_{11m}, the radicand in (2.15.8a) becomes zero, and hence the phase change for the wave at the interface between the film and the substrate also becomes zero. For $\theta < \theta_{11m}$, the radicand in (2.15.8a) becomes negative, and there is no total internal reflection at the interface. It is clear that a wave with $\theta < \theta_{11m}$ cannot be a waveguide mode for this film. The condition

$$\theta_m \geqslant \arcsin(n_1/n) \tag{2.15.13}$$

limits the number of waveguide modes that may propagate in a particular thin-film waveguide. For example, in a Ta_2O_5 film of thickness $d = \lambda = 0.78$ μm deposited on a glass substrate, four waveguide modes ($m = 0, 1, 2, 3$) are possible.

Field Distribution in Waveguide Modes. According to (2.15.7), the distribution of the field along the y-axis in the m-th order waveguide mode inside the film is described by a function of the type

$$w_m(y) = 2U \cos(b_m y). \tag{2.15.14}$$

It can be shown (see, for example, [75]) that the function $w_m(y)$ assumes the value

$$w'_m = 2U \cos(\varphi_m/2), \tag{2.15.15a}$$

at the upper boundary of the film, and the value

$$w''_m = 2(-1)^m U \cos(\psi_m/2) \tag{2.15.15b}$$

at the lower boundary of the film. The field in the substrate and in the medium immediately above the film decreases exponentially (with distance from the film boundary). The field distribution above the film may be expressed in the form

$$w_m(Y) = w'_m \exp\left(-\sqrt{\beta_m^2 - (kn_2)^2}\, Y\right), \tag{2.15.16a}$$

where the coordinate Y is increased from the top of the film. The distance

$$p_m = [\beta_m^2 - (kn_2)^2]^{-1/2} \tag{2.15.17a}$$

is the distance from the top of the film, where the field is attenuated to $1/e$ of its value. The field distribution in the substrate is similar in nature to the distribution above the film:

$$w_m(Y') = w''_m \exp\left(\sqrt{\beta_m^2 - (kn_1)^2}\, Y'\right); \tag{2.15.16b}$$

where the coordinate Y' is measured from the bottom of the film. The distance

$$P_m = [\beta_m^2 - (kn_1)^2]^{-1/2} \tag{2.15.17b}$$

is the distance from the bottom of the film where the field is attenuated to $1/e$ of its value.

Figure 2.96 shows the *field distribution* for the first four waveguide modes ($m = 0, 1, 2, 3$). The lower part of the figure shows the passage to a zigzag ray for each of the modes under consideration. It should be noted that the field distribution inside the film is not symmetric with respect to the horizontal line passing exactly through

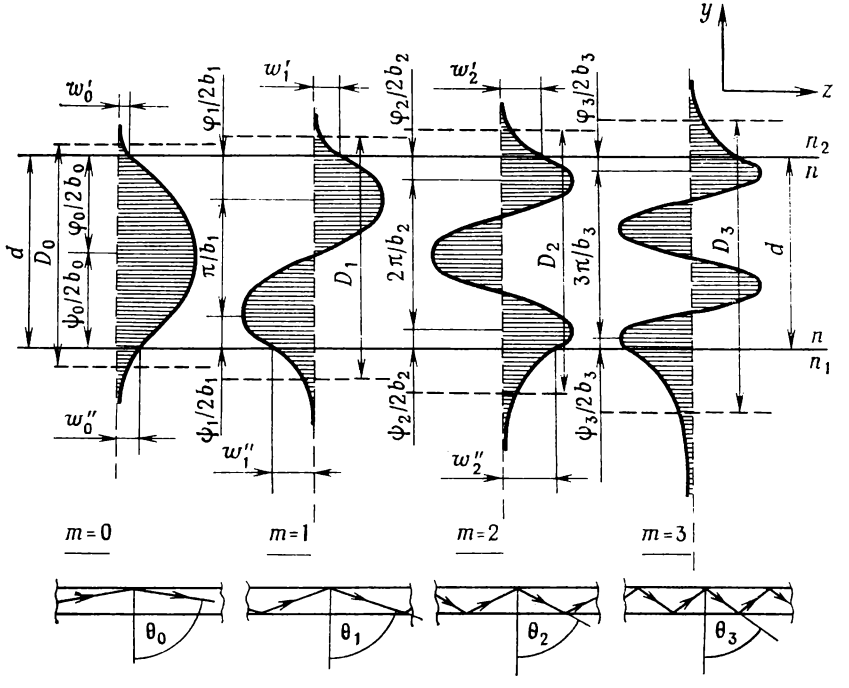


Fig. 2.96

the middle of the film, but rather displaced somewhat towards the lower boundary of the film. This is due to the inequality $n_2 < n_1$, (if $n_2 > n_1$, the distribution is displaced towards the upper boundary of the film, while it will be symmetrical for $n_2 = n_1$). Using the inequality $n_2 < n_1$, and the formulas (2.15.8), it can be easily concluded that $\varphi_m > \psi_m$, and consequently (see (2.15.15)),

$$| w_m' | < | w_m'' |. \qquad (2.15.18)$$

The boundary conditions (2.15.15) completely define the position of the cosine curve (2.15.14) on the y-axis, describing the field distribution inside the film[61].

[61] Only one of the conditions (2.15.15) is enough for defining the position of the cosine curve on the y-axis.

The field distributions above the upper boundary and below the lower boundary of the film are even more asymmetric. This is due to the inequality (2.15.18), as well as to the inequality

$$p_m < P_m, \tag{2.15.19}$$

which is also a consequence of the inequality $n_2 > n_1$. The field in the substrate decreases with distance from the boundary at a slower rate than in the medium above the film. It is also evident from Fig. 2.96 that the effect of the field outside the film increases with increasing index m defining the order of the mode.

In accordance with (2.15.10), we can express the film thickness through a relation of the form

$$d = (m\pi/b_m) + (\psi_m/2b_m) + (\varphi_m/2b_m). \tag{2.15.20}$$

It can be seen from Fig. 2.96 that the segment $d'_m = m\pi/b_m$ is the distance between the farthest extrema of the cosine curve (2.15.14). Inside this segment, the cosine curve turns to zero m times. Thus, it is quite obvious that the number of nodes in the field distribution is equal to the order of the waveguide mode.

The exponential decrease in the field with distance from the field boundary outwards should not suggest an attenuation of the field as a result of absorption in the substrate (or in the medium above the film). As a matter of fact, there is no energy flux along the y-axis for waveguide modes. In this case, the entire light flux propagates only along the z-axis (i.e. along the film), but the transverse dimension of the flux exceeds the film thickness d by an amount $p_m + P_m$ (for the m-th order waveguide mode) approximately. In this connection, the concept of the *effective thickness* is introduced for the m-th order mode of a thin-film waveguide:

$$D_m = d + p_m + P_m. \tag{2.15.21}$$

Boundaries corresponding to the effective thickness D_m are shown by horizontal dashed lines in Fig. 2.96.

Injection and Extraction of Radiation for a Thin-Film Waveguide. A very small film thickness ($d \approx 1$ μm) creates certain difficulties both for injecting radiation into a film as well as for extraction of radiation from the film. Two methods for injection (extraction) of radiation are frequently used. These are the prism method and the diffraction method[62].

In the prism (tunnel) method, a trihedral prism is placed over the film in such a way that there is a small gap of thickness Δ, of the order of a fraction of the radiation wavelength ($\Delta \approx 0.2\lambda$) between the base of the prism and the film surface[63]. In order to introduce the

[62] The method of injecting (extracting) radiation through a gradually narrowing film edge is also used (see, for example, [73, 78]).

[63] The gap between the prism and the film may have a varying thickness (wedge-shaped gap).

radiation into the film, the initial collimated light beam is directed towards the prism in such a way that it undergoes the total internal reflection at its base (Fig. 2.97*a*). It is well known that for the total internal reflection, the field of the reflected light may *penetrate* the

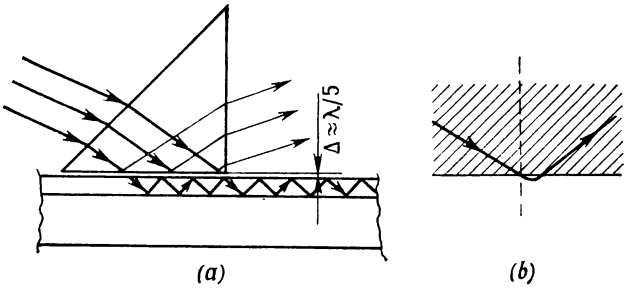


Fig. 2.97

reflecting surface up to a fraction of the wavelength (Fig. 2.97*b*). Using this phenomenon, an effective transfer of light energy from the prism to the film (or in the reverse direction) can be realised.

In the diffraction method, a phase diffraction grating is applied near the ends of the film. The period of this grating is matched with the radiation wavelength. Injection (extraction) of the radiation is caused by diffraction in this case.

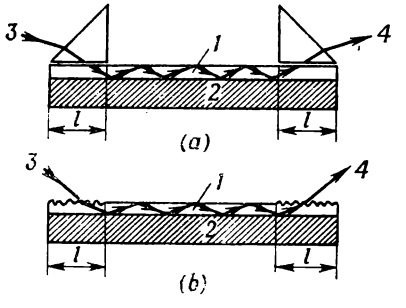


Fig. 2.98

Fig. 2.98 shows schematically the application of (a) prism and (b) diffraction methods for injecting and extracting radiation. Here, *1* is a thin film, *2*—the substrate, *3*—the input radiation (radiation injected into the film), and *4*—the output radiation (radiation extracted from the film). In both cases, the contact between the external radiation and the radiation in the film occurs over a comparatively long distance l. This circumstance predetermines (under the condition of matching of the angle of incidence of output radiation with the angle θ_m of the corresponding waveguide mode) a sufficiently high efficiency in transmission energy, which is higher than 50% (the efficiency of the prism method may be as high as 80-90%).

An analysis of various methods of injection and extraction of radiation for a thin-film waveguide is carried out, for example, in [73, 75]. We shall now give a somewhat detailed description of the prism method.

Operating Principle of the Coupling Element Prism-Film. The principle of operation of this element is shown in Fig. 2.99. The dashed line in the prism corresponds to the plane front of the light wave incident on the base of the prism. This front is shown at the moment the light wave arrives at the point *1* of the prism base. In accordance with the above-mentioned effect of the emergence of field of reflected wave beyond the reflecting surface, this wave excites a zigzag wave in the film at point *1'*. This zigzag wave, propagating along the film, will traverse a distance s from the line $1'1''$ to the line $2'2''$ in time

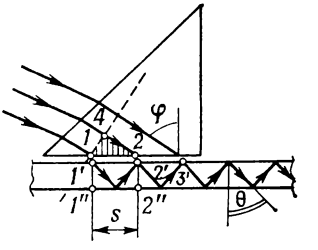


Fig. 2.99

$$\tau_1 = s/v, \qquad (2.15.22)$$

where v is the velocity of propagation of radiation along the film in the direction of the z-axis, given by the formula (2.15.6). Propagating inside the prism, the wavefront will traverse the distance between the point *4* and the point *2* (this distance is equal to $s \sin \varphi$, see Fig. 2.99) in time

$$\tau_2 = \frac{s \sin \varphi}{cn_3} \qquad (2.15.23)$$

where n_3 is the refractive index of the prism.

As the wavefront incident on the base of the prism is displaced, the zigzag waves will be excited successively at different points of the film: *1'*, *2'*, *3'*, ... If the condition

$$\tau_1 = \tau_2 \qquad (2.15.24)$$

is satisfied, the moment of excitation of the wave at any point of the film will *coincide* with the moment of arrival at this point of the wave propagating along the film. Consequently, the excited wave will be *in phase* with the wave already existing in the film; thus apparently causing an amplification of the latter. The condition (2.15.24) is called the *matching* condition. Taking into account (2.15.6), (2.15.22), and (2.15.23), this condition may be written in the form

$$n \sin \theta = n_3 \sin \varphi. \qquad (2.15.25)$$

It can be seen from (2.15.25) that by choosing the value of the ratio n_3/n, as well as the angle φ, we can satisfy the matching condition for a definite angle θ, i.e. for a definite waveguide mode. Thus, the prism method of introducing radiation in a film leads, in principle, to the excitation of any given waveguide mode.

Distributed Feedback. Suppose that the refractive index of an active element is *spatially modulated* in the direction of its optical

axis (z-axis)

$$n(z) = n_0 + \Delta n \cos(2\pi z/\Lambda), \qquad (2.15.26)$$

where the period Λ of spatial modulation is of the same order of magnitude as the radiation waveguide. In this case, the so-called *distributed feedback* ensured generation without a resonator with reflecting mirrors.

The distributed feedback principle is based on *Bragg's reflection* of light waves by the periodic structure formed inside the active element as a result of spatial modulation of its refractive index. The dashed lines in Fig. 2.100 depict the arbitrary reflecting planes of periodic structure. The distance between adjacent planes is equal to the period Λ of spatial modulation. We consider the normally

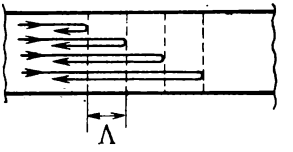


Fig. 2.100

incident light waves as they are reflected back at an isolated system of planes. The mutual amplification of the reflected waves will take place if the condition

$$\boxed{2\Lambda n = m\lambda} \qquad (2.15.27)$$

is satisfied, n being the refractive index of the active element and m being an integer (in actual practice, it is enough to consider the value $m = 1$). The condition (2.15.27) is the Bragg's reflection condition in this case.

Thus, instead of reflection of light waves at the resonator mirrors placed near the ends of the active elements (or at the ends themselves), we can use Bragg's reflection at the periodic structure *throughout the length* of the active element. As a result, a highly selective feedback is created according to wavelength. This feedback is called *distributed feedback* (abbreviated as DFB). A DFB laser generates radiation whose wavelengths λ satisfy the condition (2.15.27) and lie within the gain width.

It should be noted that structures with regular inhomogeneities whose period is comparable with the length of the electromagnetic wave are widely used for amplification and generation of radiation in the microwave region (see, for example, [79]). Such structures are rather easy to fabricate, since their period is of the order of 1-10 mm. In the x-ray region, such periodic structures have been provided by

nature—in the form of a crystal lattice[64]. In the optical wavelength region, a periodic structure having a period of about 1 μm is required. The possibility of obtaining such structures (in the form of thin-film optical waveguides) appeared first only in the seventies with the development of microelectronics. The first DFB laser was constructed in 1971 [81]. The basic principle and properties of such lasers have been described, for example, in [73, 82-84].

Spatial modulation of the *refractive index* of an active element is just one of the methods for creating a DFB laser. Other methods are based on spatial modulation of the *amplification factor* or on

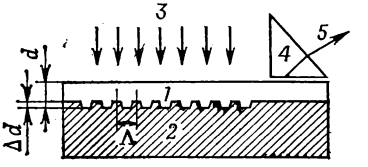


Fig. 2.101

the modulation of *geometric parameters* (cross section of the active element). The problems of practical realisation of different methods of constructing DFB in the optical region have been considered, for example, in [83].

Thin-film DFB Lasers. A *thin-film laser* is one of the main elements used in integrated optics. The active element of such a laser is an activated thin film. Apparently, we cannot use a resonator with reflecting mirrors in such a laser. In this case, distributed feedback is often employed.

Quite often, the active film in a *thin-film DFB laser* is a film of gelatine in which an activator, for example, rhodamine 6G[65], has been dissolved. Such a laser is shown in Fig. 2.101 [85]. Here, *1* is a film of gelatine with rhodamine 6G ($d \approx 1$ μm), *2*—a substrate with corrugated surface ($\Delta d \approx 0.01$ μm, $\Lambda \approx 1$ μm), *3*—the pumping radiation (second harmonic of an Nd-laser, $\lambda_p = 0.53$ μm), *4*—a prism for extracting the radiation from the film, and *5*—the output radiation. Distribution feedback is ensured in this case by periodic variation in the *thickness of the active film* due to the corrugated surface of the substrate. Corrugation of the substrate surface is carried out by chemical etching through a mask obtained by the photolithographic method.

The method of spatial modulation of the amplification factor of the active film through a periodic variation of the *intensity* of laser

[64] The possibility of creating a DFB laser in the x-ray region by using the periodic structure of a crystal lattice was first indicated in 1965 [80].

[65] In addition to thin-film DFB organic dye lasers, the semiconducting thin-film DFB lasers are also quite widely employed.

pumping along the optical axis is quite interesting. For this purpose, we can use, for example, the pumping diagram shown in Fig. 2.102*a*. Here, *1* is a collimated light beam from the laser used for pumping, *2*—a beam splitting film, *3*—totally reflecting mirrors, and *4*—the active film being pumped. Two coherent light beams are incident on the surface of the film (2φ is the angle between the directions of propagation of the beams). Consequently, an interference pattern is formed on the surface of the film; the period of interference fringes is given by

$$\Lambda = \lambda_p/2 \sin \varphi \qquad (2.15.28)$$

where λ_p is the wavelength of the radiation used for pumping of the film. The periodic variation of the illumination of the film surface leads to a corresponding spatial modulation of its amplification factor.

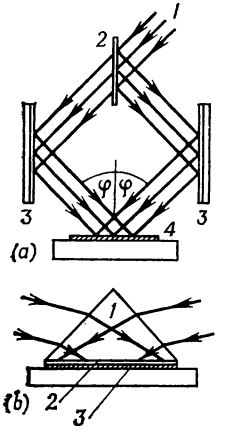


Fig. 2.102

By altering the mutual position of the mirrors *3* and the film *4* shown in Fig. 2.102*a*, we can continuously vary the angle φ and hence the modulation period Λ (see (2.15.28)). Since the generation wavelength of a thin-film DFB laser is determined by the modulation period Λ, (see (2.15.27)), a *continuous tuning* of the wavelength of radiation generated by such a laser can be accomplished.

Figure 2.102*b* shows another diagram for spatial modulation of the amplification factor of the active film by using the interference of light beams illuminating the film. Here, *1* is a prism, *2*—an immersion film, and *3*—the active film. The use of a prism in this diagram leads to an n_3 fold decrease in the modulation period Λ as compared to the diagram shown in Fig. 2.102*a* (n_3 is the refractive index of the prism).

The possibility of a continuous tuning of the generation frequency (by controlling the parameters of the periodic structure) is not the only advantage of a DFB laser. Selectivity for photon states *over the entire* length of the active element quite naturally leads to improved spectral and spatial properties of the generated radiation. It is well known that the DFB lasers are already superior in this respect to the ordinary (cavity) lasers based on similar active media[66].

Thin-Film Lasers Employing a Periodic Structure as a Resonator Mirror. Figure 2.103 shows a thin-film laser, in which Bragg's reflection of the light ray is realised not along the entire length of the film, but just near the ends [84]. Here, *1* is the active part of the

[66] Of course, as far as the energy parameters (efficiency, threshold characteristics) are concerned, the DFB lasers are inferior to ordinary lasers.

film, *2*—the parts with periodically varying film thickness, and *3*—the substrate. The parts denoted by *2* function like mirrors in ordinary laser resonators. They ensure a partial return of the radiation to the film (through Bragg's reflection). Besides, these parts serve as a phase diffraction grating and partially extract the radiation from the film (in the form of laser radiation).

Unlike a DFB laser, the active element here does not have a periodic inhomogeneity. Such thin-film lasers are called *lasers employing*

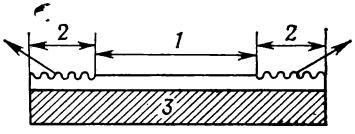


Fig. 2.103

a periodic structure as a resonator mirror. Such lasers are also interesting because the lengths of the active part and the parts with periodic structure, as well as the period of the latter, may be changed independently, and hence an optimal version with maximum suppression of undesirable modes and with an extremely narrow spectral line of generation may be obtained in principle.

Chapter Three

DYNAMICS OF LASER PROCESSES

The investigation of the *dynamics of processes* which determine the physical nature of laser operation under different conditions has assumed an ever increasing significance with advancing laser technology. This is primarily connected with a need to create lasers with *prescribed* parameters of radiation like the pulse energy, pulse duration, mean power and peak power, pulse repetition frequency, etc. The problem of creating lasers with extremal characteristics, for example, the problem of creating *superpower* lasers, has a considerable practical significance. It is important to ensure generation *stability* under various conditions, as well as a good reproducibility of radiation parameters from pulse to pulse. Investigation of dynamics of laser processes is of prime importance for *controlling the laser parameters*, a problem of great practical significance. It should also be noted that these investigations are closely related to the study of the *actual* space-time structure of laser radiation. This is extremely important for interpretation of nonlinear optical phenomena including those which form the basis of parametric oscillators, optical harmonics generators, Raman lasers, etc.

With the help of the existing lasers, we can obtain light pulses of different durations—*millisecond*, *microsecond*, *nanosecond*, or *picosecond* pulses. Single as well as multiple pulses have been generated. The latter are characterised by different pulse repetition frequencies (in the range up to about 10 MHz, and up to several gigahertz with mode synchronisation). The peak power of the generated pulses has a wide range—up to 10^{12} W and higher.

Pulsed laser radiation is widely applied in a number of technological processes connected with the treatment of materials, optical detection and ranging of objects, communication, measuring techniques, data processing systems, various physical, chemical and biological investigations, medicine, etc. It should be noted that a decrease in the pulse duration and an increase in the pulse steepness of lasers is necessary, for example, for a high-temperature plasma heating (controlled thermonuclear synthesis). An increase in the decay rate of short light pulses is essential for an investigation of relaxation processes as well as for solving the problems of modern measuring techniques. A comparatively longer pulse duration may, however, be necessary in a number of technological problems, e.g. in holography and for pumping of parametric oscillators.

One of the earliest systematic descriptions of non-stationary (transient) laser generation has been given in [1]. See also [2-6].

3.1. GENERAL REMARKS ABOUT LASER OPERATING CONDITIONS

In actual practice, laser generation is a *pulsed* operation, and it cannot be described without a consideration of the dynamics of such processes. But even in the case of *continuous* generation, the dynamics of processes plays a significant role. Strictly speaking, laser generation is always non-stationary. Stationary generation is nothing more than idealisation, which is useful for description of specific real situations only to a certain approximation.

Reasons for Instability of Laser Generation. The *non-stationary pumping*, like pumping by flash lamp radiation, or pulsed discharge, is apparently the reason behind unstable generation. Another equally apparent reason is the purposeful time variation of the unfavourable losses (active *Q-modulation* of the resonator), or favourable losses (*load modulation*). Instability of generation may lead to the introduction of *nonlinear elements* in the resonator, for example, a saturable resonance absorber (bleachable filter)[1].

These reasons for instability of generation are connected with a purposeful "interference" in the generation process. Besides, certain factors beyond our control are also responsible for this instability. These factors may be either technical or physical.

The factors of *technical* nature involve the *instability* of resonator parameters, the active medium, and the pumping system (for example, non-uniform heating of the active element during pulsed pumping, or vibrations of resonator mirrors). Investigations have revealed an important role of technical instabilities. It was found that a laser is highly sensitive to different types of perturbations of its parameters (see [9, 10], as well as [4]).

Turning to the *physical* factors, let us first point out the *multimode nature* of laser radiation observed in most practical cases. Each mode has a different structure of the field in the resonator, and a different value for the gain and the loss factor. The generation conditions depend on the number of simultaneously excited modes. Generally speaking, the participation of each new mode in generation is accompanied by a violation of the stability of generation kinetics [11]. At different moments of time, the radiation energy may be distributed among modes in different ways—more favourable conditions may first result in generation of some modes, and later of the other modes (see, for example, [12]).

It should be further remarked that the transition probabilities per unit time between the levels of active centres have finite magnitudes. This means that the processes of population and depopula-

[1] Introduction of a bleachable filter in the resonator, generally speaking, leads to a decreased stability in stationary generation, and under certain conditions may even cause undamped pulses of radiation (see, for example, [7, 8]).

tion of laser levels have a certain time lag (*persistence*). This means that the increase in the inverse population density of levels caused by pumping does not stop as soon as the threshold of the inverse population density is attained. The radiation appearing in the generation process reduces the inversion population density to below the threshold level. Consequently, *periodic variations* in the inverse population density are observed near its threshold value, leading to *fluctuations* in the radiation power [2].

It should also be taken into consideration that laser radiation is generated as a result of selective amplification of primary luminescence. In other words, *random processes* of spontaneous emission serve as the fundamental principle. The irregular picture in time and space, defined by these processes, becomes ordered as the laser starts generating. This ordering, however, is not complete. It should be noted that the bleachable filter in the resonator, which is characterised by a sufficiently small relaxation time, has a tendency to underline (isolate, accentuate) the most intense fluctuations in the initial distribution of the radiation field (see, for example, [13, 14]).

Free Oscillations. Suppose that a laser generator contains only an active element and no nonlinear elements or elements whose properties change under the influence of external signals. In this case, *free oscillations* are said to be generated in the resonator. This term is in fact a combination of several different conditions, their common point being that there is no special control over the oscillations, or any outside influence on them. In particular, there is no Q-modulation (active or passive) of the resonator. Free oscillations may take place both for pulsed as well as continuous pumping.

The most interesting situation of free oscillations arises in solid-state lasers. Free radiation in a solid-state laser is, as a rule, a train of relatively short pulses, or, as is customarily to say, *spikes*[2]. The duration of an individual spike is equal to 10^{-7}-10^{-6} sec (0.1-1 μsec), its power may attain values up to 10^4-10^5 W. The time interval between two adjacent spikes is about 1-10 μsec.

Figure 3.1 shows three types of oscillograms for the solid-state laser radiation corresponding to three types of pulsations (three types of spikes) [4]: (a) *regular damped* pulsations with generation at a constant power, (b) *regular undamped* pulsations, and (c) *irregular undamped* pulsations[3].

Although spikes were observed in the laser output radiation intensity in the first experiments with ruby lasers in 1960 [15], their nature continues to be a subject of investigation even today (see,

[2] Power fluctuations are less pronounced in gas lasers.

[3] In the case of pulsed pumping, undamped pulsations exist over an interval of time corresponding to the duration of the pumping pulse. For solid-state lasers, its duration is equal to 0.1-1 msec. In dye lasers shorter pumping pulses—up to 1 μsec are used; this is necessary in order to reduce the effect of triplet-triplet absorption.

for example, [16-18]). On the basis of a single-mode model of a laser, it can be shown that the regular damped pulsations are connected with *transition* processes accompanying the beginning of generation upon the arrival of the next pumping pulse. In other words, these pulsations are connected with the abovementioned effect of time-lag in the processes of population and depopulation of levels [1, 2]. The *multimode nature* of generation has a considerable influence on the

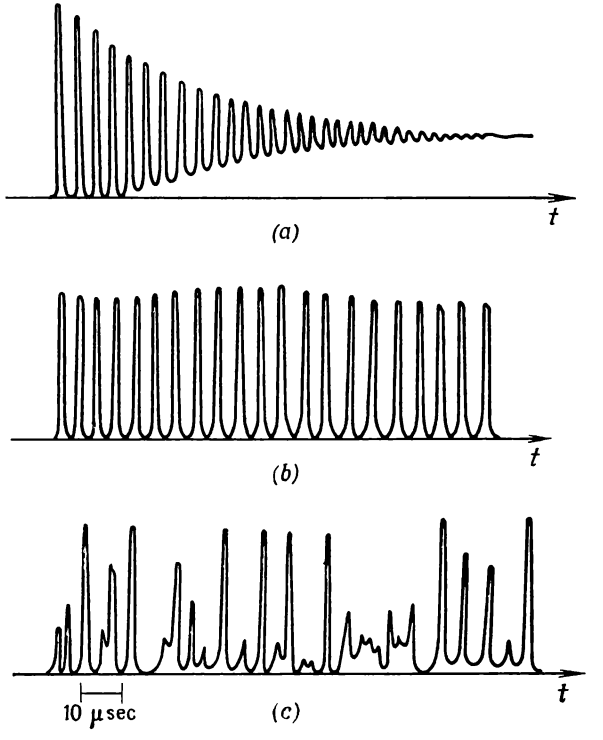


Fig. 3.1

spiking behaviour of the laser [4, 11, 16-20]. In particular, the existence of several modes may bring about disorder in the pulsation diagram.

The nature of *undamped* pulsations has remained unclear to a large extent. Investigations of solid-state spike lasers and the properties of Nd:YAG lasers have confirmed the assumption put forth in [9] that undamped pulsations are connected mainly with the effect of resonator instability on the dynamics of the laser, and hence are mainly of a technical nature. For an Nd:YAG laser, direct evidence was obtained, connecting undamped pulsations with the resonator

mirror vibrations and with non-uniform (in time) heating of the active element [21]. Undamped pulsations may also be connected with multimode generation [16].

Giant-Pulse Generation for Active Q-modulation of a Resonator. By using *Q-modulation* of a laser resonator with pulsed pumping, short and powerful light pulses were first obtained in 1962 [22, 23]. By controlling the Q-factor of a resonator, high level of unfavourable losses is first attained, i.e. the generation threshold is specially *raised*. This helps in the creation of a significant inversion of population density in the active medium. Next, with the help of an outside signal, the loss level, and hence the generation threshold *are quickly reduced* to their lowest possible value. Consequently, the initial value of the inverse population density turns out to be considerably *higher* than the new threshold corresponding to small losses. Under these conditions, a *single* short light pulse of high power (*giant pulse*) is emitted instead of multiple spikes.

The power of a giant pulse is higher, the larger the extent to which the initial inverse population density (for a low Q-factor of the resonator) is increased over the threshold value (corresponding to a high Q-factor of the resonator). The power of giant pulses obtained in practice is as high as 10^9 W[4]. The duration of a giant pulse is of the order of 10-100 nsec. The minimum duration of a pulse may be around 1-3 nsec (see, for example, [24]).

In order to attain this generation, a *modulator* (*loss switch*) controlled by an external signal is placed in the laser resonator. Under the influence of this signal, the modulator quickly changes the level of unfavourable losses in the resonator (transition from a state corresponding to higher losses to a state corresponding to lower losses, and vice versa). Since such transitions are made under *external* influence, this Q-modulation of the resonator is called *active* modulation. Various types of modulators can be used. The first ones to be used were *mechanooptic* modulators. These were followed by acoustooptic modulators [25-28].

A modulator usually works as a *controlled optical shutter*. The passage through the shutter, and hence losses in the resonator are controlled through an external signal. If the shutter is "open", the losses are low (the resonator has a low Q). In some cases, the quickly rotating resonator mirror plays the role of a modulator (mechanooptic type modulator). Obviously, the switching from "closed" to "open" position of the shutter should be synchronised with the pumping pulses: the shutter should "open" when a sufficiently high inverse population density of laser levels has been obtained.

Figure 3.2 shows the process of growth of a giant pulse upon active Q-modulation of the resonator. The curve P vs. t describes the

[4] A further increase in the pulse power is obstructed by spontaneous emission and superluminescence, which increase with increasing the initial inverse population density.

time variation of the power of the generated radiation. The time variations of the Q-factor of the resonator (Q vs. t) and of the inverse population density (N vs. t) have also been shown in this figure. In the initial state, we have a low Q ($Q = Q_{min}$) and a high initial inverse population density ($N = N_1$). Under the influence of the controlling signal, the Q-factor begins to increase and hence the threshold value of the inverse population density (not shown in the figure) begins to decrease. As soon as the threshold value decreases to the level N_1, the generation begins. This moment of time

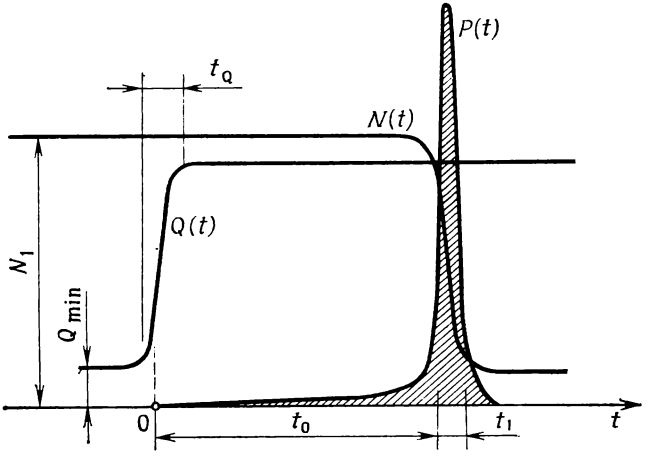


Fig. 3.2

has been chosen as the initial moment ($t = 0$) in the figure, from which it is apparent that the process of giant pulse generation consists of two stages: a relatively long stage of *slow* (linear) pulse growth (the duration t_0 of this stage is $\sim$100 nsec), and a short stage of *rapid* (nonlinear) pulse growth (the duration of this stage is $t_1 \sim$ $\sim$ 10 nsec). Nearly all the pulse energy is emitted during the second stage, hence it is customary to measure the duration of the giant pulse by the duration of this stage (i.e. by the magnitude of t_1). It should be noted that a decrease in the inverse population density takes place practically during the stage of rapid pulse growth only.

Let us denote by t_Q the interval over which the Q-factor increases from its minimum to its maximum value (*Q-switching time*). If $t_Q \ll t_0$, a *rapid* Q-switching to a higher value is indicated. Figure 3.2 corresponds to such a case. The process of pulse growth upon a rapid Q-switching to a high value is usually calculated, assuming for the sake of simplicity that the Q-factor increases *instantaneously*

[29]. If the time t_Q is of the same order as t_0, it is necessary to take into account the actual rate of Q-increase [30, 24][5].

For a sufficiently slow Q-switching to a higher value, the generation picture is considerably altered: instead of a *single* pulse, *several* pulses with gradually decreasing power and increasing duration may appear (Fig. 3.3). The time interval between successive pulses gradually increases from 100 nsec to 1 μsec.

Giant-Pulse Generation for Passive Q-modulation of a Resonator. *Passive* Q-modulation is based on the application of *nonlinear elements* whose characteristics vary with radiation power generated in the active element. *Bleachable filters*, i.e. optical shutters

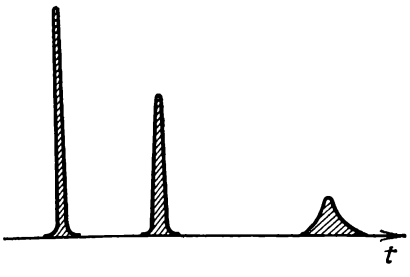


Fig. 3.3

operating on the nonlinear optical effect of bleaching of the medium[6] are widely used. Besides nonlinear filters, nonlinear cells based on the stimulated Brillouin principle of scattering, semiconducting mirrors whose reflection coefficient depends on the intensity of the incident light beam, etc. are also used [4].

The idea of using bleachable media in quantum electronics was put forth in 1964 [31]. It was soon applied in practice for obtaining giant pulses in a ruby laser (see, for example, [32])[7].

Figure 3.4 shows the growth of a giant pulse for passive Q-modulation of a pulse-pumped laser resonator. Q-modulation is attained by using a bleachable filter. The curve P vs. t describes the time variation of the radiation power. The time variation of the coefficient of resonant absorption by filter at laser frequency ($\varkappa_a$ vs. t) and of inverse population density of active medium levels (N vs. t) are also shown in the same figure. The initial state corresponds to the unbleached filter ($\varkappa_a = \varkappa_{0a}$). The threshold of inverse population

[5] Strictly speaking, the time t_0 depends on t_Q. Hence it is more correct to compare t_Q with time $\tau_0 = 2L/c$, corresponding to a round-trip through the resonator, instead of t_0 [24]. If $t_Q \ll \tau_0$, the Q-switching is considered as *rapid*; but if $t_Q \gg \tau_0$, the Q-switching is considered to be *slow*.

[6] The term *phototropic shutters* is also used.

[7] Giant-pulse lasers with bleachable filters have been discussed in [2, 6].

density is quite high for this state (we denote it by $N_{\text{thr.max}}$). With the arrival of pumping radiation at the active element, the magnitude of N will increase. As soon as it attains the value $N_{\text{thr.max}}$, generation will start[8]. This moment of time is chosen as the starting point ($t = 0$) in the figure. Like in the case of active Q-modulation, the giant-pulse formation takes place in two stages: the long stage of *slow* (linear) growth (t_0 is the duration of this stage) and the short stage of *rapid* (nonlinear) growth (duration of this stage is t_1). For passive Q-modulation, the stage of linear growth is

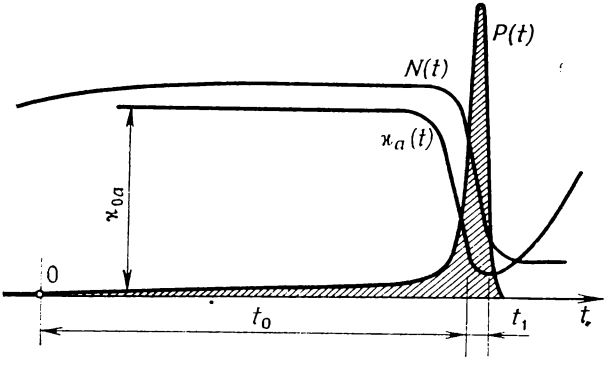


Fig. 3.4

an order of magnitude longer than for active modulation, and is now of the order of 1 μsec. This is due to the fact that the pulse growth in this stage takes place for passive Q-modulation under *high-loss* conditions. From the figure, it is apparent that the filter is bleached only in the second (nonlinear) stage of the pulse growth. The duration of the second stage is about 10 nsec (same as for active modulation).

After the giant-pulse emission, the coefficient of resonant absorption of the filter again increases on account of spontaneous transitions in the filter. The time T_a during which the filter returns to the initial (unbleached) state is called the *relaxation time of the filter.*

Longitudinal Mode Locking (Ultrashort Light Wave Generation). Creation of Q-modulation lasers was an important step in the development of laser technology. The next important step is connected with the creation of *longitudinal mode-locking* lasers.

Let us suppose that a laser radiation contains m longitudinal modes whose frequencies are *equidistant* and separated by Ω from each other (it should be recalled that $\Omega = \pi v/L$, L being the length

[8] Giant-pulse generation in a laser with a bleachable filter is possible only if certain conditions are satisfied. These conditions will be considered later (see Sec. 3.8).

of the resonator). The gain line width $\Delta\omega$ is connected with Ω and m through the apparent relation $\Delta\omega = \Omega m$. We assume that the modes are *phased-locked*, i.e. the phase difference between any two adjacent modes has a definite fixed value. In this case, there will be a mutual *interference* of longitudinal modes[9], giving rise to a *train of ultrashort light pulses*. The duration τ of an individual pulse is described by the gain line width or, in other words, as the mode-locking number

$$\tau \sim 1/\Delta\omega = 1/\Omega m.$$

The power of an ultrashort pulse turns out to be about m times greater than the average radiation power in the absence of mode locking. The ultrashort pulse repetition period T is expressed through the frequency interval between the locked-in modes:

$$T \sim 1/\Omega.$$

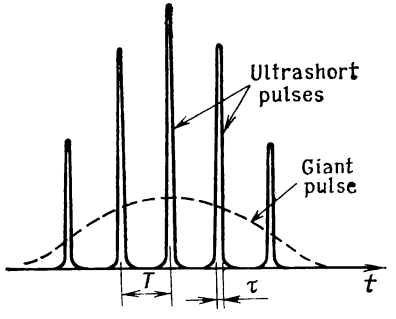


Fig. 3.5

In the presence of longitudinal mode locking, a giant pulse is converted into a train of ultrashort (superpower) pulses. Figure 3.5 shows an approximate comparison between a giant pulse and a train of ultrashort pulses in a pulsed pumping laser[10]. The duration of this pulse train in time is nearly equal to the duration t_1 of the giant pulse. Thus, the number of ultrashort pulses may be estimated by the ratio t_1/T.

For generation of ultrashort light pulses, two basic conditions have to be satisfied. Firstly, a laser must generate a fairly large number of longitudinal modes[11]. Secondly, these modes must be equidistant in frequency and synchronised in phase.

In order to satisfy the first condition, it is necessary to have a fairly *wide* gain line and, besides, to take special measures to prevent the possible *selection* of longitudinal modes in the resonator (the mode selection in this case is an undesirable effect). The gain linewidth $\Delta\omega$ is about 10^{11} sec^{-1} for a ruby laser, 10^{12} sec^{-1} for an Nd-laser, and 10^{13}-10^{14} sec^{-1} for organic-dye lasers. Assuming $\Omega \sim 10^8$ sec^{-1}, we find that the maximum possible (under condition that selection has been prevented) number of longitudinal modes is equal to 10^3,

[9] The term *mode locking* is sometimes applied for this.

[10] The mention of pulsed pumping is not coincidental. As a matter of fact, giant pulses are realised under conditions of pulsed pumping. As regards mode locking, it can be realised in lasers with pulsed pumping as well as with continuous pumping.

[11] In principle, at least three longitudinal modes are required for mode locking.

10^4, 10^5-10^6 respectively for the lasers mentioned above. It would appear that for $m = 10^6$ the ultrashort light pulse must have a duration $\tau \sim (\Omega m)^{-1} \sim 10^{-14}$ sec (10^{-5} nsec). In actual practice, however, it is not possible to get pulses of shorter duration than about 10^{-3} nsec since an increasing gain linewidth inevitably leads to a violation of the requirement of equidistance between longitudinal mode frequencies[12], thus naturally deteriorating the synchronisation conditions[13]. The duration of ultrashort light pulses actually obtained in practice is about 10^{-2}-10^{-3} nsec, their power being as high as 10^{12} W.

For a phase locking of longitudinal modes, *active* as well as *passive* locking methods are used. In the first case, a forced periodic modulation is applied to parameters of a resonator whose frequency is equal to, or a multiple of, the frequency Ω. In the second case, a bleachable filter or a nonlinear dielectric is used inside a resonator. In this case, it is significant that the filter should have a *very small relaxation time*, so that the condition $T_a < T$ is satisfied. While considering passive mode locking, the term *mode self-locking* is often applied.

The first experimental results on active longitudinal mode locking were obtained in a He-Ne laser [33]. In 1966, it was shown [34] that a passive mode locking (*mode self-locking*) is possible in a laser with a quickly-relaxing bleachable filter under certain conditions. The question of generating ultrashort light pulses by active or passive longitudinal mode locking, and their properties have been discussed, for example, in [35-41].

In the case of *free generation*, self-locking of longitudinal modes is also possible due to nonlinear properties of the active medium [42-45][14].

Transverse Mode Locking. According to (2.9.21), transverse modes in a resonator with spherical mirrors are characterised by an equidistant set of resonance frequencies, with a spacing equal to $\Omega = v \arccos \sqrt{g_1 g_2}/L$, L being the resonator length, g_1 and g_2, its generalised parameters. Equidistance of frequencies is a necessary condition for mode locking. The fact that this condition may be satisfied not only for *longitudinal*, but also for *transverse* modes, indicates the possibility of a transverse mode locking.

While the *longitudinal* mode locking generates a train of ultrashort light pulses (in other words, it leads to a periodic modulation *in time* of the generated light power), the *transverse* mode locking leads to a redistribution of the generated light power in a direction

[12] In this connection, we can mention the frequency pulling effect, considered in Sec. 2.12.

[13] According to fluctuation concepts, an inordinate increase in the number of longitudinal modes deteriorates the synchronisation conditions even in the case of equidistant frequencies (see Sec. 3.11).

[14] In this case, the term *spontaneous locking* is sometimes used.

perpendicular to the resonator axis (in other words, a *space modulation* of light power must be observed). In the absence of transverse mode locking, the axis of the light beam generated by the laser coincides with the optical axis of the resonator. In the case of transverse mode locking, such a coincidence occurs only at certain moments of time. Transverse mode locking means that the cross-section of the generated light beam (*generation zone*) starts a *periodic motion* in the plane of the mirror with a frequency Ω corresponding to the difference in the frequencies of locked modes. This effect was first predicted in [46], and is discussed in detail in [47].

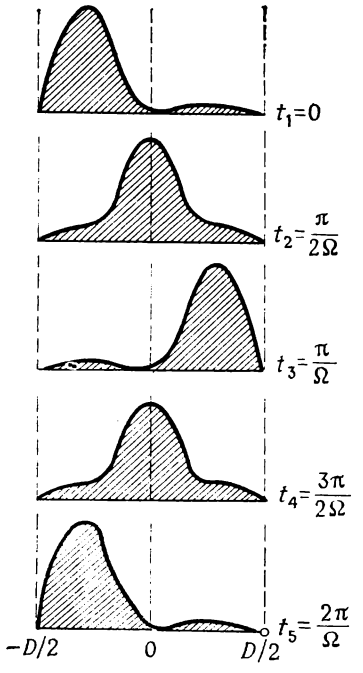


Fig. 3.6

Experimental confirmation of the existence of transverse mode locking is given, for example, in [48, 49] for gas lasers and in [50-52] for solid-state lasers. Figure 3.6 shows the intensity distribution for the generated radiation over the diameter D of the resonator mirror, taken from [51] and obtained for a locking of three lowest transverse modes for several successive moments of time:

$$t_1 = 0; \quad t_2 = \pi/2\Omega; \quad t_3 = \pi/\Omega;$$
$$t_4 = 3\pi/2\Omega; \quad t_5 = 2\pi/\Omega.$$

It can be seen from the figure that the generation zone oscillates in the plane of the mirror with a period $T = 2\pi/\Omega$.

Investigation of the transverse mode locking effect is certainly interesting from a practical point of view. Transverse mode-locked lasers may be quite promising for applications in *opto-electronics*, in communication systems, and in optical data processing.

Cavity Dumping. This is also known as *load modulation* and *favourable loss modulation*. Unlike Q-switching of a resonator, the *favourable* and not *unfavourable* losses are controlled in this case.

For cavity dumping, a laser with a *high Q-resonator* is used, the resonator mirrors having a reflection coefficient close to unity. A high-speed *modulator* (switch) of favourable losses, which can be controlled externally, is placed in the resonator. This is meant for *dumping* a part of the radiation from the resonator. Modulators (switches) of both acoustooptic as well as electrooptical type are

used. *Continuous* pumping is normally employed in cavity dumping lasers.

Suppose that the modulator of favourable losses is not switched on while the pumping is going on. Under these conditions, if the inverse population density of laser levels exceeds the relatively low generation threshold of a high resonator, there will be an increase in the photon density inside the resonator (due to predominance of induced emission over resonant absorption at the laser transition, and over losses). Continuous pumping will keep the inverse population density of the laser levels above the generation threshold. In this case, even though the generation is actually taking place, the radiation is confined within the resonator.

Further, let us assume that a modulator of favourable losses is switched on for a short interval of time. This leads to extraction of a short pulse from the resonator, i.e. the resonator partially "dumps" the photons accumulated in it.

Comparing cavity dumping with active Q-switching we remark that in the latter case, the photon density in the resonator is very low in the initial state (when Q is low). The laser is then *below* the generation threshold corresponding to high losses. Upon switching Q to a higher value, the generation begins to develop and the output pulse begins to form simultaneously. It should be noted that the formation of this pulse starts from the spontaneous background (noise level), thus accounting for a relatively long stage of linear growth (see Fig. 3.2).

Unlike Q-switching, the cavity dumping is characterised by a high Q in the initial state; the laser is *above* the generation threshold corresponding to low losses. The generation takes place even before the output pulse begins to form, and the cavity is full of photons. It should be emphasised that while for Q-switching the generation starts *after* the controlling signal has been applied to the modulator, for cavity dumping the modulator is switched on in the laser which is *already operating*. This considerably *reduces* the output pulse formation time (there is no prolonged linear stage in the pulse growth). Consequently, we can obtain light pulse trains of *higher* frequencies.

During cavity dumping of photons, the laser must remain above the generation threshold corresponding to a high Q-state. This requirement restricts the duration of time interval for which the modulator may be switched on.

The oscillations of inverse population density of laser levels for cavity dumping are considerably *weaker* than for Q-switching. This is due to the fact that the generation threshold in the initial state, and hence the initial inverse population density in the case of cavity dumping are *considerably lower* than for Q-switching.

If the radiation is extracted from the cavity at the wavelength of the laser transition in the active medium, the load is called *linear*.

In actual practice, radiation corresponding to the wavelength of the *second harmonic*[15] is also extracted from the cavity. Since the power of second harmonic radiation is proportional to the square of the power of the fundamental-mode radiation (in the approximation of the given field), the term *quadratic* load is used. This is a special case of *nonlinear* load.

The possibility of cavity dumping by using a fast acousto-optic modulator has been discussed in [53]. A detailed description of this process in the case of a continuously pumped Nd:YAG laser is given in [54-57]. Cavity dumping in a dye laser with *pulsed* pumping is considered in [58].

It has been shown in [55] that cavity dumping in a continuously pumped Nd:YAG laser gives a mean output power equal to the maximum power of continuous generation; the frequency of the light pulse train ranges between 100 kHz to tens of mega-Hertz[16]. For the sake of comparison, it may be indicated that the maximum frequency of the pulse train for continuous pumping in case of Q-switching is approximately 50 kHz [59].

Pulse Train Generation in a Continuously Pumped Laser. In actual practice, it is frequently required to have a regularly controlled *train of light pulses* following one after another at a sufficiently high frequency. For this purpose, a *continuous* pumping generation is used.

Continuously pumped Nd:YAG lasers have been extensively investigated in [54-57, 59-64]. The mean power of output radiation for them is about 1-10 W. Maximum value of the mean output power may be as high as several hundreds watts [61].

Active Q-switching of the resonator was first used for pulse generation in continuously pumped lasers. To begin with, a mechanico-optical modulator in the form of a rotating mirror was used [60]. However, such a method of modulation was found to be of little interest for the case of continuous pumping on account of poor stability of amplitude from pulse to pulse (this is due to poor reproduction of the position of the reflecting plane of the rotating mirror). The acoustooptic modulators, which came into operation later, were found to be quite suitable. They helped in obtaining extremely high frequencies of pulse trains, $f \sim 50$ kHz [59].

The pulse generator in a continuously pumped single-mode laser for active Q-switching of the resonator has the following energy and time characteristics: pulse train frequency $f \sim 10$ kHz, pulse duration $t_1 = 100$ nsec-1 μsec, peak power $P_{max} \sim 10^3$ W, average output power $P_{av} \sim 1$-10 W (note that $P_{av} \sim P_{max} t_1 f$). This regime may be used even for frequencies $f < 10$ kHz; however, if f is lower

[15] This is the *second harmonic cavity generation*. To attain this, a frequency doubler for radiation generated in the active element is introduced in the cavity.

[16] The maximum power of continuous generation is the generation power of a continuously pumped laser without loss modulation, and with an optimal reflection coefficient of the output mirror.

than about 5 kHz, the efficiency of the laser decreases. This decrease is greater, the lower the value of f [59, 62]. As mentioned earlier, the frequency f has an upper limit of about 50 kHz. The existence of an upper frequency limit is due to the existence of a long stage of linear growth of the output pulse.

In order to get a pulse train with a recurrence frequency above 50 kHz, we must ensure a quicker growth of pulse intensity. For this purpose, the generated pulse may be "cut off" at the point where the intensity begins to decrease, and so a sufficiently high radiation density (as well as a relatively high inverse population density of laser levels) may be retained inside the resonator.

In this case the generation will start not from the noise level but from the radiation level, retained in the resonator as a result of pulse "cut-off". Such a method helps in increasing the frequency f up to about 100 kHz [63].

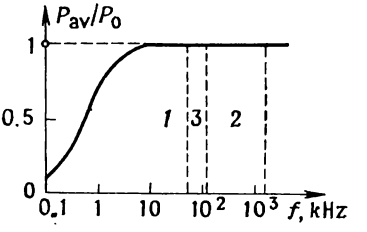


Fig. 3.7

Another method of increasing f is the *cavity dumping*. The frequencies f obtained in this case are limited *from above* just by the rate of accumulation of radiation in the cavity (the accumulation time corresponds to the time spent in several passes of the radiation through the cavity). It has been mentioned above that if the average output power is equal to the maximum power of continuous generation, the frequencies f acquire a *lower* limit: the inequality $f > 100$ kHz must be satisfied [55, 56]. As a matter of fact, the requirement of conservation of average output power for low pulse repetition frequencies leads to the necessity of dumping an extremely large number of pulse photons from the cavity. Consequently, the inverse population density of laser levels may turn out to be lower than the generation threshold. Typical characteristics for cavity dumping are: pulse repetition frequency $f \sim 100$ kHz-10 MHz, pulse duration $t_1 \sim 10$-100 nsec, average output power $P_{av} \sim 1$-10 W.

Figure 3.7 shows the dependence P_{av}/P_0 vs. f, where P_0 is the maximum power of continuous generation [55]. Three regions have been isolated in the figure: *1* is the frequency region utilised for Q-switching ($f \leqslant 50$ kHz), *2* is the region utilised for cavity dumping (100 kHz $\leqslant f \leqslant$ 10 MHz), *3* is the region between the upper frequency limit for Q-switching and the lower frequency limit for cavity dumping. Both Q-switching as well as cavity dumping are unstable in region *3*.

Applying a deeper load modulation (by ensuring a more efficient cavity dumping for one pulse), stable generation may be obtained in region *3* [57]. On the other hand, as mentioned above, a pulse "cut-off" may lead to a stable Q-switching in this region.

Negative Feedback for Obtaining Microsecond Pulses. As a modification of Q-switching for a pulsed-pumping laser cavity, we can mention generation using *negative feedback* for controlling the load and shape of a giant light pulse[17]. Negative feedback has a braking influence on the growth of the induced emission process which appears as a result of Q-switching of the resonator to a higher value. Consequently, the removal of inversion in the active medium (and hence the formation of the output pulse) takes a *longer* time. The duration of a light pulse can thus be increased by about two orders of magnitude—to several microseconds instead of tens of nanoseconds (upon a manifold decrease in the pulse energy).

There are different possible ways of getting a negative feedback for increasing the duration of a giant pulse [65]. In the *electrooptical* method, Q-switching is attained through an electrooptical shutter whose opening is changed by modulating voltage used for switching on the shutter, as well as by the *feedback signal* proportional to the intensity of cavity radiation. When the shutter is "opened", the intensity of the output radiation begins to increase. Correspondingly, the intensity of feedback signal also begins to increase, and hence the shutter opening is reduced thus bringing to halt the growth of the light pulse. The pulse duration increases with increasing sensitivity of the photodetector in the feedback circuit (with increasing ratio of the intensity of feedback to the intensity of the output radiation incident on the photodetector), as well as with decreasing Q-switching rate.

Negative feedback may be obtained by placing *nonlinear elements* in the resonator. Nonlinear losses in such lasers may be caused by different nonlinear optical effects: two-photon absorption of light, second harmonic generation, induced Raman scattering, etc. [65]. By way of an example, let us consider the *two-photon absorption of light* in a semiconductor.

Suppose that a semiconductor plate, whose forbidden bandwidth ΔE satisfies the condition $\hbar\omega < \Delta E < 2\hbar\omega$ (ω is the frequency of laser transition in the active medium), is placed in a resonator. This condition is satisfied, for example, in a ruby laser by CdS, and in the case of Nd-lasers by CdSe and GaAs. With the help of an optical shutter, we can Q-switch the resonator to a higher value, thus causing the growth of intensity of radiation generated in the active element. With increasing radiation intensity, the probability of a two-photon absorption of this radiation by the semiconducting plate will increase. In other words, the transparency of the plate for generated radiation *will decrease*. The stronger the absorption of light in the semiconductor, the more effective the check on the growth of photon density in the resonator, and hence the slower the

[17] The feedback is called *negative* if the losses increase with increasing radiation intensity.

rise in induced transition probability. Consequently, the processes of removal of inversion in the active medium and the formation of the light pulse are staggered in time. The duration of the generated pulse increases with decreasing Q-switching rate and with increasing pulsed pumping energy.

Before concluding this section, it may be remarked that the introduction of a negative feedback may help in *stabilising* the laser parameters. The electrooptical feedback was used as early as 1962 for smoothing the spikes in the ruby laser radiation [66]. For the same purpose we can use nonlinear absorbers in which the losses increase with increasing intensity of radiation (see, for example, [67]). Investigations of second harmonic cavity generation in Nd:YAG lasers show that the introduction of a negative feedback leads to a sharp decrease in the sensitivity of the output radiation to small loss modulation on account of a transformation into second harmonic. This may lead to a smoothing of phase-frequency characteristics of the laser [68].

3.2. APPROXIMATE EQUATIONS DESCRIBING THE DYNAMICS OF LASER PROCESSES (BALANCE EQUATIONS)

To a first approximation, the dynamics of processes may be described by *balance equations*. Such equations have already been applied in Secs. 1.1 and 1.2 while considering the population of laser levels under stationary conditions. The system of balance equations helps in getting a time dependence for inverse population density of laser levels and the generated radiation power.

Differential Equation for the Light Flux Density. We shall be considering the *one-dimensional* case—a monochromatic radiation propagates in the active medium along the z-axis (along the optical axis of the laser). The *density of light flux* propagating along the direction of the z-axis is denoted by $S_+ (z, t)$, while the density of flux propagating in the opposite direction is denoted by $S_- (z, t)$. Let us consider the increment ΔS_+ in the flux S_+ as it propagates from the point z to $z + \Delta z$. Using Bouguer's differential law, we can write

$$\Delta S_+ = [\varkappa (z, t) - \eta_1] S_+ (z, t) \Delta z + q (z, t) \Delta z. \qquad (3.2.1)$$

According to this equation, the increment in the flux density during its passage from z to $z + \Delta z$ consists of three components:

(a) $\varkappa (z, t) S_+ (z, t) \Delta z$ is the increase in flux density on account of an amplification of radiation by active centres (it should be recalled that $\varkappa (z, t)$ is the amplification factor of the active medium);

(b) $-\eta_1 S_+ (z, t) \Delta z$ is the decrease in the flux density due to absorption by inactive centres as well as scattering of radiation (η_1 is the coefficient of unfavourable losses);

(c) $q(z, t)\,\Delta z$ is the increase in the flux density due to luminescence (spontaneous emission).

In view of its small magnitude, the last term is usually neglected, and the following simpler equation is used:

$$\Delta S_+ = [\varkappa(z, t) - \eta_1]\, S_+(z, t)\,\Delta z. \qquad (3.2.2)$$

The propagation of flux from the point z to $z + \Delta z$ requires a time $\Delta t = \Delta z/v$, where v is the velocity of light in the active medium. Thus, $\Delta S_+ = S_+(z + \Delta z, t + \Delta t) - S_+(z, t)$. The increase in the flux density is due to two reasons: a variation in the flux density with distance, and with time. The first cause leads to the term $\frac{\partial S_+}{\partial z}\Delta z$ in the expression for the increase ΔS_+, while the second contributes the term $\frac{\partial S_+}{\partial t}\frac{\Delta t}{\Delta z}\Delta z = \frac{1}{v}\frac{\partial S_+}{\partial t}\Delta z$. Thus,

$$\Delta S_+ = S_+(z+\Delta z,\ t+\Delta t) - S_+(z, t) = \left(\frac{\partial S_+}{\partial z} + \frac{1}{v}\frac{\partial S_+}{\partial t}\right)\Delta z. \qquad (3.2.3)$$

Taking (3.2.3) into account, Eq. (3.2.2) can be rewritten as

$$\frac{\partial S_+}{\partial z} + \frac{1}{v}\frac{\partial S_+}{\partial t} = [\varkappa(z, t) - \eta_1]\, S_+(z, t). \qquad (3.2.4)$$

Denoting the cross section of the induced transition in the generation channel by σ, we can write, in accordance with Eq. (1.1.3),

$$\varkappa(z, t) = \sigma N(z, t) \qquad (3.2.5)$$

where $N(z, t)$ is the inverse population density of laser levels. Consequently, the differential equation (3.2.4) for the flux density S_+ assumes the form

$$\frac{\partial S_+}{\partial z} + \frac{1}{v}\frac{\partial S_+}{\partial t} = [\sigma N(z, t) - \eta_1]\, S_+(z, t). \qquad (3.2.6a)$$

The differential equation for the flux density S_- has an analogous form:

$$-\frac{\partial S_-}{\partial z} + \frac{1}{v}\frac{\partial S_-}{\partial t} = [\sigma N(z, t) - \eta_1]\, S_-(z, t). \qquad (3.2.6b)$$

Equations (3.2.6) contain three unknown functions: $S_+(z, t)$, $S_-(z, t)$, and $N(z, t)$. Let us now consider the third missing equation in these unknowns.

Differential Equations for Inverse Population Density. (Three-Level and Four-Level Lasers). Let us consider the *three-level diagram* shown in Fig. 3.8. The following notation has been used: w is the probability of induced transitions in the generation channel (channel *2-1*), w_p is the probability of induced transitions in the channel *1-3* (probability of transitions induced by the pumping radiation), $1/\tau$ is the probability of spontaneous transitions in the generation channel, $1/\tau_{31}$ and $1/\tau_{32}$ are the probabilities of sponta-

neous transitions in the channels *1-3* and *2-3* respectively (all probabilities are per unit time). We denote the population density of the i-th level by n_i (z, t), and the total number of active centres per unit volume by n'. The *balance equations* for the population densities n_1, n_2, and n_3 have the following form:

$$\left.\begin{aligned}
\frac{\partial n_1}{\partial t} &= w(n_2 - n_1) - w_p(n_1 - n_3) + \frac{n_2}{\tau} + \frac{n_3}{\tau_{31}}; \\
\frac{\partial n_2}{\partial t} &= -w(n_2 - n_1) + \frac{n_3}{\tau_{32}} - \frac{n_2}{\tau}; \\
\frac{\partial n_3}{\partial t} &= w_p(n_1 - n_3) - \frac{n_3}{\tau_{32}} - \frac{n_3}{\tau_{31}}.
\end{aligned}\right\} \qquad (3.2.7)$$

(It should be noted that $\partial n_1/\partial t + \partial n_2/\partial t + \partial n_3/\partial t = 0$. This is quite natural, since the sum $n_1 + n_2 + n_3 = n'$ is independent of time. Subtracting the first equation (3.2.7) from the second, we get

$$\frac{\partial (n_2 - n_1)}{\partial t} = -2w(n_2 - n_1) + w_p(n_1 - n_3) - 2\frac{n_2}{\tau} + n_3\left(\frac{1}{\tau_{32}} - \frac{1}{\tau_{31}}\right). \qquad (3.2.8)$$

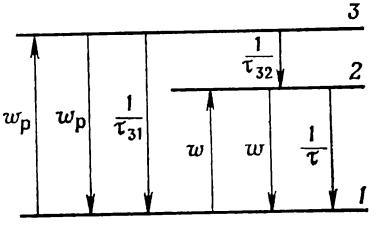


Fig. 3.8

We now use the so-called *two-level approximation*, i.e. we assume that the active centres practically do not accumulate at level *3* (having arrived at level *3*, they quickly leave it, and go over mainly to level *2*). This means that the conditions

$$n_3 \ll n_1; \quad \partial n_3/\partial t \approx 0; \quad \tau_{32} \ll \tau_{31} \qquad (3.2.9)$$

are satisfied. In this case, the three-level diagram is reduced to a *two-level* diagram (i.e., $\partial n_2/\partial t \approx -\partial n_1/\partial t$).

Using (3.2.9), the third equation in (3.2.7) may be written in the form

$$w_p n_1 = n_3/\tau_{32}. \qquad (3.2.10)$$

Taking into account (3.2.9) and (3.2.10), we can rewrite Eq. (3.2.8) in the form

$$\partial (n_2 - n_1)/\partial t = -2w(n_2 - n_1) + 2w_p n_1 - 2n_2/\tau. \qquad (3.2.11)$$

We assume that

$$N = n_2 - n_1. \qquad (3.2.12)^{18}$$

[18] For the sake of simplicity, we assume that the laser levels have identical degeneracy ($g_2/g_1 = 1$). It follows from this, in particular, that the Einstein coefficients (and hence the cross sections) are equal for both induced transitions in the generation channel: for induced emission and resonant absorption by active centres.

Considering that $n_3 \ll n_1$, we can put $n_1 + n_2 = n'$, and hence $n_1 = (n' - N)/2$, $n_2 = (n' + N)/2$. As a result, Eq. (3.2.11) assumes the form

$$\partial N/\partial t = -2wN + w_p (n' - N) - (n' + N)/\tau,$$

or, finally,

$$\partial N/\partial t = -(w_p + 2w + \tau^{-1}) N + n' (w_p - \tau^{-1}). \qquad (3.2.13)$$

Let us now consider the *four-level* diagram, where the optical pumping takes place in the channel *0-3*, and the generation occurs in the channel *2-1*. As in the case of a three-level diagram, we shall be using the two-level approximation, assuming that the active centres after arriving at level *3* quickly move over to the metastable level *2*. In addition, we shall assume that the lower laser level *1* is rapidly depopulated (the rate of $1 \to 0$ transition is quite high). Under such simplification, we can easily get the following differential equation for the inverse population density N (in this case, $N = n_2 - n_1 \sim n_2$)[19]

$$\partial N/\partial t = -(w_p + w + \tau^{-1}) N (z, t) + n' w_p. \qquad (3.2.14)$$

Here, w and w_p are probabilities of induced transitions in the generation and pumping channels respectively, and $1/\tau$ is the probability of spontaneous transitions in the generation channel.

Complete System of Partial Differential Balance Equations. It should be recalled that the cross section σ of a process is the probability w of the process per unit time divided by the flux density I of the photons responsible for this process:

$$\sigma = w/I. \qquad (3.2.15)$$

Since $I = (S_+ + S_-)/\hbar\omega$, where $\hbar\omega$ is the energy of one photon, we get

$$\sigma = w\hbar\omega/(S_+ + S_-). \qquad (3.2.16)$$

Further, taking into account that $w = B (S_+ + S_-)/v$, where B is the Einstein coefficient for induced processes in the generation channel, we get the following familiar expression for the cross section σ (see Sec. 2.1) from Eq. (3.2.16):

$$\sigma = B\hbar\omega/v. \qquad (3.2.17)$$

Combining (3.2.6) and (3.2.13), and taking into account Eq. (3.2.16), we arrive at the *complete system of balance equations for*

[19] The derivation of Eq. (3.2.14) is based on the same principles as were used for deriving Eq. (3.2.13). For details, see, for example, [1].

a three-level laser (in the framework of two-level approximation):

$$\begin{aligned}
&\frac{\partial S_+}{\partial z}+\frac{1}{v}\frac{\partial S_+}{\partial t}=[\sigma N(z,\ t)-\eta_1]\,S_+(z,\ t);\\
&-\frac{\partial S_-}{\partial z}+\frac{1}{v}\frac{\partial S_-}{\partial t}=[\sigma N(z,\ t)-\eta_1]\,S_-(z,\ t);\\
&\frac{\partial N}{\partial t}=-\left[w_{\mathrm{p}}+\frac{2\sigma}{\hbar\omega}(S_++S_-)+\frac{1}{\tau}\right]N+n'\left(w_{\mathrm{p}}-\frac{1}{\tau}\right)
\end{aligned} \qquad (3.2.18)$$

For a *four-level laser*, the last equation in the system (3.2.18) must be replaced by the equation

$$\frac{\partial N}{\partial t}=-\left[w_{\mathrm{p}}+\frac{\sigma}{\hbar\omega}(S_++S_-)+\frac{1}{\tau}\right]N+n'w_{\mathrm{p}}. \qquad (3.2.19)$$

Let us consider the boundary conditions for the functions S_+ and S_-. For this purpose, we turn to Fig. 3.9 where the active element of length L with specially prepared faces has been schematically



Fig. 3.9

shown. The reflection coefficients of the faces are equal to R_1 (for $z = 0$) and R_2 (for $z = L$). The boundary conditions have the form

$$S_+(0,\ t)=R_1S_-(0,\ t);\quad S_-(L,\ t)=R_2S_+(L,\ t). \qquad (3.2.20)$$

Averaged Balance Equations (Rate Equations). Yet another simplification is used when balance equations are applied. This simplification is connected with the *averaging* of inverse population densities and of light flux density over the length of the active medium (more precisely, over the length of the resonator). First of all, we assume that

$$S_+ + S_- = S;\qquad S_+ - S_- = S'. \qquad (3.2.21)$$

Adding the first two equations in the system (3.2.18) and taking into account (3.2.21), we find that

$$\partial S'/\partial z + v^{-1}\,\partial S/\partial t = [\sigma N(z,\ t) - \eta_1]\,S(z,\ t).$$

Integrating this equation over the length of the active medium, we get

$$\begin{aligned}
&S'(L,\ t)-S'(0,\ t)+\frac{1}{v}\frac{\partial}{\partial t}\int_0^L S(z,\ t)\,dz\\
&=\sigma\int_0^L N(z,\ t)\,S(z,\ t)\,dz-\eta_1\int_0^L S(z,\ t)\,dz.
\end{aligned} \qquad (3.2.22)$$

Using angle brackets $\langle \ldots \rangle$ for denoting the averaged functions $\left(\langle f \rangle = \frac{1}{L} \int_0^L f(z, t,) \, dz \right)$, we can rewrite (3.2.22) in the form

$$S'(L) - S'(0) + (L/v)\, d\langle S \rangle / dt = \sigma L \langle NS \rangle - \eta_1 L \langle S \rangle. \quad (3.2.23)$$

While averaging, it was assumed that the properties of the active medium are uniform in space, so that neither σ nor η_1 depend on the coordinate z.

It can be shown (for example, see [1]) that the following approximate relation is quite effective for considering real situations:

$$\langle NS \rangle \sim \langle N \rangle \langle S \rangle. \quad (3.2.24)$$

Taking this approximation into account, we can rewrite (3.2.23) in the form

$$S'(L) - S'(0) + (L/v)\, d\langle S \rangle / dt = L(\sigma \langle N \rangle - \eta_1) \langle S \rangle. \quad (3.2.25)$$

It can be easily seen that the density of light flux emerging from the resonator S_{out} is given by

$$\begin{aligned} S_{out} &= [S_+(L) - S_-(L)] + [S_-(0) - S_+(0)] \\ &= S'(L) - S'(0). \end{aligned} \quad (3.2.26)$$

Using the coefficient of favourable losses η_2 (see Sec. 2.1), S_{out} may be written in the form

$$S_{out} = L \langle S \rangle \eta_2, \quad (3.2.27)$$

where, it may be recalled,

$$\eta_2 = (1/2L) \ln (1/R_1 R_2). \quad (3.2.28)$$

Comparing (3.2.27) and (3.2.26), we find that

$$S'(L) - S'(0) = L \langle S \rangle \eta_2,$$

using which, Eq. (3.2.25) may be written in the form

$$(L/v)\, d\langle S \rangle / dt = L\sigma \langle S \rangle \langle N \rangle - L(\eta_1 + \eta_2) \langle S \rangle. \quad (3.2.29)$$

Thus, *averaging over the length of the active medium* leads to a considerable simplification of the system of balance equations. Instead of a system of *three* partial differential balance equations, we now have a system of *two* averaged equations:

$$\left.\begin{aligned} \frac{1}{v}\frac{d}{dt}\langle S \rangle &= \sigma \langle S \rangle \langle N \rangle - (\eta_1 + \eta_2) \langle S \rangle; \\ \frac{d}{dt}\langle N \rangle &= -\frac{2\sigma}{\hbar\omega} \langle S \rangle \langle N \rangle - \left(w_p + \frac{1}{\tau} \right) \langle N \rangle + n' \left(w_p - \frac{1}{\tau} \right). \end{aligned}\right\} \quad (3.2.30)$$

Averaged balance equations are also called *rate* equations.

Since, as a rule, we shall be using only the averaged balance equations, angle brackets will be omitted. While considering time func-

tions appearing in the balance equations, we shall assume that the averaging over space has already been carried out. Taking this into consideration and introducing the notation

$$K = w_p \tau, \tag{3.2.31}$$

the system of averaged balance equations (3.2.30) for a *three-level* laser may be rewritten in the following form:

$$\left.\begin{aligned} &\frac{1}{v}\frac{d}{dt}S = \sigma S(t)\,N(t) - (\eta_1 + \eta_2)\,S(t); \\ &\frac{d}{dt}N = -\frac{2\sigma}{\hbar\omega}S(t)\,N(t) - \frac{N(t)}{\tau}(K+1) + \frac{n'}{\tau}(K-1). \end{aligned}\right\} \tag{3.2.32}$$

For a *four-level* laser, the second equation in the system (3.2.32) should be replaced by the equation

$$\frac{d}{dt}N = -\frac{\sigma}{\hbar\omega}S(t)\,N(t) - \frac{N(t)}{\tau}(K+1) + \frac{n'}{\tau}K. \tag{3.2.33}$$

Statz-De Mars Equations. While deriving the system of equations (3.2.32), certain assumptions were made about the level diagram of an active centre. In a *more general* form (not depending on the choice of a particular level diagram), balance equations were formulated by Statz and De Mars in 1960 [69]. *The Statz-De Mars system of equations* has the following form:

$$\boxed{\begin{aligned} &\frac{d}{dt}M = B'M(t)\,N(t) - \frac{M(t)}{T}; \\ &\frac{d}{dt}N = -\beta B'M(t)\,N(t) + \frac{N_0 - N(t)}{T_1}. \end{aligned}} \tag{3.2.34}$$

The required functions here are the *inverse population density* $N(t)$ (as in (3.2.32)) and the *photon density* $M(t)$ at the generation frequency. The quantity $M(t)$ can be easily expressed in terms of the light flux density $S(t)$. As a matter of fact, dividing $S(t)$ by the velocity v of propagation of radiation, we get the radiation density. Dividing further by the photon energy $\hbar\omega$, we get the photon density $M(t)$. Thus

$$M(t) = S(t)/v\hbar\omega. \tag{3.2.35}$$

The following parameters appear in the Statz-De Mars equations: $B' = B\hbar\omega$ is the Einstein coefficient for induced transitions in the generation channel multiplied by the photon energy, T is the photon lifetime in the resonator determined by the sum of favourable and unfavourable losses (in accordance with (2.3.10), this time related to the Q-factor of the resonator as follows: $T = Q/\omega$); T_1 is the *longitudinal relaxation* time (relaxation of the difference in the

population densities of levels)[20]; $1/T_1$ is the variation probability for the difference in population densities of levels on account of relaxation processes, β is an integer describing the change in the difference in the population densities of laser levels upon emission of one photon, and N_0 is the equilibrium inverse population density in the absence of generation (the physical significance of this parameter is described below).

Statz-De Mars equations have a clear physical explanation. The *first equation* means that the photon density in a resonator *increases* as a result of induced transitions in the generation channel (on account of a predominance of induced emission over resonant absorption) and *decreases* on account of losses in the resonator. The rate of *increase* is equal to the product of inverse population density N and the probability of induced emission per unit time, w. Taking into account Eq. (3.2.35), we get $w = BS/v = B\hbar\omega M = B'M$, and hence the rate of increase is equal to $wN = B'MN$, which is reflected by the first of the Statz-De Mars equations. The rate of decrease in the photon density is equal to M/T, i.e. is inversely proportional to the Q-factor of the resonator. It should be noted that the quantity $1/T$ is quite simply expressed through the coefficients of favourable and unfavourable losses:

$$1/T = v(\eta_1 + \eta_2). \tag{3.2.36}$$

The *second Statz-De Mars equation* means that the inverse population density *decreases* on account of induced emission and *increases* due to the predominant effect of pumping over the effect of depopulation of the upper laser level as a result of relaxation processes. The rate of decrease is equal to $\beta B'MN$, and the rate of increase is equal to $(N_0 - N)/T_1$.

It is necessary to discuss in detail the parameter N_0, defined above as the equilibrium inverse population density in the absence of generation. Suppose that conditions which are known to exclude generation are satisfied (for example, the resonator is misaligned). Suppose that under these conditions a constant power pumping takes place. If there were no relaxation processes (if the spontaneous depopulation of levels were absent), the inverse population density N in this case should rise until all active centres cross the upper laser level ($N = n'$). However, the relaxation processes always take place. Hence the function $N(t)$ increases and tends to a certain constant value (less than n') at which the increase in N due to pumping and the decrease in N due to relaxation processes *compensate each other*. The constant value of inverse population density is N_0. It should be noted that the higher the pumping power, the higher the value of N_0, apparently, at which the above mentioned compen-

[20] For a description of longitudinal and transverse relaxation, see, for example, Sec. 5.7 in [70].

sation occurs. Hence N_0 is sometimes also called the *pumping parameter*.

It should be noted that the second Statz-de Mars equation, as can be easily seen, has a solution, $N = N_0$, if we assume $M = 0$ (no generation) and $dN/dt = 0$ (the pumping and relaxation processes compensate each other).

It is sometimes preferable (see, for example, [54, 59, 68]) to use the functions $F(t) = \hbar\omega M(t)$ and $N'(t) = \hbar\omega N(t)$ instead of $M(t)$ and $N(t)$. These functions describe the radiation energy density (at the generation frequency) stored in the field inside the resonator and in the inverted active centres respectively. In this case, the Statz-De Mars system of equations (3.2.34) may be written in the form

$$\left.\begin{aligned} dF/dt &= BF(t)\,N'(t) - \xi F(t); \\ dN'/dt &= R - \lambda N'(t) - \beta BF(t)\,N'(t). \end{aligned}\right\} \qquad (3.2.34a)$$

Here $\xi = 1/T$; $\lambda = 1/T_1$; $R = N_0\hbar\omega/T_1$.

Comparison of the Statz-De Mars Equations and the System of Averaged Balance Equations. Let us compare the Statz-de Mars equations with the system of balance equations (3.2.32). Using the relations (3.2.17), (3.2.35), and (3.2.36) and the relation $B' = B\hbar\omega$, the Statz-De Mars equations (3.2.34) can be rewritten in the form

$$\left.\begin{aligned} \frac{d}{dt}S &= v\sigma S(t)\,N(t) - v(\eta_1 + \eta_2)\,S(t); \\ \frac{d}{dt}N &= -\beta\frac{\sigma}{\hbar\omega}S(t)\,N(t) - \frac{N(t)}{T_1} + \frac{N_0}{T_1}. \end{aligned}\right\} \qquad (3.2.37)$$

The first equation in this system *is identical* to the first equation in the system (3.2.32). The second equations in these systems are slightly different due to the fact that a specific (in this case, three-level) diagram of laser levels has been considered in (3.2.32). Comparing the second equations in the systems (3.2.37) and (3.2.32), we conclude that for a *three-level* laser

$$\beta = 2; \quad T_1 = \tau/(K+1); \quad N_0 = n'(K-1)/(K+1). \qquad (3.2.38)$$

Comparing the second equation in (3.2.37) with Eq. (3.2.33), we get a similar result for a *four-level* laser:

$$\beta = 1; \quad T_1 = \tau/(K+1); \quad N_0 = n'K/(K+1). \qquad (3.2.39)$$

We shall now explain the results obtained for β and T_1. Since the lower laser level (level *1*) in a three-level diagram is also the ground level, the difference in the population densities of laser levels upon generation of photons in the channel *2-1* will decrease not only due to a decrease in the population density of the upper level, but also due to an increase in the population density of the lower levels Upon generation of one photon, the difference in population densitie.

should thus decrease by 2 (hence $\beta = 2$). In a four-level diagram the decrease in the difference in laser level population densities is due only to a decrease in the population density of the upper laser level, since the active centres from the lower laser level quickly go over to the ground level. Hence in this case $\beta = 1$.

The equation for longitudinal relaxation time T_1 can be easily understood if we rewrite it in the form

$$1/T_1 = (K + 1)/\tau = w_p + 1/\tau.$$

It is apparent from this that the total relaxation probability $1/T_1$ is composed of the pumping probability and the relaxation probability in the generation channel.

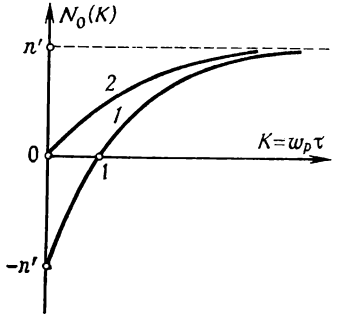


Fig. 3.10

The N_0 vs. K dependence defined by the relations (3.2.38) and (3.2.39) is graphically represented in Fig. 3.10. Curves *1* and *2* correspond to a three-level and a four-level laser respectively. The figure demonstrates the increase in pumping parameter N_0 with increasing pumping power (more precisely, with increasing value of $K = w_p\tau$).

Threshold Inverse Population Density and Generation Condition. The threshold value of the inverse population density, at which the generation process starts (we shall denote it by N_{thr}), is obviously defined by the condition

$$dM_1/dt > 0.$$

Using the first of equations (3.2.34), we get

$$N > 1/B'T, \tag{3.2.40}$$

and hence

$$N_{thr} = 1/B'T = 1/B\hbar\omega T. \tag{3.2.41}$$

Since, as we have already mentioned, $T = Q/\omega$, we can write in accordance with (3.2.41)

$$N_{thr} = 1/B\hbar Q. \tag{3.2.42}$$

The threshold value of the inverse population density is inversely proportional to the Q-factor of the resonator.

Taking into account (3.2.17) and (3.2.36), the expression (3.2.41) for the threshold value of inverse population density may also be written in the following form:

$$N_{thr} = (\eta_1 + \eta_2)/\sigma. \tag{3.2.43}$$

For generation, it is essential that the threshold value of inverse population density should not exceed the value N_0 for a given pump-

ing power. This means that the *generation condition* (*self-excitation condition*) may be written in the form

$$\boxed{N_0 > N_{\text{thr}}} \tag{3.2.44}$$

or, taking (3.2.43) into account,

$$\sigma N_0 > (\eta_1 + \eta_2). \tag{3.2.45}$$

Note that the condition (3.2.45) has been encountered earlier. In view of the condition (2.1.10), we get

$$\varkappa_0 > (\eta_1 + \eta_2)$$

(this is the condition of the initial gain $\varkappa_0$ surpassing the loss level determined by the sum of the coefficients of favourable and unfavourable losses). The inequality (3.2.45) is consistent with (2.1.10) if the initial gain $\varkappa_0$ is written, in accordance with (2.1.2), in the form[21]

$$\varkappa_0 = \sigma N_0. \tag{3.2.46}$$

For a *three-level* laser, the generation condition (3.2.45) may be written, with the help of Eqs. (3.2.38), in the form of the inequality

$$\sigma n' (K - 1)/(K + 1) > (\eta_1 + \eta_2) \tag{3.2.47}$$

or, alternatively

$$K > [\sigma n' + (\eta_1 + \eta_2)]/[\sigma n' - (n_1 + \eta_2)]. \tag{3.2.48}$$

This leads to the *threshold* value for the probability w_p (characterising the threshold pumping power):

$$w_{p\,\text{thr}} = \frac{K_{\text{thr}}}{\tau} = \frac{\sigma n' + (\eta_1 + \eta_2)}{\tau [\sigma n' - (\eta_1 + \eta_2)]}. \tag{3.2.49}$$

Using (3.2.39), we can write the generation condition (3.2.45) in a form applicable to a *four-level* laser:

$$\sigma n' K/(K + 1) > (\eta_1 + \eta_2)$$

or

$$K > (\eta_1 + \eta_2)/[\sigma n' - (\eta_1 + \eta_2)]. \tag{3.2.50}$$

The *threshold* value for the probability w_p in this case assumes the form

$$w_{p\,\text{thr}} = \frac{K_{\text{thr}}}{\tau} = \frac{\eta_1 + \eta_2}{\tau [\sigma n' - (\eta_1 + \eta_2)]}. \tag{3.2.51}$$

Comparing (3.2.49) and (3.2.51), we find that for a four-level diagram, the pumping threshold is lower than for a three-level diagram

[21] Using (3.2.38) and taking into account the nature of "two-level approximation", the expression (2.1.13) for the initial gain can be easily obtained from (3.2.46).

(subject to the condition that the parameters σ, τ, n', η_1, and η_2 have identical values in both cases).

Dimensionless Form of the Statz-De Mars Equations. The Statz-De Mars equations are often written in a form employing only *dimensionless* quantities, namely:

$$\left.\begin{aligned} &t' = t/T_1 \text{ — dimensionless time} \\ &m(t') = \beta B' T_1 M(t'T_1) \text{ — dimensionless field intensity} \\ &n(t') = N(t'T_1)/N_{\text{thr}} \text{ — ratio of the inverse population density to its threshold value } (n = B'TN) \\ &\alpha = B'TN_0 = N_0/N_{\text{thr}} \text{ — dimensionless pumping parameter} \\ &G = T_1/T \text{ — ratio of the relaxation time for the difference in population densities to the lifetime of a photon in the resonator} \end{aligned}\right\} \quad (3.2.52)$$

It can be easily seen that upon transition to dimensionless quantities, the Statz-De Mars equations (3.2.34) assume the following form:

$$\boxed{\begin{aligned} dm/dt' &= Gm(n-1); \\ dn/dt' &= \alpha - n(m+1). \end{aligned}} \quad (3.2.53)$$

Here, it must be remembered that $\frac{\partial}{\partial t} = T_1^{-1} d/dt'$.

The compactness of dimensionless notation makes it quite convenient for analysis of processes occurring in a laser. In particular, the *generation condition* (3.2.44) may be written as follows in the dimensionless form:

$$\boxed{\alpha > 1.} \quad (3.2.54)$$

Contribution of Spontaneous Emission to Field Intensity. Using the dimensionless form of notation we shall show how to take into account the contribution to the field intensity in the balance equations from the part of spontaneous emission that falls in the excited resonator mode (this corresponds to the inclusion of the term $q(z, t)\,\Delta z$ in (3.2.1)). It should be noted that in spite of its relatively small quantitative contribution, spontaneous emission may significantly influence the nature of processes occurring in a laser.

The term Gmn in the first equation in (3.2.53) takes into account the contribution of *induced processes* (induced emission and resonant

absorption). Going over to *spontaneous emission*, we must, firstly, exclude the field factor m. Secondly, the dimensionless difference n in the laser level population densities should be replaced by the dimensionless upper laser level population density (we denote it by n_u). Finally, while considering the change in the Einstein coefficient upon a transition from induced to spontaneous emission, a correction factor ε should be introduced. Thus, the required contribution from spontaneous emission may be introduced in the first of equations (3.2.53) through an additional term $G\varepsilon n_u$. Since

$$n_u \approx (n + n'')/2, \text{ where } n'' = n'/N_{\text{thr}}, \tag{3.2.55}$$

the "spontaneous term" may be written in the form $G\varepsilon\,(n + n'')$ (the factor 1/2 is taken care of in the factor ε). Taking into account the contribution due to spontaneous emission, the *balance equations* in the dimensionless form will appear as follows:

$$\left.\begin{aligned} dm/dt' &= Gm\,(n - 1) + G\varepsilon\,(n + n''); \\ dn/dt' &= \alpha - n\,(m + 1). \end{aligned}\right\} \tag{3.2.56}$$

Table 3.1 gives characteristic numerical values of parameters appearing in (3.2.56), as applied to two solid-state lasers, the ruby laser and activated Nd-laser [4].

TABLE 3.1

Type of laser	Parameters			
	α	G	ε	n''
Ruby laser	30	10^5	10^{-13}	100
Nd-laser	2	10^4	10^{-15}	1

General Remarks on the Method of Balance Equations. Balance equations, like the Statz-De Mars equations, are sometimes called *point equations*. Neglecting spatial variables, these equations essentially describe the *point model* of a laser, i.e. one in which the entire space occupied by the active medium may be reduced to a single point. Changes in space are not taken into account here, only the time variations are considered. This considerably restricts the potentialities of this method. Thus, for example, the balance equations are unsuitable for considering spatially inhomogeneous active media; they do not permit a consideration of spatial inhomogeneity of inverse population density and a number of other spatial effects.

It should be emphasised that in the balance equation method, we do not consider the amplitude or phase of the field, but just its *intensity*. Hence in the generated radiation we do not consider *phase relations* and interference effects connected with them. Thus the

balance equations are not suitable for calculating spectral or angular properties of radiation, nor for analysing coherent nonlinear optical phenomena.

In spite of this, the balance equation method is found to be quite useful for studying the dynamics of lasers. It is found that such a simplified approach leads to a fairly correct analysis of a number of questions connected with the *time* variation of parameters of a *single-mode* laser and its radiation. In particular, the balance equation method reveals the main features of the dynamics of free generation and giant pulse generation processes, including processes in lasers with a bleachable filter. Balance equations are also used for a study of *multimode* lasers [4, 71, 72].

Confining ourselves to the above qualitative remarks, we observe that a fairly rigorous analysis of the *conditions of applicability* of balance equations is given in [4, 73, 74]. These conditions for a single-mode laser include, in particular, the requirement that the transverse relaxation time T_2 (relaxation time of polarisation of the medium) be small in comparison to the longitudinal relaxation time T_1, as well as to the life time T of a photon in the resonator:

$$T_2 \ll T_1; \quad T_2 \ll T. \tag{3.2.57}$$

In solid state lasers, the inequalities (3.2.57) are always satisfied. The following values of time are characteristic for such lasers: $T_1 \sim 10^{-3}$-10^{-4} sec, $T \sim 10^{-8}$ sec, $T_2 \sim 10^{-12}$ sec.

Laser as a Distributed Self-Oscillating System. A more rigorous approach to laser dynamics, taking into account the development of processes not only *in time* but also *in space*, is based on the use of *Maxwell's equations* for describing radiation and of *quantum mechanical equations* for describing matter (the so-called *semiclassical* theory; see, for example, [1, 4, 75]). Within the framework of such an approach, it is possible to fill the "gaps" in the method of balance equations, i.e. to take into account phase relations and to consider interference effects in the resonator of a multimode laser. Semiclassical approach helps in the analysis of dynamics of multimode, especially two-mode, lasers [17, 75-77].

It is advisable to demonstrate, at least roughly, the semiclassical approach to the dynamics of a multimode laser. The laser may be treated as a self-oscillating system with a distributed negative resistance (see [75], as well as [78, 79]). Let us restrict the consideration to a one-dimensional case, assuming that the radiation propagates strictly along the resonator axis (along the z-axis), and that variation in the field in a direction perpendicular to the axis may be neglected. In this case, the *wave equation* for the component of the electric field vector has the following form for an empty resonator without losses:

$$\frac{\partial^2 E}{\partial z^2} - \frac{1}{c^2}\frac{\partial^2 E}{\partial t^2} = 0. \tag{3.2.58}$$

We express $E(z, t)$ as a sum of longitudinal modes:

$$E(z, t) = \sum_n A_n(t) \sin(k_n z), \tag{3.2.59}$$

where $k_n = n\pi/L$, L being the length of the resonator. The relation (3.2.59) takes into account the boundary conditions $E(0, t) = E(L, t) = 0$. Substituting (3.2.59) in (3.2.58), we get

$$d^2A_n/dt^2 + \Omega_n^2 A_n = 0, \tag{3.2.60}$$

where $\Omega_n = n\pi c/L$.

While considering *losses* in a resonator, we must include the term $\frac{dA_n}{dt}\omega_0/Q_n$, ($Q_n$ is the Q-factor of the n-th mode) in the left-hand mode of Eq. (3.2.60). In the case of an *active* resonator, yet another term appears in Eq. (3.2.60). This term is expressed in terms of electric polarisation $P(z, t)$, which *supplies* the field distributed along the z-axis. This term has the form [78]

$$4\pi \frac{d^2P_n}{dt^2}, \text{ where } P_n(t) = \frac{2}{L}\int_0^L P(z, t) \sin(k_n, z)\, dz.$$

Thus, Eq. (3.2.60) should be replaced by the following equation, describing the n-th longitudinal mode in an active resonator with losses:

$$\frac{d^2A_n}{dt^2} + \frac{\omega_0}{Q_n}\frac{dA_n}{dt} + \Omega_n^2 A_n + 4\pi \frac{d^2P_n}{dt^2} = 0. \tag{3.2.61}$$

The functions $A_n(t)$ and $P_n(t)$ are expressed in the form

$$A_n(t) = E_n(t) \cos[\omega_n t + \varphi_n(t)]; \tag{3.2.62a}$$

$$P_n(t) = C_n(t) \cos[\omega_n t + \varphi_n(t)] + S_n(t) \sin[\omega_n t + \varphi_n(t)], \tag{3.2.62b}$$

where $E_n(t)$ and $\varphi_n(t)$ are the amplitude and phase of the n-th mode, varying slowly over a period $2\pi/\omega_0$. The functions $C_n(t)$ and $S_n(t)$ are also assumed to be slowly varying. The relations (3.2.62) are substituted in (3.2.61) and terms with second order derivatives of slowly varying functions are neglected. The coefficients of $\cos[\omega_n t + \varphi_n(t)]$ and $\sin[\omega_n t + \varphi_n(t)]$ are then put equal to zero separately, and terms containing $\frac{\omega_0}{Q_n}\frac{dE_n}{dt}$, $\frac{dE_n}{dt}\frac{d\varphi_n}{dt}$, $E_n\frac{\omega_0}{Q_n}\frac{d\varphi_n}{dt}$ are neglected. Considering that $\omega_n + \frac{d\varphi_n}{dt}$ may be taken as equal to Ω_n, we finally get the following equations for the amplitude and phase of the n-th mode:

$$\left.\begin{aligned} \frac{dE_n}{dt} + \frac{1}{2}\frac{\omega_0}{Q_n}E_n &= -2\pi\omega_0 S_n; \\ \left(\frac{d\varphi_n}{dt} + \omega_n - \Omega_n\right)E_n &= -2\pi\omega_0 C_n. \end{aligned}\right\} \tag{3.2.63}$$

These equations are called *reduced equations* or *self-consistent equations.*

In the next step, we express the polarisation (more precisely, the functions C_n and S_n) in terms of mode amplitudes. For this purpose, we employ a quantum mechanical description of the material of the active element with the help of *density matrix*[22]. For relatively small field intensities in the resonator (close to self-excitation threshold), the dependence of C_n and S_n on the mode amplitude may be written in the form [78]

$$-2\pi\omega_0 S_n = \alpha_{0n}E_n - \beta_n E_n^3 - \sum_{m\neq n} \theta_{nm}E_n E_m^2, \qquad (3.2.64a)$$

$$-2\pi\omega_0 C_n = \sigma_n E_n + \rho_n E_n^3 + \sum_{m\neq n} \tau_{nm}E_n E_m^2, \qquad (3.2.64b)$$

where α_{0n}, β_n, σ_n, ρ_n, θ_{nm}, and τ_{nm} are coefficients depending on Ω_n, the degree of inverse population of levels, relaxation time for upper and lower laser levels, and the absorption line width. The physical significance of these coefficients, whose numerical values have been calculated in [75] for a gas laser, has been discussed in [78]. Taking Eqs. (3.2.64) into consideration, the reduced equations (3.2.63) assume the form

$$\left.\begin{aligned} \frac{dE_n}{dt} &= \left(\alpha_{0n} - \frac{\omega_0}{2Q_n}\right) E_n - \beta_n E_n^3 - \sum_{m\neq n} \theta_{nm}E_n E_m^2; \\ \frac{d\varphi_n}{dt} + \omega_n &= \Omega_n + \sigma_n + \rho_n E_n^2 + \sum_{m\neq n} \tau_{nm}E_m^2. \end{aligned}\right\} \qquad (3.2.65)$$

It can be easily seen that the coefficient α_{0n} is the amplification factor for the n-th mode. The condition for self-excitation of the n-th mode has the form $\alpha_{0n} > \omega_0/2Q_n$. The coefficients θ_{nm} and τ_{nm} play the role of coupling factors, describing the interaction of modes.

3.3. FREE GENERATION. REGULAR DAMPED PULSATIONS OF RADIATION POWER

Pregeneration Stage. For the sake of simplicity, we shall consider a pumping pulse of rectangular shape, the duration of the pulse is t_p, the moment $t = 0$ corresponds to the switching on of the pumping pulse. We denote by t_{thr} the time from the moment of pulse switching to the moment when generation begins. During the passage of this time, an accumulation of active centres takes place at the upper laser level, until the inverse population density increases to the threshold value $N_{thr} = (\eta_1 + \eta_2)/\sigma$.

[22] The density matrix is described in [80]. The application of a density matrix for describing interaction of radiation with the active medium has been described in [75, 79].

At the *pregeneration stage*, we should put $S = 0$ ($M = 0$) in the *balance equations*. Considering a three-level laser, we get from (3.2.32)

$$dN/dt = [n'(K-1) - N(t)(K+1)]/\tau. \qquad (3.3.1)$$

For a rectangular pumping pulse, the quantity K may be considered as a constant (during pumping). Using this, we can easily get a solution of Eq. (3.3.1) in the following form:

$$N(t)/n' = 2K(K+1)^{-1}\{1 - \exp[-(K+1)\,t/\tau]\} - 1. \qquad (3.3.2)$$

For $t = 0$, we have $N = -n'$. As $t \to \infty$, $N(t)$ asymptotically tends to the value $N_0 = n'(K-1)/(K+1)$ (Fig. 3.11). It follows from

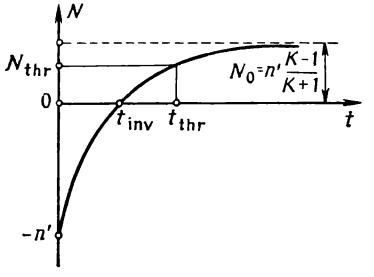


Fig. 3.11

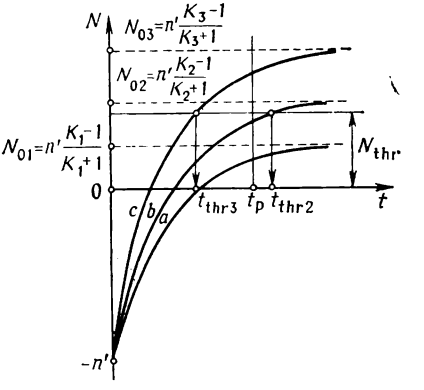


Fig. 3.12

Eq. (3.3.2) that the time t_{inv}, when the function $N(t)$ passes through zero (see the figure) is equal to

$$t_{inv} = \tau(K+1)^{-1} \ln[2K/(K-1)]. \qquad (3.3.3)$$

Generation begins as soon as the function $N(t)$ attains the value N_{thr}. Consequently,

$$t_{thr} = \frac{\tau}{K+1} \ln\left[\frac{2K}{K+1}\left(\frac{n'}{N_0 - N_{thr}}\right)\right]. \qquad (3.3.4)$$

From Fig. 3.11 it is obvious that the necessary condition for generation is given by $N_0 > N_{thr}$. This condition has been discussed in Sec. 3.2, where it was shown that we can write it in the form (3.2.48). It follows from this that the pumping power must be higher than the threshold value given by the right-hand side of the inequality.

Figure 3.12 shows the curve N vs. t for three different situations corresponding to *different pumping power*: (a) the pumping power is lower than the threshold level ($K_1 < K_{thr}$), (b) the pumping power

is just slightly higher than the threshold value ($K_2 \geqslant K_{\text{thr}}$), and (c) the pumping power is sufficiently high ($K_3 > K_{\text{thr}}$). The horizontal dashed lines correspond to different values of the pumping parameter N_0. The solid horizontal line corresponds to the value N_{thr}. It can be easily seen that N_0 increases with increasing pumping power. Generation becomes possible for $N_0 > N_{\text{thr}}$. With increasing value of K, the time t_{thr} decreases. Taking into consideration the fact that although generation is possible in case (b), it does not occur since $t_{\text{thr}\,2} > t_{\text{p}}$ (the pumping pulse terminates before the threshold value of the inverse population density is attained).

It should be noted that in the limit $K \gg 1$, we may take $N_0 \approx n'$. In this case, Eq. (3.3.4) gives

$$t_{\text{thr}} = \frac{1}{\omega_{\text{p}}} \ln \frac{2n'\sigma}{n'\sigma - (\eta_1 + \eta_2)}. \tag{3.3.5}$$

Transition Rrocesses Accompanying Generation (Regular Damped Pulsations of Radiation Power). *Generation* is accompanied by *transition processes* leading to *regular damped* pulsations of generated radiation power. An analysis of these pulsations has been carried out by several authors [1, 2, 4, 73, 81-86].

Let us turn to the system of *balance equations* (3.2.32). With the help of (3.2.43), this system can be written in the form

$$\left.\begin{aligned} \frac{dS}{dt} &= v\sigma\,[N(t) - N_{\text{thr}}]\,S(t); \\ \frac{dN}{dt} &= -\frac{2\sigma}{\hbar\omega}\,S(t)\,\dot{N}(t) - \frac{N(t)}{\tau}(K+1) + \frac{n'}{\tau}(K-1). \end{aligned}\right\} \tag{3.3.6}$$

Let us consider the system (3.3.6) *in the vicinity of stationary* values S_{st} and N_{st}. For this purpose, we write

$$S(t) = S_{\text{st}} + \Delta S(t); \quad N(t) = N_{\text{st}} + \Delta N(t) \tag{3.3.7}$$

and assume that

$$\Delta S(t) \ll S_{\text{st}}; \quad \Delta N(t) \ll N_{\text{st}}. \tag{3.3.8}$$

The values S_{st} and N_{st} are obtained by putting $dS/dt = 0$ and $dN/dt = 0$ in (3.3.6):

$$N_{\text{st}} = N_{\text{thr}}; \quad S_{\text{st}} = \frac{\hbar\omega}{2N_{\text{thr}}\sigma}\left[\frac{n'}{\tau}(K-1) - \frac{N_{\text{thr}}}{\tau}(K+1)\right]. \tag{3.3.9}$$

Substituting (3.3.7) into (3.3.6) and using (3.3.9), we get

$$\left.\begin{aligned} \frac{d}{dt}\Delta S &= v\sigma S_{\text{st}}\Delta N + v\sigma\Delta S\Delta N; \\ \frac{d}{dt}\Delta N &= -\frac{2\sigma}{\hbar\omega}(N_{\text{st}}\Delta S + S_{\text{st}}\Delta N) - \frac{\Delta N}{\tau}(K+1) \\ &\quad - \frac{2\sigma}{\hbar\omega}\Delta S\,\Delta N. \end{aligned}\right\} \tag{3.3.10}$$

Taking (3.3.8) into account, we neglect terms with $\Delta S \Delta N$. Consequently, the system of equations is *linearised*, i.e. is converted from a *nonlinear* to *linear* system (in ΔS and ΔN):

$$\left.\begin{aligned} \frac{d}{dt}\Delta S &= v\sigma S_{st}\,\Delta N; \\ \frac{d}{dt}\Delta N &= -\frac{2\sigma}{\hbar\omega}(N_{st}\,\Delta S + S_{st}\,\Delta N) - \frac{\Delta N}{\tau}(K+1). \end{aligned}\right\} \quad (3.3.11)$$

Eliminating ΔN from (3.3.11), we get the following differential equation in $\Delta S\ (t)$:

$$\frac{d^2}{dt^2}\Delta S + \left(\frac{2\sigma}{\hbar\omega}S_{st} + \frac{K+1}{\tau}\right)\frac{d}{dt}\Delta S + 2\frac{v\sigma^2}{\hbar\omega}S_{st}N_{st}\,\Delta S = 0. \quad (3.3.12)$$

Substituting (3.3.9) in this equation, taking (3.2.38) into consideration, and using the relation

$$v\sigma = (TN_{thr})^{-1}, \quad (3.3.13)$$

which follows from (3.2.17) and (3.2.41), we finally get

$$\frac{d^2}{dt^2}\Delta S + \frac{N_0}{N_{thr}T_1}\frac{d}{dt}\Delta S + \frac{1}{TT_1}\left(\frac{N_0}{N_{thr}} - 1\right)\Delta S = 0. \quad (3.3.14)$$

The solution of Eq. (3.3.14) is sought in the form

$$\Delta S\ (t) = C \exp\ (pt). \quad (3.3.15)$$

Substituting (3.3.15) in (3.3.14), we get the following equation in the parameter p (*characteristic equation*):

$$p^2 + \frac{N_0}{N_{thr}T_1}p + \frac{1}{TT_1}\left(\frac{N_0}{N_{thr}} - 1\right) = 0. \quad (3.3.16)$$

The roots of this equation are

$$p_{1,2} = -(N_0/2N_{thr}T_1) \pm \sqrt{D}/2, \quad (3.3.17)$$

where

$$D = (N_0/N_{thr}T_1)^2 - 4\,[(N_0/N_{thr}) - 1]/TT_1.$$

Let us assume that the inequality

$$D < 0 \quad (3.3.18)$$

is satisfied. This is possible if

$$4\,(T_1/T)\,[(N_0/N_{thr}) - 1] > (N_0/N_{thr})^2 \quad (3.3.19)$$

or (if we go over to parameters G and α introduced in Sec. 3.2),

$$4G\,(\alpha - 1) > \alpha^2. \quad (3.3.20)$$

The data given in Table 3.1 show that the inequality (3.3.20), and hence (3.3.18), must be satisfied conservatively.

If the inequality (3.3.18) is satisfied, the roots of the characteristic equation are found to be *complex*. In this case the solution of Eq.

(3.3.14) may be written in the following form if we take (3.3.17) into consideration:

$$\Delta S = \exp(-N_0 t/2N_{\text{thr}}T_1)\,[C\exp(i\sqrt{|D|}\,t/2) + C^*\exp(-i\sqrt{|D|}\,t/2)]. \tag{3.3.21}$$

It can be easily seen that the expression (3.3.21) describes *regular damped* pulsations with pulse repetition frequency

$$\Omega = \frac{\sqrt{|D|}}{2} = \frac{N_0}{2N_{\text{thr}}T_1}\left[4\frac{T_1}{T}\left(\frac{N_{\text{thr}}}{N_0}\right)^2 \times \left(\frac{N_0}{N_{\text{thr}}} - 1\right) - 1\right]^{1/2}. \tag{3.3.22}$$

The pulse amplitude decreases exponentially with a time constant given by

$$t_{\text{damp}} = 2T_1 N_{\text{thr}}/N_0. \tag{3.3.23}$$

Figure 3.13 shows the regular damped pulses described by Eq. (3.3.21). The moment $t = 0$ in the figure corresponds to the beginning of generation.[23]

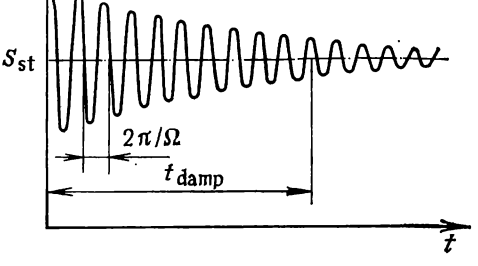


Fig. 3.13

Using the dimensionless parameters G and α, we can rewrite the relations (3.3.22) and (3.3.23) in the form (assuming $G \gg 1$)

$$\Omega = (\alpha/2T_1)\sqrt{4G(\alpha-1)/\alpha^2 - 1} \approx \sqrt{G(\alpha-1)}/T_1; \tag{3.3.24}$$

$$t_{\text{damp}} = 2T_1/\alpha. \tag{3.3.25}$$

For a ruby laser, for example, $\alpha = 30$, $G = 10^5$, $T_1 \approx 10^{-3}$ sec. Consequently, $\Omega \approx 10^6$ sec^{-1}, $t_{\text{damp}} \approx 10^{-4}$ sec.

The above discussion is based on the relations (3.3.8). However, in the initial stages of growth of generation, these inequalities are

[23] We assume that $t_{\text{damp}} \ll t_p$, hence the pulses are damped before the termination of pumping pulse.

not satisfied, hence pulses corresponding to transition processes should be considered, strictly speaking, not on the basis of the *linear* system of equations (3.3.11), but rather on the basis of the *nonlinear* system (3.3.10). Figure 3.14 shows a characteristic curve obtained on the basis of a rigorous calculation of damped pulses in a ruby laser with the help of a computer. It can be easily seen that the real picture of pulses at the initial stage of their growth is considerably different from the picture shown in Fig. 3.13.

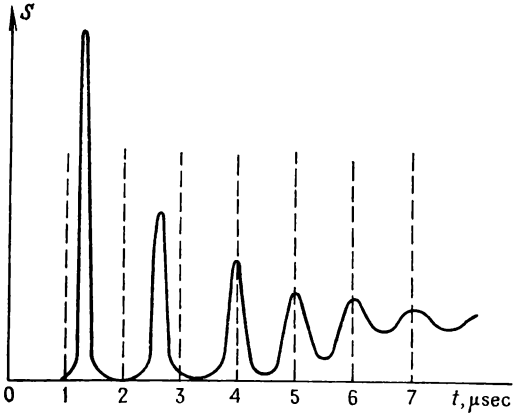


Fig. 3.14

Taking into consideration the above remarks, we shall carry out a more rigorous analysis of regular damped pulsations in a solid-state laser. For this purpose, we shall be using the Statz-De Mars equations in the dimensionless form (i.e. Eq. (3.2.53))[24].

Phase Portrait of a Free-running Solid-state Laser. In accordance with Eqs. (3.2.53), a laser as a dynamic system is described by two functions of time n (t') and m (t'). We define the *plane of laser states* (i.e. the *phase plane*) as the plane in which parameters n and m serve as Cartesian coordinates. At any moment of time, the state of a laser is "represented" by a certain point on the phase plane (*representative point*). With the passage of time, a representative point describes on the phase plane a certain curve called the *phase trajectory*. The family of possible phase trajectories is called the *phase-plane* portrait of the given dynamic system.

[24] Of course, we could have considered the damped pulsations on the basis of the Statz-De Mars equations in dimensionless form from the very beginning. However, we thought that the correct procedure would be to start the analysis not on the basis of the system of equations (3.2.53), but the system (3.2.32) which must appear to an inexperienced reader as more specific and more descriptive from a physical point of view.

If a laser is described in Eqs. (3.2.53), its phase trajectories may be found from the equation

$$\boxed{\frac{dm}{dn} = G\,\frac{m\,(n-1)}{\alpha-(m+1)\,n}}, \qquad (3.3.26)$$

which is obtained by dividing the first of Eqs. (3.2.53) by the second. One of such phase trajectories is shown in Fig. 3.15. It gives an idea about the phase portrait of the laser described by the Statz-De Mars balance equations.

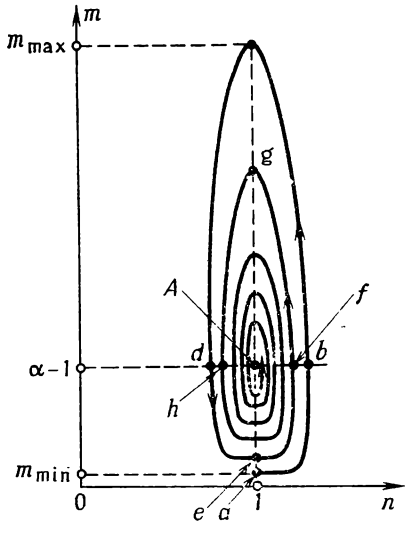


Fig. 3.15

For the case considered in Fig. 3.15, the representative point moves along a *spiral* winding up at the point A whose coordinates are given by

$$n_A = 1; \quad m_A = \alpha - 1. \qquad (3.3.27)$$

The point A "represents" the state of the laser corresponding to *stationary generation*. This can be easily confirmed by putting $dm/dt' = 0$ and $dn/dt' = 0$ in (3.2.53)[25].

The spiral shown in the figure starts at the point a with coordinates

$$n_a = 1; \quad m_a = m_{min}. \qquad (3.3.28)$$

The point a is the state at which the threshold of inverse population density is attained for the first time (after beginning of the pumping), and hence this point corresponds to the moment when generation starts. The intensity of the field m_{min} at this moment is determined by spontaneous transitions. It should be remembered that $m_{min} \ll 1$.

At this moment of time, the generation of the first spike begins. As the representative point moves from a to c along the phase trajectory, the spike power increases, attaining its maximum value at the point c (coordinates of the point are given by $n_c = 1$, $m_c = m_{max}$). The power of the first spike decreases beyond this point, falling to a value slightly higher than m_{min} (point e in the figure) at which stage the generation of the second spike begins. To each spike in the laser radiation there corresponds one loop in the spiral. The fact that the spiral approaches the point A with each winding

[25] The relations (3.3.27) are the dimensionless form of relations (3.3.9) (subject to the condition that $N_0 = n'\,(K-1)/\,(K+1)$).

means that a gradual damping takes place in the pulses of radiation field intensity as well as of inverse population density.

The phase portrait of a laser shown in Fig. 3.15 is "unfolded" in time in Fig. 3.16 where the functions m and n are plotted against time t' ($t' = t/T_1$). The point $t' = 0$ corresponds to the moment when generation begins, the dashed lines indicate the pregeneration state of these curves.[26] The interval of time t'_0 corresponds to the initial stage of generation of the first spike (*linear* growth of generation), the interval t'_1 describes the effective duration of the spike,

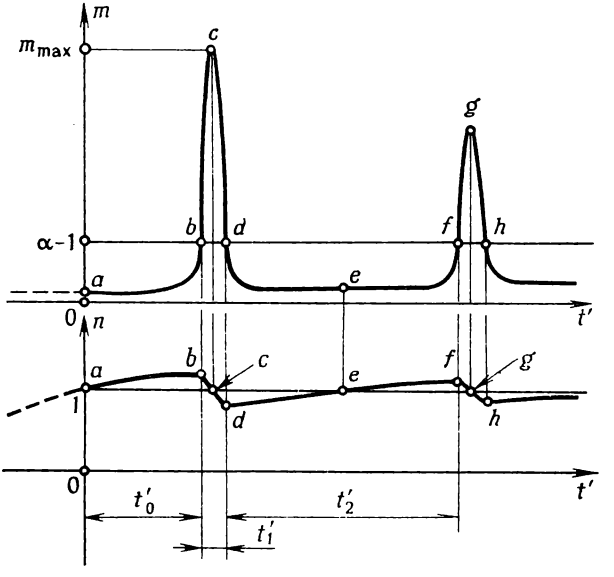


Fig. 3.16

and t'_2 is the effective time interval between two successive spikes. The figure clearly demonstrates a certain synchronism between the pulsations of inverse population density and those of radiation field intensity. It also shows that the velocity of the representative point along the phase trajectory in Fig. 3.15 is not constant: the lower parts of the spiral (for example the section *a-b* or *d-f*) are covered by the representative point much more slowly than the upper parts (for example the sections *b-d* or *f-h*). It is apparent from Fig. 3.16 that $(t'_2 \approx 2t'_0) \gg t'_1$. The farther from the abscissa axis the representative point is on the phase plane, the higher its velocity.

Let us introduce the notation $\nu = n - n_A = n - 1$. For free generation, the magnitude of ν is much smaller than unity ($\nu_{max} \approx$

[26] The nature of inverse population density in the pregeneration stage has been discussed earlier; see Fig. 3.12.

≈ 0.1). Other numerical data characterising free generation in two types of solid-state lasers are given in Table 3.2 [4].

TABLE 3.2

Type of laser	Parameters				
	T_1, sec	t'_1	$t'_2 \approx 2t'_0$	m_{max}	m_{min}
Ruby laser	2×10^{-3}	7×10^{-4}	8×10^{-3}	700	10^{-9}
Nd-laser	2×10^{-4}	2.5×10^{-3}	0.16	30	3×10^{-13}

Structure of Phase Portrait of a Laser. *Characteristic points* in the phase portrait structure for a free-running laser may be revealed without solving Eq. (3.3.26). For this, it is necessary to first *examine the behaviour of phase trajectories near a singular point* corresponding to stationary generation (point A in Fig. 3.15). More specifically, the system of balance equations must be linearised in the vicinity of the singular point, and *the type of the singular point must be revealed* by considering the roots of the characteristic equation obtained as a result of this linearisation [87]. This plan of action is discussed in Appendix 5 where six different types of singular points have been considered.

Linearisation of the system of equations (3.2.53) in the vicinity of the singular point (3.3.27) leads to the following system of equations

$$\left.\begin{aligned} d\mu/dt' &= G(\alpha-1)\nu; \\ d\nu/dt' &= -\alpha\nu-\mu. \end{aligned}\right\} \qquad (3.3.29)^{27}$$

Here, $\mu(t') = m(t') - m_A = m - (\alpha - 1)$, $\nu(t') = n(t') - n_A = n - 1$, and $\mu \ll m_A$, $\nu \ll n_A$. The characteristic equation corresponding to the system (3.3.29) has the form

$$p^2 + \alpha p + G(\alpha - 1) = 0. \qquad (3.3.30)$$

The roots of this equation are given by (cf. (3.3.17))

$$p_{1,2} = -\frac{\alpha}{2} \pm \frac{1}{2}\sqrt{\alpha^2 - 4G(\alpha - 1)}. \qquad (3.3.31)$$

Since, as mentioned above, the inequality

$$4G(\alpha - 1) \gg \alpha^2 \qquad (3.3.32)$$

is valid, we get

$$p_{1,2} = -\frac{\alpha}{2} \pm i\sqrt{G(\alpha-1)}. \qquad (3.3.33)$$

[27] This system of equations corresponds to the system (3.3.11) represented in the dimensionless form.

The characteristic equation in this case has *complex roots with a negative real part.* This means (see Appendix 5) that we have a singular point of *stable focus* type. The nature of phase trajectories in the vicinity of such a singular point is shown in Fig. A.5.1*d* in Appendix 5 (cf. Fig. 3.15).

Thus, we have determined the nature of phase trajectories *in the vicinity of a singular point* with coordinates $n_A = 1$, $m_A = \alpha - 1$. Further, a number of additional conclusions may be drawn about the structure of a phase portrait, starting with the form of Eq. (3.3.26):

(a) the straight line $m = 0$ (i.e. the abscissa axis in the phase plane) is one of the possible phase trajectories;

(b) since $G \gg 1$, the inclination of phase trajectories must be high ($dm/dn \gg 1$) all over the phase plane except regions adjoining the straight lines $n = 1$ and $m = 0$;

(c) at all points on the straight line $n = 1$, the tangent to the phase trajectory must be horizontal ($dm/dn = 0$).

Summing up all these remarks, we can easily arrive at the structure of the phase portrait shown in Fig. 3.15. For this, it is necessary simply to use the additional information that the following inequalities are valid for free generation:

$$(n - 1) < 0.1; \quad m_{max} \gg (\alpha - 1). \tag{3.3.34}$$

Analysis of Pulse Diagram on the Basis of Balance Equations. Considering the *stage of linear growth of generation of the first spike* (corresponding to the region *a-b* of the phase trajectory in Fig. 3.15), we take into account the fact that $m < (\alpha - 1)$, and hence neglect the quantity m in the right-hand side of the second equation (3.2.53). Consequently, we get the following system of balance equations

$$\left.\begin{aligned} dm/dt' &= Gm\,(n-1); \\ dn/dt' &= \alpha - n. \end{aligned}\right\} \tag{3.3.35}$$

Assuming that the moment $t' = 0$ corresponds to the beginning of generation ($n\,(0) = 1$, $m\,(0) = m_{min}$), we get, after integrating the second equation in (3.3.35),

$$n\,(t') = \alpha - (\alpha - 1)\exp(-t'). \tag{3.3.36}$$

The magnitude of t' changes from 0 to t'_0 (t'_0 is the duration of the generation stage under consideration; see Fig. 3.16). Since $t'_0 = 0.01\text{-}0.1$ (see Table 3.2), we may put $\exp(-t') = 1 - t'$, and hence rewrite (3.3.36) in the form

$$v\,(t') = n\,(t') - 1 = (\alpha - 1)\,t'. \tag{3.3.37}$$

Thus, in the region *a-b* of the phase trajectory the inverse population density increases *linearly* with time. Hence the growth of generation corresponding to this part of the phase trajectory is called the *linear* stage.

Taking into account Eq. (3.3.37), we can rewrite the first of Eqs. (3.3.35) in the form $dm/dt' = G(\alpha - 1)\, mt'$. Integrating this equation between 0 to t', we get

$$\ln (m(t')/m_{\min}) = {}^1/_2 G(\alpha - 1)(t')^2. \tag{3.3.38}$$

Eliminating the time from Eqs. (3.3.37) and (3.3.38), we get

$$\nu(t') = [(2(\alpha - 1)/G) \ln (m(t')/m_{\min})]^{1/2}. \tag{3.3.39}$$

Substituting $m = \alpha - 1$ in (3.3.39), we get an estimate for ν_{max}

$$\nu_{max} = [(2(\alpha - 1)/G) \ln ((\alpha - 1)/m_{\min})]^{1/2}. \tag{3.3.40}$$

Substituting $\nu = \nu_{max}$ in (3.3.37), we get an estimate for t_0':

$$t_0' = \nu_{max}/(\alpha - 1). \tag{3.3.41}$$

In order to use these relations, we must know the parameter $m_{\min}$ in addition to the parameters G and α. For estimating $m_{\min}$, we must use the system of equations (3.2.56), which considers the contribution of *spontaneous emission* to the field intensity (the quantity m in the second equation of this system may be neglected). The approximate expression for $m_{\min}$ has the form [4]

$$m_{\min} \approx (1 + n'')\varepsilon \sqrt{\frac{G}{\alpha - 1}}. \tag{3.3.42}$$

It should be noted that although the magnitude of $m_{\min}$ is quite small (see Table 3.2) it is very important to take this quantity into account while considering generation. We suppose that there are no spontaneous transitions (nor any fluctuations), so that $m_{\min} = 0$. In this case, the representative point will be moving *all the time* along the phase trajectory coinciding with the abscissa axis, i.e. with straight line $m = 0$. Spontaneous transitions are necessary in order to ensure a non-zero $m_{\min}$, even though it is very small. Thus the representative point is pushed from the trajectory $m = 0$ to one of the phase trajectories which shift upwards in the phase plane with increasing n. Hence spontaneous transitions are of great importance, since they *qualitatively* change the manner in which the representative point moves on the phase plane.

Next, let us consider the generation stage corresponding to the region *b-c* of the phase trajectory in Fig. 3.15. Using the variable $\nu = n - 1$ and considering that $\nu \ll 1$, we can rewrite the initial system (3.2.53) of balance equations in the form

$$\left.\begin{aligned} dm/dt' &= Gm\nu; \\ d\nu/dt' &= \alpha - (m + 1). \end{aligned}\right\} \tag{3.3.43}$$

From this, it follows that

$$dm/d\nu = Gm\nu/[\alpha - (m + 1)]$$

and hence

$$\int_{\alpha-1}^{m_{max}} \frac{\alpha-(m+1)}{m}\,dm = G\int_{v_{max}}^{0} v\,dv \qquad (3.3.44)$$

(integration is carried out over the section *b-c* of the phase trajectory). Considering that $m_{max} \gg (\alpha - 1)$, we get from (3.3.44),

$$m_{max} \approx Gv_{max}^2/2. \qquad (3.3.45)$$

This result may be written in the following form if we take into account Eq. (3.3.40):

$$m_{max} \approx (\alpha - 1)\ln[(\alpha - 1)/m_{min}]. \qquad (3.3.46)$$

Using the second equation in (3.3.43), we can get an estimate for time t_1' characterising the duration of the generation stage corresponding to the region *b-d* of the phase trajectory (in other words, the *effective duration of the spike*):

$$t_1' \approx (2/Gv_{max})\ln[2Gv_{max}^2/(\alpha - 1)]. \qquad (3.3.47)$$

Free Generation in a Multimode Laser. Some Remarks. It was mentioned in Sec. 3.1 that in addition to *regular damped* power pulsations, *irregular* and *undamped* pulsations are also observed. The irregularity of pulses may be due, in particular, to *multimode* laser radiation[28].

It was shown above that the generation of the first spike has a relatively long initial stage of linear growth. The duration t_0' of this stage is considerably longer than the duration t_1' of the spike itself (see Table 3.2). Further, it should be noted that the threshold values of inverse population density (the value $(\eta_1 + \eta_2)/\sigma$), and hence the parameters α and m_{min}, are different for different modes. This means that the first spike generation will start at different instants of time for different modes, and the durations of the stages of linear growth of generation will also be different for different modes. Consequently the generation of different modes may start at different instants of time, and the spike of one mode may radiate before the termination of the linear growth stage of another mode. In the latter case, the emission of the spike of the first mode will violate the conditions for the growth of the spike of the second mode, since the emission process inevitably affects the inverse population density. All this may lead to *irregularities* in the observed picture of power pulses.

[28] Free generation in a multimode laser has been discussed, for example, in [4, 11, 18-20, 88].

3.4. UNSTABLE RESONATOR LASER. UNDAMPED PULSATIONS OF RADIATION POWER

By an *unstable resonator* we mean a resonator whose Q-factor is subjected to a *weak modulation* either deliberately (for example, with the help of acoustooptic or electrooptical cells), or inadvertantly (due to various technical factors, which, as a rule, appear under actual working conditions of a laser). Significantly, even a slight instability in resonator parameters may considerably affect the laser action.

Balance Equations for a Laser with a Periodically Varying Q-factor of the Resontator.[29] Let us suppose that the Q-factor of a resonator varies *periodically* with a certain frequency ω_M:

$$Q(t) = Q_0 (1 - \beta \cos \omega_M t), \tag{3.4.1}$$

the depth of Q-switching is assumed to be fairly small (*weak* Q-switching):

$$\beta \ll 1. \tag{3.4.2}$$

We can rewrite the first of the Statz-De Mars equations (3.2.34) in the following form with the help of (3.4.1):

$$dM/dt = B'MN - M\omega/Q_0 (1 - \beta \cos \omega_M t)$$

or, with the help of (3.4.2), in the form

$$dM/dt = B'MN - (M/T_0)(1 + \beta \cos \omega_M t), \tag{3.4.3}$$

where $T_0 = Q_0/\omega$. Going over to the dimensionless form of notation, we can transform Eq. (3.4.3), in accordance with (3.2.52), into the form

$$dm/dt' = GMn - Gm (1 + \beta \cos \omega'_M t'), \tag{3.4.4}$$

where $\omega'_M = \omega_M T_1$; $G = T_1/T_0$.

Thus, for a *weak periodic* Q-switching of the resonator, the system of *balance equations* (written in the dimensionless form) may be expressed in the form

$$\boxed{\begin{aligned} dm/dt' &= Gm (n - 1 - \beta \cos \omega'_M t'); \\ dn/dt' &= \alpha - n (m + 1) \end{aligned}}. \tag{3.4.5}$$

This system of equations does not have stationary solutions, since it contains time in an explicit form (term $-Gm\beta \cos \omega'_M t'$ in the first equation of the system). The nature of processes described by Eqs. (3.4.5) depends to a large extent on the magnitude of the modulation parameter β, as well as on the ratio ω'_M/Ω', where

$$\Omega' = \sqrt{G(\alpha - 1)} \tag{3.4.6}$$

[29] A single-mode laser with periodically varying Q-factor of the resonator has been discussed, for example, in [9, 10, 17, 21, 89-91].

is the frequency of damped pulsations for $\beta = 0$, expressed in the dimensionless form (see (3.3.24) as well as (3.3.33)). The parameter Ω' is called the *eigenfrequency* of relaxation oscillations of the laser about the equilibrium position.

We assume that the pumping is weak ($\alpha \gg 1$) and that the laser is above the generation threshold for just a part of the modulation period ($\beta > (\alpha - 1)$). We also assume that $\omega'_M \ll \Omega'$ (low-frequency Q-switching). The dependence m vs. t', calculated under these conditions with the help of Eq. (3.4.5), is shown in Fig. 3.17 [21]. Specifically, $\alpha = 1.01$; $\beta = 0.1$, $\omega'_M = 0.45$; $\Omega' = 4.5$; and $G = 2 \times 10^3$. It can be seen from the figure that radiation appears in the form of a *train of damped* spikes. The repetition frequency of these spike-

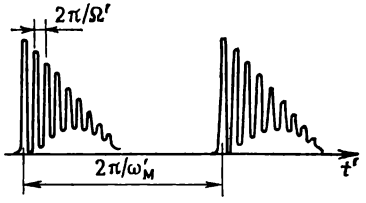


Fig. 3.17

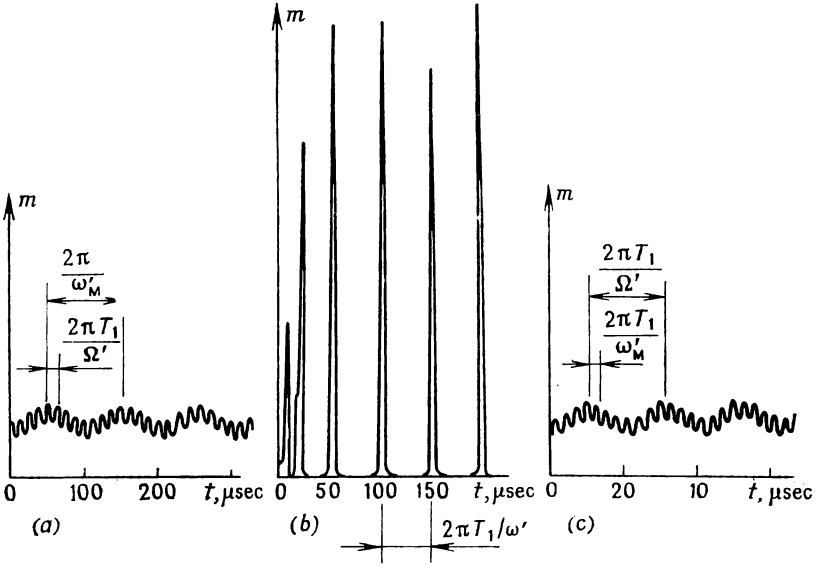


Fig. 3.18

trains is the modulation frequency. The beginning of generation is accompanied every time by the excitation of a train of damped spikes.

Next, we consider the situation when $\beta < (\alpha - 1)$. Figure 3.18 shows the m vs. t dependence, calculated on the basis of Eq. (3.4.5) or three different values of the ratio ω'_M/Ω': (a) $\omega'_M/\Omega' = 0.1$;

(b) $\omega'_M/\Omega' = 2$; (c) $\omega'_M/\Omega' = 10$ (in all these cases, $\alpha = 2$, $\beta = 10^{-3}$, $T_1 = 2 \times 10^{-3}$ sec, and $G = 6 \times 10^5$). It can be easily seen that *undamped pulsations* of radiation power appear in the cases considered in Fig. 3.18. In Fig. 3.18*a* and 3.18*c*, the pulse has two main components—the *low-frequency* one and the *high-frequency* one. The low-frequency component in Fig. 3.18*a* corresponds to the modulation frequency (frequency ω'_M), while the high-frequency component corresponds to the natural oscillation frequency (frequency Ω'). In the case (c), the reverse situation takes place. Case (b) where the modulation frequency is close to the natural oscillation frequency is most interesting. The pulses in this case have a large amplitude.

In all the cases shown in Fig. 3.18, there is a certain *adjustment* of pulse frequency by the modulation frequency. In particular, this adjustment in the case (b), where the spike repetition frequency ω' is equal to $\omega'_M/8$ (i.e. *synchronisation* of spikes is observed at frequency $\omega'_M/8$). The periodic Q-switching of the resonator thus helps in an *ordering* of the laser generation process [92, 93].

Small Amplitude Pulsations. We represent the functions $n(t')$ and $m(t')$ in the form

$$n(t') = 1 + \nu(t'); \quad m(t') = \alpha - 1 + \mu(t'), \tag{3.4.7}$$

where $\nu(t')$ and $\mu(t')$ are respective deviations of functions from their values corresponding to the solutions of the unperturbed stationary system (3.3.27). We assume that the amplitude of pulsations of field intensity and the inverse population density are small:

$$\nu \ll 1; \quad \mu \ll (\alpha - 1). \tag{3.4.8}$$

Substituting (3.4.7) in (3.4.5) and taking into account (3.4.8) as well as the inequality (3.4.2), the system of balance equations can be linearised in the neighbourhood of point $(1, \alpha - 1)$ of the phase plane. This gives

$$\left.\begin{aligned} d\mu/dt' &= G(\alpha - 1)(\nu - \beta \cos \omega'_M t'); \\ d\nu/dt' &= -\mu - \alpha\nu. \end{aligned}\right\} \tag{3.4.9}$$

Eliminating ν, we get the following differential equation in μ:

$$\frac{d^2\mu}{dt'^2} + \alpha \frac{d\mu}{dt'} + G(\alpha - 1)\mu = G(\alpha - 1)\beta[\omega'_M \sin \omega'_M t' - \alpha \cos \omega'_M t']. \tag{3.4.10}$$

It can be easily seen that for $\beta = 0$, Eq. (3.4.10) turns into Eq. (3.3.14) written in the dimensionless form.

The solution of Eq. (3.4.10) is sought in the form

$$\mu(t') = \mu_1 \exp(i\omega'_M t') + \mu_1^* \exp(-i\omega'_M t'). \tag{3.4.11}$$

It should be noted that the right-hand side of Eq. (3.4.10) may be expressed in the form of the sum of terms containing either

$\exp(i\omega'_M t')$ or $\exp(-i\omega'_M t')$, since

$$\sin \omega'_M t' = \frac{1}{2i}(e^{i\omega'_M t'} - e^{-i\omega'_M t'});$$

$$\cos \omega'_M t' = \frac{1}{2}(e^{i\omega'_M t'} + e^{-i\omega'_M t'}).$$

The function $\mu_1 \exp(i\omega'_M t')$ will be a solution of Eq. (3.4.10) if only the term with $\exp(i\omega'_M t')$ is retained in its right-hand side. Taking this into account, we can easily get the following expression for μ_1:

$$\mu_1 = \frac{1}{2} G(\alpha - 1)\beta \frac{\alpha + i\omega'_M}{\omega'^2_M - G(\alpha - 1) - i\omega'_M \alpha}. \qquad (3.4.12)$$

This equation has *resonance properties*. The resonance occurs when the Q-modulation frequency ω'_M satisfies the condition

$$\omega'_M = \sqrt{G(\alpha - 1)}. \qquad (3.4.13)$$

In accordance with (3.4.6), this means that the modulation frequency is equal to the natural vibration frequency of the system.

If the resonance condition (3.4.13) is satisfied, we get from (3.4.12) (considering that $G \gg \alpha$)

$$\mu_{1max} = G(\alpha - 1)\beta/2\alpha. \qquad (3.4.14)$$

It should be remembered that the results obtained here are valid only under the condition that the pulse amplitude is *small* (see condition (3.4.8)). This means, in particular, that the following inequality must be satisfied:

$$\mu_{1max} \ll (\alpha - 1).$$

Taking into account the relation (3.4.14), this inequality may be written in the form

$$\beta \ll 2\alpha/G. \qquad (3.4.15)$$

Possibility of Realising Large Amplitude Undamped Pulses. Using the above-mentioned case of *small amplitude* pulses, we can draw certain conclusions about the conditions for realising *large amplitude* undamped pulses. Firstly, the modulation frequency must be close to the natural frequency of the system (*resonance condition*). Secondly, the modulation depth should not be *too low*. In order to get large amplitude undamped pulses, it is essential that the following condition (cf. (3.4.15)) is satisfied

$$\beta \gtrsim 2\alpha/G. \qquad (3.4.16)$$

Since $\alpha/G \approx 10^{-4}$, it follows from (3.4.16) that the modulation parameter β must be of the order of, or greater than, 10^{-4}.

These remarks confirm the m vs. t dependence shown in Fig. 3.18*b*. The pulse frequency ω' has a certain *integral* ratio to the modulation

frequency ω_M' (in the Figure, $\omega' = \omega_M'/8$), indicating the parametric nature of the pulse excitation mechanism.

Thus, while considering a weakly periodic Q-switching of the resonator, two qualitatively different situations must be isolated. The first situation is realised if the condition (3.4.15) is satisfied (*low amplitude pulses*). In this case, although μ increases in the vicinity of the resonance, it remains much below the stationary value $\alpha - 1$, and the generated pulse repetition frequency is equal to the Q-modulation frequency. The second situation arises when the condition (3.4.16) is satisfied (*large amplitude pulses*). The amplitude μ in this case has a large value near the resonance ($\mu_{max} \gg (\alpha - 1)$), and the pulse repetition frequency has an integral ratio to the Q-modulation frequency.

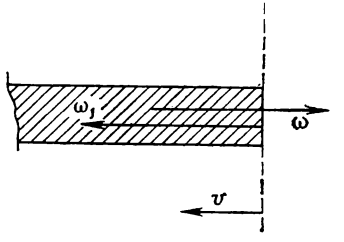


Fig. 3.19

Periodic Q-switching for a Uniform Motion of the Reflecting Surface. It is noteworthy that the periodic Q-switching of a resonator takes place, in particular, for a *uniform motion* along the optical axis of a reflecting surface, for example, the output mirror plane, or the end face of the active element [9, 10]. This effect can be easily explained by considering *the longitudinal Doppler effect.*

Suppose that the end face of an active element moves with velocity v along the resonator axis (see Fig. 3.19 where the dashed line shows the cross section of this plane). Let ω be the frequency of the light wave *traversing* through the moving plane, and ω_1 be the frequency of the wave *reflected* from this plane. According to the Doppler effect

$$\omega_1 = \omega + \Delta\omega_D = \omega + 2\omega v/c. \qquad (3.4.17)$$

Thus, the motion of the reflecting plane leads to the appearance in the resonator of *additional* waves with frequencies $\omega \pm \Delta\omega_D$ besides the wave with frequency ω (the amplitudes of these additional waves depend on the reflection coefficient of the plane).

The existence of additional (Doppler) components leads to a modulation of the light flux density. By considering the expression for flux density

$$S = [E_0 e^{-i\omega t} + \beta E_0 e^{-i(\omega+\Delta\omega_D)t}] \text{ [coml. conj.]},$$

we can easily detect a term of the type $S = 2 \mid E_0 \mid^2 \beta \cos(\Delta\omega_D t)$ in it. This may be associated with the *periodic modulation* of the Q-factor of the resonator under the condition that the modulation frequency is equal to

$$\omega_M = \Delta\omega_D' = 2\omega v/c. \qquad (3.4.18)$$

This situation may be described by balance equations (3.4.5), where

$$\omega'_{\mathrm{M}} = 2T_1\omega v/c, \tag{3.4.19}$$

and the modulation parameter β must be expressed through the reflection coefficient of the active reflecting planes.

Using (3.4.19), we can find an expression for the velocity of motion of the reflecting plane at which the resonance condition (3.4.13) is satisfied (*resonance velocity*)

$$v_{\mathrm{res}} = c\sqrt{G(\alpha-1)}/2\omega T_1. \tag{3.4.20}$$

Assuming the values $G = 10^5$, $\alpha = 30$, $T_1 = 2 \times 10^{-3}$ sec, $\omega = 3 \times 10^{15}$ sec^{-1} for a ruby laser, we get $v_{\mathrm{res}} = 4.5$ cm/sec from (3.4.20). In actual practice the resonance velocity for a ruby laser varies between 1 and 10 cm/sec.

Periodic Q-modulation by Heating the Active Element. Heating of the active element by absorption of pumping radiation changes the value of its refractive index (see Sec. 2.13). This may also result in a periodic modulation of the Q-factor of a resonator.

Suppose that the temperature of the active element changes with time at a rate of dT/dt. The *optical length* l_{opt} of the active element in this case will change at a rate of

$$dl_{\mathrm{opt}}/dt = l\eta\, dT/dt, \tag{3.4.21}$$

where l is the geometrical length of the element, and η is the temperature coefficient of its refractive index (this coefficient was denoted by dn/dT in Sec. 2.13).[30] Consequently, a periodic modulation of the resonator Q-factor will take place, the modulation frequency being determined by a formula similar to (3.4.19):

$$\omega'_{\mathrm{M}} = 2T_1\,(\omega/c)\, dl_{\mathrm{opt}}/dt. \tag{3.4.22}$$

Substituting (3.4.21) in (3.4.22), we get

$$\omega'_{\mathrm{M}} = 2T_1\,(\omega/c)\, l\eta\, dT/dt. \tag{3.4.23}$$

The analogy between the formulae (3.4.19) and (3.4.22) means, in particular, that the resonance rate of change in the optical length of the active element must be defined by a similar expression to the one for the resonance velocity of the reflecting surface, i.e. the expression (3.4.20) (in other words, both resonance velocities are identical). It was mentioned above that v_{res} for a ruby laser assumes values between 1 and 10 cm/sec. It can be easily seen that the dl_{opt}/dt, defined by the expression (3.4.21) falls in this interval for a ruby laser. Actually for $l = 10$ cm, $\eta = 1.4 \times 10^{-5}$ K^{-1}, $dT/dt = 10^4$ K/sec, we get $dl_{\mathrm{opt}}/dt = 1.4$ cm/sec.

[30] The thermal expansion of the active element is neglected. Besides, we do not consider the effects connected with the non-uniform heating of the element. It is also assumed that the magnitude of dT/dt is identical at all points of its cross section.

Nature of Undamped Pulses for Free Generation. It was shown above that undamped pulses arise upon a weak periodic modulation of the resonator Q-factor. Significantly, such a Q-modulation may be achieved not only by using special modulating elements in the resonator, but also by the motion of reflecting planes, or by rapid temperature variations of the active element. The last point means that a periodic Q-modulation, and hence the undamped pulses, may arise in the *free generation* case as a result of motion (vibrations) of reflecting planes caused by random processes, as well as through a rapid heating of the active element by absorption of the pumping radiation pulse. The fact that the actual velocity of the reflecting surfaces, as well as the rate of heating of the active element are not constant, is of no practical significance since the build-up of strong pulsations upon attainment of resonance takes place very rapidly, over a period of about 10 μsec only. For excitation of strong pulsations, it is necessary that the velocity of reflecting planes should be close to the resonance velocity at least for a comparatively short period.

Thus, the model of a single-mode laser with an unstable resonator may be used to reveal the important role of the instabilities of technical nature as one of the reasons behind the emergence of *undamped* laser radiation intensity pulsations.

3.5. ACTIVE MODULATION OF THE RESONATOR Q-FACTOR

In the preceding section, we have considered the effect of *weak* modulation of the resonator Q-factor on the dynamics of a laser. Let us now turn to the question of *deep* Q-switching which ensures a giant pulse generation in a laser (upon pulsed pumping) or a regular pulse train generation (upon continuous pumping). We shall consider three types of active Q-switching: *Mechanooptic* [26, 60], *electrooptical* [25-27], and *acoustooptic* [25, 28, 59].

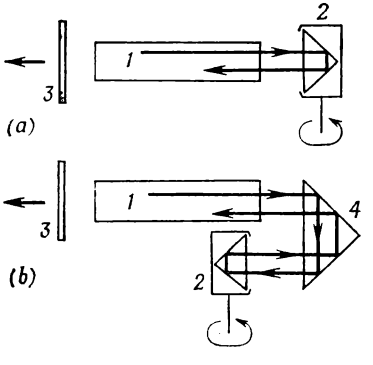


Fig. 3.20

Mechanooptic Q-switching. In this method of Q-switching, rotating reflecting planes are frequently employed. Two diagrams of mechano-optical Q-switching have been shown in Fig. 3.20 by way of an example. Here, *1* is the active element, *2*—a totally reflecting prism, rotating around an axis perpendicular to the resonator axis, *3*—the output resonator mirrors, and *4*—an additional (immovable) totally reflecting prism. The rotating prism *2* ensures a high Q of the resonator only for a short time. The angle of rotation of the prism

for which Q falls to half its maximum values is of the order of 1′. For an angular velocity of rotation of the prism of the order of 10^3 rev/sec, the Q-switching time is of the order of 100 nsec. Introduction of additional optical elements may increase the effective angular velocity of rotation of the prism (without any change in the real rotation rate). Thus in Fig. 3.20*b*, the effective angular velocity of rotation is twice the real value.

Electrooptical Q-switching. This method of Q-switching is based on the electro-optical *effect*, which consists in a change in the refractive index of the medium under the action of an external electric field. There are two types of electrooptical effect—the *quadratic* one (*Kerr effect*) and the *linear* one (*Pockels effect*). In the first case, the change in refractive index is proportional to the square of the electric intensity of the external field, while in the second case, it is proportional to the field intensity[31]. Pockels effect appears only in crystals which do not have a centre of symmetry. As an example, we may mention the uniaxial crystals KDP (chemical formula KH_2PO_4), and DKDP (chemical formula KD_2PO_4 or, more precisely, $KH_{2-2x}D_{2x}PO_4$ where x is the degree of deuteration).

Let us consider the electrooptical Q-switching of a resonator on the basis of the *Pockels effect*. First of all, we shall explain the basic idea behind this effect.

Figure 3.21 shows the *optical indicatrix* of a uniaxial crystal, having the form of an ellipsoid of revolution around the optical axis OO; n_o and n_e are the refractive indices for the ordinary and extraordinary waves respectively (these are the principal refractive indices of the crystal). For DKDP and KDP crystals, $n_o = 1.49$, $n_e = 1.46$ for light of wavelength 1 μm approximately and at a temperature of 20°C[32].

Let us apply an external electric field to the crystal along the OO axis. Under the action of this field, the optical indicatrix of the crystal is converted from an ellipsoid of revolution into a triaxial ellipsoid (the crystal turns from *uniaxial* into *biaxial*). Figure 3.22 shows the cross section of the optical indicatrix by a plane perpendicular to the OO axis (perpendicular to the direction of the applied field): the dashed line shows the cross section *before* the field is switched on while the solid line shows the cross section *after* the field has been switched on. The principal refractive indices of the crystal after switching on the field are n_1, n_2, and n_e; the principal dielectric axes are X, Y, and Z (Z-axis is perpendicular to the plane of the figure). Pockels effect in this case is described by the relations

$$n_1 = n_o + n_o^3 rE/2; \quad n_2 = n_o - n_o^3 rE/2, \tag{3.5.1}$$

[31] Pockels effect and Kerr effect have been described, for example, in [25, 70].

[32] Optical properties of crystals used in electrooptics and nonlinear optics, have been summarised in [94].

where E is the electric field, and r is one of the electro-optical constants of the crystal.

We shall examine the *longitudinal* Pockels effect, when light propagates along the direction of the field (i.e. perpendicular to the plane of Fig. 3.22). In this case, two linearly polarised waves will

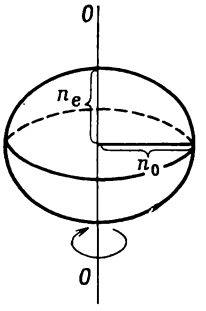


Fig. 3.21

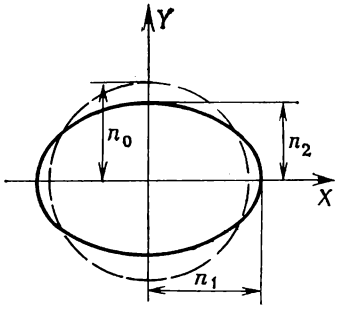


Fig. 3.22

propagate in the crystal, their polarisation being along the X-axis (wave velocity c/n_1) and the Y-axis (wave velocity c/n_2), respectively. With the help of the relation (3.5.1), we can find the phase difference between these two waves after the light has traversed a distance l inside the crystal:

$$\Delta\varphi = 2\pi l\,(n_1 - n_2)/\lambda_0 = 2\pi n_o^3 r U/\lambda_0. \qquad (3.5.2)$$

Here, λ_0 is the wavelength of light in vacuum and $U = El$ is the voltage applied to the crystal (l is the length of the crystal along OO

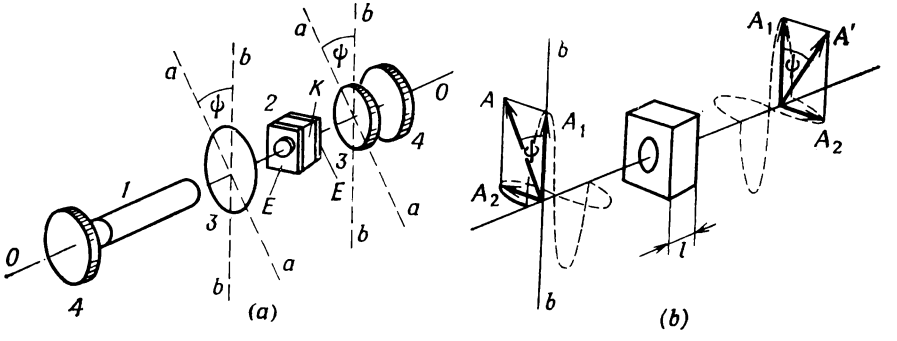


Fig. 3.23

axis). For a DKDP crystal, $r = 2.6 \times 10^{-11}$ m/V, while for a KDP crystal, $r = 1 \times 10^{-11}$ m/V.

Figure 3.23*a* shows a Q-switched laser based on the Pockels effect. Here, *1* is the active element, *2*—the Pockels cell (K is a DKDP

crystal, E—the electrodes), *3*—linear polarisers, and *4*—the resonator mirrors. The direction of polarisation of light passing through the polariser (the direction *aa* in the figure) forms an angle ψ with the direction of the principal dielectric axis X of the crystal (direction *bb* in the figure).

Suppose that a voltage is applied to the crystal (Pockels cell is switched on). In this case, the light waves polarised along the X-axis and the Y-axis, after passing through the cell, appear with a *phase difference* $\Delta\varphi$ with respect to each other, as described by the formula (3.5.2). Consequently, the linearly polarised light beam entering the Pockels cell will be converted into an elliptically polarised beam upon leaving the cell. Suppose that a voltage has been applied to the cell so that $\Delta\varphi = \pi$. Such a voltage is called *half-wave* voltage and is denoted by $U_{\lambda/2}$. It follows from (3.5.2) that

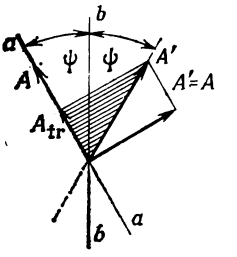


Fig. 3.24

$$U_{\lambda/2} = \lambda_0/(2n_0^3\, r). \qquad (3.5.3)$$

When the half-wave voltage is applied, the beam polarisation at the outlet of the cell *remains linear*, although the direction of the polarisation is *turned* by an angle 2ψ with respect to the initial direction. This can be clearly seen in Fig. 3.23*b*, where A is the amplitude vector of the wave at the entrance of the cell, and A′ is the corresponding vector as the beam leaves the cell. We consider the wave entering the cell as a superposition of two linearly polarised waves with refractive indices n_1 (amplitude vector A_1) and n_2 (amplitude vector A_2). Since for $U = U_{\lambda/2}$ these waves shift in phase by a half wavelength upon passing through the cell, one of the amplitude vectors (A_1 or A_2) must reverse its direction.

As a result of a rotation by 2ψ of the direction of polarisation, the light wave leaving a Pockels cell may only partially traverse through the second polariser. The intensity of the wave transmitted through the second polariser (denoted by A_{tr}^2) is related to the intensity of the wave passing through the first polariser (intensity A^2) through

$$A_{tr}^2/A^2 = \cos^2 2\psi, \qquad (3.5.4)$$

which is apparent from Fig. 3.24.

Thus when the Pockels cell shown in Fig. 3.23*a* is switched on, the losses increase in comparison to the case when the cell is switched off. The maximum increase in losses upon switching on the cell is attained for $\psi = \pi/4$. In this case $A_{tr}^2 = 0$, and the shutter is completely closed. Upon switching off the Pockels cell (upon removing the voltage across its electrodes), a rapid and considerable increase in the Q-factor of the resonator is observed. The Q-switching time is

determined by the rate of change of voltage applied to the Pockels cell, and is of the order of several nanoseconds.

Acoustooptic Q-switching. An acoustooptic shutter works on the principle of *ultrasonic optical diffraction.* Suppose that a plane ultrasonic wave, induced by a piezoelectric transducer, propagates in a certain medium (solid or liquid). This leads to a mechanical stress in the medium, due to local compressions and rarefactions. These stresses influence the refractive index through *photoelastic effect.* Consequently, alternate layers with different refractive indices are formed in the medium (the period in space is equal to the length Λ of the acoustic wave), travelling in the medium with the velocity of sound. A light wave passing through such a medium is diffracted by the periodic structure in space, due to the periodically varying refractive index.

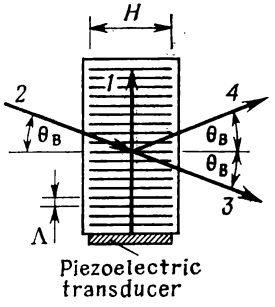


Fig. 3.25

Assuming that an acoustic wave of frequency Ω propagates along the y-axis, we can express the refractive index in the form

$$n(y, t) = n + \Delta n \sin[(2\pi y/\Lambda) - \Omega t]. \tag{3.5.5}$$

Here, n is the refractive index of the medium in the absence of an ultrasonic wave, and Δn is the amplitude of variation of refractive index. The magnitude of Δn is determined by the amplitude of elastic deformation with which it is connected through the elastooptic constants of the medium. The amplitude of elastic deformation, in turn, depends on the power P_a of the acoustic wave [25].

We assume that the following inequality is satisfied

$$l\lambda/\Lambda^2 > 1, \tag{3.5.6}$$

where λ is the wavelength of light in the medium, and l is the length of acoustooptic interaction (the path traversed by the light beam in the volume of the medium occupied by the sound wave). If the condition (3.5.6) is satisfied, *Bragg's diffraction*[33] takes place.

The principle behind an acoustooptic shutter operating on the basis of Bragg's diffraction is illustrated in Fig. 3.25. Here, H is the width of the acoustic beam, the numbers *1*, *2*, *3*, and *4* denote the direction of propagation of an acoustic beam, incident light beam, transmitted light beam, and the diffracted light beam, respectively (the refraction of light at the boundary of the shutter has not been

[33] If $l\lambda/\Lambda^2 \ll 1$, *Raman-Nath diffraction* takes place [28]. As a rule, this type of diffraction does not take place in acoustooptic shutters.

shown in the figure). Bragg's angle θ_B is defined by the relation

$$\sin \theta_B = \lambda/2\Lambda. \tag{3.5.7}$$

The shutter is oriented in the resonator of the laser in such a way that the direction of the incident light beam inside the shutter conforms to the condition (3.5.7). If the piezoelectric transducer is switched off, the light beam passes through the shutter without changing its direction (open shutter). Upon switching on the piezoelectric transducer, the incident light beam (of intensity I_0) will be partially converted into a diffracted beam (of intensity I_1), whose direction forms an angle $2\theta_B$ with the direction of the incident beam. The closer the ratio I_1/I_0 to unity, the lower the transmission through the shutter in the direction of the incident light beam. The ratio I_1/I_0 is a measure of the *efficiency* of an acoustooptic shutter.

In the *plane* wave approximation, the following relation holds (see [28]).

$$\frac{I_1}{I_0} = \sin^2\left(\frac{\pi}{\lambda_0 \cos\theta_B}\sqrt{\frac{P_a l}{2H} M_2}\right). \tag{3.5.8}$$

Here, λ_0 is the wavelength of light in vacuum, M_2 is called the *acoustooptic Q-factor*:

$$M_2 = n^6 p^2/\rho v^3,$$

where p is the elastooptic constant for the medium, ρ is the density of the medium, and v is the velocity of sound. It follows from (3.5.8) that $I_1/I_0 = 1$ if the acoustic power P_a assumes the value

$$P_{0a} = ((\lambda_0^2 \cos^2\theta_B)/2M)\,(H/l) \tag{3.5.9}$$

In this case a 100% conversion of incident light beam into diffracted light beam takes place (the shutter is completely closed).

The results (3.5.8) and (3.5.9) are valid for *plane* waves. In actual practice, however, we have to deal with *converging* (or *diverging*) waves. Upon diffraction of waves, a complete deviation of the incident light beam is not possible in principle, hence in actual practice, the ratio I_1/I_0 does not attain the value equal to unity.

Let us assume that the light beam is *Gaussian* and that an acoustooptic shutter is placed at the beam constriction, having a radius ρ_0. The efficiency of such a shutter depends on the magnitude of the parameter a, defined by the relation [95]:

$$a = (2\lambda/\pi\rho_0)\,(H/\Lambda). \tag{3.5.10}$$

The factor $2\lambda/\pi\rho_0$ is the angle of divergence of the Gaussian light beam with the radius of constriction ρ_0 (see (2.7.5)), and Λ/H is the angle of divergence of the acoustic beam. Consequently, a is the ratio of angles of divergence of the optical and acoustic beams. Figure 3.26*a* shows the dependence of I_1/I_0 on P_a for a few values of the parameter a, while Fig. 3.26*b* shows the dependence of I_1/I_0 on a

for $P_a = P_{0a}$. For a given acoustic power, the efficiency of a shutter is the higher, the lower the parameter a. The curve in Fig. 3.26*a*, drawn for $a = 0$ corresponds to the formula (3.5.8). Other curves have been obtained by considering diffraction of Gaussian light beams [28].

Let us denote by Δt the *switching* time of an acoustooptic shutter, i.e. the time during which a diffracted beam appears or, conversely, disappears. It may be estimated as the time during which an acoustic wave traverses a distance d equal to the diameter of the light beam: $\Delta t \approx d/v$. Assuming that $d = 0.2$ cm, $v = 6 \times 10^5$ cm/sec (fused quartz), we get $\Delta t \approx 300$ nsec. In order to decrease Δt, we must decrease d; that is why the acoustooptic shutter is placed at the constriction of the incident light beam. The smaller the radius of the constriction, the lower the value of Δt, and hence the faster the response of the shutter. However, it should be remembered that with decreasing radius of the constriction, the divergence of the light beam increases (the parameter a increases), and consequently the efficiency of the shutter decreases. In actual practice, it is preferable to work at values of parameter a that are close to unity.

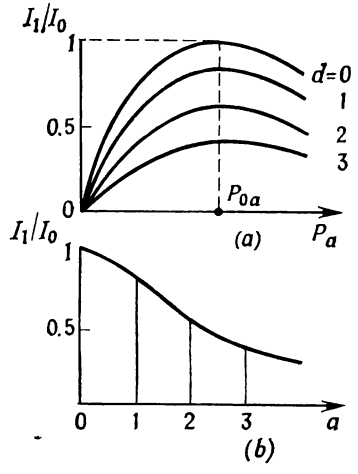


Fig. 3.26

Acoustooptic shutters made of fused quartz have found wide applications. Fused quartz is characterised by a high degree of transparency. However, it has a low acoustooptic Q-factor; hence it is necessary to employ a relatively high acoustic power ($P_a \approx 50$ W at frequencies 25-50 MHz).

Comparison between Acoustooptic and Electrooptic Q-Switching. Table 3.3. gives a comparison of main properties of acoustooptic and electrooptic shutters. It is apparent from the table that the minimum losses (losses for the open position of the shutter) in the case of acoustooptic shutters are about an order of magnitude lower than for electrooptic ones, and are of the order of 0.1%. The electrooptical shutters close very well (maximum losses in these are 100%), while the acoustooptic shutters close considerably worse. The switching time for electrooptic shutters is two or even three orders less than for acoustooptic shutters and is about a few nanoseconds.

Acoustooptic shutters are mainly used in *continuously* pumped lasers while the *pulse-pumped* lasers employ the electrooptical shutters. This is connected with the properties of the shutter and with the fact that pulse-pumped lasers are characterised by considerably higher values of gain in comparison to continuously pumped lasers.

In this connection, it should be noted that the optimal transmission coefficient of the output mirror is usually just a few per cent for continuously pumped lasers, while for pulse-pumped lasers it exceeds 50%.

TABLE 3.3

Properties	Shutters	
	Electrooptical	Acoustooptic
Minimum losses, %	1-3	0.1-0.3
Maximum losses, %	≈ 100	20-60
Speed, nsec	$\leqslant 5$	10^2-10^3

For low gain values characteristic of continuously pumped lasers, a breakdown in generation is possible even for comparatively low losses introduced by the shutter in the resonator. Hence for such lasers, we can effectively use acoustooptic shutters, which have the lowest losses in the open position. The fact that these shutters cannot be closed well is of no importance if the light pulse repetition frequency is quite high (5-50 kHz for a continuously pumped Nd:YAG laser). However, for low pulse repetition frequencies or, more significantly, for single pulses, the loss introduced by the acoustooptic shutter in the closed position may be found to be insufficient for the breakdown of generation in a continuously pumped laser (and hence for Q-switching). A proper closing of the shutter is especially important in pulse-pumped lasers. In this case, the fact that a shutter in the open position may introduce comparatively high losses (of the order of a few per cent) is not important, the only important thing is that the shutter should close properly and thus ensure a breakdown of generation for large values of the gain factor. Hence electrooptic shutters are preferable in pulse-pumped lasers.

It was mentioned earlier that for a faster operation of acoustooptic shutters, we must use light beams with small constriction radius, and place the shutter at the constriction of the beam. In pulse lasers this requirement leads to a strong heating of the shutter (and even to its destruction).

Modulation of Favourable Losses. The concept of *Q-switching* is usually connected with the modulation of *unfavourable* losses. A special term, *cavity-dumping*, is used for describing modulation of *favourable* loss (see Sec. 3.1). From a more general point of view, according to which the Q-switching of a resonator is determined by favourable as well as unfavourable losses, the modulation of favourable losses may be considered as one of the versions for active modulation of the Q-factor of the resonator.

A fast-operating acoustooptic fused quartz shutter intended for cavity dumping has been described in [53]. The shutter switching

time of 5 nsec is attained by focussing the light beam. The radius of the beam at the shutter is 20 μm. Such a shutter (playing the role of a modulator of favourable losses in this case) is shown in Fig. 3.27. Here, *1* is the active element; *2*, *3*, and *4* are highly reflecting mirrors; *5* is a shutter placed at the centre of the sphere corresponding

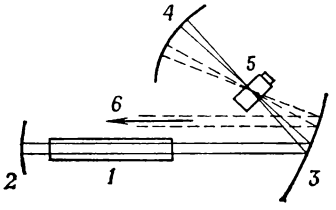


Fig. 3.27

to the surface of the mirror *4*; and *6* is the beam extracted from the resonator when the shutter is switched on. The solid lines show the light beam when the shutter is switched off, while the dashed lines show the beam obtained after switching on the shutter.

3.6. GIANT PULSE GENERATION IN THE CASE OF ACTIVE MODULATION OF THE RESONATOR *Q*-FACTOR

Main Time Stages[34]. The growth of a giant pulse can be conveniently examined by considering the main time stages in the generation process.

In Fig. 3.28 (cf. Fig. 3.2), three time dependences are shown in the upper half of the figure: the inverse population density (N vs. t curve), the threshold inverse population density (N_{thr} vs. t curve), the resonator Q-factor (the dashed line, Q vs. t curve). The latter two curves are interconnected, since in accordance with (3.2.42), $N_{\text{thr}}(t) = [B\hbar Q(t)]^{-1}$. The Q-factor varies from its minimum value $Q_{\min}$ (*high losses*) to maximum value Q (*low losses*). The time that elapses in the Q-switching process is denoted by t_Q. Correspondingly, the threshold inverse population density changes from the maximum value $N_{0\,\text{thr}}$ to its minimum value N_{thr}. The lower curve in the figure describes the time dependence of the photon density in the generated radiation (M vs. t dependence). Let us consider three successive stages: the pumping stage, and the linear and nonlinear stages of generation growth.

The *pumping stage* precedes the generation ($N(t) < N_{\text{thr}}(t)$). The inverse population density $N(t)$ increases as a result of pumping. At a certain moment of time (indicated as t_{sw} in the figure),

[34] Giant pulse generation for a rapid Q-switching is discussed in [1-4], see also [24, 29, 96-98].

the Q-factor of the resonator begins to increase rapidly, and hence the generation threshold begins to decrease rapidly. A decrease in the threshold results in the intersection of curves N vs. t and N_{thr}

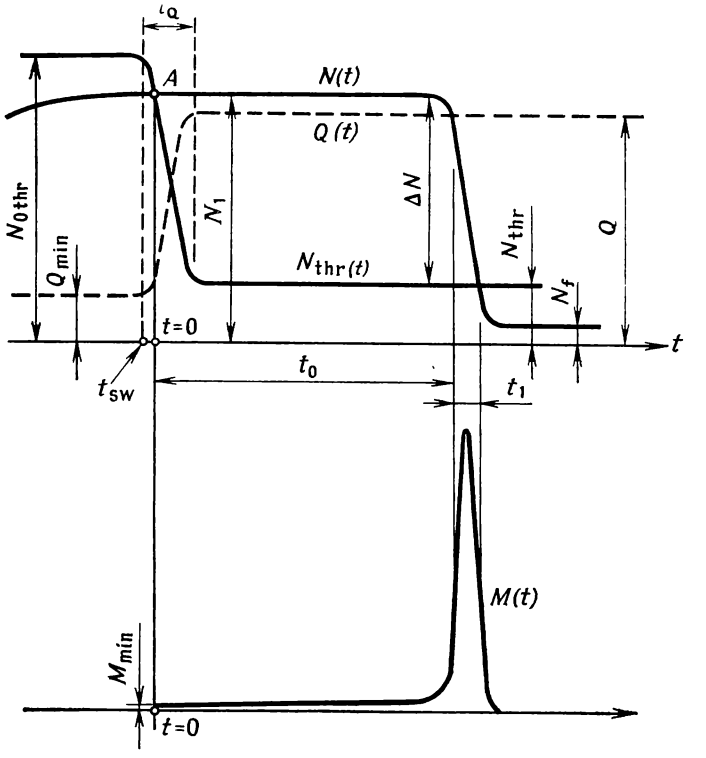


Fig. 3.28

vs. t. The instant of time corresponding to the point of intersection A (see Fig. 3.28) is the moment when generation begins. It is indicated as the instant $t = 0$ in the figure.

The duration of the *linear (slow) growth of generation* is denoted by t_0. It is characterised by a practically constant value of the inverse population density (we denote this value by N_1; strictly speaking, $N_1 = N(0)$). Since for the case of *rapid* Q-switching considered in this case, $t_Q \ll t_0$, the Q-factor already attains its maximum value at the initial stage of the linear growth of generation, so that the growth of generation takes place under the conditions of *low losses*. At the beginning of generation (i.e. at the moment $t = 0$), the photon field density caused by the spontaneous processes assumes the value M_{min}. At the linear generation stage, the function

$M(t)$ increases very slightly and only towards the end of this stage a rapid growth indicating the onset of the nonlinear stage begins.

The *nonlinear (rapid) growth of generation* has a duration t_1 which is much smaller than t_0, the duration of the linear stage (see Fig. 3.28). During this stage, the inverse population density falls to its minimum value N_f, which is less than the final threshold value N_{thr}. Practically the whole energy concentrated in the giant pulse is emitted during this stage.

The necessary condition for increasing the energy of the giant pulse is to increase the difference $N_1 - N_{thr}$ (this difference is denoted as ΔN in the figure). For this purpose, it is necessary, firstly, to ensure a large value of the difference $N_{0\,thr} - N_{thr}$, i.e. a deep Q-switching. Secondly, a high pumping intensity is essential so that the pumping parameter N_0 (and hence the magnitude $N(t)$) approaches the value $N_{0\,thr}$. Thirdly, and finally, it is essential to coincide the moment t_{sw} of Q-switching with the pumping pulse—the Q-factor must start increasing after $N(t)$ attains a value fairly close to its limiting value N_0 (for the given pumping power) as a result of pumping.

Balance Equations. Instantaneous Q-Switching. Let us consider the time dependence of the Q-factor of a resonator:

$$Q(t) = Q/f(t) = \omega T/f(t). \tag{3.6.1}$$

Here, Q is the maximum value of the Q-factor, T is the corresponding photon lifetime in the resonator, and $f(t)$ is a certain function of time, changing from $f(0) = Q/Q_{min}$ to 1.[35] Taking into account Eq. (3.6.1), the system of balance equations (3.2.34) may be rewritten in the following form:

$$\left.\begin{aligned} dM/dt &= B'MN - Mf(t)/T; \\ dN/dt &= -\beta B'MN + (N_0 - N)/T_1. \end{aligned}\right\} \tag{3.6.2}$$

Further, we observe that the growth time for the giant pulse (including the linear stage) is much smaller than T_1.[36] Hence the term $(N_0 - N)/T_1$ may be neglected in (3.6.2), i.e. the relaxation and pumping processes may not be taken into consideration during the giant pulse emission period. Consequently, the system of balance equations is considerably simplified:

$$\left.\begin{aligned} dM/dt &= B'MN - Mf(t)/T; \\ dN/dt &= -\beta B'MN. \end{aligned}\right\} \tag{3.6.3}$$

It should be emphasized that the relaxation and pumping processes are of prime importance at the *pregeneration stage*. On account of the relatively short duration of the giant pulse *generation stage*,

[35] For the sake of simplicity, it is assumed that the Q-switching instant and the start of generation (the instants t_{sw} and $t = 0$) coincide.

[36] It should be recalled (see Sec. 3.1) that $t_0 + t_1 \approx 10^{-7}$ sec.

these processes are not significant in this stage. The giant pulse generation process terminates before any noticeable variation in the inverse population density takes place due to relaxation and pumping processes.

Going over to the dimensionless form of notation, we can use the relations (3.2.52), where T and N_{thr} are values of parameters corresponding to the state with highest Q-factor. The system of equations (3.6.3) then assumes the following form:

$$\left.\begin{aligned} dm/dt' &= Gm\,[n - f(t')]; \\ dn/dt' &= -mn. \end{aligned}\right\} \tag{3.6.4}$$

We shall assume that the Q-switching is *instantaneous*. In this case, the function f may be written in the form

$$f(t') = \begin{cases} Q/Q_{\min}; & t' \leqslant 0; \\ 1; & t' > 0. \end{cases} \tag{3.6.5}$$

Thus, at the generation stage ($t' > 0$), we have $f = 1$. Consequently, we arrive at the following system of balance equations:

$$\boxed{\begin{aligned} dm/dt' &= Gm\,(n-1); \\ dn/dt' &= -mn. \end{aligned}} \tag{3.6.6}$$

Suppose that in addition to the Q-switch, the resonator contains a *nonlinear* element providing a *negative feedback*. This may be done in order to increase the duration of the giant pulse. A semiconductor crystal with *two-photon absorption* at the generation frequency may be used as the nonlinear element. In this case, the first equation in the system (3.6.6) acquires an additional term which takes into account nonlinear losses in the resonator. This term is proportional to the square of the field intensity in the resonator. In this case, the system of equations (3.6.6) assumes the form

$$\left.\begin{aligned} dm/dt' &= Gm\,(n-1) - gm^2; \\ dn/dt' &= -mn. \end{aligned}\right\} \tag{3.6.7}$$

Here g is a certain parameter characterising the two-photon absorption in a nonlinear element.

Phase-field Portrait of a Laser for Instantaneous Q-switching. Dividing the first equation in (3.6.6) by the second, we get

$$dm/dn = -G\,(n-1)/n. \tag{3.6.8}$$

Integrating, we get

$$\int_{m_1}^{m} dm = -G \int_{n_1}^{n} dn \left(1 - \frac{1}{n}\right), \tag{3.6.9}$$

where

$$n_1 = n\,(0) = N_1/N_{\text{thr}}; \quad m_1 = m\,(0) = M_1 \beta B' T_1. \tag{3.6.10}$$

Consequently, we arrive at the following equation for the *phase trajectories* of a laser in the case of instantaneous Q-switching:

$$m = m_1 + G\,[n_1 - n - \ln(n_1/n)]. \tag{3.6.11}$$

Putting $dm/dt' = 0$, we find from (3.6.6) that the *maximum* value of field intensity corresponding to the peak power of the giant pulse is attained for $n = 1$. Substituting $n = 1$ into (3.6.11), we get this maximum value

$$m_{max} = G\,(n_1 - 1 - \ln n_1) \tag{3.6.12}$$

(the term m_1 on the right-hand side of Eq. (3.6.11) may be neglected in this case, since $m_{max} \gg m_1$).

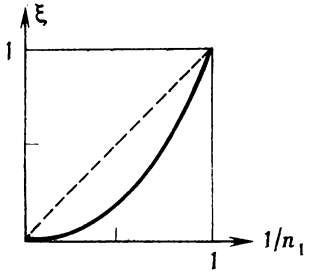


Fig. 3.29

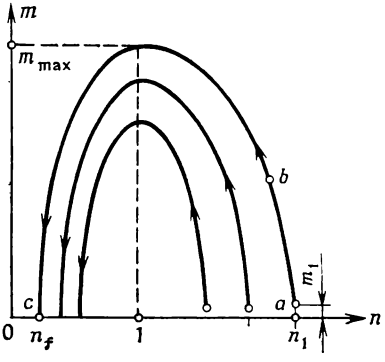


Fig. 3.30

The inequality $N_1 - N_{thr} > 0$ is apparent. It follows hence that the quantity n_1, being the ratio N_1/N_{thr}, must be greater than unity:

$$n_1 > 1. \tag{3.6.13}$$

We denote by n_f the ratio N_f/N_{thr}, where N_f is the *final* inverse population density attained at the end of the giant pulse emission. In order to find n_f, we put $m = 0$ in (3.6.11). This gives

$$n_f + \ln(n_1/n_f) = n_1 + m_1/G. \tag{3.6.14}$$

Neglecting the second term on the right-hand side of this equation which is much smaller than the first, and introducing the notation $\xi = n_f/n_1$, we can rewrite (3.6.14) in the form

$$\xi = 1 + \ln \xi/n_1. \tag{3.6.15}$$

Figure 3.29 shows the ξ vs. $1/n_1$ dependence defined by the relation (3.6.15). It is apparent from the figure that $\xi < 1/n_1$, i.e.

$$n_f < 1. \tag{3.6.16}$$

Thus, $N_f < N_{thr}$, which indicates a certain time lag in the pulse emission. At the instant when the decaying function $N(t)$ attains its threshold value N_{thr}, the generation *does not terminate* since the photons that are still present in the resonator continue to induce emission by the excited active centres.

The higher the ratio N_1/N_{thr}, the lower the ratio N_f/N_{thr}. For example, for $n_1 = N_1/N_{thr} = 2$, we get $\xi = 0.2$ and consequently $n_f = N_f/N_{thr} = 0.4$. For $n_1 = 3.5$, we get $\xi = 0.04$ and hence $n_f = 0.14$.

Summing up the results obtained above, we can easily build up a *phase diagram* for a laser in the case of instantaneous Q-switching. This diagram is shown in Fig. 3.30. The three phase trajectories shown in the figure correspond to three different values of n_1 (three different ratios N_1/N_{thr}).

One of the phase trajectories is broken into two parts, corresponding to the *linear* stage (*a-b*) and the *nonlinear* stage (*b-c*) of generation. This division of the trajectory is approximate[37], the ordinate of the point *b* is chosen equal to half the maximum value of the field intensity for the given phase trajectory. The velocity of the representative point along the phase trajectory is not constant: the point traverses the relatively short path *a-b* during a period of time t_0' and a longer path *b-c* during t_1', although $t_1' \ll t_0'$.

Analysis of the Linear Generation Growth Stage. In this stage of generation, we assume that

$$n = n_1 = \text{const}. \tag{3.6.17}$$

Besides, we take into consideration the contribution of *spontaneous radiation*. For this purpose, the first equation in (3.6.6) is replaced by the equation

$$dm/dt' = Gm\,(n_1 - 1) + G\varepsilon\,(n_1 + n''), \tag{3.6.18}$$

which is obtained from (3.2.56) by taking (3.6.17) into consideration. Equation (3.6.18) can be rewritten in the form

$$dm/(m + \delta) = G\,(n_1 - 1)\,dt', \tag{3.6.19}$$

where $\delta = \varepsilon\,(n_1 + n'')/(n_1 - 1)$. Integration of this equation gives

$$\int_{m_1}^{m} \frac{dm}{m+\delta} = G\,(n_1 - 1) \int_0^{t'} dt'.$$

Consequently, we get

$$m\,(t') = (m_1 + \delta) \exp\,[G\,(n_1 - 1)\,t'] - \delta. \tag{3.6.20}$$

[37] It is impossible to indicate a clear-cut demarcation between the linear and nonlinear generation stages.

It can be shown (see, for example, [4]), that

$$m_1 = \varepsilon (n_1 + n'') \Big/ \left(\frac{Q}{Q_{\min}} - n_1 \right). \tag{3.6.21}$$

Since $(Q/Q_{\min} - n_1) \gg (n_1 - 1)$ as a rule, it follows from (3.6.21) that $m_1 \ll \delta$. Hence (3.6.20) may be written in the form

$$m(t') = \delta [\exp [G (n_1 - 1) t'] - 1]. \tag{3.6.22}$$

It may be considered that formula (3.6.22) describes quite well ohe part of the curve $m(t')$ which corresponds to the shaded area tn Fig. 3.31. The duration t_0' of this stage is treated as the duration if linear growth of generation.

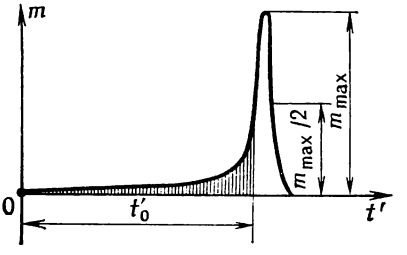


Fig. 3.31

Substituting $m = m_{max}/2$ in (3.6.22), we can evaluate the magnitude of t_0':

$$t_0' = [1/G (n_1 - 1)] \ln (m_{max}/2\delta) \tag{3.6.23}$$

(we consider that $\delta \ll m_{max}$). Using Eq. (3.6.12), we can transform (3.6.23) into

$$t_0 = t_0' T_1 = \frac{T}{n_1 - 1} \ln \frac{G (n_1 - 1 - \ln n_1)}{2\varepsilon (n_1 + n'')/(n_1 - 1)}. \tag{3.6.24}$$

Let us consider a specific numerical example: $T = 10^{-8}$ sec, $n_1 = 3.5$, $n'' = 10^2$, $G = 10^5$, and $\varepsilon = 10^{-13}$. In this case, the expression (3.6.24) gives $t_0 = 1.5 \times 10^{-7}$ sec $= 150$ nsec.

Energy Characteristics of a Giant Pulse. Taking Eqs. (3.2.27) and (3.2.35) into account, the power P of the generated radiation may be expressed in the form

$$P = S_{out}\, s = \hbar\omega v \eta_2 M V \tag{3.6.25}$$

where s is the illuminating area of the end face of the active element, and V is the volume taking part in the generation. Using (3.2.36) and (3.2.52), we can rewrite (3.6.25) in the form

$$P = \frac{\eta_2}{\eta_1 + \eta_2} \frac{Gm}{\beta B T_1^2} V = \frac{\eta_2}{\sigma N_{thr}} \frac{Gm}{\beta B T_1^2} V. \tag{3.6.26}$$

Introducing the dimensionless output power

$$p = P\left[\frac{\eta_2}{\sigma N_{\text{thr}}}\,\frac{V}{\beta B T_1^2}\right]^{-1}, \tag{3.6.27}$$

we can rewrite (3.6.26) in the form

$$p = Gm. \tag{3.6.28}$$

Using (3.6.12), we get an expression for the *maximum* value of the output power (in dimensionless form)

$$p_{\max} = Gm_{\max} = G^2 (n_1 - 1 - \ln n_1). \tag{3.6.29}$$

Let us examine the possibility of increasing the value of $p_{\max}$. In this connection, it should be recalled that $n_1 = N_1/N_{\text{thr}} = B\hbar N_1 Q$. From this, two ways of increasing the value of n_1 can be visualised: by increasing N_1 or by increasing Q. Since the function $F(n_1) = n_1 - 1 - \ln n_1$ increases monotonically with increasing n_1 (in the region $n_1 > 1$ which is of interest to us), and G^2 does not depend on N_1, it follows that the output peak power must increase with increasing N_1 (with increasing pumping power). It should be remembered that an increase in N_1 is restricted by the magnitude of n' ($N_1 < n'$), i.e. the inverse population density cannot apparently exceed the limit when all the active centres have been transferred to the upper laser level.

Let us assume, however, that we prefer to fix N_1 and increase Q. Considering that $G = T_1\omega/Q$, we can rewrite (3.6.29) in the form

$$p_{\max}(Q) = (a^2/Q^2)(bQ - 1 - \ln bQ), \tag{3.6.30}$$

where $a = T_1\omega$ and $b = B\hbar N_1$.

Equating the derivative $dp_{\max}/dQ$ to zero, we can obtain an *optimal* value Q_{opt} for the Q-factor of the resonator, which results in *maximum* output peak power. It can be easily seen that Q_{opt} is defined by the equation

$$bQ_{\text{opt}} - 1 = 2 \ln bQ_{\text{opt}}. \tag{3.6.31}$$

whence

$$bQ_{\text{opt}} = n_{\text{opt}\,1} = 3.5. \tag{3.6.32}$$

It is useful to rewrite the result (3.6.29) in a form which does not use dimensionless quantities. Besides, it should be remembered that

$$\eta_2 = (1/2L) \ln (1/R),$$

where L is the resonator length, and R is the coefficient of reflection of the output mirror (the second mirror is considered to be totally reflecting). Using (3.6.27), we get the following relation from (3.6.29):

$$P_{\max} = \frac{1}{4}\hbar\omega N_1 vs \ln\frac{1}{R}\left[1 - \frac{N_{\text{thr}}}{N_1}\left(1 + \ln\frac{N_1}{N_{\text{thr}}}\right)\right]. \tag{3.6.33}$$

Putting $N_1/N_{thr} = 3.5$, we get an expression for the *maximum* output peak power of the pulse:

$$P_{max}^{max} = 0.1\hbar\omega N_1 vs \ln (1/R). \tag{3.6.34}$$

Let us now estimate the energy of the emitted giant pulse. If during the process of emission, the inverse population density decreases from N_1 to N_f, it means that $(1/\beta)(N_1 - N_f)$ photons were generated per unit volume of the active medium. Multiplying this number by the photon energy $\hbar\omega$, the generating volume V of the active medium, and the ratio $\eta_2/(\eta_1 + \eta_2)$ describing the fraction of the generated light energy emerging from the resonator mirror in the form of useful radiation, the giant pulse energy is given by

$$U = (\hbar\omega/\beta)\, V (N_1 - N_f)\, \eta_2/(\eta_1 + \eta_2). \tag{3.6.35}$$

Duration and Shape of a Giant Pulse. As has been mentioned above, the main part of pulse energy is emitted at the stage of nonlinear growth of generation, hence by the *pulse duration* we mean the duration t_1 of this stage. In order to estimate the value of t_1, we divide the pulse energy U by its peak power P_{max}:

$$t_1 \approx U/P_{max}. \tag{3.6.36}$$

In accordance with (3.6.35), we can write U in the form

$$U = (\hbar\omega/\beta)\, VN_{thr}\, (n_1 - n_f)\, \eta_2/(\eta_1 + \eta_2), \tag{3.6.37}$$

while P_{max} can be written in accordance with (3.6.26) and (3.6.29), as follows

$$P_{max} = \frac{\eta_2}{\eta_1+\eta_2} \frac{V}{\beta B T_1^2} G^2 (n_1 - 1 - \ln n_1). \tag{3.6.38}$$

Dividing (3.6.37) by (3.6.38), we get

$$t_1 = \hbar\omega B N_{thr} \frac{T_1^2}{G^2} \frac{n_1 - n_f}{n_1 - 1 - \ln n_1}.$$

Considering that $\hbar\omega B = \sigma v$, $N_{thr} = 1/Tv\sigma$, and $G = T_1/T$, we finally get

$$t_1 = T\,(n_1 - n_f)/(n_1 - 1 - \ln n_1). \tag{3.6.39}$$

Let us consider a numerical example: $T = 10^{-8}$ sec, $n_1 = 3.5$, $n_f = 0.1$. In this case, we get $t_1 = 2.8 \times 10^{-8}$ sec $= 28$ nsec.

Neglecting n_f which is small in comparison with n_1, we can rewrite Eq. (3.6.39) in the form

$$1/t_1 = (1/Tn_1)\,(n_1 - 1 - \ln n_1) \tag{3.6.40}$$

or, considering that $n_1 = B\hbar N_1 Q$,

$$1/t_1 = (\text{const}/Q^2)\,(bQ - 1 - \ln bQ), \tag{3.6.41}$$

where $b = B\hbar N_1$. Comparing (3.6.41) and (3.6.30), we find that the peak pulse power and the reciprocal of its duration have an *identical* dependence on Q. The pulse duration attains a minimum value *for the same value of Q-factor*, for which the peak pulse power has maximum value (i.e. for $bQ_{opt} = n_1^{opt} = 3.5$). It follows from this that a decrease in the peak power of a giant pulse with increasing Q in the region $bQ > 3.5$ is due to a protraction of the pulse.

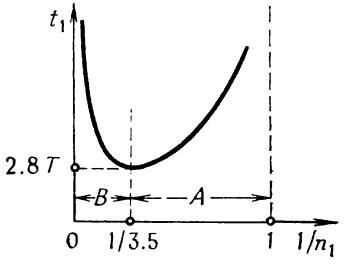


Fig. 3.32

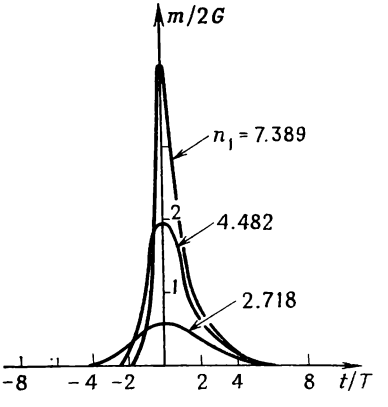


Fig. 3.33

Figure 3.32 shows the dependence of the giant pulse duration on $1/n_1$, as described by Eq. (3.6.40). In the region A, a protraction of pulse with decreasing n_1 is explained by a slower increase in the number of photons in the resonator as the generation threshold approaches, thus *increasing the pulse growth time.* In the region B, a protraction of pulse with increasing n_1 is explained by a *protraction of the pulse decay* with decreasing losses.

It can be easily seen that the pulse *form* inevitably changes with increasing n_1. As a matter of fact, an increase in n_1 leads to a decrease in the pulse growth time, while the decay time must increase for sufficiently large values of n_1. If for small values of n_1 a giant pulse has a *symmetric* form approximately, a transition to *asymmetric* form is inevitable with increasing n_1, when the pulse growth time becomes considerably less than the pulse decay time. This is clearly seen from Fig. 3.33 which shows the giant pulse form obtained for three different values of n_1 with the help of a computer [97]. The instant of time corresponding to the peak pulse power is chosen each time at the starting moment.

Giant Pulse Generation for Different Q-switching Times. The balance equations *averaged* over the length of the resonator (Statz-De Mars equations) give a correct description of the generation process only when the duration of the pulse is greater than the time

spent in a round-trip of the radiation through the resonator. In order to consider generation of sufficiently short pulses (duration less than 10 nsec) it is essential to consider the *spatial* effects. In such a case, balance equations cannot be used.

A more correct approach is based on the use of *partial differential* balance equations (in other words, the balance equations which are not averaged over the length of the resonator). The radiation density and the inverse population density appearing in these equations depend not only on *time* but also on the *longitudinal spatial*

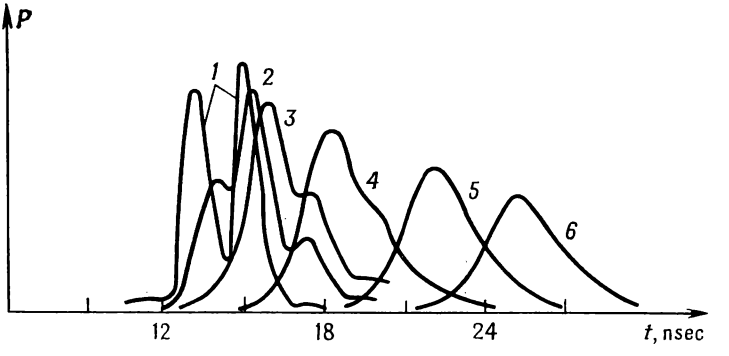


Fig. 3.34

coordinate. This kind of approach has been adopted in [24], where the following system of partial differential balance equations is used:

$$\left.\begin{aligned} \frac{\partial S_+}{\partial z}+\frac{1}{v}\frac{\partial S_+}{\partial t}&=(\sigma N-\eta_1)\,S_+;\\ -\frac{\partial S_-}{\partial z}+\frac{1}{v}\frac{\partial S_-}{\partial t}&=(\sigma N-\eta_1)\,S_-;\\ \frac{\partial N}{\partial t}&=-2\,\frac{\sigma N}{\hbar\omega}(S_++S_-). \end{aligned}\right\} \qquad (3.6.42)$$

This is the familiar system (3.2.18) in which the last equation has been modified in accordance with the specific nature of the problem (the relaxation and pumping processes during the giant pulse emission have not been taken into account). On the basis of numerical analysis of balance equations (3.6.42) carried out with the help of a computer, the form of the light pulse has been found out for *different* values of Q-switching time t_Q (Fig. 3.34). This figure shows the dependence of light pulse power P on time t (the instant $t = 0$ indicates the onset of generation) for values of t_Q equal to 1.5 nsec (curve *1*), 3 nsec (curve *2*), 10 nsec (curve *3*), 20 nsec (curve *4*), 40 nsec (curve *5*), and 60 nsec (curve *6*). Let us denote as τ_0 the time

taken by radiation for a round-trip through the resonator. In this case $\tau_0 \approx 2$ nsec. It can be easily seen from the figure that for a *rapid* Q-switching ($t_Q \leqslant \tau_0$), the generated pulse acquires a *substructure* modulated with a period of the order of τ_0. This substructure is due to a non-stationary redistribution of the field intensity and the inverse population density along the length of the active element.

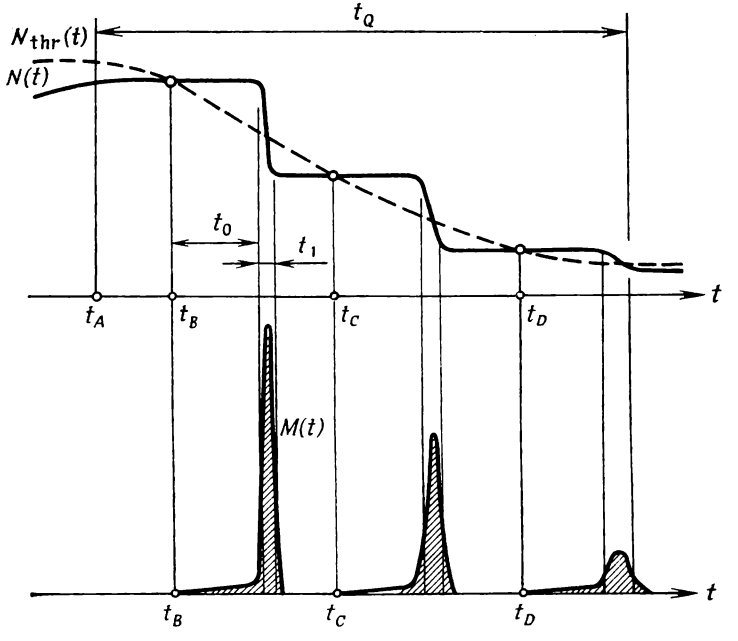


Fig. 3.35

An *increase* in Q-switching time leads to the disappearance of this substructure of the giant pulse, as well as to an increase in the linear pulse growth time (t_0) and a decrease in the pulse energy. The latter is due to the fact that for $t_Q > t_0$, the generation takes place under conditions of high losses.

For a *sufficiently slow* Q-switching (when $t_Q \gg t_0$), *several* light pulses may be independently generated [1]. The dynamics of processes[3] taking place in this case is shown in Fig. 3.35. The function $N(t)$ is shown in the upper half of the figure and the dashed line depicts the function $N_{thr}(t)$ corresponding to a slow growth of the resonator Q-factor. The lower half of the figure shows the function $M(t)$ whose shape indicates the emission of the three pulses consid-

[38] In this case (just like in the case of instantaneous Q-switching), we can use the *averaged* balance equations.

ered in this case. The instant of time t_A indicates the beginning of variation in the inverse population density (the Q-factor begins to increase at this moment). At the instant t_B, the curves N vs. t and N_{thr} vs. t intersect, and the generation of the first pulse begins, passing successively the stages of linear (duration t_0) and nonlinear (duration t_1) growth. As a result of the emission of the first pulse, the inverse population density falls below the threshold level. The continuing decrease in the threshold level results in another intersection of the N vs. t and N_{thr} vs. t curves at the instant t_C. This instant corresponds to the generation of the second pulse. Later, at

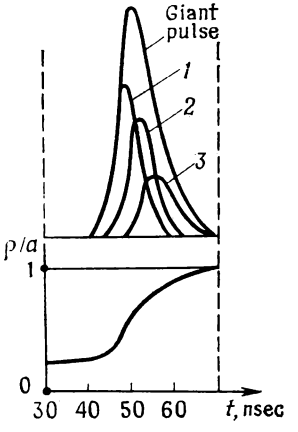


Fig. 3.36

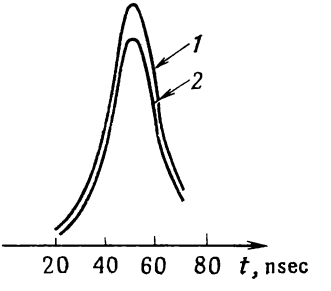


Fig. 3.37

the instant t_D, the third pulse begins to form. The process of pulse emission is terminated when a constant value of threshold level corresponding to the maximum Q-factor is established.

Pulse Growth in a Direction Perpendicular to the Resonator Axis. A nonuniform distribution of the inverse population density along the cross section of the active element leads to a certain growth of the generation process in a direction perpendicular to the resonator axis. For a higher initial inversion in the axial region of the active element, the generation starts near the axis and propagates outwards over a certain period of time, ultimately engulfing the entire volume of the active element, which is filled with the modes excited in the resonator. A giant pulse may be treated as the sum of pulses emitted by various regions in the cross section of the active element. These pulses are displaced along the time axis, and each of them has a duration lower than the duration of the entire giant pulse. Figure 3.36 illustrates this situation [29]. The fine structure of the giant pulse in a ruby laser (with an instantaneous Q-switching), depicted in the upper half of the figure, consists of three

pulses: *1* is the pulse emitted by the central region of the end face of the active element (the radius of this region is given by $0.5a$, where a is the radius of the entire illuminating face), *2* and *3* are pulses emitted by circular regions of the end face, formed by rings of radii $0.5a$, $0.75a$ and $0.75a$, a respectively. The lower half of the figure shows the $\rho(t)/a$ vs. t curve, $\rho(t)$ being the radius of the generation region at the moment t. In the linear generation growth stage, generation takes place in the axial region of the active element. With the onset of nonlinear stage, generation grows in the transverse direction. With increasing gain of the active medium and decreasing aperture, the duration of the process of "spreading" of generation over the cross-section of the active element decreases.

A considerable decrease in the duration of this process takes place in lasers with *unstable resonators*, whose nature ensures a rapid growth of generation from the axis of the active element towards the periphery. Figure 3.37 shows the fine structure of a giant pulse in a ruby laser with an unstable resonator [99]. Here, *1* is the pulse formed in the axial region (with a radius of $0.5a$), while *2* is the pulse formed in the remaining volume of the active element. For the case considered in this figure, we can actually consider that there is a *simultaneous* generation from the entire transverse cross section of the active element (pulse *2* lags behind pulse *1* by just 1 nsec).

3.7. BLEACHABLE FILTER LASERS

Bleachable Filter. A *bleachable filter* is a nonlinear resonance absorber capable of a reversible change in the absorption coefficient under the action of a sufficiently high intensity light beam of a certain frequency. A bleachable filter consists of molecules (atoms) which resonantly absorb radiation at the transition frequency for a given laser. These molecules (atoms) are called *absorbing centres.* The basic principle behind a bleachable filter is the nonlinear optical effect of *bleaching of the medium*: the initially opaque medium becomes transparent (bleached) as the intensity of the radiation incident on it increases.

Solutions of organic dyes like cyanine (phthalocyanine and kryptocyanine) dyes and polymethine dyes are frequently used as bleachable media. Cyanine dyes are used in ruby lasers, while polymethine dyes are used in activated Nd-lasers (see, for example, [6, 100-103].

While considering the interaction of radiation with absorbing centres, a *two-level* or *three-level* model is employed for the bleachable medium. We shall consider the *two-level model* below.

The energy difference between the absorbing centre levels must correspond to the frequency ω of the transition in the active centre of the laser. At the initial stage, all the absorbing centres are situated at the lower level, and the filter has maximum opaqueness

(*unbleached* state of the filter). In this state

$$n_{1a} = n'_a; \quad n_{2a} = 0,$$

where n'_a is the total number of absorbing centres per unit volume; and n_{1a} and n_{2a} denote the population density of the lower and upper levels of the absorbing centre respectively[39]. Irradiation of the filter by light of generation frequency leads to resonant absorption and induced emission, accompanied by transitions of absorbing centres between the two levels considered above. Since $n_{2a} < n_{1a}$, resonant absorption will be predominant, and thus the difference $(n_{1a} - n_{2a})$ will gradually decrease, i.e. the filter starts *getting bleached*. For a sufficiently high intensity of radiation, the difference $(n_{1a} - n_{2a})$ in population densities may become equal to zero. In this case, the coefficient of resonant absorption also becomes zero, and we get the *maximum bleaching* of the filter:

$$n_{1a} = n_{2a} = n'_a/2.$$

Upon termination of the radiation, the relaxation processes ensure a return of the absorbing centres to the lower level. Consequently, the filter returns to its initial (unbleachable) state.

Balance equations for the population density of the absorbing centre levels for a two-level case may be written in the form

$$\left.\begin{aligned} \frac{dn_{2a}}{dt} &= B_a n_{1a} \frac{S}{v_a} - B_a n_{2a} \frac{S}{v_a} - \frac{n_{2a}}{T_{1a}}; \\ \frac{dn_{1a}}{dt} &= B_a n_{2a} \frac{S}{v_a} - B_a n_{1a} \frac{S}{v_a} + \frac{n_{2a}}{T_{1a}}. \end{aligned}\right\} \tag{3.7.1}$$

Here, S is the density of the light flux averaged over the length of the filter, B_a is the Einstein coefficient for induced transitions between levels of an absorbing centre, v_a is the velocity of light in the filter, and T_{1a} is the longitudinal relaxation time for the filter ($1/T_{1a}$ is the probability of spontaneous transitions from the upper level to the lower one).

We introduce the inverse population density for the levels of an absorbing centre

$$N_a = n_{2a} - n_{1a}.$$

The quantity N_a is negative, since $n_{2a} < n_{1a}$. Substracting the second equation from the first one in (3.7.1) and considering that $n_{1a} + n_{2a} = n'_a$, we get

$$dN_a/dt = -2B_a N_a S/v_a - (N_a + n'_a)/T_{1a}. \tag{3.7.2}$$

It should be noted that in the initial state (at the moment $t = 0$) $N_a(0) = -n'_a$.

[39] The index a in the notation used here indicates that the corresponding quantity characterises the bleachable filter.

Next, we introduce the linear *coefficient $\varkappa_a$ of resonant absorption of the filter*. By analogy with (3.2.5), we can write

$$\varkappa_a = -\sigma_a N_a, \tag{3.7.3}$$

where σ_a is the cross section of induced transitions between the levels of the absorbing centre. By analogy with (3.2.9), we get

$$\sigma_a = B_a \hbar\omega / v_a. \tag{3.7.4}$$

The quantity

$$\varkappa_{0a} = -\sigma_a N_a (0) = \sigma_a n_a' \tag{3.7.5}$$

is the *initial* coefficient of resonant absorption, i.e. the absorption coefficient of the filter in the initial (unbleached) state.

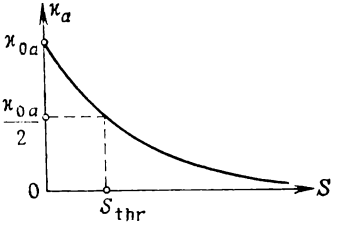


Fig. 3.38

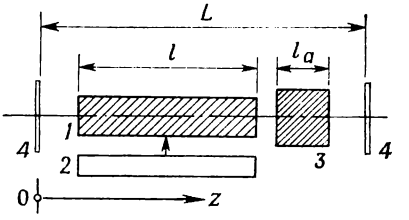


Fig. 3.39

Taking into account (3.7.3) and (3.7.5), we can rewrite (3.7.2) in the form

$$\frac{d\varkappa_a}{dt} = -2B_a\varkappa_a \frac{S}{v_a} + \frac{\varkappa_{0a} - \varkappa_a}{T_{1a}}. \tag{3.7.6}$$

For the *stationary* state ($d\varkappa_a/dt = 0$), we get

$$\varkappa_a (S) = \frac{\varkappa_{0a}}{1 + (S/S_{thr})}, \tag{3.7.7}$$

where

$$S_{thr} = v_a / 2B_a T_{1a} = \hbar\omega / 2\sigma_a T_{1a} \tag{3.7.8}$$

is conventional threshold density of the light flux, at which the coefficient of resonant absorption is reduced to half its value. The $\varkappa_a$ vs. S dependence given by formula (3.7.8) is shown in Fig. 3.38.

The *total* absorption coefficient η_a for the filter is the sum of the coefficients of *resonant* and *nonresonant* absorption:

$$\eta_a (S) = \varkappa_a (S) + \eta_{1a}. \tag{3.7.9}$$

The nonresonance absorption coefficient η_{1a} is independent of S. It is connected with the absorption of radiation by those molecules (atoms) of the filter which are not absorbing centres, and hence may be called the *coefficient of unfavourable losses in the filter*.

Differential Equation for the Averaged Density of Light Flux. Figure 3.39 shows a bleachable filter laser. Here, *1* is the active

element, *2*—the pumping system, *3*—the bleachable filter, and *4*—the resonator mirrors. We introduce the following notations: l, l_a, and l, represent the lengths of the active element, the filter, and the resonator, respectively; $v = c/n$ and $v_a = c/n_a$ are the velocity of light in the active element and that in the filter, respectively.

In order to obtain a differential equation for the *averaged* light flux density over the length of the resonator under consideration, we use Eq. (3.2.25) which can be rewritten in the following form with the help of (3.2.26):

$$S_{\text{out}} + \frac{l}{v}\frac{d\langle S\rangle}{dt} = l\sigma\langle N\rangle\langle S\rangle - l\eta_1\langle S\rangle. \tag{3.7.10}$$

In order to generalise Eq. (3.7.10) to the case of a laser with a filter (applicable for the case shown in Fig. 3.39), it should be considered that while averaging the flux density over the length of the resonator, it is necessary to take into consideration different properties of the active element and the filter. In the present case, we get

$$\int_0^L \frac{\partial S(z,t)}{\partial t}\frac{dz}{v(z)} = \left[\frac{l}{v} + \frac{l_a}{v_a} + \frac{L-(l+l_a)}{c}\right]\frac{d\langle S\rangle}{dt};$$

$$\int_0^L \sigma(z)N(z,t)S(z,t)\,dz = l\sigma\langle N\rangle\langle S\rangle + l_a\sigma_a\langle N_a\rangle\langle S\rangle;$$

$$\int_0^L \eta_1(z)S(z,t)\,dz = l\eta_1\langle S\rangle + l_a\eta_{1a}\langle S\rangle.$$

It can be seen from here that the following equation is equivalent to Eq. (3.7.10):

$$S_{\text{out}} + \left[\frac{l}{v} + \frac{l_a}{v_a} + \frac{L-(l+l_a)}{c}\right]\frac{d\langle S\rangle}{dt}$$

$$= l\sigma\langle N\rangle\langle S\rangle + l_a\sigma_a\langle N_a\rangle\langle S\rangle - l\eta_1\langle S\rangle - l_a\eta_{1a}\langle S\rangle. \tag{3.7.11}$$

Let us introduce the *filling factor* for the active medium in the resonator:

$$\mu = \frac{ln}{ln + l_a n_a + [L-(l+l_a)]} = \frac{l/v}{l/v + l_a/v_a + [L-(l+l_a)]/c}. \tag{3.7.12}$$

Using this factor and omitting the angle brackets $\langle\ldots\rangle$ in order to simplify the notation, we can rewrite Eq. (3.7.11) in the form

$$S_{\text{out}} + \frac{l}{\mu v}\frac{dS}{dt} = l\left(\sigma N + \frac{l_a}{l}\sigma_a N_a\right)S - l\left(\eta_1 + \frac{l_a}{l}\eta_{1a}\right)S. \tag{3.7.13}$$

Further, considering that in accordance with (3.2.27), $S_{\text{out}} = -lS\eta_2$, we get

$$\frac{1}{\mu v}\frac{dS}{dt} = \left(\sigma N + \frac{l_a}{l}\sigma_a N_a\right) S - \left(\eta_1 + \frac{l_a}{l}\eta_{1a} + \eta_2\right) S. \tag{3.7.14}$$

Equation (3.7.14) is a generalisation of the first equation in (3.2.32) for the case of a bleachable laser.

Finally, let us introduce the parameter T which denotes the lifetime of a photon in the resonator:

$$T = [\mu v\,(\eta_1 + (l_a/l)\,\eta_{1a} + \eta_2)]^{-1}. \tag{3.7.15}$$

Equation (3.7.14) may now be written in the form

$$dS/dt = \mu v \sigma N S - \mu v\,(l_a/l)\,\sigma_a N_a S - (1/T)\,S, \tag{3.7.16}$$

or, if we take (3.7.3) into account,

$$dS/dt = \mu v \sigma N S - \mu v\,(l_a/l)\,\varkappa_a S - (1/T)\,S. \tag{3.7.17}$$

Complete System of Balance Equations for a Bleachable Filter Laser. The complete system of balance equations must include Eq. (3.7.17) or (3.7.16) for averaged density of light flux in the resonator, the balance equation for the active element, and the balance equation for a bleachable filter. As the balance equation for the *active element*, we choose the second equation in (3.2.37), while Eq. (3.7.6) is chosen as the balance equation for the *filter*. Thus, the complete system of balance equations for a bleachable filter laser has the following form:

$$\boxed{\begin{aligned} \frac{dS}{dt} &= \mu v \sigma N S - \mu v \frac{l_a}{l}\varkappa_a S - \frac{1}{T} S; \\ \frac{dN}{dt} &= -\beta \frac{\sigma}{\hbar\omega} N S + \frac{N_0 - N}{T_1}; \\ \frac{d\varkappa_a}{dt} &= -2\frac{\sigma_a}{\hbar\omega}\varkappa_a S + \frac{\varkappa_{0a} - \varkappa_a}{T_{1a}}. \end{aligned}} \tag{3.7.18}$$

The required functions in this system are the density of the light flux in the resonator, $S(t)$, the inverse population density in the active element, $N(t)$, and the resonance absorption coefficient in the filter, $\varkappa_a(t)$. Of course, instead of the last function, we can also consider the inverse population density in the filter, i.e. the function $N_a(t)$.

It should be recalled that the time T_1 is determined by the pumping probability w_p and the probability of spontaneous transitions, $1/\tau$, in the generation channel:

$$1/T_1 = w_p + 1/\tau \tag{3.7.19}$$

while the *pumping parameter* N_0 is defined (for a three-level laser) by the relation

$$N_0 = n' (w_p\tau - 1)/(w_p\tau + 1). \tag{3.7.20}$$

Let us write the system of equations (3.7.18) in the *dimensionless form*, using the dimensionless time t' ($t' = t/T_1$; $d/dt = T_1^{-1}d/dt'$), the dimensionless field intensity

$$m(t') = \beta B T_1 S(t')/v = \beta\sigma T_1 S(t')/\hbar\omega, \tag{3.7.21a}$$

the dimensionless inverse population density in the active element,

$$n(t') = \mu v\sigma T N(t'), \tag{3.7.21b}$$

and the dimensionless inverse population density $n_a(t')$ in the filter, given by

$$n_a(t') = -\mu v T \varkappa_a(t')\, l_a/l. \tag{3.7.21c}$$

Taking into account Eq. (3.7.21), the system of balance equations (3.7.18) may be written in the following form:

$$\left.\begin{aligned} \frac{dm}{dt'}\frac{1}{T_1} &= \frac{n}{T}m + \frac{n_a}{T}m - \frac{1}{T}m; \\ \frac{dn}{dt'}\frac{1}{T_1} &= -\frac{m}{T_1}n + \frac{1}{T_1}(\mu v\sigma T N_0 - n); \\ \frac{dn_a}{dt'}\frac{1}{T_1} &= -\frac{2\sigma_a}{\beta\sigma}\frac{m}{T_1}n_a + \frac{1}{T_{1a}}\left(-\mu v\frac{l_a}{l}T\varkappa_{0a} - n_a\right). \end{aligned}\right\} \tag{3.7.22}$$

With the help of the dimensionless parameters[40]

$$G = T_1/T; \quad \delta = T_1/T_{1a}; \quad \rho = 2\sigma_a/\beta\sigma; \tag{3.7.23}$$

$$\alpha = \mu v\sigma T N_0; \tag{3.7.24}$$

$$\alpha_a = -\mu v T \varkappa_{0a} l_a/l = -\mu v T \sigma_a n_a' l_a/l. \tag{3.7.25}$$

The system of equations (3.7.22) assumes the form

$$\boxed{\begin{aligned} dm/dt' &= Gm(n + n_a - 1); \\ dn/dt' &= \alpha - n(m+1); \\ dn_a/dt' &= \alpha_a\delta - n_a(\rho m + \delta). \end{aligned}} \tag{3.7.26}$$

The system of balance equations (3.7.18) (or its dimensionless form (3.7.26)) is essential for considering the development of processes in a *single-mode bleachable filter laser* [2, 4, 7, 17, 104, 105][41].

[40] It should be recalled that the dimensionless parameters G and α have already been used, for example, in Eq. (3.2.52).

[41] A generalisation of the system of balance equations for the *multimode* case has been carried out in [106]; see also [4].

Steady-state Solutions of the System of Balance Equations. In order to consider the *stationary* case, we get

$$dm/dt' = 0; \quad dn/dt' = 0; \quad dn_a/dt' = 0.$$

The system of equations (3.7.26) then assumes the form

$$\left.\begin{aligned} &m(n+n_a-1)=0;\\ &n=\alpha/(1+m);\\ &n_a=\alpha_a/[1+(\rho/\delta)\,m]. \end{aligned}\right\} \tag{3.7.27}$$

It can be easily seen that this system has three solutions:

$$(A)\ m_A=0; \quad n_A=\alpha; \quad n_{aA}=\alpha_a; \tag{3.7.28}$$

$$\left.\begin{aligned} &(B)\ m_B=(1/2)\left[\Phi+\sqrt{\Phi^2+4(\delta/\rho)(\alpha+\alpha_a-1)}\,\right],\\ &\text{where } \Phi=\alpha-1+(\delta/\rho)(\alpha_a-1);\\ &n_B=\alpha/(1+m_B);\\ &n_{aB}=\alpha_a/[1+(\rho/\delta)\,m_B]; \end{aligned}\right\} \tag{3.7.29}$$

$$\left.\begin{aligned} &(C)\ m_C=(1/2)\left[\Phi-\sqrt{\Phi^2+4(\delta/\rho)(\alpha+\alpha_a-1)}\,\right];\\ &n_C=\alpha/(1+m_C);\\ &n_{aC}=\alpha_a/[1+(\rho/\delta)\,m_C]. \end{aligned}\right\} \tag{3.7.30}$$

The solution (3.7.28) describes the steady state which is usually the *initial* one. In this state, there is no generation ($m_A = 0$), the active element is characterised by a high value of the inverse population density ($n_A = \alpha$), and the filter is in the unbleachable state ($n_{0A} = \alpha_a$). The *generation* may be described by either of the solutions (3.7.29) and (3.7.30), but it is essential that the value of m_B (or m_C) obtained from (3.7.29) (or (3.7.30)) must have a physical meaning, i.e. must be *real* and *nonnegative*:

$$\mathrm{Im}\{\bar{m}\}=0; \quad \bar{m}\geqslant 0. \tag{3.7.31}$$

Here, $\bar{m}$ represents any steady-state solution for the field intensity, having a physical sense.

It is very important to examine the solutions (3.7.28)-(3.7.30) from the point of view of *stability*. It should be recalled that if a state is non-stationary even slight fluctuations in the value of m (as well as in the values of n and n_a) may irreversibly remove the system from a given state, while in the steady state, the system will always return to the state under consideration. In order to examine the stability of a certain stationary state ($\bar{m}$, $\bar{n}$, $\bar{n}_a$), we put

$$m=\bar{m}+\Delta m, \quad n=\bar{n}+\Delta n, \quad n_a=\bar{n}_a+\Delta n_a, \tag{3.7.32}$$

where Δm, Δn, and Δn_a are small deviations of the respective quantities from their stationary values. Substituting (3.7.32) into (3.7.26),

we consider that $\bar{m}$, $\bar{n}$, and $\bar{n}_a$ satisfy the system of equations (3.7.27), and neglect products of the type $\Delta m \Delta n$ as quantities having a second order of smallness. Consequently, we get the following system of *linear* differential equations for functions $\Delta m\,(t')$, $\Delta n\,(t')$, and $\Delta n_a\,(t')$[42]:

$$\left.\begin{aligned} d\,\Delta m/dt' &= G(\bar{n}+\bar{n}_a-1)\,\Delta m + G\bar{m}\,\Delta n + G\bar{m}\,\Delta n_a;\\ d\,\Delta n/dt' &= -\bar{n}\,\Delta m - (\bar{m}+1)\,\Delta n;\\ d\,\Delta n_a/dt' &= -\bar{n}_a\rho\,\Delta m - (\rho\bar{m}+\delta)\,\Delta n_a. \end{aligned}\right\}$$

Characteristic equation corresponding to this system of linear differential equations may be written in the form

$$\begin{vmatrix} G(\bar{n}+\bar{n}_a-1)-p & G\bar{m} & G\bar{m}\\ -\bar{n} & -(\bar{m}+1)-p & 0\\ -\bar{n}_a\rho & 0 & -(\rho\bar{m}-\delta)+p \end{vmatrix} = 0. \tag{3.7.33}$$

This is a third-order algebraic equation, whose roots can be given as p_1, p_2, and p_3. If the *real* parts of all these roots are *negative*, the state $(\bar{m}, \bar{n}, \bar{n}_a)$ is *stationary*. If even one of the roots has a positive real part, the state under consideration will be non-stationary [87].

It should be emphasized that under certain conditions (for certain values of the parameters G, ρ, δ, α, and α_a), both stationary oscillation states (3.7.29) and (3.7.30) are unstable. This means that even for *stationary pumping* and *stability* of parameters of the active element, filter, and resonator, the oscillations in a laser with a bleachable filter may be *non-stationary*. In other words, the presence of a bleachable filter inside a resonator may lead to instability of stationary oscillations.

Instability of Initial Stationary State and the Condition for Self-excitation of Generation in a Bleachable Filter Laser. The question of stability (instability) of an initial stationary state (3.7.28) is of utmost importance for exploring the possibility of self-excitation of oscillations in a bleachable filter laser. Let us suppose that the state (3.7.28) is stable. In this case the fluctuations in the density of the field and the inverse population density cannot lead to laser action. Irrespective of the increase in the pumping intensity, the filter laser invariably remains close to the initial state (3.7.28). In other words, the stability of the state (3.7.28) means that the

[42] The procedure followed here is called *linearisation* of a system of nonlinear equations in the neighbourhood of a steady-state solution. Such a procedure was adopted earlier (in Sec. 3.3) while considering free generation.

pumping of the active element by itself (without any additional influence on the system) cannot cause generation in a bleachable filter laser. In order for generation *to occur* during pumping of the active element, the state (3.7.28) must be *unstable.*

The characteristic equation (3.7.33) assumes the following form for the state (3.7.28):

$$\begin{vmatrix} G(\alpha+\alpha_a-1)-p & 0 & 0 \\ -\alpha & -1-p & 0 \\ -\alpha_a\rho & 0 & -\delta-p \end{vmatrix} = 0$$

or,

$$[G(\alpha+\alpha_a-1)-p](-1-p)(-\delta-p)=0. \qquad (3.7.34)$$

The roots of this equation are given by

$$p_1 = G(\alpha+\alpha_a-1); \quad p_2=-1; \quad p_3=-\delta. \qquad (3.7.35)$$

All these roots are *real*, p_2 and p_3 being *negative.* It follows from this that the question about stability (instability) of the state (3.7.28) is connected with the negative (positive) value of the root p_1. This state will be *unstable* if the root is *positive*, i.e. if

$$\boxed{\alpha > (-\alpha_a+1).} \qquad (3.7.36)$$

The condition (3.7.36) is the *necessary condition for self-excitation* of oscillations in a bleachable filter laser. It should be noted that in the absence of a filter, the condition (3.7.36) is transformed into the generation condition (3.2.54).

Let us now consider the physical significance of the condition (3.7.36). Using (3.7.23), this condition can be rewritten in the form $\sigma N_0 > [\varkappa_{0a}(l_a/l) + (1/\mu v T)]$, or, if we take (3.7.15) into account, in the form

$$\boxed{\sigma N_0 > \left(\varkappa_{0a}\frac{l_a}{l}+\eta_1+\eta_{1a}\frac{l_a}{l}+\eta_2\right).} \qquad (3.7.37)$$

The product σN_0 is the initial gain $\varkappa_0$. Consequently, the condition (3.7.37) is just the familiar condition (2.1.10) for a bleachable filter laser. This condition means that for self-excitation of oscillations, it is essential that the initial gain should exceed the loss level, which in this case is the sum of the initial coefficient of resonant absorption of the filter, the coefficients of unfavourable losses in the active element and the filter, and the coefficient of favourable losses connected with the extraction of radiation through the resonators. The coefficients related to the filter are taken per unit length of the active element, i.e. are multiplied by l_a/l.

Generation by Soft and Hard Excitation. The condition $\mathrm{Im}\{\bar{m}\} = 0$ (see (3.7.31)) means that the inequality

$$\{[\alpha - 1 + (\delta/\rho)(\alpha_a - 1)]^2 + 4(\delta/\rho)(\alpha + \alpha_a - 1)\} \geqslant 0 \quad (3.7.38)$$

must be satisfied. Together with the requirement $\bar{m} \geqslant 0$, the inequality (3.7.38) defines the conditions under which generation is possible in a bleachable filter laser. Significantly, these conditions are *less rigid* than the conditions defined by the inequality (3.7.36).

In Fig. 3.40, three regions marked as I, II, and III are isolated in the (α, α_a) plane (only the negative values of the parameter α_a and positive values of the parameter α are considered). The straight line *1* in the figure satisfies the equation

$$\alpha + \alpha_a - 1 = 0, \quad (3.7.36a)$$

while the broken curve *2* satisfies the equation

$$[\alpha + 1 + (\delta/\rho)(\alpha_a - 1)]^2 + 4(\delta/\rho)(\alpha + \alpha_a - 1) = 0. \quad (3.7.38a)$$

The point C has coordinates

$$\alpha' = (1 - \delta/\rho)^{-1}; \quad \alpha_a' = -(\delta/\rho)(1 - \delta/\rho)^{-1}. \quad (3.7.39)$$

This is the tangency point for the straight line *1* and the curve *2*.

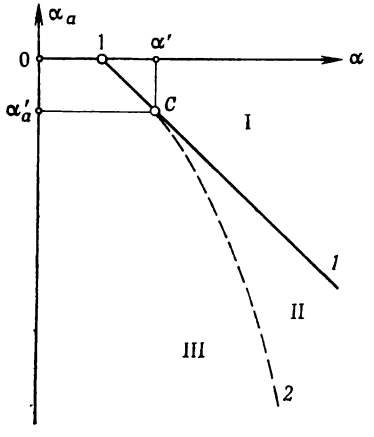


Fig. 3.40

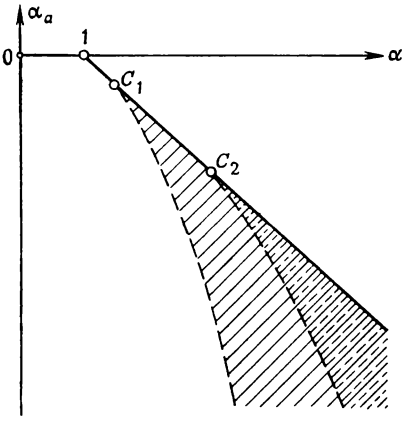


Fig. 3.41

The condition (3.7.36) is satisfied in the region I in Fig. 3.40. This is the region of *self-excitation of generation* in a laser with a filter. In region III, the condition (3.7.38) and the additional requirement $\bar{m} \geqslant 0$ are not satisfied (i.e., the conditions (3.7.31) are not satisfied in the region III). This is the region in which generation is *generally impossible* in a filter laser. In region II, generation is possible but self-excitation is impossible. In this case, in order to induce generation,

it is necessary *to irradiate the filter* by radiation from an auxiliary source like an additional laser, besides pumping the active element. Such a method of inducing generation is called *hard excitation*, while the term *soft excitation* is used for the self-excitation. Thus, the regions I, II, and III shown in Fig. 3.40 are regions of generation by soft excitation, generation by hard excitation, and no generation respectively. The straight line *1* is called the *threshold line* while the curve *2* is called the *boundary curve.*

The necessary condition for the existence of the hard excitation generation region is given by

$$\delta/\rho < 1. \tag{3.7.40}$$

The lower the ratio δ/ρ, the larger the region of generation by hard excitation. This is illustrated in Fig. 3.41. The point C_1 in the figure corresponds to the case when $\delta/\rho \ll 1$; this region of generation by hard excitation is shaded by continuous lines. As δ/ρ increases (i.e. as this ratio approaches unity), the point C_1 moves downwards along the straight line $\alpha + \alpha_a - 1 = 0$, and goes to infinity for $\delta/\rho = 1$. The figure shows another point, C_2, with a somewhat higher ratio δ/ρ than for the point C_1. The corresponding region of generation by hard excitation is shaded by alternating continuous and broken lines.

Stability (instability) of Stationary States for Generation by Soft Excitation. If the condition of generation by soft excitation (condition (3.7.36)) is satisfied, we get $\Phi < \sqrt{\Phi^2 + 4(\delta/\rho)(\alpha+\alpha_a-1)}$, and hence $m_B < 0$. This means that in the region of generation by soft excitation only the stationary solution (3.7.29) is possible (in the region of generation by hard excitation, both solutions (3.7.29) and (3.7.30) are possible).

The stability of solutions (3.7.29) and (3.7.30) has been examined by a number of authors (see, for example, [7, 104, 105], as well as [2, 4]). We shall now give some results of these investigations, confining ourselves to the case of generation by *soft* excitation. (This requires a consideration of the solution (3.7.29)[43] only.)

It can be shown that the straight line

$$\alpha + \rho\delta\alpha_a = 0 \tag{3.7.41}$$

isolates the region in the (α, α_a) plane where the solution (3.7.29) is stable in all cases. This region is called the *absolute stability* region, and is situated above the straight line (3.7.41). Below this straight line, unstable stationary states (3.7.29) are *possible.*

If $\rho\delta < 1$, the straight lines $\alpha + \rho\delta\alpha_a = 0$ and $\alpha + \alpha_a - 1 = 0$ do not intersect (in the region of negative values of the parameter α_a)—see Fig. 3.42*a*. The region shaded by continuous lines marks

[43] It should be noted that the solution (3.7.30) is always unstable. Hence an analysis of the stability of stationary oscillations in any case is reduced to an analysis of the stability of the solution (3.7.29).

the boundary of the region of absolute stability while the dashed lines mark the boundary of the region of generation by soft excitation (self-excitation). In this case, the region of generation by self-excitation is entirely *within* the region of absolute stability.

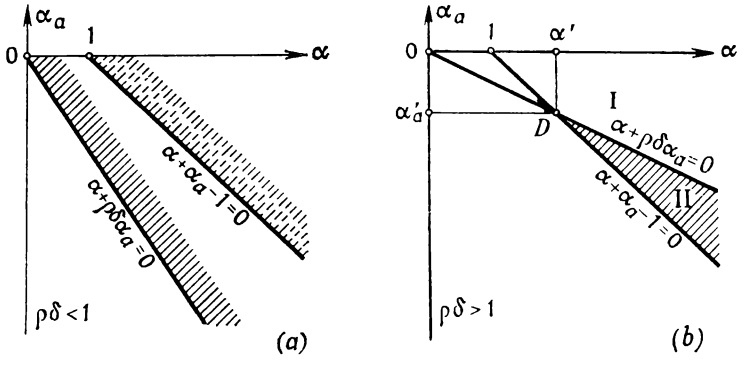


Fig. 3.42

A more interesting (and practically more important) situation arises when

$$\rho\delta > 1. \tag{3.7.42}$$

In this case, the straight lines $\alpha + \rho\delta\alpha_a = 0$ and $\alpha + \alpha_a - 1 = 0$ intersect (Fig. 3.42*b*). The point of intersection D has coordinates

$$\alpha' = \rho\delta/(\rho\delta - 1); \quad \alpha'_a = -1/(\rho\delta - 1). \tag{3.7.43}$$

In this case an *overlapping* of the regions of self-excited generation and instability is possible. Region I in Fig. 3.42*b* is the region where self-excitation and absolute stability are combined. In region II (shown shaded in the figure), *self-excitation* may exist together with the *instability of stationary oscillations.* In order to specify the condition of instability it is convenient to consider separately the cases $\rho \gg \delta$, $\rho \approx \delta$, and $\rho \ll \delta$.

If $\rho \gg \delta$, the stationary solution (3.7.29) may be

$$m_B = \alpha - 1; \quad n_B = 1; \quad n_{aB} = \delta\alpha_a/\rho\,(\alpha - 1). \tag{3.7.44}$$

Substituting these values in the characteristic equation (3.7.33) we arrive at the following *instability condition*:

$$-\alpha_a > (\rho/G\delta)\,\alpha\,(\alpha - 1), \tag{3.7.45}$$

isolating a certain region of instability within the region II in Fig. 3.42*b* (this region of instability is not shown in the figure).

If $\rho \ll \delta$, the stationary solution (3.7.29) may be written in the form

$$m_B = \frac{\alpha + \alpha_a - 1}{1 - \alpha_a}; \quad n_B = 1 - \alpha_a; \qquad n_{aB} = \alpha_a \left(1 - \frac{\rho}{\delta} \frac{\alpha + \alpha_a - 1}{1 - \alpha_a}\right). \tag{3.7.46}$$

In this case, the *instability condition* for stationary oscillations has the form

$$-\alpha_a > \delta\alpha/G\rho\ (\alpha - 1). \tag{3.7.47}$$

If $\rho \approx \delta$, the stationary solution (3.7.29) is given by the relations

$$m_B = \alpha + \alpha_a - 1; \quad n_B = \alpha/(\alpha + \alpha_a); \quad n_{aB} = \alpha_a/(\alpha + \alpha_a). \tag{3.7.48}$$

This leads to the following *instability condition*:

$$-\alpha_a > \alpha/\rho\delta. \tag{3.7.49}$$

This inequality may be written in the form

$$\alpha + \rho\delta\alpha_a < 0.$$

Hence the instability region of stationary oscillations in this case is identical to the region II shaded in Fig. 3.42*b*.

Generation in a Bleachable Filter Laser. First of all, it must be remarked that two types of generation are possible—by *soft* excitation, and by *hard* excitation. In the latter case, an external illumination source is needed for additional bleaching of the filter. Generation by hard excitation is possible only for $\delta < \rho$.

If the condition (3.7.42) is satisfied, i.e. if $\rho\delta > 1$, it is advisable to isolate two regions in the (α, α_a) plane, shown in Fig. 3.42*b* as regions I and II. If the parameters α and α_a are in region I, the generation (by soft excitation) will be attained in the following manner: oscillations are self-excited as soon as the pumping increases the inverse population density n in the active element to its threshold value $(-\alpha_a + 1)$. The instant t' of the beginning of generation is thus described by the relation

$$n\ (t') = -\alpha_a + 1. \tag{3.7.50}$$[44]

If certain conditions are satisfied (these conditions will be discussed in the following section), the generation will be of *single pulse* type, and a *giant pulse* will be emitted. Periodic generation of giant pulses is obtained in this case for stationary pumping. If the conditions for giant pulse generation are not satisfied, *damped pulses* of radiation may arise, resulting in stationary oscillations.

[44] In the absence of a filter, the expression (3.7.50) is converted into the familiar relation $n\ (t') = 1$; see, for example, (3.3.28).

Suppose that parameters α and α_a are inside region II shown in Fig. 3.42*b*, being in the *instability* region of stationary oscillations. As in the previous case, oscillations are self-excited as soon as the pumping ensures that the condition (3.7.50) is satisfied. The generation has a specific nature, which is connected with the instability of stationary oscillations. In this case, *undamped* radiation *pulses* as well as *giant pulses* may be emitted.

3.8. GIANT PULSE GENERATION FOR PASSIVE *Q*-MODULATION OF THE RESONATOR

Among the various methods of *passive* Q-modulation in a resonator, let us isolate the methods based on the application of bleachable filters. The bleachable filter lasers have been discussed in the previous section. We shall now consider the conditions which ensure *giant pulse generation* in such lasers, and discuss the nature of this process.

Conditions for Ensuring Giant Pulse Generation in a Bleachable Filter Laser. Giant pulse generation presumes a large value for the coefficient of resonant absorption $\varkappa_{0a}$ in the filter (for small values of $\varkappa_{0a}$, a bleaching of the filter leads to a small increase in Q). Since, in accordance with (3.7.5), $\varkappa_{0a} = \sigma_a n_a'$, an increase in the coefficient $\varkappa_{0a}$ means an increase in the density of absorbing centres n_a', and in the cross section σ_a of induced transitions in the filter. In terms of dimensionless parameters, an increase in the initial resonant absorption coefficient of the filter means an increase in the parameter $|\alpha_a|$. It is obvious, however, that an inordinate increase in $|\alpha_a|$ cannot be permitted, since this would lead to a breakdown of the condition (3.7.36) of self-excitation of oscillations, which can be written in the form

$$|\alpha_a| < (\alpha - 1). \tag{3.8.1}$$

We must set the standards by which the quantity $|\alpha_a|$ should be large. To begin with, the peak power of a giant pulse is several orders of magnitude higher than the peak power of a free generation spike. This means that the increase in the initial inverse population density over the threshold value corresponding to the bleached filter (i.e. the quantity $|\alpha_a|$) must be several orders of magnitude higher than the quantity ν_{max} encountered first in Sec. 3.3 during a discussion of free generation. Using (3.3.40), we arrive at the following inequality:

$$|\alpha_a| \gg \sqrt{(\alpha-1)/G}\,. \tag{3.8.2}$$

Combining (3.8.1) and (3.8.2), we get the *necessary condition for self-excitation* of a giant pulse:

$$\sqrt{(\alpha-1)/G} \ll |\alpha_a| < (\alpha-1). \tag{3.8.3}$$

It should be recalled that for a ruby laser, $\alpha = 30$, $G = 10^5$, so that the condition (3.8.3) assumes the form $0.01 \ll |\alpha_a| < 30$. For

an Nd-activated laser, $\alpha = 2$, $G = 10^4$. In this case, the condition (3.8.3) can be written as $0.01 \ll |\alpha_a| < 1$. Thus, in order that the condition (3.8.3) be satisfied for the cases considered here, it is necessary that

$$|\alpha_a| \approx 1. \tag{3.8.4}$$

It is well known that a high speed of Q-switching is necessary for giant pulse generation. In the present case, it means that the filter should be bleached quite rapidly, i.e. the derivative dn_a/dt' should be high. The sufficient condition for this derivative to be high is given, as can be easily seen from (3.7.26), by

$$\rho \gg 1 \tag{3.8.5}$$

or,

$$\sigma_a \gg \sigma. \tag{3.8.6}$$

Thus, the cross section of induced transitions in the filter must be *considerably higher* than the cross section of induced transitions in the active element. A value of $\rho \approx 10^4$ is normally attained in actual practice.

The condition (3.8.5) (or (3.8.6)) together with the condition (3.8.3) determines the basic requirements imposed on the parameters of a "bleachable filter laser", which are necessary for self-excitation of a giant pulse.

It should be noted that an important case from the application point of view when the inequality (3.7.42) is satisfied, in conjunction with (3.8.5) means that the following inequality holds:

$$\delta < 1 \tag{3.8.7}$$

or, otherwise,

$$T_1 < T_{1a}, \tag{3.8.8}$$

which is the same as

$$(w_p + 1/\tau) > 1/T_{1a}. \tag{3.8.9}$$

This means that the relaxation probability in a filter is usually less than the sum of the probabilities of pumping and relaxation in the active element. In other words, relatively *slowly relaxing* bleaching filters are normally used. Only in such filters can the highest degree of bleaching be realised.

Giant Pulse Growth in a Bleachable Filter Laser. The instant of beginning of generation is the instant of time when the relation (3.7.50) is satisfied, i.e. the instant when the generation condition is satisfied for a resonator with an unbleached filter. As for the case of active Q-modulation, the process of giant pulse generation may be divided into two stages—the long stage of *linear* growth of oscillations (having a duration t_0) and the brief stage of *nonlinear* growth of oscillations (having a duration t_1). (In this connection, see Fig. 3.4 and the remarks made in Sec. 3.1.) It should be recalled

that $t_0 \approx 10^3 - 2 \times 10^3$ nsec, which is an order of magnitude *higher* than the duration of the linear stage for active modulation, and $t_1 \approx 10$-30 nsec, which is in accordance with the duration of the nonlinear stage for active modulation.

The stage of linear growth of oscillations is marked by the amplification of primary luminescence. This process corresponds to the growth of a free generation spike at constant losses corresponding to an unbleached filter. The resonant absorption coefficient of the filter and the inverse population density in the active element remain practically unchanged over this stage. The intensity of radiation increases at this stage according to a nearly exponential

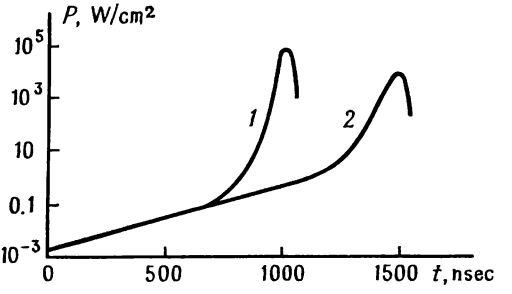


Fig. 3.43

law, increasing from values of the order of 10^{-4} W/cm^2 at the beginning of this stage to values of the order of 1-10 W/cm^2 at the end of the stage.

The *duration of the linear stage* depends to a considerable extent on the magnitude of the parameter ρ as well as on $\varkappa_{0a}$, the absorption coefficient of the filter in the unbleached state. A decrease in ρ without any change in the parameters of the active medium is connected with a decrease in the cross section σ_a of induced transitions in the filter. In accordance with (3.7.8), a decrease in σ_a leads to an increase in S_{thr}. Thus, a higher radiation density is required for bleaching the filter in the case of a decrease in the value of the parameter ρ. Consequently, a longer stage of linear growth of oscillations is necessary. Figure 3.43 shows the experimental curves [6] indicating the growth of a giant pulse in a ruby laser using two different filters: *1* is a filter based on a solution of chlorinated gallium phthalocyanine in chlorobenzene ($\rho = 1.6 \times 10^4$), while *2* is a filter based on a solution of chlorinated aluminium phthalocyanine in ethanol ($\rho = 0.8 \times 10^4$). In the first case, the duration of the linear stage of growth of oscillations is equal to 10^3 nsec, and in the second case, it is equal to 1.5×10^3 nsec.

With increasing absorption coefficient $\varkappa_{0a}$, the magnitude of $|\alpha_a|$ increases, and in accordance with (3.7.50), the initial inverse

population density in the active element, at which the generation begins, also increases. The higher this inverse population density, the faster the growth of the linear stage of oscillations, and hence the shorter the duration of this stage. Figure 3.44 shows an experimental curve [6] illustrating a decrease in time t_0 with increasing $\varkappa_{0a}$. The initial transmission T_0 of the filter, defined in terms of $\varkappa_{0a}$ and l_a through the formula $T_0 = \exp(-\varkappa_{0a} l_a)$, is plotted along the abscissa axis.

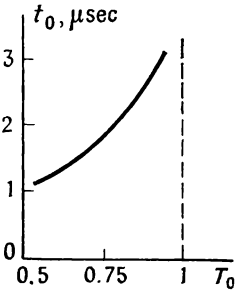


Fig. 3.44

Balance Equations; Analogy with the Case of Instantaneous Q-switching.[45] Taking into account the comparatively short duration of the giant pulse growth stage,[46] we can neglect, as in the case of active Q-modulation (see Sec. 3.6), the pumping and relaxation processes in the active element (and the filter) in the balance equations. Consequently, the system of *balance equations* in the dimensionless form (3.7.26) may be written as follows:

$$\boxed{\begin{aligned} dm/dt' &= Gm(n + n_a - 1); \\ dn/dt' &= -nm; \\ dn_a/dt' &= -n_a \rho m. \end{aligned}} \qquad (3.8.10)$$

Dividing the third equation in (3.8.10) by the second, we get

$$dn_a/dn = \rho n_a/n,$$

or,

$$dn_a/n_a = \rho dn/n. \qquad (3.8.11)$$

Let us integrate Eq. (3.8.11) from the moment of beginning of generation to a certain arbitrary instant of time. At the moment of beginning of generation, $n_a = \alpha_a$, $n = 1 - \alpha_a$ (see (3.7.50)). Hence we get

$$\int_{\alpha_a}^{n_a} \frac{dn_a}{n_a} = \rho \int_{1-\alpha_a}^{n} \frac{dn}{n}.$$

From this, it follows that

$$n_a = \alpha_a (n/n_1)^\rho, \text{ where } n_1 = 1 - \alpha_a. \qquad (3.8.12)$$

[45] The giant pulse generation in a single-mode filter laser is considered, for example, in [2, 107-109].

[46] This duration, even if we take into account the stage of linear growth, is approximately 10^{-6} sec, which is considerably lower than T_1, and even more so than T_{1a} (it should be recalled that $T_1 = 10^{-3}$-10^{-4} sec).

Using the result (3.8.12), we eliminate n_a from Eqs. (3.8.10). This leads to the following balance equations:

$$\left.\begin{aligned} dm/dt' &= Gm\,[n+\alpha_a\,(n/n_1)^{\rho}-1]; \\ dn/dt' &= -mn. \end{aligned}\right\} \qquad (3.8.13)$$

From Eqs. (3.8.13), we can easily obtain an equation for phase trajectories in a giant-pulse laser with a bleachable filter. Dividing the first equation in (3.8.13) by the second, we get

$$\frac{dm}{dn} = -G\,\frac{n+\alpha_a\,(n/n_1)^{\rho}-1}{n}. \qquad (3.8.14)$$

Integration of this equation leads to

$$\int_{m_1}^{m} dm = -G\int_{n_1}^{n} dn\left[1+\frac{\alpha_a}{n_1^{\rho}}\,n^{\rho-1}-\frac{1}{n}\right].$$

Consequently, we get the following equation for *phase trajectories*:

$$m = m_1 + G\left(n_1 - n - \ln\frac{n_1}{n} + \frac{\alpha_a}{\rho}\,\frac{n_1^{\rho}-n^{\rho}}{n_1^{\rho}}\right). \qquad (3.8.15)$$

Let us compare Eq. (3.8.15) with Eq. (3.6.11) for the phase trajectories of a laser upon *instantaneous Q-switching*. The only difference between these two equations is that there is an additional term $\alpha_a\,(n_1^{\rho} - n^{\rho})/\rho n_1^{\rho}$ within the brackets in the right-hand side of the equation in the case of a filter. If the condition (3.8.5) is satisfied, this term may be neglected by taking into account Eq. (3.8.4). Consequently, we arrive at the phase portrait of a laser, shown in Fig. 3.30. We find that the condition (3.8.5) really ensures an "instantaneous" Q-switching in a laser with a bleachable filter.

Starting with the established *analogy with the case of instantaneous Q-switching*, we use the relation (3.6.12) in order to express the *peak* value $m_{\max}$ of the field intensity. Considering that $n_1 = 1 - \alpha_a$, we get from (3.6.12),

$$m_{\max} = G\,[-\alpha_a - \ln(1-\alpha_a)]. \qquad (3.8.16)$$

According to (3.8.4), $1 - \alpha_a \approx 2$, which is close to the value $n_1 = 3.5$ used in Sec. 3.6 while discussing active Q-modulation. Hence it is not surprising that the energy characteristics of giant pulses, obtained for active and passive Q-modulation turn out to be quite similar.

Comparison Between Giant Pulse Generation for Active and Passive *Q*-switching; Combined *Q*-switching. We have mentioned above a certain analogy between these two generation processes. In both cases, the giant pulse has a relatively long stage of linear growth of generation, over which the inverse population density remains

practically unchanged, and a short stage of nonlinear growth of generation during which the main part of the energy contained in the giant pulse is emitted. In both cases, the giant pulses have quite similar parameters like the pulse duration (determined by the duration of the nonlinear stage), the peak power, and energy. In balance equations for a bleachable filter laser, a nearly complete analogy is observed with the case of rapid (instantaneous) Q-switching for $\rho \gg 1$.

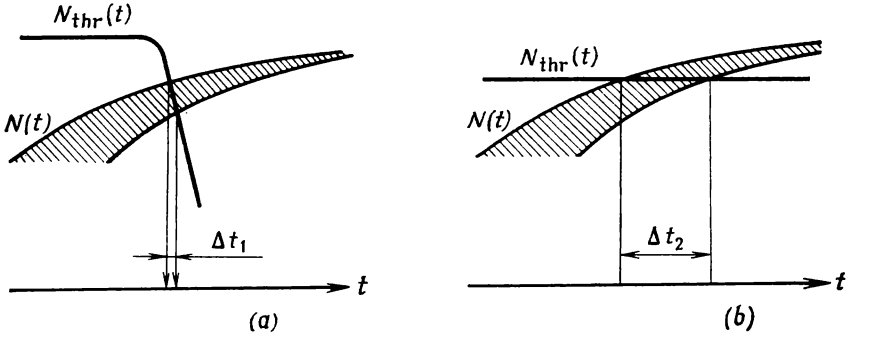


Fig. 3.45

At the same time, each giant pulse generation has its own *specific nature*. For *active Q-switching*, generation starts at the instant when the threshold inverse population density is reduced to the inverse population density caused by pumping at this moment. It should be recalled that $N_{thr}(t) = 1/B\hbar Q(t)$. By controlling the time variation of the Q-factor, we can also control the time variation of the generation threshold N_{thr} and thus fix fairly accurately the moment of the beginning of generation with respect to the external signal, within 10 nsec for electrooptical shutters and up to 100 nsec for mechanooptical shutters with a rotating prism.

The generation of giant pulse for *passive Q-switching* starts at the moment of time when the inverse population density caused by pumping increases gradually up to its threshold value determined by the losses in a resonator with an unbleached filter. This threshold value is determined by the relation (3.7.50):

$$N_{thr} = \frac{l_a}{l}\frac{\sigma_a}{\sigma}n_a' + \frac{\eta_1 + (l_a/l)\,\eta_{1a} + \eta_2}{\sigma}. \qquad (3.8.17)$$

In this case, the moment of beginning of generation can be changed by merely controlling the time variation of the pumping intensity. The moment of beginning of generation cannot be fixed, however, in this case with an arbitrary degree of accuracy. The time of beginning of generation, measured from the moment of switching on

the pumping lamp, strongly varies from flash to flash (from pulse to pulse), the fluctuation may be as high as 10^{-5}-10^{-4} sec.

These remarks are illustrated in Fig. 3.45. Suppose that the N vs. t curve, rising in the process of pumping, fluctuates from flash to flash within the area shown shaded in the figure. Figure 3.45*a* shows the intersection of the functions $N(t)$ and $N_{thr}(t)$ for active Q-switching (for a rapid Q-switching to a higher value), while 3.45*b* refers to the passive Q-switching. In the first case the time variation of the generation threshold is controllable, while in the second case, the generation threshold does not vary with time. It can be easily seen that the interval over which the moments of beginning of generation are spread for passive Q-switching is much wider than for active Q-switching: $\Delta t_2 \gg \Delta t_1$.

In order to fix more accurately the moment of beginning of generation and to improve the reproducibility of the processes in time, *combined Q-switching* is used, i.e. a bleachable filter and an active Q-switching are simultaneously used. As a rule, the presence of a bleachable filter increases the speed of Q-switching, and improves the radiation parameters. The active type switch fixes the moment of beginning of generation and facilitates an ordering of the appearance of pulses from flash to flash. By way of a specific example, Table 3.4 contains data on parameters of a giant pulse in a ruby laser for three different cases [6]. It can be seen that combined Q-switching in this case increases the energy and the peak power of the pulse and decreases its duration.

TABLE 3.4

Type of switching	Energy, J	Duration, nsec	Power, MW
Active Q-switching with rotating prism	0.35	43	8
Passive Q-switching with phthalocyanine dye	0.4	20	20
Combination Q-switching	0.6	16	37

It has been mentioned above that for passive Q-switching, the duration of the stage of linear growth of oscillations is nearly an order of magnitude higher than for active Q-switching. This is due to the fact that for *active Q-switching* generation over the linear stage grows practically under the conditions of *low losses in the resonator* (in the case of a rapid Q-switching), while for *passive Q-switching* the generation over the linear stage is accompanied by *high losses.* The difference between these two processes of giant pulse generation is clearly illustrated in Fig. 3.46 where the M vs. t and N_{thr} vs. t dependences are compared for each process (*a* represents the active

modulation for a rapid Q-switching to a higher value, while b represents the passive modulation). Physically, it is clear that a rapid decrease of losses in the case of active Q-switching facilitates (accelerates) the growth of oscillations. This is reflected in a decrease (in comparison to the case of passive Q-switching) in the duration of the linear stage.

Figure 3.47 shows the experimental curves for the time dependence of the radiation power for active (curve *1*) and passive (curve *2*) Q-switching in a ruby laser [6]. The time is measured from the moment the generation starts, and a logarithmic scale has been

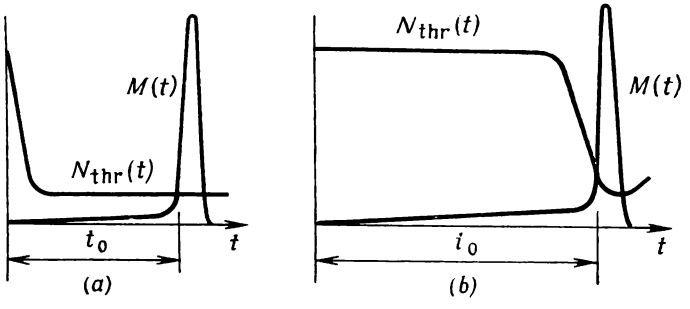


Fig. 3.46

chosen for plotting the power. It is apparent from the figure that an increase in the duration of the linear stage for passive Q-switching leads to an increase in the level of power from which the giant pulse growth starts in the nonlinear stage. This level is about three orders of magnitude higher than for the case of active Q-switching.

Natural Selection of Longitudinal Modes for Passive Q-Switching. By considering the model of a *multimode* laser [106, 110], it can be shown that a *strong competition* between different modes arises as a result of the comparatively long stage of linear growth of oscillations in a laser with a bleachable filter. Consequently, some modes are damped, while some others are amplified and reach the stage of nonlinear growth of oscillations. It has been shown [110] that a relative difference of just 10^{-3} in the Q-factor for two modes may result in the intensity difference between these two modes of about an order of magnitude at the beginning of bleaching of the filter, for a 2×10^3 nsec duration of the linear stage. Thus, even an insignificant random difference in Q-factors may lead to a sharp amplification of individual modes.[47]

[47] It has been mentioned more than once that laser radiation has a *fluctuation origin*, since the primary radiative processes are spontaneous processes. One of the peculiarities of bleachable filter lasers is that the fluctuation nature of laser radiation is sharply manifested in them.

The competition between different modes, which manifests itself at the stage of linear growth leads to a considerable decrease in the number of modes conserved in the radiation field at the beginning of bleaching of the filter. The number of modes conserved is found to be an order of magnitude lower than the number of modes existing at the moment when generation starts[48]. In this connection, the effect of *natural selection* of longitudinal modes for passive Q-switching is said to take place.

This effect takes place upon a significant *narrowing of the generation spectrum* of the laser (since the modes situated near the centre of the gain curve are predominantly conserved). Figure 3.48 shows the dependence of the effective width of the generation spectrum

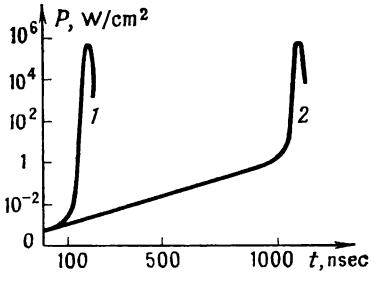


Fig. 3.47

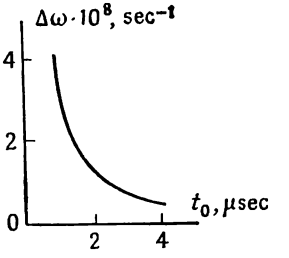


Fig. 3.48

on the duration of the stage of linear growth of generation [6]. The longer the duration of the linear stage, the stronger the effect of natural selection of longitudinal modes and, hence, the narrower the generation spectrum. That is why the generation spectrum of a laser for passive Q-switching is found to be considerably narrower than for active Q-switching.

3.9. LONGITUDINAL MODE LOCKING (ULTRASHORT LIGHT PULSE GENERATION)

Phase locking of longitudinal modes in a laser helps in creating pulses of duration 10^{-2}-10^{-3} nsec with a peak power up to 10^{12} W, i.e. the *ultrashort light pulses*[49].

Following the publication of the fundamental work by De Maria *et al.* [34] in 1966, investigations of longitudinal mode locking have been intensified steadily. A detailed analysis of these questions has been given in [38, 39, 111-113].

[48] According to the estimates given in [39], the number of longitudinal modes in an Nd-laser decreases from 3×10^4 to 6×10^2.

[49] It should be recalled that general remarks about the generation of ultrashort pulses were made in Sec. 3.1; some numerical data have also been given there.

Basic Ideas Behind Longitudinal Mode Locking. The simplest idea concerning the longitudinal mode locking may be explained as follows. Let us suppose that m longitudinal modes have been excited in a resonator, and the following two conditions are satisfied: firstly, the modes are *equidistant*, i.e. the difference between the frequencies of two successive modes is constant (we denote this frequency difference by Ω); secondly, the modes are *phase-locked*, i.e. the phase difference between two successive modes is constant (we denote this phase difference by Φ). We number all modes in order of increasing frequency using the integral index k which assumes the values $-(m-1)/2$, $-(m-1)/2+1$, $-(m-1)/2+2$, ..., $(m-1)/2$ (it is assumed that m is odd, although this is not essential). The mode with index $k=0$ is called the central mode, and we denote its frequency and phase by ω_0 and φ_0 respectively (this mode lies at the centre of the gain curve). The frequency and phase of any arbitrarily chosen k-th mode may then be written in the form

$$\omega_k = \omega_0 + k\Omega; \quad \varphi_k = \varphi_0 + k\Phi. \tag{3.9.1}$$

Using (3.9.1), we get the following simplified expression for the resonator field (considering just the time dependence):

$$E(t) = \sum_{k=-(m-1)/2}^{(m-1)/2} E_k \exp[i(\omega_0 + k\Omega)t + i(\varphi_0 + k\Phi)]. \tag{3.9.2}$$

For the sake of simplicity, we shall assume that $E_k = E_0$ for all k. (This is not true in actual practice, since the initial gain depends on frequency. However, this assumption does not alter the basic aspects of the problem.) In this case, the relation (3.9.2) may be written in the form

$$E(t) = E_0 G(t) \exp[i(\omega_0 t + \varphi_0)], \tag{3.9.3}$$

where, as can be easily seen, the function

$$G(t) = \sum_{k=-(m-1)/2}^{(m-1)/2} \exp[ik(\Omega t + \Phi)] \tag{3.9.4}$$

is the sum of m terms of the geometric progression with a common ratio $q = \exp[i(\Omega t + \Phi)]$ and the first term $a_1 = \exp[-i(m-1) \times \times (\Omega t + \Phi)/2]$. Using the formula for the sum of a geometric progression, we get

$$G(t) = a_1 \frac{q^m - 1}{q - 1}$$

$$= \exp\left[-i\frac{m-1}{2}(\Omega t + \Phi)\right] \frac{\exp[im(\Omega t + \Phi)] - 1}{\exp[i(\Omega t + \Phi)] - 1}$$

$$= \frac{\exp[im(\Omega t + \Phi)/2] - \exp[-im(\Omega t + \Phi)/2]}{\exp[i(\Omega t + \Phi)/2] - \exp[-i(\Omega t + \Phi)/2]}.$$

Considering that $\sin \xi = (e^{i\xi} - e^{-i\xi})/2i$, we can write the above result in the form

$$G(t) = \frac{\sin [m(\Omega t + \Phi)/2]}{\sin [(\Omega t + \Phi)/2]} \tag{3.9.5}$$

or, changing the moment from which the time is measured, we get

$$\boxed{G(t) = \frac{\sin (m\Omega t/2)}{\sin (\Omega t/2)}.} \tag{3.9.6}$$

It follows from (3.9.3) that the function $G(t)$ may be considered as an envelope for the field amplitude with a carrier frequency ω_0. In other words, the field in a resonator "composed" of m locked longitudinal modes is *amplitude modulated* by the function $G(t)$. The nature of this modulation is defined by the expression (3.9.6).

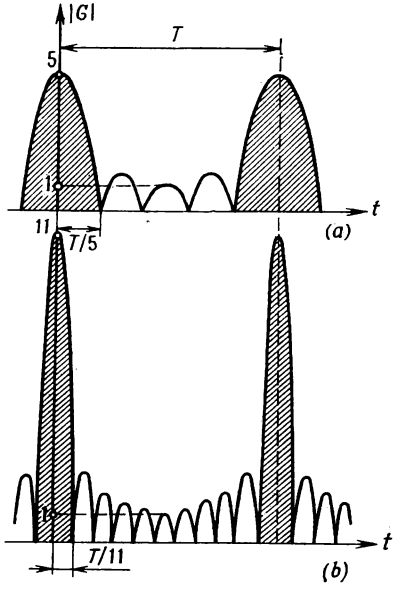


Fig. 3.49

Figure 3.49 shows the form of the function $|G(t)|$ obtained from the expression (3.9.6) for (a) $m = 5$ and (b) $m = 11$. In both these cases the amplitude E_0 of an individual mode is taken equal to unity. The time T is called the *modulation period* (it is also called the *resonator period*); it corresponds to the frequency difference Ω between adjacent modes:

$$T = 2\pi/\Omega. \tag{3.9.7}$$

It can be seen from the figure that with increasing number m of locked modes, the envelope $G(t)$ assumes a form corresponding to a *train of light pulses* having an amplitude mE_0 and duration T/m. Each pulse is followed by the next one after an interval T (see shaded pulses in the figure). The larger the number m, the larger the amplitude and the shorter the duration of these light pulses.

If the modes were not locked, the radiation power would be given by

$$P_{\text{unlocked}} \approx mE_0^2. \tag{3.9.8}$$

For the case of mode locking, we get a different result for peak power:

$$P_{\text{locked}} = (mE_0)^2 = mP_{\text{unlocked}}. \tag{3.9.9}$$

Consequently, the peak power of radiation in the case of locking of m modes increases m times over the case when mode locking does not occur.

Thus, the interference of m longitudinal modes, which are equidistant in frequency and are phase-locked, leads (for sufficiently large m) to the laser radiation assuming the nature of a train of quite short and quite powerful light pulses which follow one another with a time interval T equal to the resonator period, the duration of an individual pulse is equal to about T/m[50].

Nonselective Cavity. Apparently, the necessary condition for longitudinal mode locking is the simultaneous excitation of a sufficiently large number of such modes[51]. In this case, the *multifrequency* generation is of basic importance.

The *maximum possible* number of longitudinal modes in a cavity is determined by the well-known relation

$$m = \Delta\omega/\Omega = \Delta\omega L/\pi v, \tag{3.9.10}$$

where $\Delta\omega$ is the gain linewidth, L is the resonator length, and v is the velocity of light in the medium filling the resonator. Taking (3.9.10) into account, the resonator period $T = 2\pi/\Omega$ may be represented in the form

$$T = 2L/v \tag{3.9.11}$$

the duration of the ultrashort pulse may be estimated as

$$\tau \approx T/m = 1/\Delta\omega. \tag{3.9.12}$$

Characteristic values of $\Delta\omega$ and m for some lasers are given in Sec. 3.1. It should be recalled that $\Delta\omega \approx 10^{11}$ sec^{-1}, $m \approx 10^3$ for a ruby laser, and $\Delta\omega \approx 10^{12}$ sec^{-1}, $m \approx 10^4$ for an Nd-laser. These figures show that for a longitudinal mode locking in the lasers under consideration, it is possible in principle to obtain light pulses of duration 10^{-2}-10^{-3} nsec.

In order to put this possibility into practice, it is necessary to prevent selection of longitudinal modes in the resonator. We are speaking here of the *interference* selection of modes (see Sec. 2.11), which always takes place in ordinary resonators owing to the presence of several additional reflecting surfaces in them (for example, the end faces of the active element, mirror plates, etc.). In order to prevent the interference mode selection, the *nonselective cavities* are used: all reflecting coatings are applied to wedge-shaped surfaces, and the ends of the active element are cut at Brewster's angle. Such a resonator is shown in Fig. 3.50. Here, *1* is the active element,

[50] This situation corresponds to the ideal case of *complete mode locking* (see Sec. 3.11).

[51] It will be shown in Sec. 3.11 that an inordinate increase in the number of longitudinal modes must lead to a worsening of the conditions for their locking.

2—the mirrors on wedge-shaped substrates, and α—Brewster's angle. The thick broken line shows the passage of a light ray through the resonator. In a nonselective cavity, there are no additional reflecting surfaces perpendicular to the light ray, only two reflecting planes form the resonator (the cross sections of these planes are denoted by the straight lines AA in the figure)[52].

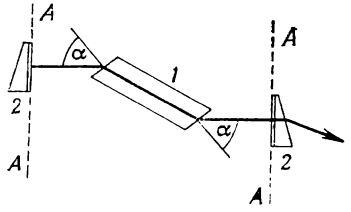


Fig. 3.50

Active Mode Locking. In order to link the phases of longitudinal modes we turn to *periodic modulation* of the parameters of a resonator with frequency equal to, or a multiple of, the difference between frequencies of adjacent modes. Since this modulation is carried out under the influence of external signals applied to the electrooptical or acoustooptic switch inside the resonator, the mode locking is called *active*.

Suppose that the amplitude of the central mode is periodically modulated with a frequency Ω. In this case, the mode under consideration may be represented in the form

$$E(t) = E_0 (1 + \beta \cos \Omega t) \exp [i (\omega_0 t + \varphi_0)], \tag{3.9.13}$$

where β is the modulation thickness ($0 < \beta \leqslant 1$). Since

$$\cos \Omega t = [\exp (i\Omega t) + \exp (-i\Omega t)]/2,$$

the expression (3.9.13) may be rewritten in the following form:

$$\begin{aligned} E(t) = E_0 \exp [i (\omega_0 t + \varphi_0)] \\ + (\beta E_0/2) \exp [i (\omega_0 + \Omega) t + i\varphi_0] + (\beta E_0/2) \\ \times \exp [i (\omega_0 - \Omega) t + i\varphi_0]. \end{aligned} \tag{3.9.14}$$

Thus we see that a periodic amplitude modulation with a frequency Ω leads to a conversion of the carrier mode at frequency ω_0 into three *phase-locked modes* at frequencies ω_0, $\omega_0 + \Omega$, and $\omega_0 - \Omega$.

If the modulation frequency Ω is chosen equal to the difference in frequencies of two adjacent modes excited in the laser, the marginal frequencies $\omega_0 + \Omega$ and $\omega_0 - \Omega$ will coincide, apparently, with frequencies of modes adjacent to the central mode. In this case, the second and third terms on the right-hand side of (3.9.14) will play the role of driving forces for these adjacent modes. Consequently, these adjacent modes will be generated in phase with the central

[52] It is useful to emphasise that while in Sec. 2.11 we considered special measures to be taken for intensifying the frequency selection of modes (thus finally ensuring a single-mode generation), we now require, on the contrary, measures for excluding the selection.

mode. In other words, these modes will be *locked* with the central mode.

In case when the modulation frequency is n times the difference between the frequencies of adjacent modes, we get a locking of modes with frequencies differing by more than n times the intermode interval.

The first experiments on active mode locking were carried out in 1965 using a He-Ne laser [33]. Similar experiments were later conducted mainly in solid-state lasers (see, for example, [114]) as well as organic dye lasers (see [115]). Active locking of longitudinal modes has been analysed in [112, 113][53].

Passive Mode Locking (Self-Mode Locking). The periodic modulation of resonator parameters may be carried out not only by an external signal, but also automatically to a certain extent—by *nonlinear mode beat response.* For this purpose, it is necessary to have a *nonlinear element* in the resonator, for example, a bleachable filter. In principle, the nonlinear properties of an active element may be used. In such cases a *passive* mode locking or *self*-mode locking takes place.

Bleachable filters are quite frequently applied[54]. Each pair of longitudinal modes excited in a laser with a filter will periodically modulate the coefficient of resonant absorption in the filter with a frequency equal to the difference between the frequencies of the modes under consideration. This, in turn, leads to an amplitude modulation of all modes. Consequently, as in the case of active locking, a definite link between phases of different modes may be attained.

Self-locking of longitudinal modes in a bleachable filter laser may also be considered from other points of view, by using the concept of *fluctuation.* For such an approach, the generation of ultrashort light pulses may be considered as a result of *separation* by the filter of the *highest intensity* fluctuations of the radiation field from the initial spontaneous noise and the *suppression* of the other (lower intensity) fluctuations. Fluctuation concepts have been developed in [13, 14, 39, 116]; see also [111]. An explanation of the self-mode locking on the basis of these concepts is now widely accepted; such an approach permits a consideration of self-mode locking in a systematic and comprehensive way. We shall consider the fluctuation concept in detail in Sec. 3.11.

For self-mode locking, practically the same diagram of a bleachable filter laser is used for the case of giant pulse generation. The following three points are *specific* to this case. Firstly, the *i* nterfer-

[53] Acoustooptic active locking of longitudinal modes is described in detail in Sec. 3.12.

[54] The effect of natural selection of longitudinal modes in a bleachable filter laser, discussed in Sec. 3.8, does not exclude the possibility of a passive mode locking; see Sec. 3.11.

ence mode selection must be prevented, i.e. a non-selective cavity should be used. Secondly, the bleachable filter must have a *short relaxation time* (in comparison with the resonator period):

$$T_{1a} < T. \qquad (3.9.15)^{55}$$

Thirdly, some specific requirements must be satisfied regarding the configuration of the set-up, e.g. the resonator length and the shape of individual elements and their mutual arrangement [40, 117]. In particular, it is expedient to place the bleachable filter in the vicinity of the output mirror of the resonator.

Figure 3.51 shows a typical set-up of a self-mode locking laser. Here, *1* is the active element, *2*—the bleachable filter (a cuvette

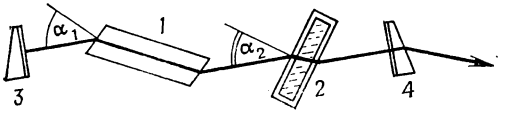


Fig. 3.51

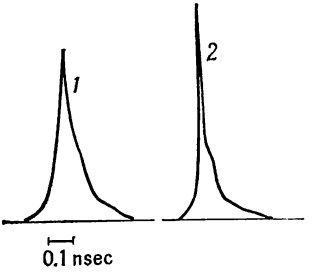


Fig. 3.52

filled with a solution of a fast relaxing dye), *3* and *4*—the reflecting and output resonator mirrors on wedge-shaped substrates, and α_1 and α_2—Brewster's angles for the active element and the cuvette, respectively.

Self-locking of longitudinal modes by using bleachable filters has been extensively investigated in experiments with Nd- and ruby lasers (see, for example, [34-37, 118]).

Combination Method of Mode Locking. The properties of ultrashort light pulses obtained for passive mode locking (self-mode locking) differ from the properties of pulses obtained for active mode locking. For passive locking, it is possible to attain a pulse duration close to the limiting duration determined by the width of the gain line. For active mode locking the pulse duration is formed to be considerably longer (by an order of magnitude or more). On the other hand, for passive mode locking, the time during which an ultrashort light pulse train is created may fluctuate between 10 and 100 μsec. The pulse parameters are reproduced from one pumping pulse to another just with a certain degree of probability. For active mode locking, however, the pulses are characterised by a high degree of stability of parameters.

[55] This condition will be proved in Sec. 3.11.

Optimal results are sought by using the method of *combination* mode locking. In this case, a bleachable filter and an active mode locker are placed inside the resonator. A combination of a filter (which serves as a passive mode locker) and an active Q-switch is also used. A combination of an electrooptical mode locker with a bicomponent medium containing two types of particles, viz. the active centres and the resonant absorption centres, has been considered in [119]. A self-mode locking laser has been investigated in [120] for the case when the resonator contains an electrooptical Q-switch in addition to the bleachable filter. The possibility of achieving self-mode locking is discussed in [121] under the conditions when the resonator Q-factor can be controlled with the help of a set of phototropic and mechanooptical shutters.

In Fig. 3.52, a comparison of light pulses obtained for the case of active and combination locking of longitudinal modes [119] has been shown. Pulse *1* is obtained in a ruby laser using an electrooptical mode locker based on a lithium niobate crystal. Pulse *2* is obtained in the same laser under the condition that a bleachable filter (a solution of kryptocyanine in ethyl alcohol) is used in addition to an electrooptical locker. The duration of the pulses *1* and *2* is 0.1 nsec and 0.01 nsec respectively (the pulse duration was estimated by the width of the spectrum). In both cases, the time from the moment of mode-locker switching to the moment when the pulse attains its maximum power is established with an accuracy up to 1 nsec.

Methods of Reducing the Relaxation Time for Bleachable Filters. The need for using rapidly relaxing bleachable filters (see condition (3.9.15)) predetermines the development of methods for *decreasing the relaxation time in dyes.* For this purpose we use the dependence of lifetime of excited states of dye molecules on the properties of the surroundings, like the nature of the solvent, its temperature, viscosity, etc. [122]. The dependence of the relaxation time of polymethine dye on the *nature of the solvent* has been discussed in [123]. It is shown that by using different solvents, a five-fold variation in the relaxation time can be achieved.[56]

A reduction in the lifetime of an excited state on account of a change in the external conditions is called *luminescence quenching.* For this purpose, we can use the effect of *concentration quenching (self-quenching)* arising as a result of increasing the dye concentration in the solution [124]. This effect is connected with the formation of associates (consisting of several dye molecules) in the concentrated solution. These associates do not luminesce upon excita-

[56] The effect of the nature of a solvent on the relaxation time of a filter is connected with the existence of nonradiative processes of deactivation of the state S_1 of the dye molecule as a result of *internal conversion*, i.e. through a transfer of vibrational energy to the surroundings (see Sec. 1.3).

tion, but rather give away their excitation energy rapidly to the inactive complexes as a result of resonant interaction with them.

The possibility of reducing the relaxation time in a bleachable filter by exciting *superluminescence* [125] or *generation* [126] in the dye solution should be specially mentioned here. In the latter case, the cuvette with the dye is placed in a *special resonator* whose optical axis forms a certain angle with the optical axis of the main resonator. The active element radiation serves as a sort of transverse optical pumping for the dye. Generation in the dye solution contained in a special resonator ensures a relatively rapid relaxation of the filter.

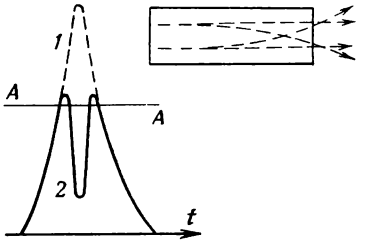


Fig. 3.53

Effect of the Self-focusing of Light. The generation of superpower pulses may be accompanied by auxiliary nonlinear optical effects, in particular, the *self-focusing of light*. A change in the time structure of ultrashort light pulses in an Nd-laser has been experimentally observed. This may be attributed to self-focusing of radiation in the active element (see, for example, [127]). Let us consider Fig. 3.53 in this connection, where curve *1* describes the shape a light pulse would have in the absence of self-focusing. The straight line AA fixes the level of power corresponding to the threshold of self-focusing effect. When the power of a pulse during its generation attains this threshold value, the self-focusing of radiation takes place, leading to higher losses as the light gets scattered through the lateral face of the active element (see the right-hand part of the figure). These losses are highest for the most intense part of the light pulse. This causes a *dip* in the part of the pulse corresponding to its highest intensity. Hence the shape of the light pulse is described not by curve *1* but by curve *2* (see the figure).

It can be seen from the figure that self-focusing not only changes the shape of a light pulse, but also restricts its peak power. The question of limiting the power of the generated radiation due to self-focusing is very important when estimating the limiting energy characteristics of lasers [128, 129]. Self-focusing limits the intensity of the generated power at a level equal to about 10^9 W/cm^2 (for normally used laser diagrams).

The possibility of using self-focusing for *reducing the duration* and *increasing the contrast*[57] of ultrashort light pulses has been discussed

[57] The contrast of an ultrashort light pulse is measured as the ratio of the peak pulse power to the level of nonsynchronised background power. Increasing the contrast in fact means an increase in the degree of synchronisation of radiation.

in [130], and illustrated in Fig. 3.54. Here, *1* is the medium in which the self-focusing of radiation takes place, *2*—the absorbing screen of a relatively small diameter, *3*—the input light pulse (in general, it may be a group of pulses of different intensities), and *4*—the output light pulse. The lower intensity part of the input light pulse *3* does not undergo self-focusing and is mainly absorbed by the screen *2*. As a result of a broadening of the beam on account of self-focusing, the higher intensity part of the light beam escapes the screen *2*. Hence the output pulse *4* must be shorter and in sharper contrast than the input pulse *3*.

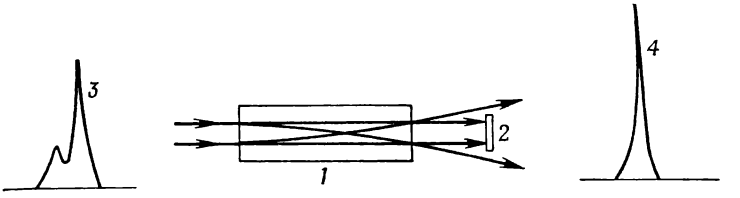


Fig. 3.54

It has been shown in [130] that instead of an absolutely opaque screen of a small diameter it is better to use an inhomogeneous screen, whose transparency K increases with distance r from the axis according to the law $K(r) = K(0) \exp(r^2/a^2)$, where a is the diameter of the screen. Such a screen ensures that losses are minimum for the highest intensity part of the pulse. This results not only in a decrease in the pulse duration, but also in an increase in its peak power. In this case, the self-focusing effect plays a positive role, leading to a decrease, and not an increase, in the losses (for the highest intensity part of the light pulse).

It should be noted that a spatially inhomogeneous screen does not necessarily have to be absorbing. Instead of an absorbing screen, we may use an amplifying medium characterised by a spatially inhomogeneous gain factor.

3.10. MEASUREMENT OF DURATION OF ULTRASHORT LIGHT PULSES

Basic Methods for Investigating Pulse Structure. A growing interest in the investigation of mode-locking in lasers is closely related to an analysis of methods of measuring the duration of ultrashort light pulses. The well-established oscillographic methods cannot be used in this case, since their resolution is limited to 0.1 nsec. There are two types of methods for measuring pulses of the order of 10^{-2}–10^{-3} nsec, called *direct* and *indirect* methods.

Indirect methods were the first to be proposed and developed. In this connection, we can mention two articles published in 1967: the first one [131] is connected with the second harmonic excitation by two light beams, the second one [132] is based on the measurement of the luminescence track in the case of a two-photon absorption. The latter method (called the *two-photon method* or the *collision method*) has been widely applied because of its simplicity.

While using indirect methods for measuring the structure of light pulses, we measure not the pulse parameters but some *integral*

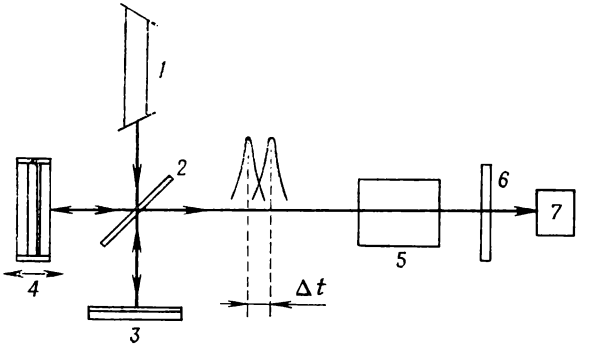


Fig. 3.55

quantities, for example, the *intensity correlation functions*[58]. These methods have a limited scope since they do not permit a unique determination of the pulse shape [111].

Direct measurement methods based on the application of optoelectronic converters were successfully developed in the early seventies for high-speed processes [111]. Photoelectron recorders having a time resolution of 10^{-2}-5×10^{-3} nsec were created. An optoelectronic converter with a cycloidal time base, having a resolution up to 5×10^{-4} nsec was constructed in 1972.

The problem of recording the high intensity radiation, as well as the field itself, is of considerable practical interest. In other words, the problem consists in recording information not only about the amplitude, but also the phase of a laser radiation. For this purpose, the *holographic* method of nonstationary wave fields was proposed in 1971. This method provides maximum information about the passage in time of a signal, including information about the amplitude, phase, as well as the signal spectrum [111].

Method Based on Second Harmonic Generation. The principle behind this indirect method of measuring the duration of an ultrashort pulse is illustrated in Fig. 3.55. Here, *1* is the laser, *2*—a beam

[58] Indirect methods of time measurement are also called *correlation* methods.

splitting plate which converts the initial laser pulse into two pulses, *3*—a fixed mirror, *4*—a movable mirror, *5*—a nonlinear crystal in which the *second harmonic generation* takes place, *6*—a filter transmitting only the second harmonic, and *7*—a photodetector. Mirrors *3* and *4* ensure that both light pulses into which the initial pulse splits at the plate *2* arrive at the nonlinear crystal. The time delay Δt for one pulse with respect to the other may be varied with the help of the movable mirror *4*.

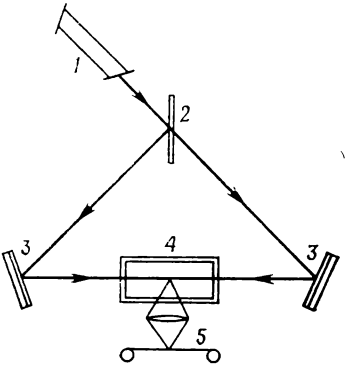


Fig. 3.56

For $\Delta t = 0$, the two light pulses completely overlap. In this case, the light power in the nonlinear crystal is maximum, hence the photodetector registers a comparatively high intensity second harmonic pulse.

Let us denote the effective duration of an ultrashort light pulse as τ. For $\Delta t > \tau$, light pulses do not overlap, and the intensity of the second harmonic sharply decreases. If $E_\omega(t)$ is the field of one of the light pulses falling on the nonlinear crystal, the pulse field for the second harmonic emerging from the crystal may be given in the form

$$E_{2\omega}(t) = \text{const}\,[E_\omega(t) + E_\omega(t + \Delta t)]^2$$
$$= \text{const}\,[E_\omega^2(t) + E_\omega^2(t + \Delta t) + 2E_\omega(t)\,E_\omega(t + \Delta t)]. \quad (3.10.1)^{59}$$

For $\Delta t > \tau$, the correlation term $2E_\omega(t)\,E_\omega(t + \Delta t)$ vanishes, and the power of the second harmonic decreases.

Thus, in order to measure τ, the time delay Δt should be gradually increased from zero, and the intensity of the second harmonic pulse should be observed. Time Δt at which this intensity sharply decreases corresponds to the duration τ of the pulse.

The Two-Photon Method. As mentioned above, this method is based on the observation of *luminescence for a two-photon absorption*[60]. The basic principle behind this method is illustrated in Fig. 3.56. Here, *1* is the laser, *2*—a beam-splitting plate which converts the initial pulse into two pulses, *3*—the mirrors, *4*—a cuvette filled with the dye solution (for example, Rhodamine 6G) which luminesces as

[59] It should be recalled that the field of the second harmonic is proportional to the square of the field intensity of the principal wave (in the approximation of the given field).

[60] The term *two-photon luminescence method* is also sometimes used. However, this is not a correct nomenclature. since luminescence here is the ordinary one-photon process.

a result of the *two-photon absorption* of light, and *5*—a photographic camera for recording the luminescence track in the cuvette with dye. The intensity of luminescence for two-photon absorption is proportional to the fourth power of the field amplitude. Hence it is possible to photograph a fairly sharp track, whose length Δl corresponds to the time interval over which the two beams propagating towards each other upon reflection from mirrors *3* overlap to a considerable extent. This time interval is equal to $\tau/2$ (τ is the duration of the light pulse). Obviously,

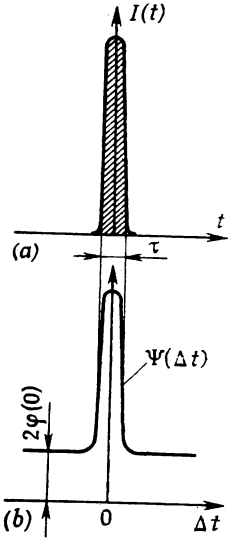


Fig. 3.57

$$\tau = 2\Delta l/v, \qquad (3.10.2)$$

where v is the velocity of light in the dye solution. This method is in fact based on instantaneous measurement in *space* of the duration of the light pulse.

This method is widely applied for investigation of laser mode locking, hence we shall describe it in somewhat greater detail. The luminescence output for two-photon absorption is proportional to the square of the intensity of exciting radiation:

$$I_{\text{lum}}(z) = \text{const} \int I^2(z,\ t)\, dt \qquad (3.10.3)$$

(the z-axis is chosen as the direction of propagation of light in the cuvette filled with the dye solution, and z is the distance from the centre of the cuvette. Denoting the light field of the signal under investigation by $E(t) \exp(i\omega t)$, the quantity $I^2(z, t)$ appearing in (3.10.3) may be represented in the form

$$I^2(z, t) = \left\{\left[E\left(t-\frac{z}{v}\right)\exp\left(i\omega\left(t-\frac{z}{v}\right)\right)\right.\right.$$
$$\left.\left.+E\left(t+\frac{z}{v}\right)\exp\left(i\omega\left(t+\frac{z}{v}\right)\right)\right][\text{compl. conj.}]\right\}^2. \qquad (3.10.4)$$

Here, we have considered two light pulses propagating towards each other along the z-axis with a velocity v.

It can be shown [111] that a substitution of Eq. (3.10.4) in (3.10.3) leads finally to the result

$$I_{\text{lum}}(z) = \text{const}\left[2\int_0^{t_{\text{meas}}} I^2(t)\, dt + 4\int_0^{t_{\text{meas}}} I(t)\, I\left(t+2\frac{z}{v}\right) dt\right], \qquad (3.10.5)$$

where t_{meas} is the measurement time. Introducing the delay time $\Delta t = 2z/v$ instead of the variable z, we get the following expression

from (3.10.5) for the luminescence track observed in the cuvette:

$$\Psi(\Delta t) = \frac{1}{t_{meas}}\left[2\int_0^{t_{meas}} I^2(t)\,dt + 4\int_0^{t_{meas}} I(t)\,I(t+\Delta t)\,dt\right]. \quad (3.10.6)$$

Using the special notation

$$\varphi(\Delta t) = \frac{1}{t_{meas}}\int_0^{t_{meas}} I(t)\,I(t+\Delta t)\,dt, \quad (3.10.7)$$

for the *correlation intensity function*, the result (3.10.6) may be rewritten in its final form as follows:

$$\Psi(\Delta t) = 2\varphi(0) + 4\varphi(\Delta t). \quad (3.10.8)$$

We assume that the intensity $I(t)$ of the light pulse under investigation is of the form shown in Fig. 3.57*a*. Using (3.10.6) we can find the function $\psi(\Delta t)$ describing the luminescence track. This function has a form shown in Fig. 3.57*b*. In accordance with (3.10.8), the maximum emission intensity is three times the intensity of the pulse at those places in the track where the light pulses arriving for opposite direction do not overlap. Measuring the width of the emission intensity pulse, we can find the required quantity τ.

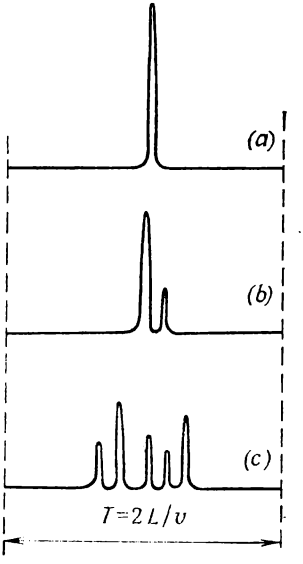


Fig. 3.58

It should be recalled that in actual practice, we measure the length Δl of the bright part of the luminescence track instead of Δt. The two are connected through the relation $\Delta t = 2\Delta l/v$.

Complete and Incomplete Mode Locking and Measurements of Time. The indirect methods discussed above for measuring the duration of ultrashort light pulses have a significant drawback which cannot be realised at once[61]. These methods are applicable only when a single pulse is generated during the resonator period which is equal to $2L/v$. This kind of a situation is characteristic of active mode locking. For passive mode locking, instead of a single pulse over the resonator period, we may get a *group* (and an irregular

[61] The potentialities of the two-photon method were not properly exploited in literature for a long time. Occasionally, unfounded conclusions were drawn about the duration of ultrashort light pulses on the basis of data obtained by this method.

one, too) of several pulses, on account of fluctuations in the process of mode self-locking. Figure 3.58 illustrates certain situations that may be encountered in the case of self-mode locking. In this connection, the terms *complete* and *incomplete* (*partial*) mode locking are introduced. Figure 3.58*a* illustrates the case corresponding to *complete* mode locking (a *single* ultrashort light pulse is generated over the resonator period). Figures 3.58*b* and 3.58*c* illustrate cases corresponding to *partial* mode locking, the *extent* of locking being higher for the case shown in Fig. 3.58*b*. For partial mode locking, an ultrashort light pulse may be obtained against a *background* of unlocked radiation, whose power has a weak time dependence. The higher the power of the unlocked background, the lower the extent of mode locking and hence the less the contrast between ultrashort pulses.

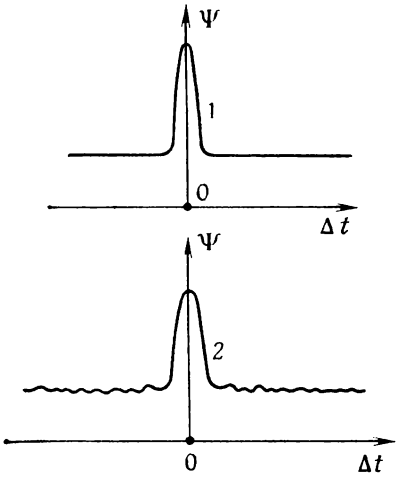


Fig. 3.59

Significantly, the indirect methods (including the two-photon method) for the measurement of ultrashort pulse duration cannot distinguish between complete and partial mode locking[62]. This is a serious drawback in the application of these methods for mode locking studies. In order to illustrate this aspect, let us compare the results of computations of the function $\Psi(\Delta t)$, with the help of formula (3.10.6), for the cases shown in Figs. 3.58*a* and 3.58*c*. These results are shown in Fig. 3.59 (curves *1* and *2* respectively) [111]. Obviously, the difference between the luminescence tracks shown in Fig. 3.59 lies in that additional weak maxima appear in the second case (for partial locking), but it is hard to distinguish these from the noise in the recording instruments.

It should be emphasised that indirect methods of measurement provide information only about the *characteristic* time interval during which the intensity of radiation changes. It is not possible to establish whether the radiation over the resonator period consists of one or several short pulses, nor can the ratio of the peak power of an ultrashort pulse to the power of the unlocked background (in case the latter is present), be established with the help of these methods. Hence it is important to develop the direct methods of time measurements, using superfast photo recorders with opto-electronic converters.

[62] A detailed critical analysis of the potentialities of the indirect methods of time measurements in mode locking investigations is given in [111].

Method Based on Measurement of Signal Spectrum Structure. In order to distinguish between the generation of a single short pulse and multi-pulse generation during the resonator period, we can use the method based on the measurement of the structure of corresponding *frequency spectra* [124]. Suppose that several pulses are generated during the resonator period. In this case, the Fourier transform of the radiation field (spectrum) will contain *oscillations* which are

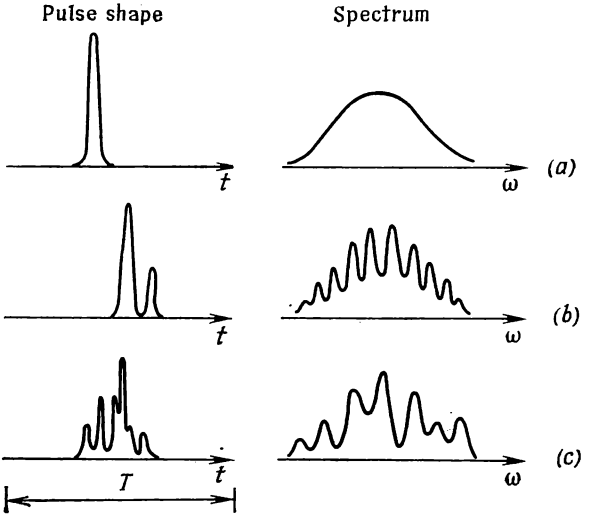


Fig. 3.60

defined by the time intervals between pulses. The smaller these intervals, the higher the frequency of spectral oscillations. If a single pulse is formed over the resonator period, the spectrum will be described by a smooth function (without oscillations).

Figure 3.60 shows a comparison between the spectral structure for complete (Fig. 3.60*a*) and partial (Fig. 3.60*b*, *c*) mode locking [124]. It can be easily seen that the structure of the signal spectrum in Fig. 3.60*b* and *c* is considerably different from the spectral structure in Fig. 3.60*a*.

3.11. ANALYSIS OF SELF-LOCKING OF LONGITUDINAL MODES IN A BLEACHABLE FILTER LASER BASED ON FLUCTUATION CONCEPTS

Fluctuation concepts for investigating self-locking longitudinal modes have been discussed in [13, 14, 39, 111, 115].

Qualitative Description of the Physical Picture. Two main points must be considered while investigating the physical picture of self-

mode locking when the resonator contains a bleachable filter. The *first* point concerns the appearance of a radiation field profile at the stage preceding the bleaching of the filter[63]. This profile contains a large number of fluctuations in intensity with different amplitude, and is characterised by the presence of a *periodic correlation* at the instants t and $t + T$, where T is the resonator period. This field profile is called *initial*. The process of its formation from the noise will be explained at a later stage. The *second* point concerns the *narrowing* and *accentuation* (selection) of individual, most powerful

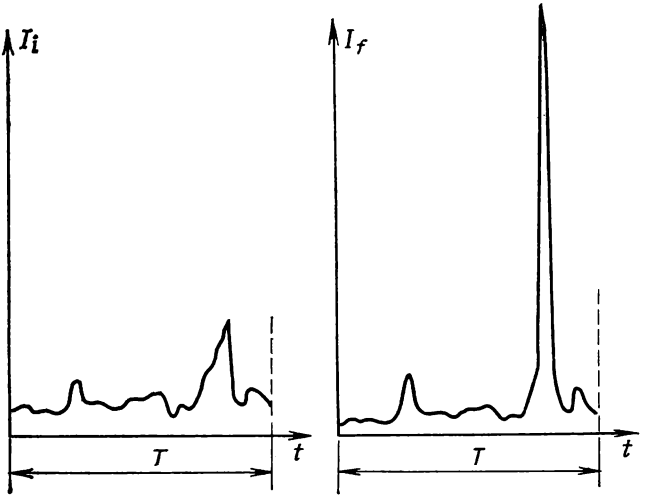


Fig. 3.61

fluctuations during the process of bleaching (at the stage of nonlinear growth of generation), and a simultaneous *suppression* of the other, weaker fluctuations. Consequently, the field profile is considerably altered. Finally, only a few (or even a single) short intense spikes are retained over the resonator period. Figure 3.61 shows a comparison between a certain initial profile $L_1(t)$ and the characteristic final profile $I_f(t)$ over one resonator period T. The variation in the profile as a result of interaction of radiation with the filter during bleaching can be clearly seen in the figure.

We shall now examine the *selective* action of a bleachable filter on the initial field profile. The condition (3.7.37) for self-excitation of oscillation in a laser with a filter can be rewritten in the following form:

$$(\varkappa_0 - \eta_{\text{nonlin}} - \eta_{\text{lin}}) > \eta_2. \qquad (3.11.1)$$

[63] This stage consists, in turn, of the pumping stage and the stage of linear growth of generation.

Here, $\varkappa_0$ is the initial gain; $\eta_{\text{nonlin}} = (l_a/l)\,\varkappa_{0a}$ is the product of resonant absorption coefficient of the unbleached filter and the ratio l_a/l or, in other words, the *nonlinear* loss factor; $\eta_{\text{lin}} = \eta_1 + (l_a/l)\eta_{1a}$ is the unfavourable loss factor in the active element and the filter or, in other words, the *linear* loss factor, and η_2 is the favourable loss factor.

We assume that the condition (3.11.1) is not satisfied for a given pumping power, and that a high intensity pulse from the initial profile is travelling towards the filter. If this pulse bleaches the filter, the inequality (3.11.1) can be replaced by the inequality

$$(\varkappa_0 - \eta_{\text{lin}}) > \eta_2 \qquad (3.11.2)$$

which can be easily satisfied for the given pumping power. This means that the condition of self-excitation of oscillations will be satisfied for this high intensity pulse.

It is extremely important that the condition of self-excitation should be satisfied for the high intensity pulse only. For this purpose, it is necessary that the filter should relax quite rapidly, or, in other words, it should be quickly slammed after the passage of the high intensity pulse through it. In this case, the weaker pulse following the high intensity pulse can no longer pass through the filter (and hence cannot be amplified).[64]

The significance of the condition (3.9.15) now becomes clear. In order to perform selective operation (accentuation of high intensity pulses and suppression of weak initial pulses) a filter must have a *high speed*, i.e. it should quickly return to the unbleached state from the bleached state. If the filter remains in the bleached state for some time, then in addition to the high intensity pulse, weaker pulses will also pass through the filter and will be amplified upon passing through the active element.

In the presence of a high speed filter, we get a picture of a *single* light pulse "flitting" from one mirror to another (in the resonator). The amplitude of this pulse initially increases, and then gradually decreases (as the pumping pulse energy transferred to the active element gets consumed). Each time after an interval of $2L/v$, equal to the time required for a round-trip through the resonator, this pulse will approach the output mirror and will partially emit radiation. Consequently, the laser output radiation will be a *train of light pulses* separated by an interval of time $T = 2L/v$ (Fig. 3.62*a*).

This ideal situation does not take place under real conditions. Firstly, a real filter has a time lag, and may not be able to slam just in front of the weaker pulse immediately following the high intensity pulse. In this case, a light pulse train shown in Fig. 3.62*b* will be observed. Secondly, fluctuations in the initial field profile may re-

[64] It is assumed that the power of this weak pulse is not sufficient to bleach the filter.

sult in two or more initial pulses having nearly identical intensities, which will then be equally accentuated by the filter. Consequently, two or more short pulses of high intensity may be formed over the resonator period (Fig. 3.62*c*). It should be noted that Fig. 3.62*a* corresponds to a complete mode locking, while Figs. 3.62*b* and *c* correspond to a partial mode locking.

Spectral and Time Description of Mode-locking. The above description of the generation of ultrashort light pulses in a laser with a bleachable filter may be considered as a *time-based description.* In this case, the generation of a train of ultrashort pulses may be considered as the process of regular emission (with period of repetition equal to $T = 2L/v$) of a part of the energy of a powerful fluctuation spike in the field profile, isolated and accentuated by the bleachable filter. The concept of a powerful pulse flitting in a resonator may be used for the case of active mode locking. It should be recalled that the losses in the resonator due to the locker are modulated by the control signal, and vary periodically with a frequency $1/T$. The pulse "flitting" in the resonator will obviously pass through the locker each time at the instant corresponding to minimum losses.[65]

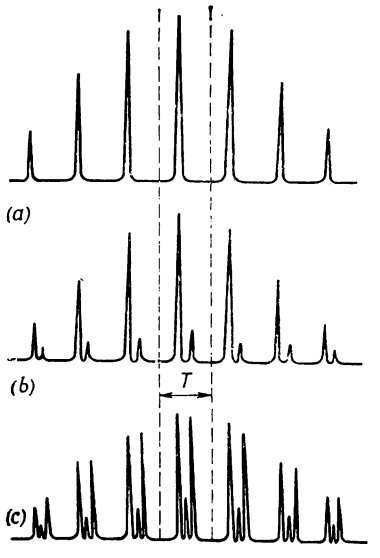


Fig. 3.62

Besides the above description, a *spectral description* of ultrashort light pulse generation is also used, when the pulse train formation is considered as the result of interference of a large number phase-locked modes, equidistant in frequency (see Sec. 3.9 as well as Sec. 3.1). The first experimental results for ultrashort pulse generation were explained by using the spectral approach, and it was in this context that the term mode locking was first employed. This term means a *phasing of spectral components.* The time-based approach, using the concept of a powerful pulse "flitting" in a resonator and separated from the noise either randomly (passive locking) or by a locker (active locking), was developed somewhat later.

The periodic correlation at the instants t and $t + T$ characterising the initial field profile corresponds in the spectral language to

[65] The time-based description of active locking of longitudinal modes is given in Sec. 3.12.

formation of set of discrete modes with equidistant frequencies $\omega_k = \omega_0 \pm 2\pi k/T$. We assume that the frequency interval between the phases of the modes is $\Delta\omega$, corresponding to the width of the gain line. It can be easily seen that if the phases of modes depend linearly on the mode number ($\varphi_k = \varphi_0 \pm 2\pi kt/T$), i.e. if the modes are phase-locked, a single light pulse with period

$$\tau \approx 1/\Delta\omega \qquad (3.11.3a)$$

is formed over the resonator period. This means that the spectral approach is equivalent to the time-based approach if a single pulse is formed during the resonator period, i.e. if there is a *complete* mode locking.

In the case of *partial* mode locking, the spectral approach is not so suitable. As a matter of fact, only a *part of the spectrum* (and not the entire spectrum, as in the case of complete locking) is responsible for the formation of ultrashort pulses in the case of partial locking. This leads to the following relation instead of (3.11.3a):

$$\tau > 1/\Delta\omega \text{ or, otherwise, } \tau \approx 1/\Delta\omega_{\text{locked}},$$
$$\text{where } \Delta\omega_{\text{locked}} < \Delta\omega. \qquad (3.11.3b)$$

The spectral approach does not provide an answer for the question whether a single high-intensity pulse is isolated (over the resonator period) from the initial fluctuation picture. Thus, the time-based approach must be considered as *more comprehensive* and *systematic*. It permits an analysis of the physical picture of phenomena at various stages of interaction of radiation with the filter (both before and during bleaching). Moreover, we can also consider the *conditions for complete locking*, i.e. conditions under which the probability of generation of a single high-intensity light pulse over the resonator period is quite high.

Initial Profile of Radiation Field. The initial field profile is formed as a result of *spontaneous* processes. Owing to fluctuations in processes, the radiation intensity will fluctuate, and the minimum period of fluctuations at the beginning of oscillations will be given by $\tau_{\text{fluct}} \approx 1/\Delta\omega$, where $\Delta\omega$ is the width of the gain line of the active element.

Significantly, no definite ordering takes place in this fluctuation picture. As a matter of fact, a certain fraction of spontaneously emitted photons will be returned by the mirrors to the active medium, thus causing a partial regenerative noise amplification. As the inverse population density approaches its threshold value, the fraction of photons returning in this manner will increase. Consequently, the contribution of the amplified noise will exceed the contribution of direct spontaneous emission, and so a *periodic correlation* of the field takes place at instants of time separated by intervals equal to the time required for a round-trip of radiation through the resonator (i.e. equal to the resonator period T). Thus, even

before the threshold value is attained in a laser, discrete longitudinal modes appear in the frequency interval $\Delta\omega$ corresponding to the width of the gain line. Adjacent modes are separated by the frequency $\Omega = 2\pi/T$. During the *linear* growth of oscillations, a natural selection of longitudinal modes takes place, leading to a narrowing down of the spectrum (see Sec. 3.8). At the moment of bleaching of the filter, the spectral width $\Delta\omega_0$ is much smaller than the initial width $\Delta\omega$.

Suppose that the initial field profile is formed by m equidistant longitudinal modes ($m = \Delta\omega_0/\Omega$). Significantly, the phases of modes at this stage are independent and are randomly distributed. Hence the field in the resonator is a *Gaussian noise*, whose intensity I fluctuates around a certain mean value $\langle I\rangle$. The probability that the intensity attains the value I is given by the formula

$$\omega(I) = \exp(-I/\langle I\rangle)/\langle I\rangle \tag{3.11.4}$$

which follows from the Gaussian distribution of the field amplitude, if we consider that the intensity is proportional to the square of the amplitude.[66]

Let us denote by w_ν the probability of fluctuation spike having an intensity higher than ν times the average intensity. The probability may be found by using the relation

$$w_\nu = \int_{\nu\langle I\rangle}^{\infty} w(I)\, dI. \tag{3.11.5}$$

Substituting (3.11.4) in (3.11.5), we get

$$w_\nu = \exp(-\nu). \tag{3.11.6}$$

Since the frequency of fluctuations with any intensity is equal to $\Delta\omega_0/2\pi$ in the order of magnitude, the fluctuation spike of intensity $I \geqslant \nu\langle I\rangle$ must appear on the average over an interval of time τ_ν, determined by the relation

$$\tau_\nu \approx 2\pi/\Delta\omega_0 w_\nu. \tag{3.11.7}$$

Substituting (3.11.6) into (3.11.7) we get

$$\tau_\nu \approx (2\pi/\Delta\omega_0)\exp(\nu) \tag{3.11.8}$$

or, if we take (3.9.12) into account,

$$\tau_\nu \approx (T/m)\exp(\nu). \tag{3.11.9}$$

Taking into consideration the periodicity of initial field profile, we find that in order to get a spike of intensity $I \geqslant \nu\langle I\rangle$, it is necessary that the time interval τ_ν should not exceed the resonator

[66] Application of Gaussian distribution for describing fluctuation processes is discussed in detail in [133].

period T:

$$\tau_\nu \leqslant T. \tag{3.11.10}$$

The maximum value of ν may be estimated from the condition $\tau_\nu \approx \approx T$, or from the condition $m \approx \exp(\nu)$ by taking into consideration (3.11.9). Thus

$$\nu \approx \ln m. \tag{3.11.11}$$

If the initial field profile includes $m \approx 10^3$ longitudinal modes, it is possible, in accordance with (3.11.11), to get fluctuation spikes whose intensity is nearly an order of magnitude higher than the mean radiation intensity.

It should be noted that in accordance with (3.11.9), the time interval τ_ν decreases with increasing mode number m, and hence the probability of the appearance of such spikes increases. Significantly, this means an increased probability of the appearance of *two* or *more* spikes during the resonator period. Thus an increase in the number of longitudinal modes has its advantages as well as disadvantages, the latter being a decreased probability of complete self-mode locking.

Naturally, the occurrence of high-intensity short pulses in the initial radiation profile cannot be interpreted as a self-mode locking effect. This is because the mean part of the radiation energy is concentrated in the background of average spikes and not in the spikes of maximum intensity. In the process of self-mode locking (occurring at the stage of bleaching of the filter), the field profile significantly changes due to a redistribution of the radiation energy: the weaker spikes are suppressed while the high-intensity pulses are additionally augmented (and also become narrower); see Fig. 3.61.

Nonlinearity Index. The extent of variation of the field profile during the process of interaction of radiation with the filter during the bleaching stage depends on the magnitude of the *nonlinearity index* p defined by the following relation:

$$\boxed{p-1=\eta_{\text{nonlin}}/[\varkappa-(\eta_{\text{nonlin}}+\eta_{\text{lin}})].} \tag{3.11.12}$$

It follows from (3.11.12) that the effect of field profile variation may be enhanced by increasing the nonlinear loss factor η_{nonlin} or by reducing the difference between the gain and the total loss factor $[\varkappa - (\eta_{\text{nonlin}} + \eta_{\text{lin}})]$. Both these cases have a simple physical explanation. In the first case, the action of the filter is augmented *for a single passage* of radiation through the resonator. This may be achieved by increasing the density of the absorbing centres in the filter as well as the cross section of resonant absorption. In the second case, the *number of passes* accompanied by the field profile variation increases (in other words, the number of passes accompa-

nied by a bleaching of the filter increases; we call such passes *favourable*). It is quite obvious that the number of such passes will be the lower, the higher the increase in the gain factor $\varkappa$ over the sum of the loss factors $\eta_{\text{nonlin}} + \eta_{\text{lin}}$. If this difference is quite large, the filter may be bleached over just a single passage. Consequently, in order that the number of favourable passes be quite large, the following condition must be satisfied:

$$\varkappa \geqslant (\eta_{\text{nonlin}} + \eta_{\text{lin}}). \tag{3.11.13}$$

This condition means that the laser must operate in the *near*-threshold conditions.

The values of the parameter p lie between 20 and 100 for ruby and Nd-lasers [111].

Transformation of Field Profile Upon Interaction of Radiation with the Filter at the Bleaching Stage. It can be shown [111] that the final field profile $I_f(t)$, established after a complete bleaching of the filter, is connected with the initial profile $I_1(t)$ through the relation

$$I_f = \text{const}\ (I_1)^p. \tag{3.11.14}$$

If $p = 1$, the field profile does not change. In order to change the field profile, it is necessary that $p > 1$. As mentioned before, the increase in the difference $(p - 1)$ enhances the effect of variation of radiation field profile.

In accordance with (3.11.14), the change in the initial field profile upon interaction between radiation and the filter at the bleaching stage takes place in two directions. *Firstly*, each spike of the initial intensity has a *shorter duration* (is contracted) by about $\sqrt{p}$ times. This can be demonstrated by considering a *Gaussian* spike:

$$I_1(t) = \text{const} \exp\left[-(t - t_0)^2/\tau_1^2\right] \tag{3.11.15}$$

(τ_1 is the initial spike duration). Substituting (3.11.15) into (3.11.14), we get

$$I_f(t) = \text{const} \exp\left[-p\,(t - t_0)^2/\tau_1^2\right] = \\ = \text{const} \exp\left[-(t - t_0)^2/\tau_f^2\right]. \tag{3.11.16}$$

It is obvious from this that the final spike duration τ_f is $\sqrt{p}$ times less than the initial duration:

$$\tau_f = \tau_1/\sqrt{p}. \tag{3.11.17}$$

It should be observed that in the spectral language, the effect of spike concentration means the appearance of *new spectral components*[67]. In other words, the above-mentioned decrease in the dura-

[67] This observation is valid only when the relation (3.11.3a) is satisfied, i.e. if a complete mode locking takes place. If the duration of a pulse is considerably longer than the reciprocal of the width of frequency spectrum, the contraction of the pulse does not lead to the appearance of any new spectral components.

tion of radiation intensity spikes means a certain *increase* in the width of frequency spectrum. This broadening of the spectrum compensates the contraction of spectrum at the stage of linear growth of oscillations caused by natural selection of longitudinal modes.

Secondly, if any two intensity spikes in the initial profile are characterised by the ratio I_i'/I_i'', this ratio assumes the form $(I_i'/I_i'')^p$ in the final profile. Hence,

$$I_f'/I_f'' = (I_i'/I_i'')^p. \tag{3.11.18}$$

The result (3.11.18) follows from (3.11.14). It means that the difference in spike intensities in the initial field profile *is considerably amplified* (if $p \gg 1$) during the bleaching of the filter. In other words, the filter really augments the highest-intensity initial spikes.

It should be noted that of the two effects mentioned above (the effect of spike contraction and the effect of augmentation of high-intensity spikes), only the second effect may be clearly linked to the phasing of longitudinal modes. It is possible to build a model of a laser in which self-mode locking is not accompanied by a spectral broadening [111]. In this connection, it should be recalled that a pulse contraction may not lead to new spectral components in the case of a partial mode locking.

On the Possibility of Mode Locking in the Case of the Second Harmonic Generation. Self-mode locking may be observed in principle in any system where a *nonlinear* transformation of the radiation field is attained. In particular, it is possible to use the transformation of the fundamental harmonic of the radiation into the *second harmonic*. In this case, Eq. (3.11.14) assumes the form

$$I_{f,\,2\omega} = \text{const}\,(I_{1,\,\omega})^2. \tag{3.11.19}$$

In the present case $p = 2$. It has been proved experimentally that the second harmonic radiation from unlocked pumping radiation is actually partially locked.

For locking of natural frequency radiation, we may use the *intracavity generation of the second harmonic* [134]. This method of locking is based on the existence of two processes which take place simultaneously in the resonator. These processes are the doubling of the fundamental harmonic frequency and the generation of the difference frequency (i.e. the frequency equal to the difference between the frequencies of the second and fundamental harmonics). In this case, we get

$$I_f = \text{const}\,(I_1)^3. \tag{3.11.20}$$

Unlike (3.11.19), the nonlinearity index in this case is higher: $p = 3$. It should also be observed that I_1 as well as I_f correspond to the fundamental harmonic radiation in this case.

The highest values of the parameter p (of the order of 10-100) are obtained only with the help of bleachable filters. Hence the

most efficient method of self-mode locking is based on the bleaching of medium in lasers with bleachable filters.

Conditions for Complete Mode Locking. Let us formulate the conditions under which there is a high probability of generation, in the final field profile, of only one high-intensity spike over the resonator period. Qualitatively, these conditions result from the above discussion.

The *first condition* is that the filter must have a *high speed*, i.e. it must be "slammed" quickly after the passage of the high-intensity spike through it.

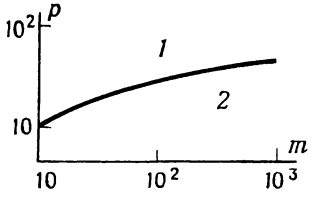


Fig. 3.63

The *second condition* requires a sufficiently large value of the nonlinear index p. It should be recalled that for this purpose it is necessary to increase the nonlinear loss factor to ensure a near-threshold laser generation. The higher the parameter p, the more selective the filter (the greater the augmentation of high-intensity spikes and the suppression of weaker spikes), and hence the more probable the generation of only one high-intensity spike in the final profile over the resonator period.

The *third condition* is that the number of modes in the radiation interacting with the filter should not be very high. Otherwise, the probability of *several* spikes of comparable intensities appearing over the resonator period will considerably increase.

Besides these fundamental conditions, there are several auxiliary conditions, for example, the exclusion of the frequency-pulling effect and the self-focusing of radiation.

A quantitative analysis of the conditions for a complete self-locking of longitudinal modes is given in [14]. The results of this analysis are shown in Fig. 3.63. The theoretical curve drawn in the (m, p) plane, where p is the nonlinearity index and m is the number of longitudinal modes subjected to locking, is the boundary between the regions of complete (region 1) and partial (region 2) locking. It is obvious from the figure that the condition of an increased value of the parameter p is more critical than the condition of a comparatively low value of m.

3.12. TIME-BASED DESCRIPTION OF ACTIVE LONGITUDINAL MODE LOCKING IN A LASER WITH A UNIFORMLY BROADENED GAIN LINE [68]

Statement of the Problem; Basic Assumptions. Active locking of longitudinal modes in continuously pumped lasers is usually ac-

[68] This section has been written in collaboration with V. K. Novokreshchenov.

complished with the help of an acoustooptic modulator[69]. Assuming that the gain line of the active element is uniformly broadened, let us analyse this problem from a time-based approach [112, 113, 135, 136].

We shall be considering the motion of a Gaussian ultrashort light pulse in a resonator containing an acoustooptic modulator, see Fig. 3.64. (Here, *1* is the active element, *2*—the acoustooptic modulator, and *3*—the resonator mirrors.) The motion of a light pulse from the initial reference plane P is indicated by arrows in the figure. Making use of certain assumptions (see below), we can calculate the parameters of the pulse after its passage through the active element and the modulator (taking into account the losses). By the parameters of a pulse we mean its period, average power, and the time shift with respect to the moment corresponding to zero losses in the modulator. By finding the difference in the values of any parameter between the *final* (after a round-trip through the resonator) and the *initial* pulses, and by dividing this difference by the time required for a round-trip, we can get the derivative of this parameter with respect to time [135]. Consequently, we get a system of differential equations describing the mode-locking process. An analysis of this system leads to the determination of the region of *instability* for the said regime [136].

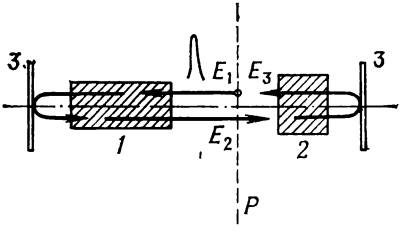


Fig. 3.64

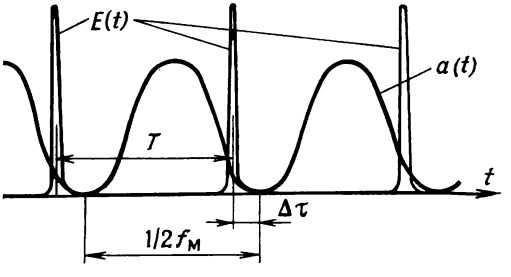


Fig. 3.65

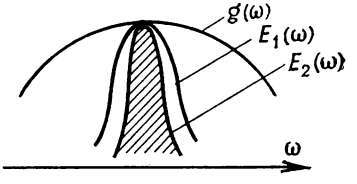


Fig. 3.66

Figure 3.65 shows the time variation of losses caused by an acoustooptic modulator in a resonator (curve $a(t)$) and the unfolding in time of the generated ultrashort light pulse train (curve $E(t)$).

[69] By modulator we mean a mode locker. It will be shown below that it differs from the Q-switch (acoustooptic shutter) considered in Sec. 3.5.

It should be recalled that the output laser radiation is generated in the form of a pulse train due to partial emission of the energy of a "flitting" high-intensity light pulse in the resonator every time the pulse is reflected from the output mirror. The notation used in the figure is as follows: T is the pulse repetition period or the resonator period (time required for a round-trip through the resonator), $2f_m$ is the loss modulation frequency, f_m is the frequency of the voltage applied to the modulator (frequency of the controlling signal), and $\Delta\tau$ is the time shift for the pulse with respect to the zero-loss instant. In the case of mode locking, $1/2f_m = T$ and optimum conditions of generation are attained for $\Delta\tau = 0$.

Basic assumptions: (A) the spectral width of the pulse is much smaller than the width of the gain line (see Fig. 3.66, where $g(\omega)$ is the contour of the gain line, $E_1(\omega)$ is the envelope of the pulse spectrum at the entrance to the active element, and $E_2(\omega)$ corresponds to the pulse after passing through the active element); (B) the pulse duration is much less than the pulse repetition period, and (C) the pulse parameters change little over a round-trip through the resonator. The assumption (A) is important for considering the transformation of a pulse in the *active element*, while assumption (B) is important for considering the pulse transformation in the *modulator*. But for these conditions, the Gaussian shape of the pulse "flitting" in the resonator would not be retained[70]. Assumption (C) is necessary in order that the ratio of difference in the values of parameters of final and initial pulses to the time required for a round-trip through the resonator be exactly equal to the derivative of the parameter with respect to time.

Variation in a Light Pulse upon Its Passage Through the Active Element and the Modulator. As proposed in [112], we represent the initial light pulse in the form

$$E_1(t) = (E_0/2)\exp(-\alpha t^2)\exp(i\omega_p t), \qquad (3.12.1)$$

where ω_p is the central frequency of the pulse spectrum, and the parameter α determines the pulse period τ_p and its spectral width Δf_p:

$$\tau_p = \sqrt{2\ln 2/\alpha}\,; \qquad \Delta f_p = \sqrt{2\alpha\ln 2}/\pi. \qquad (3.12.2)$$

In order to consider the transformation of the pulse upon its passage through the active element in the frequency space, it is conveniently to change over from the function $E_1(t)$ to its Fourier transform:

$$E_1(\omega) = F[E_1(t)] = (E_0/2)\sqrt{\pi/\alpha}\exp[-(\omega-\omega_p)^2/4\alpha] \qquad (3.12.3)$$

[70] These assumptions permit a retention of terms up to the second order only in the series expansion of the functions $g(\omega)$ and $a(t)$, thus ensuring that the Gaussian shape of the pulse is conserved.

(the operator F accomplishes the Fourier transformation). After a round-trip through the active element the light pulse (we denote this pulse by $E_2(t)$) is described by the relation

$$E_2(t) = F^{-1}\{g(\omega)\, F[E_1(t)]\}, \tag{3.12.4}$$

where $g(\omega)$ is the gain factor for the amplitude upon a round-trip through the active element[71]; it has the following form:

$$g(\omega) = \exp\left[g \Big/ \left(1 + 2i\frac{\omega - \omega_0}{\Delta\omega}\right)\right] \tag{3.12.5}$$

(ω_0 is the central frequency of the gain contour and $\Delta\omega$ is the width of the gain contour at half its height).

After a round-trip through the modulator, the light pulse $E_3(t)$ may be written in the form

$$E_3(t) = E_2(t)\, a(t - B), \tag{3.12.6}$$

where $B = 2g/\Delta\omega$ is the lag in the active element, and the function $a(t)$ describing the time dependence of losses imparted by the modulator has a Gaussian form according to the assumption (B):

$$a(t) = \exp[-(2\delta_0 + 2\delta_1\omega_m t + 2\delta_2\omega_m^2 t^2)]. \tag{3.12.7}$$

Here $\omega_m = 2\pi f_m$, and parameters δ_3, δ_1, and δ_2 are expressed in terms of β, the diffractional efficiency of the modulator for a single passage (also called the loss modulation depth) as

$$\delta_0 = \beta \sin^2\varphi; \quad \delta_1 = \beta \sin 2\varphi; \quad \delta_2 = \beta \cos 2\varphi, \tag{3.12.8}$$

where $\varphi = \pi\Delta\tau/T$. It should be noted that the relations (3.12.8) are valid under the condition that β is small ($\beta \ll 1$).

Next, we consider the pulse delay during its propagation in free space, as well as the favourable and unfavourable energy losses during a round-trip through the resonator. The losses may be taken into account by a suitable choice of the effective reflection coefficient R of the output mirror. Consequently, we get

$$E_4(t) = (1/2)\ln(1/R)\, E_3(t - 2L/c), \tag{3.12.9}$$

where L is the optical length of the resonator.

Substituting (3.12.1) into (3.12.4), then (3.12.4) into (3.12.6) and finally (3.12.6) into (3.12.9), we can determine the pulse shape and its position in time *after a full-round through the resonator.* Dividing the difference between the values of a parameter corresponding to the final pulse (3.12.9) and the initial pulse (3.12.1) by the time of passage through the resonator, we can find the derivative of this parameter with respect to time.

[71] The difference between the gain $g(\omega)$ and the amplification factor $\varkappa(\omega)$ used in the preceding sections must be clearly understood. The latter describes the amplification of intensity, and not amplitude. Besides, it corresponds to a unit length of the active element.

System of Differential Equations Describing the Establishment of Mode Locking. Carrying out the procedure described above and using the balance equation for the gain factor, we get the following system of differential equations [136][72]:

$$\left.\begin{aligned} dK/d\tau &= 2\delta_2 - 2\mu^2 K^2 g;\\ d\varphi/d\tau &= \mu g + \Delta - (2\delta_1/K);\\ dI/d\tau &= I(4g - 2\ln(1/R) - 8\delta_0);\\ dg/d\tau &= \zeta g_0 - \zeta g(I+1). \end{aligned}\right\} \qquad (3.12.10)$$

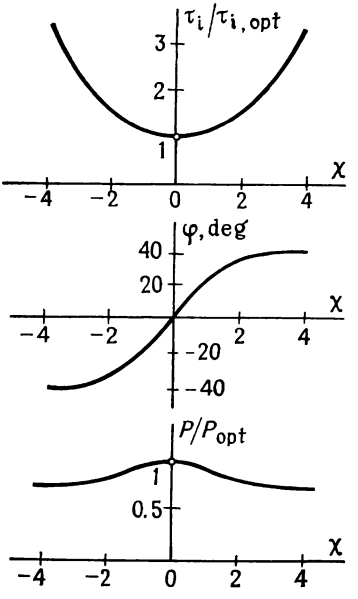


Fig. 3.67

Here, $\tau = tf_m$; $K = (2\ln 2/\pi^2)(T/\tau_1)^2$; g_0 and g represent the initial and saturation gain; $I = P/P_s$, P and P_s being the average mode locking power and the saturation parameter for the active medium (the latter is the power for which the gain is halved); $\mu = 4f_m/\Delta f$, $\Delta f = \Delta\omega/2\pi$; $\xi = 1/\tau_u f_m$, $1/\tau_u$ is the probability of relaxation of the upper laser level; $\Delta = 2\pi[(4Lf_m/c) - 1]$ is the relative detuning of the frequency of the modulating signal. The balance equation mentioned above is the fourth equation in the system (3.12.10) (cf. the second equation in the system (3.2.53)). Putting the derivatives in (3.12.10) equal to zero, we get a system of equations for *stationary* mode locking. As an illustration, Fig. 3.67 shows the stationary parameters of a typical mode-locked Nd:YAG laser. The parameters have been plotted as functions of the degree of detuning of the frequency of modulation signal, χ, defined by the relation

$$\chi = (f_m - f_{m\,opt})/(c/4L - f_{m\,opt}),$$

where

$$f_{m\,opt} = [(4L/c) + \ln(1/R)/\pi\Delta f]^{-1}.$$

The subscript "opt" corresponds to optimal mode locking for which a pulse crosses the modulator under zero loss conditions.

[72] An attempt has been made in [135] to obtain such a system of equations. However, the assumptions used in [135] regarding the time invariance of the gain in the active element is incorrect. Hence, unlike the system (3.12.10), the system of equations in [135] does not provide an adequate description of the instability region.

The system (3.12.10) permits a determination of the *instability region* mode locking with respect to small perturbations by examining the stability of the stationary solution of the system[73]. The *characteristic* equation for the system (3.12.10) has the form

$$\begin{vmatrix} -4\delta_2/K-p & -4\delta_1 & -2\delta_2/g & 0 \\ 2\delta_1/K & -4\delta_2/K-p & \mu & 0 \\ 0 & 0 & -\zeta(1+I)-p & -\zeta g \\ 0 & -8/\delta_1 & 4I & -p \end{vmatrix} = 0. \quad (3.12.11)$$

In order to identify the instability regions in this case, it is necessary to define the regions where the *real part* of at least one of the

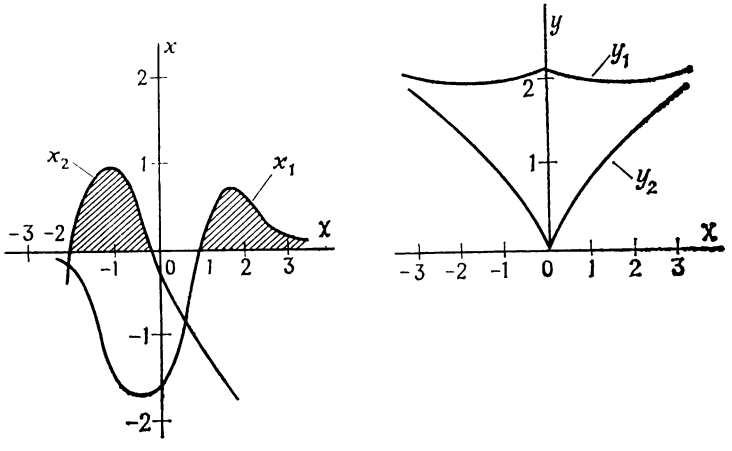


Fig. 3.68

roots may be given by $p_{1,2} = x_1 \pm iy_1$, $p_{3,4} = x_2 \pm iy_2$. The dependences x_1 vs. χ, x_2 vs. χ, y_1 vs. χ, and y_2 vs. χ for an Nd:YAG laser are shown in Fig. 3.68. The regions of values of χ corresponding to the shaded areas under the x vs. χ curve are the instability regions for mode locking. It is obvious from the figure that the allowed values of χ for detuning (for which mode locking is stable to perturbations) are quite small. Hence in actual practice a fairly rigid stabilisation of the frequency of the modulating signal and the optical length of the resonator are necessary, failing which an automatic frequency control should be applied.

We shall now discuss a qualitative picture explaining the origin of instability in mode locking. Suppose that $f_m > f_{m\,opt}$. In this

[73] It should be recalled that a similar investigation was carried out in Sec. 3.7.

case, an increase in f_m will lead to increased losses because the pulses will be passing through the modulator at instants of time which are far removed from the zero-loss stage (in other words, φ will increase). This will lead to a decrease in the value of $f_{m\,opt}$ and to a further increase in detuning and a phase shift φ. Consequently, with increasing f_m, the value of $f_{m\,opt}$ decreases (the frequency $f_{m\,opt}$, instead of remaining stabilised, "runs" downwards) and thus the detuning increases. This effect corresponds to an internal *positive* feedback which results in the loss of stabilisation in mode locking. In this case, the generation occurs in the form of chaotic spikes.

For $f_m < f_{m\,opt}$, this mechanism corresponds to a *negative* feedback. It should appear that this should stabilize the laser action. However, it is well known [68] that there is a phase shift between small oscillations of losses and gain near the resonance frequency by nearly 180°. Consequently, at frequencies close to resonance frequencies, the negative feedback becomes positive and causes instability in mode locking.

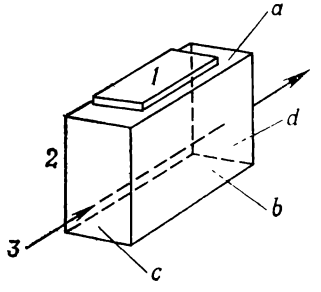


Fig. 3.69

Remarks About Phase (Electrooptical) and Amplitude (Acoustooptic) Mode Locking. Historically, the *phase* lockers based on *electrooptical* crystals were the first to be fabricated. In these lockers, an alternating high-frequency field (with a frequency close to the intermode beat frequency) leads to a modulation of the delay of an ultrashort light pulse upon its passage through the synchronizer, which corresponds to the phase locking of phase trains. At the present time, phase lockers have been practically replaced by *acoustooptic* mode lockers which bring about an *amplitude* modulation of resonator losses at a frequency close to the intermode beat frequency [137].

Amplitude mode lockers have the following advantages over phase lockers: lower losses owing to the application of optically transparent materials, a supply voltage having a frequency twice as low (owing to the use of a *standing* ultrasonic wave), the convenience of matching in the RF section and a low supply voltage (the control voltage in amplitude mode lockers is about 10 V and about 100 V in phase lockers), insignificant heating, and the absence of phase uncertainty in the pulse train. In connection with the last advantage, it should be mentioned that in phase locking of modes, even slight perturbations may lead to a phase change of 180° in the pulse train with respect to the modulating signal [112].

It is well known that upon diffraction of light by a *travelling* ultrasonic wave for a constant ultrasonic power input, an amplitude

modulation of the transmitted light flux does not take place. Hence, unlike acoustooptic Q-switches, the acoustooptic mode lockers employ a *standing* ultrasonic wave and not a travelling one. Upon diffraction of light by such a wave, an amplitude modulation of the light flux takes place in such a wave at a frequency equal to twice the frequency of the modulating signal.

As in the case of acoustooptic Q-switches, *Bragg's diffraction* is employed in acoustooptic mode lockers. The ratio of intensity I_1 of the light passing through the locker to the intensity I_0 of the incident light is given by

$$\frac{I_1}{I_0} = \cos^2 \left[\frac{\pi}{\lambda} \sqrt{2P_a \frac{l}{H} M_2} \sin (2\pi f_m t) \right]. \qquad (3.12.12)$$

This relation is similar to Eq. (3.5.8). The difference between the two is because of the fact that a standing ultrasonic wave is used in this case instead of a travelling one.

Figure 3.69 illustrates the working of an acoustooptic mode locker. Here, *1* is a piezoelectric transducer, *2*—a prism made of fused quartz, and *3*—the direction of propagation of light pulses. The faces *a* and *b* of the quartz prism are parallel to each other (to ensure the creation of a standing wave), while faces *c* and *d* are inclined at a small angle with respect to each other (to prevent the selection of longitudinal modes). The acoustooptic mode locker is an optical element placed inside the resonator of a continuously pumped Nd:YAG laser. In view of the small gain in such lasers, the limiting allowed optical losses in the lockers should not exceed 0.5-1%, taking into account the antireflection coating.

APPENDIX 1

Hermite Polynomials

Hermite Polynomials in Differential Form. We expand the function $H(x, t) = \exp(2xt - t^2)$ into a power series in the neighbourhood of the point $t = 0$:

$$\exp(2xt - t^2) = \sum_{n=0}^{\infty} H_n(x) \frac{t^n}{n!}. \tag{A.1.1}$$

The coefficients $H_n(x)$ of this expansion are essentially *Hermite polynomials*:

$$H_n(x) = \frac{\partial^n}{\partial t^n} H(x, t)\Big|_{t=0}. \tag{A.1.2}$$

The function $H(x, t)$ is called the *generating function* for Hermite polynomials, and can be written in the form

$$\begin{aligned} H(x, t) = \exp(2xt - t^2) &= \exp(x^2) \exp[-(x-t)^2] \\ &= \exp(x^2) \exp[-(x+u)^2], \end{aligned}$$

Substituting this function into (A.1.2), we get

$$\begin{aligned} \frac{\partial^n}{\partial t^n} H(x, t)\Big|_{t=0} &= (-1)^n \frac{\partial^n}{\partial u^n} H(x, u)\Big|_{u=0} \\ &= \exp(x^2)(-1)^n \frac{\partial^n}{\partial u^n} \exp[-(x+u)^2]\Big|_{u=0} \\ &= \exp(x^2)(-1)^n \frac{\partial^n}{\partial x^n} \exp[-(x+u)]\Big|_{u=0}. \end{aligned}$$

Thus,

$$\boxed{H_n(x) = \exp(x^2)(-1)^n \frac{\partial^n}{\partial x^n} \exp(-x^2)}. \tag{A.1.3}$$

The first few polynomials can be written in the following form:

$$H_0(x) = 1; \quad H_1(x) = 2x; \quad H_2(x) = 4x^2 - 2;$$
$$H_3(x) = 8x^3 - 12x; \quad H_4(x) = 16x^4 - 48x^2 + 12.$$

It should be observed that $H_n(-x) = (-1)^n H_n(x)$.

Recurrence Formulas. It follows from (A.1.1) that

$$\frac{\partial}{\partial t} H(x, t) = \sum_{n=0}^{\infty} \frac{H_n(x)}{n!} n t^{n-1}.$$

On the other hand,

$$\frac{\partial}{\partial t} H = \frac{\partial}{\partial t} \exp(2xt - t^2) = 2(x - t) H(x, t).$$

This gives

$$2(x-t)\sum_{n=0}^{\infty}\frac{H_n(x)}{n!}t^n=\sum_{n=0}^{\infty}\frac{H_n(x)}{n!}nt^{n-1}. \tag{A.1.4}$$

Equating the coefficients of t^n, we get from (A.1.4)

$$2x\frac{H_n}{n!}-2\frac{H_{n-1}}{(n-1)!}=\frac{H_{n+1}}{n!}$$

or

$$\boxed{2xH_n-2nH_{n-1}=H_{n+1}}. \tag{A.1.5}$$

Next, differentiating $H(x, t)$ with respect to x, we get

$$\frac{\partial}{\partial x}H(x, t)=\sum_{n=0}^{\infty}\frac{dH_n}{dx}\frac{t^n}{n!}.$$

On the other hand,

$$\frac{\partial}{\partial x}H=\frac{\partial}{\partial x}\exp(2xt-t^2)=2tH(x, t).$$

Consequently,

$$2t\sum_{n=0}^{\infty}\frac{H_n(x)}{n!}t^n=\sum_{n=0}^{\infty}\frac{dH_n}{dx}\frac{t^n}{n!}.$$

Equating the coefficients of t^n, we get

$$\frac{2H_{n-1}}{(n-1)!}=\frac{1}{n!}\frac{dH_n}{dx}$$

or

$$\boxed{2nH_{n-1}=dH_n/dx.} \tag{A.1.6}$$

Differential Equation for Hermite Polynomials. Differentiating Eq. (A.1.5), we get

$$\frac{dH_{n+1}}{dx}=2H_n+2x\frac{dH_n}{dx}-2n\frac{dH_{n-1}}{dx}. \tag{A.1.7}$$

Differentiating Eq. (A.1.6), we get

$$2n\frac{dH_{n-1}}{dx}=\frac{d^2H_n}{dx^2}. \tag{A.1.8}$$

In accordance with (A.1.6), we have

$$\frac{dH_{n+1}}{dx}=2(n+1)H_n. \tag{A.1.9}$$

Substituting (A.1.8) and (A.1.9) in (A.1.7), we get

$$2(n+1)H_n=2H_n+2x\frac{dH_n}{dx}-\frac{d^2H_n}{dx^2}. \tag{A.1.10}$$

Thus, the differential equation for $y = H_n(x)$ can be written in the following form:

$$\boxed{\frac{d^2y}{dx^2} - 2x\frac{dy}{dx} + 2ny = 0} \,. \tag{A.1.11}$$

Degree of Orthonormal Completeness of Hermite Polynomials. Hermite polynomials are orthonormalised over the interval $-\infty < x < \infty$. We shall prove that

$$\boxed{\int_{-\infty}^{\infty} H_n(x)\, H_m(x) \exp(-x^2)\, dx = \sqrt{\pi}\, 2^n n! \delta_{nm}} \tag{A.1.12}$$

where δ is the Kronecker delta. For this purpose, we consider

$$N = (-1)^n \int_{-\infty}^{\infty} H_m(x) \frac{d^n}{dx^n} \exp(-x^2)\, dx = (-1)^n H_m(x) \frac{d^{n-1}}{dx^{n-1}} \exp(-x^2)\Big|_{-\infty}^{\infty}$$

$$+ (-1)^{n+1} \int_{-\infty}^{\infty} \frac{dH_m}{dx} \frac{d^{n-1}}{dx^{n-1}} e^{-x^2} dx$$

$$= (-1)^{n+1} \int_{-\infty}^{\infty} \frac{dH_m}{dx} \frac{d^{n-1}}{dx^{n-1}} e^{-x^2} dx.$$

Integrating m times by parts, we get

$$N = (-1)^{n+m} \int_{-\infty}^{\infty} \frac{d^m H_m}{dx^m} \frac{d^{n-m}}{dx^{n-m}} \exp(-x^2)\, dx. \tag{A.1.13}$$

The derivative $d^m H_m / dx^m$ can be easily found:

$$\frac{dH_m}{dx} = 2mH_{m-1};$$

$$\frac{d^2H_m}{dx^2} = 2m \frac{dH_{m-1}}{dx} = 2m \cdot 2(m-1) H_{m-2};$$

$$\frac{d^3H_m}{dx^3} = 2m \cdot 2(m-1) \frac{dH_{m-2}}{dx} = 2^3 m(m-1)(m-2) H_{m-3};$$

$$\cdots\cdots\cdots\cdots\cdots\cdots\cdots\cdots\cdots\cdots$$

$$\frac{d^m H_m}{dx^m} = 2^m m(m-1)(m-2) \ldots 2 \cdot 1 \cdot H_0 = 2^m m!. \tag{A.1.14}$$

Substituting (A.1.14) into (A.1.13), we get

$$N = (-1)^{n+m} 2^m m! \int_{-\infty}^{\infty} \frac{d^{n-m}}{dx^{n-m}} \exp(-x^2)\, dx. \tag{A.1.15}$$

The integral on the right-hand side of this equation vanishes for $n > m$. For $n = m$, this integral turns into Poisson's integral $\int_{-\infty}^{\infty} \exp(-x^2)\,dx = \sqrt{\pi}$. The equality (A.1.12) is thus proved.

Modified Hermite Polynomials (Hermite-Gauss Polynomials). These polynomials are defined as follows:

$$\boxed{\psi_n(x) = (2^n n!\,\sqrt{\pi})^{1/2}\, H_n(x) \exp(-x^2/2)}. \qquad \text{(A.1.16)}$$

It can be easily shown by using (A.1.12) that

$$\boxed{\int_{-\infty}^{\infty} \psi_n(x)\,\psi_m(x)\,dx = \delta_{nm}}. \qquad \text{(A.1.17)}$$

Differentiating the relation (A.1.16) twice, we get

$$\frac{d^2\psi_n}{dx^2} = (2^n n!\,\sqrt{\pi})^{-1/2} \exp(-x^2/2) \times \left[\frac{d^2 H_n}{dx^2} - 2x\frac{dH_n}{dx} + (x^2-1)\,H_n\right].$$

Using (A.1.10), we get

$$\frac{d^2\psi_n}{dx^2} = (2^n n!\,\sqrt{\pi})^{-1/2} \exp\left(-\frac{x^2}{2}\right)(x^2-1-2n)\,H_n$$

or

$$\frac{d^2\psi_n}{dx^2} = (x^2-1-2n)\,\psi_n.$$

Thus the differential equation for $y = \psi_n(x)$ is of the form

$$\boxed{\frac{d^2y}{dx^2} + (2n+1-x^2)\,y = 0}. \qquad \text{(A.1.18)}$$

APPENDIX 2

Gaussian Beams in Free Space

Assuming that the aperture effects are absent, we can write (see (2.7.7)) $u(x, y, z) = v(x, z)\,v(y, z)$, where

$$v(x, z) = \sqrt{B(z)} \int_{-\infty}^{\infty} \exp\left[-(\xi/\rho_0)^2 + i(\pi/\lambda z)(x-\xi)^2\right] d\xi,$$

$$B(z) = -i(A/\lambda z) \exp(i2\pi z/\lambda). \qquad \text{(A.2.1)}$$

Equation (A.2.1) can be written in the form

$$v(x,\ z)=\sqrt{B(z)}\int\limits_{-\infty}^{\infty}\exp\left[-(a\xi+b)^2+c\right]d\xi, \tag{A.2.2}$$

where it can be easily seen that

$$a(z)=\sqrt{1-i(\pi\rho_0^2/\lambda z)}/\rho_0;$$

$$b(x,\ z)=i\,\frac{\pi\rho_0 x}{\lambda z}\left[\frac{1+i(\pi\rho_0^2/\lambda z)}{1+(\pi\rho_0^2/\lambda z)^2}\right]^{1/2};$$

$$c(x,\ z)=i\,\frac{\pi x^2/\lambda z}{1+(\pi\rho_0^2/\lambda z)^2}-x^2\,\frac{(\pi\rho_0/\lambda z)^2}{1+(\pi\rho_0^2/\lambda z)^2}.$$

Introducing the integration variable $\tau = a\xi + b$, we get

$$v(x,\ z)=[\sqrt{B(z)}/a(z)]\exp[c(x,\ z)]\int\limits_{-\infty}^{\infty}e^{-\tau^2}d\tau$$

$$=\exp[c(x,\ z)]\sqrt{\pi B(z)}/a(z).$$

Thus,

$$u(x,\ y,\ z)=\exp[c(x,\ z)+c(y,\ z)]\,\pi B(z)/a^2(z).$$

Substituting the above expressions for $B(z)$, $a(z)$, $c(x,\ z)$ into this equation (the expression for $c(y,\ z)$ is obtained from the expression for $c(x,\ z)$ by replacing x by y), we get the result (2.7.8).

APPENDIX 3

Stable and Unstable Spherical Waves in an Unstable Resonator

Let R be the solution of Eq. (2.10.20a). This equation has the form

$$R=(AR+B)/(CR+D). \tag{A.3.1}$$

Let us add a small perturbation ΔR to R. As a result of a round-trip of the radiation through the resonator, the initial perturbation ΔR is converted into the perturbation δR, which is defined by the relation

$$\frac{A(R+\Delta R)+B}{C(R+\Delta R)+D}=R+\delta R. \tag{A.3.2}$$

If $|\delta R| < |\Delta R|$, the perturbation *is damped* as the radiation propagates along the resonator. Hence the solution R of Eq. (A.3.1) is *stable*. For $|\delta R| > |\Delta R|$, on the contrary, the perturbation *increases*, thus indicating the *instability* of the solution. Equation (A.3.2) can be transformed as follows:

$$R+\delta R=\left(\frac{AR+B}{CR+D}+\frac{A\,\Delta R}{CR+D}\right)\Big/\left(1+\frac{C\,\Delta R}{CR+D}\right).$$

Using (A.3.1) and considering that $C\Delta R \ll (CR + D)$, we get

$$R+\delta R\approx\left(R+\frac{A\,\Delta R}{CR+D}\right)\left(1-\frac{C\,\Delta R}{CR+D}\right)\approx R+\left(\frac{A-CR}{CR+D}\right)\Delta R.$$

Thus

$$\frac{\delta R}{\Delta R}=\frac{A-CR}{CR+D}. \tag{A.3.3}$$

Equation (A.3.1) is known to have two solutions:

$$R=\frac{1}{2C}[A-D\pm\sqrt{(A+D)^2-4}]. \tag{A.3.4}$$

The plus sign corresponds to the solution (2.10.22a), while the minus sign corresponds to the solution (2.10.22b). Using (A.3.4), we can transform the right-hand side of the relation (A.3.3) as follows:

$$\frac{A-CR}{CR+D}=\frac{(A+D)\mp\sqrt{(A+D)^2-4}}{(A+D)\pm\sqrt{(A+D)^2-4}}.$$

If $(A+D)>2$, we get

$$\frac{(A+D)-\sqrt{(A+D)^2-4}}{(A+D)+\sqrt{(A+D)^2-4}}<1,$$

$$\frac{(A+D)+\sqrt{(A+D)^2-4}}{(A+D)-\sqrt{(A+D)^2-4}}>1.$$

Hence for $(A+D)>2$, the solution (2.10.22a) is stable, while the solution (2.10.22b) is unstable.

The reverse situation arises if $(A+D)<-2$.

APPENDIX 4

Jones' Matrices

For a polarised light wave, the two-component *Jones vector* $\begin{pmatrix}E_x\\E_y\end{pmatrix}$ defines the state of polarisation, E_x and E_y being the components of the electric wave vector. Introducing the amplitude and phase of the wave, we can express the Jones vector in the form $\begin{pmatrix}A_x e^{i\varphi_x}\\A_y e^{i\varphi_y}\end{pmatrix}$. For linearly polarised light, $\varphi_x=\varphi_y$.

Suppose that an optical element (polariser, birefringent plate, etc.) alters the polarisation of the light wave. Suppose that the new Jones vector has the form $\begin{pmatrix}E'_x\\E'_y\end{pmatrix}$. In terms of the original Jones vector, the new vector may be written in the form $\begin{pmatrix}E'_x\\E'_y\end{pmatrix}=\begin{pmatrix}a_{xx}&a_{xy}\\a_{yx}&a_{yy}\end{pmatrix}\begin{pmatrix}E_x\\E_y\end{pmatrix}$, where $\begin{pmatrix}a_{xx}&a_{xy}\\a_{yx}&a_{yy}\end{pmatrix}$ is the *Jones matrix* describing the optical element under consideration.

If a light wave passes successively through *several* optical elements, the resulting Jones matrix is the *product* of the corresponding matrices written in the inverse order to that of the passage of the optical ray through the optical elements.

For a linear polariser, whose transmission plane passes through the z-axis and the x-axis (z-axis is the direction of the wave propagation), the Jones matrix can be written in the form $M_1=\begin{pmatrix}1&0\\0&0\end{pmatrix}$, while for a polariser having yz-plane of transmission, $M_2=\begin{pmatrix}0&0\\0&1\end{pmatrix}$.

In order to get the Jones matrix for a *polariser* whose plane of polarisation forms an angle α with the xz plane, let us consider the transformation of the Jones vector upon a transition from the system of coordinate axes x, y to the system x', y', inclined at an angle α to the former. For the sake of simplicity, we

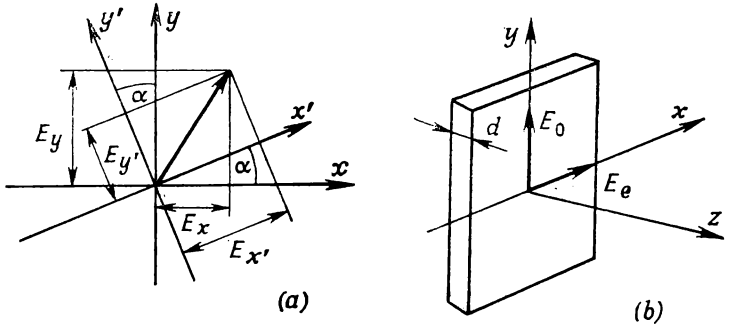


Fig. A.4.1

consider the linearly polarised light. Figure A.4.1*a* shows the projections of the vector **E** on the axes x, y as well as on the axes x', y'. It can be seen from the figure that

$$E_{x'} = E_x \cos\alpha + E_y \sin\alpha; \quad E_{y'} = -E_x \sin\alpha + E_y \cos\alpha.$$

Thus

$$\begin{pmatrix} E_{x'} \\ E_{y'} \end{pmatrix} = \begin{pmatrix} \cos\alpha & \sin\alpha \\ -\sin\alpha & \cos\alpha \end{pmatrix} \begin{pmatrix} E_x \\ E_y \end{pmatrix}.$$

The matrix

$$M(\alpha) = \begin{pmatrix} \cos\alpha & \sin\alpha \\ -\sin\alpha & \cos\alpha \end{pmatrix}$$

is the matrix reducing the Jones vector to the system of axes inclined at an angle α to the initial system.

If the transmission plane of a polariser forms an angle α with the xz-plane, its Jones matrix has the form

$$M_{x\alpha} = M(-\alpha) \begin{pmatrix} 1 & 0 \\ 0 & 0 \end{pmatrix} M(\alpha)$$

$$= \begin{pmatrix} \cos\alpha & -\sin\alpha \\ \sin\alpha & \cos\alpha \end{pmatrix} \begin{pmatrix} 1 & 0 \\ 0 & 0 \end{pmatrix} \begin{pmatrix} \cos\alpha & \sin\alpha \\ -\sin\alpha & \cos\alpha \end{pmatrix} = \begin{pmatrix} \cos^2\alpha & \cos\alpha\sin\alpha \\ \cos\alpha\sin\alpha & \sin^2\alpha \end{pmatrix}.$$

The Jones vector is first reduced to the polariser axes, after which the action of the polariser is taken into consideration. Finally, we return to the initial system of axes.

Suppose that a light wave passes through a *birefringent* plate of thickness d, the optical axis of the plate coinciding with the x-axis (see Fig. A.4.1*b*). We denote the refractive index for the *ordinary* and the *extraordinary* wave by n_0 and n_e respectively. The extraordinary wave is polarised along the x-axis while the ordinary wave is polarised along the y-axis. Upon passing through the plate, the phase of the x-component of the Jones vector (i.e. the phase of the extraordinary wave) acquires an increment $\varphi_e = \omega n_e d/c$, while the phase of the y-com-

ponent (i.e. the phase of the ordinary wave) acquires an increment $\varphi_0 = \omega n_0 d/c$. Consequently,

$$\begin{pmatrix} E'_x \\ E'_y \end{pmatrix} = \begin{pmatrix} \exp(i\varphi_e) & 0 \\ 0 & \exp(i\varphi_0) \end{pmatrix} \begin{pmatrix} E_x \\ E_y \end{pmatrix}.$$

The matrix

$$M(\varphi) = \begin{pmatrix} \exp(i\varphi_e) & 0 \\ 0 & \exp(i\varphi_0) \end{pmatrix}$$

is the Jones matrix for a birefringent plate, oriented in such a way that its optical axis coincides with the x-axis.

If the optical axis of the plate forms an angle α with the x-axis, the Jones vector must be reduced to a system of axes inclined at an angle α to the initial system. After passing through the plate, the vector must be brought back to the initial system of axes. The Jones matrix in this case is the product of the matrices: $M(-\alpha)\, M(\varphi)\, M(\alpha)$.

APPENDIX 5

Singular Points of a Two-dimensional Dynamic System

Suppose that a dynamic system is described by a certain *nonlinear* system of equations:

$$\left.\begin{aligned} dm/d\tau &= F(m, n); \\ dn/d\tau &= \Phi(m, n), \end{aligned}\right\} \qquad (A.5.1)$$

where $m(\tau)$ and $n(\tau)$ are functions of time τ, being the dynamic parameters of the system.

Let $m = m_A$ and $n = n_A$ be the coordinates of one of the *singular points* of the system. Considering the *neighbourhood* of this singular point, we can write

$$m(\tau) = m_A + \mu(\tau); \quad n(\tau) = n_A + \nu(\tau), \qquad (A.5.2)$$

where μ and ν are first-order infinitesimals. Substituting (A.5.2) in (A.5.1), and neglecting the terms containing the second and higher order infinitesimals, we get the following system of *linear* equations instead of (A.5.1):

$$\left.\begin{aligned} d\mu/d\tau &= a\mu + b\nu; \\ d\nu/d\tau &= c\mu + d\nu. \end{aligned}\right\} \qquad (A.5.3)$$

The solution $\mu(\tau)$ (and similarly $\nu(\tau)$) of this system is sought in the form

$$\mu(\tau) = C_1 \exp(p_1\tau) + C_2 \exp(p_2\tau),$$

where p_1 and p_2 are the roots of the *characteristic equation*

$$p^2 + p(a + d) + (ad - bc) = 0. \qquad (A.5.4)$$

Six qualitatively different situations are possible, corresponding to six different types of singular points. Figure A.5.1 shows the phase portraits in the neighbourhood of these points:

Fig. A.5.1*a* corresponds to a singular point of *stable node* type (in this case, the roots p_1 and p_2 are real and negative);

Fig. A.5.1*b* corresponds to a singular point of *unstable node* type (the roots p_1 and p_2 are real and positive);

Fig. A.5.1*c* corresponds to a singular point of the *saddle* type (the roots p_1 and p_2 are real and opposite in sign);

Fig. A.5.1*d* corresponds to a singular point of *stable focus* type (the roots p_1 and p_2 are complex and their real parts are negative);

Fig. A.5.1*e* corresponds to a singular point of *unstable focus* type (the roots p_1 and p_2 are complex and their real parts are positive);

Fig. A.5.1*f* corresponds to a singular point of the *centre* type (the roots p_1 and p_2 are imaginary).

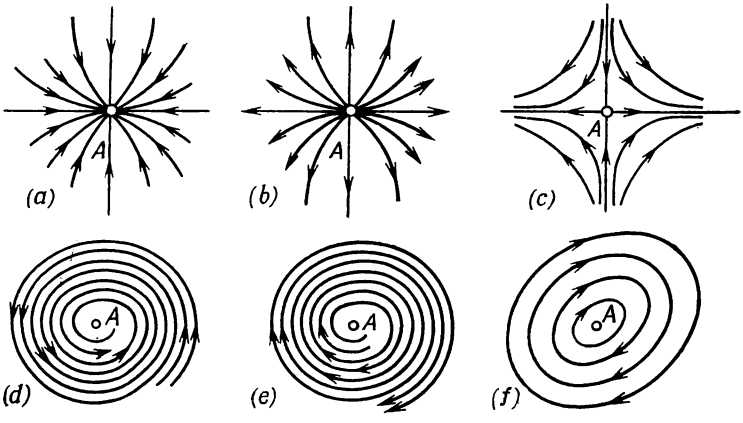


Fig. A.5.1

The state of a system represented by a singular point in Figs. A.5.1*a* and *d* is *stable*. Any arbitrary ejection of the system from this state brings it to a phase trajectory which returns the system to the initial state without any change. On the contrary, the state of the system represented by the singular point in Figs. A.5.1*b*, *c*, and *e* is *unstable*. Any arbitrarily small perturbation brings the system to a trajectory which takes it away from the initial state. In Fig. A.5.1*f*, we can speak about the stability of the state represented by the singular point in the sense that for sufficiently small perturbations, the system is found to be on a phase trajectory in the vicinity of the initial state.

REFERENCES

CHAPTER ONE

1. Tarasov, L. V., *Physical Principles of Quantum Electronics.* Sov. Radio, Moscow, 1976 (in Russian).
2. Bates, D. R. (Ed.), *Atomic and Molecular Processes.* Academic Press, N.Y.-London, 1962.
3. Vainshtein L. A., I. I. Sobel'man, and E. A. Yukov, *Electronic Excitation Cross Sections of Atoms and Ions.* Nauka, Moscow, 1973 (in Russian).
4. Prokhorov, A. M. (Ed.), *Handbook of Lasers* (in two volumes), Vol. I. Sov. Radio, Moscow, 1978 (in Russian).
5. Petrash, G. G., *Usp. Fiz. Nauk*, **105**, 4, 645 (1971). Isayev, A. A., G. G. Petrash, *Trudy FIAN SSSR*, **81**, 3 (1975).
6. Mikhailin, V. V., S. P. Chernov, and A. V. Shepelev, *Kvant. Electronika*, 5, 8, 1759 (1978); P. L. Kzonka, *ibid*, p. 1749.
7. Ishchenko, E. F. and Yu. M. Klimkov, *Lasers.* Sov. Radio, Moscow, 1968 (in Russian).
8. Ryabov, S. G., G. N. Toropkin, and I. F. Usoltsev, *Quantum Electronics Instruments.* Sov. Radio, Moscow, 1976 (in Russian).
9. Koechner, W., *Solid-state Laser Engineering.* Springer-Verlag, N.Y.-Heidelberg-Berlin, 1976.
10. Mikaelyan, A. L., M. L. Ter-Mikaelyan, and Yu. G. Turkov, *Solid-State Lasers.* Sov. Radio, Moscow, 1967 (in Russian).
11. Stepanov, B. I. (Ed.), *Computation Methods in Lasers* (in two volumes), Vol. II. Nauka i Tekhnika, Minsk, 1968 (in Russian).
12. Mak, A. A., Yu. A. Anan'ev, and B. A. Ermakov, *Usp. Fiz. Nauk*, **92**, 3, 373 (1967).
13. Görlich, P., H. Karras, G. Kötitz, and R. Lehmann, *Spectroscopic Properties of Activated Laser Crystals.* Akademie-Verlag, Berlin, 1966.
14. Kaminskii, A. A., *Laser Crystals.* Nauka, Moscoskw, 1975 (in Russian).
15. Belostotskii, B. R., Yu. V. Lyubavskii, and V. M. Ovchinnikov, *Fundamentals of Laser Engineering.* Sov. Radio, Moscow, 1972 (in Russian).
16. Belostotskii, B. R. and A. S. Rubanov, *Thermal Conditions in Solid-state Lasers.* Energiya, Moscow, 1973 (in Russian).
17. Ryabtsev, N. G., *Materials of Quantum Electronics.* Sov. Radio, Moscow, 1972 (in Russian).
18. Jonson, L. F., L. G. Van Uitert, J. J. Rubin, and R. A. Thomas, *Phys. Rev.*, **133A**, 1, 494 (1964).
19. Tolstoi, M. N., in: *Spectroscopy of Crystals.* Nauka, Moscow, 1970 (in Russian).
20. Voron'ko, Yu. K., A. A. Kaminskii, V. V. Osiko, and A. M. Prokhorov, *Izv. Akad. Nauk SSSR. Series Inorganic Materials*, **2**, 7, 1161 (1966).
21. Kaminskii, A. A., *Izv. Akad. Nauk SSSR. Series Inorganic Materials*, **7**, 5, 904 (1971).
22. Maiman, T. H., *Nature*, **187**, 4736, 493 (1960).
23. Frish, S. E., *Optical Atomic Spectra.* Fizmatgiz, Moscow-Leningrad, 1963 (in Russian).
24. Bilak, V. I., N. R. Dokuchaev, A. M., Onishchenko, V. A. Pashkov, A. I. Petrov, M. F. Stelmakh, and N. P. Chernousov, *Kvant. Electronika*, **2**, 5, 1050 (1975).
25. Stepanov, B. I. and A. N. Rubinov, *Usp. Fiz. Nauk*, **95**, 1, 45 (1968).
26. Bass. M., T. Deutsch, and M. Weber, *Usp. Fiz. Nauk*, **105**, 3, 521 (1971).
27. Schäfer, F. P. (Ed.), *Dye Lasers.* Springer-Verlag, Berlin-Heidelberg-N.Y., 1973.

28. Tomin, V. I., N. A. Nemkovich, and A. N. Rubinov, *Kvant. Elektronika*, 5, 5, 986 (1978).
29. Rabinowitz, P., S. Jacobs, and G. Gould, *Appl. Optics*, **1**, 4, 513 (1962).
30. Rautian, S. G. and I. I. Sobel'man, *Zh. Eksp. Teor. Fiz.*, **41**, 6, 2018 (1961).
31. Mikheev, L. D., *Kvant. Electronika*, **5**, 6, 1189 (1978).
32. Kasper, J. V. and G. C. Pimental, *Appl. Phys. Letters*, **5**, 11, 231 (1964).
33. Golger, A. L., L. I. Gudzenko, and S. I. Yakovlenko, *Kvant. Elektronika*, 5, 9, 1982 (1978).
34. Bennett, W. R., Jr., Chemical Lasers, in: *J. Appl. Optics. Suppl.* (1965); G. Gould, Chemical Lasers, in: *Appl. Optics Suppl.* (1965); A. L. Bloom, *Proc. IEEE*, **54**, 10, 1262 (1966).
35. Allen, L. and D. G. C. Jones, *Principles of Gas Lasers*. Butterworth, London, 1967.
36. Eletskii, A. V. and B. M. Smirnov, *Gas Lasers*. Atomizdat, Moscow, 1971 (in Russian).
37. Pestov, E. G. and G. M. Lapshin, *Quantum Electronics*. Voenizdat, Moscow, 1972 (in Russian).
38. Strakhovskii, G. M. and A. V. Uspenskii, *Fundamentals of Quantum Electronics*. Vysshaya Shkola, Moscow, 1979 (in Russian).
39. Kitaeva, V. F., A. I. Odintsov, and N. N. Sobolev, *Usp. Fiz. Nauk*, **99**, 3, 361 (1969).
40. Landau, L. D. and E. M. Lifschitz, *Quantum Mechanics* (Non-relativistic Theory). Pergamon Press, Oxford, 1977.
41. Javan, A., W. R. Bennett, and D. R. Herriott, *Phys. Rev. Letters*, **6**, 3, 106 (1961).
42. Patel, C. K. N., *Phys. Rev. Letters*, **13**, 21, 617 (1964).
43. Tychinskii, V. P., *Usp. Fiz. Nauk*, **91**, 3, 389 (1967).
44. Sobolev, N. N. and V. V. Sokovikov, *Usp. Fiz. Nauk*, **91**, 3, 425 (1967).
45. Patel, C. K. N., *Sci. Am.*, **219**, 2233 (1968).
46. Kuz'min, G. P., *Radiotekh. i Electronika*, **18**, 8, 1553 (1973).
47. Basov, N. G., E. M. Belenov, V. A. Danilychev, and A. F. Suchkov, *Usp. Fiz. Nauk*, **114**, 2, 213 (1974).
48. Danilychev, V. A., O. M. Kerimov, and I. B. Kovsh, *Trudy FIAN SSSR*, 85, 49 (1976).
49. Fenstermacher, C. A., M. I. Nutter, I. C. Rink, and K. Boyer, *Bull. Am. Phys. Soc.*, **16**, 42 (1971).
50. Basov, N. G., E. M. Belenov, V. A. Danilychev, and A. F. Suchkov, in: *Quantum Electronics*, No. 3 (N. G. Basov, Ed.), *Sov. Radio*, Moscow, 1971 (in Russian).
51. Galaktionov, I. I., V. Yu. Gorelov, and I. V. Podmoshenskii, *Kvant. Electronika*, **3**, 12, 2570 (1976).
52. Batyrbekov, G. A., V. A. Danilychev, I. B. Kovsh, M. P. Mardenov, and M. U. Khasenov, *Kvant. Electronika*, **4**, 5, 1166 (1977).
53. Basov, N. G. and A. N. Oraevskii, *Zh. Eksp. Teor. Fiz.*, **44**, 5, 1742 (1963).
54. Basov, N. G., A. N. Oraevskii, and V. A. Shcheglov, *Zh. Tekh. Fiz.*, **37**, 2, 339 (1967).
55. Losev, S. A., *Gasdynamic Lasers*. Springer-Verlag, Berlin-Heidelberg-N.Y., 1981.
56. Konyukhov, V. K., *Kvant. Electronika*, **4**, 5, 1014 (1977).
57. Konyukhov, V. K. and A. M. Prokhorov, *Pis'ma v Sh.E.T.F.*, **3**, 11, 435 (1966).
58. Oraevskii, A. N., *Zh. Eksp. Teor. Fiz.*, **42**, 2, 177 (1963).
59. Talroze, V. L., *Kinetika i Kataliz*, 5, 1, 11 (1964).
60. Tijoev, M. S., V. T. Platonenko, and R. V. Khokhlov, *Usp. Fiz. Nauk*, **100**, 4, 641 (1970).
61. Basov, N. G., V. I. Igoshin, E. P. Markin, and A. N. Oraevskii, in: *Quantum Electronics*, No. 2 (N. G. Basov, Ed.), Sov. Radio, Moscow, 1971 (in Russian).
62. Oraevskii, A. N., *Zh. Eksp. Teor. Fiz.*, 55, 10, 1423 (1968).

63. Cool, T. A., F. J. Falk, and R. R. Stephens, *Appl. Phys. Letters*, 15, 10, 318 (1969).
64. Pollack, M. A., *Appl. Phys. Letters*, 8, 9, 237 (1965).
65. Gerasimov, Yu. A., G. N. Kashnikov, V. K. Orlov, A. K. Piskunov, Yu. V. Romanenko, and A. V. Taran, *Kvant. Electronika*, 2, 1, 140 (1975).
66. Bashkin, A. S., A. N. Oraevskii, V. N. Tomashev, and N. N. Yuryshev, *Kvant. Electronika*, 3, 2, 362 (1976).
67. Bashkin, A. S., N. L. Kupriyanov, and A. N. Oraevskii, *Kvant. Electronika*, 4, 5, 1063 (1977).
68. Smirnov, B. M., *Atomic Collisions and Elementary Processes in Plasma.* Atomizdat, Moscow, 1968 (in Russian).
69. Gudrenko, L. I. and S. I. Yakovlenko, *Plasma Lasers.* Atomizdat, Moscow, 1978 (in Russian).
70. Gudrenko, L. I., L. A. Shelepin, and S. I. Yakovlenko, *Usp. Fiz. Nauk*, 114, 3, 457 (1974); *Trudy FIAN SSSR*, 83, 100 (1975).
71. Zhukov, V. V., E. L. Latush, V. S. Mikhalevskii, and M. F. Sam, *Kvant. Electronika*, 4, 6, 1249 (1977); V. V. Zhukov, V. S. Kucherov, E. L. Latush, and M. F. Sam, *Kvant. Elektronika*, 4, 6, 1257 (1977).
72. Frank-Kamenetskii, D. A., *Lectures on Plasma Physics*, Atomizdat, Moscow, 1968 (in Russian).
73. Kondrat'ev, V. N., *Rate Constants in Gaseous Phase Reactions.* Nauka, Moscow, 1971 (in Russian).

CHAPTER TWO

1. Tarasov, L. V., *Physical Principles of Quantum Electronics (Optical Region).* Sov. Radio, Moscow, 1976 (in Russian).
2. Prokhorov, A. M. (Ed.), *Handbook of Lasers* (in two volumes), Vol. II. Sov. Radio, Moscow, 1978 (in Russian).
3. Stepanov, B. I. (Ed.), *Computation Methods in Lasers* (in two volumes), Vol. I. Nauka i Tekhnika, Minsk, 1968 (in Russian).
4. Gerrard, A. and J. M. Burch, *Introduction to Matrix Methods in Optics.* J. Wiley and Sons, London-N.Y.-Sydney-Toronto, 1975.
5. Mandelshtam, L. I., *Lectures on Theory of Oscillations.* Nauka, Moscow, 1972.
6. Zhabotinskii, M. E. (Ed.), *Quantum Electronics: Small Encyclopaedia.* Sov. Encyclopaedia, Moscow, 1969 (in Russian).
7. Marcuse, D., *Light Transmission Optics.* Van Nostrand Reinhold Co., N.Y., 1972.
8. Prokhorov, A. M. (Ed.), *Handbook of Lasers* (in two volumes), Vol. I. Sov. Radio, Moscow, 1978 (in Russian).
9. Maitland, A. and M. H. Dunn, *Laser Physics.* North-Holland Publishing Co., Amsterdam-London, 1969.
10. Bennett, W. R., Jr., *Appl. Optics*, 1, 24 (1962).
11. Dmitriev, V. G., B. M. Umanskii, and N. V. Shkunov, in: *Quantum Electronics*, (N. G. Basov, Ed.), No. 2. Sov, Radio, Moscow, 1966 (in Russian).
12. Mikaelyan, A. L. and V. V. Dyachenko, *Kvant. Electronika*, 1, 4, 937 (1974).
13. Mikaelyan, A. L., M. L. Ter-Mikaelyan, and Yu. G. Turkov, *Solid-state Lasers.* Sov. Radio, Moscow, 1967 (in Russian).
14. Vainshtein, L. A., *Open Resonators and Open Waveguides.* Sov. Radio, Moscow, 1966 (in Russian).
15. Kogelnik, H. and T. Li., *Appl. Optics*, 5, 10, 1550 (1976).
16. Ishchenko, E. F. and Yu. M. Klimkov, *Lasers.* Sov. Radio, Moscow, 1968 (in Russian).
17. Goncharenko, A. M., *Gaussian Light Beams.* Nauka i Tekhnika, Minsk, 1977 (in Russian).
18. Prokhorov, A. M., *Zh. Eksp. Teor. Fiz.*, 34, 6, 1658 (1958).

19. Dicke, R. H., *Molecular Amplification and Generation Systems and Methods.* US Pat. 2851652, 1958.
20. Schawlow, A. L. and C. H. Townes, *Phys. Rev.*, **29**, 1940 (1958).
21. Landsberg, G. S., *Optics*, Nauka, Moscow, 1976 (in Russian).
22. Boyd, C. D. and J. P. Gordon, *Brit. Sci. Tech. Journ.*, **40**, 2, 489 (1961).
23. Gordon, J. P. and H. Kogelnik, *Brit. Sci. Tech. Journ.*, **43**, 6, 2873 (1964).
24. Privalov, V. E. and S. A. Fridrikhov, *Usp. Fiz. Nauk*, **97**, 3, 377 (1969).
25. Fyodorov, B. F., A. G. Sheremetyev, and V. N. Umnikov, *Laser Gyroscope.* Mashinostroeniye, Moscow, 1973 (in Russian).
26. Bychkov, S. I., D. P. Luk'yanov, and A. I. Bakalyar, *Laser Gyroscope.* Sov. Radio, Moscow, 1975 (in Russian).
27. Borovnikov, V. A. and B. E. Kinber, *Geometrical Theory of Diffraction.* Svyaz, Moscow, 1978 (in Russian).
28. Boyd, G. and H. Kogelnik, *Brit. Sci. Tech. Journ.*, **41**, 4, 1347 (1962).
29. Goodman, J. W., *Introduction to Fourier Optics.* McGraw-Hill Book Co., San Francisco-N.Y., 1968.
30. Fox, A. and T. Li, *Brit. Sci. Tech. Journ.*, **40**, 2, 453 (1961).
31. Gradshtein, I. S. and I. M. Ryzhik, *Tables of Integrals, Sums, Series, and Products*, Nauka, Moscow, 1971 (in Russian).
32. Kogelnik, H., *Brit. Sci. Tech. Journ.*, **44**, 3, 455 (1965).
33. Vakhitov, N. G., V. A. Zenkin, V. R. Kushnir, and N. V. Shkunov, *Elektr. Tekhnika, Series* 10, *Kvantovaya Electronika*, 1, 24 (1975).
34. Goubau, G. and F. Schwering, *IRE Trans.*, **AP-9**, 248 (1961).
35. Kogelnik, H., *Appl. Optics*, **4**, 12, 1562 (1965).
36. Tien, P., J. Gordon, and J. Whinnery, *Proc. IEEE*, **53**, 2, 129 (1965).
37. Deschamps, G. A. and P. E. Mast, in: Proceedings of the Symposium on Quasi-Optics, New York, 1964.
38. Siegman, A. E., *Proc. IEEE*, **53**, 3, 277 (1965).
39. Siegman, A. E. and R. Arrathoon, *IEEE Journ.*, **QE-3**, 4, 156 (1967).
40. Anan'ev, Yu. A., N. A. Sventsitskaya, and V. E. Sherstobitov, *Zh. Eksp. Teor. Fiz.*, **55**, 1, 130 (1968).
41. Bergstein, L. *Appl. Optics*, **7**, 3, 495 (1968).
42. Sanderson, R. L. and W. Streifer, *Appl. Optics*, **8**, 10, 495 (1968).
43. Siegman, A. E., *Appl. Optics.*, **13**, 2, 353 (1974).
44. Anan'ev, Yu. A., in: *Quantum Electronics* (N. G. Basov, Ed.) No. 6. Sov. Radio, Moscow (in Russian).
45. Fox, A. C. and T. Li, in: *Proceedings of the III International Congress on Quantum Electronics*, New York, Columbia Univ. Press, 1964.
46. Anan'ev, Yu. A. and V. E. Sherstobitov, in: *Quantum Electronics* (N. G. Basov, Ed.) No. 3, Sov. Radio, Moscow, 1971 (in Russian).
47. Anan'ev, Yu. A., V. N. Chernov, and V. E. Sherstobitov, in: *Quantum Electronics* (N. G. Basov, Ed.) No. 4, Sov. Radio, Moscow, 1971 (in Russian).
48. Anan'ev, Yu. A., G. N. Vinokurov, L. V. Kovalchuk, N. A. Sventsitskaya, and V. E. Sherstobitov, *Zh. Eksp. Teor. Fiz.*, **58**, 3, 786 (1970).
49. Golubeva, N. S., L. F. Krinitsyna, L. S. Orbachevskii, and V. I. Rozhdestvin, *Kvant. Electronika*, **4**, 1, 49 (1977).
50. Galutva, G. V. and A. I. Ryazantsev, *Selection of Types of Vibration and Frequency Stabilization in Lasers.* Svyaz, Moscow, 1972 (in Russian).
51. Anan'ev, Yu. A., *Usp. Fiz. Nauk*, **103**, 4, 705 (1971).
52. Bonch-Bruevich, A. M., N. N. Kostin, and V. A. Khodovoi, *Optika i Spectroskopiya*, **24**, 6, 1014 (1968).
53. Basov, N. G. and V. S. Letokhov, *Pis'ma v Zh. E.T.F.*, **2**, 1, 6 (1966).
54. White, A., *Brit. Sci. Tech. Journ.*, **45**, 2, 339 (1966).
55. Bakeev, A. A. and N. V. Cheburkin, *Radiotekh. i Electronika*, **14**, 7, 1302 (1969).
56. Averbakh, V. S., S. N. Vlasov, and V. I. Talanov, *Izv. Vuzov SSSR. Radiofizika*, **10**, 9, 10, 1333 (1967).

57. Shurkliff, W. A., *Polarised Light, Production and Use.* Harvard Univ. Press, Cambridge, Mass., 1962.
58. Molchanov, V. Ya. and G. V. Skrotskii, in: *Quantum Electronics* (N. G. Basov, Ed.) No. 4, Sov. Radio, Moscow, 1971 (in Russian).
59. Letokhov, V. S., *Pis'ma v Zh. E.T.F.*, **6**, 4, 597 (1967).
60. Bennett, W. R., in: *Proceedings of the III International Congress on Quantum Electronics*, New York, Columbia Univ. Press, 1964.
61. Belostotskii, B. R. and A. S. Rubanov, *Thermal Conditions in Solid-state Lasers*, Energiya, Moscow, 1973 (in Russian).
62. Sukhorukov, A. P., in: *Nonlinear Processes in Optics* (R. V. Khokhlov, Ed.). Nauka, Novosibirsk, 1970.
63. Maldutis, E. K., Yu. I. Reksnis, and S. V. Sakalauskas, *Kvant. Electronika*, **2**, **11**, 2493 (1975).
64. Zheltov, G. I. and Yu. A. Polkanov, in: *Quantum Electronics and Laser Spectroscopy* (A. M. Samson, Ed.). Nauka i Tekhnika, Minsk, 1974 (in Russian).
65. Vigasin, A. A. and A. P. Sukhorukov, *Kvant. Electronika*, **2**, 3, 519 (1975).
66. Vorob'ev, V. V. and V. V. Shemetov, *Kvant. Electronika*, **2**, 7, 1428 (1975).
67. Bykov, V. P., N. G. Vakhytov, V. K. Novokreshchenov, and N. V. Shkunov, in: *Quantum Electronics* (N. G. Basov, Ed.), No. 2, Sov. Radio, Moscow, 1971 (in Russian).
68. Kushnir, V. R., A. N. Nemkov, and N. V. Shkunov, *Kvant. Electronika*, **2**, 6, 1312 (1975).
69. Kushnir, V. R., *Kvant. Electronika*, **2**, 6, 1312 (1975).
70. Mikaelyan, A. L. and V. V. Dyachenko, *Pis'ma v Zh. E.T.F.*, **16**, 25 (1972).
71. Glushchenko, N. F., V. V. Dyachenko, A. L. Mikaelyan, and P. P. Tsaryev, *Kvant. Electronika*, **4**, 4, 783 (1977).
72. Born, M. and E. Wolf, *Principles of Optics.* Pergamon Press, Oxford, 1964.
73. Zolotov, E. M., V. A. Kiselev, and V. A. Sychugov, *Usp. Fiz. Nauk*, **112**, 2, 231 (1974).
74. Itskhoki, I. Ya, *Zarubezhnaya Radioelectronika*, **9**, 99 (1975).
75. Barnoski, M. K. (Ed.), *Introduction to Integrated Optics.* Plenum Press, N.Y.-London, 1974.
76. Kogelnik, H., *Usp. Fiz. Nauk*, **121**, 4, 695 (1977).
77. Tamir, T. (Ed.), *Integrated Optics.* Springer-Verlag, Berlin-Heidelberg-N.Y., 1975.
78. Zolotov, E. M., V. M. Pelekhatyi, and A. M. Prokhorov, *Kvant. Elektronika*, **3**, 7, 1478 (1976).
79. Brillouin, L. and M. Parodi, *Propagation des Ondes dans les Milieux Périodiques.* Dunod, Paris, 1956.
80. Rivlin, L. A., *Pis'ma v Zh. E.T.F.*, **1**, 7 (1965).
81. Kogelnik, H. and C. V. Shank, *Appl. Phys. Letters*, **18**, 4, 152 (1971).
82. Kogelnik, H. and C. V. Shank, *J. Appl. Phys.*, **43**, 5, 2328 (1972).
83. Luk'yanov, V. N., A. T. Semenov, N. V. Shelkov, and S. D. Yakubovich, *Kvant. Elektronika*, **2**, 11, 2373 (1975).
84. Tang, C. L. in: *Introduction to Integrated Optics* (M. K. Barnoski, Ed.). Plenum Press, N.Y.-London, 1974.
85. Deryugin, L. N., O. I. Ovcharenko, V. E. Sotin, and T. K. Chekhlova, *Kvant. Elektronika*, **2**, 9, 2073 (1975).

CHAPTER THREE

1. Mikaelyan, A. L., M. L. Ter-Mikaelyan, and Yu. G. Turkov, *Solid-state Lasers.* Sov. Radio, Moscow, 1967 (in Russian).
2. Stepanov, B. I. (Ed.), *Computation Methods in Lasers* (in two volumes), Vol. II. Nauka i Tekhnika, Minsk, 1968 (in Russian).
3. Mashkevich, V. S., *Kinetic Theory of Lasers.* Nauka, Moscow, 1971 (in Russian).

4. Khanin, Ya. I., *Laser Dynamics* (*Quantum Radiophysics, Vol.* 2). Sov. Radio, Moscow, 1975 (in Russian).
5. Rivlin, L. A., *Dynamics of Semiconductor Laser Radiation.* Sov. Radio, Moscow, 1976 (in Russian).
6. Pilipovich, V. A. and A. A. Kiselev, *Bleachable Filter Lasers.* Nauka i Tekhnika, Minsk, 1975 (in Russian).
7. Morozov, V. N. and A. N. Oraevskii, *Zh. Tekh. Fiziki*, **37**, 5, 947 (1967).
8. Voropaev, N. D. and A. N. Oraevskii, *Izv. Vuzov SSSR, Radiofizika*, 8, 2, 409 (1965).
9. Vinokurov, G. N., N. M. Galaktionova, V. F. Egorova, A. A. Mak, B. M. Sedov, and Ya. I. Khanin, *Zh. Eksp. Teor. Fiz.*, **60**, 2, 489 (1971).
10. Livshits, B. L., *Zh. Eksp. Teor. Fiz.*, **59**, 2 (8), 156 (1970).
11. Kirsanov, B. P., A. M. Leontovich, and A. M. Mozharovskii, *Kvant. Electronika*, 1, 10, 2211 (1974).
12. Tang, C., H. Statz, and G. De Mars, *J. Appl. Phys.*, **34**, 8, 2289 (1963).
13. Letokhov, V. S., *Zh. Eksp. Teor. Fiz.*, 55, 5 (11), 1943 (1968).
14. Kuznetsova, T. I., *Zh. Eksp. Teor. Fiz.*, **57**, 11, 1673 (1969).
15. Collins, R., D. Nelson, A. Schawlow, W. Bond, C. G. B. Garrett, and W. Kaiser, *Phys. Rev. Letters*, 5, 7, 303 (1960).
16. Dementyev, V. A., T. N. Zubarev, and A. N. Oraevskii, *Trudy FIAN SSSR*, **91**, 237, (1977).
17. Belenov, E. M., V. N. Morozov, and A. N. Oraevskii, *Trudy FIAN SSSR*, 52, 237 (1970).
18. Golyaev, Yu. D., Ph. D. Thesis, Moscow State University, Moscow, 1973.
19. Leontovich, A. M. and V. L. Churkin, *Zh. Eksp. Teor. Fiz.*, **59**, 1 (7), 7 (1970).
20. Akhmanov, S. A., Yu. D. Golyaev, and V. G. Dmitriev, *Zh. Eksp. Teor. Fiz.*, **62**, 1, 13 (1972).
21. Golyaev, Yu. D. and S. V. Lantratov, *Kvant. Elektronika*, **1**, 10, 2197 (1974).
22. McClung, F. and R. Hellwarth, *J. Appl. Phys.*, 33, 3, 828 (1962).
23. Hellwarth, R., in: *Lasers* (A. Levine, Ed.), Vol. I, New York, 1966.
24. Dmitriev, V. G., I. Ya. Itskhoki, and E. M. Shvom, *Elektron. Tekhnika, ser.* 10: *Kvant. Elektronika*, 1, 30 (1975).
25. Mustel, E. R. and V. N. Parygin, *Methods of Modulation and Scanning of Light.* Nauka, Moscow, 1970 (in Russian).
26. Belostotskii, B. R., Yu. V. Lyubavskii, and V. M. Ovchinnikov, *Fundamentals of Laser Engineering*, Sov. Radio, Moscow, 1972 (in Russian).
27. Lisitsa, M. P., *Kvantovaya Elektronika*, Inst. Semiconductors, Acad. Sci. Ukr. SSR, 6, 3, (1972).
28. Magdich, L. N. and V. Ya. Molchanov, *Acoustooptic Instruments and Their Applications*, Sov. Radio, Moscow, 1978 (in Russian).
29. Letokhov, V. S. and A. F., Suchkov, *Trudy FIAN SSSR*, **43**, 169 (1968).
30. Mikaelyan, A. L. and Yu. G. Turkov, *Radiotekh. i Elektronika*, **9**, 4, 743 (1964).
31. Rivlin, L. A., *Zh. Eksp. Teor. Fiz.*, **47**, 8, 624 (1964).
32. Bret, G. and F. Gires, *Appl. Phys. Letters*, **4**, 10, 173 (1964).
33. Hargrove, L., R. Fork, and M. Pollack, *Appl. Phys. Letters*, 5, 1, 4 (1965).
34. De Maria, A., D. Stetser, and H. Heunau, *Appl. Phys. Letters*, 8, 7, 174 (1966).
35. Malyshev, V. I., A. S. Markin, and A. A. Sychev, *Pis'ma v Zh. E.T.F.*, 6, 2, 503 (1967).
36. Weber, H., *J. Appl. Phys.*, 39, 13, 6041 (1968).
37. Kaitmazov, S. D., I. K. Krasyuk, P. P. Pashinin, and A. M. Prokhorov, *Dokl. Akad. Nauk SSSR*, **180**, 6, 1331 (1968).
38. De Maria, A., W. Glenn, M. Brienza, and M. Mack, *Proc. IEEE*, **57**, 1, 2, (1969).
39. Zeldovich, B. Ya. and T. I. Kuznetsova, *Usp. Fiz. Nauk*, **106**, 1, 47 (1972).
40. Markin, A. S., *Trudy FIAN SSSR*, 56, 3, (1971).

41. Gurevich, G. L. and L. K. Ingel, *Izv. Vuzov SSSR. Radiofizika*, **17**, 2, 219 (1974).
42. Morozov, V. N., V. V. Nikitin, and A. A. Sheronov, *Pis'ma v Zh. E.T.F.*, **7**, 9, 327 (1968).
43. Lyon, D., E. George, and H. Haus, *Appl. Phys. Letters*, **17**, 11, 474 (1970).
44. Bondarenko, A. N., G. V. Krivoshchekov, V. M. Semibalamut, V. A. Smirnov, and M. F. Stupak, *Izv. Vuzov SSSR. Radiofizika*, **14**, 10, 1615 (1971).
45. Khanin, Ya. I., *Kvant. Elektronika*, 5, 3, 590 (1978).
46. Austin, D. H., *IEEE Journ.*, **QE-4**, 6, 420 (1968).
47. Signore, R., *Revue de Physique Appliquee*, 8, 33 (1973).
48. Smith, P., *Appl. Phys. Letters*, **13**, 7, 235 (1968).
49. Arkelyan, V. S., N. V. Karlov, and A. M. Prokhorov, *Pis'ma v Zh. E.T.F.*, **10**, 6, 279 (1969).
50. Michon, M., J. Ernest, and R. Auffer, *IEEE Journ.*, **QE-5**, 2, 125 (1969).
51. Dukhovnyi, A. M., A. A. Mak, and V. A. Fromzel, *Zh. Eksp. Teor. Fiz.*, **59**, 10, 1165 (1970).
52. Dmitriev, V. G., E. A. Shalaev, and E. M. Shvom, *Kvant. Elektronika*, **2**, 8, 1834 (1975).
53. Maydan, D., *J. Appl. Phys.*, **41**, 4, 1552 (1970).
54. Chesler, R. B. and D. Maydan, *J. Appl. Phys.*, **42**, 3, 1028 (1971).
55. Maydan, D. and R. B. Chesler, *J. Appl. Phys.*, **42**, 3, 1031 (1971).
56. Moran, J. M., *IEEE Journ.*, **QE-12**, 10, 639 (1976).
57. Konvisar, P. G., S. R. Rustamov, O. O. Silichev, and A. A. Fomichev, *Abstracts of the VIII All-Union Conference on Coherent and Nonlinear Optics*, Tbilisi, 1976.
58. Morton, R. G., M. E. Mack, and I. Itzkan, *Appl. Optics*, **17**, 20, 3268 (1978).
59. Chesler, R. B., M. A. Karr, and J. E. Geusic, *Proc. IEEE*, 58, 1899 (1970).
60. Geusic, J. E., M. L. Hensel, and R. G. Smith, *Appl. Phys. Letters*, 6, 175 (1965).
61. Koechner, W., *Rev. Sci. Instr.*, **41**, 12, 1699 (1970).
62. Baldwin, G. D., *IEEE Journ.*, **QE-7**, 6, 220 (1971).
63. Konvisar, P. G. and A. A. Fomichev, *Trudy MFTI, ser. Radiotechnika i Elektronika*, Part 1, 83 (1972).
64. Konvisar, P. G., S. R. Rustamov, and A. A. Fomichev, *Kvant. Elektronika*, **1**, 3, 667 (1974).
65. Arsen'ev, V. A., I. N. Matveev, and N. D. Ustinov, *Kvant. Elektronika*, **4**, 11, 2309 (1977).
66. Marschall, F. R. and O. L. Roberts, *Proc. IRE*, **50**, 10, 2108 (1962).
67. Gryaznov, Yu. M. and A. A. Chastov, *Zh. Prikl. Spektr.*, **16**, 4, 658 (1972).
68. Dmitriev, V. G. and V. K. Novokreshchenov, *Kvant. Elektronika*, **4**, 7, 1582 (1977).
69. Statz, H. and G. De Mars, in: *Quantum Electronics* (C. H. Townes, Ed.), Columbia Univ. Press, New York, 1960.
70. Tarasov, L. V., *Physical Principles of Quantum Electronics (Optical Region)*. Sov. Radio, Moscow, 1976 (in Russian).
71. Menne, T., *IEEE Journ.*, **QE-2**, 2, 38 (1966).
72. Morozov, V. N., *Kvant. Elektronika*, **1**, 3 (1974).
73. Genkin, V. N. and Ya.I. Khanin, *Izv. Vuzov SSSR. Radiofizika*, 5, 3, 423 (1962).
74. Tang, C., *J. Appl. Phys.*, **34**, 10, 2935 (1963).
75. Lamb, W. E., *Phys. Rev.*, **134**, 1429 (1964).
76. Ostrovskii, L. A., *Zh. Eksp. Teor. Fiz.*, **48**, 4, 1087 (1965).
77. Ostrovskii, L. A., *Zh. Eksp. Teor. Fiz.*, **49**, 5 (11), 1535 (1965).
78. Migulin, V. V. (Ed.), *Basic Principles of the Theory of Vibrations*. Nauka, Moscow, 1978 (in Russian).
79. Maitland, A. and M. H. Dunn, *Laser Physics*. North-Holland Publishing Co., Amsterdam-London, 1969.
80. Landau, L. D. and E. M. Lifshitz, *Quantum Mechanics (Non-relativistic Theory)*. Pergamon Press, Oxford, 1977.

81. Makhov, G., *J. Appl. Phys.*, **33**, 1, 202 (1962).
82. Sinnet, D., *J. Appl. Phys.*, **33**, 4, 1578 (1962).
83. Korobkin, V. V. and A. V. Uspenskii, *Zh. Eksp. Teor. Fiz.*, **45**, 4 (10), 1003 (1963).
84. Uspenskii, A. V., *Radiotekh. i Elektronika*, **9**, 4, 747 (1964).
85. Oraevskii, A. N. and A. V. Uspenskii, *Trudy FIAN SSSR*, **31**, 96 (1965).
86. Bespalov, V. I. and A. V. Gaponov, *Izv. Vuzov SSSR. Radiofizika*, **8**, 1, 70 (1965).
87. Andronov, A. A., A. A. Witt, and S. E. Khaikin, *Theory of Vibrations.* Fizmatgiz, Moscow, 1965 (in Russian).
88. Statz, H. and C. Tang, *J. Appl. Phys.*, **35**, 5, 1377 (1964).
89. Morosov, V. N. and A. N. Oraevskii, *Izv. Vuzov SSSR. Radiofizika*, **9**, 4, 710 (1966).
90. Tsikunov, V. N., *Zh. Eksp. Teor. Fiz.*, **58**, 5, 1646 (1970).
91. Vinokurov, G. N., *Optika i Spektroskopia*, **31**, 3, 472 (1971).
92. De Maria, A. and R. Gagosz, *Proc. IRE*, **56**, 6, 1522 (1962).
93. Kozlov, V. K., E. R. Mustel, and V. N. Parygin, *Radiotekh. i Elektronika*, **14**, 5, 875 (1969).
94. Nikogosyan, D. N., *Kvant. Elektronika*, **4**, 1, 5 (1977).
95. Maydan, D., *IEEE Journ.*, **QE-6**, 1, 15 (1970).
96. Prokhorov, A. M., *Radiotekh. i Elektronika*, **8**, 6, 1073 (1963).
97. Wagner, W. and B. Lengyel, *J. Appl. Phys.*, **34**, 7, 2040 (1963).
98. Menat, M., *J. Appl. Phys.*, **36**, 1, 73 (1965).
99. Golubeva, N. S., L. F. Krinitsyna, L. S. Orbachevskii, and V. I. Rozhdestvin, *Kvant. Elektronika*, **4**, 1, 49 (1977).
100. Sorokin, P., J. Luzzi, J. Lankard, and G. Pettit, *IBM J. Res. Dev.*, **8**, 2, 182 (1964).
101. Armstrong, J., *J. Appl. Phys.*, **36**, 2, 471 (1965).
102. Ermakov, B. A. and A. V. Lukin, *Zh. Prikl. Spektr.*, **4**, 5, 410 (1966).
103. Gross, L. and M. Cheng, *J. Appl. Phys.*, **38**, 5, 2290 (1967).
104. Roshchin, R. V., *Izv. Vuzov SSSR., Radiofizika*, **16**, 7, 1006 (1973).
105. Bespalov, V. I. and E. I. Yakubovich, *Izv. Vuzov SSSR. Radiofizika*, **8**, 5, 909 (1965).
106. Sushchik, M. M. and G. I. Freidman, *Izv. Vuzov SSSR. Radiofizika*, **9**, 5, 919 (1966).
107. Erickson, L. and A. Szabo, *J. Appl. Phys.*, **37**, 13, 4953 (1966).
108. Szabo, A. and R. Stein, *J. Appl. Phys.*, **36**, 5, 1562 (1965).
109. Borovich, B. L., V. S. Zuev, and V. A. Shcheglov, *Zh. Eksp. Teor. Fiz.*, **49**, 4 (10), 1031 (1965).
110. Sooy, W., *Appl. Phys. Letters*, **7**, 2, 36 (1965).
111. Kuznetsova, T. I., *Trudy FIAN SSSR*, **84**, 62 (1975).
112. Kulzenga, D. J. and A. E. Siegman, *IEEE Journ.*, **QE-6**, 11, 694 (1970).
113. Siegman, A. E. and D. J. Kulzenga, *Opto-Electronics*, **6**, 1, 43 (1974).
114. Osterink, L. and J. Foster, *J. Appl. Phys.*, **39**, 9, 4136 (1968).
115. Gutfeld, von, R., *Appl. Phys. Letters*, **18**, 11, 481 (1971).
116. Letokhov, V. S., *Zh. Eksp. Teor. Fiz.*, **55**, 9, 1077 (1968).
117. Lariontsev, E. G. and V. N. Serkin, *Kvant. Electronika*, **1**, 10, 2166 (1974).
118. Kuznetsova, T. I., V. I. Malyshev, and A. S. Markin, *Zh. Eksp. Teor. Fiz.*, **52**, 2, 438 (1967).
119. Krivoshchekov, G. V., N. G. Nikulin, and V. A. Smirnov, *Kvant. Elektronika*, **2**, 9, 2019 (1975).
120. Vartapetov, S. K., V. I. Vovchenko, I. K. Krasyuk, and P. P. Pashinin, *Kvant. Elektronika*, **3**, 11, 2450 (1976).
121. Altshuler, G. B., V. B. Krasev, and S. F. Sharlai, *Kvant. Elektronika*, **4**, 4, 878 (1977).
122. Terenin, A. N., *Dye Photenics.* Nauka, Leningrad, 1967 (in Russian).
123. Babenko, V. A., V. D. Kovin, V. I. Malyshev, and A. A. Sychev, *Kvant. Elektronika*, **1**, 5, 1228 (1974).
124. Sychev, A. A., *Trudy FIAN SSSR*, **84**, 3 (1975).

125. Babenko, V. A., V. I. Malyshev, A. A. Sychev, and A. N. Shibanov, *Kvant. Elektronika*, 2, 9, 1923 (1975).
126. Abakumov, G. A., A. I. Antipov, A. P. Simonov, A. D. Shiltsyn, and V. V. Fadeev, *Kvant. Elektronika*, 4, 11, 2442 (1977).
127. Zherikhin, A. N., P. G. Kryukov, Yu. A. Matveets, and S. V. Chekalin, *Kvant. Elektronika*, 1, 4, 956 (1974).
128. Vlasov, S. N. and Yu. K. Verevkin, *Kvant. Elektronika*, 3, 5, 991 (1970).
129. Zherkhin, A. N., Yu. A. Matveets, and S. V. Chekalin, *Kvant. Elektronika*, 3, 7, 1585 (1976).
130. Lariontsev, E. G. and V. N. Serkin, *Kvant. Elektronika*, 2, 7, 1481 (1975).
131. Armstrong, J., *Appl. Phys. Letters*, 10, 1, 16 (1967).
132. Giordmaine, J., P. Rentzepis, S. Shapiro, and K. Wecht, *Appl. Phys. Letters*, 11, 7, 216 (1967).
133. Landau, L. D. and E. M. Lifshitz, *Lehrbuch der Teoretischen Physik, Bd. 5. Statistische Physik*. Akademie Verlag. Berlin, 1966.
134. Dmitriev, V. G., A. N. Denisov, and E. A. Shalaev, *Kvant. Elektronika*, 5, 11, 2479 (1978).
135. Barnes, N. R., *J. Appl. Phys.*, 45, 3, 1291 (1974).
136. Novokreshchenov, V. K. and S. R. Rustamov, *Abstracts of the I All-Union Conf. on Problems of Controlling the Parameters of Laser Radiation*, Tashkent, 1978.
137. Rice, R. R., G. H. Burkhart, and J. R. Teague, *J. Appl. Phys.*, 47, 7, 3045 (1976).

INDEX

Absorption of radiation,
 triplet-triplet, 34
 two-photon, 316
activator, 24
active centres, 59
active medium, 53, 9ff
amplification factor, 9
approximation
 geometrical (optics), 99
 two-level, 231

Bragg's reflection, 210

Caustic, 159, 162
cavity dumping, 224, 227, 269
cavity, nonselective, 307
coefficient(s)
 Einstein, 77, 235
 gain, 77
 loss, 77
condition(s),
 of creating stationary inversion, 21
 pulse generation, 19
conversion,
 internal, 34
 singlet-triplet, 34
creation of inversion,
 direct, 61f
 indirect, 61f

De-exitation,
 chemical, 14
 electronic, 14
 through adiabatic expansion, 14
depopulation of levels, radiative, 13
diagram, four-level, 29, 232
diffraction,
 Bragg, 266
 Raman-Nath, 267
 mirror-edge, 171
dispersion prism, 35
distributed feedback (DFB), 210f

Effect,
 Doppler, 184
 longitudinal, 260
 edge, 172
 electro-optical, 267
 frequency pulling, 183, 187, 223
 hole burning, 87, 183ff
 Kerr, 263
 photoelastic, 266
 piezooptic, 191
 Pockels, 263
 longitudinal, 264
 thermal lens, 87
efficiency, 10
electric discharge,
 afterglow, 69
 arc, 40
 glow, 40f
 non-self-sustained, 51
 pulsed, 40
 quasi-stationary, 40
 self-sustained, 50, 59
 stationary, 40
electron excitation,
 cascade, 44
 direct, 44
 step-by-step, 44
energy level(s),
 atomic, 28
 excitation, 25
 ground, 25
 laser,
 lower, 25, 27f
 upper, 25, 27f
energy-liberating element (ELE), 70
equation(s)
 balance, 11, 22, 229, 231, 245, 253, 256, 272, 284, 296
 averaged, 233, 237
 complete system of, 232
 characteristic, 247, 290, 343
equation(s)
 Fox-Li integral, 118
 Maxwell, 242
 parabolic, 140
 point, 241
 rate, 233
 reduced, 244
 self-consistent, 244
 Statz-De Mars, 235, 237, 240, 250, 256

first, 236
second, 236
of thin lens, 102
wave, 242
excitation of generation,
hard, 292
soft, 292

Fabry-Perot interferometer, 34, 177
filling factor, 286
filter, bleachable, 309, 311
formula, recurrence, 336
Franck-Condon principle, 37
frequency selection, 175ff
Fresnel number, 95ff, 155, 162
equivalent, 171, 173
Fresnel zone, 96
function, correlation intensity, 317

Gain, initial, 73, 75f
frequency dependence, 78
gain line, 78
gain saturation, 87, 187
Gaussian beam, 134ff, 140, 168, 267
complex parameters, 139
in free space, 339
phase shift, 156
in stable resonators, 151
transformation and matching, 142, 145f, 148f
Gaussian noise, 324
Gaussian spike, 326
giant pulse generation, 270ff

Hermite polynomials, 336
degree of orthonormal completeness, 338
differential equations for, 337

Index, nonlinearity, 325
induced emission, 9
inverse population density, 9
inversion of active medium, 9
inversion threshold, 23

Jones matrix(ces), 181, 341ff
Jones vector, 181

Kirchhoff-Huygens diffraction integral, 117

Laser(s),
argon, 41ff
creation of inversion, 42f
atomic, 39
bleachable filter, 309, 319f
generation, 295ff
instability, 290
single-mode, 288
chemical, 15ff, 58ff
CO, 63
DF-CO_2, 62
on electronic transitions, 64
CO_2, 46
creation of inversion, 47
collision, 17, 49
compressed gas, 51
copper-vapour, 46
electroionisation, 50ff
Ar + N_2, 53
CO, 53
CO_2, 52f
compressed xenon, 53
electron beam, 66
four-level, 330
gas, 50
with wide-band optical pumping, 36ff
gas-discharge, 39f, 56, 66
gasdynamic, 54ff
CO_2, 55f
efficiency, 58
geometrical optics, 165
helium-neon, 44
ionic, 16, 39
liquid, 15f, 30
molecular, 16, 39, 66
multimode, 242, 255, 303
Nd, 241, 304, 307, 326
Nd:YaG, 27ff, 43
noble-gas molecular, 19
nuclear pumping, 66
organic dye, 30ff
optical pumping, 32
photochemical, 38
photodissociation, 16, 37
iodine, 38
plasma, 16, 64
based on electronic transitions, 72
Sr-He, 211
plasmachemical, 72
plasmadynamic, 66, 70
plasmamechanical, 66
pulsed, 66
plasma, 69
Q-switched, 264
recombination, 65

laser(s),
reactor, 69
ruby, 261, 241
semiconductor, 15, 30
single-mode, 242
solid-state, 15f, 20f, 24, 249
thin-film, 201, 211f
DFB, 211
three-level, 230, 239
unstable resonator, 256
waveguide resonator, 196
laser level depopulation, 67
laser resonator, 73ff

Matrix, 24
method,
Fox-Li iterative, 116
initiation,
by electric discharge, 59
by electron impact, 59
photoionization, 59
thermal, 59
ionisation, 53
photoionisation, 53
for investigating pulse structure,
based on second harmonic generation, 314
collision, 314
direct, 313f
holographic, 314
indirect, 313f
two-photon, 314
luminescence, 313
mode(s),
longitudinal, 223
phase-locked, 308
transverse,
electrical, 202
magnetic, 201
wavequide, 196, 200
parasitic, 197
mode locking, 223
acoustooptic, 334
active, 308f
combination method, 310f
complete, 307, 317f, 323, 328
electro-optical, 334
incomplete, 317f
longitudinal, 305f
amplitude modulation, 304
partial, 323
passive, 309
phase, 334
spectral, 322
spontaneous, 223
stationary, 332
time-based, 322, 328
model, four-level, 10
inversion condition, 11f

Optical cavity, 73f
optical resonator, 78f
active, 86
passive, 86
role in laser, 83
optical resonator,
vibrational modes, 82f
longitudinal, 82
transverse, 82
organic dyes, 30f
output mirror, 93

Period, modulation (resonator), 306
phase advance, 78
phase corrector, 143
phase locking, 304
phase shift, 80, 118
pinch effect, 71
plasma, degree of ionisation, 41
ionised, 65
recombination, 64f
polariser, 342
population inversion, 9ff
pumping,
chemical, 13, 15
continuous coherent, 32
electro-ionisation, 13
non-stationary, 215
optical, 13, 15
coherent, 20
efficiency, 24
incoherent, 20, 33
quantum efficiency, 24
pulsed, 17
recombination, 13, 15, 64
pumping,
by self-sustained discharge, 15
stationary, 11
thermal, 13, 15, 54
pumping rate, 22, 76, 81

Q-factor, 218f
acoustooptic, 267
Q-switching, 262f
acoustooptic, 262, 266, 268, 226
active, 300f,
combined, 300, 302
electro-optical, 263, 268
instantaneous, 272, 299

mechanooptical, 262
passive, 296, 300f, 303
quantum yield, 10
quenching,
concentration, 311
luminescence, 311

Reflecting diffraction grating, 35
resonator(s)
active, 189
astigmatic, 136
asymmetric, 133, 154
resonator(s)
concentric, 98
condition for stability, 103
confocal, 98, 123, 129, 153, 159, 161
consisting of two spherical mirrors, 120
coupled, 178
diaphragm, 132, 162
equivalent, 128, 161
half waveguide, 198
non-confocal, 122
open, 98f, 100, 116f
detuning, 112f
modes, 94
Q-factor, 91ff
stable, 101, 103
transverse modes, 119
unstable, 92, 101, 103
passive, 189
plane-parallel, 98, 154
Q-factor, 256
active modulation, 270ff
Q-modulation, 215
active, 218
passive, 220
ring, 98
selective, 34, 117
semiconcentric, 98
semiconfocal, 98
stability diagram, 104
resonator(s),
unstable, 153f, 163, 165, 340
ABCD law, 168
geometrical optics losses, 165
telescopic, 170
waveguide, 195
cavity, 197
plane, 197
radiation field, 323
relaxation time, 310f

Second-harmonic generation, 327
selection rules, 13
self-focusing of light, 312
self-mode locking, 309, 319
singular points, 343
spectral selective element, 34
spectrum,
absorption, 28
luminescence, 29
spherical waves,
stable, 340
unstable, 346
Stark's splitting, 28, 43
states of molecules,
electronic, 33
rotational, 33
singlet, 33
triplet, 33
vibrational, 33
superluminescence, 312

Temperature,
discharge, 40
electron, 40
thermal lens, 190
transformation matrix, 106, 109
transitions,
dipole, 75
magneto-dipole, 75
non-optical, 15
optically allowed, 75
optically forbidden, 75f
purely rotational, 39
quadrupole, 75
self-terminating, 17f
vibration-rotation, 39, 49, 59

Ultrasonic wave,
standing, 335
travelling, 334

Vibrational modes
asymmetric, 47
deformation, 47
symmetric, 47
vibrations of CO_2 molecule,
asymmetric, 58
symmetric deformation, 58

Waveguide, thin-film, 200ff

TO THE READER

Mir Publishers would be grateful for your comments on the content, translation and design of this book. We would also be pleased to receive any other suggestions you may wish to make.
Our address is: Mir Publishers,

2 Pervy Rizhsky Pereulok,
I-110, GSP, Moscow, 129820,
USSR.

Printed in the Union of Soviet Socialist Republics

ALSO FROM MIR PUBLISHERS

Nuclear Physics, Vols. I-II

Yu. SHIROKOV, D. Sc. and N. YUDIN, Cand.Sc.

This is the second edition of a comprehensive course of general nuclear physics for undergraduates specializing in physics. It is an up-to-date survey of all fields of experimental and theoretical nuclear physics and physics of elementary particles. Theoretical results are explained to make them comprehensible to readers not familiar with quantum mech nics and the theory of relativity.

Problems in Atomic and Nuclear Physics

I. IRODOV, Cand.Sc. (Phys.-Math.)

The book is directed at undergraduates taking general courses in atomic and nuclear physics. It contains, however, a sufficient number of problems lying outside a general course to make it helpful in studies of some special courses just as well. Over a thousand problems are subdivided in 17 sections embracing all major domains of atomic and nuclear physics. The answers and solutions take up over one third of the volume. Many of them are provided with detailed explanations.

About the Author

Professor Lev Vasilyevich Tarasov of the Institute of Electronic Engineering in Moscow has been working in the fields of quantum electronics and optics, as well as popularization of science. He is author of about a dozen textbooks and monographs dealing with different aspects of problems concerning these fields. Besides he has about 100 scientific publications to his credit. Owing to their lucid style, and clarity of expression the books written by Prof. Tarasov enjoy a wide popularity both in the Soviet Union and abroad. Besides English, his books have been translated into French, Spanish, German, Japanese, Hungarian and Tamil.

OTHER BOOKS FOR YOUR LIBRARY

Calculus. Basic Concepts for High Schools

by L. TARASOV, Cand. Sc.

The book presents an exposition of the fundamental concepts and definitions of calculus taught to high school students. It is written in the form of an animated explicatory dialogue between the AUTHOR and the READER. The book will be useful supplement for standard textbooks on algebra and fundamentals of calculus.